Diurnal variation in nicotine-mediated behaviour, cholinergic signalling and gene expression in the rodent brain

A thesis submitted to The University of Manchester for the degree of

Doctor of Philosophy

in the Faculty of Biology, Medicine and Health

2021

Abigail J C Pienaar

School of Medical Sciences

Division of Diabetes, Endocrinology and Gastroenterology

Table of Contents

WORD COUNT: 68 841 (excluding References and Appendices)

List of Figures

List of Tables

List of Abbreviations

Abbreviation	Definition
3V	Third ventricle
5-HT	Serotonin (5-hydroxytryptamine)
AAV	Adeno-associated virus
ACh	Acetylcholine
AChE	Acetylcholinesterase
AChR	Acetylcholine receptor
aCSF	Artificial cerebrospinal fluid
ANOVA	Analysis of variance
ATP	Adenosine triphosphate
AVP	Arginine vasopressin
BAC	Bed nucleus of the anterior commissure
BH	Benjamini-Hochberg
bHLH	Basic helix–loop–helix
CCH	Cross-correlation histogram
ChAT	Choline acetyltransferase
ChR2	Channelrhodopsin
CNQX	Cyanquixaline (6-cyano-7-nitroquinoxaline-2,3-dione)
CNO	Clozapine-N-oxide
CNS	Central nervous system
CRY	Cryptochrome
DA	Dopamine
DD	Constant darkness
DHβE	Dihydro-β-erythroidine hydrobromide
DL-AP5	DL-2-Amino-5-phosphonopentanoic acid
DNA	Deoxyribonucleic acid
DR	Dorsal Raphe
EIF2	Eukaryotic initiation factor 2
EYFP	Enhanced Yellow Fluorescent Protein
FC	Fold-change
FR	Fasciculus retroflexus
GABA	Gamma-aminobutyric acid
GHT	Geniculohypothalamic tract
Glu	Glutamate
GLuR	Glutamate receptor
GRP	Gastrin-releasing peptide
HCN	Hyperpolarization-activated cyclic nucleotide–gated
HNF4A	Hepatocyte nuclear factor-4-alpha
hr-MRI	Ultra-high resolution Magnetic Resonance Imaging
IGL	Intergeniculate leaflet
IGF-1	Insulin-like growth factor 1
IPA	Ingenuity Pathway Analysis
IPN	Interpeduncular nucleus
ipRGC	Intrinsically photosensitive retinal ganglion cell
LD	Light / dark cycle
LDTg	Laterodorsal tegmental nucleus
LGN	Lateral geniculate nucleus
LHb	Lateral habenula
MD	Mean difference
MEA	Multielectrode array
MHb	Medial habenula

MHb-IPN	Medial habenulo-interpeduncular pathway
MIII	Oculomotor nucleus
Min	Minutes
MnR	Median Raphe
MOp	Primary motor area of the cortex
MSDB	Medial septum / nucleus of the diagonal band
MUA	Multi unit activity
NAc	Nucleus accumbens
nAChR	Nicotinic acetylcholine receptor
ND	Neutral density
NDB	Nucleus of the diagonal band
NFIL3	Nuclear factor, interleukin 3 regulated
Nic	Nicotine
NMDA	N-methyl-D-aspartate
NPY	Neuropeptide Y
PACAP	Pituitary adenylate cyclase-activating polypeptide
PAS	Period-Arnt-Sim
PBS	Phosphate-buffered saline
PCA	Principal component analysis
PCR	Polymerase chain reaction
PER	Period
pHb	Peri-habenular region
pMEA	Perforated multielectrode array
RBE	ROR-binding elements
REM	Rapid eye movement
Rev-Erb	Nuclear receptor subfamily 1 group D member
RHT	Retinohypothalamic tract
RM	Repeat measures
RNA	Ribonucleic acid
ROR	Retinoic acid-related orphan receptor
SCN	Suprachiasmatic nucleus
SFi	Septofimbrial nucleus
SM	Stria medullaris
SP	Substance P
SUA	Single unit activity
TS	Triangular septum
TTX	Tetrodotoxin
UMI	Unique Molecular Identifier
VAChT	Vesicular acetylcholine transporter
VIP	Vasoactive intestinal polypeptide
VTA	Ventral tegmental area
ZT	Zeitgeber time

Abstract

Circadian rhythms are ubiquitous throughout biology. In mammals, these rhythms are centrally orchestrated by the master pacemaker, the suprachiasmatic nuclei (SCN), which aligns rhythms in internal physiology with the external geophysical time. In addition, there are other brain structures outside of the SCN which are also capable of generating endogenous oscillations in gene expression and neuronal activity, and thus control the timing of diverse processes such as mood regulation, rest-activity cycles, feeding behaviour and other aspects of the brain's reward system. Interestingly, accumulating evidence suggests that smoking behaviours are also modulated by the time of day, indicating that the circadian system might be controlling the endogenous cholinergic pathways underlying these behaviours. Therefore, to investigate this possibility, the overall aim of this thesis was to explore how the time of day impacts the key brain circuitry mediating nicotine's effects, specifically within the medial habenula (MHb).

We began by investigating daily variation in behavioural responses to nicotine in rats. We found that there was significant diurnal variation in nicotine-evoked changes in locomotor behaviour which appeared to be dependent on the level of arousal of the animal. These experiments support the idea that there is a rhythmic component to the circuitry underlying nicotine responses.

The next aim was to explore circadian variation in cholinergic signalling at the network level. These studies focussed specifically on the MHb, a small structure of the epithalamus, which is implicated both as a critical mediator of smoking behaviours and has also been identified as a potential circadian oscillator. We explored circadian variation in mouse MHb neuronal activity and cholinergic signalling through the use of both *ex*- and *in vivo* electrophysiological approaches. *Ex vivo*, we found evidence of rhythmicity in spontaneous firing activity, even in the absence of SCN input, and diurnal variation in responses to nicotine. We further confirmed rhythmicity in MHb neuronal activity *in vivo*, and revealed that MHb cholinergic neurons integrate both circadian and photic information, which could contribute to the rhythmic drive in nicotine addiction behaviours.

Finally, we investigated the molecular mechanisms driving the diurnal variation in MHb properties. We generated a diurnal transcriptomic profile of mouse MHb tissue, and whilst we did not find evidence for robust rhythms in molecular clock gene expression, we did however find a group of rhythmic transcripts which were associated with hormone signalling and mechanisms regulating synaptic plasticity that may underlie rhythms in MHb function.

Overall the results presented in this thesis indicate that there is certainly rhythmic control of rodent MHb activity, response to nicotine and cholinergic output. This highlights the MHb as a potential site for diurnal modulation of goal-directed behaviours including those related to nicotine addiction, which has implications both for the treatment of nicotine addiction as well as other mood disorders which might be modulated through this structure.

Declaration

No portion of the work referred to in the thesis has been submitted in support of an application for another degree or qualification of this or any other university or other institute of learning.

Copyright Statement

Contributions from Collaborators

All experiments and analysis were performed by AP other than the following:

Chapter 2: AP designed the experiments in collaboration with Professor Joanna Neill.

Chapter 3: AP designed the experiments in collaboration with Professor Timothy Brown and Professor Hugh Piggins. Professor Timothy Brown wrote the LabView programs for control of the light stimuli during electrophysiological experiments and the Matlab scripts for processing the data.

Chapter 4: AP designed the experiments in collaboration with Professor Timothy Brown. Professor Timothy Brown wrote the LabView programs for control of the light and optogenetic stimuli during electrophysiological experiments and the Matlab scripts for processing the data, and assisted with some of the data processing.

Chapter 5: AP designed the experiments in collaboration with Professor Hugh Piggins.

Acknowledgements

First, I'd like to thank Prof. Tim Brown, whose supervision over the past few years has been invaluable. Thank you for your direction and guidance throughout the project, and for your insightful comments on this thesis – as well as taking me on at short notice! This thesis would not have been possible without your help.

Secondly, I'd like to thank Prof. Hugh Piggins, who first offered me the chance to undertake my PhD. Thank you for continued supervision and support even over long distances.

Sincere thanks to Prof. Jo Neill for her guidance in a field that was new for me, and for offering me great mentorship even over a short time.

Thanks to all the assorted members of the Lucas and Brown labs, who have been there to offer advice and commiseration when experiments failed, and encouragement to carry on.

Finally, I have to acknowledge my family, friends and partner. I am privileged to have the best support network around me, and it is due to their unwavering support that this thesis was even possible. These may have been some of the most challenging years of my life, but you've kept my chin up, wine glass full and constantly reminded me of a life beyond the lab. Thank you all.

The Author

i) Journal publications

Mouland, J. W., Pienaar, A., Williams, C., Watson, A. J., Lucas, R. J., & Brown, T. M. (2021). Extensive cone-dependent spectral opponency within a discrete zone of the lateral geniculate nucleus supporting mouse color vision. *Current Biology*, *31*(15), 3391-3400.e4. https://doi.org/10.1016/j.cub.2021.05.024

Pienaar, A., Walmsley, L., Hayter, E., Howarth, M., & Brown, T. M. (2018). Commissural communication allows mouse intergeniculate leaflet and ventral lateral geniculate neurons to encode interocular differences in irradiance. *The Journal of Physiology*, *596*(22), 5461–5481. https://doi.org/10.1113/JP276917

Hanna, L., Walmsley, L., Pienaar, A., Howarth, M., & Brown, T. M. (2017). Geniculohypothalamic GABAergic projections gate suprachiasmatic nucleus responses to retinal input. *The Journal of Physiology*. https://doi.org/10.1113/JP273850

Cehajic-Kapetanovic, J., Eleftheriou, C., Allen, A. E., Milosavljevic, N., Pienaar, A., Bedford, R., Davis, K. E., Bishop, P. N., & Lucas, R. J. (2015). Restoration of Vision with Ectopic Expression of Human Rod Opsin. *Current Biology: CB*, *25*(16), 2111–2122. https://doi.org/10.1016/j.cub.2015.07.029

ii) Conference presentations

Pienaar, A., Baño-Otálora, B., Belle, M., Piggins, H.D., (2019). Daily variation in electrophysiological sensitivity to nicotine within the medial habenula [Poster session]. British Neuroscience Association Conference, Dublin, Ireland.

Pienaar, A., Baño-Otálora, B., Piggins, H.D., (2018). Daily variation in electrophysiological and behavioural sensitivity to nicotine [Poster session]. Sleep and Circadian Neuroscience Institute Summer School, Oxford, UK.

Pienaar, A., Cehajic-Kapetanovic, J., Davis, K.E., Bishop, P.N., Lucas, R.J., (2015). Measuring visual acuity and assessing the efficacy of optogenetic therapy in mice using a voluntary behaviour paradigm [Poster session]. ARVO Annual Meeting, Denver, Colorado, USA.

iii) Funding and Awards

British Neuroscience Association Conference, Dublin (2018) – Runner up poster prize (£50)

Biotechnology and Biological Sciences Research Council Doctoral Training Partnership Award (2017 – 2021)

Presidents Doctoral Scholar Award (2017 – 2021)

1 General Introduction

1.1 The circadian timekeeping system

Throughout history, a feature of life on Earth has been its constant and predictable rotation around its axis, reliably generating a transition from light to dark to light every 24 hours. As organisms evolved to better suit their environment, many developed mechanisms of anticipating this change from dark to light and synchronising their physiology and behaviour to optimal times (Bell-Pedersen et al., 2005). These oscillatory processes are diverse, ranging from rhythms in cell division as demonstrated in cyanobacteria (Johnson and Golden, 1999), rhythms in leaf movement to maximise photosynthesis during the day in plants (Creux and Harmer, 2019), to the pronounced sleep-wake cycles demonstrated in most mammals (Fuller et al., 2006). A key feature of circadian rhythms is that they are self-sustained – rather than being driven in response to a changing environment, rhythms will recur with a period close to 24 hours even in the absence of any time cues (for example, in constant darkness) (Vitaterna et al., 2001).

Since the 2017 Nobel Prize in Physiology or Medicine was awarded to Jeffrey C. Hall, Michael Rosbash and Michael W. Young for their work on uncovering the molecular mechanisms controlling circadian rhythmicity, circadian biology has been cemented as a fundamental component of the study of life on Earth. The circadian system is vital for maintaining physiological harmony, and can be more readily appreciated when this internal system becomes out of sync with the geophysical time. Jet-lag is a commonly experienced outcome of perturbations in entrainment, and causes poor sleep and suboptimal performance (Reid and Abbott, 2015). However, longer term circadian misalignments can have serious health consequences: shift work can increase the risks of developing metabolic disorders (Brum et al., 2015) and is even classed as a probable carcinogen (Erren et al., 2019).

1.1.1 Molecular components of the circadian clock

Cellular timekeeping relies on a transcription-translation feedback loop of core “clock genes” which oscillate with a period close to 24 hours (Buhr and Takahashi, 2013). The cellular mechanism driving these rhythms relies on molecular autoregulatory feedback loops, which may have evolved independently several times throughout history (Bhadra et al., 2017), demonstrating how important circadian rhythms are for conferring evolutionary fitness. The discovery of clock genes in the 1990s revealed the ubiquitous nature of the circadian molecular clock (Takahashi, 2017), with virtually all cells expressing these genes and thus having the capacity for rhythm

generation. Indeed, one study revealed that in the mouse, 43% all protein-coding genes demonstrated circadian rhythmicity in at least one of twelve organs (Zhang et al., 2014), and similarly an investigation of 64 tissues in the baboon found that the majority (>80%) of protein-coding genes show daily rhythms in expression in at least one tissue (Mure et al., 2018). Together, these studies underscore the pervasive nature of the circadian control of the transcriptome.

Figure 1.1 summarises the mammalian molecular clock. In mammals, the activating arm of this transcription-translation feedback loop involves the proteins CLOCK and BMAL1 (otherwise known as ARNTL), both basic helix-loop-helix (bHLH) Period-Arnt-Sim (PAS)-type transcription factors (Gekakis et al., 1998; Honma et al., 1998). These proteins heterodimerize in the cytoplasm and translocate to the nucleus, to bind E-boxes upstream of their target genes (Hao et al., 1997; Takahashi, 2017). This triggers the transcription of the proteins PERIOD (PER, encoded by *Per1, Per2, Per3*) and CRYPTOCHROME (CRY, encoded by *Cry1, Cry2)*, initiating the repressive arm of the cycle (Kume et al., 1999; Shearman et al., 2000). Once PER and CRY proteins are expressed, they too heterodimerize, and translocate to the nucleus to inhibit transcription of CLOCK:BMAL1, thus repressing their own transcription (Michael et al., 2017). In addition, PER and CRY are regulated by the serine-threonine kinases Casein kinase 1δ (CK1δ) and CK1ε (Etchegaray et al., 2009; Lee et al., 2001), which controls their degradation through phosphorylation and sets the speed of the clock (Yang et al., 2017). As the PER:CRY complexes are degraded, this relieves the inhibition on the activating arm of this loop and so the cycle begins again, running with 24 hour period (Takahashi, 2017).

The mammalian molecular clock is further regulated by additional genes and feedback loops. In the second major transcriptional loop, CLOCK:BMAL1 proteins induce expression of the nuclear receptors REV-ERBα and REV-ERBβ (encoded by *Nr1d1* and *Nr1d2*), which compete with the RAR-related orphan receptors RORα, RORβ, and RORγ for binding sites on the *BMAL1* gene (Preitner et al., 2002). Thus, the competition for ROR-binding elements (RBE) provides further regulation of transcription (Sato et al., 2004). In the third loop, CLOCK:BMAL1 and CRY1 activate D-box binding protein (DBP), driving transcription in genes which contain D-boxes including *RORα*, *RORβ*, and *RORγ* (Ripperger and Schibler, 2006; Stratmann et al., 2010). The REV-ERB and ROR target gene, nuclear factor interleukin-3 regulated protein (NFIL3), inhibits D-box dependent transcription (Ueda et al., 2005).

Together, these loops work to drive downstream recurrent rhythms in gene expression. The core clock genes can bind to thousands of regulatory targets (Sun et al., 2020), depending on the function of the tissue – for example, clocks in the pancreas regulate insulin release and glucose

homeostasis (Sadacca et al., 2011), whilst clocks in the heart influence heart rate and blood pressure (Crnko et al., 2019). However, they rely on a master pacemaker in order to ensure the correct timing of these processes.

1.1

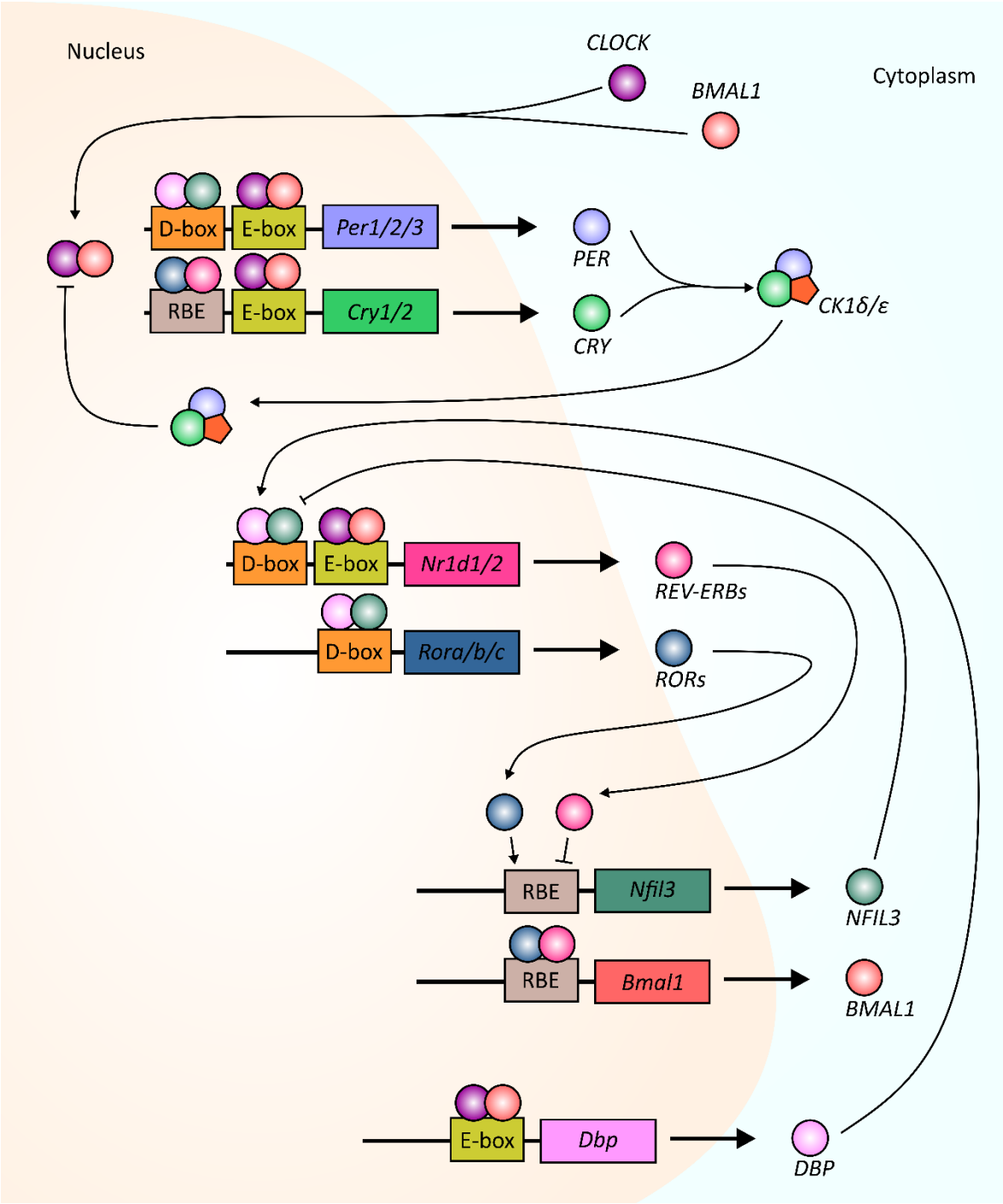

Figure 1.1 The mammalian molecular clock

A simplified diagram of the core autoregulatory feedback loops driving the mammalian molecular clock. BMAL1 and CLOCK bind the DNA of target genes at E-boxes to drive expression of PER and CRY proteins in the primary positive arm of the loop, and the REV-ERBs and DBPs in the accessory loops. PER and CRY form heterodimers in the cytoplasm and translocate to the nucleus to inhibit the transcription of *Clock* and *Bmal1*, thus repressing their own transcription and forming the negative arm of the feedback loop. REV-ERBα/β and RORα/β/γ compete to bind at the RBE sites and drive rhythmic transcription of *Bmal1* and *Nfil3*. Figure adapted from Takahashi, 2017.

1.1.2 The mammalian master clock is the suprachiasmatic nucleus

Despite most cells containing the molecular clock machinery for generating endogenous rhythms, they rely on a master clock to synchronise the oscillations and keep physiological processes aligned with the external environment (Hastings et al., 2019). In mammals, the master pacemaker is the suprachiasmatic nucleus of the hypothalamus (SCN). The SCN receives information that signals the time of the external day, known as 'Zeitgebers' ('time-givers'), and fine-tunes its period accordingly to match the perceived geophysical time. In mammals, the principal Zeitgeber is light (Meijer and Schwartz, 2003), but the SCN can also entrain to food intake (Mistlberger, 2011), social interaction (Grandin et al., 2006) and exercise (Tahara et al., 2017).

1.1.3 Anatomy and connectivity of the SCN

In humans, each SCN nuclei is comprised of approximately 42 000 neurons (Hofman et al., 1996), and 10 500 in mice (Abrahamson and Moore, 2001), located bilaterally either side of the third ventricle (3V), directly above the optic chiasm. Traditionally the SCN has been subdivided into 'core' and 'shell' subregions based on afferent connectivity and neuropeptide co-expression (Hastings et al., 2018; Moore, 1983), although SCN neurons are believed to near uniformly express the neurotransmitter gamma aminobutyric acid (GABA). This terminology originated with studies of hamster SCN, although analogous subdivisions also apply to other rodent species. Hence, vasoactive intestinal peptide (VIP) and gastrin-releasing peptide (GRP) expression defines the ventral or core part of SCN, while cells that express arginine vasopressin (AVP) are found in the dorsal or shell part (see Figure 1.2).

Information regarding the light / dark cycle is sent to the SCN via inputs from the retina, which primarily innervate the ventral/core subregion (Moore and Lenn, 1972). In mammals, this light information is transduced both through the visual pathway of the retina, using rods and cones, and also through the intrinsically photosensitive retinal ganglion cells (ipRGCs). ipRGCs are a specialised subset of ganglion cells which express the light sensitive photopigment melanopsin (Berson, 2003). Melanopsin tracks slow changes in global irradiance which occurs over the course of the day (Paul and Brown, 2019), and sends signals to the SCN via the retinohypothalamic tract (RHT) (Hattar et al., 2006). This signal is transmitted by releasing glutamate (Glu) and pituitary adenylyl cyclase activating peptide (PACAP) to retinorecipient neurons in the SCN, mediating photic entrainment (Astiz et al., 2019). The SCN also receives information about non-photic cues (e.g. arousal) via two major pathways: the geniculohypothalamic tract (GHT) transmits signals from the intergeniculate leaflet (IGL) by releasing GABA and neuropeptide Y (NPY; Janik and

Mrosovsky, 1994), and the median raphe signals to the SCN through release of serotonin (5-HT; Meyer-Bernstein and Morin, 1996).

Individual SCN neurons maintained as dispersed cultures will maintain rhythms in spontaneous firing rates and gene expression, as driven through their molecular clocks (Hastings et al., 2019), although they will not necessarily remain synchronised with each other. However, when explants containing the whole, intact SCN are removed from the brain and maintained *in vitro*, the SCN will sustain synchronised molecular and electrical oscillations indefinitely with remarkable precision (Patton et al., 2016). This exemplifies one of the unique properties of the SCN: cells remain in synchrony due to their extraordinary intercellular coupling (Maywood, 2020). This is thought to be driven primarily through the paracrine release of VIP from core neurons, which signal to neurons in the shell (Maywood et al., 2011). In addition, the GABAergic nature of the majority of cells within the SCN also facilitates coupling between the core and shell (Albus et al., 2005). AVP and GRP further serve to provide synchronising signals within the SCN and preserve rhythmicity (Maywood, 2020). Thus, the network of neurons within the SCN are able to produce a single coherent output to transmit time information throughout the brain and to peripheral oscillators (Guilding and Piggins, 2007).

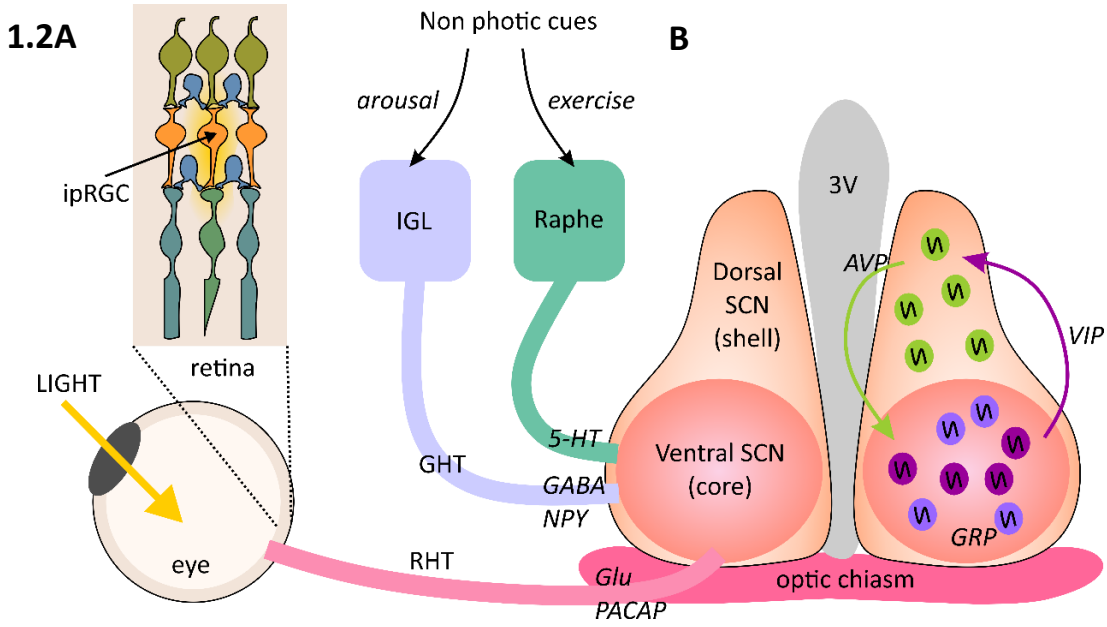

Figure 1.2 Connectivity and synchronization in the mammalian master clock

A) Light is the primary Zeitgeber of the SCN, and information about the time of day is conferred through the ipRGCs of the retina along the RHT, although the SCN can also entrain to non-photic cues.
B) The SCN ventral/core region is the primary retinorecipient region, defined by cells expressing VIP and GRP. These neuropeptides signal to the dorsal/shell region, which primarily contains neurons expressing AVP, which in turn signal to the core. In addition, most neurons of the SCN are GABAergic, further facilitating intercellular coupling. This ensures the rhythms of the SCN neurons remain synchronised.

1.1.4 Outputs from the SCN

In the SCN, the rhythmic gene expression of the molecular clock drives rhythms in the electrophysiological properties of these cells, generating higher excitability during the day and reducing action potential firing at night (Belle et al., 2009a; Schwartz et al., 1983), regardless of whether the animal is diurnal or nocturnal. This rhythm in electrical activity facilitates the communication of circadian information to clocks located in multiple brain regions and across the body via both neuronal and humoral mechanisms (Buijs et al., 2016). In this way, the SCN is able to orchestrate the cellular rhythms to keep the clocks aligned both with each other and entrained to external time.

Interestingly, whilst the electrophysiological output of the SCN signals external 'day' time rather than the animal's active/wake phase, downstream from the SCN these signals are subject to change depending on the animal's temporal niche. This is most clearly seen in the behavioural locomotor rhythms triggered by the SCN. For nocturnal rodents, peak spontaneous activity is

phase-locked to the trough of ensemble SCN activity, whilst the nadir of behavioural activity coincides with the peak of SCN activity (Houben et al., 2014). In diurnal species, these behavioural outcomes are reversed (Bano-Otalora et al., 2021a; Sato and Kawamura, 1984).

1.1.5 Extra-SCN oscillators within the mammalian brain

The mammalian circadian system is organised as a hierarchical structure, with the SCN as the master pacemaker regulating the 'lesser clocks' within this system. Within the brain there is a network of multiple structures demonstrating circadian oscillations in activity, which can be classified as either semiautonomous oscillators or slave oscillators (Guilding and Piggins, 2007). Semiautonomous oscillators are capable of producing circadian rhythms in clock genes autonomously but depend on the SCN to maintain synchronicity between cells. Slave oscillators on the other hand lack the ability to produce endogenous cellular rhythms, but will produce circadian activity driven by either the master or semiautonomous clocks.

Brain regions can be considered rhythmic based either on rhythms in electrical activity, expression of the core clock machinery, rhythmic gene expression, or indeed if they regulate rhythmic activity (J. R. Paul et al., 2020). Today, there is an abundance of regions in the brain that have been identified as displaying either diurnal or circadian oscillatory properties (Begemann et al., 2020). One recent review listed 33 structures from across the nocturnal rodent brain which demonstrated daily molecular rhythms (J. R. Paul et al., 2020), although the majority of these were under diurnal conditions and therefore are not necessarily 'circadian'. Nonetheless, circadian rhythmicity as evidenced through bioluminescence reporter studies has been demonstrated in at least 14 isolated rat brain regions (Abe et al., 2002). However, as yet, for most of these structures there is only limited evidence of oscillation, often with few time points or only with one experimental approach. Nonetheless, such data certainly point to the ubiquity of rhythms across the brain.

These clocks act together to regulate a variety of neural systems, including memory (Snider et al., 2018), reward (DePoy et al., 2017a) and arousal (Fuller et al., 2006). For example, many processes underlying memory function are modulated by the circadian system, with processes such as learning, memory consolidation and retrieval all fluctuating according to the time of day (Albrecht and Stork, 2017; Rawashdeh et al., 2018). Across multiple animals, from cockroaches to rats, most types of memory are formed and recalled optimally during the active phase (Hartsock and Spencer, 2020), although this is contrary in the case of aversive memories (Albrecht and Stork, 2017; Li et al., 2015). In mice at least, the rhythms in memory retrieval for a contextual fear conditioning task persist even in constant darkness, supporting the idea that it is circadian clocks

modulating these fluctuations (Chaudhury and Colwell, 2002). Local molecular clocks are also thought to drive daily oscillations in synaptic plasticity, the molecular mechanism underpinning memory (Hartsock and Spencer, 2020). Processes such as membrane excitability (Belle et al., 2009b; Chaudhury et al., 2005; Jones et al., 2018; Parekh et al., 2018), neuronal morphology (Barth et al., 2010; Girardet et al., 2010; Ikeda et al., 2015; Liston et al., 2013; Petsakou et al., 2015; Weber et al., 2009) and intracellular signalling (Eckel-Mahan et al., 2008; Hatori and Panda, 2010; Rawashdeh et al., 2016; Zhang et al., 2010) all demonstrate rhythmicity which may also be dependent on the molecular circadian clock.

Circadian rhythms in arousal contribute to both the pronounced sleep-wake cycles seen in many animals (Schwartz and Klerman, 2019) as well as circadian rhythms in alertness (Valdez et al., 2005), selective attention (Horowitz et al., 2003) and changes in emotional state (Fisk et al., 2018). These processes are thought to be driven by neurons in many areas including the basal forebrain (Villano et al., 2017) which also projects to the SCN (Bina et al., 1993). Overall, the functional consequences of these circadian rhythms in arousal lead to improved performance during the active phase and suboptimal performance during the inactive phase (Valdez, 2019).

Rhythms in reward processing will be explored in more detail later (see sections 1.4.1 and 1.4.2), but ultimately both local clocks in the reward circuitry (DePoy et al., 2017b; Hood et al., 2010; Jansen et al., 2012) as well as behavioural rhythms driven by the SCN (Siemann et al., 2021) produce daily fluctuations in reward behaviours. As such, processes such as motivation (Acosta et al., 2020; Murray et al., 2009), reward anticipation (Byrne et al., 2019) and reinforcement (Webb et al., 2015; Whitton et al., 2018) are all known to fluctuate over the day. Interestingly, there is some evidence to suggest that the cholinergic system may also be under circadian influence (Hut and Van der Zee, 2011). This presents an intriguing area for research, given how the cholinergic system has wide ranging roles in arousal (Jones, 2020), reward (de Kloet et al., 2015), memory (Haam and Yakel, 2017) and autonomic function.

1.2 Cholinergic signalling in the mammalian brain

In the peripheral nervous system, acetylcholine (ACh) acts as a conventional neurotransmitter, producing direct excitatory responses at the neuromuscular junction and autonomic ganglia (Picciotto et al., 2012). It is involved in a number of fundamental biological processes including cardiovascular control, energy homeostasis, respiration and secretion through sweat glands (De Biasi, 2002; Falk et al., 2020).

Cholinergic signalling is also widespread throughout the central nervous system (CNS), and ACh-containing neurons are found in many brain nuclei including the basal forebrain complex (Gielow and Zaborszky, 2017), the pedunculopontine and laterodorsal tegmental nuclei (LDTg) (Wang and Morales, 2009) and the medial habenula (MHb) (Ren et al., 2011). Cholinergic transmission is facilitated through either projection neurons targeting distal sites or local circuit interneurons (Chen et al., 2010), which project widely across the brain (Picciotto et al., 2012). Reflecting this extensive innervation, cholinergic signalling is consequently involved in many diverse functions including synaptic plasticity (McKay et al., 2007), arousal (Jones, 2008), attention (Luchicchi et al., 2014) and reward (de Kloet et al., 2015). However, unlike in the peripheral nervous system, ACh produces primarily neuromodulatory effects in the CNS, rather than acting through direct excitatory responses (Ito and Schuman, 2008). These neuromodulatory effects are mediated through a number of processes including altering neuronal excitability, modulating presynaptic release of neurotransmitters, and coordinating firing between neurons (Dannenberg et al., 2017).

1.2.1 Mechanisms of signalling through acetylcholine receptors

ACh acts through two classes of receptor, either the fast nicotinic ACh receptors (nAChRs) or slow-activated muscarinic receptors (Picciotto et al., 2012). Both the muscarinic ACh receptors and nAChRs are expressed widely throughout the peripheral and central nervous system. Like other ionotropic ligand-gated channels, nAChRs have low affinity for their endogenous ligand (here, ACh) and will rapidly open the channel following agonist binding (Hurst et al., 2013). This allows influx of cations through the channel pore which increases the excitability of the cell, allowing for the rapid, high frequency signalling found at synapses (Picciotto et al., 2012). Interestingly, however, cholinergic axo-axonal synapses are relatively rare in the mammalian brain (Brown, 2019; Descarries et al., 1997) and are instead more commonly found at pre-, peri- and extra-synaptic sites (Hurst et al., 2013). This is consistent with the idea that ACh primarily signals through “volume transmission”: rather than being mediated through traditional synaptic machinery, effects are instead mediated through slow diffusion through the extracellular space to target sites distal from the site of ACh release (Colangelo et al., 2019).

The metabotropic muscarinic acetylcholine receptors on the other hand, are prototypical members of the seven transmembrane G protein-coupled receptor superfamily (Brown, 2019). ACh binding will activate the guanine nucleotide binding protein (G protein) and a produce a variety of biochemical signalling cascades (Picciotto et al., 2012). There are five distinct muscarinic receptor subtypes in the mammalian CNS: three subtypes (M1, M3, M5) are coupled to $G_{q/11}$ G proteins and activate phospholipase C following ACh binding, whilst two subtypes (M2, M4)

preferentially couple to $G_{i/o}$ proteins to inhibit adenylate cyclase (Lebois et al., 2018). Muscarinic receptors are located both pre- and postsynaptically, and can therefore produce diverse effects on a brain circuit (Picciotto et al., 2012).

1.2.2 Cholinergic signalling in the circadian system

The interaction between the cholinergic system and the circadian system has been studied for decades. In fact, ACh was one of the first neurotransmitters suggested as a regulator of circadian rhythms (Hegazi et al., 2019). ACh was previously hypothesized to mediate the effects of light on the SCN (Earnest and Turek, 1985; Hut and Van der Zee, 2011), as carbachol (a cholinergic agonist) injected into lateral ventricles produced similar effects on activity rhythms as those seen in response to light pulses (Zatz and Brownstein, 1979) and in turn, light pulses produced increased ACh release in the SCN (Murakami et al., 1984). However, these theories were largely dismissed as direct application of ACh to the SCN did not produce circadian phase changes that mimicked light pulses (Buchanan and Gillette, 2005), and the role of cholinergic inputs to the SCN remains largely unclear (Dojo et al., 2017).

Nonetheless, several aspects of the cholinergic system demonstrate daily fluctuations. ACh levels show diurnal oscillation in the rodent brain, peaking during the early subjective day (Hanin et al., 1970), and ACh release in the cortex is higher during the dark phase than the light phase (Jiménez-Capdeville and Dykes, 1993; Kametani and Kawamura, 1991). In freely-moving rats, increased ACh levels in the striatum, hippocampus and cortex correspond to the beginning of the dark phase, as measured through microdialysis (Day et al., 1991). However, rhythms in ACh content within the SCN are not sustained under constant conditions (Murakami et al., 1984; Rusak and Bina, 1990). Today, ACh is considered a neuromodulator of arousal, somewhat paradoxically producing increased transmission during waking and rapid eye movement sleep (Van Erum et al., 2019). A direct connection exists between cholinergic neurons of the brainstem and forebrain which projects to the SCN (Yamakawa et al., 2016). This connection appears to regulate activity patterns in response to changing light / dark cycles. There is widespread ACh receptor expression within the SCN, including several nAChR subtypes (O'Hara et al., 1998) and all of the five muscarinic ACh receptor subtypes (Basu et al., 2016; Bina et al., 1993; Dojo et al., 2017; Yang et al., 2010). Thus, whilst ACh is no longer considered critical for driving rhythms in the SCN, there is instead evidence that rhythms in the SCN may drive circadian rhythms in cholinergic signalling and function.

1.3 Neurobiology of nicotine reward and dependence

Not only is it important to understand the cholinergic system within the context of endogenous ACh signalling, but this system can also be altered by nicotine, the psychoactive component found within both tobacco and e-cigarettes. Despite a wealth of public information campaigns encouraging individuals to quit (Kuipers et al., 2020) and the public broadly perceiving the serious health risks posed by cigarettes (Czoli et al., 2017), tobacco addiction remains one of the greatest threats to public health today. In the UK, smoking is still a major factor underlying a number of hospital admissions: between 2019 and 2020, 21% of all respiratory diseases, 14% of all circulatory diseases and 9% of all cancers were estimated to be attributable to smoking (NHS Digital, 2020). Furthermore, whilst general trends have seen a global decline in smoking rates (World Health Organization, 2019), there has been an increase in popularity of e–cigarettes among young people which increases the risk of starting smoking (Barrington-Trimis et al., 2016). Smoking remains a huge risk in low- and middle-income countries, which make up the majority of worldwide tobacco users (World Health Organization, 2021) and causes a range of devastating health problems, affecting almost every organ within the body (Benowitz, 2009). Therefore, further investigation into the pharmacological properties of nicotine remains as essential as ever.

1.3.1 Neuronal nicotinic acetylcholine receptors

Inhalation of smoke from cigarettes (or vapour from electronic nicotine delivery systems) allows for rapid absorption of nicotine in the lungs (Benowitz, 2010). Here, nicotine transiently activates nAChRs on the sensory nerves of the lung alveoli and pulmonary circulatory system (Kiyatkin, 2014), producing effects on the cardiovascular and metabolic system (Tsai et al., 2020). Once in arterial circulation, nicotine is rapidly transported to the brain and crosses the blood brain barrier easily (Tega et al., 2018), where it binds and activates neuronal nAChRs. It is through these neuronal nAChRs that nicotine produce its well-known reinforcing properties (de Kloet et al., 2015), as well as its less well characterised effects.

The exact pharmacological and functional properties of the neuronal nAChRs are determined according the composition of the subunits that form their distinct pentameric structure (Leslie et al., 2013). As depicted in Figure 1.3, mammalian neuronal nAChRs are ligand-gated cation channels comprised of five subunits formed around an aqueous central pore (Wittenberg et al., 2020). nAChR subunits follow the conventional structure of other cys-loop ligand-gated cation channels, consisting of a long, hydrophilic extracellular binding domain, three hydrophobic transmembrane domains (M1-3), followed by an intracellular loop and a fourth transmembrane

region (M4) terminating with the short extracellular carboxyl domain (Dani, 2015). There are nine α subunits (α2-7, α9-10) and three β subunits (β2-4) that are expressed in the mammalian nervous system (Zoli et al., 2015), which can form either homopentameric (five identical subunits) or heteropentameric (at least one α and one β subunit) structures. Agonist binding sites are located at the interface between two α subunits or between an α and a β subunit (Gotti et al., 2009; Zoli et al., 2018) although more recent studies have demonstrated unorthodox binding sites in heteromeric nAChRs (Wang and Lindstrom, 2018). Homopentameric receptors therefore have five binding sites, although not all of them need to be occupied for activation of the channel (Andersen et al., 2013). Most heteropentameric structures however, only have two binding sites located at the interface between each pair of α and β subunits (Zoli et al., 2018). There is therefore enormous diversity between these receptors: expression patterns, cationic permeability and pharmacological function are all dictated by the composition of the subunits (Dani, 2015).

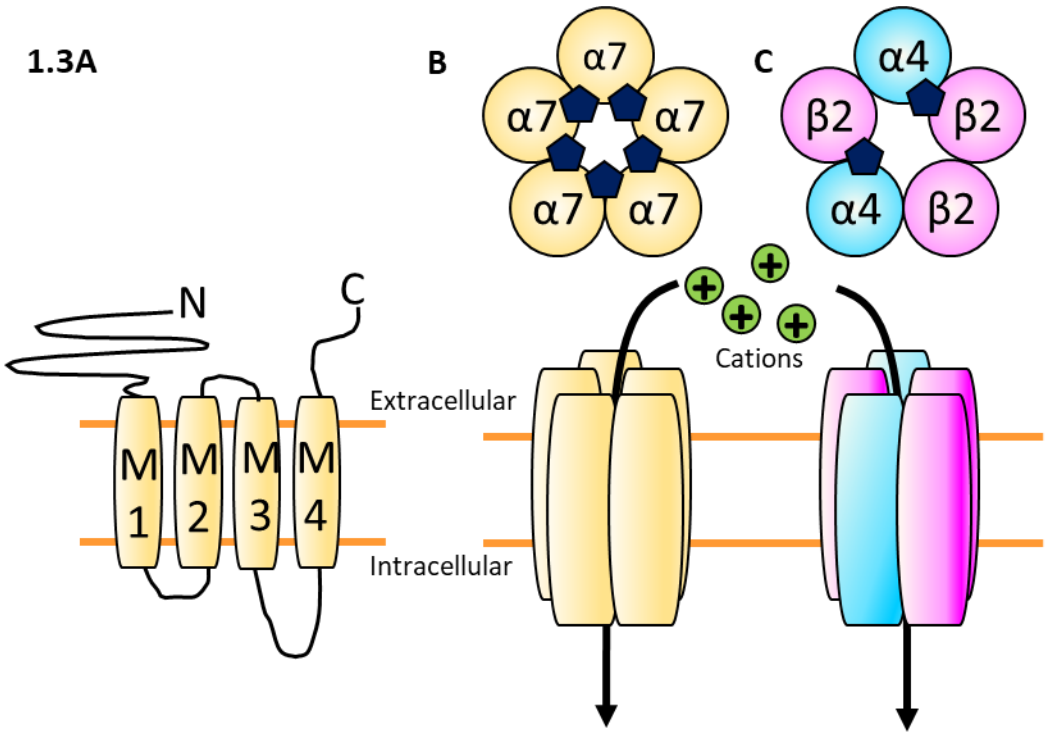

Figure 1.3 Structure of nAChRs.

A) Each nAChR subunit is composed of four transmembrane domains (M1-M4), an extracellular amino-terminus (N) and carboxy-terminus (C), and an intracellular loop between M3-M4.
B - C) Neuronal nAChRs are composed of 5 subunits and can either be (B) homomeric, such as α7-nAChrs, or (C) heteromeric, composed of at least one type of α subunit plus one type of β subunit, for example α4β2-nAChRs. This dictates the number of binding sites available. The subunits assemble to form a cation permeable pore. ACh binding sites depicted as dark blue pentagons.

When the endogenous ligand, ACh, or an exogenous agonist such as nicotine, binds to the extracellular portion of the nAChR subunit, the channel undergoes a conformational change into the active state, allowing cationic influx for several milliseconds and depolarizing the cell (Dani, 2015). Following activation of the channel, the channel will either return to resting state or a desensitized state, where the channel cannot be activated even following ligand binding (Wittenberg et al., 2020). Once again, the kinetics of desensitization are dependent on the subunits of each channel. Brief exposure to ACh, or acute nicotine exposure, favours synchronous opening of the channel's pore (Dani, 2015). However, long-term exposure to low doses of nicotine for several seconds, such as is obtained through smoking, will cause activation and lead to significant desensitization of the receptors (de Kloet et al., 2015). Nicotine promotes desensitization because unlike ACh, which is rapidly hydrolysed through the actions of acetylcholinesterase (AChE; Silman and Sussman, 2008), nicotine remains in the synapse and renders the nAChRs unresponsive to further ligand binding (Wittenberg et al., 2020).

Neuronal nAChRs can be located both pre or postsynaptically, where they act to modulate neurotransmitter release or promote fast excitatory transmission respectively (Dani and Bertrand, 2007; McGehee et al., 1995; Wonnacott, 1997). Furthermore, as nAChRs are so widespread, nicotine can drive opposing modulatory influences on the same circuit if both excitatory and inhibitory inputs are activated (Zoli et al., 2015). It is the interplay between different nAChRs subtypes, located in different regions within the brain, which results in the complex actions of nicotine on the brain.

1.3.2 Acute effects of nicotine on the reward pathways of the brain

Nicotine binds to nAChRs in the brain, causing the release of neurotransmitters. One such neurotransmitter, dopamine (DA), acts on the mesolimbic reward pathways of the brain, producing the pleasurable effects of nicotine inhalation which are critical for driving the reinforcing effects of smoking (Picciotto and Kenny, 2021). This pathway is thought to represent a common mechanism through which all drugs of abuse produce their acute rewarding and reinforcing effects (Feltenstein and See, 2008).

Nicotine will enhance reward signals most prominently by activating mesocorticolimbic dopaminergic neurons in the ventral tegmental area (VTA) which project to the nucleus accumbens (NAc), although nicotine can influence neural circuits throughout the brain due to the widespread nature of cholinergic systems (Benowitz, 2008). Under physiological conditions, VTA dopaminergic neurons will be activated following salient stimuli that predict reward, and these same neurons are inhibited when expected rewards are omitted (Dani and De Biasi, 2013). In this

way behaviours that lead to rewards are reinforced, and nicotine will 'hijack' this circuit to reinforce associations and behaviours driving self-administration (Xia et al., 2017). Generating this pleasurable experience is key to establishing the tobacco smoking habit (Kenny and Markou, 2006).

When nicotine first arrives into the midbrain, it particularly excites the high-affinity α4β2* receptors which are located somatodendritically on both dopaminergic neurons and GABAergic interneurons in the VTA (Wills and Kenny, 2021), as shown in Figure 1.4. Nicotine binding to the α4β2* nAChRs directly depolarizes the VTA dopaminergic neurons projecting to dopaminergic neurons in the NAc, increasing their firing activity and release of DA in the NAc (Brody et al., 2009; Zhang et al., 2009). Simultaneously, nicotine activates the α4β2* naChRs located presynaptically on the GABAergic interneurons. This causes the GABAergic neurons to depolarize and increase the inhibitory drive onto VTA dopaminergic neurons (Johnson and North, 1992; Picciotto and Mineur, 2014). Nicotine will also activate presynaptic nAChRs, such as the lower-affinity α7 receptors, enhancing excitatory glutamatergic projections onto both the GABA and DA neurons in the VTA (Mansvelder and McGehee, 2000).

The coincidental increase in presynaptic glutamate signalling with postsynaptic depolarisation and firing of the dopaminergic neurons induces long term synaptic potentiation of glutamatergic afferents onto the dopaminergic neurons and increased responsiveness to nicotine (Mansvelder et al., 2002). This will subsequently lead to the VTA neurons altering their firing patterns from tonic to phasic burst firing in response to nicotine, which further enhances downstream dopamine release in the NAc (Mao et al., 2011; Ostroumov and Dani, 2018). In addition, the α4β2* nAChRs on the GABAergic interneurons are mostly desensitized shortly after potentiation of the excitatory projections to the DA neurons, reducing inhibition on these neurons (Dani, 2015). In addition, multiple other nAChRs are also thought to act on this circuit, although their mechanisms are less well characterized (Wills and Kenny, 2021). Thus, the reinforcing signal produced by nicotine through increased DA in the VTA and NAc is the result of a multitude of nAChRs altering various neurotransmitters across the brain.

Interestingly, due to the dichotomous nature of nicotine, the pleasurable experience of nicotine is not guaranteed. At higher doses, unpleasant experiences such as nausea occur in humans, and there is evidence that initial sensitivity to these noxious effects can indicate the risk of developing a daily smoking habit (Sartor et al., 2010). Indeed, both rodents and humans will titrate their intake of the drug to account for higher or lower doses of nicotine to avoid these aversive properties but still experience the reward (Fowler et al., 2011; Lynch and Carroll, 2001).

1.4

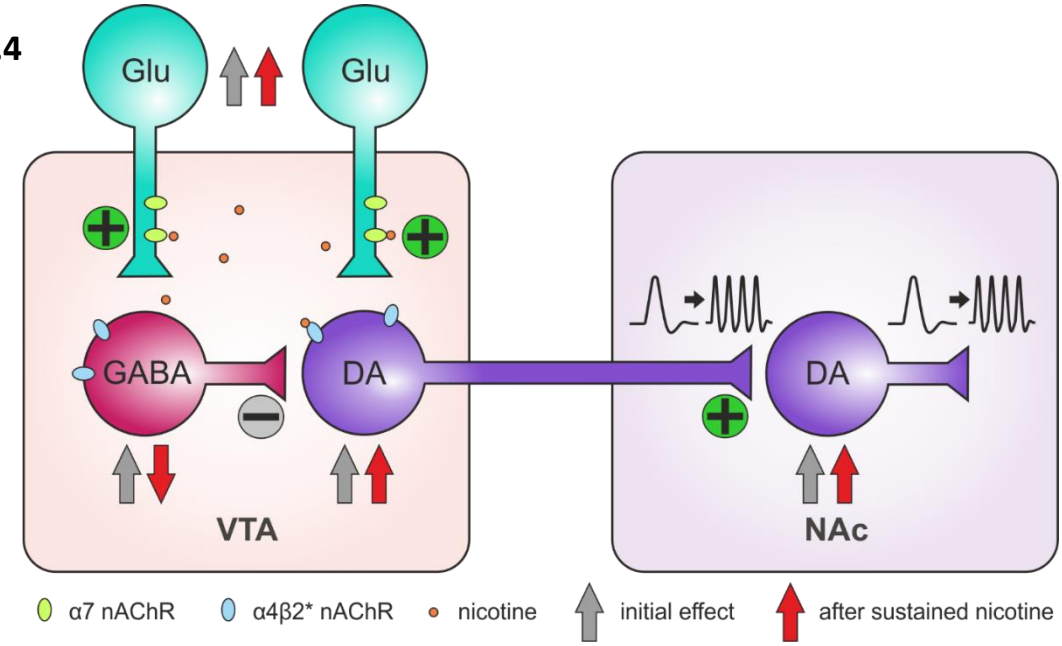

Figure 1.4 Schematic representation of the action of nicotine in the VTA and NAc

Initially, nicotine acts on postsynaptic α4β2*nAChRs, directly activating VTA DA and GABA neurons. Simultaneous activation of presynaptic α7 nAChRs potentiates glutamatergic inputs and enhances inhibitory GABAergic projections from interneurons. Overall, this leads to increased tonic and bursting activity of VTA DA neurons. Following sustained nicotine exposure, α4β2* nAChRs desensitize rapidly, reducing inhibition from the GABA interneurons. The coincidence of presynaptic and postsynaptic excitation can induce long term potentiation and will cause the DA neuron to increase firing activity from tonic to phasic bursting, also contributing to the increased activity of the VTA DA neurons.

A series of studies with transgenic mice suggests that these aversive properties are mediated not only by the mesoaccumbens reward pathway but additional circuits, such as the medial habenulo-interpenduncular (MHb-IPN) pathway (Antolin-Fontes et al., 2015; Picciotto and Kenny, 2021; Wills and Kenny, 2021). Mice lacking the α5 nAChR subunit were less sensitive to the noxious nature of nicotine usually experienced at high doses. However, virus-mediated re-expression of α5 nAChR subunit in the MHb-IPN was able to restore aversion to nicotine and limit nicotine intake in these mice (Fowler et al., 2011). Similarly, knockdown of α3* nAChRs in the MHb-IPN increases self-administration of intravenous nicotine in rats (Elayouby et al., 2021). Mice engineered to express hypofunctional β4 nAChRs also showed increased nicotine intake (Ślimak et al., 2014). On the other hand, mice overexpressing the β4 subunit demonstrated increased sensitivity to the aversive properties of nicotine, which was reversed by selective expression of the β4 subunit in the MHb (Frahm et al., 2011; Harrington et al., 2016). Recently, a study using transgenic mice with reduced excitatory output from MHb cholinergic neurons showed these mice had increased rates of nicotine self-administration, implicating these neurons as moderators of the aversive properties of nicotine (Souter et al., 2021). Together this suggests that nicotine

intake is at least partially mediated by the MHb-IPN pathway, with nicotine acting here to evoke avoidance and limit consumption.

1.3.3 Repeated exposure to nicotine produces neuroadaptations

Repeated and prolonged exposure to nicotine will produce diverse adaptive measures in the circuitry underlying the addictive process, ranging from effects on motivational systems, to memory and associative learning (De Biasi and Dani, 2011; Wittenberg et al., 2020). One of the most important neuroadaptations in response to repeated nicotine exposure is the increased expression of subtype-specific nAChRs (Benwell et al., 1988; Perry et al., 1999). This upregulation of receptors is thought to be a possible compensatory mechanism to account for the repeated desensitization of high sensitivity nAChR subtypes following nicotine activation (De Biasi and Dani, 2011; Giniatullin et al., 2005). The upregulation of nAChRs begins after around 10 days of long-term nicotine exposure and is thought to be achieved through post-translational mechanisms, as changes in mRNA levels have not been observed following this process (Cooper and Henderson, 2020; Henderson and Lester, 2015). Upregulation differs according to nAChR subtype, cell type, brain region and administration protocols (Wittenberg et al., 2020). As the brain adapts to the new circuits and neuroadaptations following repeat exposure to nicotine, a new homeostatic equilibrium is reached. This condition is reliant on the availability of nicotine in the system, and so sudden discontinuation of nicotine intake will contribute to the symptoms of withdrawal.

1.3.4 Factors driving nicotine addiction

A persons susceptibility to developing nicotine dependence is influenced by multiple factors including genetics (El-Boraie and Tyndale, 2021), socioeconomic background (Chen et al., 2019), mental illness (Kutlu et al., 2015) as well as the complex psychopharmacological actions of nicotine within the brain. In addition to acting on the reward pathways in the brain, nicotine also acts on the systems regulating appetite (Calarco and Picciotto, 2020), mood (Picciotto et al., 2015) and attention (Picciotto and Kenny, 2021), all of which further contribute to the maintained motivation to continue smoking.

Previous twin and candidate gene association studies demonstrated that addiction susceptibility has a strong genetic component, and this has been further validated through human genome-wide association studies (Hall et al., 2013; Karkowski et al., 2000). Genome-wide association studies comb the entire genome of a population, searching through hundreds of thousands of genetic variants (typically single nucleotide polymorphisms) that may be associated with a particular trait. Usually involving control and affected populations of sample sizes of at least 1000,

these high-throughput genetic studies have yielded numerous interesting results: in the majority of genes encoding the multiple different nAChR subunits, at least one variant has been associated with an aspect of smoking-related behaviour (Greenbaum and Lerer, 2009). However, it is the genetic associations between the α3, α5 and β4 nAChR subunit genes encoded within the *CHRNA3/CHRNA5/CHRNB4* gene cluster and nicotine dependence over any other nAChR genes which have produced the most convincing results (Greenbaum and Lerer, 2009). Association studies at this cluster have provided evidence that variants here are strongly involved in both increased smoking quantity and nicotine dependence (Berrettini and Doyle, 2012; Bierut, 2011; Saccone et al., 2007; Thorgeirsson et al., 2008) as well as the age of smoking initiation (Stevens et al., 2008; Weiss et al., 2008). The association with several genetic variants within this cluster and multiple nicotine dependent phenotypes further confirms that these three subunits are key to driving nicotine addiction, and warrants further investigation as potential therapeutic targets. In particular, as the MHb-IPN pathway has the highest concentrations of α5, α3 and β4 nAChR subunits in the mammalian brain (Grady et al., 2009), this highlights the importance of this pathway in mediating nicotine behaviours. In an innovative study, Gallego et al generated mice that overexpressed the human *CHRNA5/CHRNAA3/CHRNAB4* gene cluster to increase function of the α3β4 nAChR, but only in regions with endogenous expression of these receptors. These mice therefore had increased nicotine binding sites and displayed increased sensitivity to acute nicotine exposure, as well as increasing their voluntary intake of nicotine in a self-administration paradigm (Gallego et al., 2012).

As well as genetic susceptibility, nicotine addiction is thought to be underpinned by the balance between the pleasurable sensations of nicotine driving positive reinforcement and avoidance of the unpleasant symptoms associated with withdrawal (Allen et al., 2008; Lüscher, 2016; Xia et al., 2017). In fact, sensitivity to these unpleasant symptoms are a major predictor in whether an individual's attempts to quit smoking will be successful (West et al., 1989). Another key factor underlying the success of smoking cessation attempts are the severity of cravings, as this is one of the most frequent motives cited by smokers as their reason for smoking (Piasecki et al., 2007) and the intensity of these cravings is a predictor of relapse risk (Shiffman et al., 1997).

1.3.5 Circuits underlying nicotine withdrawal

After chronic exposure to nicotine, the neuroadaptive changes in gene expression and protein synthesis lead to withdrawal symptoms if access to nicotine is withdrawn (Koob and Le Moal, 2001; Pidoplichko et al., 2004). Either spontaneous abstinence or mecamylamine-precipitated nicotine withdrawal will manifest in both somatic (physical) and affective (mood-related) effects,

and can be observed in both rodents and humans (Malin and Goyarzu, 2009). In humans, withdrawal is characterized by affective symptoms such as irritability, anxiety, and fatigue or entail physical symptoms such as bradycardia, gastrointestinal discomfort and mouth ulcers (Wills and Kenny, 2021). In rodents, affective symptoms will typically be measured as anxiety-like behaviours, elevated reward thresholds and conditioned place aversion (Antolin-Fontes et al., 2015). Rodent somatic signs of withdrawal include rearing, shaking and scratching (Changeux, 2010), hyperalgesia (Grabus et al., 2005) and changes in locomotor activity (Hildebrand et al., 1997).

Nicotine withdrawal is mediated in part through the mesolimbic pathway. Withdrawal from nicotine is associated with reduced levels of DA in the NAc, reflecting the changes in DA release and reuptake mechanisms (Duchemin et al., 2009). These changes in DA signalling occur within the same time frame as the occurrence of both somatic and affective withdrawal symptoms, and so are thought to contribute (Hadjiconstantinou and Neff, 2011). Other neurotransmitters such as 5-HT and noradrenaline, known to contribute to withdrawal symptoms in other substances of abuse, may also be involved (Bruijnzeel et al., 2010).

However, recent evidence increasingly points to the MHb-IPN axis as the crucial circuit mediating withdrawal. It is now thought that chronic exposure to nicotine upregulates α6 and α4 subunits in the ventral portion of the MHb, increasing excitatory inputs to the IPN during withdrawal (Molas et al., 2017a). Yamaguchi et al demonstrated that ventral MHb projections to the central core of the IPN mediates anxiety behaviours, and that ablating glutamatergic inputs specifically from the triangular septum (which normally innervate the ventral MHb) impairs these anxiety behaviours (Yamaguchi et al., 2013). It has been suggested that nAChRs on these neurons may well be mediating anxiety-like behaviours at this axis, in particular during withdrawal as nicotine-induced currents in the MHb are upregulated (Pang et al., 2016). The mechanisms underlying withdrawal symptoms however, are not yet fully characterized.

1.4 Is the circadian system influencing nicotine addiction behaviours?

1.4.1 Circadian regulation of reward circuitry in humans

There is sensible reasoning behind assuming the reward system varies according to the time of day. “Natural rewards”, such as food and sex, are not available with equal abundance at all times of the day. Therefore matching motivation and reward systems to the diurnal profile of availability in these systems could confer an evolutionary advantage (Murray et al., 2009).

However, it is still not certain the degree to which natural rewards and drugs of abuse share the same underlying mechanisms (DePoy et al., 2017a).

If the circadian system is regulating the reward circuitry, one could expect to find similar rhythmic patterns in reward-related behaviours or features of the reward circuitry. There is a range of evidence to support this in humans (Webb et al., 2015). For example, studies using fMRI have found diurnal variation in activity in reward-related brain areas of male subjects (Byrne et al., 2017). There is also evidence that alcohol consumption (Arfken, 1988), cocaine (Erickson et al., 1998) and nicotine intake (Benowitz et al., 1982; Mooney et al., 2006) all vary according to the time of day, and there is evidence of diurnal variation in cue-induced drug craving among recently abstinent heroin users (Ren et al., 2009). Interestingly, one study investigated hospital admissions arising from drug overdoses from a range of substances and found a clear time of day effect, with overdose most common in the early evening, suggesting rhythmicity in the effects of these drugs (Raymond et al., 1992).

There is also less direct evidence linking the clock to the reward system in humans. Sleep disruption (Brower, 2003; Fakier and Wild, 2011; Fisk and Montgomery, 2009; Teplin et al., 2006), alterations in clock genes (Kovanen et al., 2010; Sjöholm et al., 2010) and perturbations in circadian rhythms (Conroy et al., 2012; Vescovi et al., 1992) are all associated with an increased tendency towards developing substance abuse disorders. There is evidence from human studies that chronotypes with an 'eveningness' preference are more likely to consume psychoactive substances (Adan, 1994; Fisk and Montgomery, 2009; Logan et al., 2018), although the reason for this relationship remains unclear (Haynie et al., 2017; Tavernier et al., 2015).

Elucidating the role of the circadian system in human disorders is complicated, as circadian phase and chronotype are both typically measured using subjective self-reporting rather than objective biological measures (Logan et al., 2014). Furthermore, determining whether time of day effects on addiction behaviours originate from the circadian system, social factors or the sleep-wake cycle is challenging. Therefore, the majority of evidence linking the circadian and reward systems comes from laboratory rodent studies.

1.4.2 Circadian regulation of reward circuitry in rodents

Similarly to humans, animal models also demonstrate diurnal variation in the rates of self-administration of many substances of abuse, including cocaine (Bass et al., 2010; Nakamura et al., 2011), alcohol (Perreau-Lenz et al., 2012), morphine (Deneau et al., 1969) and nicotine (O'Dell et al., 2007) suggesting diurnal variations in the mechanisms driving the reinforcing properties of

these substances (Webb et al., 2015). There is also apparent circadian modulation in the behavioural effects of drugs of abuse, as demonstrated through conditioned place preference (Kurtuncu et al., 2004; Webb et al., 2009) or the locomotor effects produced by psychomotor stimulants (Bovet et al., 1967; Evans et al., 1973; Gaytan et al., 1998).

Core circadian clock genes are expressed within the mesocorticolimbic system (Logan et al., 2014; Rosenwasser, 2010), and brain structures of the reward circuitry show rhythmic activity patterns and neurochemistry (Begemann et al., 2020; McClung, 2007; J. R. Paul et al., 2020), suggesting downstream regulation from the clock. For example, clock gene expression within the VTA is well documented (Hampp et al., 2008; Li et al., 2010; McClung et al., 2005; Mendoza and Challet, 2014), although expression is not consistently rhythmic *ex vivo* (Webb et al., 2009). The VTA also demonstrates diurnal variation in several markers of dopaminergic activity, including monoamine oxidase enzymes (Hampp et al., 2008) and tyrosine hydroxylase (Webb et al., 2009), as well as daily fluctuation in DA receptor expression and DA synthesis (Tamura et al., 2021). Interestingly, these circadian rhythms can be altered by chronic nicotine administration (Pietila et al., 1995). Evidence of circadian regulation of VTA electrical activity is somewhat controversial, as many studies failed to find rhythmicity in this area or find contradictory results (J. R. Paul et al., 2020; Sidor et al., 2015). However, later studies showed rhythmic DA neuron firing in anaesthetized rats (Domínguez-López et al., 2014) and rhythmic multiunit activity in the VTA of freely-moving mice which persisted in constant conditions (Fifel et al., 2018). As yet the source of these circadian variations remains unclear (Webb et al., 2015), but could be due to either an endogenous clock in the VTA, or from projections from an upstream circadian clock – both the habenula and the SCN present potential sites (Mendoza and Challet, 2014).

It should also be noted that there is a bidirectional relationship between DA signalling and circadian rhythmicity (Grippo and Güler, 2019), whereby it is now thought that DA signalling is able to modulate circadian activity and *vice versa*. For example, the ability to entrain to timed food availability is dependent on the SCN (Stephan et al., 1979; Stokkan et al., 2001) and is thought to be regulated by DA signalling in the striatum (Gallardo et al., 2014). Grippo and colleagues have shown that the SCN receives direct input from DA neurons projecting from the VTA and activation of DA neurons in the VTA increases the rate of photoentrainment (Grippo et al., 2017). Together, this suggest that dopamine receptors in the SCN may modulate aspects of both photic and non-photic resetting.

1.4.3 Circadian influences on nicotine-dependent behaviours in humans

Whilst there is ample evidence to suggest the circadian system influences the reward circuitry of the brain, research has tended to be biased towards select drug types, including cocaine, amphetamine and alcohol (Engmann, 2021). Only limited research has been carried out into circadian influences on mechanisms driving nicotine intake. Nonetheless, there is evidence from human and animal studies to suggest that both nicotine intake and sensitivity to the effects of nicotine follow a daily rhythm.

In humans, smoking intake varies systematically across the day (Chandra et al., 2011). Both cigarettes and nicotine gum have similar patterns of use, with heaviest use in the morning and lowest during the night (Benowitz et al., 1982; Benowitz and Jacob, 1984; Mooney et al., 2006). However, another study has shown that cigarettes smoked during the early morning are puffed less intensively than at other times of the day (Grainge et al., 2009).

As well as rhythmicity in nicotine intake, other evidence suggests circadian control of the circuits mediating nicotine cravings and withdrawal. A study examining the cravings of both *ad libitum* smokers, abstinent participants with a nicotine replacement patch or abstinent participants with placebo showed that both abstinent groups exhibited circadian patterns of craving intensity which peaked during the evening – although cravings in the smoking group did not vary over the three days of the study in a diurnal fashion, and there was no pattern found in withdrawal measures (Teneggi et al., 2002). Another study of 200 participants showed that whilst smoking, craving and withdrawal symptoms varied according to the time of day, and abstinent participants showed notably increased evening cravings compared to other times of day (Perkins et al., 2009). It seems that daily rhythms in cravings and withdrawal leads to rhythms in relapse following an attempt to stop smoking (Shiffman et al., 1997; Ussher and West, 2003). For example, an investigation of nicotine patch users found lapses were more likely during the afternoon and evening (Ussher & West, 2003). One study sought to cluster individuals with different temporal patterns of cigarette smoking, and found that the group with higher evening smoking were at greater risk of lapsing (Chandra et al., 2007)

Chronotype, a natural inclination towards morning or evening activity and set by the circadian clock, may also influence an individual's susceptibility to smoking. A study of Finnish adolescents showed that evening-types find it harder to quit smoking (Heikkinen et al., 2009), whilst a study of Japanese university students showed evening-types are more likely to smoke than their morning-type counterparts (Ishihara et al., 1985). These findings are further corroborated by a study into Finnish adult twins who found that evening-types were much more likely to be current or lifetime

smokers and far less likely to stop smoking (Broms et al., 2011). “Social jetlag” has been proposed as the mechanism that links later chronotype to smoking, whereby an individual has a mismatch between biologically-preferred sleeping hours and conventional social schedules such as school or work, leading to accumulated sleep debt (Wittmann et al., 2006). In addition, several studies have shown that smoking rates are higher in night-shift workers, a population who experience significant circadian disruption (Bae et al., 2017; Y.-M. Cho et al., 2019; van Amelsvoort et al., 2006).

Together, the evidence from human studies indicates a significant relationship between the circadian cycle and nicotine-related behaviours. However, these studies are not able to reveal the mechanisms driving these rhythms, and as discussed earlier, are also at risk of confounding factors such as stress, sleep disorders and mood disorders, which can alter the sleep-wake cycle and alter drug use (Engmann, 2021). Establishing whether there is a true rhythm underlying nicotine behaviours could lead to better smoking cessation treatment by taking this factor into consideration.

1.4.4 **Circadian influences on nicotine-dependent behaviours in rodents**

There are surprisingly few animal studies investigating time of day patterns in sensitivity to the effects of nicotine. Studies in rats able to self-administer nicotine at will showed diurnal patterns of intake, with self-administration corresponding to the middle of the dark phase (O’Dell et al., 2007). In rats, there is also a tendency for nicotine to produce the greatest increases in locomotor activity during the light phase, but effects produced during the dark phase are not consistent across studies (Bovet et al., 1967; Kita et al., 1986; Morley and Garner, 1990), and may depend on the administration protocol. Williams et al found circadian variation in rat hypothermic response to nicotine, with greater sensitivity during the light phase than dark (Williams et al., 1993). In mice, there is similar uncertainty. In one study, nicotine-dependent hypolocomotion and hypothermia in response to acute nicotine was greatest late in the light phase and lowest in the late dark phase (Mexal et al., 2012). An alternative study showed that chronic nicotine produced the greater hyperactivity during the latter portion of the dark phase (King et al., 2004).

In addition, there is evidence that the endogenous cholinergic system varies according to the time of day. Markus et al (2003) showed that α7 nAChRs were decreased in rat cerebellum during the dark phase (as shown through availability of α-bungarotoxin binding sites), although stimulating these receptors at this time conversely led to increased glutamate release compared with stimulation during the light phase. There are also rhythms in cholinergic markers such as choline acetyltransferase (ChAT; responsible for ACh synthesis), AChE (the enzyme which degrades ACh)

or the vesicular acetylcholine transporter (VAChT) (Berrard et al., 1995; Hut and Van der Zee, 2011; Jenni-Eiermann et al., 1985; Nordberg and Wahlström, 1980; Perry et al., 1977). However, these studies were mostly performed in the 1970s and 1980s, and are limited due to few time point measurements and coarse spatial resolution – often the whole brain or cortex.

1.5 The Habenula

The habenula complex is a small bilateral structure of the mammalian dorsal diencephalic conduction system, a major pathway linking the limbic forebrain and monoaminergic midbrain reward centres (Metzger et al., 2021; Sutherland, 1982). The habenula has been highly conserved across vertebrate evolution (Concha and Wilson, 2001), from lamprey to humans (Stephenson-Jones et al., 2012). Across species, the role of this conserved circuitry appears to be modulating reward processing and regulating behaviour (Mathuru, 2017). The habenula itself can be divided into two substructures, the lateral (LHb) and medial habenula (MHb) which are both functionally and neurochemically distinct (Klemm, 2004). However, in the mammalian habenula, both nuclei are now thought to play a role in mediating the aversive properties of distinct drugs of abuse.

1.5.1 The lateral habenula

Interest in the habenula has had resurgence in recent years, following the breakthrough work of Matsumoto and Hikosaka in 2007, which finally demonstrated a clear function of the habenula (Fakhoury, 2018). Despite a wealth of earlier studies which detailed the neurocircuitry of the structure in the 1970s and 1980s, the role of the habenula remained elusive (Sutherland, 1982). This was in part due to its small size (the very name '*habenula*' comes from the Latin for '*little rein'*) which meant that lesion studies often obliterated the whole complex and made distinguishing the individual contributions of the MHb or LHb difficult (Aizawa et al., 2011). In their paper, Matsumoto and Hikosaka performed electrophysiological recordings from awake and behaving monkeys and showed that the neurons in the LHb would increase their firing activity when an expected reward was not delivered, and this was exactly opposed by dopaminergic neurons in the midbrain, which decreased activity to the same stimulus – thus forming the 'circuit of disappointment' (Matsumoto and Hikosaka, 2007). This firmly implicated the LHb in regulating 'negative reward' and motivation (Hikosaka et al., 2008) and generated extensive research into this structure and its role in regulating the reward systems of the brain (Hu et al., 2020; Proulx et al., 2014). Today, the LHb is also linked to cognition (Mathis et al., 2017; Mizumori and Baker, 2017), pain (Shelton et al., 2012), motor output and maternal behaviours (Hikosaka, 2010), and is

now a therapeutic target in the treatment of depression as well as schizophrenia (Boulos et al., 2017).

The LHb has also been linked to the circadian system (Baño-Otálora and Piggins, 2017; Salaberry et al., 2019) and may act as a semi-independent circadian oscillator (Guilding et al., 2010). Evidence shows that the LHb has rhythmic expression of the clock gene *Per2* as demonstrated through *in vitro* luciferase reporter experiments (Guilding et al., 2013, 2010) or real-time quantitative PCR assays (Zhao et al., 2015). In addition, the LHb demonstrates rhythmic expression of c-fos (an indication of neuronal activity; M. J. Paul et al., 2011; Tavakoli-Nezhad & Schwartz, 2006), daily variation in electrophysiological properties when examined *in vitro* (Park et al., 2017; Sakhi et al., 2014b; Zhao and Rusak, 2005) and *in vivo* (Zhao and Rusak, 2005) and receives indirect photic inputs which may serve to provide timing information (Hattar et al., 2006; Sakhi et al., 2014b; Zhao and Rusak, 2005).

1.5.2 The medial habenula

In contrast to the LHb, the MHb remains largely understudied, and relatively little is known of its functions (Lee et al., 2019; Viswanath et al., 2013). The MHb is an area rich in cholinergic neurons and is the site of dense expression of many nAChRs, some of which are uncommon throughout the rest of the brain (Grady et al., 2009; Ren et al., 2011). Due to these unique characteristics and the downstream reward targets of the MHb, research into this brain structure has primarily focussed on its role in nicotine addiction, which has finally seen the MHb generate a peak in research activity (Fowler et al., 2011; Frahm et al., 2011; Velasquez et al., 2014). A series of experiments with transgenic mice, as well as investigations with pharmacological agents and even studies into the human genome have firmly implicated the MHb and its projection target, the IPN as critical components of nicotine addiction.

Interestingly, the MHb is also a site of interest for research into other substances of abuse such as cocaine (López et al., 2019), morphine (Glick et al., 2006), and alcohol (Hwang et al., 2004), suggesting the MHb could be part of a common addiction pathway (McLaughlin et al., 2017). In addition, previous studies have indicated that the MHb has some of the properties of a circadian oscillator, making this a promising candidate for mediating the circadian influences on the circuits driving nicotine behaviours.

1.5.3 The peri-habenular region

The peri-habenular region (pHb) is a small region located immediately adjacent to the LHb (Huang et al., 2019). This region of the dorsal thalamus has only recently been unrecognized, and has

been implicated in the SCN-independent pathway inducing the effects of light on mood (Maruani and Geoffroy, 2022). A subpopulation of ipRGCs project directly to the pHb (Fernandez et al., 2018; Hattar et al., 2006; Morin and Studholme, 2014), and these neurons in turn project to the limbic emotional processing ventromedial prefrontal cortex and the dorsal and ventral striatum, brain regions previously identified as involved in mood-regulation (Francis and Lobo, 2017; Meng et al., 2014; Shrestha et al., 2015). Fernandez and colleagues used an ultradian light / dark cycle to abolish molecular clock rhythmicity in the pHb through an ipRGC-dependent circuit, which then produced depressive behaviours in mice (Fernandez et al., 2018). Importantly, the mood alterations triggered by the aberrant lighting schedule could be blocked by inhibition of pHb neurons. A later study showed that light delivered specifically during the night promoted depressive-like behaviours, driven through the ipRGC-pHb circuit (An et al., 2020). As yet it is unclear how the pHb might communicate with the adjacent habenular structure, although it has been reported that a subset of pHb neuron collaterals appeared to project into the LHb (Fernandez et al., 2018) and another recent studied has shown pHb neurons projecting to the MHb (Brock et al., 2022)

1.5.4 Anatomical organisation of the MHb

The MHb is composed of a highly diverse neuronal population, much more densely packed than those in the LHb (Kim and Chang, 2005). The MHb can broadly be divided through expression of neurotransmitters and receptors (Antolin-Fontes et al., 2015). The dorsal third of the MHb is largely composed of neurons which express substance P (SP) with glutamate (Melani et al., 2019), whereas the cells of the ventral portion of the MHb co-express ACh with glutamate (Ren et al., 2011; Wagner et al., 2014). The MHb is also characterised by abundant expression of several different nAChR subtypes (Perry et al., 2002), in fact studies have suggested that as many as 90% of MHb neurons express nAChRs (Sheffield et al., 2000). The majority of nAChRs in the ventral portion of the MHb contain the α3 and β4 subtypes (Gahring et al., 2004; Grady et al., 2009; Quick et al., 1999). Other subtypes, such as the α4, α6, β2 and β3, are localized in a gradient across the structure (Shih et al., 2014). This suggests that subdivisions of the MHb have distinct neurophysiology and will differ in their sensitivity to nicotine.

The gradients in neurotransmitter and receptor expression evident across the MHb has seen the MHb divided into at least five subnuclei (Aizawa et al., 2012; Aizawa and Zhu, 2019; Wagner et al., 2016). Recently, two studies performed single-cell transcriptional profiling of mouse habenula, and identified 5-6 clusters of MHb neurons (Hashikawa et al., 2020; Wallace et al., 2020). These clusters had distinct transcriptional profiles and anatomical distribution, the locations of which

largely matched the subdivisions defined in previous studies (Wagner et al., 2016). At least two of these clusters were shown to be functionally distinct as they had clear differences in some electrophysiological properties (Hashikawa et al., 2020). However, the majority of these divisions are yet to be meaningfully translated into differences in the electrophysiological character of the neurons (Kim and Chang, 2005; Kim and Chung, 2007; Sakhi et al., 2014a).

1.5.5 **Connectivity of the MHb**

The MHb receives inputs from a diverse range of brain areas. In the 1980s, many neuroanatomical and histological studies were carried out in order to identify the connectivity of this area. However, owing in part to its small size, many of these earlier studies failed to differentiate between the medial and lateral substructures of the habenula, instead only drawing broad conclusions on the nucleus as a whole. Recent advances have allowed for a finer examination of the inputs and have revealed the diversity of signals projecting to the MHb, although there is still some conflicting evidence as to the nature of the inputs the MHb receives. Figure 1.5 summarizes the inputs and outputs of the MHb which have been functionally confirmed.

The triangular septum (TS), septofimbrial nucleus (SFi) and the bed nucleus of the anterior commissure (BAC) are all categorized as areas of the posterior septum, and are a source of upstream signalling to the MHb. The TS and SFi were considered to be the source of purinergic inputs to the MHb (Edwards et al., 1992; Sperlágh et al., 1998), as lesions in the TS and SFi led to reductions in release of the neurotransmitter adenosine triphosphate (ATP). It was also suggested glutamate could be co-released along this same TS-MHb pathway (Robertson & Edwards, 1998). Later, Yamaguchi et al performed selective elimination of glutamatergic neurons within the posterior septum (including the TS) to demonstrate that both the BAC and the TS project and release glutamate to the MHb, and that furthermore these parallel pathways are anatomically and functionally distinct: the BAC projects exclusively to the dorsal MHb whilst the TS projects exclusively to the ventral MHb (Yamaguchi et al., 2013). A later study performed by Otsu et al extended this work, and they showed that the inputs to the MHb from the posterior septum were exclusively glutamatergic (Otsu et al., 2018), refuting the earlier studies that suggested the posterior septum as a purinergic source.

Despite the abundance of nAChRs in the MHb, so far it has proved difficult to establish a direct cholinergic source of projections to the MHb. Early lesion and tracing studies implicated both the TS and SFi nucleus as potential sources of cholinergic input (Contestabile and Fonnum, 1983; Fonnum and Contestabile, 1984). However, there is little evidence for cholinergic neurons in

either the TS or the SFi, as demonstrated through a lack of ChAT expression in these areas (Lein et al., 2007).

The medial septum/nucleus of the diagonal band (MSDB) has also been implicated as a source of ACh input (Contestabile and Fonnum, 1983). However, there has been no further confirmation of this pathway: whilst it is indeed true that there is an abundance of cholinergic neurons within the MSDB (Ahmed et al., 2019), there is no evidence that they project to the MHb. Instead, cholinergic MSDB neurons project to other septal regions and the hippocampus (Agostinelli et al., 2019; Li et al., 2018). However, the MSDB contributes GABAergic neuronal signalling to the ventral MHb, as has been functionally demonstrated through optogenetic approaches (Choi et al., 2016; Qin and Luo, 2009). A recent tracing study has demonstrated glutamatergic projections from the MS to the MHb, although this has not been functionally confirmed yet (Zhang et al., 2018). Studies also indicate afferent connections to the MHb from other brain structures, including the VTA, preoptic area and nucleus basalis of Meynert (Herkenham and Nauta, 1979), locus coerulus and superior cervical ganglion (Gottesfeld, 1983), as well as the NAc and median raphe nucleus (Sutherland, 1982).

The majority of MHb efferents reach the IPN along the core of the fasciculus retroflexus (FR) (Lecourtier and Kelly, 2007), and largely maintain topographic organisation: lateral MHb neurons innervate dorsal IPN, medial MHb sends innervate ventral IPN and the dorsal SP neurons of the MHb project to the ipsilateral lateral IPN (Contestabile et al., 1987; Herkenham and Nauta, 1979; Qin and Luo, 2009). Axons from the MHb intertwine and loop throughout the IPN structure before terminating in the ipsilateral IPN (Herkenham and Nauta, 1977). The MHb may also send *en passant* axonal boutons through the LHb (Kim and Chang, 2005). Recent evidence also shows that the MHb sends sparse but direct projections to the 5-HT neurons of the median raphe and dorsal raphe (Ogawa et al., 2014).

The IPN itself is an unpaired structure which spans the midline at the posterior part of the midbrain (Beretta et al., 2012). Although the MHb provides most of the inputs to the IPN, this region is also innervated by the locus coerulus (Shibata et al., 1986), the medial prefrontal cortex (Takagishi and Chiba, 1991), the nucleus of diagonal band (Contestabile and Flumerfelt, 1981), mesencephalic raphe nuclei (Marchand et al., 1980) and other areas (Antolin-Fontes et al., 2015; McLaughlin et al., 2017; Morley, 1986). The majority of IPN neurons express the enzyme glutamate decarboxylase, and so are presumably GABAergic in nature (Hsu et al., 2013), although early immunohistochemical analysis also found neurons expressing 5-HT and glutamate (Hemmendinger and Moore, 1984). The IPN sends projections to midbrain monoaminergic reward

areas such as the dopaminergic neurons of the VTA and serotonergic neurons of the dorsal and median raphe nucleus (Klemm, 2004; Lima et al., 2017; Metzger et al., 2021; Xu et al., 2021). Recent studies have also shown the IPN projects to the serotonergic neurons of the LDTg (Hsu et al., 2013; Wolfman et al., 2018). Like the MHb, IPN neurons also have exceptionally dense expression of nAChRs located both presynaptically and postsynaptically (Beiranvand et al., 2014; Grady et al., 2009; Mulle et al., 1991), but in particular express the α5, α2 and β4 nAChR subunits (Hsu et al., 2013; Zhao-Shea et al., 2013).

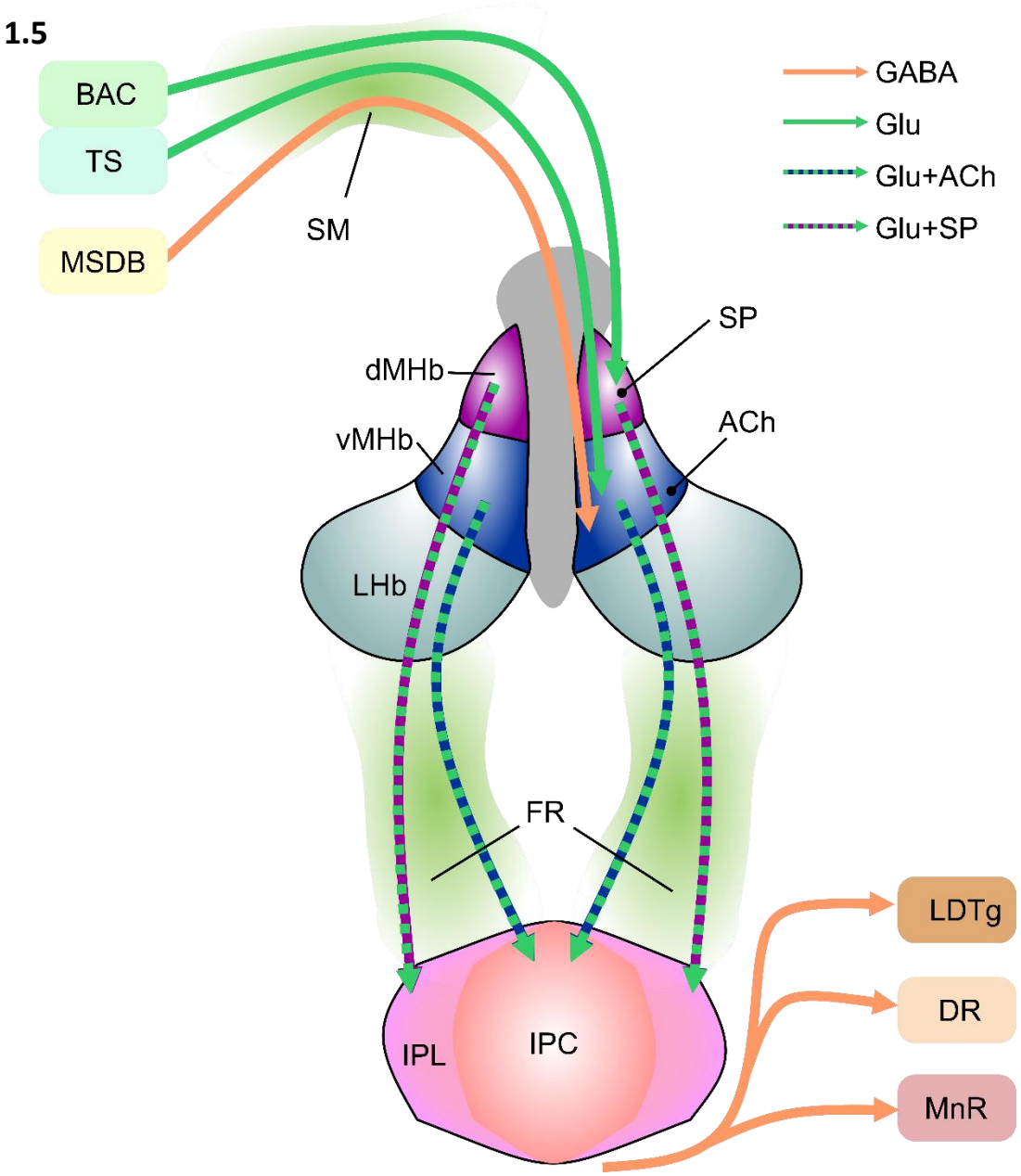

Figure 1.5 Simplified schematic illustration of the MHb-IPN circuit showing the main afferent and efferent projections of the MHb and the distributions of neurotransmitters.

The MHb receives glutamatergic input from the bed nuclei of the anterior commissure (BAC) and triangular septal nucleus (TS) of the posterior septum, and GABAergic input from the medial septum/nucleus of the diagonal band (MSDB) through the stria medullaris (SM). BAC inputs terminate in the dorsal MHb (dMHb) and TS and MSDB inputs terminate in the ventral MHb (vMHb). The majority of MHb outputs extend through the fasciculus retroflexus (FR) to the IPN, maintaining topographic organisation: neurons in the dMHb express substance P (SP) and glutamate and send projections to the ipsilateral lateral portion of the IPN (IPL), whereas neurons in the vMHb co-express acetylcholine and glutamate and project to the central core of the IPN (IPC). GABAergic neurons project from the IPN to downstream reward pathways such as the lateral dorsal tegmental nucleus (LDTg) and median and dorsal raphe nuclei (MnR, DR).

1.5.6 Electrophysiological properties of MHb neurons

Cholinergic neurons of the MHb display spontaneous tonic firing activity independent of inputs, generated by hyperpolarization-activated cyclic nucleotide-gated (HCN) pacemaker channels (Görlich et al., 2013). This pacemaker activity is facilitated by the neurotransmitter ATP (He et al., 2014), and can be modulated by GABAergic inputs through the opposing modulatory activity of $GABA_A$ receptors and $GABA_B$ receptors, also found in the neurons of the MHb (Kim and Chung, 2007). Cholinergic axons from the MHb form a particular type of synapse in the IPN, where both left and right MHb innervate a single disc-shaped IPN dendrite ("crest" synapses; Lenn et al., 1983).

An interesting feature of MHb cholinergic neurons is that MHb axon terminals within the IPN co-express ACh and glutamate vesicular transport machinery (Aizawa et al., 2012; Frahm et al., 2015; Herkenham and Nauta, 1977). Optogenetic studies have demonstrated that these neurotransmitters can be co-released depending on the mode of stimulation: brief stimulation produces glutamate-mediated fast postsynaptic effects whilst only high frequency, sustained stimulation of the cholinergic fibres produces slow responses in nAChRs, consistent with the 'volume transmission' model of ACh signalling (Ren et al., 2011). In this model, high levels of AChE at sites of ACh release degrade the neurotransmitter quickly, preventing spillover to receptors in more distal sites (Antolin-Fontes et al., 2015). AChE is found in high concentration at the synapses of MHb cholinergic neurons on to the IPN (Flumerfelt and Contestabile, 1982), and so high frequency stimulation of the MHb is needed to produce enough ACh for signalling. It is thought that volume transmission onto presynaptic nAChRs on MHb terminals facilitates excitatory presynaptic glutamate release (Frahm et al., 2015; Girod et al., 2000) as well as modulating GABA release (Covernton and Lester, 2002).

Some recent studies have demonstrated that neurons in the MHb vary in their electrophysiological character depending on the time of day, and may well be under the influence of circadian inputs (Sakhi et al., 2014a; Zhao and Rusak, 2005). This particular property of the MHb will be discussed in more detail later.

1.5.7 Physiological functions of the MHb

The MHb is positioned as a relay centre between multiple afferent and efferent connections, and it is therefore likely that not all the roles of the MHb have been truly elucidated yet. Research has so far primarily been focussed on how the MHb modulates nicotine addiction behaviours, although it has also been linked to a number of motivation and mood-related behaviours.

The MHb has been implicated in both anxiety- and fear-related behaviours, after a study in mice ablating two different subsets of neurons in the MHb impaired these behaviours separately (Yamaguchi et al., 2013). Glutamatergic neurons projecting from the TS to the ventral portion of the MHb are involved in regulating anxiety-related behaviours, whilst glutamatergic neurons originating in the BAC terminate in the dorsal portion of the MHb and instead regulate fear responses (Yamaguchi et al., 2013). These findings extended the work of Agetsuma et al, which showed that genetically silencing neurons in the zebrafish homolog of the MHb impaired experience-dependent fear responses (Agetsuma et al., 2010). MHb cholinergic neurons can also control expression of aversive memories, as mice with conditional deletion of presynaptic cannabinoid type 1 receptors in the MHb (which enhances cholinergic neurotransmission) are less likely to demonstrate freezing responses in cued and contextual fear conditioning experiments (Soria-Gómez et al., 2015). Finally, in a recent experiment, transgenic mice with reduced excitability in MHb cholinergic neurons demonstrated anxiogenic behaviours and interestingly, reduced interest in novel social stimuli (C.-H. Cho et al., 2019).

The MHb has also been linked to depression-like behaviours in rodents. Selective ablation of BAC inputs to the MHb generates increased fear responses in mice following electric shock presentation (Yamaguchi et al., 2013), suggesting that fear responses are driven through the SP neurons in the dorsal MHb. However, one study knocked down ChAT gene in the ventral MHb, thus inactivating cholinergic neurons in this area, and found that this induced symptoms of anhedonia which could be linked with dopaminergic activity in the VTA (Han et al., 2017). Interestingly, this same study also showed that human suicide victims diagnosed with major depressive disorder also showed a significant reduction in genes encoding for proteins of cholinergic transmission. However, an alternative study found that MHb lesions reversed anhedonia behaviours in a rat model of depression (Xu et al., 2018). Clearly, more research is needed to resolve these seemingly contradictory findings as to MHb contributions to depression.

Recent evidence has accumulated to suggest that the MHb is involved in motivation and regulating drive to perform voluntary exercise. Hsu et al used mice where the neurons in the dorsal MHb were developmentally eliminated, and showed that this genetic model had reduced motivation to perform voluntary exercise (Hsu et al., 2014). These same mice had decreased wheel-running activity but normal home cage activity, suggesting the dorsal MHb is specifically involved in motivation to perform elective exercise, rather than producing motor deficits (Hsu et al., 2017). Lesions in the dorsal MHb also caused a longer circadian period of wheel-running activity, although there was no change in the circadian period of home cage activity (Hsu et al., 2017). Other studies showed that optogenetic activation of the MHb via septal afferents (and

therefore projecting to the ventral MHb) produced anxiolysis and increased locomotion in mice (Otsu et al., 2018), and optogenetic activation of MHb cholinergic neurons decreases the motivational drive to explore novel stimuli (Molas et al., 2017b). Most recent work has also extended these findings to rats: rats bred for low voluntary wheel-running behaviour had maturational deficiencies in the MHb compared with rats that showed high levels of wheel-running (Grigsby et al., 2018).

Nicotine is known to have cognition enhancing effects. However, despite the MHb-IPN circuit presenting one of the highest densities of nAChR expression in the brain (Grady et al., 2009), there are surprisingly few studies which have investigated whether the MHb is involved in some aspects of cognition (Lecourtier and Kelly, 2007). In one study, mice with genetic lesions of the MHb demonstrated deficits in reversal learning (Kobayashi et al., 2013). A recent investigation showed that mice lacking the habenula-specific G-protein gamma subunit Gng8 had long-term memory deficit and increased social novelty preferences, and these behaviours were driven through reduced cholinergic transmission in the MHb-IPN pathway (Lee et al., 2021).

1.5.8 The MHb is critical in mediating nicotine withdrawal

As discussed previously, a key driver in sustained cigarette use and continued nicotine dependence is avoidance of the unpleasant symptoms associated with withdrawal. Throughout this chapter, evidence from transgenic mice studies and human genetic studies has already indicated that the MHb-IPN is important in regulating nicotine behaviours, in particular in regulating nicotine intake by mediating the aversive properties of nicotine. However, a wealth of studies has now firmly implicated the MHb-IPN circuit as a critical mediator in nicotine withdrawal (Lee et al., 2019; McLaughlin et al., 2017; Wills and Kenny, 2021).

Withdrawal is mediated through nAChR signalling. The MHb-IPN axis is therefore highly sensitive to this effect due to its abundance of nAChR subtypes (Grady et al., 2009). Indeed, infusion of nicotinic antagonist mecamylamine directly in the MHb (Salas et al., 2009) or the IPN (Zhao-Shea et al., 2015) precipitates withdrawal symptoms in both nicotine-dependent and nicotine-naïve mice. Importantly, mecamylamine injections into other brain areas, including the VTA and median raphe, do not produce withdrawal symptoms in these mice (Zhao-Shea et al., 2015). This clearly indicates the MHb is involved in control of withdrawal signals, and is further evidence that the MHb is involved in mediating normal anxiety-related behaviours. Interestingly, inhibiting the HCN channels responsible for the endogenous pacemaking activity of the MHb cholinergic neurons is able to precipitate both somatic and affective withdrawal-like behaviours, even in mice not exposed to nicotine (Görlich et al., 2013).

Extended nicotine exposure produces neuroadaptation and upregulation of nAChRs, but affects different subunits in different ways, therefore producing changes in nAChR function and cell signalling in a region-specific manner (Wills and Kenny, 2021). Of the nAChRs in the MHb, the α4* and α6* nAChRs expressed in the ventral MHb are the most sensitive to upregulation following chronic nicotine treatment (Arvin et al., 2019; Pang et al., 2016), and this has also been confirmed in experiments using rats that have previously undergone extended nicotine self-administration (Jin et al., 2020). Cholinergic neurons of the ventral MHb, in particular those expressing α6 and α4 nAChR subunits, have been implicated in the heightened anxiety associated with nicotine withdrawal: optogenetically silencing MHb cholinergic neurons that project to the IPN reduces withdrawal-induced anxiety behaviours (Zhao-Shea et al., 2015), whereas transgenic mice engineered to have hypersensitive α4* nAChRs expressed in MHb cholinergic neurons show increased anxiety behaviours, which are restored to normal levels following mecamylamine injection (Pang et al., 2016). These nAChRs are upregulated following prolonged nicotine exposure, presumably leading to increased activation of the cholinergic neurons during withdrawal and subsequent activation of the IPN following the co-release of ACh and glutamate.

Optogenetic activation of GABAergic neurons in the IPN (which may well be activated by signalling from the upstream MHb ordinarily) can drive withdrawal symptoms even in nicotine-naïve mice (Zhao-Shea et al., 2013). Further, β4* nAChR subunits are upregulated in the somatostatin-expressing GABAergic neurons of the IPN in nicotine-dependent mice (Zhao-Shea et al., 2013). The somatostatin-positive GABAergic neurons of the IPN project to the median raphe and LDTg, two areas of serotonergic signalling, which may therefore be involved in withdrawal (Hsu et al., 2013). Interestingly, these same somatostatin-expressing neurons are also known to express α5* nAChRs, and chronic nicotine activation of these receptors drives increased gene expression to mediate feedback inhibition of MHb inputs to the IPN - ultimately enhancing the motivational properties of nicotine (Ables et al., 2017).

Thus, the MHb is an area of the brain that warrants further examination, as research here may contribute to therapies to alleviate withdrawal symptoms and encourage people to stop smoking.

1.5.9 The MHb as a potential circadian oscillator

As previously discussed, there are several brain areas outside of the SCN that have the capacity for rhythmic oscillation (Begemann et al., 2020; J. R. Paul et al., 2020). The LHb is now commonly regarded as one such structure (Bano-Otalora et al., 2021b; Salaberry and Mendoza, 2015). However, the MHb equally demonstrates several of these characteristics, although whether it also functions as an extra-SCN circadian oscillator remains under-explored.

Recent research has demonstrated that there may well be a strong circadian influence on the cells of the MHb. Early studies using *in vitro* hybridisation demonstrated moderate expression of core clock gene mRNA in both rat (Shieh, 2003) and hamster MHb (Yamamoto et al., 2001). Two studies of *ex vivo* tissue containing portions of mouse MHb examined *Per2* expression through bioluminescent reporter proteins, but reported slightly contradictory findings. Landgraf et al reported rhythmic bioluminescence sustained over several days, with higher amplitudes than that of the adjoining LHb (Landgraf et al., 2016a). In contrast, Guilding et al saw only very weak expression of *Per2* fluorescence and weak temporal rhythms compared to the LHb, and they suggested that the rhythms in the MHb might be driven by the cells in the ependymal layer (Guilding et al., 2010). Most recently, a study using *in situ* hybridization found rhythmic expression of both *Per1* and *Per2* in the MHb, albeit with lower amplitude than in the SCN (Olejniczak et al., 2021).

In addition to expression of the molecular clock components, there is also evidence of oscillation in electrical properties in MHb neurons. Rhythmic c-fos expression in MHb has been demonstrated in both hamster (Paul et al., 2011) and diurnal grass rats (Shuboni-Mulligan et al., 2019). Zhao and Rusak performed *in vivo* extracellular single unit recordings in rats, observing that MHb neurons increased their firing rate from morning to early evening (Zhao and Rusak, 2005), although they did not find significant variation in MHb neuron firing rates when they performed recordings *in vitro.* Nonetheless, later experiments using whole-cell patch clamp recordings reported rhythmic spontaneous firing activity in mouse MHb neurons, even in the absence of connections with the SCN (Sakhi et al., 2014a). Notably, this variation in discharge rate over 24 hours was absent in recordings from the MHb of *Cry1-2* knockout mice, indicating that the rhythms are dependent on a functional molecular clock (Sakhi et al., 2014a). This apparent discrepancy between the two studies could be down to the methodological differences: Zhao and Rusak built up a population profile over 24 hours by recording from neurons pooled across tissue slices prepared 12 hours apart, whereas Sakhi et al recorded for shorter durations from slices recorded at different points throughout the 24-hour cycle. Clearly, further work to characterise the circadian profile of electrical activity in the MHb is needed.

In addition, other studies have demonstrated circadian activity within the habenula at large, but it is unclear which substructure might be responsible. One study examined the wheel-running activity of hamsters following transection of the FR (thus severing outputs from both LHb and MHb), and found that the procedure lengthened the circadian rest-activity pattern when in constant darkness, implicating the habenula as a modulator of these rhythms (Paul et al., 2011). An alternative study reported expression of *Per1, Per2 and Bmal1* in the LHb but reported that

they could not discount the possibility of MHb tissue inclusion in their samples (B. Zhang et al., 2016).

Interestingly, there is also evidence that neurons in the habenula are light-responsive, and this has been documented across several species including salmon (Eilertsen et al., 2021), pigeon (Semm and Demaine, 1984), mouse (Sakhi et al., 2014b), rat (Zhao and Rusak, 2005) and even humans (Kaiser et al., 2019). As yet, the function of these light responses is not clear, but they may well modulate mood-related behaviours or could indeed serve to convey information about the time of day (Milosavljevic, 2019).

In zebrafish, neurons in the habenula respond to a change in ambient illumination (both lights on and lights off) in either an excitatory or inhibitory manner, which can be further classified as sustained or transient (Cheng et al., 2017). Sakhi et al performed *in vivo* electrophysiology in mice and also found photic responses in the LHb and a region just outside of the habenula borders, which may correspond to the pHb (Sakhi et al., 2014b). In the LHb the light responses were particularly sluggish, suggesting a polysynaptic pathway generating the responses, in comparison to the much quicker responses found in the region outside of the LHb. They also demonstrated that the responses were not well correlated with the ambient illumination, instead being driven primarily by visual contrast. In rats, Zhao and Rusak performed *in vivo* electrophysiology and demonstrated light responses found across both the MHb and the LHb to long pulses of binocular illumination from dark. These responses were shown to be dependent on the time of day in the LHb, although this was not shown in the MHb. Interestingly, a recent study investigating the light responsive properties of the human habenula also seems to corroborate this finding, with a decrease in habenula activation following a change in the light conditions irrespective of the direction as opposed to the levels of retinal illumination (Kaiser et al., 2019), although the spatial resolution of this study was unable to distinguish between MHb and LHb, so it remains to be seen which portion of the habenula is contributing to this effect.

In mice, there are at least two circuits which may be responsible for driving light responses in the habenula. M1 type ipRGCs project directly from the retina to the pHb, the region immediately lateral to the LHb (Fernandez et al., 2018; Hattar et al., 2006; Morin and Studholme, 2014). The proximity of this projection to the habenula has led to suggestion LHb uses light to regulate behaviours along this indirect pathway (Salaberry et al., 2019). Therefore, it is possible the MHb can access this photic information in a similar way. A different class of ipRGCs, the M4 type, are part of a disynaptic circuit conveying light information to the LHb (Huang et al., 2019). Neurons from the retina project to the lateral geniculate (LGN) / IGL of the thalamus, synapsing with

neurons which terminate in the LHb, as demonstrated through retrograde tracer experiments. Activation of this pathway improved depressive-like behaviours in mice and firmly implicated this circuit as a potential mechanism for the anti-depressive effects of light therapy. It should be noted that this study did not appear to examine whether such projections from the thalamus also terminated in the MHb, so this may well provide a mechanism for MHb responses to light as well.

Together, there is considerable evidence in support of the MHb as an oscillatory structure. The evidence for circadian activity in these parameters begs the question of where this circadian control might originate from and whether the MHb itself is another semi-autonomous clock of the mammalian nervous system.

1.6 Summary and aims

Collectively, this evidence points to there being a circadian influence on the cholinergic circuitry of the MHb-IPN axis, which has potential implications for nicotine-dependent behaviours. Smoking and nicotine-reinforced tobacco consumption in humans is still a major cause of early death around the world, and therefore research into the mechanisms driving this behaviour is of crucial importance. Indeed, not only could an understanding of the circadian influences on the MHb generate more effective strategies for smoking cessation in humans, this could also have implications for other substances of abuse which may use a common circuit of withdrawal (Neugebauer et al., 2013). Furthermore, if there is circadian control over cholinergic systems outside of the MHb, this could have consequences for a broad range of other behavioural outputs and processes, such as learning and memory, anxiety and the sleep-wake cycle (Picciotto et al., 2012). However there remain a number of unanswered questions as identified throughout this chapter. The time of day at which nicotine's effects are most potent remains inconclusive. Whilst there is certainly evidence that the MHb is rhythmic, work so far has not determined the extent to which these rhythms are dependent on a circadian clock, and further investigations to characterise the diurnal rhythm in electrophysiological properties is needed. Finally, although outputs of the MHb that are mediated through nicotine and the cholinergic system are rhythmic, as yet evidence that the MHb is the site of diurnal fluctuations in cholinergic signalling is lacking. This thesis sets out to address these questions.

This thesis is presented in the 'alternative format', with chapters presented in the format of published papers. The overall aim of this thesis is to examine how the time of day alters the circuitry mediating nicotine's effects, in particular by using the nocturnal rodent as an experimental model.

Although there is some evidence of diurnal variation in sensitivity of the effects of nicotine, this area remains underexplored. Therefore, the next chapter (Chapter 2) begins by investigating how acute nicotine affects the locomotor behaviour of rats at different times of day.

Next, Chapter 3 aims to further investigate time of day differences in cells of the MHb, using an *in vitro* preparation. We examine both short-term and long-term cellular behaviour for evidence of rhythmicity in the absence of the SCN. As an area of dense nAChR expression, we also set out to investigate how time of day alters the effects of nicotine within this brain structure, and in particular explore the contribution of a particular nAChR subunit to this pattern.

Building on findings from Chapter 3, experiments in Chapter 4 were designed to confirm rhythmicity in MHb function *in vivo*. Moreover, a particular aim here was to characterise the circadian and light-dependent activity of cholinergic neurons within the MHb and determine whether this differed from other classes of MHb neurons.

Finally, Chapter 5 attempts to elucidate the mechanisms of diurnal variation evident within the MHb. Using RNA sequencing, these studies examine how the transcriptional profile of the MHb varies over 24 hours to identify which genes may exhibit rhythmic expression driving the oscillations previously observed within this structure.

2 Daily variation in behavioural sensitivity to nicotine in rats

2.1 Abstract

Nicotine addiction is highly prevalent worldwide. Both human and animal studies provide evidence that the brain's reward circuitry is under circadian control and reveal daily rhythms in consumption of and/or responses to many drugs of abuse, including nicotine. To date, however, relatively few studies have investigated diurnal variations in response to nicotine in rodent models. To address this, we examined how nicotine impacts rodent behavioural activity according to the time of day. Spontaneous locomotion (both horizontal and vertical activity) of female Lister Hooded rats was measured using automated infrared photo beam cages. Rats were injected with one of four doses of nicotine (0.0, 0.1, 0.2, 0.4 mg / kg) and nicotine-evoked changes in locomotion were compared between defined time points across the day / night cycle. These experiments revealed that stimulatory effects of nicotine on ambulation were most apparent during the mid-late day, coinciding with the periods when rats were least spontaneously active. By contrast, time points at which the rats were least spontaneously active tended to lead to a decreased sensitivity towards suppressive effects of nicotine, whereas robust decreases in rearing activity were clear at time points when the rats were highly spontaneously active. Together, these experiments demonstrate that the acute effects of nicotine on rat locomotion are dependent on the time of day, highlighting the need for researchers to carefully control for circadian variation when assessing the actions of nicotine in laboratory rodents.

2.2 Introduction

Smoking and tobacco addiction remains a major concern for public health, leading to 96000 premature deaths in UK alone each year (West, 2017). Nicotine, the main psychoactive and addictive component of tobacco (Jackson et al., 2015), binds to nicotinic acetylcholine receptors in the brain, producing pleasurable effects through activation of the reward centres in the mesolimbic pathway (Benowitz, 2010). Repeat exposure to nicotine produces neuroadaptation, which gives rise to the unpleasant symptoms associated with withdrawal following smoking cessation (Changeux, 2010; De Biasi and Dani, 2011). Accordingly, development of addiction to nicotine is the net result of balancing the positive reinforcing actions of nicotine with the avoidance of the aversive effects of withdrawal (Dani and De Biasi, 2013). Given the impacts of tobacco use on heath, a better understanding of these systems underlying nicotine withdrawal and addiction clearly remain as vital as ever.

Currently, there is evidence that the brain's reward circuitry is under circadian control; many drugs of abuse demonstrate a daily rhythm in rates of self-administration including alcohol (Perreau-Lenz et al., 2012), heroin (Negus et al., 1995; Phillips et al., 2013) and cocaine (Abarca et al., 2002; Sleipness et al., 2005). This suggests that the mechanisms driving drug intake also exhibit diurnal variation (Webb et al., 2015). For example, the mesolimbic reward pathway has been shown to express clock genes and exhibits rhythms in neuronal excitability (McClung, 2007; Rosenwasser, 2010). One further point to note is that the circadian system may be regulating addiction through less direct routes, such as through circadian regulation of more generalised processes, including arousal and motivation. For example, research from both human and animal studies show that extracellular concentrations of the neuromodulator adenosine are strongly correlated with time awake, and decline following sleep (Porkka-Heiskanen et al., 2000; Urry and Landolt, 2015). This modulator of arousal typically fluctuates in a circadian-dependent fashion, following the sleep-wake cycle (Lazarus et al., 2019) and is also known to regulate alcohol intake (Nam et al., 2012) and many other drug-related behaviours (Ballesteros-Yáñez et al., 2018). Motivation to seek rewarding stimuli also varies cyclically across the day (Mendoza and Challet, 2014; Webb, 2017). Together these studies demonstrate how circadian regulation of reward system exist on several direct and indirect routes. However, only limited research has been carried out into circadian influences on mechanisms driving nicotine intake.

Interestingly, there is evidence from human studies to suggest that smoking behaviours may have a biological rhythm. Smoking intake varies systematically across the day (Chandra et al., 2011). Both smoking and nicotine gum use follows a similar diurnal pattern with heaviest use during the

morning (Benowitz et al., 1982; Mooney et al., 2006). Smoking intensity also shows diurnal variation, with cigarettes smoked during the night and early morning being puffed less intensively (Grainge et al., 2009). However, human patterns of nicotine intake are difficult to interpret as they may not be truly circadian in nature, but could instead reflect responses to social cues such as working schedules or other societal conventions. A large study of over 200 participants found that whilst smoking, craving and withdrawal symptoms varied according to the time of day (although this was only compared between three broad time points) and abstinent participants showed notably increased evening cravings compared to other times of day (Perkins et al., 2009). Similarly, an investigation of nicotine patch users found lapses were more likely during the afternoon and evening (Ussher and West, 2003). Current treatments, including nicotine patches, do not account for the diurnal variation in craving intensity. Establishing whether there is a true rhythm underlying nicotine signalling could lead to better smoking cessation treatment by taking this factor into consideration.

Analogous to the rhythms in human consumption indicated above, nicotine self-administration in rats follows a circadian pattern with greater intake during the dark phase than the light (O'Dell et al., 2007). Only a few animal studies have so far investigated diurnal or circadian variation in sensitivity to the effects of nicotine, however, and as yet there is no consensus as to the time of day at which nicotine is most potent. An early study from 1967 showed nicotine injected during the light phase increased the wheel-running behaviour of rats during the following 12 hour light phase, whereas injections during the dark phase produced either no effect or a decrease in activity during the 12 hours of darkness (Bovet et al., 1967). Similarly, a later study by Morley and Garner examined the effects of chronic nicotine infusion on rat locomotion by implanting minipumps, and saw increased activity during the light phase, but no change in activity during the dark phase (Morley and Garner, 1990). Williams et al found diurnal variation in nicotine-induced hypothermia in male rats, with strongest actions during the light phase (Williams et al., 1993). Mexal et al found the activity-depressing actions of acute nicotine on mouse ambulatory activity was greatest during the latter portion of the light phase, when animals were at their least active (Mexal et al., 2012), while an alternative study has demonstrated that mice are most susceptible to the locomotor stimulating effects of chronic nicotine during the latter portion of the dark phase (King et al., 2004). On the other hand, a further study showed that the nicotine-induced depressant effect on rat locomotion during the first 20 mins following injection had greatest effect during the dark phase, whereas nicotine-evoked activity was stimulated with greatest effect between 80 - 100 min following injection at the beginning of the dark phase (Kita et al., 1986). Therefore, whilst there is certainly evidence to suggest nicotinic cholinergic signalling may be

under circadian control, additional studies are warranted to further characterise this diurnal variation.

To address this, behavioural experiments were conducted to investigate whether the acute effects of nicotine on spontaneous locomotor activity exhibit diurnal variation. Nicotine has potent but complex effects on locomotion in rats. Acute nicotine challenge has generally been found to produce biphasic effects on rat ambulatory activity – an initial depressant effect followed by a stimulatory effect (Clarke and Kumar, 1983; Matta et al., 2007; Stolerman et al., 1995). However, this initial depressant effect is highly dependent on nicotine tolerance, in some cases even a single pre-exposure is enough to eliminate this effect (Kanýt et al., 1999). The effects of nicotine on horizontal locomotor behaviour are further dependent on the interaction of other factors including age, sex, dose, strain and habituation to the arena (Elliott et al., 2004; Faraday et al., 2003; Kanýt et al., 1999; Ksir, 1994; Matta et al., 2007). Additionally, acute nicotine alters rearing behaviour (Meliska and Loke, 1984; Rodgers, 1979), which has been interpreted as a separate behavioural process to ambulation (Faraday et al., 2003; Lever et al., 2006; Qiu et al., 1992).

Therefore, this set of experiments aimed to first establish the effects of nicotine on the locomotor activity of female Lister Hooded rats, and then to investigate this action at different times of day. Female rats were used to address the previous bias for using male rats in studies investigating how nicotine effects locomotor behaviour. The studies described in this report assessed sensitivity to both the locomotor depressant actions of nicotine on rearing and the stimulatory effects on ambulation at four time points over the light / dark cycle, from which we were able to detect diurnal variation in sensitivity to an acute nicotine challenge, which appeared to be dependent on the underlying rhythms in spontaneous activity.

2.3 Materials and methods

2.3.1 **Animals**

All experiments were performed in accordance with the Animals (Scientific Procedures) Act 1986 and were approved by the University of Manchester Animal Welfare and Ethical Review Body under conducted under the authority of the Project Licence P763B36B8. All procedures were carried out in the Biological Services Facility at the University of Manchester. Eighty experimentally naïve adult female Lister Hooded rats aged between 6-8 weeks were obtained from Charles River (UK). This study used female Lister Hooded rats as previous work in this laboratory has shown that they consistently demonstrate reliable performance over a range of

cognitive tasks across the oestrous cycle (McLean et al., 2009; Sutcliffe et al., 2007), and we had originally planned to include cognitive tests as part of these experiments. Furthermore, the use of female rats facilitates social housing as they do not grow as rapidly as male rats, thus avoiding the stressful condition of individual housing (Brown and Grunberg, 1995; Hayward et al., 2017). The oestrous cycle was not taken into consideration as this has been shown not to influence nicotine's effects on locomotor activity (Kanýt et al., 1999) and nicotine itself is not thought to interfere with the oestrous cycle in female rats (Booze et al., 1999).

Upon arrival, rats were housed as groups of 5 in double level individually-ventilated cages (GR1800 Double-Decker cage, Techniplast, UK) with standard items for environmental enrichment (cardboard tube, wooden blocks, bedding material). Temperature (21 ± 2˚C) and humidity (55 ± 5 %) were kept constant. Food (standard rat chow, Special Diet Services, UK) and water were available *ad libitum* except for during the experimental procedures. Animals weighed between 175 - 200 g at the start of the experiment. In all cases, sample sizes were based on previous work (Hayward et al., 2017), but post-hoc sensitivity power analyses were carried out (e.g. for a one way ANOVA with 4 groups of 12 we have 80% power to detect effect sizes of Cohen's f = 0.498, which equates to a large effect size).

Figure 2.1 details the experimental timelines and the lighting environments used for this study. A cohort of 65 animals were habituated to the holding room for 1 week under standard 12 hr / 12 hr light / dark cycle with lights on at 07.30 and dim red light at 19.30, with a 15 min dawn / dusk period. 50 animals were used for Experiments 1, 2 and 4, and 15 rats were used for Experiment 3. A separate cohort of 15 animals, also for Experiment 3, were housed under a reversed light / dark cycle in an alternative holding room with lights on at 22.30 and dim red light at 10.30. Dim red light was used to allow safe and rapid conduction of the subcutaneous injections and to mask the light emitted from the computer within the experiment room. This also eliminated the effects of a dim light pulse during the animals dark phase which can disrupt circadian rhythms (González, 2018). Once animals had been undergone the first set of tests for Experiment 3, they were then put into the alternative light dark cycle and left to acclimatise for a further 2 weeks to entrain before retesting.

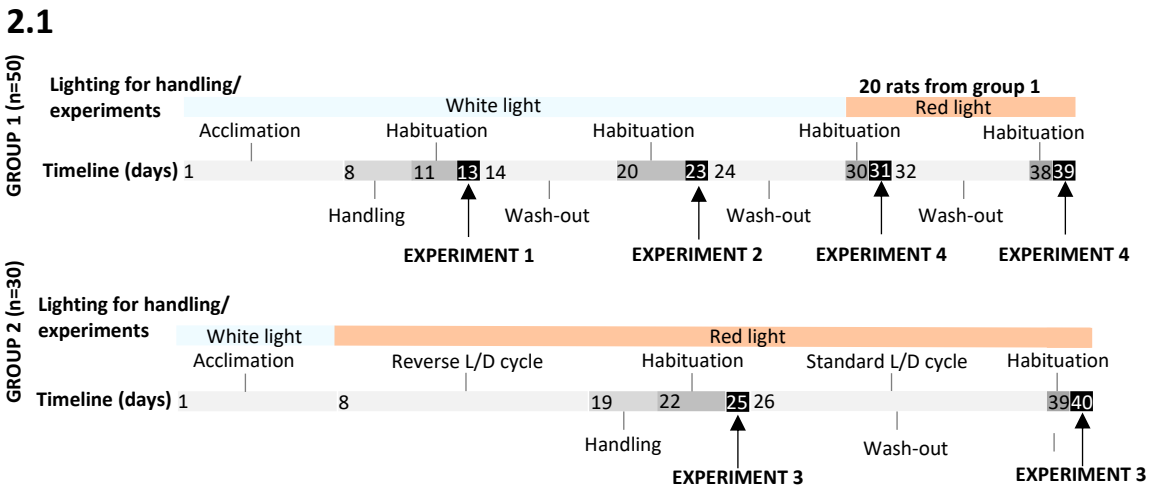

Figure 2.1 Experimental timeline of all rat behavioural studies.

A) Upon arrival, 50 naïve rats were acclimatized to the holding room on a standard light / dark cycle before handling and habituation. After experiments 1 and 2, 20 rats from this group went on to participate in experiment 4.
B) A second cohort of 30 naïve rats arrived, and half were placed into a reversed light / dark cycle. After the first test in experiment 3, rats were immediately put into a standard light / dark cycle and left for 2 weeks before retesting (or vice versa for the other 15 rats).

2.3.2 Apparatus

All experiments were performed in a dedicated test room either under white or dim red light (see specific experimental protocols for details). Locomotor activity was measured using the automated infrared Photobeam Activity System (San Diego Instruments, San Diego, CA, USA). Rats were placed individually into transparent Plexiglas chambers (H 20 cm x W 24 cm x L 44 cm) that were arranged on a single 4 x 3 rack. This allowed 10 test chambers to be run simultaneously to avoid within-cage order effects. At the beginning of each experimental session, cages were thoroughly wiped down with ethanol and a small quantity of fresh woodchips to cover the floor and absorb urine and faeces were added. Rats were pseudorandomly assigned to cages within the rack to account for the possible effects of cage position.

2.3.3 Data collection

Test chambers were set up to allow automatic measurement of locomotor activity, eliminating experimenter bias. Infrared photobeam interruptions were counted in real time using Pas764 LMA software through a dedicated computer in the experimental room. Horizontal or ambulatory activity was measured using the infrared beams positioned 5 cm apart on the cage floor (X axis: 2 x 4 beams; Y axis: 2 x 8 beams). Vertical or rearing activity was measured using the beams

elevated 14cm above the cage floor (Y axis only: 2 x 8 beams). Activity was recorded continuously and collected as cumulative counts every 5 min. The experimenter and the computer were set out of sight of the cages, and during experiments performed under red light the screens were covered with red filters and set to the dimmest screen brightness to prevent light pollution disrupting the circadian system.

Animals were transported to the test room in their home cages at least 15 min before being placed in the test cage. The experimenter remained silently in the room for the course of the experiments. Care was taken not to disturb the animals (although checks of suspected erroneous beam breaks were made). Animals were immediately returned to their home cages at the end of the experiment.

2.3.4 Drugs

Drug doses were calculated based on the free weight of nicotine. -(-)Nicotine ditartrate (Tocris, UK) was dissolved in 0.9% saline made up fresh on the day of the experiment. Injections were administered subcutaneously into the flank of the animal at a volume of 1 ml / kg before they were immediately returned to the test arena. Control animals received an injection of saline vehicle alone. There was at least a 7 day wash out period between drug administration to avoid tolerance to acute nicotine doses (Stolerman et al., 1973) and interference with the circadian cycle (Gillman et al., 2010).

2.3.5 Experiment 1: Nicotine's effects on locomotor activity in minimally habituated rats

Fifty rats were used for this initial study. Rats were habituated to the standard holding room for 1 week before daily handling sessions were conducted for a further week. Rats were also habituated to the test cages during the 2 days immediately preceding the experiment day, which exposed animals to the test cages first for 30 min and 60 min the next day.

Rats were pseudorandomly assigned to 1 of 4 dose groups such that within each home cage of 5 rats there was at least 1 rat from each group. The nicotine dose groups (0.0 mg / kg, n = 12; 0.1 mg / kg, n = 13; 0.2 mg / kg, n = 13; 0.4 mg / kg, n = 12) were selected to cover the range of effective doses used widely within the existing literature to facilitate comparison with previous studies (Clarke and Kumar, 1983; Ksir, 1994; Stolerman et al., 1973).

All behavioural experiments took place under standard white light during the mid day (ZT 4 – 8). Locomotor activity was recorded during the 30 min habituation period before administration of

nicotine. Individual rats were immediately returned to the same cage following injection and activity was recorded for a further hour.

2.3.6 Experiment 2: Nicotine's effects on locomotor activity in extensively habituated rats

This experiment was performed to determine if extensive habituation to the arena would reveal nicotine-evoked changes in locomotor activity not uncovered during Experiment 1. Nicotine's effects on locomotor activity are known to be affected by pre-exposure to the arena. If rats are not habituated to the test cage, nicotine tends to suppress activity, whereas rats that have been habituated to the arena tend to demonstrate locomotor activation (Ksir, 1994; Matta et al., 2007; Palmatier et al., 2003). In the initial investigation into nicotine's effects on locomotor activity, rats failed to demonstrate the expected increases in activity associated with nicotine despite having been habituated to the arena beforehand. We postulated that they may need further habituation to the arena in order to observe this effect, in particular as Lister Hooded rats demonstrate higher levels of novelty-induced exploratory behaviour than other strains (Clemens et al., 2014).

As such, the procedures were largely the same as those outlined in Experiment 1, but with further habituation steps. Animals remained in the same dose groups as in Experiment 1. Following a week long washout period, animals were further habituated to the test cages. For the 3 days prior to the experiment, animals were left to habituate to the arena for 1 hr every day. During the experiment, rats were placed in the test cages and locomotor activity was recorded for a full hour before injection. Activity was then recorded for a further hour after the animals were returned to the test cages.

2.3.7 Experiment 3: Comparing nicotine-evoked locomotor activity during the mid day and mid night

This study was designed to investigate how the time of day influenced nicotine-evoked locomotor activity. As such, experimental procedures were performed either during the mid day as in the previous two experiments (ZT 4 - 8) or mid night (ZT 16 - 20). Thirty rats were used for this portion of the study. The test procedure was largely the same as in Experiment 2, although the lighting conditions were altered.

Rats were split into 2 cohorts of 15 rats and following the week of acclimatisation to the animal unit, one cohort was placed into the alternative holding room under the reversed lighting schedule. Rats were left for at least 10 days to allow for circadian entrainment before 3 days of handling sessions performed at different times during the circadian cycle to avoid any possible

disruption to their behavioural rhythms (although it should be noted that previous work suggests that low cognitive tasks including handling do not significantly alter nocturnal rats circadian cycle; Gritton et al., 2009). A further 3 days of hour-long habituation sessions where rats were left in the test cage followed, before locomotor activity was recorded the next day. To account for possible effects of repeat exposure to the test, one cohort were tested during the light phase first and then the dark phase whilst the second cohort were tested during the dark phase first. After the first experimental session, animals were rehoused in the opposite light / dark cycle and left to entrain for a further 2 weeks prior to the second test session.

Exposure to light during the animals' dark phase is known to alter their circadian rhythms and can affect their locomotor behaviour (Fonken et al., 2013; Shigeyoshi et al., 1997; Studholme et al., 2013) and so to keep circadian disruption to a minimum as far as possible, all experiments were performed under dim red light. Furthermore, lighting conditions themselves have been shown to affect locomotor activity (Tatem et al., 2014; Valle, 1970). Therefore, to allow comparisons between day and night responses to activity, even tests carried out during the light phase were performed in dim red light. Animals were transported from the holding room to the test room on a trolley under a light proof blanket to further eliminate sources of light pollution.

Rats were once again pseudorandomly assigned to 1 of 4 nicotine dose groups (0.0 mg / kg, n = 8; 0.1 mg / kg, n = 6; 0.2 mg / kg, n = 8; 0.4 mg / kg, n = 8) which received the same nicotine dose during the mid day and mid night experiments. One rat from the saline control group was later excluded from the experiment due to experimenter error in recording the data collection in the software. Groups were balanced such that there were equal numbers of rats tested first at each time point within each dose group.

2.3.8 Experiment 4: How time of day influences nicotine-evoked changes in locomotor activity during the early and late day

Twenty rats were randomly selected from the cohort used in Experiments 1 and 2 to investigate how 0.4 mg / kg nicotine evoked changes in locomotor activity are different between the early day (ZT 0 - 4) or late day (ZT 8 - 12). 0.4 mg / kg was chosen as the dose was shown to be reliable at producing changes in locomotor activity as demonstrated in the previous experiments. Ten animals received saline and 10 received 0.4 mg / kg nicotine injection at both time points. Test order was once again counterbalanced to account for any possible effects of repeat exposure, with half the animals being tested first in the early morning, and then in the late day following 7 days washout.

As these rats had already been extensively habituated to the test cages during Experiments 1 and 2, rats only had one further hour long habituation session the day before testing. The test procedure was largely the same as in Experiment 3, with an hour of habituation before injection and a further hour to record the locomotor activity, but all procedures were performed under dim red light.

2.3.9 Data analysis

Since the initial depressant effects of nicotine are known to show a strong tolerance effect (Kanýt et al., 1999), and the present experiment involved several repeat exposures to nicotine, horizontal activity occurring 30 – 60 min post drug was taken as the primary measure for assessing effects of nicotine on ambulatory behaviour. Similarly, to investigate how nicotine altered rearing activity, vertical beam breaks were totalled across the 30 – 60 min epoch following injection. Habituation phase activity was calculated as the total horizontal beam breaks counted during the period immediately before injections.

Data were collected automatically as beam breaks every 5 min over the course of the entire test session. However, during some experiments it was noted that there seemed to be erroneous rearing data being collected, which were confirmed at the completion of the behavioural test and therefore the data was not included in subsequent analysis (i.e. after the rat was removed from the cage, occasionally the system would still register vertical beam breaks, which would produce approximately 10 fold higher counts than the other chambers). This meant that for each experiment, between 1 - 5 animals were excluded from each group and were thus not included in the analysis of rearing behaviour (either before or after nicotine challenge), although they were not excluded from the horizontal behaviour analysis. In addition, one rat from the 0.1 mg /kg dose group managed to escape her cage during the experiment and was excluded entirely from analysis in Experiment 2. The total number of rats included in each analysis is indicated in the time course figures throughout this report.

2.3.10 Statistical analysis

Data were exported to Microsoft Excel for initial examination and all statistical analysis was performed in GraphPad Prism v9.1.2 (GraphPad, USA). Data were examined for normality using D'Agostino & Pearson normality test and visualisation of the data distribution with Q-Q plots. Time course activity profiles were analysed with two-way mixed effects ANOVAs (Factors: Time, Dose) with Dunnett's post-hoc tests to detect differences from the vehicle control group. One-way ANOVAs were run to compare horizontal or vertical activity between dose groups, followed

by Dunnett's post-hoc tests. For investigations into time of day influences on nicotine-evoked locomotor activity, two-way mixed effects ANOVAs were employed (Factors: Dose, Time of day). In the cases where vertical activity counts were missing (due to false beam break counting), data was analysed using a mixed effects model instead of repeat measures ANOVA as implemented through GraphPad Prism v9.1.2. This mixed model employs a compound symmetry covariance matrix, fit using Restricted Maximum Likelihood. Both the two-way ANOVAs or mixed effects model were followed by Dunnett's post-hoc tests when examining differences from the vehicle control group or Holm-Šídák's s post-hoc tests for other comparisons. An alpha level of 0.05 was applied to all statistical tests. All graphs were produced using GraphPad Prism v9.1.2.

2.4 Results

2.4.1 Experiment 1 – Nicotine-evoked locomotor behaviour in minimally habituated rats

Experiment 1 was designed to establish the effects of nicotine on locomotor activity of female Lister Hooded rats, so as to establish an appropriate dose for testing nicotine sensitivity across the circadian cycle. Figure 2.2A-B shows the time course of both horizontal and vertical activity during both the pre-drug habituation period and the 60 min following acute nicotine challenge. Horizontal activity was characterised by high initial activity which steadily declined until administration of the drug, which caused a spike in activity. Two-way mixed effects ANOVA revealed a significant Time x Drug interaction (F (51, 782) = 1.94, p = 0.0001) with reduced horizontal activity relative to vehicle in the five minutes immediately following injection (Dunnett's post-hoc tests). This was similar for the vertical activity, with nicotine producing reduced rearing behaviour in the first five minute following injection (two-way mixed effects ANOVA, Time x Drug: F (51, 544) = 2.68, p < 0.0001; Dunnett's post-hoc tests). All nicotine dose groups had similar horizontal and vertical activity levels in the 30 min habituation period immediately before exposure to the drug (Figure 2.2C-D; horizontal: one-way ANOVA, F (3, 46) = 2.03, p = 0.12; vertical: F (3, 32) = 0.109, p = 0.95).

When the activity counts were totalled for the 30 – 60 min period following the injection, significant effects of nicotine on locomotor activity were not detectable across the dose range tested for either ambulatory (Figure 2.2E; one-way ANOVA, F (3, 46) = 1.85, p = 0.15) or rearing behaviours (Figure 2.2F; one-way ANOVA, F (3, 32) = 1.53, p = 0.22).

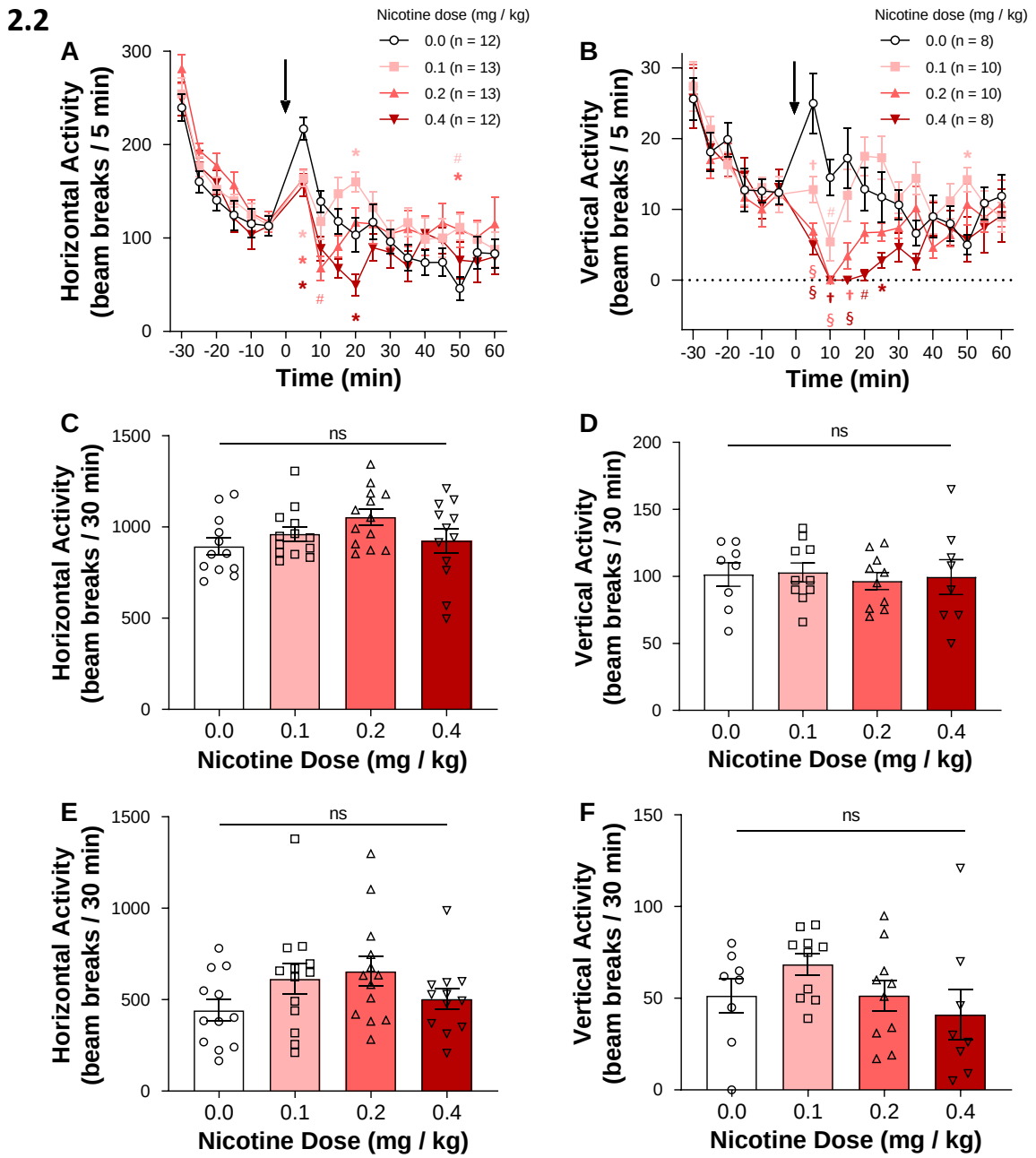

Figure 2.2 Changes in spontaneous locomotor behaviour following acute nicotine challenge in minimally habituated rats. Rats were habituated to the test cage for two sessions (totalling 1.5 hr) prior to the test.

A – B) Time course profiles of both the horizontal (A) and vertical activity (B) during the 30 min habituation period and 60 min following nicotine challenge (indicated by the arrow at 0 min). Activity was measured at 5 min intervals, and nicotine-treated groups were compared with the vehicle group at each time point by two-way mixed effects ANOVA with Dunnett's post-hoc tests. The number of rats in each dose group (n) are shown above the graph (some data was excluded from the vertical activity analysis due to faulty equipment).

C - D) Average horizontal (C) and vertical (D) beam breaks recorded during 30 min pre-drug habituation period. All groups had similar activity (one-way ANOVA).

E - F) Average horizontal (E) and vertical (F) beam breaks recorded 30 - 60 min after nicotine injection. Nicotine did not appear to affect activity (one-way ANOVA).

Data is presented as the mean ± SEM. Graphs display significant differences from vehicle group in post-hoc testing; * $p < 0.05$; # $p < 0.01$; † $p < 0.001$; § $p < 0.0001$.

2.4.2 Experiment 2 - Nicotine-evoked locomotor behaviour in extensively habituated rats

Following further extensive habituation to the test cages, horizontal and vertical activity counts were measured for 1 hr before and 1 hr immediately after rats were challenged with either saline or nicotine. Here, again, two-way mixed effects ANOVA revealed a significant Time x Dose interaction for horizontal activity (F (69, 1035) = 2.70, $p < 0.0001$) with most groups showing reduced activity relative to vehicle in the ten minutes immediately following injection and increased activity at later time points (Figure 2.3A; Dunnett's post-hoc tests). Vertical activity was similarly analysed, once more revealing a significant interaction (two-way mixed effects ANOVA; Time x Dose: F (69, 621) = 1.59, $p = 0.0027$) with a rats injected with nicotine reducing rearing relative to controls in the first five minutes (Figure 2.3B; Dunnett's post-hoc tests). In this case, however, inspection of the data indicated reduced variability compared to the previous experiment that used less extensive habituation. Once again, there were no significant differences found between the groups during the pre-drug habituation phase for either horizontal (Figure 2.3C; one-way ANOVA, F (3, 45) = 0.856, $p = 0.47$) or vertical activity counts (Figure 2.3D; one-way ANOVA, F (3, 27) = 1.50, $p = 0.24$).

In contrast to Experiment 1, when the total horizontal activity counts recorded 30 - 60 min after injection were compared using a one-way ANOVA, a significant between-group difference became detectable (Figure 2.3E; F (3, 45) = 2.89, $p = 0.046$). Hence, there was a tendency for activity to increase in a dose-dependent manner, with the highest dose of nicotine producing a significant increase in locomotor activity in comparison to the control group (mean difference, MD = 284.7 ± 96.8, $p = 0.014$, Dunnett's post-hoc tests). However, as can be seen in Figure 2.3F, rearing behaviour broadly followed a similar dose-response pattern to that shown in less extensively habituated animals (Experiment 1). There was no significant effect of nicotine on vertical activity (one-way ANOVA, F (3, 27) = 1.23, $p = 0.32$).

2.3

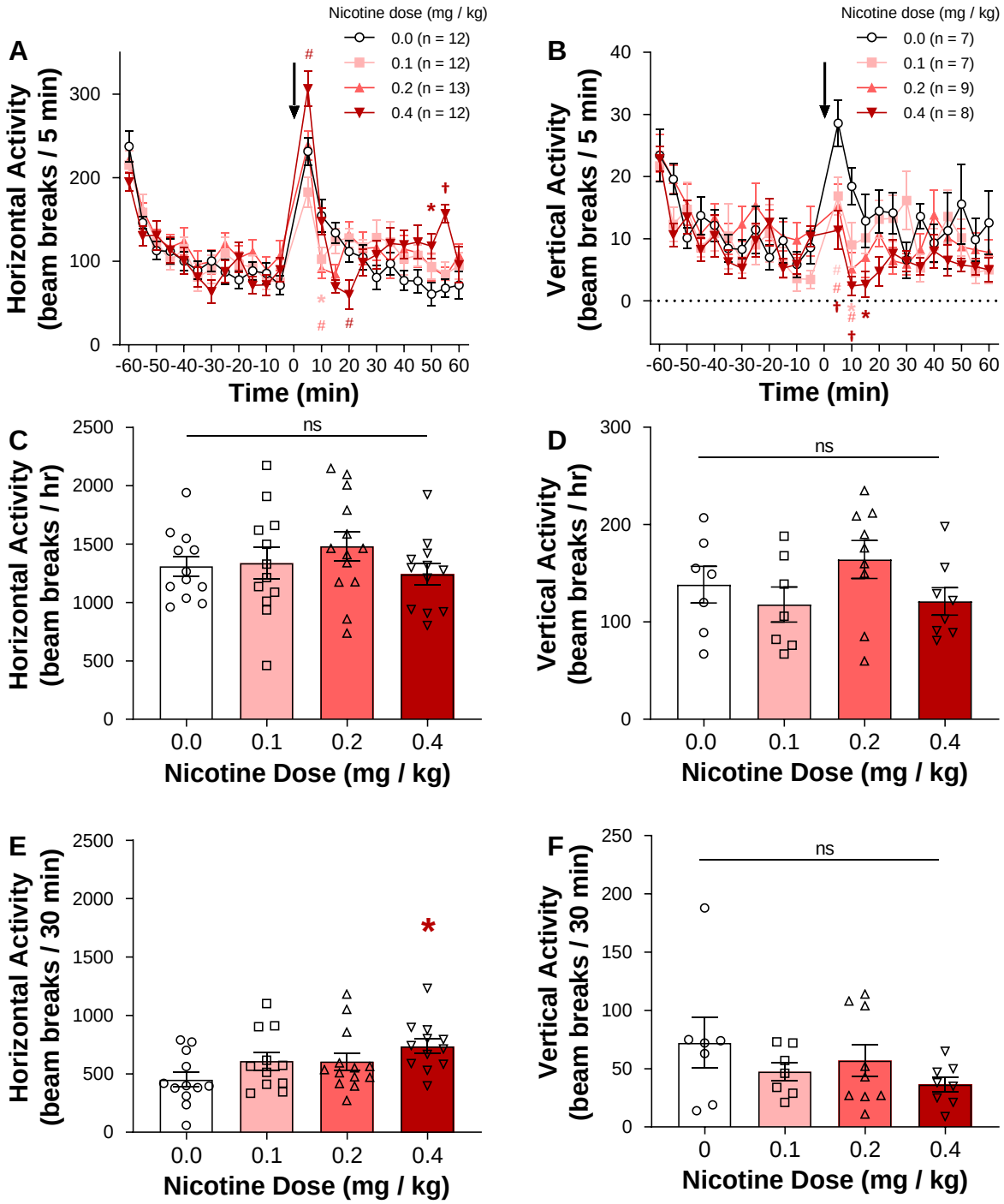
A
Horizontal Activity (beam breaks / 5 min)
Nicotine dose (mg / kg)
0.0 (n = 12)
0.1 (n = 12)
0.2 (n = 13)
0.4 (n = 12)
Time (min)
B
Vertical Activity (beam breaks / 5 min)
Nicotine dose (mg / kg)
0.0 (n = 7)
0.1 (n = 7)
0.2 (n = 9)
0.4 (n = 8)
Time (min)
C
Horizontal Activity (beam breaks / hr)
ns
Nicotine Dose (mg / kg)
D
Vertical Activity (beam breaks / hr)
ns
Nicotine Dose (mg / kg)
E
Horizontal Activity (beam breaks / 30 min)
Nicotine Dose (mg / kg)
F
Vertical Activity (beam breaks / 30 min)
ns
Nicotine Dose (mg / kg)

Figure 2.3 Changes in spontaneous locomotor behaviour following acute nicotine challenge in extensively habituated rats. Rats were habituated the test cage for 1 hr / day for 3 days prior to testing.

A – B) Time course profiles of both the horizontal (A) and vertical activity (B) during the 1 hr habituation period and 1 hr following nicotine challenge (indicated by the arrow at 0 min). Activity was measured at 5 min intervals, and nicotine-treated groups were compared with the vehicle group at each time point by two-way mixed effects ANOVA with Dunnett's post-hoc tests. The number of rats in each dose group (n) are shown above the graph (some data was excluded from the vertical activity analysis due to faulty equipment).
C - D) Average horizontal **(**C) and vertical (D) beam breaks recorded during 1hr pre-drug habituation period. All groups had similar activity (one-way ANOVA).
E - F) Average horizontal (E) and vertical (F) beam breaks recorded 30 - 60 min after nicotine injection. 0.4 mg/ kg significantly increased ambulatory activity relative to the control group. There did not appear to be any significant changes to rearing behaviour (one-way ANOVA).
Data is presented as the mean ± SEM. Graphs display significant differences from vehicle group in post-hoc testing; *, $p < 0.05$; #, $p < 0.01$; †, $p < 0.001$.

2.4.3 Experiment 3 - Nicotine dependent changes in locomotor behaviour during mid day and mid night

Locomotor activity was tested in rats following 3 days of habituation during mid day (ZT 4 - 8) or mid night (ZT 16 - 20). To minimise disruption of the animals circadian rhythm, and to allow comparisons between day and night responses to activity, tests carried out during the light phase and dark phase were performed in dim red light. Another dose-response curve for nicotine's effects on locomotor activity was therefore carried out under these conditions.

Figure 2.4A-B shows the time course horizontal activity profiles of all the nicotine dose groups recorded during either the mid day or mid night, again echoing the general patterns observed in Experiments 1 and 2. A two-way mixed effects ANOVA failed to reveal a significant interaction between Dose and Time for the horizontal activity data collected during the mid day (F (69, 598) = 1.20, $p = 0.13$). There was not a significant main effect of dose (F (3, 26) = 0.107, $p = 0.95$) although there was a significant main effect of time (F (7.120, 185.1) = 23.97, $p < 0.0001$). In contrast, a two-way mixed effects ANOVA of the horizontal activity collected during the night revealed a significant interaction of Dose and Time (F (69, 598) = 1.805, $p = 0.0002$) such that nicotine decreased ambulation in relative to controls in most dose groups during 5-10 minutes following injection, and this suppression lessened across the remainder of the experiment (Dunnett's post-hoc tests).

Rats had increased spontaneous ambulatory behaviour when tested during the mid night compared to the mid day. As presented in Figure 2.4C, examination of the horizontal activity counts generated during the hour long pre-drug habituation with a two-way mixed effects ANOVA highlighted a significant main effect of Time of day (F (1, 26) = 26.47, $p < 0.0001$) but not of Dose or any interaction effects. The average number of horizontal beam breaks was significantly greater during the night than the day (MD = 495.6 ± 96.3).

As depicted in Figure 2.4D, horizontal activity during the 30 – 60 min following injections was dependent on both the time and the nicotine dose. As expected, responses observed for the tests performed during the day resembled those for Experiment 2 (which were conducted at the same time of day but under brightly lit conditions), with higher doses of nicotine tending to increase activity. Interestingly, opposite effects were seen during the night, with nicotine tending to decrease activity in a dose-dependent manner. The two-way mixed effects ANOVA revealed a significant interaction between Dose and Time of day (F (3, 26) = 3.523, p = 0.029). Holm-Šídák's post-hoc tests showed that none of the nicotine-injected dose groups had significantly different horizontal activity to the control group either during the day or the night. However, the post-hoc tests indicated that the vehicle and 0.1 mg / kg nicotine-injected groups had significantly greater activity levels during the mid night compared to the mid day (0.0 mg / kg, MD = 352.9 ± 75.1, p = 0.0003; 0.1 mg / kg, MD = 353.8 ± 86.7, p = 0.0011), and this time of day effect was not seen in either of the groups injected with the highest doses of nicotine. Instead, locomotor activity stayed at levels intermediary between the day-night variation of vehicle-injected animals. Hence nicotine appeared to modulate the normal diurnal regulation of locomotor activity.

2.4

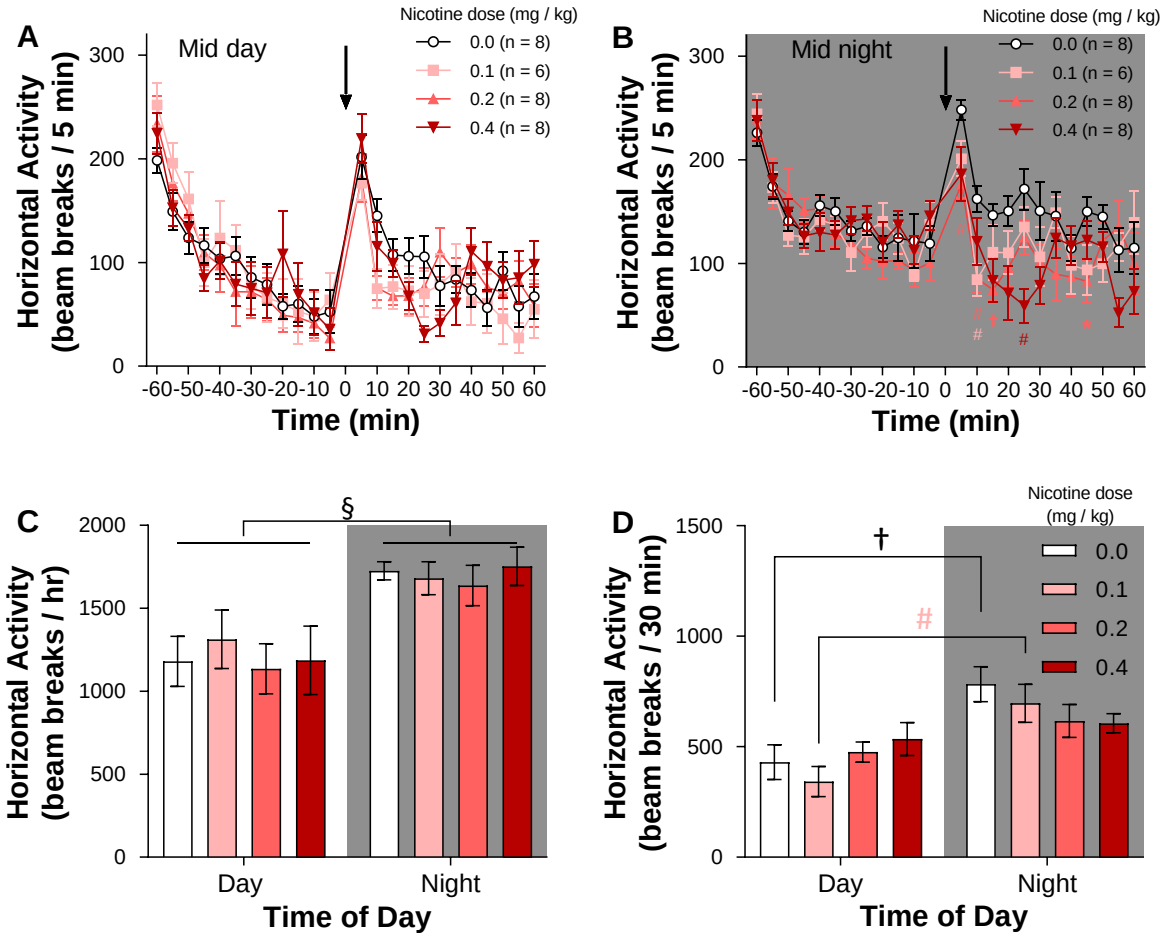

Figure 2.4 Changes in spontaneous ambulatory behaviour following nicotine challenge at mid day and mid night.

A – B) Horizontal activity before and after nicotine challenge (indicated by the arrow at 0 min) measured over 2 hrs at 5 min intervals, recorded during the mid day (ZT 4 - 8) (A) or mid night (ZT 16 – 20) (B). Nicotine-treated groups were compared with the vehicle group at each time point by two-way mixed effects ANOVA with Dunnett's post-hoc tests. The number of rats in each dose group (n) are shown above the graph.

C - D) Average horizontal beam breaks recorded during 1hr pre-drug habituation period (C) or 1 hr following injection (D) during either the mid day or mid night. Horizontal activity was consistently greater during the night but there was no difference between dose groups during the habituation period (two-way mixed effects ANOVA). However, following nicotine challenge, the two highest doses of nicotine appeared to abolish the day night variation in activity levels seen in the vehicle group.

Data is presented as the mean ± SEM. Data collected during the mid day is presented on white panels, data collected during the mid night presented on shaded panels. Graphs display significant differences from vehicle group in post-hoc tests unless otherwise indicated; *, $p < 0.05$; #, $p < 0.01$; †, $p < 0.001$; §, $p < 0.0001$.

Diurnal variation in rearing activity, however, did not follow the same pattern as ambulatory behaviour. A two-way mixed effects ANOVA indicated a significant interaction between Dose and Time for vertical activity counts recorded during the mid day (Figure 2.5A; F (69, 391) = 2.51, p < 0.0001) and mid night (Figure 2.5B; F (69, 414) = 1.83, p = 0.0002). In both cases, nicotine induced a strong suppression of rearing activity immediately following the injection, although this suppression seemed to be longer lasting during the mid day (Dunnett's post-hoc tests).

There was a time of day effect on spontaneous rearing behaviour, as shown in Figure 2.5C. Vertical activity measured during the habituation period had a significant main effect of Time of day (mixed effects model, F (1, 13) = 29.51, p = 0.0001), such that average vertical activity counts were almost 50 % greater when experiments were performed during the mid night compared to the mid day (MD = 96.4 ± 17.7). However, there were no significant main effects of dose groups (F (3, 22) = 2.34, p = 0.10) or any interaction effects (F (3, 13) = 2.20, p = 0.14).

In contrast to the time of day effects on horizontal activity, examination of the rats' post-drug rearing behaviour showed that high doses of nicotine produced consistent suppressive effects during both the mid day and the night, producing reduced rearing relative to the vehicle group at both time points (Figure 2.5D). Analysis using a mixed effects model revealed a significant main effect of Dose group (F (3, 22) = 4.56, p = 0.012) and Time of day (F (1, 13) = 11.0, p = 0.0055), although the interaction between these factors was not significant (F (3, 13) = 2.13, p = 0.14). Subsequent post-hoc tests showed that in this instance, only the highest dose of nicotine significantly reduced vertical activity counts relative to controls during the day (Dunnett's post-hoc tests).

2.5

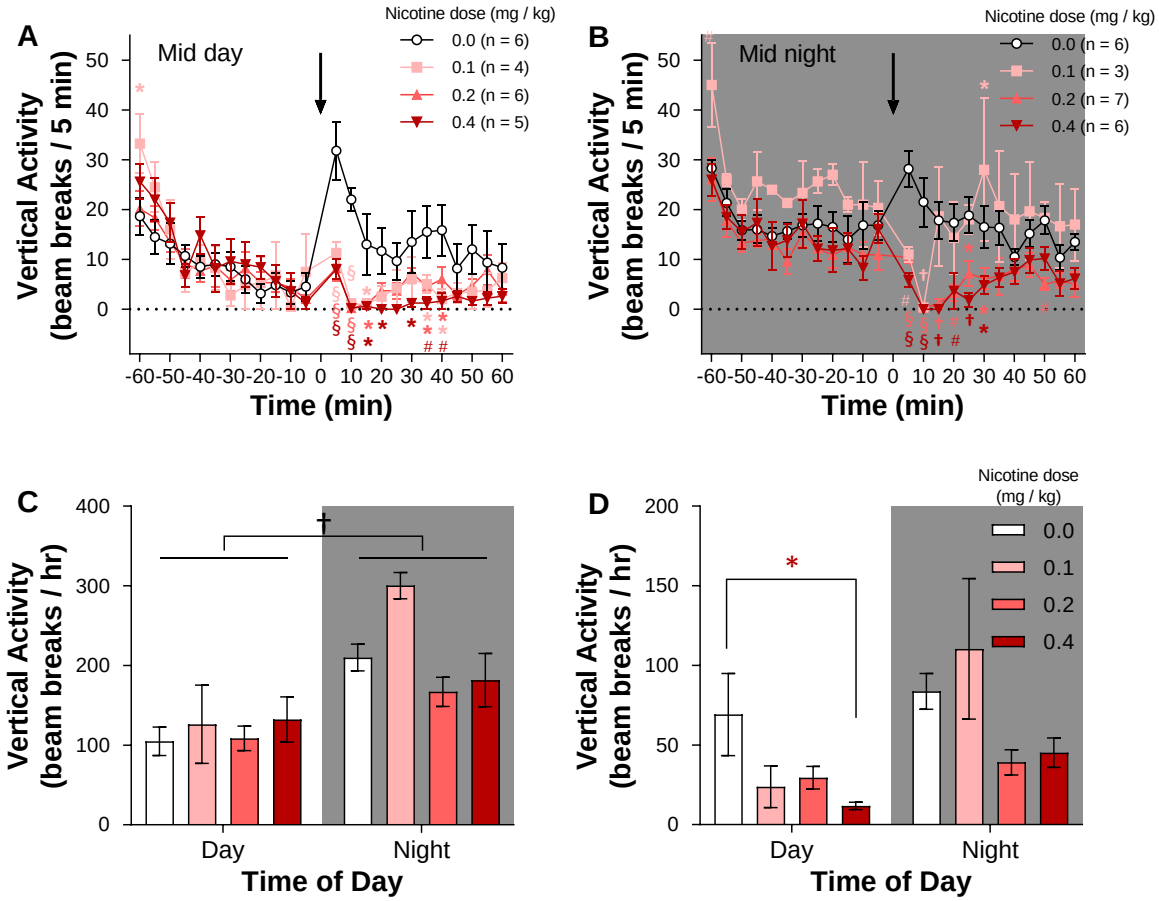

Figure 2.5 Changes in spontaneous rearing behaviour following nicotine challenge at mid day and mid night.

A – B) Vertical activity before and after nicotine challenge (indicated by the arrow at 0 min) measured over 2 hrs at 5 min intervals, recorded during the mid day (ZT 4 - 8) (A) or mid night (ZT 16 – 20) (B). Nicotine-treated groups were compared with the vehicle group at each time point by two-way mixed effects ANOVA with Dunnett's post-hoc tests. The number of rats used for each dose group (n) are displayed on the time course graph (some data was excluded from the vertical activity analysis due to faulty equipment).

C - D) Average vertical beam breaks recorded during 1 hr pre-drug habituation period (C) or 1 hr following injection (D) during either the mid day or mid night. During the habituation period, vertical activity was consistently greater during the night but there was no difference between dose groups (mixed effects analysis). Following nicotine challenge, the highest dose of nicotine reduced rearing activity relative to controls only during the day, and did not significantly change the rearing behaviour during the night (mixed effects analysis, Dunnett's post-hoc tests)

Data is presented as the mean ± SEM. Data collected during the mid day is presented on white panels, data collected during the mid night is presented on shaded panels. Graphs display significant differences from vehicle group in post-hoc testing unless otherwise indicated; *, $p < 0.05$; #, $p < 0.01$; †, $p < 0.001$; §, $p < 0.0001$.

2.4.4 Experiment 4 - Nicotine dependent changes in locomotor behaviour during early day and late day

In the final experiment, locomotor activity was tested either during 4 hours immediately after lights on (early day, ZT 0 – 4) or the 4 hours preceding lights off (late day, ZT 8 – 12). Animals received either vehicle or 0.4 mg / kg nicotine at both time points.

Investigation of the time course activity profiles using a two-way mixed effects ANOVA revealed a significant interaction between Time and Dose for activity recorded during both the early day (Figure 2.6A; F (23, 414) = 3.87, $p < 0.0001$) and late day (Figure 2.6B; F (23, 414) = 4.09, $p < 0.0001$). However, post-hoc analysis revealed differences in the nicotine-evoked activity between the early and late day. During the early day, there was a tendency for suppression of activity relative to vehicle-injected controls immediately following injection, whereas during the late day there tended to be increased activity relative to controls during the latter portion of the experiment instead (Holm-Šídák's post-hoc tests).

Two-way mixed effects ANOVAs investigating the pre-drug habituation sessions confirmed that spontaneous ambulatory behaviour was dependent on the time of day. As expected, there was a significant main effect of Time of day on total horizontal activity (Figure 2.6C; F (1, 18) = 11.1 p = 0.0037) such that experiments performed during the early day resulted in greater horizontal activity when compared to the late day (MD = 351.5 ± 105.5). There was no effect of Dose (F (1, 18) = 0.417, p = 0.53) or a significant interaction (F (1, 18) = 3.40, p = 0.061) between these factors on horizontal activity.

During the final 30 min of the experiment following injection, horizontal activity levels were affected by both exposure to nicotine and the time of day (Figure 2.6D). In this case, a two-way mixed effects ANOVA indicated that there was a significant main effect of Dose (F (1, 18) = 5.50, p = 0.031) although the main effect of Time of day was not significant (F (1, 18) = 3.69, p = 0.071). The expected interaction also approached significance (F (1, 18) = 4.33, p = 0.052) and post-hoc analysis revealed that nicotine only produced a significant increase in locomotor activity relative to saline injected controls during the late day (MD = 273.4 ± 88.8, p = 0.0079; Holm-Šídák's post-hoc test).

2.6

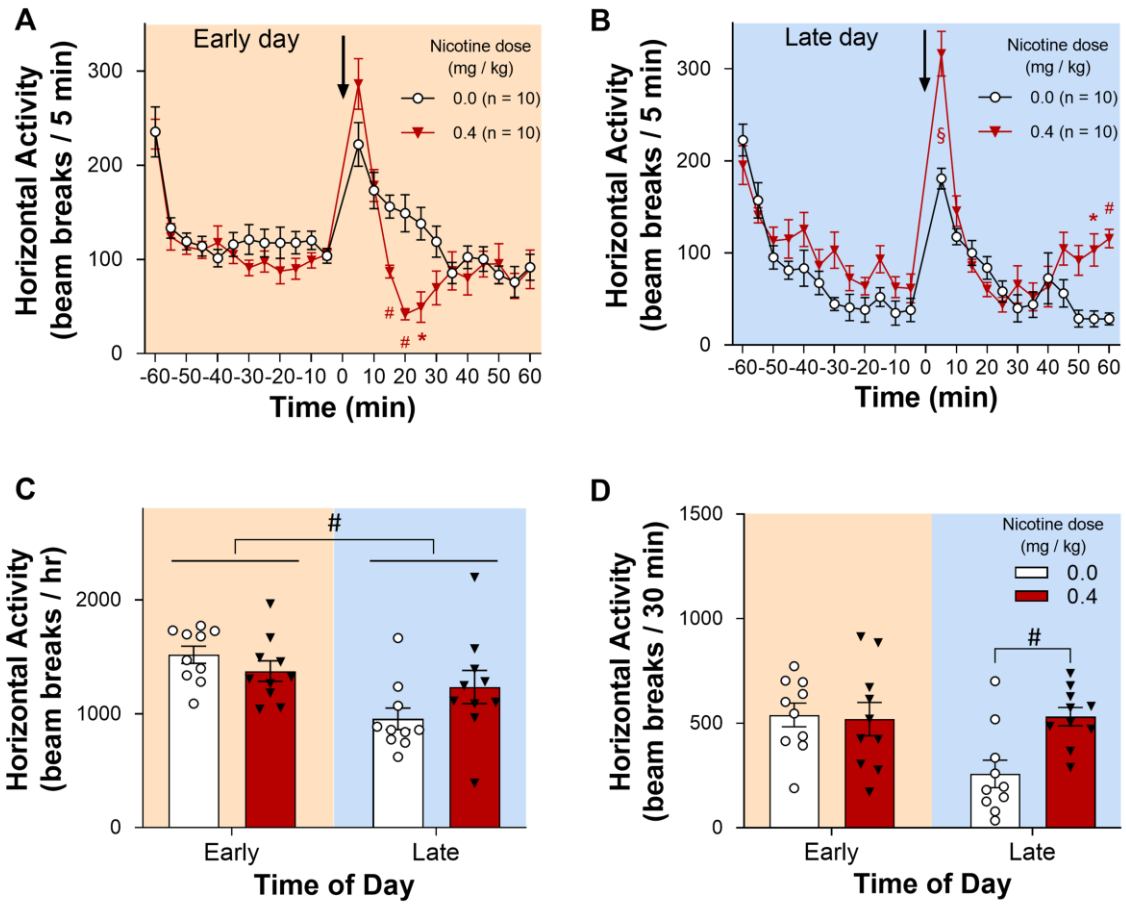

Figure 2.6 Changes in spontaneous ambulatory behaviour following nicotine challenge during the early and late day.

A – B) Horizontal activity before and after nicotine challenge (indicated by the arrow at 0 min) measured over 2 hrs at 5 min intervals, recorded during the early day (ZT 0 - 4) (A) or late day (ZT 8 – 12) (B). Nicotine-treated animals were compared with the vehicle group at each time point by two-way mixed effects ANOVA followed by Holm-Šídák's post-hoc tests. The number of rats used for each dose group (n) are displayed above the time course graphs.
C - D) Average horizontal beam breaks recorded during 1 hr pre-drug habituation period (C) or 1 hr following injection (D) during either the early day or late day. Ambulatory activity was higher during the early day compared to the late day, but there were no differences between dose groups (two-way mixed effects ANOVA). Nicotine challenge evoked a significant increase in horizontal activity relative to the control group only during the late day (two-way mixed effects ANOVA, Holm-Šídák's post-hoc tests).
Data is presented as the mean ± SEM; *, $p < 0.05$; #, $p < 0.01$; †, $p < 0.001$; §, $p < 0.0001$. Data collected during the early day is presented on pale orange panels, data collected during the late day is presented on blue panels.

We also analysed the time course activity profiles of the rearing activity recorded either during the early day (Figure 2.7A) or late day (Figure 2.7B). As seen previously, two-way mixed effects ANOVAs indicated a significant interaction between Time and Dose on the rearing activity from

experiments performed during both the early day (F (23, 299) = 4.82, p < 0.0001) and late day (F (23, 253) = 5.15, p < 0.0001). In both cases, rearing activity immediately following nicotine challenge tended to be suppressed relative to controls, although this appeared to have a greater effect during the early day compared to the late day (Holm-Šídák's post-hoc tests).

Similarly to the diurnal variation in spontaneous horizontal activity between early and late day, spontaneous rearing behaviour was also dependent on the time of day. There was a significant main effect of Time of day on the pre-drug vertical activity counts, with greater rearing observed during the early day compared to the late day (Figure 2.7C; mixed effects model, F (1, 24) = 9.64, p = 0.0048; MD = 49.4 ± 15.9), mirroring the pattern observed in spontaneous horizontal activity. There was no effect of Dose (F (1, 24) = 0.249; p = 0.62) or evidence of any significant interaction between factors (F (1, 24) = 3.2, p = 0.086) for vertical activity during the habituation period.

Finally, we inspected the rearing activity of rats during the 30 – 60 min following injection at both times of day. Examination of the vertical activity counts using a mixed effects model indicated a significant interaction between Dose and Time of Day (Figure 2.7D; F (1, 9) = 10.2, p = 0.011). Consistent with the results reported in Experiment 3, suppression of rearing activity was dependent on the time of day. Here, post-hoc tests revealed that whilst the control group continued to display higher vertical activity counts during the early day compared to the late day (MD = 45.0 ± 6.9, p = 0.0002; Holm-Šídák's post-hoc test) this time of day influence on vertical activity was eliminated when comparing the rats injected with 0.4 mg / kg nicotine.

2.7

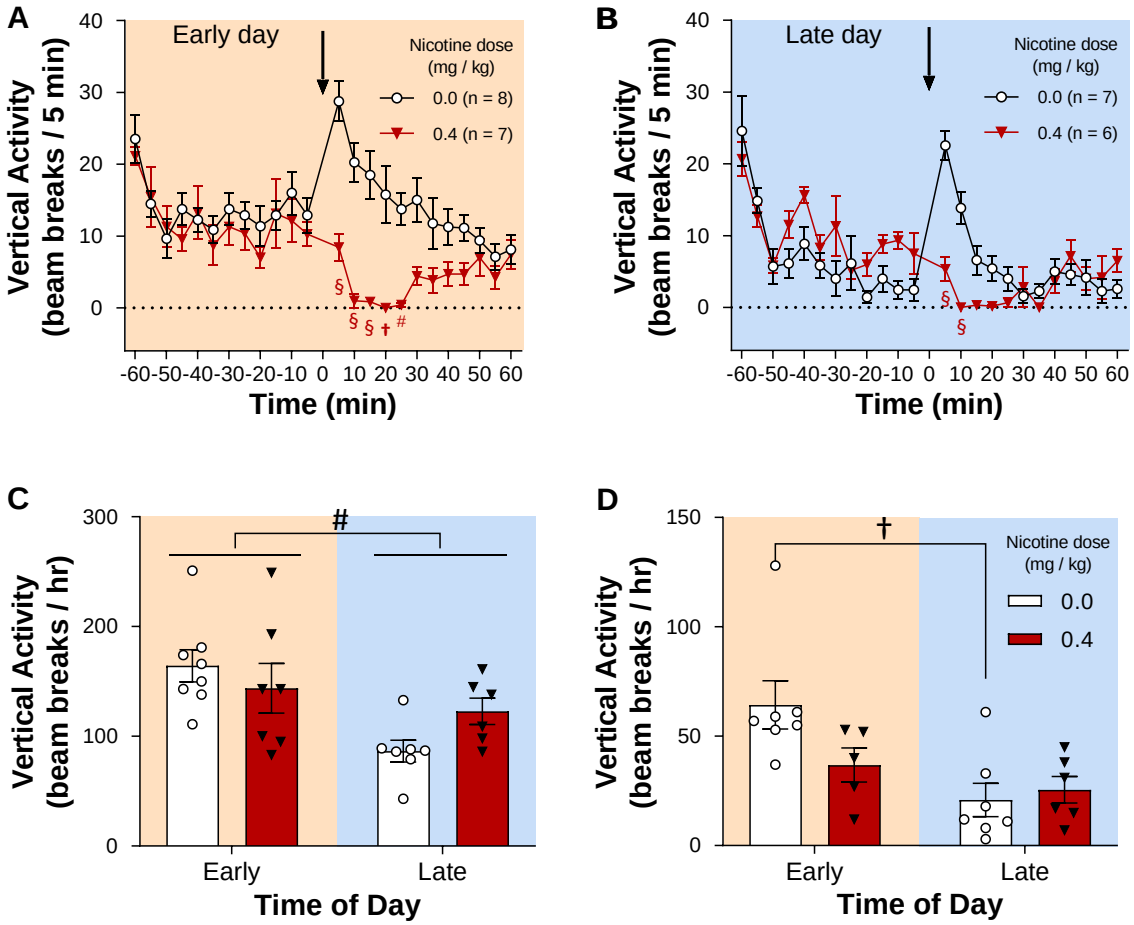

Figure 2.7 Changes in spontaneous rearing behaviour following nicotine challenge during the early and late day.

A – B) Vertical activity before and after nicotine challenge (indicated by the arrow at 0 min) measured over 2 hrs at 5 min intervals, recorded during the early day (ZT 0 - 4) (A) or late day (ZT 8 – 12) (B). Nicotine-treated animals were compared with the vehicle group at each time point by two-way mixed effects ANOVA followed by Holm-Šídák's post-hoc tests. The number of rats in each dose group (n) are displayed above the graph (some data was excluded from the vertical activity analysis due to faulty equipment).
C - D) Average vertical beam breaks recorded during 1 hr pre-drug habituation period (C) or 1 hr following injection (D) during either the early day or late day. Increased rearing activity was observed during the pre-drug habituation phase recorded during the early day compared with the late day (mixed effects model). Following nicotine challenge, the diurnal variation in rearing observed in the control group was abolished in the group injected with 0.4 mg/kg nicotine (mixed effects model, Holm-Šídák's post-hoc tests).
Data is presented as the mean ± SEM; *, $p < 0.05$; #, $p < 0.01$; †, $p < 0.001$; §, $p < 0.0001$. Data collected during the early day is presented on pale orange panels, data collected during the late day is presented on blue panels.

2.5 Discussion

Many drugs of abuse are known to vary their actions depending on the time of day (Abarca et al., 2002; Negus et al., 1995; Phillips et al., 2013; Sleipness et al., 2005), and there is some evidence from both humans (Chandra et al., 2011; Grainge et al., 2009; Gries et al., 1996; Mooney et al., 2006; Perkins et al., 2009; Ussher and West, 2003) and animals (Kita et al., 1986; Mexal et al., 2012; O'Dell et al., 2007; Williams et al., 1993) to suggest that nicotine also exhibits diurnal variation in its acute effects. However, there remains a relative lack of studies investigating how the actions of nicotine vary over the course of the day in rodent models (Mexal et al., 2012). Therefore, this report aimed to answer the question of whether cholinergic signalling exhibits diurnal variation at the behavioural level, and therefore investigated nicotine-evoked changes in locomotor activity in the rat at different time points across the circadian cycle. The data reported here demonstrate that there is indeed a significant time of day influence on nicotine-evoked changes in locomotor activity, on both ambulatory and rearing behaviour. We found that animals had reduced sensitivity to the locomotor depressant effects on vertical activity during periods when the animal was less active (here, during the late day), whilst sensitivity to the stimulatory effects of nicotine on horizontal activity were greatest at this time.

Taken together, these results further support the hypothesis that there is diurnal variation in response to nicotine. Thus, this study builds on the work of previous reports demonstrating diurnal variation in nicotine-evoked changes in locomotor activity in rodents (Bovet et al., 1967; King et al., 2004; Kita et al., 1986; Mexal et al., 2012). However, the data presented here suggest that the two behavioural outputs affected by nicotine (horizontal and vertical activity) may be differentially regulated by the time of day. This study also extends the work put forward by Prus et al (2008) which shows that nicotine's acute effects on locomotion vary depending on the individuals baseline level of arousal, but our experiments show that this theory could be further extrapolated to be dependent on the daily rhythmic activity cycle. Together, these results highlight the need to consider time of day when investigating the actions of nicotine in laboratory rodents.

2.5.1 Nicotine produces biphasic effects on horizontal locomotor activity even in minimally habituated rats

In the present study, time course data recapitulated the biphasic effects of nicotine on horizontal locomotor activity which has been reported in previous studies in naïve rats (Clarke and Kumar, 1983; Matta et al., 2007; Wiley et al., 2015). Whereas horizontal activity exhibited a monotonic

decrease over the 60 min epoch following vehicle injection, high dose of nicotine generally produced an initial suppression below levels seen in controls, followed by a rebound stimulation 30-60 min following injection. This profile was somewhat unexpected as previous studies have suggested that the initial suppression is only detectable in animals that have not been habituated to the arena (Ksir, 1994; Matta et al., 2007). The fact that this suppression was observed across all the studies suggests that the suppressive actions of nicotine are not purely reliant on the novelty-seeking behaviour of unhabituated rats, or that the strong response to vehicle may have obscured some group differences. Instead, however, we think it likely to be a reflection of ataxia: during these experiments the experimenter would frequently observe that some rats were experiencing short-lasting hind limb ataxia, a behaviour which has been previously reported as an effect of acute exposure to nicotine (Clarke and Kumar, 1983; Faraday et al., 2003; Stolerman et al., 1973). This behavioural observation was not formally scored and was therefore not included in the results, nonetheless it likely explains the initial activity suppressant effects observed in the first 30 minutes following the injection of nicotine. In addition, this depressant effect suggests that rats did not develop tolerance to nicotine across the course of this study, and so were "naïve-like" for each nicotine challenge, despite previous reports which suggests rats develop rapid tolerance to the suppressive effects of nicotine after even a single dose (Kanýt et al., 1999).

2.5.2 Female Lister Hooded rats need extensive habituation to reveal stimulatory actions of nicotine on horizontal activity

Habituation to the arena prior to nicotine challenge is generally considered to increase the chances of observing the stimulatory effects of nicotine (Ksir et al., 1985; Matta et al., 2007). Despite the fact that all animals had been previously exposed to the arena on two separate occasions, a significant stimulatory effect of nicotine on locomotor activity was not detected during Experiment 1. This was unexpected, as previous studies examining this effect have found that a habituation session of only 90 min is sufficient to reveal the stimulatory effects of nicotine in naïve male Sprague-Dawley rats (O'Neill et al., 1991). We hypothesized that our rats were not sufficiently habituated and thus performed further exposure to the arena before subsequent retesting in Experiment 2, which then produced the expected increase in ambulation. It could be argued that this result was due to sensitization (where previous exposure to nicotine produces a larger subsequent stimulatory effect) although this seems less likely as the depressant effects of nicotine on horizontal activity (considered to be highly subject to sensitization) were still evident. One factor contributing to this result may be that Lister Hooded rats are known to be generally more active than other commonly used laboratory strains when placed in a novel environment (Clemens et al., 2014) and so this could be a strain dependent effect. However, one study in male

Lister Hooded rats was able to show significant stimulatory effects of nicotine 40 – 60 min post injection in animals entirely unhabituated to the test apparatus (Clarke and Kumar, 1983), so instead this effect could be sex dependent.

Pharmacological research has previously been dominated by male animal models (Beery, 2018; Beery and Zucker, 2011), therefore it is imperative to address the relative dearth of female rodent neuroscience studies. Most of the previous work investigating locomotor responses and nicotine in Lister Hooded rats has been performed in males (Alderson et al., 2008, 2005; Clarke and Kumar, 1983; Mirza et al., 2000; Reavill and Stolerman, 1990; Shoaib et al., 1994; Stolerman et al., 1995, 1973) whereas we used females, which could explain why our results needed such further habituation to reveal the stimulatory actions of nicotine. Nicotine's effects have been shown to vary by sex: Long Evans female rats are more sensitive to the activity enhancing effects of nicotine than males, but this is not the case in Sprague-Dawleys (Faraday et al., 2003). Interestingly, female Lister Hooded rats have been shown to have higher levels of locomotion than their male counterparts (Lynn and Brown, 2009), lending further evidence to the idea that the extensive habituation required to reveal the stimulatory effects of nicotine in this study may be sex and strain dependent. These findings highlight the importance of researchers characterizing nicotine's actions on locomotor activity within their own experimental set-up.

The activating effects of nicotine were only reliably observed at the highest dose tested, whereas other studies have demonstrated nicotine can increase activity at doses lower than 0.4 mg / kg (Ksir, 1994; Schochet et al., 2004). However, these previous studies were performed in male Sprague-Dawley rats, which again may explain why this report failed to find effects of nicotine on lower doses: nicotine's effects are known to vary by strain, and age of rats (Elliott et al., 2004; Faraday et al., 2003). Indeed, there is evidence that Lister Hooded rats, as used in this study, demonstrate a blunted locomotor response to nicotine compared with Sprague-Dawley rats (Iyaniwura et al., 2001). Further, only the highest dose of nicotine used in our experiments revealed a significant reduction in rearing activity relative to controls, indicating this system is equally sensitive to the actions of nicotine as the stimulatory effects of nicotine on horizontal activity.

2.5.3 Nicotine-evoked changes in ambulatory activity are dependent on the time of day and the underlying rhythms in arousal

As expected, the pre-drug habituation data from Experiments 3 and 4 demonstrated the underlying day / night variation in both ambulatory (Figures 2.4C and 2.6C) and rearing behaviours (Figures 2.5C and 2.7C), with increased activity during the animal's dark phase and the

hours immediately following light on and reduced activity levels during the mid to late light phase. This was similarly reflected in the diurnal variation in horizontal activity following saline injection, as shown in Figure 2.8A. Previous work examining the circadian rhythms of home cage locomotor activity of Lister Hooded rats has demonstrated that activity peaks during the dark phase and in the hours immediately following lights on, with lowest activity during the mid- to late day (Clemens et al., 2014; McDermott and Kelly, 2008). Therefore, together these results suggest that the injection of saline did not alter the diurnal variation in spontaneous activity during the 30 – 60 minutes post injection.

However, when examining how nicotine altered these behaviours between time points there appeared to be a time of day effect. Statistical analysis of horizontal data following nicotine challenge during both the day and night (Figure 2.4D) suggested that nicotine eliminated the time of day influence on horizontal activity levels such that at high doses, nicotine produced stimulatory effects during the day (when pre-drug activity is low) and an inhibitory effect during the night (when pre-drug activity is high). Similarly, there was evidence of a time of day effect on horizontal activity compared between early and late day (Figure 2.6D), with nicotine only increasing activity relative to controls during the late day – when animals were less active in general. Taking the evidence of Experiments 3 & 4 together provides evidence of diurnal variation in sensitivity to the stimulatory effects of nicotine such that these effects are most pronounced during portions of the light / dark cycle when the rats are least active (i.e., during the hours immediately preceding lights off). This can be more clearly visualized in Figure 2.8A, which summarises the horizontal activity of vehicle-injected and 0.4 mg / kg nicotine-injected rats 30 – 60 min after administration of the drugs. Interestingly, it appears that nicotine was able to override the underlying circadian rhythm in activity. The mechanism behind this effect currently remains unclear.

Furthermore, this result is consistent with the work of Kita et al (1986) who showed that 0.5 mg / kg nicotine injected in male Wistar rats produced a stimulatory effect 40 – 60 min post injection during the light phase but had a depressant effect during the dark phase. Of particular relevance to note is the finding that even between the first 4 hr of lights on and last 4 hr before lights off, which is the period when most rodent experimental procedures are conducted, there was significant variation in sensitivity to nicotine. Thus, circadian variation is another variable that contributes to the variability in nicotine-evoked changes in locomotor activity reported in the literature (Matta et al., 2007), and as such should be carefully controlled for when assessing the effects of nicotine on rodents.

2.8

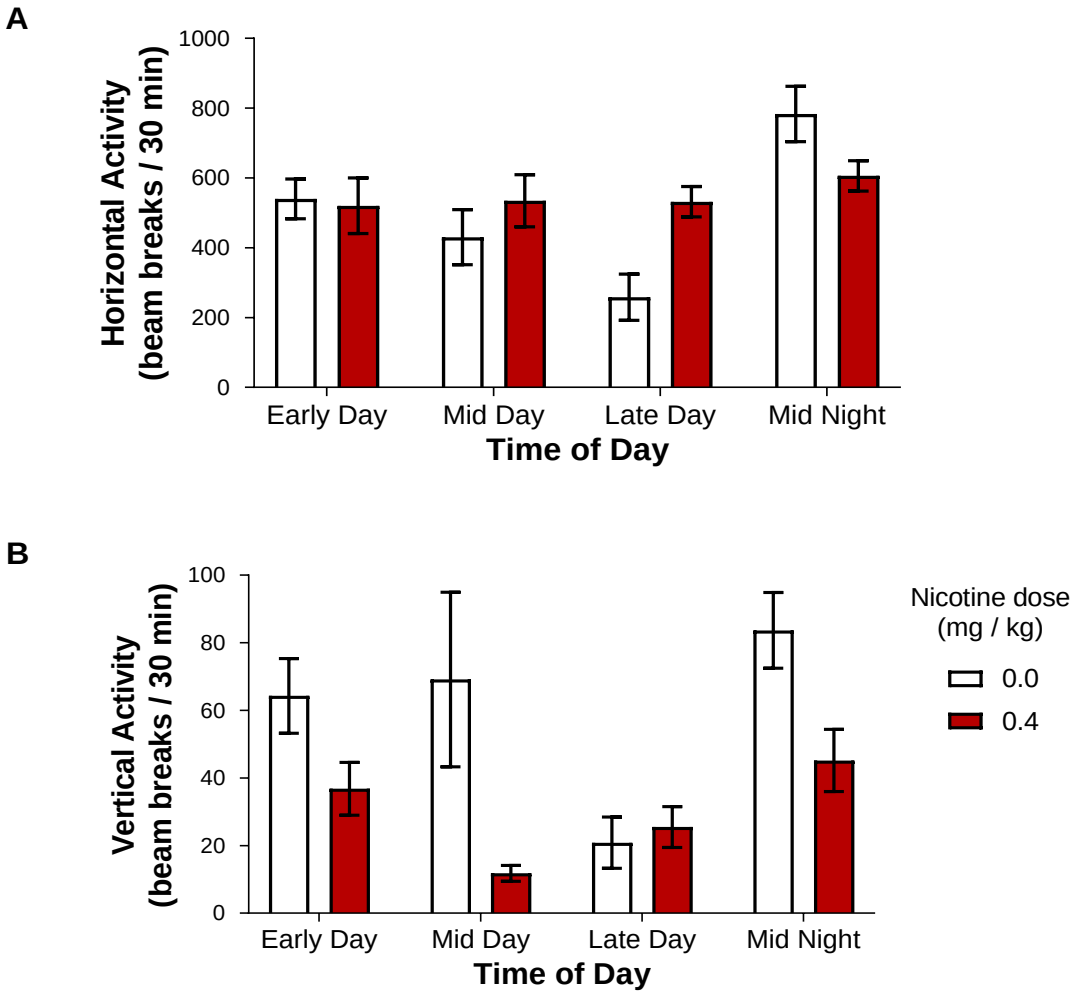

Figure 2.8 Summary of the relationship between time of day and locomotor activity for saline-injected and nicotine-injected rats. This figure combines the data from Experiments 3 and 4, in order to visualize how activity during the 30 – 60 min following injection changes across the 4 time points examined in this study.

A) Vehicle control groups exhibit a clear diurnal rhythm in horizontal activity, which is blunted in the rats injected with 0.4 mg / kg nicotine. Nicotine either increased or suppressed ambulation depending on the time of day.
B) Similarly, the control group displayed diurnal variation in rearing activity. The rats injected with 0.4 mg / kg nicotine also showed a similar diurnal variation in their rearing, and tended to either suppress or not affect vertical activity relative to controls depending on the time of day.
Data is presented as the mean ± SEM.

2.5.4 Nicotine suppresses rearing behaviour, but this effect is dependent on the underlying rhythms in arousal

In contrast to ambulatory behaviour, nicotine produced exclusively depressant effects on rearing behaviour as has been previously described in the literature (Jandová et al., 2013; Jerome and Sanberg, 1987; Ksir, 1994; Rodgers, 1979). However, the magnitude of this depression varied in size depending on the time of day as demonstrated in Experiments 3 and 4 (Figures 2.5D and 2.7D). This suppression effect was not seen during the late day, which coincides with the period when Lister Hooded rats are at their least active (McDermott and Kelly, 2008). Therefore these results support the idea of diurnal variation in sensitivity to nicotine-evoked rearing suppression, with maximal suppression occurring at points in the day / night cycle when rats are at their most active, as illustrated in Figure 2.8B. This raises the possibility that the time of day influenced effects of nicotine result from a changing activity baseline, rather than from a change in cholinergic signalling mechanisms as such.

These findings may be somewhat limited by the reduced sample size for vertical activity counts. Due to hardware issues with some test chambers, in some cases vertical activity count data had to be discarded due to excessive noise. Therefore, investigations into vertical activity draw on smaller group sizes than the studies of horizontal activity. Importantly, however, these results can still be considered to be a representative sample – as animals were preassigned test chambers randomly before the start of the experiments.

2.5.5 Nicotine-evoked suppression of rearing and stimulation of ambulation are distinct systems

Rearing and ambulation are considered to represent different, dissociative aspects of behaviour. Horizontal activity is thought to reflect arousal levels and nicotine is thought to produce its stimulatory effects by promoting dopamine release in the mesolimbic system (Benwell and Balfour, 1992; Di Chiara, 2000), and the initial depressant effects of nicotine are thought to originate in the nucleus accumbens (Welzl et al., 1990). On the other hand, vertical activity is a measure of exploratory behaviour (Lever et al., 2006), which is also correlated with dopamine levels in the nucleus accumbens (Adermark et al., 2015). Reduced rearing can indicate increased anxiety (Lever et al., 2006), and it has been postulated that nicotine-evoked suppression in rearing is a measure of the aversive or anxiogenic effects of nicotine (Adermark et al., 2015; Casarrubea et al., 2015). Therefore it is interesting to consider that whilst nicotine produced aversive effects at all time points tested in this study, the decreased size of the effect seen during the late day could indicate rhythms in the aversive properties of nicotine. Interestingly, the habenula has been

implicated in control of locomotor activity cycles (Paul et al., 2011), is known to be a critical mediator of the aversive properties of nicotine (Molas et al., 2017; Pang et al., 2016) and has evidence of rhythmicity (Sakhi et al., 2014; Salaberry and Mendoza, 2015; Zhao and Rusak, 2005). Accordingly the habenula presents an interesting neural structure that could be a potential site for the integration of these pathways.

The evidence from this study suggests that the rhythm in sensitivity to nicotine-evoked suppression of rearing appears to be distinguished from the rhythm in sensitivity to nicotine-evoked ambulatory stimulation. This extends the work of previous publications which demonstrate that these behaviours are dissociative and represent different neural systems (Lever et al., 2006; Sturman et al., 2018) and indeed, nicotine may produce these effects through multiple pathways (Balfour, 2009; Meliska and Loke, 1984; Vezina et al., 2007).

2.5.6 **Limitations of the study**

One caveat of this work is that animals were maintained on a light / dim red light cycle rather than light / total dark. Rats maintain the capacity for visual discrimination under red light (Nikbakht and Diamond, 2021; Niklaus et al., 2020) and even dim red light during the dark phase can disrupt circadian rhythms relative to controls kept in absolute darkness at night (Dauchy et al., 2015). Therefore, it is likely that these animals are not representative of all Lister Hooded rats in terms of their circadian cycle. However, rats still exhibited the anticipated day / night variation in locomotor activity as previously described in the literature (McDermott and Kelly, 2008). Therefore, we expect that disruption to their circadian system was minimal, and so the broad findings from this work remain largely generalizable – although perhaps caution should be taken in extrapolating any meaning from the absolute circadian times to any further studies. Instead, we suggest that the data from this study and the previous work it builds on is enough to suggest that nicotine-evoked changes in locomotor activity are influenced by the circadian system. Further experiments with greater temporal resolution would be needed to make any precise claims about exactly which times of day are most effective for revealing nicotine's effects on locomotor activity.

It also remains to be seen whether these differences are truly circadian. For a rhythm to be considered truly circadian in nature, it must be endogenously generated and persist even without environmental Zeitgebers such as the light / dark cycle (Vitaterna et al., 2001). The evidence presented in this study is certainly compatible with a circadian origin, but further experiments would be required to rule out the possibility that the observed daily variation in nicotine responses are passively driven by the environmental light / dark cycle.

In addition, we should be cautious in our interpretations of behaviour based purely on the read outs of horizontal or vertical beam-breaks. One drawback of using a fully-automated activity monitoring system is that measuring activity in this way does not allow for distinguishing between behaviours. For example, a lack of beam-breaking activity could reflect an animal remaining still, or it could reflect that the animal has fallen asleep or indeed that it has become ataxic. Nicotine's ataxic effects are thought to be centrally mediated in mice (Kita et al., 1988) but the precise route of action in rats remains underexplored. Therefore, although previous studies have claimed that the ataxic effects of nicotine last less than 20 minutes (Clarke and Kumar, 1983; Shoaib and Stolerman, 1996), in line with the observations of the experimenter in this study, we cannot be certain that these effects are not contributing to the behaviours recorded during the final 30 minutes of the test.

2.5.7 **Conclusions**

To summarise, the data produced from this study support and extend previous work demonstrating that the acute effects of nicotine on rat locomotion are dependent on the time of day, highlighting the need for researchers to carefully control for circadian variation when assessing the actions of nicotine in laboratory rodents. Here we find that the peak sensitivity to nicotine stimulatory effects on ambulation occur during the latter portion of the light phase of the light / dark cycle, when activity and arousal levels are dampened. In contrast, when rats are at their most spontaneously active, nicotine tended to suppress ambulatory activity. Nicotine consistently produced suppressive effects in rearing behaviour, which were most apparent during the rat's active phase. The different time of day influences over these two nicotine-evoked locomotor behaviours suggests they may be mediated by separate cholinergic signalling pathways, and indeed that the circadian system may differentially contribute to these daily rhythms in nicotine sensitivity. Further, with the timings of both rearing and ambulatory behaviours, it appears that the balance between them is changing as a function of the time of day. Further work to understand how the circadian system contributes to diurnal variation in nicotinic cholinergic signalling may yield insights into the aversive and addictive properties of nicotine, and as such lead to more effective nicotine cessation therapies.

2.6 References

Abarca, C., Albrecht, U., Spanagel, R., 2002. Cocaine sensitization and reward are under the influence of circadian genes and rhythm. Proc. Natl. Acad. Sci. U.S.A. 99, 9026–9030. https://doi.org/10.1073/pnas.142039099

Adermark, L., Morud, J., Lotfi, A., Jonsson, S., Söderpalm, B., Ericson, M., 2015. Age-contingent influence over accumbal neurotransmission and the locomotor stimulatory response to acute and repeated administration of nicotine in Wistar rats. Neuropharmacology 97, 104–112. https://doi.org/10.1016/j.neuropharm.2015.06.001

Alderson, H.L., Latimer, M.P., Winn, P., 2008. A functional dissociation of the anterior and posterior pedunculopontine tegmental nucleus: excitotoxic lesions have differential effects on locomotion and the response to nicotine. Brain Struct Funct 213, 247–253. https://doi.org/10.1007/s00429-008-0174-4

Alderson, H.L., Latimer, M.P., Winn, P., 2005. Involvement of the laterodorsal tegmental nucleus in the locomotor response to repeated nicotine administration. Neuroscience Letters 380, 335–339. https://doi.org/10.1016/j.neulet.2005.01.067

Balfour, D.J.K., 2009. The Neuronal Pathways Mediating the Behavioral and Addictive Properties of Nicotine, in: Henningfield, J.E., London, E.D., Pogun, S. (Eds.), Nicotine Psychopharmacology, Handbook of Experimental Pharmacology. Springer, Berlin, Heidelberg, pp. 209–233. https://doi.org/10.1007/978-3-540-69248-5_8

Ballesteros-Yáñez, I., Castillo, C.A., Merighi, S., Gessi, S., 2018. The Role of Adenosine Receptors in Psychostimulant Addiction. Frontiers in Pharmacology 8.

Beery, A.K., 2018. Inclusion of females does not increase variability in rodent research studies. Current Opinion in Behavioral Sciences, Sex and Gender 23, 143–149. https://doi.org/10.1016/j.cobeha.2018.06.016

Beery, A.K., Zucker, I., 2011. Sex Bias in Neuroscience and Biomedical Research. Neurosci Biobehav Rev 35, 565–572. https://doi.org/10.1016/j.neubiorev.2010.07.002

Benowitz, N.L., 2010. Nicotine Addiction. N Engl J Med 362, 2295–2303. https://doi.org/10.1056/NEJMra0809890

Benowitz, N.L., Kuyt, F., Jacob, P., 1982. Circadian blood nicotine concentrations during cigarette smoking. Clin. Pharmacol. Ther. 32, 758–764.

Benwell, M.E., Balfour, D.J., 1992. The effects of acute and repeated nicotine treatment on nucleus accumbens dopamine and locomotor activity. Br J Pharmacol 105, 849–856. https://doi.org/10.1111/j.1476-5381.1992.tb09067.x

Booze, R.M., Welch, M.A., Wood, M.L., Billings, K.A., Apple, S.R., Mactutus, C.F., 1999. Behavioral Sensitization Following Repeated Intravenous Nicotine Administration: Gender Differences and Gonadal Hormones. Pharmacology Biochemistry and Behavior 64, 827–839. https://doi.org/10.1016/S0091-3057(99)00169-0

Bovet, D., Bovet-Nitti, F., Oliverio, A., 1967. Action of Nicotine on Spontaneous and Acquired Behavior in Rats and Mice*. Annals of the New York Academy of Sciences 142, 261–267. https://doi.org/10.1111/j.1749-6632.1967.tb13728.x

Brown, K.J., Grunberg, N.E., 1995. Effects of housing on male and female rats: Crowding stresses males but calms females. Physiology & Behavior 58, 1085–1089. https://doi.org/10.1016/0031-9384(95)02043-8

Casarrubea, M., Davies, C., Faulisi, F., Pierucci, M., Colangeli, R., Partridge, L., Chambers, S., Cassar, D., Valentino, M., Muscat, R., Benigno, A., Crescimanno, G., Di Giovanni, G., 2015. Acute nicotine induces anxiety and disrupts temporal pattern organization of rat exploratory behavior in hole-board: a potential role for the lateral habenula. Frontiers in Cellular Neuroscience 9, 197. https://doi.org/10.3389/fncel.2015.00197

Chandra, S., Scharf, D., Shiffman, S., 2011. Within-day temporal patterns of smoking, withdrawal symptoms, and craving. Drug Alcohol Depend 117, 118–125. https://doi.org/10.1016/j.drugalcdep.2010.12.027

Changeux, J.-P., 2010. Nicotine addiction and nicotinic receptors: lessons from genetically modified mice. Nat. Rev. Neurosci. 11, 389–401. https://doi.org/10.1038/nrn2849

Clarke, P.B.S., Kumar, R., 1983. The effects of nicotine on locomotor activity in non-tolerant and tolerant rats. British Journal of Pharmacology 78, 329–337. https://doi.org/10.1111/j.1476-5381.1983.tb09398.x

Clemens, L.E., Jansson, E.K.H., Portal, E., Riess, O., Nguyen, H.P., 2014. A behavioral comparison of the common laboratory rat strains Lister Hooded, Lewis, Fischer 344 and Wistar in an automated homecage system. Genes Brain Behav. 13, 305–321. https://doi.org/10.1111/gbb.12093

Dani, J.A., De Biasi, M., 2013. Mesolimbic Dopamine and Habenulo-Interpeduncular Pathways in Nicotine Withdrawal. Cold Spring Harb Perspect Med 3. https://doi.org/10.1101/cshperspect.a012138

Dauchy, R.T., Wren, M.A., Dauchy, E.M., Hoffman, A.E., Hanifin, J.P., Warfield, B., Jablonski, M.R., Brainard, G.C., Hill, S.M., Mao, L., Dobek, G.L., Dupepe, L.M., Blask, D.E., 2015. The Influence of Red Light Exposure at Night on Circadian Metabolism and Physiology in Sprague–Dawley Rats. J Am Assoc Lab Anim Sci 54, 40–50.

De Biasi, M., Dani, J.A., 2011. Reward, Addiction, Withdrawal to Nicotine. Annu Rev Neurosci 34, 105–130. https://doi.org/10.1146/annurev-neuro-061010-113734

Di Chiara, G., 2000. Role of dopamine in the behavioural actions of nicotine related to addiction. European Journal of Pharmacology 393, 295–314. https://doi.org/10.1016/S0014-2999(00)00122-9

Elliott, B.M., Faraday, M.M., Phillips, J.M., Grunberg, N.E., 2004. Effects of nicotine on elevated plus maze and locomotor activity in male and female adolescent and adult rats. Pharmacol. Biochem. Behav. 77, 21–28.

Faraday, M.M., O'Donoghue, V.A., Grunberg, N.E., 2003. Effects of nicotine and stress on locomotion in Sprague–Dawley and Long–Evans male and female rats. Pharmacology Biochemistry and Behavior 74, 325–333. https://doi.org/10.1016/S0091-3057(02)00999-1

Fonken, L.K., Aubrecht, T.G., Meléndez-Fernández, O.H., Weil, Z.M., Nelson, R.J., 2013. Dim light at night disrupts molecular circadian rhythms and increases body weight. J. Biol. Rhythms 28, 262–271. https://doi.org/10.1177/0748730413493862

Gillman, A.G., Kosobud, A.E.K., Timberlake, W., 2010. Effects of multiple daily nicotine administrations on pre- and post-nicotine circadian activity episodes in rats. Behav. Neurosci. 124, 520–531. https://doi.org/10.1037/a0020272

González, M.M.C., 2018. Dim Light at Night and Constant Darkness: Two Frequently Used Lighting Conditions That Jeopardize the Health and Well-being of Laboratory Rodents. Frontiers in Neurology 9, 609. https://doi.org/10.3389/fneur.2018.00609

Grainge, M.J., Shahab, L., Hammond, D., O'Connor, R.J., McNeill, A., 2009. First cigarette on waking and time of day as predictors of puffing behaviour in UK adult smokers. Drug Alcohol Depend 101, 191–195. https://doi.org/10.1016/j.drugalcdep.2009.01.013

Gries, J.M., Benowitz, N., Verotta, D., 1996. Chronopharmacokinetics of nicotine. Clin. Pharmacol. Ther. 60, 385–395. https://doi.org/10.1016/S0009-9236(96)90195-2

Gritton, H.J., Sutton, B.C., Martinez, V., Sarter, M., Lee, T.M., 2009. Interactions between cognition and circadian rhythms: attentional demands modify circadian entrainment. Behav Neurosci 123, 937–948. https://doi.org/10.1037/a0017128

Hayward, A., Adamson, L., Neill, J.C., 2017. Partial agonism at the α7 nicotinic acetylcholine receptor improves attention, impulsive action and vigilance in low attentive rats. European Neuropsychopharmacology 27, 325–335. https://doi.org/10.1016/j.euroneuro.2017.01.013

Iyaniwura, T.T., Wright, A.E., Balfour, D.J., 2001. Evidence that mesoaccumbens dopamine and locomotor responses to nicotine in the rat are influenced by pretreatment dose and strain. Psychopharmacology 158, 73–79. https://doi.org/10.1007/s002130100852
Jackson, K.J., Muldoon, P.P., De Biasi, M., Damaj, M.I., 2015. New mechanisms and perspectives in nicotine withdrawal. Neuropharmacology 96, 223–234. https://doi.org/10.1016/j.neuropharm.2014.11.009
Jandová, K., Marešová, D., Pokorný, J., 2013. Fast and delayed locomotor response to acute high-dose nicotine administration in adult male rats. Physiol Res 62, S81-88. https://doi.org/10.33549/physiolres.932610
Jerome, A., Sanberg, P.R., 1987. The effects of nicotine on locomotor behavior in non-tolerant rats: a multivariate assessment. Psychopharmacology 93, 397–400. https://doi.org/10.1007/BF00187264
Kanýt, L., Stolerman, I.P., Chandler, C.J., Saigusa, T., Pöğün, Ş., 1999. Influence of Sex and Female Hormones on Nicotine-Induced Changes in Locomotor Activity in Rats. Pharmacology Biochemistry and Behavior 62, 179–187. https://doi.org/10.1016/S0091-3057(98)00140-3
King, S.L., Caldarone, B.J., Picciotto, M.R., 2004. β2-subunit-containing nicotinic acetylcholine receptors are critical for dopamine-dependent locomotor activation following repeated nicotine administration. Neuropharmacology, Frontiers in Addiction Research: Celebrating the 30th Anniversary of the National Institute on Drug Abuse. 47, 132–139. https://doi.org/10.1016/j.neuropharm.2004.06.024
Kita, T., Nakashima, T., Kurogochi, Y., 1986. Circadian variation of nicotine-induced ambulatory activity in rats. Jpn. J. Pharmacol. 41, 55–60.
Kita, T., Nakashima, T., Shirase, M., Asahina, M., Kurogochi, Y., 1988. Effects of Nicotine on Ambulatory Activity in Mice. The Japanese Journal of Pharmacology 46, 141–146. https://doi.org/10.1254/jjp.46.141
Ksir, C., 1994. Acute and chronic nicotine effects on measures of activity in rats: a multivariate analysis. Psychopharmacology 115, 105–109. https://doi.org/10.1007/BF02244758
Ksir, C., Hakan, R., Hall, D.P., Kellar, K.J., 1985. Exposure to nicotine enhances the behavioral stimulant effect of nicotine and increases binding of [3H]acetylcholine to nicotinic receptors. Neuropharmacology 24, 527–531. https://doi.org/10.1016/0028-3908(85)90058-9
Lazarus, M., Oishi, Y., Bjorness, T.E., Greene, R.W., 2019. Gating and the Need for Sleep: Dissociable Effects of Adenosine A1 and A2A Receptors. Frontiers in Neuroscience 13.
Lever, C., Burton, S., O'Keefe, J., 2006. Rearing on hind legs, environmental novelty, and the hippocampal formation. Rev Neurosci 17, 111–133.
Lynn, D.A., Brown, G.R., 2009. The Ontogeny of Exploratory Behavior in Male and Female Adolescent Rats (Rattus norvegicus). Dev Psychobiol 51, 513–520. https://doi.org/10.1002/dev.20386
Matta, S.G., Balfour, D.J., Benowitz, N.L., Boyd, R.T., Buccafusco, J.J., Caggiula, A.R., Craig, C.R., Collins, A.C., Damaj, M.I., Donny, E.C., Gardiner, P.S., Grady, S.R., Heberlein, U., Leonard, S.S., Levin, E.D., Lukas, R.J., Markou, A., Marks, M.J., McCallum, S.E., Parameswaran, N., Perkins, K.A., Picciotto, M.R., Quik, M., Rose, J.E., Rothenfluh, A., Schafer, W.R., Stolerman, I.P., Tyndale, R.F., Wehner, J.M., Zirger, J.M., 2007. Guidelines on nicotine dose selection for in vivo research. Psychopharmacology 190, 269–319. https://doi.org/10.1007/s00213-006-0441-0
McDermott, C., Kelly, J.P., 2008. Comparison of the behavioural pharmacology of the Lister-Hooded with 2 commonly utilised albino rat strains. Progress in Neuro-Psychopharmacology and Biological Psychiatry 32, 1816–1823. https://doi.org/10.1016/j.pnpbp.2008.08.004
McLean, S.L., Idris, N.F., Woolley, M.L., Neill, J.C., 2009. D1-like receptor activation improves PCP-induced cognitive deficits in animal models: Implications for mechanisms of improved

cognitive function in schizophrenia. European Neuropsychopharmacology 19, 440–450. https://doi.org/10.1016/j.euroneuro.2009.01.009
Meliska, C.J., Loke, W.H., 1984. Caffeine and nicotine: Differential effects on ambulation, rearing and wheelrunning. Pharmacology Biochemistry and Behavior 21, 871–875. https://doi.org/10.1016/S0091-3057(84)80067-2
Mendoza, J., Challet, E., 2014. Circadian insights into dopamine mechanisms. Neuroscience, The Ventral Tegmentum and Dopamine: A New Wave of Diversity 282, 230–242. https://doi.org/10.1016/j.neuroscience.2014.07.081
Mexal, S., Horton, W.J., Crouch, E.L., Maier, S.I.B., Wilkinson, A.L., Marsolek, M., Stitzel, J.A., 2012. Diurnal variation in nicotine sensitivity in mice: role of genetic background and melatonin. Neuropharmacology 63, 966–973. https://doi.org/10.1016/j.neuropharm.2012.06.065
Mirza, N.R., Misra, A., Bright, J.L., 2000. Different outcomes after acute and chronic treatment with nicotine in pre-pulse inhibition in Lister hooded rats. Eur J Pharmacol 407, 73–81. https://doi.org/10.1016/s0014-2999(00)00658-0
Molas, S., DeGroot, S.R., Zhao-Shea, R., Tapper, A.R., 2017. Anxiety and Nicotine Dependence: Emerging Role of the Habenulo-Interpeduncular Axis. Trends Pharmacol. Sci. 38, 169–180. https://doi.org/10.1016/j.tips.2016.11.001
Mooney, M., Green, C., Hatsukami, D., 2006. Nicotine self-administration: cigarette versus nicotine gum diurnal topography. Hum Psychopharmacol 21, 539–548. https://doi.org/10.1002/hup.808
Morley, B.J., Garner, L.L., 1990. Light-dark variation in response to chronic nicotine treatment and the density of hypothalamic alpha-bungarotoxin receptors. Pharmacol. Biochem. Behav. 37, 239–245.
Nam, H.W., McIver, S.R., Hinton, D.J., Thakkar, M.M., Sari, Y., Parkinson, F.E., Haydon, P.G., Choi, D.-S., 2012. Adenosine and Glutamate Signaling in Neuron–Glial Interactions: Implications in Alcoholism and Sleep Disorders. Alcoholism: Clinical and Experimental Research 36, 1117–1125. https://doi.org/10.1111/j.1530-0277.2011.01722.x
Negus, S.S., Mello, N.K., Lukas, S.E., Mendelson, J.H., 1995. Diurnal patterns of cocaine and heroin self-administration in rhesus monkeys responding under a schedule of multiple daily sessions. Behav Pharmacol 6, 763–775.
Nikbakht, N., Diamond, M.E., 2021. Conserved visual capacity of rats under red light. eLife 10, e66429. https://doi.org/10.7554/eLife.66429
Niklaus, S., Albertini, S., Schnitzer, T.K., Denk, N., 2020. Challenging a Myth and Misconception: Red-Light Vision in Rats. Animals (Basel) 10, 422. https://doi.org/10.3390/ani10030422
O'Dell, L.E., Chen, S.A., Smith, R.T., Specio, S.E., Balster, R.L., Paterson, N.E., Markou, A., Zorrilla, E.P., Koob, G.F., 2007. Extended access to nicotine self-administration leads to dependence: Circadian measures, withdrawal measures, and extinction behavior in rats. J. Pharmacol. Exp. Ther. 320, 180–193. https://doi.org/10.1124/jpet.106.105270
O'Neill, M.F., Dourish, C.T., Iversen, S.D., 1991. Evidence for an involvement of D1 and D2 dopamine receptors in mediating nicotine-induced hyperactivity in rats. Psychopharmacology 104, 343–350. https://doi.org/10.1007/BF02246034
Palmatier, M.I., Fung, E.Y.K., Bevins, R.A., 2003. Effects of chronic caffeine pre-exposure on conditioned and unconditioned psychomotor activity induced by nicotine and amphetamine in rats. Behav Pharmacol 14, 191–198. https://doi.org/10.1097/01.fbp.0000069578.37661.2a
Pang, X., Liu, L., Ngolab, J., Zhao-Shea, R., McIntosh, J.M., Gardner, P.D., Tapper, A.R., 2016. Habenula cholinergic neurons regulate anxiety during nicotine withdrawal via nicotinic acetylcholine receptors. Neuropharmacology 107, 294–304. https://doi.org/10.1016/j.neuropharm.2016.03.039

Paul, M.J., Indic, P., Schwartz, W.J., 2011. A role for the habenula in the regulation of locomotor activity cycles. European Journal of Neuroscience 34, 478–488. https://doi.org/10.1111/j.1460-9568.2011.07762.x

Perkins, K.A., Briski, J., Fonte, C., Scott, J., Lerman, C., 2009. Severity of tobacco abstinence symptoms varies by time of day. Nicotine Tob. Res. 11, 84–91. https://doi.org/10.1093/ntr/ntn003

Perreau-Lenz, S., Vengeliene, V., Noori, H.R., Merlo-Pich, E.V., Corsi, M.A., Corti, C., Spanagel, R., 2012. Inhibition of the Casein-Kinase-1-Epsilon/Delta Prevents Relapse-Like Alcohol Drinking. Neuropsychopharmacology 37, 2121–2131. https://doi.org/10.1038/npp.2012.62

Phillips, K.A., Epstein, D.H., Preston, K.L., 2013. Daily Temporal Patterns of Heroin and Cocaine Use and Craving: Relationship with Business Hours Regardless of Actual Employment Status. Addict Behav 38, 2485–2491. https://doi.org/10.1016/j.addbeh.2013.05.010

Porkka-Heiskanen, T., Strecker, R.E., McCarley, R.W., 2000. Brain site-specificity of extracellular adenosine concentration changes during sleep deprivation and spontaneous sleep: an in vivo microdialysis study. Neuroscience 99, 507–517. https://doi.org/10.1016/s0306-4522(00)00220-7

Prus, A.J., Vann, R.E., Rosecrans, J.A., James, J.R., Pehrson, A.L., O'Connell, M.M., Philibin, S.D., Robinson, S.E., 2008. Acute nicotine reduces and repeated nicotine increases spontaneous activity in male and female Lewis rats. Pharmacol Biochem Behav 91, 150–154. https://doi.org/10.1016/j.pbb.2008.06.024

Qiu, B.S., Cho, C.H., Ogle, C.W., 1992. Effects of nicotine on activity and stress-induced gastric ulcers in rats. Pharmacology Biochemistry and Behavior 43, 1053–1058. https://doi.org/10.1016/0091-3057(92)90480-4

Reavill, C., Stolerman, I.P., 1990. Locomotor activity in rats after administration of nicotinic agonists intracerebrally. Br J Pharmacol 99, 273–278. https://doi.org/10.1111/j.1476-5381.1990.tb14693.x

Rodgers, R.J., 1979. Effects of nicotine, mecamylamine, and hexamethonium on shock-induced fighting, pain reactivity, and locomotor behaviour in rats. Psychopharmacology (Berl) 66, 93–98. https://doi.org/10.1007/BF00431996

Sakhi, K., Belle, M.D.C., Gossan, N., Delagrange, P., Piggins, H.D., 2014. Daily variation in the electrophysiological activity of mouse medial habenula neurones. J Physiol 592, 587–603. https://doi.org/10.1113/jphysiol.2013.263319

Salaberry, N.L., Mendoza, J., 2015. Insights into the Role of the Habenular Circadian Clock in Addiction. Front Psychiatry 6, 179. https://doi.org/10.3389/fpsyt.2015.00179

Schochet, T.L., Kelley, A.E., Landry, C.F., 2004. Differential behavioral effects of nicotine exposure in adolescent and adult rats. Psychopharmacology 175, 265–273. https://doi.org/10.1007/s00213-004-1831-9

Shigeyoshi, Y., Taguchi, K., Yamamoto, S., Takekida, S., Yan, L., Tei, H., Moriya, T., Shibata, S., Loros, J.J., Dunlap, J.C., Okamura, H., 1997. Light-Induced Resetting of a Mammalian Circadian Clock Is Associated with Rapid Induction of the mPer1Transcript. Cell 91, 1043–1053. https://doi.org/10.1016/S0092-8674(00)80494-8

Shoaib, M., Stolerman, I.P., 1996. Brain sites mediating the discriminative stimulus effects of nicotine in rats. Behavioural Brain Research 78, 183–188. https://doi.org/10.1016/0166-4328(95)00245-6

Shoaib, M., Stolerman, I.P., Kumar, R.C., 1994. Nicotine-induced place preferences following prior nicotine exposure in rats. Psychopharmacology 113, 445–452. https://doi.org/10.1007/BF02245221

Sleipness, E.P., Sorg, B.A., Jansen, H.T., 2005. Time of day alters long-term sensitization to cocaine in rats. Brain Res. 1065, 132–137. https://doi.org/10.1016/j.brainres.2005.10.017

Stolerman, I.P., Fink, R., Jarvik, M.E., 1973. Acute and chronic tolerance to nicotine measured by activity in rats. Psychopharmacologia 30, 329–342.
Stolerman, I.P., Garcha, H.S., Mirza, N.R., 1995. Dissociations between the locomotor stimulant and depressant effects of nicotinic agonists in rats. Psychopharmacology 117, 430–437. https://doi.org/10.1007/BF02246215
Studholme, K.M., Gompf, H.S., Morin, L.P., 2013. Brief light stimulation during the mouse nocturnal activity phase simultaneously induces a decline in core temperature and locomotor activity followed by EEG-determined sleep. Am J Physiol Regul Integr Comp Physiol 304, R459–R471. https://doi.org/10.1152/ajpregu.00460.2012
Sturman, O., Germain, P.-L., Bohacek, J., 2018. Exploratory rearing: a context- and stress-sensitive behavior recorded in the open-field test. Stress 21, 443–452. https://doi.org/10.1080/10253890.2018.1438405
Sutcliffe, J.S., Marshall, K.M., Neill, J.C., 2007. Influence of gender on working and spatial memory in the novel object recognition task in the rat. Behavioural Brain Research 177, 117–125. https://doi.org/10.1016/j.bbr.2006.10.029
Tatem, K.S., Quinn, J.L., Phadke, A., Yu, Q., Gordish-Dressman, H., Nagaraju, K., 2014. Behavioral and Locomotor Measurements Using an Open Field Activity Monitoring System for Skeletal Muscle Diseases. J Vis Exp. https://doi.org/10.3791/51785
Urry, E., Landolt, H.-P., 2015. Adenosine, caffeine, and performance: from cognitive neuroscience of sleep to sleep pharmacogenetics. Curr Top Behav Neurosci 25, 331–366. https://doi.org/10.1007/7854_2014_274
Ussher, M., West, R., 2003. Diurnal variations in first lapses to smoking for nicotine patch users. Hum Psychopharmacol 18, 345–349. https://doi.org/10.1002/hup.493
Valle, F.P., 1970. Effects of strain, sex, and illumination on open-field behavior of rats. Am J Psychol 83, 103–111.
Vezina, P., McGehee, D.S., Green, W.N., 2007. Exposure to nicotine and sensitization of nicotine-induced behaviors. Prog Neuropsychopharmacol Biol Psychiatry 31, 1625–1638. https://doi.org/10.1016/j.pnpbp.2007.08.038
Vitaterna, M.H., Takahashi, J.S., Turek, F.W., 2001. Overview of Circadian Rhythms. Alcohol Res Health 25, 85–93.
Webb, I.C., 2017. Circadian Rhythms and Substance Abuse: Chronobiological Considerations for the Treatment of Addiction. Curr Psychiatry Rep 19, 12. https://doi.org/10.1007/s11920-017-0764-z
Webb, I.C., Lehman, M.N., Coolen, L.M., 2015. Diurnal and circadian regulation of reward-related neurophysiology and behavior. Physiol. Behav. 143, 58–69. https://doi.org/10.1016/j.physbeh.2015.02.034
Welzl, H., Bättig, K., Berz, S., 1990. Acute effects of nicotine injection into the nucleus accumbens on locomotor activity in nicotine-naive and nicotine-tolerant rats. Pharmacology Biochemistry and Behavior 37, 743–746. https://doi.org/10.1016/0091-3057(90)90557-X
West, R., 2017. Tobacco smoking: Health impact, prevalence, correlates and interventions. Psychol Health 32, 1018–1036. https://doi.org/10.1080/08870446.2017.1325890
Wiley, J.L., Marusich, J.A., Thomas, B.F., Jackson, K.J., 2015. Determination of behaviorally effective tobacco constituent doses in rats. Nicotine Tob Res 17, 368–371. https://doi.org/10.1093/ntr/ntu194
Williams, R.L., Soliman, K.F., Mizinga, K.M., 1993. Circadian variation in tolerance to the hypothermic action of CNS drugs. Pharmacol. Biochem. Behav. 46, 283–288.
Zhao, H., Rusak, B., 2005. Circadian firing-rate rhythms and light responses of rat habenular nucleus neurons in vivo and in vitro. Neuroscience 132, 519–528. https://doi.org/10.1016/j.neuroscience.2005.01.012

3 Daily variation in electrophysiology and sensitivity to nicotine in the MHb *in vitro*

3.1 Abstract

Circadian clock activity is widespread throughout the brain and associated with daily rhythms in most aspects of physiology and behaviour. The habenula, a small bilateral structure of the epithalamus implicated in reward and addiction processes, is one such area, demonstrating circadian rhythmicity in molecular and neuronal activity. The medial portion of the habenula (MHb) has remarkably dense expression of several different nicotinic acetylcholine receptor subunits. This has led to a wealth of research firmly implicating the MHb as a crucial centre mediating nicotine withdrawal. Intriguingly, studies in both humans and animals have provided evidence for daily rhythms in nicotine intake and withdrawal, raising the possibility of a circadian influence on the cholinergic circuits of the MHb. Therefore, we set out to investigate whether there was evidence of diurnal patterns in sensitivity to nicotine within the MHb, and to characterise time of day differences in the network properties of the MHb. Using *in vitro* electrophysiological approaches, both spontaneous firing rates and responses to nicotine were examined in mouse MHb at defined time points across the day-night cycle to investigate whether these properties were under circadian influence. These investigations revealed higher MHb spontaneous firing activity in slice recordings during early vs late projected day and correspondingly enhanced responses to nicotine application. Longer-term recordings further provided evidence of circadian rhythmicity in the activity of many MHb neurons, whose timing of peak firing was predicted by time of slice preparation rather than the animal's prior light history. Collectively these data support the notion that MHb activity and responses to nicotine are under circadian control and indicate that endogenous circadian control of this process is rapidly reset *ex vivo*. These data have potential implications for the design of future studies on the role of the MHb in circadian control of addiction and the design of novel therapies for smoking cessation.

3.2 Introduction

Rhythmic processes which oscillate with a period close to 24 hours are prevalent throughout biology (Hastings et al., 2018). These circadian rhythms confer an evolutionary advantage to a species (Vaze and Sharma, 2013), allowing an organism to adjust their physiology and behaviour in anticipation of the reliable changes in the environment that accompany the daily transition between day and night. In mammals, the central pacemaker responsible for maintaining coherent internal rhythms in processes as diverse as sleep-wake cycles (Northeast et al., 2020), heart rate (Black et al., 2019) and cognitive performance (Valdez, 2019) whilst remaining aligned with the solar time is the suprachiasmatic nucleus (SCN). The SCN receives cues about the time of day through various signals, including light (Paul & Brown, 2019), social interaction (Mistlberger and Skene, 2004) or food availability (Bechtold and Loudon, 2013). SCN neurons generate rhythms through the intracellular molecular clock, comprised of a transcription-translation feedback loop of tightly controlled expression of core clock genes, to drive circadian variation in their neuronal excitability (Brown and Piggins, 2007; Partch et al., 2014). The SCN then transmits this timing information to downstream target structures, thus keeping the rest of the brain in time (Inouye & Kawamura, 1979; Paul et al., 2016).

Whilst the SCN remains integral for the coordination of timing across brain sites, it is not unique in its capacity for generating rhythms. Many structures within in the brain oscillate in their action potential firing capability over a 24 hour period and/or exhibit rhythmic clock gene expression (Begemann et al., 2020; Guilding & Piggins, 2007; Paul et al., 2020). Interestingly, recent work has identified the habenula as one such oscillatory structure within the mammalian brain. The habenula complex is a bilateral structure of the epithalamus comprised of medial and lateral nuclei (MHb and LHb). Despite their shared inputs, the MHb and LHb differ in their connectivity, neurochemistry and function (Klemm, 2004). Both regions, however, display evidence of intrinsic timekeeping capabilities (Baño-Otálora and Piggins, 2017; Mendoza, 2007). In the case of the MHb, *in situ* hybridization studies found core clock gene mRNA is expressed at moderate levels (Shieh, 2003; Yamamoto et al., 2001) and is rhythmic (Olejniczak et al., 2021). Bioluminescent reporter studies have also provided evidence for *ex vivo* rhythmic expression of the clock gene *Per2* (Landgraf et al., 2016), although earlier studies have reported conflicting results (Guilding et al., 2010). Further, electrophysiological studies performed by Zhao and Rusak (2005) demonstrated significant rhythmicity in neural firing activity of rat MHb neurons *in vivo.* While the latter study could not detect significant rhythmicity in *ex vivo* slice preparations, a more recent study that recorded from mouse MHb slices did find clear evidence of neuronal rhythms (Sakhi et

al., 2014a). Specifically, Sakhi et al. found a diurnal variation in action potential discharge and resting membrane potential of mouse MHb neurons. Moreover, when the investigations were carried out in slices from animals lacking a functional circadian clock, time of day differences in electrophysiology were abolished, confirming their circadian basis.

The MHb is noted for its dense expression of many nicotinic acetylcholine receptor (nAChR) subtypes (Sheffield et al., 2000; Shih et al., 2014) and has one of the highest densities of nicotine binding sites within the rat brain (Mugnaini et al., 2002). Therefore perhaps unsurprisingly, much of the current research into the MHb has focussed on its role in nicotine addiction (Wills and Kenny, 2021). nAChR expression within the MHb and its downstream target, the interpeduncular nucleus (IPN), is thought to mediate both the somatic and affective symptoms of nicotine withdrawal (Görlich et al., 2013; Salas et al., 2009; Zhao-Shea et al., 2015) and the cholinergic neurons of the MHb have been shown to control withdrawal-induced anxiety (Pang et al., 2016). In addition, expression of various nAChR subunits in the MHb has been shown to regulate nicotine intake (Elayouby et al., 2021; Fowler et al., 2011; Glick et al., 2011). Intriguingly, there is evidence that many of these nicotine addiction behaviours are under circadian control: nicotine intake varies over the course of the day in both rats (O'Dell et al., 2007) and humans (Benowitz et al., 1982; Grainge et al., 2009; Mooney et al., 2006); cravings and withdrawal symptoms have rhythms in their severity (Chandra et al., 2011; Parrott, 1995; Perkins et al., 2009; Teneggi et al., 2002) and relapse rates are higher at certain times of day (Shiffman et al., 1997; Ussher and West, 2003). These diurnal variations may well be driven by circadian rhythms in cholinergic signalling.

As yet, studies specifically investigating circadian control of cholinergic signalling are limited (Hut and Van der Zee, 2011), although there is evidence from whole brain analysis in rats that acetylcholine (ACh) content peaks at ZT2 (Hanin et al., 1970), and *in vivo* microdialysis studies in rats show cortical ACh release is higher during the dark phase than the light (Kametani and Kawamura, 1991). Evidence for circadian fluctuation in nAChRs is rare (Hut & Van der Zee, 2011), and limited to studies investigating α-bungarotoxin binding sites, which show a modest rhythm in the basal hypothalamus (Morley & Garner, 1990) and the dorsolateral SCN (Fuchs & Hoppens, 1987). There is less direct evidence, such as rhythms in sensitivity to the effects of nicotine (Kita et al., 1986; Mexal et al., 2012; O'Dell et al., 2007). However, clearly this remains an avenue which warrants further exploration.

Therefore, as a site of particularly dense cholinergic innervation with evidence of some circadian properties, the MHb is an important target for understanding mechanisms of circadian control over cholinergic signalling. This has potential implications for nicotine-dependent behaviours such

as tobacco addiction, as well as broader implications for behaviours modulated by the cholinergic system. This project set out to determine if there were time of day difference in both the network properties of the MHb and at the single cell level, and investigate the long-term behaviour of individual MHb neurons for rhythmic properties. As an area of dense cholinergic innervation, we further sought to identify whether there was evidence of diurnal patterns in cholinergic signalling within this brain structure, and in particular explore the contribution of a particular nAChR subunit to this pattern in cholinergic signalling.

3.3 Materials and methods

3.3.1 Animals

Acute *in vitro* electrophysiological experiments were performed with a total of 8 male C57Bl/6J mice aged between 2-6 months (Charles River, Kent, UK). Long-term *in vitro* experiments were performed on 9 C57Bl/6J mice (7 female, 2 male; 1 male in each group) that were bred in house by the University of Manchester Biological Services Facility. The sample size was based on an initial pilot experiment which used 12 C57Bl/6J mice that were wildtype littermates bred from animals bearing several different genotypes, and showed differences in firing rate between early and late conditions. We aimed to replicate the finding in a batch of animals that were exclusively bred purely on a C57Bl/6J background. 12 mice were ordered but due to 4 experiments failing, only data from 8 animals was collected. No further data collection was possible as the equipment was not accessible after this point. All data was collected prior to the analysis.

Mice were group housed in standard home cages with food and water available *ad libitum.* The home environment was both temperature (21±2°C) and humidity (55±5%) controlled with 12 hr light / dark cycles, adjusted to allow experiments to be performed during the working day. In all cases Zeitgeber time (ZT) is used to define the projected time of the circadian clock, where ZT0 corresponds to lights on and ZT12 corresponds to lights off. All procedures were approved by the University of Manchester Ethics Committee and strictly adhered to the Animals (Scientific - Procedures) Act, 1986, conducted under the authority of Project Licences 70/8918 and PP3176367.

3.3.2 Brain slice preparation

Brain slices for both acute and long-term recordings were prepared in the same way unless otherwise specified. Mice were killed by cervical dislocation, decapitated and the skull cap carefully removed using fine surgical scissors. The brain was gently excised after severing the optic

nerve, and the cerebellum was removed with a razor blade to create a flat surface in order to mount the brain on the cutting stage. The brain was secured in place using a small amount of cyanoacrylate superglue (RS Components Ltd, UK). The stage and the brain were then immersed in ice-cold incubation artificial cerebrospinal fluid solution (aCSF, composition in mM: NaCl 95, KCl 1.8, KH2PO4 1.2, CaCl2 0.5, MgSO4 7, NaHCO3 26, glucose 15, sucrose 50 and Phenol Red 0.005 mg/L, all from Sigma-Aldrich, UK) with a pH of 7.4 and osmolality between 300-310 mosmol/kg, oxygenated with 95%O_2/5%CO_2. This high magnesium, sucrose-substituted aCSF was formulated to reduce neuronal death resulting from excitotoxicity associated with slice preparation (Moyer and Brown, 1998).

Coronal sections (200 µm for acute, 350 µm for long-term) were cut using a Campden 7000smz-2 vibrating microtome (Campden Instruments, UK). Sections containing the mid portion of the MHb (corresponding as closely to -1.82 mm from Bregma as determined using Paxinos and Franklin mouse brain atlas as possible; Paxinos & Franklin, 2003) were transferred to a petri dish containing incubation aCSF solution using modified Pasteur pipettes to avoid mechanical stress. They were left to equilibrate for 30 min at room temperature and constantly bubbled with carbogen. Finally, slices were transferred to pre-warmed (35°C) recording aCSF solution (composition in mM: NaCl 127, KCl 1.8, KH2PO4 1.2, CaCl2 2.4, MgSO4 1.3, NaHCO3 26, glucose 5, sucrose 10 and Phenol Red 0.005 mg / L) and left to recover for a further 30 min with continuous oxygenation.

Acute electrophysiological recordings were carried out in either the early day (ZT1 - 4) or late day (ZT8 - 11). These times were selected to correspond with the times Sakhi et al found the greatest difference in mean firing frequency of MHb neurons measured at different times of the day (Sakhi et al., 2014a). Mice were culled between ZT0 - 1 for electrophysiological recordings made between ZT1 – 4, or were culled between ZT6 - 8 for electrophysiological recordings made between ZT8 - 11. For long-term recordings, animals were culled in either the early day (ZT0 - 2) for recordings started during the light phase (ZT3 - 6) or were culled during the late day (ZT11 - 12) for recordings started during the dark phase (ZT13 – 15). This was to avoid culling during the dark period, which is the period during which the circadian clock is most sensitive to resetting (Gillette, 1986; Yoshikawa et al., 2005).

3.3.3 Multielectrode array recordings

Slices were transferred to the recording chamber (acute: MEA2100 system; long-term: a USB-MEA64 system with MEA1060UP-BC amplifier, both Multi Channel Systems, MCS GmbH,

Germany) and positioned over a 6 x 10 perforated micro-electrode array (pMEA, 60pMEA100/30iR-Ti, MCS GmbH). The tissue was positioned to allow recording from the MHb in both hemispheres and was kept as consistent as possible between recordings (Figure 3.1A). Slice positioning was visually confirmed under white light transillumination using a binocular Leica MZ6 microscope (Leica Microsystems, UK) with USB web cam attachment (Carl Zeiss Tessar HD 1080p, Logitech, Switzerland) for acute recordings or a GXCAM-1.3 camera attached to a dissecting microscope (GX optical, UK) for long-term recordings. A weighted harp (ALA Scientific Instruments Inc., US) placed over the tissue and perforations spaced across the array created gentle suction from the flow of aCSF which kept the tissue in place and ensured recording stability across the experiment.

The recording chamber was constantly perfused with fresh heated and oxygenated recording aCSF solution maintained at 35 °C ± 1 °C by a water bath. aCSF entered the recording chamber via two perfusion loops, a peristaltic pump driven 'top flow' and a gravity-driven 'bottom flow'. The top flow entered at a constant rate through a perfusion cannula (acute: ~ 1.8 mL / min, MCS GmbH; long-term: ~ 3 mL / min, 120S Watson-Marlow, UK) which also heated the solution (35°C), ensuring drug solutions entering through this system were heated to the same temperature as the recording chamber. Waste recording solution was removed from the recording chamber through the bottom flow and was prevented from overflowing using a suction cannula (MCS GmbH, Germany). The brain slice was left in place over the pMEA for 20 min before data collection began to allow the tissue to stabilize on the array.

3.3.4 **Pharmacological manipulation**

Drugs were stored as aliquots at -18 °C and freshly prepared to appropriate concentrations in pre-warmed recording aCSF immediately before application. All drugs were bath-applied via the perfusion cannula.

Acute recordings: in order to investigate diurnal variation in cholinergic signalling in the MHb, nicotinic modulators were applied to MHb tissue following collection of baseline data. Preliminary experiments were carried out to determine appropriate drug concentrations and application times. These experiments demonstrated that 5 µM nicotine (Nic, Sigma-Aldrich, UK) applied for 1 min generated a single peak of activity which was replicable following 45 min of wash-out, and the order of drug application did not affect response sizes. The MHb is known to express many nAChR subunits (Lee et al., 2019), including the α4β2 subunit which is heavily implicated in nicotine addiction (Picciotto and Kenny, 2021). Therefore, we chose to investigate how this

subunit might contribute to nicotine's activity in the MHb. The moderately α4β2-selective antagonist dihydro-β-erythroidine hydrobromide (DHβE, Tocris Bioscience, UK) was applied at a concentration of 10 µM for 10 - 15 min, and then a mixture of 5 µM nicotine with 10 µM DHβE was applied immediately for 1 min (DHβE+Nic). DHβE is selective for both α4β2 and α4β4 nAChR subtypes (with IC_{50}s of 0.19 and 0.37 µM, respectively), compared with α3β2, α2β4, α3β4 and α7, as determined through electrophysiological recordings of *Xenopus* oocytes or HEK cells expressing nAChRs (Chavez-Noriega et al., 2000, 1997; Harvey et al., 1996; Jensen et al., 2005). We selected these concentrations as this cocktail of DHβE with nicotine reliably generated a smaller peak of multiunit activity than nicotine alone, allowing the antagonistic effects of DHβE to be measured. Figure 3.1B-F shows a timeline of the drug application and the typical multiunit firing activity observed in response to each drug.

Long-term recordings: slice viability was confirmed at the end of the experiment through application of 20 µM N-Methyl-D-aspartate (NMDA, Tocris Bioscience, UK) bath applied for 5 min to provide evidence of tissue responsiveness.

Finally, for both acute and long-term recordings, each experiment was terminated following 5 min application of 1 µM tetrodotoxin citrate (TTX, Tocris Bioscience, UK) to confirm the recorded electrical activity recorded was exclusively originating from sodium dependent action potentials (Figure 3.1G).

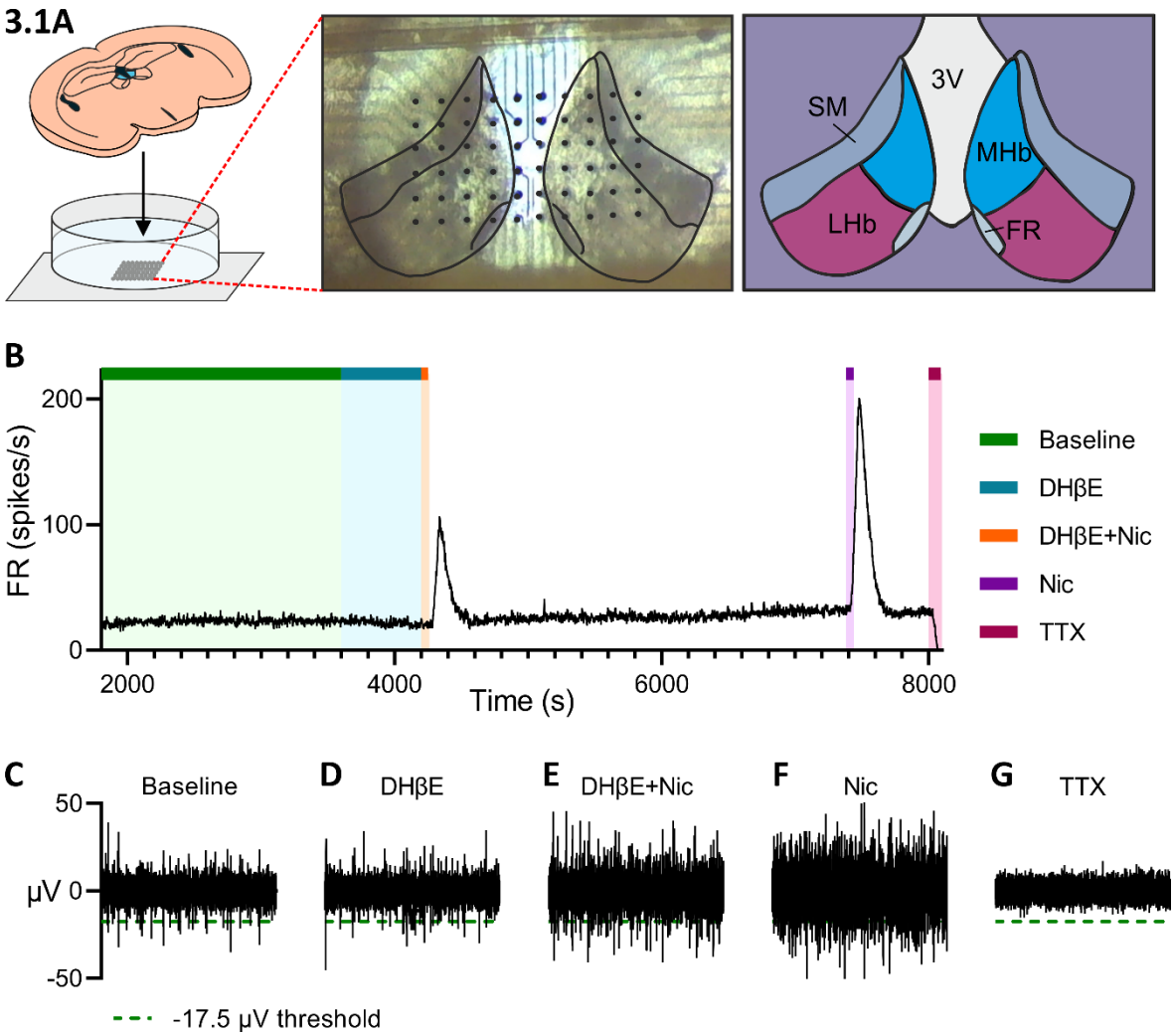

Figure 3.1 Multielectrode array experimental set up and timeline of acute experiment drug application.

A) Schematic diagram showing the positioning of the 6 x 10 pMEA array (black dots) over the MHb, demonstrating how anatomical landmarks such as the third ventricle (3V), stria medullaris (SM), lateral habenula (LHb) and fasciculus retroflexus (FR) were used to delineate channels recording with the MHb. **B)** Representative multiunit firing rate histogram of a single channel within the MHb, outlining the drug application protocol for a typical acute experiment. Baseline data was calculated as the average firing rate 30 – 60 min after the start of the recording (green bar). Firing rates were unchanged following application of 10 μM DHβE (blue bar) for 10 min but were rapidly increased in response to 5 μM nicotine with 10 μM DHβE applied for 1 min (orange bar). Following at least 45 min of washout, 5 μM nicotine (purple bar) typically produced a greater increase in firing rate than DHβE+Nic. TTX treatment (burgundy bar) abolished AP firing. Bars correspond to the duration of drug application.
C – G) Corresponding 1 s spiking activity from the same channel as in B, showing firing activity during baseline (C), application of DHβE (D), DHβE+Nic (E), Nic (F) or TTX (G). Spikes were selected if they exceeded the threshold of -17.5 μV (green dashed line).

3.3.5 Data acquisition

Titanium nitride electrodes 30 µm in diameter spaced 100 µm apart allowed parallel recordings from several neurons at once, with action potentials detected through changes in voltage at the electrodes, relative to a low impedance reference electrode. The 6 x 10 grid layout (comprising 59 active recording electrodes) allowed recording from each hemisphere of the MHb, with the other electrodes spread across the stria medullaris (SM), lateral habenula (LHb), fasciculus retroflexus (FR), hippocampus and third ventricle (3V).

For acute recordings, neural activity data was acquired with a sample rate of 25 KHz using MC_Rack v4.5.1 software (MCS GmbH). Time-stamped waveform data was collected in 10 min bins and stored for offline analysis. Spikes were extracted using MC_DataTool v2.6.15 (MCS GmbH): data was filtered (300 Hz high-pass 2^{nd} order Butterworth) and spikes selected if they exceeded the threshold of -17.5 µV.

For long-term recordings, raw activity was similarly collected using MC_Rack v4.5.1 software (MCS GmbH) but signal were sampled at 50 KHz and filtered (200 Hz high-pass 2^{nd} order Butterworth). Spikes that exceeded the threshold of -17.5 µV were extracted as timestamps of 1.5 ms duration. Spontaneous neural activity was acquired continuously for >26 hr to capture a full circadian cycle.

3.3.6 Anatomical locations

Placement of each recording channel in all experiments was confirmed by overlaid reconstructions of the known recording array geometry and histological images. Anatomical landmark brain structures such as the 3V and the white matter of the FR were used to delineate the MHb boundaries (see Figure 3.1A). A conservative approach was employed to ensure that conclusions drawn in this report are based solely on MHb activity (when specified), in particular as the surrounding brain structures such as the LHb are known to exhibit diurnal variation in electrophysiology (Sakhi et al., 2014b; Zhao and Rusak, 2005). Therefore, channels located either on the border regions between MHb and LHb or in the SM / FR were not included in the analysis.

3.3.7 Data analysis and processing

Acute: Data was exported to NeuroExplorer v5.129 (Nex Technologies, USA) to generate 1 s binned firing rate histograms and calculate mean baseline activity for each channel (or later, each isolated unit). Investigations into overall population of activity of the MHb used multiunit activity (MUA) data. Multiunit data underwent further processing to allow isolation of single units through principle components analysis-based spike sorting in Offline Sorter v3.3.5 (Plexon, USA).

This process allows the identification of groups with similar spike waveforms, indicative of the activity of distinct individual neurons generated throughout the duration of the recording. Single unit classifications were validated by reference to interspike interval and cross-correlation analysis. Well isolated units were characterised by a distinct refractory period visible in the interspike interval histogram and independence of the cross-correlograms with other isolated units or clusters of multiunit spikes.

Baseline activity was calculated as the mean number of spikes / s between 30 – 60 min after the recording was started, prior to any drug application (see Figure 3.1B). Channels or units were classed as "active" if the mean baseline activity was greater than 0.05 spikes / s. Drug responses were analysed using 1 s binned MUA or single-unit activity (SUA) histograms with Spike2 v7.09 software (Cambridge Electronic Design, UK) using a custom-written script. The change in activity following drug application was classified as a response if it exceeded 3 standard deviations from the pre-drug firing rate (mean firing frequency of 200s before drug application). Further, the response had to occur within 300s following drug application, but not occur before 100 s (this is the time taken for drug to reach the recording chamber from the infusion syringes). Mean firing frequency over 10 s at the peak of this drug response was used to determine the drug response (peak activity – 200 s baseline activity) for each channel. Nicotine responses were normalized as a fold-change of the 200 s pre-drug mean firing rate. Responses to DHβE+Nic were normalized by calculating the peak as a percentage of the peak of nicotine-evoked activity alone, and were therefore classified as either facilitated (increasing firing activity relative to nicotine alone in response to DHβE+Nic) or suppressed (decreasing firing activity relative to nicotine alone in response to DHβE+Nic).

Long term: Single units were isolated as above using Offline Sorter, following processing using custom Matlab scripts (Mathworks, MA, USA). This yielded a substantial number of units that were located in the LHb as well as the MHb, and so these were further investigated to determine daily electrophysiological activity profiles for this region in addition to the MHb. Evidence of circadian variation in electrophysiological activity was assessed for each unit whereby units were considered "rhythmic" when the firing rate activity pattern was better fit by a sinusoidal wave (with constrained periodicity of 24 - 28 hr) than a first-order polynomial function. Rhythmic units were further processed in Matlab to produce firing rate histograms (using 60 s bins and smoothed with a 1 hr boxcar filter). The bin with the maximal firing activity determined the ZT of peak firing. Data was normalised according to each unit's maximum firing rate. In order to facilitate comparison between long-term and acute recordings, we also calculated the baseline activity of

each channel or unit recorded from the long-term experiments, which was calculated as the mean number of spikes / s between 30 – 60 min after the recording was started. Channels were classed as "active" if the mean baseline activity was greater than 0.05 spikes / s.

3.3.8 Statistical analysis

Data was assessed for normality using the Shapiro-Wilks test and visualization of QQ plots, which revealed that the data was not drawn from a normal distribution. Therefore, non-parametric statistical tests are used throughout. Proportions of response classifications were compared between groups using Fisher's exact test (two-sided) or Chi-square test for groups with more than two categories. Baseline firing rates and drug responses were compared between time points using the Mann Whitney U test, unless comparing more than two groups in which case the Kruskal-Wallis test was used, followed by pairwise comparisons using Dunn's corrections for multiple comparisons. Correlations were examined using Spearman's rank correlation co-efficient, and linear regression was used to determine if relationships between baseline activity and drug-evoked responses were different between time points. Rayleigh analysis was used to calculate the circular median phase and coordination of peak firing. For these plots, the line indicates the phase vector and its length represents significance, and external histograms represent relative population density. Data is presented as the mean ± SEM throughout, both in the text and in the figures. All statistical analysis was performed using GraphPad Prism v9.1.2 (USA) apart from the calculation of Rayleigh plots, which was performed in Matlab.

3.4 Results

3.4.1 Acute electrophysiological recordings from the MHb reveal diurnal variation in spontaneous activity and sensitivity to nicotine

3.4.1.1 *Multiunit activity indicates the MHb is more spontaneously active during the early day than the late day*

To investigate whether time of day influenced the spontaneous electrical activity of the population of MHb neurons, pMEAs were used to record simultaneously from sites spread across the MHb during either the early (ZT1 – 4) or late day (ZT8 – 12). For each recording, between 5 – 9 channels were located within the projected anatomical boundaries of each hemisphere of the MHb. Spontaneous activity could be detected across the MHb, as demonstrated in Figure 3.2A, and in general activity levels were higher within the MHb than the surrounding tissue. During the 30 min period of spontaneous baseline activity, channels within the MHb fired at rates between

0.02 - 23.2 spikes / s, although this range of firing activity was more restricted for MHb channels recorded during the late day (0.00 – 11.0 spikes / s; Figure 3.2B).

The majority of channels within the MHb displayed steady spontaneous neuronal firing rates greater than 0.05 spikes / s which were abolished following the application of TTX, and were therefore classified as "active" channels. During the early day, 96.2 % of channels in the MHb were classed as active, which was a significantly greater proportion than the 81.8 % of channels active during the late day (Figure 3.2C; Fisher's exact test, $p = 0.029$).

Once channels had been classified as active, they were analysed to determine if there was a time of day influence on their baseline firing rates (Figure 3.2D). During the early day, active channels fired with an average frequency of 6.64 ± 0.83 spikes / s ($n = 50$), which was three times higher than the average baseline activity recorded during the late day ($n = 45$; $M = 2.23 \pm 0.44$ spikes /s; Mann Whitney test, $U = 554$, $p < 0.0001$).

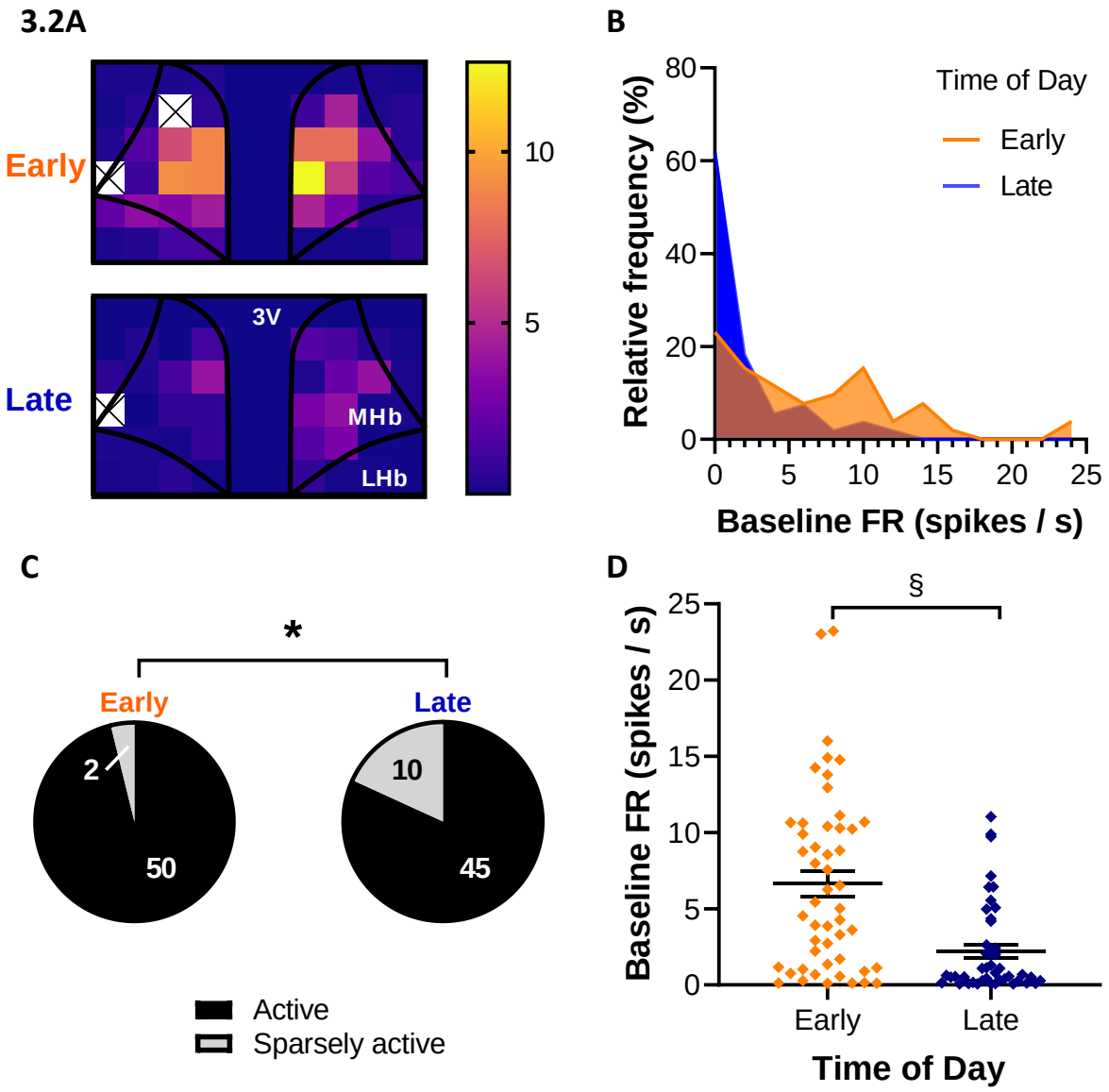

Figure 3.2 The MHb is more spontaneously active during the early day (ZT1–4) than the late day (ZT8-12).

A) Heat map of the average firing rate during the 30 min baseline period for each channel recorded either during the early (top panel) or late day (bottom panel) demonstrating the spatial distribution of spontaneous firing activity across the entire 6 x 10 pMEA array (each square represents the average firing rate for the channel calculated from 4 brain slices per time point). Anatomical landmarks are outlined to demonstrate the positioning of the array. Unfilled squares correspond to either the reference electrode (far left) or a defective channel where no data was collected.
B) Relative frequency histogram displaying the distribution of average baseline firing rates for all channels located within the MHb as a percentage of the total number of recorded channels.
C) A greater proportion of active recording sites (mean baseline firing rates > 0.05 spikes / s) than sparsely active (mean baseline firing rates < 0.05 spikes / s) are detected in the MHb during the early day than the late day (Fisher's exact test, $p = 0.029$).
D) The average baseline firing rate (FR) of active recording sites was significantly higher during the early day ($n = 50$) than the late day ($n = 45$; Mann Whitney test, $U = 554$, $p < 0.0001$).
Data is presented as the mean ± SEM. *, $p < 0.05$; §, $p < 0.0001$.

3.4.1.2 *Nicotine-evoked changes in multiunit activity are higher during the early day than the late day*

Next, we investigated whether diurnal variation could be detected in cholinergic responses across the MHb. Application of 5 µM nicotine alone for 1 min produced an excitatory response in the vast majority of MHb active channels across both time points, as shown in Figure 3.3A. Inhibitory responses were rare, and were only observed in 3 channels recorded during the early day and were absent during the late day. Subsequent analysis therefore focussed exclusively on the excitatory responses to nicotine.

The average peak increase in firing rate evoked by nicotine was significantly higher in the early day (Figure 3.3B; $n = 40$; $M = 73.3 \pm 9.1$) compared to the late day ($n = 35$; $M = 15.2 \pm 2.9$; Mann Whitney test, $U = 253$, $p < 0.0001$). However, when peak responses to nicotine were normalised (peak response divided by the corresponding 200 s pre-drug average firing rate), both time points produced a similar change in activity: channels recorded in the early day increased their firing activity by 6.1 ± 0.9 times their pre-drug activity levels, compared to 4.5 ± 0.6 times during the late day (Figure 3.3C; early, $n = 40$; late, $n = 35$; Mann Whitney test, $U = 539$, $p = 0.088$).

As both nicotine response size and spontaneous baseline firing were both greatest during the early day, we then investigated the correlation between these variables (Figure 3.3D). Spearman's rank correlation co-efficient indicated a significant positive correlation between peak nicotine response and the 200s pre-drug firing rate (early, $n = 40$; $R = 0.88$, $p < 0.0001$; late, $n = 35$; $R = 0.50$, $p = 0.0023$). Linear regression demonstrated that both the slopes and elevations describing the correlation were not significantly different between time points, suggesting the relationship between these factors does not exhibit diurnal variation (slopes, $F = 0.0669$, $DFn = 1$, $DFd = 71$, $p = 0.80$; intercepts, $F = 2.07$. $DFn = 1$, $DFd = 72$, $p = 0.15$).

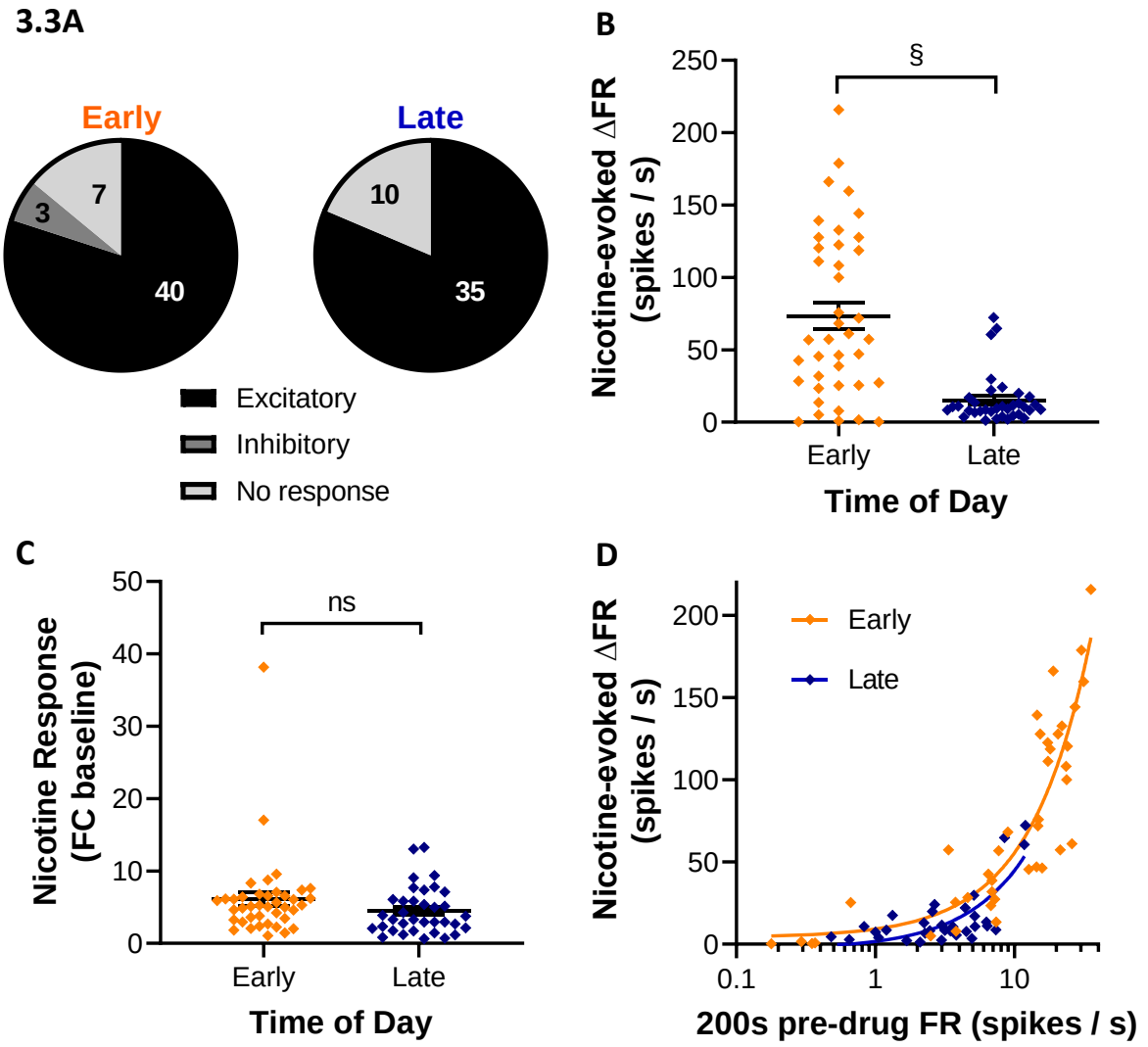

Figure 3.3 Nicotine-evoked responses in multiunit activity are greater during early day and correlate with changes in MHb spontaneous activity.

A) Pie charts showing the proportion of MHb active channels at the early or late day time points that were either excited, inhibited or showed no response to 5 µM nicotine.
B) In the early day (*n* = 40), the average increase in peak excitatory response to 5 µM nicotine was more than double that recorded during the late day (*n* = 35; Mann Whitney test, *U* = 253, *p* < 0.0001).
C) Excitatory nicotine responses for each channel were normalized to show the nicotine response as a fold-change (FC) of the 200s pre-drug firing rate baseline. There was no significant difference between response size to 5 µM nicotine during either the early (*n* = 40) or late day (*n* = 35; Mann Whitney test, *U* = 539, *p* = 0.088).
D) There is significant positive correlation between peak nicotine response and corresponding 200s pre-drug firing rate (early, *n* = 40; *R* = 0.88, *p* < 0.0001; late, *R* = 0.50, *n* = 35, *p* = 0.0023; Spearman's rank correlation). Linear regression indicated that the lines were not significantly different from each other between the early- and late-recorded channels (slopes, *F* = 0.0669, *DFn* = 1, *DFd* = 71, *p* = 0.80; intercepts, *F* = 2.07. *DFn* = 1, *DFd* = 72, *p* = 0.15).
Data is presented as the mean ± SEM. ns, *p* > 0.05; §, *p* < 0.0001; FR, firing rate.

3.4.1.3 *Effect of α4β2 nAChR subunit antagonist DHβE on multiunit activity varies between early and late day*

We also investigated whether particular receptor subunits might be driving the diurnal variation in nicotine response. 10 µM DHβE (an α4β2 nAChR antagonist) was bath applied to the brain slice for 15 min immediately prior to co-application of 5 µM nicotine with 10 µM DHβE for 1 min. DHβE alone did not produce any change in spontaneous activity (as shown in Figure 3.1B).

Channels in the MHb that were excited by nicotine alone also tended to increase spiking activity in response to the cocktail of DHβE+Nic in a similar manner. Likewise, a comparison of the peak response magnitude to DHβE+Nic at both time points also revealed a significant time of day effect (Figure 3.4A), with channels recorded during the early day producing a far greater increase in firing of 49.1 ± 8.9 spikes / s (n = 40) compared to an average response of just 7.0 ± 1.0 spikes / s (n = 35) during the late day (Mann Whitney test, U = 270, p < 0.0001). Similarly to the relationship between nicotine responses and pre-drug firing rate, Spearman's rank correlation indicated that there was a significant positive correlation between the responses to DHβE+Nic and corresponding pre-drug activity (Figure 3.4B), although this was much weaker during the late day (early, n = 40, R = 0.76, p < 0.0001; late, n = 35, R = 0.36, p = 0.034). However, in this case, linear regression indicated that the slopes differed significantly between time points suggesting that the relationship between these variables had altered between the early and late day (F = 4.173, DFn = 1, DFd = 71, p =0.045).

In order to examine the antagonistic effect produced by DHβE, we calculated the size of DHβE+Nic response as a percentage of the peak response to nicotine alone for each channel (Figure 3.4C). Overall, the average effect of DHβE was similar at each time point (Mann Whitney test, U = 671, p = 0.76). During the early day, application of DHβE+Nic produced an average response that was 63.8 ± 5.7 % of the peak response evoked by application of nicotine alone, and during the late day DHβE+Nic suppressed activity to 56.1 ± 3.9 % of the response to nicotine alone.

As can be seen in Figure 3.4C, the majority of channels demonstrated a smaller peak of firing activity in response to DHβE+Nic relative to peak nicotine response (i.e. produced a peak that was less than 100% of the nicotine-evoked peak, "suppressed"). However, there was also a minority of channels which showed a greater nicotine-evoked peak in the presence of the antagonist than without ("facilitated"). The proportion of nicotine-excited channels that were facilitated by DHβE was significantly greater during the early day than the late day (Figure 3.4D; Fisher's exact test, p = 0.0027).

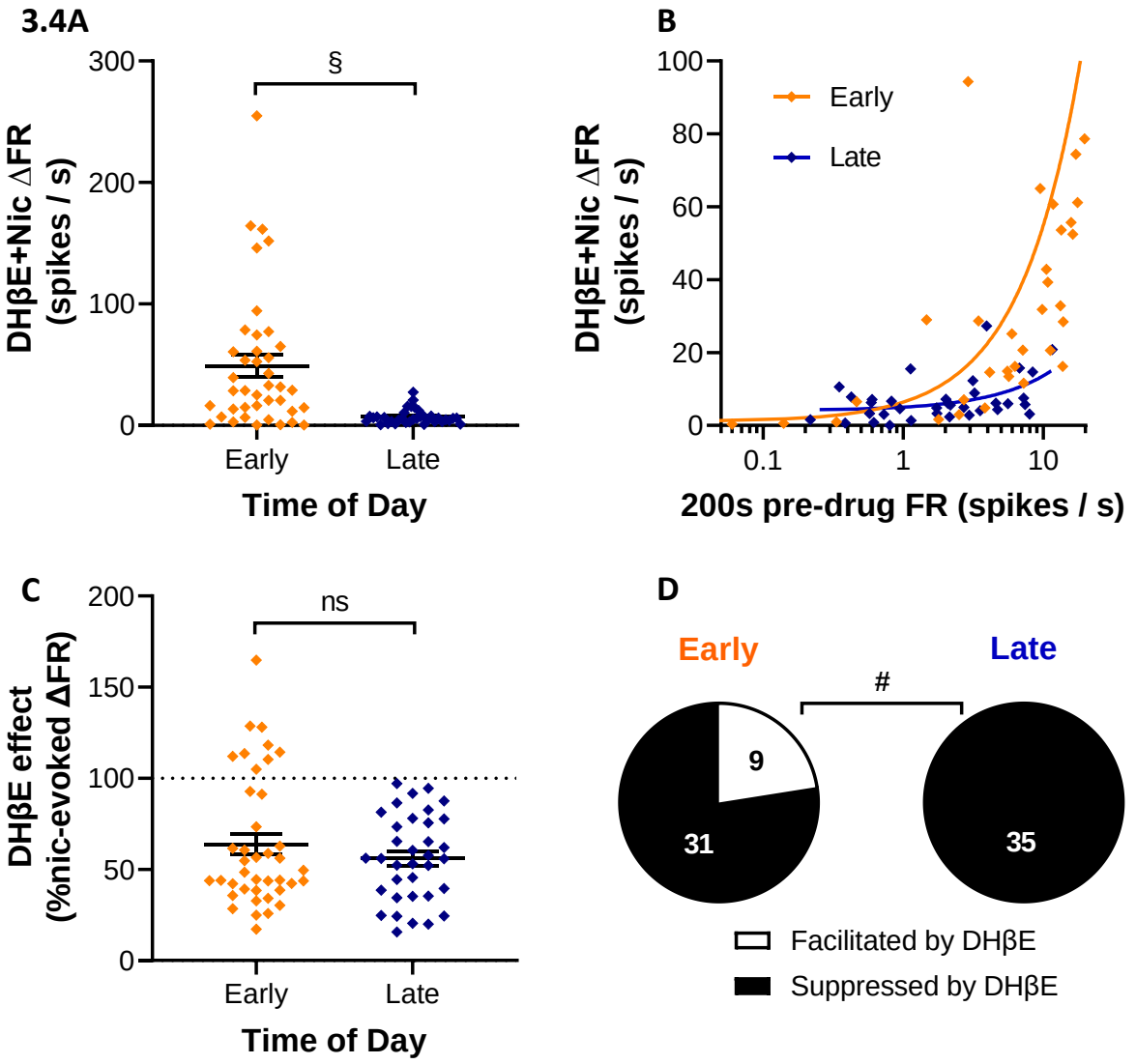

Figure 3.4 Effect of α4β2 nAChR antagonist, DHβE, varies between early and late day. Channels that produced an excitatory response to 5 µM nicotine were analysed to determine how application of 10 µM DHβE would alter this response.

A) Peak increases in firing rate following application of 5µM nicotine + 10 µM DHβE (DHβE+Nic) were greater during the early day (n = 40) than the late day (n = 35; Mann Whitney test, U = 300.5, p <0.0001).
B) There was a significant positive correlation between the responses to DHβE+Nic and the corresponding 200s average pre-drug firing rate, although this was much weaker during the late day (early, n = 40, R = 0.76, p < 0.0001; late, n = 35, R = 0.36, p = 0.034, Spearman's rank correlation). Linear regression indicated that the slopes differed significantly between time points (F = 4.173, DFn = 1, DFd = 71, p =0.045)
C) When the responses to DHβE+Nic were normalized as a percentage of the peak response to nicotine alone, there were no early-late day differences in how the antagonist attenuated nicotine's actions (early, n = 40; late, n = 35; Mann Whitney test, U = 671, p = 0.76).
D) Following application of DHβE+Nic, most channels produced smaller peak excitatory responses relative to peak nicotine response ("suppressed by DHβE"). A minority of channels produced greater peak responses in the presence of the antagonist than without ("suppressed by DHβE") which were only observed during the early day (Fisher's exact test, p = 0.0027).
Data is presented as the mean ± SEM. ns, p > 0.05; #, p < 0.01; § p < 0.0001; FR, firing rate.

3.4.1.4 *Single units isolated from the MHb do not have time of day differences in their spontaneous firing activity or responses to nicotine*

Single unit activity from individual MHb neurons was isolated from the multiunit activity recorded at each channel in order to further characterize the neural activity driving the early / late day differences in spontaneous activity reported above. A total of 69 units were successfully extracted from the 8 experiments previously analysed for multiunit activity. As shown in Figure 3.5A, there was no significant time of day effect on the average baseline firing rates of units recorded during the early day (n = 26; M = 0.86 ± 0.15 spikes / s) compared to the late day (n = 13; M = 1.27 ± 0.31 spikes /s; Mann Whitney test, U = 146, p = 0.51). The proportion of single units recorded in each location was similar between both the early and late day (Figure 3.5B; X^2 (2, N = 69) = 0.77, p = 0.68), with the majority of isolated units located in the MHb. It is interesting to note that despite recording from similar numbers of channels at both time points, we isolated fewer MHb units during the late day, although when we compared the number of units isolated per channel located in the MHb at both time points, this difference did not reach statistical significance (Mann Whitney test, U = 1209, p = 0.09).

The clear majority of units isolated from the MHb showed an excitatory response to nicotine – all but 4 units recorded during the early day (which did not produce a measurable response) increased their firing in response to application of nicotine. There was no time of day influence on the average peak excitatory response to nicotine between the early and late day (Figure 3.5C; early, n = 22; M = 4.47 ± 0.85 spikes / s; late, n = 13; M = 4.06 ± 0.84 spikes /s; Mann Whitney test, U = 126, p = 0.58). Unlike the multiunit activity, only single units recorded during the late day showed evidence of moderate correlation between nicotine-evoked change in firing activity and the corresponding pre-drug firing rate (Figure 3.5D; n = 13; Spearman's rank correlation, R = 0.66, p = 0.016). Units recorded during the early day showed only weak, non-significant correlation (n = 22; Spearman's rank correlation, R = 0.40, p = 0.064).

DHβE antagonist in combination with nicotine produced an excitatory response in all but one unit, in which it produced an inhibitory effect. Comparison of the change in firing evoked by a cocktail of DHβE+Nic between time points (Figure 3.5E) indicated that the average peak responses were similar across both early (n = 22, M = 4.65 ± 1.08 spikes / s) and late day (n = 13, M = 2.92 ± 0.56 spikes / s; Mann Whitney test, U = 136, p = 0.83). Each DHβE+Nic response was normalized as a percentage of the peak nicotine-evoked response, there was no indication of time of day effect on the average DHβE effect (Figure 3.5F; early, n = 22; M = 112.9 ± 18.0 %; late, n = 13; M = 74.3 ± 15.9 %; Mann Whitney test, U = 112, p = 0.30). DHβE antagonism produced both suppressed and

facilitated responses relative to the peak evoked by nicotine alone, with similar proportions of responses across the early and late day (Figure 3.5G; Fisher's exact test, p = 0.49).

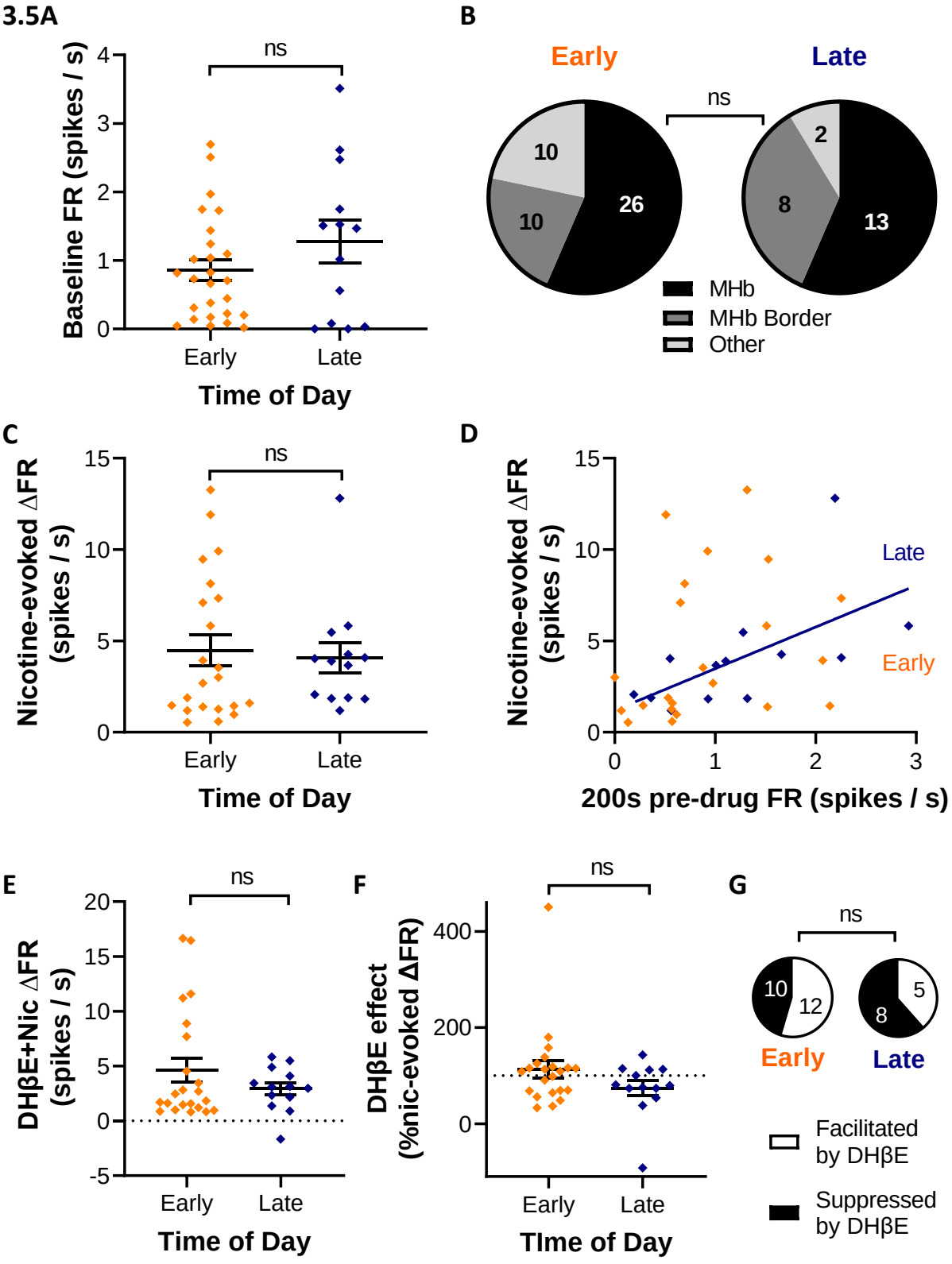

Figure 3.5 Single units isolated from the MHb do not show diurnal variation in spontaneous firing rates or nicotine-evoked responses.

A) There was no significant difference between average baseline firing rates from single units isolated in the MHb during the early (*n* = 26) or late day (*n* = 13; Mann Whitney test, *U* = 146, *p* = 0.51).
B) The proportion of single units recorded in each location was similar between the early and late day (X^2 (2, *N* = 69) = 0.77, *p* = 0.68).
C) Analysis of peak firing rates of units in response to 5 µM nicotine alone showed there was no difference between time points (early, *n* = 22; late, *n* = 13; Mann Whitney test, *U* = 126, *p* = 0.58).
D) There was moderate correlation between nicotine-evoked firing activity and the corresponding 200 s average pre-drug firing rate only for units recorded during the late day (*n* = 13; Spearman's rank correlation, *R* = 0.66, *p* = 0.016), whereas units recorded during the early day displayed only weak, non-significant correlation (*n* = 22;*R* = 0.40, *p* = 0.064, Spearman's rank correlation).
E) There was no significant difference between DHβE+Nic-evoked increase in firing across time points (early, *n* = 22; late, *n* = 13; Mann Whitney test, *U* = 136, *p* = 0.83).
F) Responses to DHβE+Nic were normalized as a percentage of the peak response to nicotine alone. There were no early-late differences in how the antagonist altered the average firing activity of isolated MHb units (early, *n* = 22; late, *n* = 13; Mann Whitney test, *U* = 112, *p* = 0.30)
G) Units were classified as either facilitated or suppressed by DHβE depending on whether they produced a larger or smaller peak response to the cocktail of DHβE+Nic relative to nicotine alone. There were equal proportions of responses at each time point (Fisher's exact test, *p* = 0.49).
Data is presented as the mean ± SEM. ns, *p* > 0.05

3.4.2 Long-term (>24 hr) electrophysiological recordings from MHb neurons demonstrate individual neurons are rhythmic but phase is reset *ex vivo*

3.4.2.1 *Single units isolated from the MHb exhibit a variety of daily profiles in electrophysiological activity*

Having demonstrated evidence for diurnal variation in spontaneous firing activity in acute recordings, we next sought to assess whether individual MHb neurons displayed circadian variation in their firing activity when recorded continuously for over 24 hr. In order to investigate whether slice preparation time influenced individual neuronal properties, we started recording from tissue either during the light phase (ZT3 – 6, "light start") or the dark phase (ZT13 – 15, "dark start"). A total of 70 cells from 6 experiments were collected from light start experiments, and 40 cells from 3 experiments were collected from dark start experiments. The majority of isolated cells were located in the MHb (see Figure 3.6A) although we also managed to record from a substantial number of units located within the LHb. As the LHb is also known to exhibit circadian variation in electrical activity (Park et al., 2017; Sakhi et al., 2014b), we also investigated how neurons in this brain structure varied their firing activity over the day. The majority of isolated units met our criteria and were thus classified as "rhythmic", with similar proportions of cells exhibiting rhythmic properties in both the MHb and the LHb (Figure 3.6B; MHb, 73.3% rhythmic;

LHb, 56.8% rhythmic; Fisher's exact test, p = 0.122). As illustrated in Figure 3.6C – D, daily electrophysiological profiles of MHb neurons were not restricted to a single pattern of firing activity.

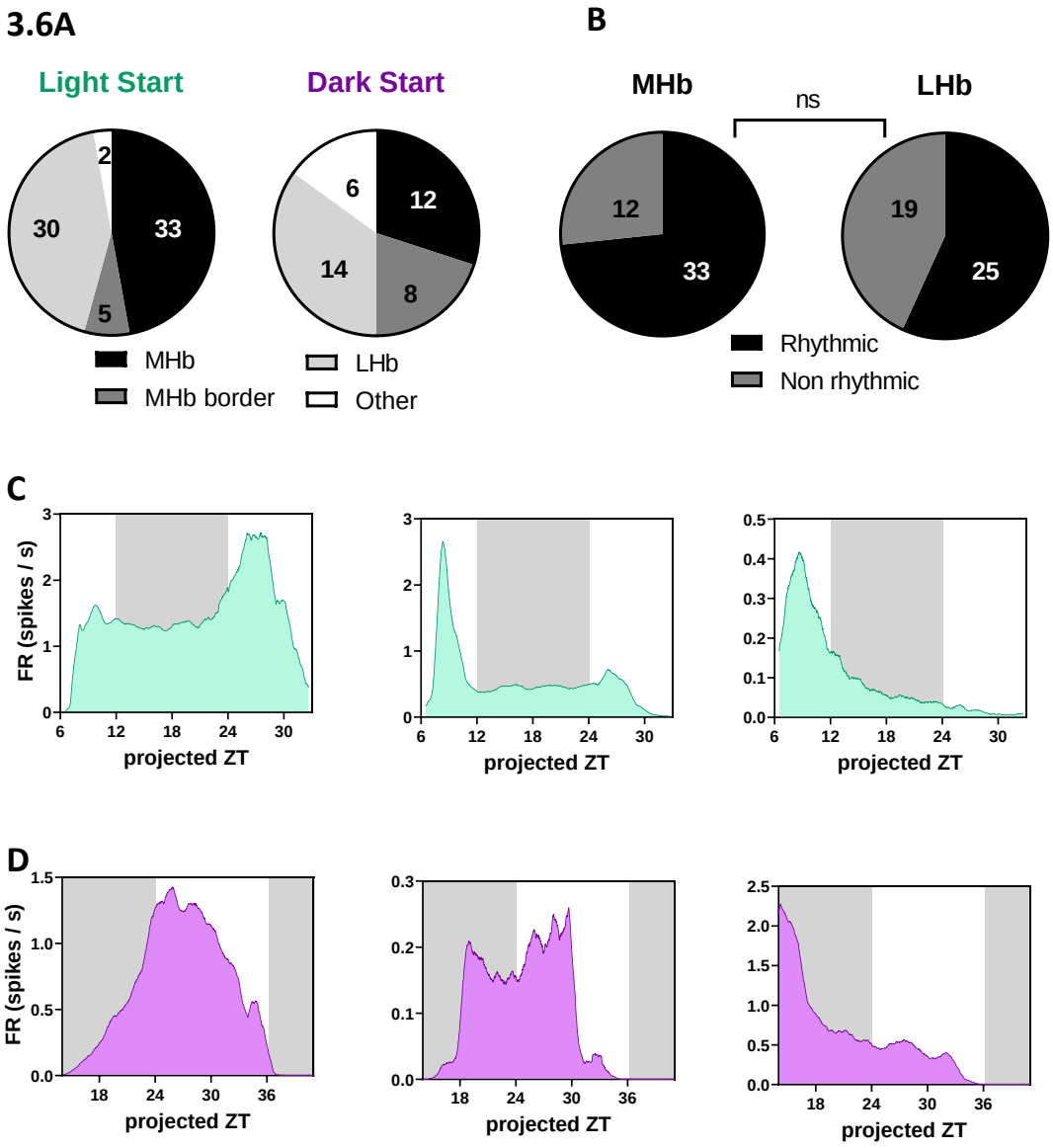

Figure 3.6 MHb neurons exhibit a wide variety of daily profiles in electrophysiological activity.

A) A total of 123 units were isolated from 9 experiments (6 light start and 3 dark start), with distributions of unit location demonstrated in the pie charts.
B) Proportion of isolated MHb and LHb cells displaying evidence of circadian variation in firing (classified as rhythmic) were compared Fisher's exact test (p = 0.1226).
C - D) Example long-term spontaneous firing activity profile of individual MHb neurons from slices prepared during the light phase (C, top three panels) or dark phase (D, bottom three panels) of the animals projected day. Shaded panels indicate the dark phase.

3.4.2.2 *MHb and LHb rhythmic activity is dependent on the time of slice preparation*

We next sought to determine how the cohort of rhythmic units might function as a population to produce a coherent rhythm in activity. As illustrated in Figure 3.7A-B, peak firing appeared to be antiphasic between slices where recording began in the light phase and those started during the dark phase. Rayleigh analysis revealed that units from slices where recording started during the light phase showed significant clustering of peak firing at ZT7.9 (Figure 3.7C; n = 22; R = 0.55, p = 0.00075), whereas units from slices where recording was started during the dark phase did not exhibit significant clustering of peak firing (Figure 3.7D; *Mdn*= ZT 19.7; n = 11; R = 0.46, p = 0.093). Hence, peak firing occurred approximately 4 hours after the start of the experiment in both cases, regardless of projected time of day.

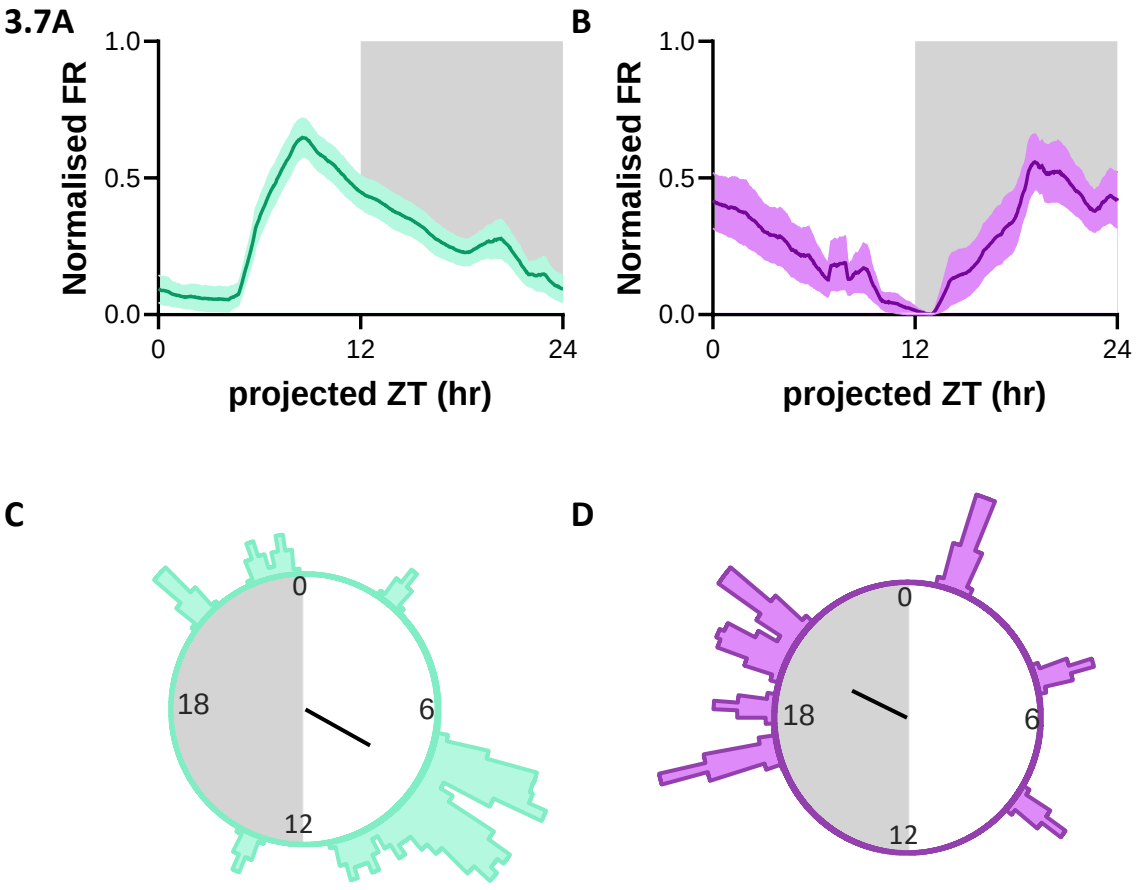

Figure 3.7 Rhythmic MHb units reset their phase following slice preparation. Long term MEA recordings were started either during the light phase (ZT3 - 6) or dark phase (ZT13 – 15).

A – B) Mean ± SEM normalised 24 hr firing rate profiles of rhythmic MHb isolated units from experiments started during the light phase (A) or dark phase (B). Shaded panels indicate the dark phase.
C – D) Rayleigh plots showing phase distribution for isolated MHb cells that exhibited evidence of circadian variation in firing from (C) light start experiments (n = 22; *Mdn* = ZT7.9; Rayleigh analysis, R = 0.55, p = 0.00075) or (D) dark start (n = 11; *Mdn* = ZT19.7; Rayleigh analysis, R = 0.46, p = 0.093. External histograms represent relative population density. Peak firing was seen approximately 4 hr after starting the experiment in both cases.

Similarly, when we examined the long-term electrophysiological profiles of units located in the LHb, light start and dark start experiments had peak firing rates that were antiphasic to each other (Figure 3.8A-B). Units from recordings started during the light phase had significant clustering of peak firing at ZT11.0 (Figure 3.8C; n = 14; Rayleigh analysis, R = 0.59, p = 0.0072). However, LHb units from experiments started during the dark phase had non-significant clustering, with the median phase of peak firing at ZT23.8 (Figure 3.8D; n = 11; R = 0.64, p = 0.0014, Rayleigh analysis). Peak firing was reached approximately 6 - 10 hr after the start of the experiment for both experiments started in the light phase and those started in the dark phase.

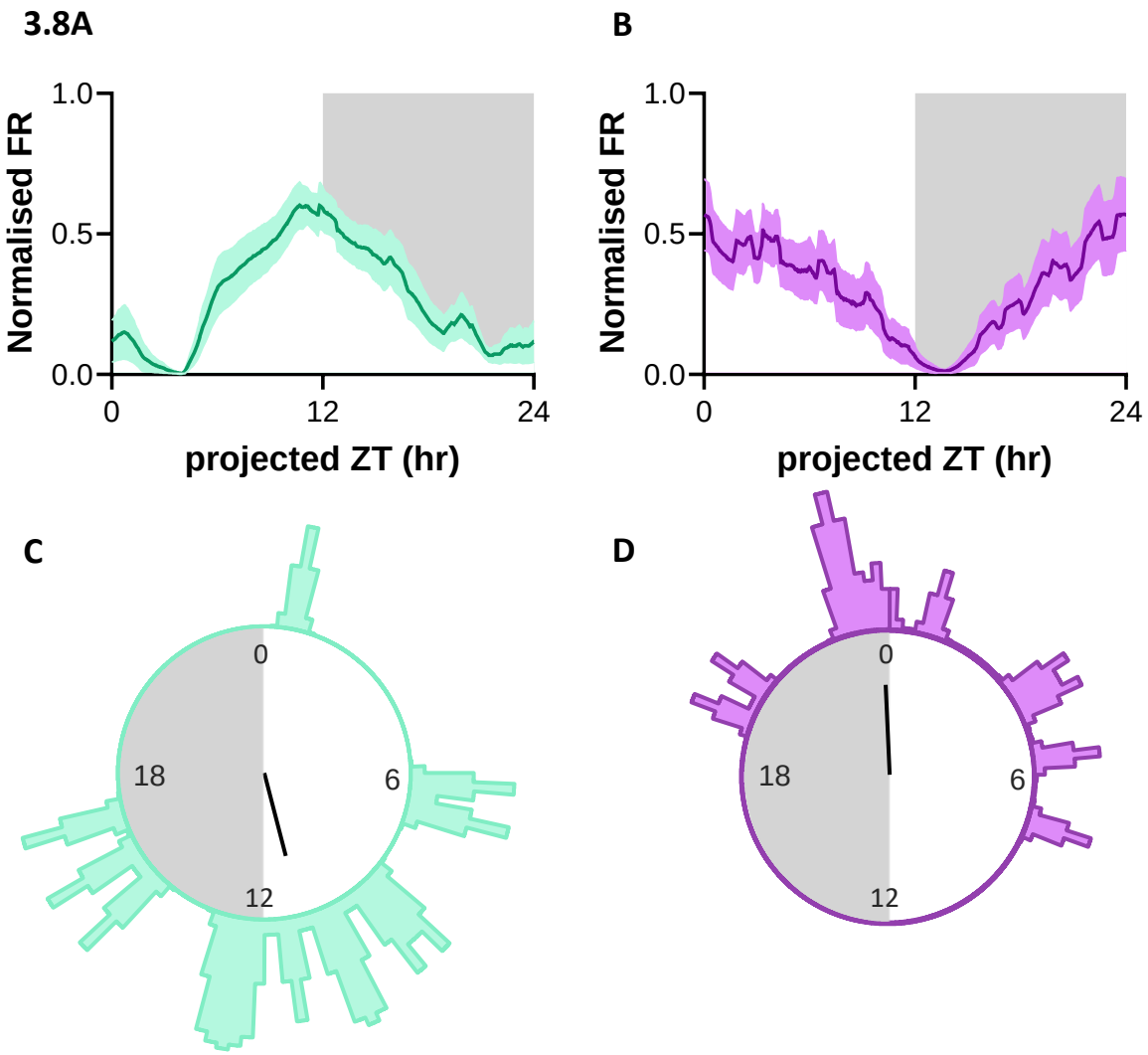

Figure 3.8 Rhythmic LHb units reset their phase following slice preparation. Long term MEA recordings were started either during the light phase (ZT 4.5 - 6.5) or dark phase (ZT 13.5 – 15).

A – B) Mean ± SEM normalised 24 hr firing rate profiles of rhythmic LHb isolated units from experiments started during the light phase (A) or dark phase (B).
C – D) Rayleigh plots showing phase distribution for isolated LHb cells that exhibited evidence of circadian variation in firing from (C) light start (*Mdn* = 11.0; n = 14; R = 0.59, p = 0.0072) or (D) dark start (*Mdn* = 23.8; n = 11; R = 0.64, p = 0.0014). External histograms represent relative population density. Peak firing was seen approximately 6 - 10 hours after starting the experiment.

3.4.2.3 *Diurnal variation in MHb spontaneous activity is apparent during the first hour of recording in long-term recordings*

It appears that in long-term recordings, electrophysiological rhythms may be reset *ex vivo*. Therefore, in order to try and identify whether the rhythms remain coherent over the timeframe used for the acute experiments, we extracted spontaneous firing activity from MHb channels recorded during long-term experiments. Average firing rates were calculated for each channel between 30 - 60 min after the recording was started, in the same way we calculated baseline firing rates for acute experiments. Similarly, we also calculated the average firing activity of individual MHb units isolated from the long-term recordings during this period (Figure 3.9A) The Mann Whitney test indicated that the baseline firing rates of MHb units were significantly higher during the mid morning (ZT3.5 – 6.5; n = 22; M = 0.93 ± 0.27 spikes /s) compared to the early night (ZT13.5 – 15.5; n = 11; M = 0.38 ± 0.23 spikes / s; Mann Whitney test, U = 61.5, p = 0.022).

Finally, we compared the baseline firing rates recorded from active channels (firing rates > 0.05 spikes/s) in the MHb during long-term recordings with those collected during the acute experiments. As illustrated in Figure 3.9B, there was clear indication of significant variation in average firing rates across the day from the multiunit activity. Firing rates were significantly higher during the early day (ZT1 – 2) compared to all other time points (Kruskal-Wallis test, H = 21.4, p <0.0001; ZT3.5 – 6.5, p = 0.012; ZT8 – 10, p = 0.0006; ZT13.5 – 15.5, p = 0.002; Dunn's multiple comparisons test), but there were no other significant differences detected.

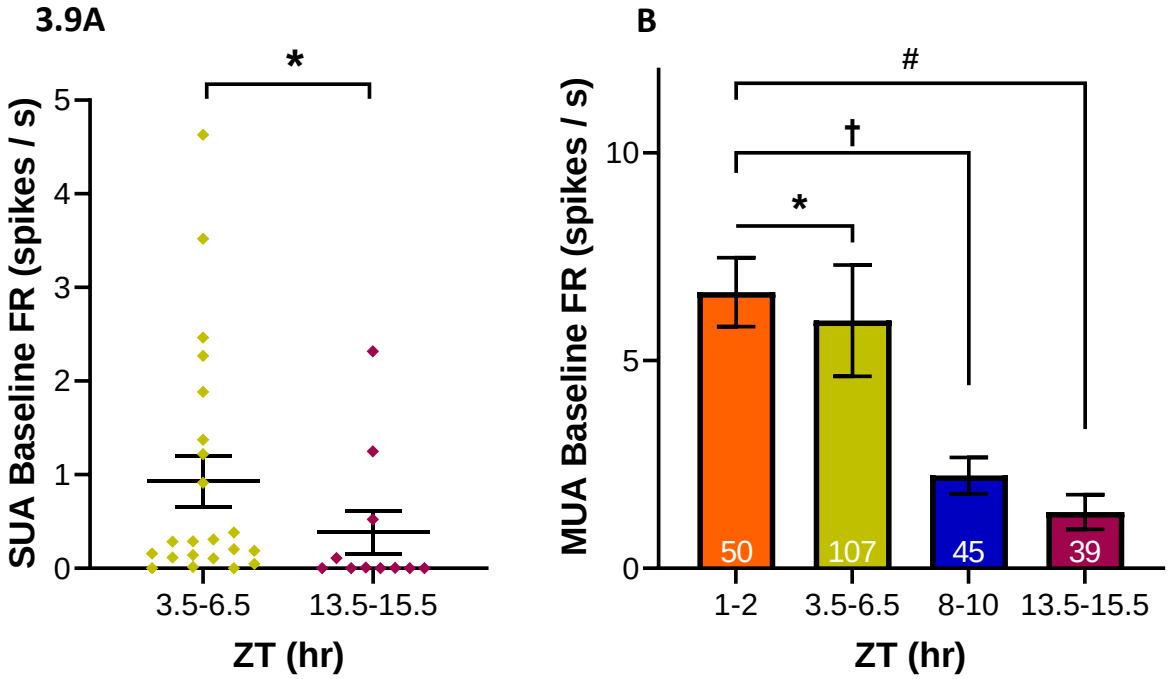

Figure 3.9 Diurnal variation in MHb firing rates is apparent 30 – 60 min after recording starts. Baseline firing rates corresponding to 30 – 60 min after recordings were started were collated from both acute and long-term experiments.

A) Average firing rates were calculated either for individual cells located in the MHb during long-term experiments started in the mid morning (ZT3.5 – 6.5) or early night (ZT13.5 – 15.5). The average baseline firing rate of the single unit activity (SUA) was significantly higher during the mid morning (n = 22) than the early night (n = 11; Mann Whitney test, U = 61.5, p = 0.022.

B) MHb baseline firing rates from multiunit activity (MUA) were significantly higher during the early day compared with all the other time points (H = 21.4, $p < 0.0001$, Kruskal-Wallis test; Dunn's multiple comparisons test). The number of MHb channels contributing to each time point are indicated in white font on the bar graph.

Data is presented as the mean ± SEM; *, $p < 0.05$; #, $p < 0.01$; †, $p < 0.001$.

3.5 Discussion

A number of brain structures show circadian variation in their electrophysiological properties (Begemann et al., 2020; Paul et al., 2020). Previous work has suggested that neurons in the MHb may also exhibit circadian rhythmicity in their bioelectric properties but this has been determined primarily through discontinuous sampling of individual neurons with patch clamping *in vitro* (Sakhi et al., 2014a) and extracellular recordings *in vivo* (Zhao and Rusak, 2005). The pMEA presents a powerful tool to capture both spatial and temporal information from the cohort activity of many neurons simultaneously, and therefore we set out to build on the work by Zhao and Sakhi and further characterise the daily electrophysiological profile of MHb neurons, investigating both the network multiunit activity as well as examining the behaviour of individual MHb neurons. In addition, there is evidence for rhythmicity in cholinergic signalling (Hut and Van der Zee, 2011) and as the MHb is a neural structure known for its dense nAChR expression, we sought to further examine the diurnal variation of cholinergic signalling within the MHb.

Here, we provide further evidence that the MHb has diurnal variation in electrophysiological activity, such that spontaneous firing activity of the neuronal population is greater in the early day than the late day. This is mirrored by an increased sensitivity to nicotine during the early rather than late day. By analysing the activity of individual neurons from this same population, it appears that this diurnal variation in spontaneous firing activity may be driven by the availability of a greater number of active neurons during the early day than in the late day, as well as an underlying change in firing rates within individual neurons. Interestingly, we find that a significant subset of MHb neurons exhibited long-term daily electrophysiological profiles consistent with circadian modulation, but the phase of the rhythm appeared to be dependent on the time elapsed since the start of the recording, rather than on the projected time of day. Since a day-night variation in firing consistent with that seen in earlier acute recordings was detected when an equivalent time window was used for analysis (30 – 60 min post start of recording), it seems the MHb rhythmic activity is rapidly reset under *ex vivo* recording conditions. Nonetheless, together, these results firmly indicate that the MHb and its response to cholinergic signals are subject to circadian modulation.

3.5.1 MHb neurons are spontaneously active and show rhythmicity in their spontaneous activity

This study demonstrated that across both the early and late day, cells within the MHb are spontaneously active, with the vast majority of the recording sites located within the MHb

detecting average spontaneous firing activity above 0.05 spikes/s. This is largely in agreement with previous studies which show that MHb neurons fire action potentials spontaneously (McCormick and Prince, 1987) and have measured the resting firing frequency of cells in the MHb to be between 0.5 and 12 spikes/s through extracellular and whole cell patch recordings (Kim and Chung, 2007). However, the frequency of firing we observed in the multiunit recordings tended to be on the lower end of this range as were the firing rates of the individual units we isolated.

One of the primary aims of this study was to build on work previously carried out by Sakhi et al who examined the electrical activity of cells in the MHb and found evidence for circadian rhythmicity in some of the bioelectric properties of neurons they classified as spontaneously active (discharging action potentials) (Sakhi et al., 2014a). They found evidence that firing rates among spontaneously active neurons was lowest during the early day but also found a clear rhythm in the proportions of cells in different spontaneous states (i.e. silent or firing), with fewer active neurons during the mid to late day. Unlike Sakhi et al, in this study we did not find a significant difference in the firing rates of individual MHb cells between early and late day. However, our data is consistent with the idea that the proportion of active cells changes over the circadian day: we found multiunit firing rates were higher during the early day and were also able to isolate more cells at this time point. Examination of the spontaneous firing rates of cells recorded from our long-term recordings also adds to this picture. Individual MHb cells had significantly greater firing activity during the mid-late morning compared with the early night, but mutiunit firing rates were unchanged between these two time points. Together this once again indicates that the overall diurnal variation in spontaneous activity of the MHb is not driven just by the change in excitability of individual cells, but that the rhythmic recruitment of active neurons is also a significant underlying factor. Of course, we cannot entirely rule out the possibility that the differences we see in the acute window are not just reflecting differential effects of resetting from the tissue collection occurring at different times of day, rather than reflecting the light history of the animal. Further experiments *in vivo* to examine if there is a rhythm in spontaneous neuronal firing activity and the phase of this activity would help to address this concern.

It should be noted that the pMEA method used in this study to generate this finding is based on ensemble activity of multiple neurons located near to the recording electrodes, whereas patch clamp experiments are based on sampling individual neurons. Sakhi et al found higher average firing rates (between 3 - 9 spikes / s) than those reported here. One limitation of recording electrophysiological activity using pMEAs is that spike sorting technologies as used in this paper can be less likely to isolate neurons with very low firing rates and instead favour frequently firing

neurons (Shoham et al., 2006). The latter is mainly an issue for very short duration recordings since it is really the number of spikes representative of a particular neuron rather than the rate *per se* which will influence how readily it can be detected. However, certain types of high firing neurons may also be harder to isolate, especially those where burst firing results in changes in extracellular spike shape. Conversely the patch technique may also bias sampling towards certain type of neurons that are easier to record from (e.g. larger cells). Hence, the overall makeup of the neural populations sampled here, could in principle differ from those contributing to data from Sakhi et al. Alternatively the patch recording technique may acutely modulate cell activity due to the associated physical disturbance of the cells and their surroundings which could account for the generally higher firing rates reported previously.

A further caveat for consideration based on the use of pMEAs in these experiments is how independent each channel truly is. In this study, we have treated individual channels as independent observations for our statistical approach, as is the convention in electrophysiological neuroscience (Society for Neuroscience, 2018). Colleagues Hanna et al performed pMEA recordings on SCN tissue slices with an experimental setup very similar to that used here (Hanna et al., 2017). Based on the known cytoarchitecture and firing rates of the SCN in comparison with their own data, they estimated the range of detection of each recording electrode to be <17 μm, well within the interelectrode distance of the 6 x 10 pMEAs (100 μm). Therefore, we can treat the signals detected at each channel as representative of distinct groups of neurons. However, these channels are not completely independent from each other. All channels recorded during a single experiment will be inherently reliant on the electrophysiological activity, quality and condition of the brain slice. To account for the possibility that differences across individuals were driving the outcomes measured, we also averaged across all channels/units recording in a single animal, and saw similar variance in the data between early and late conditions. We also examined how individual channels and units from each animal were contributing to the pooled data, and we saw no evidence that any particular experiment was driving the outcomes reported here. Therefore, we are confident that our statistical approach as used in this report was appropriate.

3.5.2 MHb neurons can sustain rhythmic patterns in their firing activity independent of the SCN

Although we did not find significant differences in the spontaneous firing rates of individual neurons when we compared between early and late day, we did find a significant reduction in firing activity of MHb cells during the early night compared to the mid-late morning. This suggests that cells in the MHb vary their average firing activity across the circadian day. This is further

supported by our finding that the majority of MHb cells isolated from long-term recordings had capacity for rhythmic variation in their spontaneous activity, even in the absence of input from the SCN, the master clock. This is consistent with previous work that demonstrates SCN-independent rhythmic activity in hypothalamic brain regions (Guilding et al., 2009).

Whilst rhythms in neuronal activity in MHb neurons are apparent in the acute recordings, it appeared that long-term rhythms we observed in this report were reset by the experimental procedure, rather than being driven according to the projected time of day. This suggests that the rhythms observed may well originate with cell intrinsic processes, or possibly inputs from local oscillatory sources, but *in vivo*, the MHb may be reliant on input from an upstream timekeeping structure to deliver signals about the time of day to keep the local rhythmic processes in sync. Previous work has successfully used long-term pMEA recordings to demonstrate rhythmic capacity of non-SCN neuronal populations where firing rate activity rhythms remain aligned with the projected time of the circadian clock (Hanna et al., 2017; S. Paul et al., 2020), although it should be noted that in these cases rhythmic cells have maintained input from the SCN in the tissue slice. The 'resetting' of rhythmic structures following separation from the SCN is a phenomenon which has been described by Harding et al, who similarly found rhythmic neural activity in the hypothalamus and thalamus that were reset by the experiment (Harding et al., 2020). This has also recently been demonstrated to be the case in the lateral geniculate nucleus (Chrobok et al., 2021), indicating that this may be a common feature of extra-SCN oscillators in the absence of direct SCN input. Further, this process of resetting may offer an explanation as to why Zhao and Rusak were unable to find evidence of rhythmicity in their *in vitro* experiments: their approach used data recorded over 24 hr from slices prepared 12 hr apart (Zhao and Rusak, 2005). If the MHb is similarly resetting in rat MHb as it was in our experiments with mouse MHb, they would likely see no rhythms due to the tissue resetting. We speculate that had they not pooled this data, they may have found population rhythms in 'day' and 'night' slices that were in antiphase as in our experiments.

It has been proposed that the LHb receives time of day information through indirect projections from the SCN via the dorsomedial hypothalamus (Stamatakis et al., 2016), or through hormone output (Baño-Otálora and Piggins, 2017) which could be similar routes by which the MHb remains entrained to external time. Alternatively there is evidence that some neurons in the MHb are photoresponsive (Zhao and Rusak, 2005), and may therefore receive information about the time of day through indirect projections from the retina (Baño-Otálora and Piggins, 2017). Therefore, it

remains to be seen how the rhythmic activity of these neurons behaves *in vivo*, when working with the cohort of time giving signals from across the brain.

Whilst the MHb and LHb largely remain morphologically and functionally distinct, both structures have evidence of rhythmicity (Baño-Otálora and Piggins, 2017). Interestingly, connectivity between these structures is asymmetrical, with a unidirectional projection from the MHb to the LHb (Kim and Chang, 2005). It has been suggested that that MHb may be modulating the clock in the LHb through this output (Baño-Otálora and Piggins, 2017). Indeed, one study investigating the rhythmic expression of *Per2* actually found that explants containing both the LHb and MHb produced stronger rhythms than LHb alone (Landgraf et al., 2016). Certainly the evidence presented in this report does not rule out the possibility of the MHb modulating LHb rhythms: although both LHb and MHb appeared to reset their rhythmic activity *ex vivo*, the LHb phase of peak activity was consistently within four hours of MHb peak phase in both experiments started during the light phase and the dark phase. Similarly, in work presented across two papers by Sakhi et al, they show that peak firing rates for LHb neurons and MHb active neurons was during the late day, and the nadir in activity was during the early day for both tissues (Sakhi et al., 2014a, 2014b). Further experiments are needed to explore whether the MHb can modulate LHb rhythmic activity, or if both structures are reliant on a common upstream oscillatory structure.

3.5.3 There are time of day influences on responses to nicotine in the MHb

The MHb is involved in signalling the aversive properties of nicotine (Frahm et al., 2011; McLaughlin et al., 2017), including withdrawal symptoms (Görlich et al., 2013; Pang et al., 2016) which interestingly also vary over the circadian day (Perkins et al., 2009). Therefore, we set out to determine whether the nicotinic pharmacological properties of this area exhibited diurnal variation. Our data reveal time of day variation in response to nicotine, with greater activation during the early day than in the late day. After smoking a cigarette, nicotine concentrations in human arterial blood can peak at 100 ng / mL (0.6 µM), depending on how intensely the cigarette is smoked (Benowitz et al., 2009; Gourlay and Benowitz, 1997; Henningfield and Keenan, 1993; Matta et al., 2007; Rose et al., 1999). The concentrations used in this experiment then are only ten-fold higher than the levels associated with smoking, and therefore the results described in this report are likely to be physiologically relevant.

Previous patch clamp studies examining how nicotine alters neuronal activity of MHb neurons demonstrated that both brief local puff application and bath application of nicotine produced increased neuronal firing in all neurons, distributed across the entire MHb structure (Lee et al., 2018). Unsurprisingly, this study confirms that the majority of channels recorded during both

early and late day altered their population firing activity in response to nicotine. This is consistent with previous studies which estimate 90 – 100 % of neurons in the MHb to express nAChR mRNA (Sheffield et al., 2000).

Importantly, this study demonstrated that nicotine application produced a greater increase in multiunit firing activity in the early day than the late day, and this was related to the underlying activity of the neuronal populations sampled: greater spontaneous activity levels were associated with larger responses to nicotine. Evidence from the isolated MHb cells indicate that individual neurons had similar firing rates between time points and firing activity in response to nicotine was similar. Therefore, the overall population effect of increased response to nicotine during the early day may be due to a recruitment of more active neurons, presenting the intriguing possibility that nAChR-expressing neurons in particular are alternately silent and then activated at specific times of the day.

In addition, evidence from the isolated MHb cells indicates that the relationship between the spontaneous activity of the cells and their response to nicotine changes between early and late day. This suggests that the pharmacological mechanisms driving these responses to nicotine might also be changing over the day. For example, this could be due to a rhythmic upregulation in nAChR expression, which has previously been reported in the basal hypothalamus (Morley and Garner, 1990) and dorsolateral SCN (Fuchs and Hoppens, 1987) of the rat through α-bungarotoxin binding site experiments, but is yet to be further explored elsewhere in the brain (Hut and Van der Zee, 2011).

In the experiments presented here, we found significant differences in the absolute change of firing rates of our neuronal population in response to nicotine, but we did not see significant time of day differences when the responses were normalised to the underlying activity of the tissue. Both measurements are important as they give different information about the underlying neural activity. However, in the broader context of considering how the MHb is involved in mediating some nicotine behaviours, perhaps it is most important that we see variation in the absolute response to nicotine between timepoints. If, for example, we saw a larger fold-change in response to nicotine in the late day, this would indicate a time of day difference in the mechanisms mediating this response – but a greater fold-change response of a neuron with low firing activity still equates to a small electrical signal. As yet there is no indication that the main target region of the MHb, the IPN, is a rhythmic structure, so it could be argued it is the absolute firing rate of neurons in the MHb that is most important for signalling diurnal variation to the downstream network. Our experiments suggest that MHb neurons exhibit diurnal variation in how they

respond to nicotine, and thus would have time of day dependent output signals to the downstream reward circuitry.

3.5.4 α4β2 nAChRs may differentially contribute to nicotinic signalling depending on the time of day

Multiple different nAChR subtypes have been functionally demonstrated in the MHb, with different subunits exhibiting different expression patterns across the MHb (although largely absent from the dorsal portion of the MHb; Shih et al., 2014). Therefore, the responses evoked by nicotine in this study are likely the aggregate responses of multiple nAChR subtypes. α4 subunit containing nAChRs are thought to be important for mediating some of the effects of nicotine, including sensitization (Tapper et al., 2004) and reinforcement (Exley et al., 2011; Pons et al., 2008) and are functionally expressed in the MHb (Fonck et al., 2009). In addition, the β2 subunit is also thought to mediate the anxiolytic effects on nicotine (Anderson and Brunzell, 2015). Therefore we also investigated how these nAChR subunits might contribute to the daily variation in nicotine signalling, through application of DHβE (a nAChR antagonist with moderate selectivity for the α4β2 nAChR).

As discussed, peak multiunit responses evoked by nicotine alone were well correlated with the pre-drug firing rate at both time points, and this relationship remained unchanged following the application of DHβE in the early day. However, during the late day, multiunit responses to DHβE+Nic were no longer as well correlated with the pre-drug activity levels, suggesting that blocking the actions of α4β2 nAChRs may have altered this relationship. In addition, we also saw that during the early day, the application of DHβE actually facilitated some of the nicotine-evoked multiunit responses, and this effect was not observed during the late day. Taken together, these results point towards the possibility that α4β2 nAChRs may have different actions between the early and late day.

It remains unclear how this nAChR subunit might alter the relationship between MHb spontaneous activity and responses to nicotine between the early and late day. Whilst the vast majority of isolated MHb neurons were excited by nicotine, blocking α4β2 nAChRs resulted in both increased and suppressed activity in firing relative to nicotine alone. This suggests that α4β2 nAChRs simultaneously act to regulate both excitatory and inhibitory signals in the tissue, either through direct postsynaptic activation or presynaptic modulation of other neurotransmitters, and depending on the synaptic connections across this network, further highlighting the complexity of nicotinic signalling within this structure. The proportion of these responses was similar at both time points, so as yet there is no indication that a particular subgroup of α4β2 nAChRs are

changing their activity over the course of the day. Further, as MHb neurons do not appear to alter their firing activity in response to DHβE+Nic according to the time of day, it seems unlikely that this underlying change in nicotine response behaviour observed during the late day following α4β2 nAChR block is due to an intrinsic decrease in sensitivity. Instead, it seems likely that as the number of active neurons are recruited, it does so with the proportion of α4β2 nAChR expressing neurons increasing too.

It is known that α4-containing neurons are restricted to the most ventrolateral portion of the MHb (Shih et al., 2014). The small size of the MHb means that even with the fine spatial resolution offered through the use of the pMEA technology, we were unable to accurately and reliably assign particular channels to this anatomical location. Future experiments to observe how neurons that are excited or inhibited by the block of α4 nAChRs are spatially distributed across the MHb could help tease out a population of MHb neurons which might be driving these diurnal changes.

3.5.5 **Summary and Conclusions**

Collectively, our data provide further evidence of diurnal variation in MHb neuronal activity, firmly cementing its importance as a circadian oscillator. We demonstrate that this variation is driven both through rhythmic oscillation of action potential firing frequency within individual MHb neurons, as well as the differential recruitment of silent and active neurons from this brain structure depending on the time of day. Furthermore, we show that there is a corresponding time of day influence on responses to nicotine within the MHb, and that the α4β2 nAChR subunit may well alter the relationship between spontaneous activity and nicotine response depending on the time of day. The MHb then, represents a potential site for circadian control of nicotine behaviour which has potential implications for the way we understand nicotine addiction, which could in turn lead to more effective strategies for smoking cessation in humans.

3.6 References

Anderson, S.M., Brunzell, D.H., 2015. Anxiolytic-like and anxiogenic-like effects of nicotine are regulated via diverse action at β2*nicotinic acetylcholine receptors. Br. J. Pharmacol. 172, 2864–2877. https://doi.org/10.1111/bph.13090

Baño-Otálora, B., Piggins, H.D., 2017. Contributions of the lateral habenula to circadian timekeeping. Pharmacology Biochemistry and Behavior, The lateral habenula. From the neuroanatomy to the implication in CNS disorders 162, 46–54. https://doi.org/10.1016/j.pbb.2017.06.007

Bechtold, D.A., Loudon, A.S.I., 2013. Hypothalamic clocks and rhythms in feeding behaviour. Trends Neurosci 36, 74–82. https://doi.org/10.1016/j.tins.2012.12.007

Begemann, K., Neumann, A.-M., Oster, H., 2020. Regulation and function of extra-SCN circadian oscillators in the brain. Acta Physiologica 229, e13446. https://doi.org/10.1111/apha.13446

Benowitz, N.L., Kuyt, F., Jacob, P., 1982. Circadian blood nicotine concentrations during cigarette smoking. Clin. Pharmacol. Ther. 32, 758–764.

Black, N., D'Souza, A., Wang, Y., Piggins, H., Dobrzynski, H., Morris, G., Boyett, M.R., 2019. Circadian rhythm of cardiac electrophysiology, arrhythmogenesis, and the underlying mechanisms. Heart Rhythm 16, 298–307. https://doi.org/10.1016/j.hrthm.2018.08.026

Brown, T.M., Piggins, H.D., 2007. Electrophysiology of the suprachiasmatic circadian clock. Progress in Neurobiology 82, 229–255. https://doi.org/10.1016/j.pneurobio.2007.05.002

Chandra, S., Scharf, D., Shiffman, S., 2011. Within-day temporal patterns of smoking, withdrawal symptoms, and craving. Drug Alcohol Depend 117, 118–125. https://doi.org/10.1016/j.drugalcdep.2010.12.027

Chrobok, L., Pradel, K., Janik, M.E., Sanetra, A.M., Bubka, M., Myung, J., Ridla Rahim, A., Klich, J.D., Jeczmien-Lazur, J.S., Palus-Chramiec, K., Lewandowski, M.H., 2021. Intrinsic circadian timekeeping properties of the thalamic lateral geniculate nucleus. J Neurosci Res. https://doi.org/10.1002/jnr.24973

Elayouby, K.S., Ishikawa, M., Dukes, A.J., Smith, A.C.W., Lu, Q., Fowler, C.D., Kenny, P.J., 2021. α3* Nicotinic Acetylcholine Receptors in the Habenula-Interpeduncular Nucleus Circuit Regulate Nicotine Intake. J Neurosci 41, 1779–1787. https://doi.org/10.1523/JNEUROSCI.0127-19.2020

Exley, R., Maubourguet, N., David, V., Eddine, R., Evrard, A., Pons, S., Marti, F., Threlfell, S., Cazala, P., McIntosh, J.M., Changeux, J.-P., Maskos, U., Cragg, S.J., Faure, P., 2011. Distinct contributions of nicotinic acetylcholine receptor subunit alpha4 and subunit alpha6 to the reinforcing effects of nicotine. Proc Natl Acad Sci U S A 108, 7577–7582. https://doi.org/10.1073/pnas.1103000108

Fonck, C., Nashmi, R., Salas, R., Zhou, C., Huang, Q., De Biasi, M., Lester, R.A.J., Lester, H.A., 2009. Demonstration of Functional α4-Containing Nicotinic Receptors in the Medial Habenula. Neuropharmacology 56, 247–253. https://doi.org/10.1016/j.neuropharm.2008.08.021

Fowler, C.D., Lu, Q., Johnson, P.M., Marks, M.J., Kenny, P.J., 2011. Habenular α5 nicotinic receptor subunit signalling controls nicotine intake. Nature 471, 597–601. https://doi.org/10.1038/nature09797

Frahm, S., Slimak, M.A., Ferrarese, L., Santos-Torres, J., Antolin-Fontes, B., Auer, S., Filkin, S., Pons, S., Fontaine, J.-F., Tsetlin, V., Maskos, U., Ibañez-Tallon, I., 2011. Aversion to nicotine is regulated by the balanced activity of β4 and α5 nicotinic receptor subunits in the medial habenula. Neuron 70, 522–535. https://doi.org/10.1016/j.neuron.2011.04.013

Fuchs, J.L., Hoppens, K.S., 1987. α-Bungarotoxin binding in relation to functional organization of the rat suprachiasmatic nucleus. Brain Research 407, 9–16. https://doi.org/10.1016/0006-8993(87)91214-5

Gillette, M.U., 1986. The suprachiasmatic nuclei: circadian phase-shifts induced at the time of hypothalamic slice preparation are preserved in vitro. Brain Res 379, 176–181. https://doi.org/10.1016/0006-8993(86)90273-8

Glick, S.D., Sell, E.M., McCallum, S.E., Maisonneuve, I.M., 2011. Brain regions mediating α3β4 nicotinic antagonist effects of 18-MC on nicotine self-administration. Eur. J. Pharmacol. 669, 71–75. https://doi.org/10.1016/j.ejphar.2011.08.001

Görlich, A., Antolin-Fontes, B., Ables, J.L., Frahm, S., Ślimak, M.A., Dougherty, J.D., Ibañez-Tallon, I., 2013. Reexposure to nicotine during withdrawal increases the pacemaking activity of cholinergic habenular neurons. Proc Natl Acad Sci U S A 110, 17077–17082. https://doi.org/10.1073/pnas.1313103110

Grainge, M.J., Shahab, L., Hammond, D., O'Connor, R.J., McNeill, A., 2009. First cigarette on waking and time of day as predictors of puffing behaviour in UK adult smokers. Drug Alcohol Depend 101, 191–195. https://doi.org/10.1016/j.drugalcdep.2009.01.013

Guilding, C., Hughes, A.T.L., Brown, T.M., Namvar, S., Piggins, H.D., 2009. A riot of rhythms: neuronal and glial circadian oscillators in the mediobasal hypothalamus. Mol Brain 2, 28. https://doi.org/10.1186/1756-6606-2-28

Guilding, C., Hughes, A.T.L., Piggins, H.D., 2010. Circadian oscillators in the epithalamus. Neuroscience 169, 1630–1639. https://doi.org/10.1016/j.neuroscience.2010.06.015

Guilding, C., Piggins, H.D., 2007. Challenging the omnipotence of the suprachiasmatic timekeeper: are circadian oscillators present throughout the mammalian brain? European Journal of Neuroscience 25, 3195–3216. https://doi.org/10.1111/j.1460-9568.2007.05581.x

Hanin, I., Massarelli, R., Costa, E., 1970. Acetylcholine concentrations in rat brain: diurnal oscillation. Science 170, 341–342. https://doi.org/10.1126/science.170.3955.341

Hanna, L., Walmsley, L., Pienaar, A., Howarth, M., Brown, T.M., 2017. Geniculohypothalamic GABAergic projections gate suprachiasmatic nucleus responses to retinal input. J. Physiol. (Lond.). https://doi.org/10.1113/JP273850

Harding, C., Bechtold, D.A., Brown, T.M., 2020. Suprachiasmatic nucleus-dependent and independent outputs driving rhythmic activity in hypothalamic and thalamic neurons. BMC Biol 18, 134. https://doi.org/10.1186/s12915-020-00871-8

Hastings, M.H., Maywood, E.S., Brancaccio, M., 2018. Generation of circadian rhythms in the suprachiasmatic nucleus. Nat Rev Neurosci 19, 453–469. https://doi.org/10.1038/s41583-018-0026-z

Hut, R.A., Van der Zee, E.A., 2011. The cholinergic system, circadian rhythmicity, and time memory. Behav. Brain Res. 221, 466–480. https://doi.org/10.1016/j.bbr.2010.11.039

Inouye, S.T., Kawamura, H., 1979. Persistence of circadian rhythmicity in a mammalian hypothalamic "island" containing the suprachiasmatic nucleus. Proc. Natl. Acad. Sci. U.S.A. 76, 5962–5966.

Kametani, H., Kawamura, H., 1991. Circadian rhythm of cortical acetylcholine release as measured by in vivo microdialysis in freely moving rats. Neuroscience Letters 132, 263–266. https://doi.org/10.1016/0304-3940(91)90316-L

Kim, U., Chang, S.-Y., 2005. Dendritic morphology, local circuitry, and intrinsic electrophysiology of neurons in the rat medial and lateral habenular nuclei of the epithalamus. J. Comp. Neurol. 483, 236–250. https://doi.org/10.1002/cne.20410

Kim, U., Chung, L., 2007. Dual GABAergic synaptic response of fast excitation and slow inhibition in the medial habenula of rat epithalamus. J. Neurophysiol. 98, 1323–1332. https://doi.org/10.1152/jn.00575.2007

Kita, T., Nakashima, T., Kurogochi, Y., 1986. Circadian variation of nicotine-induced ambulatory activity in rats. Jpn. J. Pharmacol. 41, 55–60.

Klemm, W.R., 2004. Habenular and interpeduncularis nuclei: shared components in multiple-function networks. Med. Sci. Monit. 10, RA261-273.

Landgraf, D., Long, J.E., Welsh, D.K., 2016. Depression-like behaviour in mice is associated with disrupted circadian rhythms in nucleus accumbens and periaqueductal grey. European Journal of Neuroscience 43, 1309–1320. https://doi.org/10.1111/ejn.13085

Lee, C., Lee, S., Woo, C., Kang, S.J., Kim Kwon, Y., Shin, K.S., 2018. Differential regulation of neuronal excitability by nicotine and substance P in subdivisions of the medial habenula. Anim Cells Syst (Seoul) 22, 165–171. https://doi.org/10.1080/19768354.2018.1456485

Lee, H.W., Yang, S.H., Kim, J.Y., Kim, H., 2019. The Role of the Medial Habenula Cholinergic System in Addiction and Emotion-Associated Behaviors. Front Psychiatry 10. https://doi.org/10.3389/fpsyt.2019.00100

McCormick, D.A., Prince, D.A., 1987. Acetylcholine causes rapid nicotinic excitation in the medial habenular nucleus of guinea pig, in vitro. J. Neurosci. 7, 742–752.

McLaughlin, I., Dani, J.A., De Biasi, M., 2017. The medial habenula and interpeduncular nucleus circuitry is critical in addiction, anxiety, and mood regulation. J. Neurochem. 142, 130–143. https://doi.org/10.1111/jnc.14008

Mendoza, J., 2007. Circadian clocks: setting time by food. J. Neuroendocrinol. 19, 127–137. https://doi.org/10.1111/j.1365-2826.2006.01510.x

Mexal, S., Horton, W.J., Crouch, E.L., Maier, S.I.B., Wilkinson, A.L., Marsolek, M., Stitzel, J.A., 2012. Diurnal variation in nicotine sensitivity in mice: role of genetic background and melatonin. Neuropharmacology 63, 966–973. https://doi.org/10.1016/j.neuropharm.2012.06.065

Mistlberger, R.E., Skene, D.J., 2004. Social influences on mammalian circadian rhythms: animal and human studies. Biol Rev Camb Philos Soc 79, 533–556. https://doi.org/10.1017/s1464793103006353

Mooney, M., Green, C., Hatsukami, D., 2006. Nicotine self-administration: cigarette versus nicotine gum diurnal topography. Hum Psychopharmacol 21, 539–548. https://doi.org/10.1002/hup.808

Morley, B.J., Garner, L.L., 1990. Light-dark variation in response to chronic nicotine treatment and the density of hypothalamic alpha-bungarotoxin receptors. Pharmacol. Biochem. Behav. 37, 239–245.

Moyer, J.R., Jr, Brown, T.H., 1998. Methods for whole-cell recording from visually preselected neurons of perirhinal cortex in brain slices from young and aging rats. J. Neurosci. Methods 86, 35–54.

Mugnaini, M., Tessari, M., Tarter, G., Merlo Pich, E., Chiamulera, C., Bunnemann, B., 2002. Upregulation of [3H]methyllycaconitine binding sites following continuous infusion of nicotine, without changes of α7 or α6 subunit mRNA: an autoradiography and in situ hybridization study in rat brain. European Journal of Neuroscience 16, 1633–1646. https://doi.org/10.1046/j.1460-9568.2002.02220.x

Northeast, R.C., Vyazovskiy, V.V., Bechtold, D.A., 2020. Eat, sleep, repeat: the role of the circadian system in balancing sleep-wake control with metabolic need. Curr Opin Physiol 15, 183–191. https://doi.org/10.1016/j.cophys.2020.02.003

O'Dell, L.E., Chen, S.A., Smith, R.T., Specio, S.E., Balster, R.L., Paterson, N.E., Markou, A., Zorrilla, E.P., Koob, G.F., 2007. Extended access to nicotine self-administration leads to dependence: Circadian measures, withdrawal measures, and extinction behavior in rats. J. Pharmacol. Exp. Ther. 320, 180–193. https://doi.org/10.1124/jpet.106.105270

Olejniczak, I., Ripperger, J.A., Sandrelli, F., Schnell, A., Mansencal-Strittmatter, L., Wendrich, K., Hui, K.Y., Brenna, A., Fredj, N.B., Albrecht, U., 2021. Light affects behavioral despair involving the clock gene Period 1. PLOS Genetics 17, e1009625. https://doi.org/10.1371/journal.pgen.1009625

Pang, X., Liu, L., Ngolab, J., Zhao-Shea, R., McIntosh, J.M., Gardner, P.D., Tapper, A.R., 2016. Habenula cholinergic neurons regulate anxiety during nicotine withdrawal via nicotinic acetylcholine receptors. Neuropharmacology 107, 294–304. https://doi.org/10.1016/j.neuropharm.2016.03.039

Park, H., Cheon, M., Kim, S., Chung, C., 2017. Temporal variations in presynaptic release probability in the lateral habenula. Sci Rep 7, 1–8. https://doi.org/10.1038/srep40866
Parrott, A.C., 1995. Stress modulation over the day in cigarette smokers. Addiction 90, 233–244.
Partch, C.L., Green, C.B., Takahashi, J.S., 2014. Molecular architecture of the mammalian circadian clock. Trends Cell Biol. 24, 90–99. https://doi.org/10.1016/j.tcb.2013.07.002
Paul, J.R., Davis, J.A., Goode, L.K., Becker, B.K., Fusilier, A., Meador-Woodruff, A., Gamble, K.L., 2020. Circadian regulation of membrane physiology in neural oscillators throughout the brain. European Journal of Neuroscience 51, 109–138. https://doi.org/10.1111/ejn.14343
Paul, J.R., DeWoskin, D., McMeekin, L.J., Cowell, R.M., Forger, D.B., Gamble, K.L., 2016. Regulation of persistent sodium currents by glycogen synthase kinase 3 encodes daily rhythms of neuronal excitability. Nat Commun 7, 13470. https://doi.org/10.1038/ncomms13470
Paul, S., Brown, T., 2019. Direct effects of the light environment on daily neuroendocrine control. J Endocrinol JOE-19-0302.R1. https://doi.org/10.1530/JOE-19-0302
Paul, S., Hanna, L., Harding, C., Hayter, E.A., Walmsley, L., Bechtold, D.A., Brown, T.M., 2020. Output from VIP cells of the mammalian central clock regulates daily physiological rhythms. Nat Commun 11, 1453. https://doi.org/10.1038/s41467-020-15277-x
Paxinos, G., Franklin, K.B.J., 2003. The mouse brain in stereotaxic coordinates, 2nd Edition. ed. San Diego : Academic Press.
Perkins, K.A., Briski, J., Fonte, C., Scott, J., Lerman, C., 2009. Severity of tobacco abstinence symptoms varies by time of day. Nicotine Tob. Res. 11, 84–91. https://doi.org/10.1093/ntr/ntn003
Picciotto, M.R., Kenny, P.J., 2021. Mechanisms of Nicotine Addiction. Cold Spring Harb Perspect Med 11, a039610. https://doi.org/10.1101/cshperspect.a039610
Pons, S., Fattore, L., Cossu, G., Tolu, S., Porcu, E., McIntosh, J.M., Changeux, J.P., Maskos, U., Fratta, W., 2008. Crucial role of alpha4 and alpha6 nicotinic acetylcholine receptor subunits from ventral tegmental area in systemic nicotine self-administration. J Neurosci 28, 12318–12327. https://doi.org/10.1523/JNEUROSCI.3918-08.2008
Sakhi, K., Belle, M.D.C., Gossan, N., Delagrange, P., Piggins, H.D., 2014a. Daily variation in the electrophysiological activity of mouse medial habenula neurones. J Physiol 592, 587–603. https://doi.org/10.1113/jphysiol.2013.263319
Sakhi, K., Wegner, S., Belle, M.D.C., Howarth, M., Delagrange, P., Brown, T.M., Piggins, H.D., 2014b. Intrinsic and extrinsic cues regulate the daily profile of mouse lateral habenula neuronal activity. J Physiol 592, 5025–5045. https://doi.org/10.1113/jphysiol.2014.280065
Salas, R., Sturm, R., Boulter, J., De Biasi, M., 2009. Nicotinic receptors in the habenulo-interpeduncular system are necessary for nicotine withdrawal in mice. J. Neurosci. 29, 3014–3018. https://doi.org/10.1523/JNEUROSCI.4934-08.2009
Sheffield, E.B., Quick, M.W., Lester, R.A., 2000. Nicotinic acetylcholine receptor subunit mRNA expression and channel function in medial habenula neurons. Neuropharmacology 39, 2591–2603.
Shieh, K.R., 2003. Distribution of the rhythm-related genes rPERIOD1, rPERIOD2, and rCLOCK, in the rat brain. Neuroscience 118, 831–843. https://doi.org/10.1016/S0306-4522(03)00004-6
Shiffman, S., Engberg, J.B., Paty, J.A., Perz, W.G., Gnys, M., Kassel, J.D., Hickcox, M., 1997. A day at a time: Predicting smoking lapse from daily urge. Journal of Abnormal Psychology 106, 104–116. https://doi.org/10.1037/0021-843X.106.1.104
Shih, P.-Y., Engle, S.E., Oh, G., Deshpande, P., Puskar, N.L., Lester, H.A., Drenan, R.M., 2014. Differential expression and function of nicotinic acetylcholine receptors in subdivisions of medial habenula. J. Neurosci. 34, 9789–9802. https://doi.org/10.1523/JNEUROSCI.0476-14.2014

Shoham, S., O'Connor, D.H., Segev, R., 2006. How silent is the brain: is there a "dark matter" problem in neuroscience? J Comp Physiol A 192, 777–784. https://doi.org/10.1007/s00359-006-0117-6

Society for Neuroscience, 2018. Recommendations for the Design and Analysis of In Vivo Electrophysiology Studies. J. Neurosci. 38, 5837–5839. https://doi.org/10.1523/JNEUROSCI.1480-18.2018

Stamatakis, A.M., Van Swieten, M., Basiri, M.L., Blair, G.A., Kantak, P., Stuber, G.D., 2016. Lateral Hypothalamic Area Glutamatergic Neurons and Their Projections to the Lateral Habenula Regulate Feeding and Reward. J. Neurosci. 36, 302–311. https://doi.org/10.1523/JNEUROSCI.1202-15.2016

Tapper, A.R., McKinney, S.L., Nashmi, R., Schwarz, J., Deshpande, P., Labarca, C., Whiteaker, P., Marks, M.J., Collins, A.C., Lester, H.A., 2004. Nicotine activation of alpha4* receptors: sufficient for reward, tolerance, and sensitization. Science 306, 1029–1032. https://doi.org/10.1126/science.1099420

Teneggi, V., Tiffany, S.T., Squassante, L., Milleri, S., Ziviani, L., Bye, A., 2002. Smokers deprived of cigarettes for 72 h: effect of nicotine patches on craving and withdrawal. Psychopharmacology (Berl.) 164, 177–187. https://doi.org/10.1007/s00213-002-1176-1

Ussher, M., West, R., 2003. Diurnal variations in first lapses to smoking for nicotine patch users. Hum Psychopharmacol 18, 345–349. https://doi.org/10.1002/hup.493

Valdez, P., 2019. Circadian Rhythms in Attention. Yale J Biol Med 92, 81–92.

Vaze, K.M., Sharma, V.K., 2013. On the adaptive significance of circadian clocks for their owners. Chronobiol Int 30, 413–433. https://doi.org/10.3109/07420528.2012.754457

Wills, L., Kenny, P.J., 2021. Addiction-related neuroadaptations following chronic nicotine exposure. J Neurochem 157, 1652–1673. https://doi.org/10.1111/jnc.15356

Yamamoto, S., Shigeyoshi, Y., Ishida, Y., Fukuyama, T., Yamaguchi, S., Yagita, K., Moriya, T., Shibata, S., Takashima, N., Okamura, H., 2001. Expression of the Per1 gene in the hamster: brain atlas and circadian characteristics in the suprachiasmatic nucleus. J. Comp. Neurol. 430, 518–532.

Yoshikawa, T., Yamazaki, S., Menaker, M., 2005. EFFECTS OF PREPARATION TIME ON PHASE OF CULTURED TISSUES REVEAL COMPLEXITY OF CIRCADIAN ORGANIZATION. J Biol Rhythms 20, 500–512. https://doi.org/10.1177/0748730405280775

Zhao, H., Rusak, B., 2005. Circadian firing-rate rhythms and light responses of rat habenular nucleus neurons in vivo and in vitro. Neuroscience 132, 519–528. https://doi.org/10.1016/j.neuroscience.2005.01.012

Zhao-Shea, R., DeGroot, S.R., Liu, L., Vallaster, M., Pang, X., Su, Q., Gao, G., Rando, O.J., Martin, G.E., George, O., Gardner, P.D., Tapper, A.R., 2015. Increased CRF signalling in a ventral tegmental area-interpeduncular nucleus-medial habenula circuit induces anxiety during nicotine withdrawal. Nat Commun 6, 6770. https://doi.org/10.1038/ncomms7770

4 Medial habenula cholinergic neuronal responses are modulated by time of day and visual information

4.1 Abstract

The habenular complex is a small structure of the epithalamus, comprised of both medial and lateral nuclei (MHb and LHb), which receives afferent connections from the limbic forebrain and sends efferent projections to midbrain regions involved in reward signalling. In particular, the MHb has been implicated in regulating nicotine withdrawal, due in part to its notably dense expression of cholinergic neurons and nicotinic receptors. Neurons in the MHb have been reported to exhibit circadian and/or light-dependent changes in activity but it remains unclear whether such properties differ across specific MHb neuronal subpopulations, including cholinergic cells. To address this, we used an optogenetic approach to identify MHb cholinergic neurons in combination with *in vivo* multielectrode recordings of spontaneous and light-evoked activity at different times of day. We show that cholinergic neurons of the MHb vary both their steady state firing rates and excitability in an opposing manner according to the time of day, with reduced spontaneous activity and enhanced evoked responses during the early night. In addition, we demonstrate that subsets of MHb cholinergic neurons exhibit slow and sustained increases or decreases in firing in response to diffuse increases in ocular illumination. Finally, via analysis of simultaneously recorded pairs of MHb neurons, we show the cholinergic population tend to display particularly highly correlated activity (and therefore coordinated neuronal output), consistent with shared synaptic inputs. In sum, these data indicate that MHb cholinergic neurons integrate both circadian and photic information, which may contribute to a rhythmic drive in nicotine addiction behaviours.

4.2 Introduction

The habenular complex is a small yet surprisingly heterogeneous structure of the epithalamus comprised of two major subregions, the medial and lateral habenula (MHb and LHb respectively), which differ in both their genetic expression and anatomical connectivity (Klemm, 2004; Viswanath et al., 2013). The MHb itself can be further divided into several subregions based on morphology (Andres et al., 1999) and neurotransmitter expression (Aizawa et al., 2012). Neurons within the dorsal portion of the MHb primarily express substance P and receive inputs from the bed nucleus of the anterior commissure (Yamaguchi et al., 2013), whilst neurons in the ventral portion are mostly comprised of cholinergic neurons and receive inputs mainly from the triangular septum (Herkenham and Nauta, 1977; Otsu et al., 2018). There are several other brain regions which may also project to the MHb (McLaughlin et al., 2017), and whilst a number of neurotransmitters are thought to drive these afferent connections, only a few studies have functionally confirmed these inputs (Choi et al., 2016; Otsu et al., 2018; Qin and Luo, 2009). Both dorsal and ventral portions of the MHb send projections along the fasciculus retroflexus to distinct target regions within the interpeduncular nucleus (IPN), which then in turn regulates mid and hind brain reward centres (McLaughlin et al., 2017). Thus, the MHb is well placed to act as a relay centre, regulating mood and motivational behaviours.

The MHb cholinergic neurons that project to the IPN comprise one of the major cholinergic pathways within the central nervous system (Lee et al., 2019). In addition, the MHb is noted for its remarkably dense expression of multiple different nicotinic receptor subtypes (Grady et al., 2009; Sheffield et al., 2000; Shih et al., 2014). Due in part to these characteristics, much of the research into the MHb has focussed on its role in nicotine addiction (McLaughlin et al., 2017). A wealth of studies employing knock-out mice, optogenetic and pharmacological approaches have now firmly demonstrated the MHb-IPN pathway as critical for mediating the aversive symptoms of nicotine withdrawal (Fowler et al., 2013; Pang et al., 2016; Salas et al., 2009; Zhao-Shea et al., 2013). Conversely, the endogenous functions of the MHb are less well-established, although recent work suggests that the MHb is involved in regulating mood, including fear (Yamaguchi et al., 2013; Zhang et al., 2016), depression (Han et al., 2017; Xu et al., 2018) and anxiety (Koppensteiner et al., 2016; Molas et al., 2017a). Further characterization of cholinergic neurons in the MHb could then lead not only to important developments for treatments for nicotine withdrawal symptoms, but could potentially be involved in regulating mood disorders.

MHb cholinergic neurons have been shown to corelease both glutamate and acetylcholine (ACh) (Frahm et al., 2015; Ren et al., 2011), and demonstrate pacemaker activity driven by hyperpolarization-activated cyclic nucleotide-gated (HCN) channels (Görlich et al., 2013). Previous work investigating the neurons of the MHb has provided evidence of diurnal variation in their spontaneous firing (Sakhi et al., 2014a; Zhao and Rusak, 2005), and previous research from our own investigations has yielded evidence of a diurnal influence on cholinergic signalling within the MHb *in vitro* (see previous chapter). A subpopulation of rat MHb neurons are known to respond to retinal illumination (Zhao and Rusak, 2005), although as yet it has not been determined if this reflects cholinergic and/or other neuronal sub-groups.

Intriguingly, there is evidence of rhythmic modulation driving the reward-related behaviours with which the MHb is thought to be involved, and it is well known that light can have drastic impacts on mood regulation (LeGates et al., 2014; Milosavljevic, 2019). There is diurnal variation in both nicotine withdrawal symptoms in humans (Chandra et al., 2011; Perkins et al., 2009; Teneggi et al., 2002) and nicotine intake in rats (O'Dell et al., 2007). Mood regulation is thought to be under control of the circadian system (McClung, 2013) and there is evidence for endogenous rhythms in fear-conditioned learning which suggests fear is regulated by time of day as well (Albrecht and Stork, 2017; Chaudhury and Colwell, 2002).

Therefore, as a site of potential integration between circadian signals, visual inputs and cholinergic signalling, we set out to further characterize the cholinergic neurons of the MHb, using a targeted optogenetic approach. First, we characterize the opsin expression and circadian behaviour of mice expressing channelrhodopsin (ChR2) under the control of a ChAT-cre driver (driving expression within cholinergic cells), before examining the responses of cholinergic neurons both *in vitro* and *in vivo*. We investigate whether they are modulated by the time of day, and whether these neurons are responsive to retinal illumination. Finally, we probe synaptic communication between pairs of neurons in the MHb.

4.3 Methods

4.3.1 **Transgenic mice**

Figure 4.1 illustrates the breeding strategy employed to produce our transgenic mice. For optogenetic control of cholinergic neuron activity specifically, we took advantage of the Cre-lox system and generated ChAT-Cre;Ai32 transgenic mice in order to drive expression of the light-activated ChR2 protein only in neurons which express choline acetyltransferase (ChAT), the

enzyme critical for acetylcholine synthesis and used as a marker for cholinergic neurons (Naciff et al., 1999). This mouse line was generated by crossing ChAT-Cre mice (ChAT-Cre: B6;129S6-Chat$^{tm1(cre)Lowl}$/J, Jax stock number 006410; Rossi et al., 2011) with Ai32 mice exhibiting Cre recombinase-dependent ChR2/EYFP fusion protein expression (Ai32: 129S-Gt(ROSA)26Sor$^{tm32(CAG-COP4*H134R/EYFP)Hze}$/J, Jax stock number 012569; Madisen et al., 2012). We chose the ChAT-Cre mouse model generated via internal ribosome entry site rather than lines created using bacterial artificial chromosome methods, as these alternatives have been shown to have behavioural deficits and increased ChAT expression compared to wildtypes (Chen et al., 2018), as well as ectopic ChR2 expression in the retina (Cui et al., 2020).

Only offspring that were heterozygous for both genotypes were used for both *in vitro* and *in vivo* electrophysiological experiments to avoid the behavioural and protein expression deficits associated with homozygous offspring (Chen et al., 2018). Littermates that were wildtype for the ChAT-Cre gene (Ai32 mice) were used as littermate controls for the wheel-running experiments. Mice that were heterozygous for the ChAT-Cre gene only (ChAT-cre mice) were used for brain injection experiments to ensure restricted expression of the viral gene construct to cholinergic cells.

Mice of both sexes were used throughout this study. Mice were group-housed in standard home cages (in groups of 2-6) with food and water available *ad libitum* unless otherwise specified. The home environment was both temperature (21 ± 2°C) and humidity (55 ± 5%) controlled with 12 hr light / dark cycles, adjusted to allow experiments to be performed during the working day. Animals were left to entrain to their light / dark cycle for at least 2 weeks in all cases. In all cases Zeitgeber time (ZT) is used to define the projected time of the circadian clock, where ZT0 corresponds to lights on and ZT12 corresponds to lights off. All procedures were approved by the University of Manchester Ethics Committee and strictly adhered to the Animals (Scientific Procedures) Act, 1986, under Project Licences 70/8918 and PP3176367.

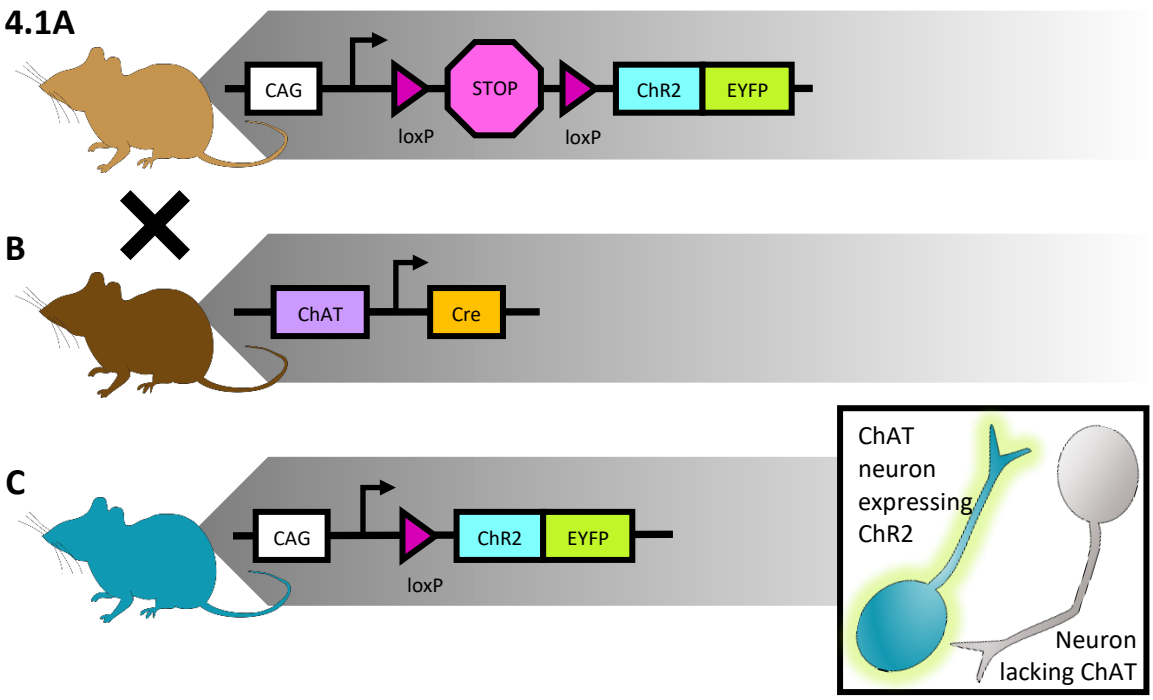

Figure 4.1 Cre-dependent expression of channelrhodopsin (ChR2) in neurons expressing choline acetyltransferase (ChAT).

A) In Ai32 mice: loxP sites flank a stop cassette preceding the ChR2-EYFP fusion protein, preventing its expression.
B) In ChAT-Cre mice: cre-recombinase is expressed under the control of the ChAT promoter.
C) Crossing Ai32 mice with ChAT-Cre mice produces ChAT-Cre;Ai32 mice: if ChAT is expressed during the lifetime of the cell, cre-dependent recombination removes the stop cassette, allowing permanent expression of ChR2-EYFP under control of the CAG promoter.

4.3.2 Immunohistochemical analysis of expression specificity

Two male ChAT-Cre;Ai32 mice aged 60 days were used to characterize the expression profile of ChAT and ChR2-EYFP through immunohistochemistry following transcardial perfusion. Mice were anaesthetized with 20% urethane in saline delivered via intraperitoneal injection. Blinking and withdrawal reflexes were tested to ensure surgical plane of anaesthesia before an initial transverse incision was made using surgical scissors below the sternum to reveal the xiphoid cartilage. Once the diaphragm was exposed, cuts were made across the ribs on both sides of the body to allow the ribcage to be retracted and clamped out of the way. Holding the heart with forceps, a small gavage needle connected to the perfusion pump (313S Watson-Marlow, UK) was inserted into the left ventricle of the heart. A small cut was made to the right atrium to allow the

outflow of blood. 0.9% saline was perfused into the heart at a rate of 10 mL / min until the liver became pale in colour (approximately 3 min), before 4% paraformaldehyde (PFA) was infused for a further 3-5 min. Following perfusion and decapitation, the skull cap was removed and the brain gently excised.

Brains were left in 4% PFA overnight and were transferred to 30% sucrose solution within 24 hr for cryoprotection. After 3 days in 30% sucrose, brains were sectioned on a freezing sledge microtome (8000 Sledge; Bright Instruments, UK) to collect 40 µm thick coronal or sagittal slices. Every other section was collected sequentially in phospho-buffered saline (PBS).

4.3.2.1 *Immunohistochemistry*

Double-staining on free floating sections was performed, with sections kept protected from light and under gentle agitation using a shaker at all steps. Sections were permeabilised in 1% Triton™ X-100 (Sigma-Aldrich, UK) in PBS (1% PBS-T) for 5 min, and the solution was replaced 4 times. Sections were then incubated in blocking solution (10% normal donkey serum, Sigma Aldrich, in 1% PBS-T) for 3 hr at room temperature (21 °C). Next, sections were left in primary antibody solution diluted in 2.5% normal donkey serum with 0.2% PBS-T overnight at 4 °C (goat polyclonal anti-ChAT 1:100, #AB144P, Merck-Millipore; chicken polyclonal anti-GFP 1:10000, #A10262, Thermofisher). The next day, sections were washed 4 times in 0.2% PBS-T for 15 min before incubation with the secondary antibody in 2.5% normal donkey serum (donkey anti-goat igG Alexa fluor 555, 1:500, #A32816, Thermofisher; donkey anti-chicken IgY, FITC, 1:400, #SA1-72000, Thermofisher). Finally, sections were washed 4 times in PBS for 10 min before they were mounted onto slides using vectashield hardset (H1500, Vector Labs, Peterborough UK) containing nuclear dye 4',6-Diamidine-2'-phenylindole dihydrochloride (DAPI) to allow for easier visualisation of tissue cytoarchitecture. The slides were processed through a slide scanner (Laser 2000, UK) in the University of Manchester Bioimaging facility, and the images were acquired using CaseViewer V2.4 software (3DHISTECH, Hungary).

4.3.3 **Wheel-running locomotor activity**

As we planned on using ChAT-Cre;Ai32 mice to investigate circadian influences on neuronal responses, we first assessed the circadian behaviour of these animals. Circadian period and locomotor activity were compared between male and female ChAT-Cre;Ai32 mice and Ai32 littermates using voluntary wheel-running behaviour (4 mice per group). Mice aged between 54 and 98 days at the start of the experiment were singly housed in light-tight cabinets to allow the light to be carefully controlled, with food and water *ad libitum*. Mice also had *ad libitum* access to

a cardboard running wheel (82 mm diameter, depth 57 mm, Vettech), connected to a computer. Activity counts were assessed by counting wheel revolutions, which were acquired in 60 s bins using The Chronobiology Kit (Stanford Software Systems, Santa Cruz, CA).

Mice were allowed to acclimatize to the cage and the running wheel for 3 days prior to data collection (note: mice were already on the same 12 hr light / 12 hr dark schedule before being housed in the cabinets). After 10 days of 12 hr light / 12 hr dark (LD1), cages were cleaned and then mice were left in constant darkness for 10 days (DD) in order to determine the animals free-running endogenous period. Finally, following a further cage change, mice were then returned to the 12 hr light / 12 hr dark cycle once more (LD2). The health and welfare of the mice were checked on a daily basis, at irregular times of day and with the use of infrared goggles (ATN NVG-7, Armasight Inc., NH, USA) if the animals were in dark. This prevented the animals entraining to any regular disruption or introducing unwanted phase shifts (Mrosovsky, 1988). For the ChAT-Cre; Ai32 male mice, a computer error meant that data collection was paused for 2 days during LD2, so animals were left in the wheel-running cages for a total of 12 days to allow 10 days of data collection.

Circadian tau was determined by χ^2-periodogram (Sokolove and Bushell, 1978) using the inbuilt function in KitAnalyze v1.06 (Stanford Software Systems, Santa Cruz, CA). Rhythm robustness was assessed under LD by quantifying the percentage of variance that was accounted for by a rhythmic component, either with a tau of 24 hr under LD conditions or the circadian tau of the animal for analysis of DD conditions (Mouland et al., 2019). Grouped data were analysed by two-way ANOVAs, followed by Holm-Šídák's post-hoc tests using Graphpad Prism v9.1.2 (USA).

4.3.4 **Viral tracing of cholinergic neurons**

In order to try and identify an upstream source of cholinergic input to the MHb, we performed unilateral injections of a viral construct (AAV2retro-DIO-ChR2-EYFP; Addgene) into the right MHb of ChAT-Cre mice to generate retrograde ChAT-cre restricted AAV expression of ChR2 fused to EYFP. A total of 4 male ChAT-Cre mice were used for this study, aged 75 days on the day of the surgery.

Mice were anaesthetized using 1% isofluorane in O_2, and secured in a stereotaxic frame. Buprenorphine analgesia (0.01mg / kg, Vetergesic; Ceva Animal Health Ltd, UK) in 0.9% sterile saline was delivered via a subcutaneous injection, before the skull was exposed using a scalpel. 25% hydrogen peroxide (Sigma Aldrich) was carefully applied to the skull surface to facilitate

visualization of Bregma and Lambda. A computerised microinjection robot was used to complete all aspects of the craniotomy and virus injection (Drill and 473 Microinjection Robot: Neurostar, Tübingen, Germany). The microinjector was fitted with a pulled glass capillary needle loaded with the virus, checking for air bubbles. Next, injection coordinates were input to the software (-1.82 mm posterior to Bregma, 0.2 mm lateral to the midline, -2.5 mm ventral to the brain surface, coordinates based on the Stereotaxic Mouse Brain Atlas, Paxinos & Franklin, 2003, as demonstrated in Figure 4.4A). Scaling and calibration of the skull was performed individually for each mouse to account for rotation of the skull and inter-individual differences in brain sizes. Following scaling, the injection robot performed the craniotomy using a 1.6 mm drill bit directly above the injection site, before the microinjector needle was slowly lowered into the brain to the desired location. 69 nL of the virus solution was delivered slowly at a rate of 25 nL / s and the needle was left in place for a further 5 min to reduce chances of virus bleeding out along the route of the injector. The needle was slowly raised out of the brain, and the incision site was closed with sutures. Additional topical pain relief was applied to the wound (Emla; Aspen Phama, Ireland) and recovery was monitored. Following surgery, animals were singly housed to avoid fighting and reduce the chance of the wounds reopening.

The viral construct used was double floxed ChR2-EYFP plasmid DNA under control of the EF1a promoter, packaged into AAV viral vectors (pAAVrg-EF1a-double floxed-hChR2(H134R)-EYFP-WPRE-HGHpA, Addgene viral prep # 20298). These were produced with the rAAV2-retro helper plasmid (Addgene #81070), which allows robust retrograde access and transgene delivery to projection neurons (Figure 4.4B).

After a 4 week period to allow for transfection, mice were killed by transcardial perfusion and brain tissue collected for imaging as described above. Sections were double-stained for ChAT and EYFP to allow visualisation of the cholinergic retrograde projections from the MHb, using the same immunofluorescence protocol as previously described.

4.3.5 *In vitro* electrophysiology

Ten ChAT-Cre; Ai32 mice (6 female and 4 male) aged between 62 – 113 days old were used to perform initial investigations into optogenetic activation of cholinergic neurons. Five mice were culled at ZT 6 to allow data collection to be performed during the subjective day (ZT 8 - 10) and 5 mice were culled at ZT 14 for experiments performed during the subjective night (ZT 16 - 18). However, as the number of units isolated were sparse, data was combined and we did not look for differences between time points. 300 µm thick coronal brain slices were prepared as described

in the previous chapter (section 3.3.2). Briefly, brains were extracted from mice following cervical dislocation, and transferred to ice-cold, oxygenated cutting solution (composition in mM: NaCl 95, KCl 1.8, KH2PO4 1.2, CaCl2 0.5, MgSO4 7, NaHCO3 26, glucose 15, sucrose 50 and Phenol Red 0.005 mg/L) before slicing using a 7000 smz-2 vibrating microtome (Campden Instruments, UK). Slices were then left to incubate for at least 20 min in constantly oxygenated artificial cerebrospinal fluid solution (aCSF; composition in mM: NaCl 127, KCl 1.8, KH2PO4 1.2, CaCl2 2.4, MgSO4 1.3, NaHCO3 26, glucose 5, sucrose 10 and Phenol Red 0.005 mg / L) before placing in the recording chambers. Time stamped action potentials were sampled at 50 KHz, filtered (200 Hz high-pass 2nd order Butterworth) and neuronal signals were acquired with the threshold for action potentials set at –16.5 µV, using MC_Rack v4.5.1 software (MCS GmbH, Germany). Single units were isolated using Offline Sorter v3.3.5 (Plexon, USA), following processing using custom Matlab scripts.

4.3.5.1 *Optogenetic stimulation*

Tissue slices containing the MHb were placed over a 6 x 10 perforated micro-electrode array (pMEA; 60pMEA100/30iR-Ti, MCS) to allow simultaneous recording of sites across both the MHb and the LHb. Cholinergic neurons were optogenetically targeted by blue LED flashes delivered through an optic fibre (200 µm thick, 465 nm LED; 800 $mWmm^{-2}$ at the fibre tip; PlexBright; Plexon) placed directly above the tissue, approximately 100 µm above the tissue surface. Following 30 min stabilization period, blue light flashes were continuously delivered as a ramped 10 ms pulse every 10 s with MC Stimulus II (Multi channel systems) for the duration of the recording (see Figure 4.5B). The ramped pulse approach was used (as in Paul et al., 2020), to prevent synchronous spiking across neighbouring neurons which can render single unit isolation challenging.

4.3.5.2 *Pharmacological manipulation*

MHb cholinergic neurons are known to co-release both glutamate and acetylcholine (Frahm et al., 2015; Ren et al., 2011). Therefore, in order to determine if responses to photostimulation were due to direct activation or indirect activation via synaptic connections, we next aimed to pharmacologically isolate cholinergic neuron activity. Following an hour of optogenetic stimulation alone, we continued to drive optogenetic activation of cholinergic neurons in the presence of glutamate receptor antagonists (GluR blockers, DL-2-Amino-5-phosphonopentanoic acid, DL-AP5, 50 µM; 6-cyano-7-nitroquinoxaline-2,3-dione, CNQX, 20 µM, both Sigma Aldrich) for 30 min, and then another 30 min with GluR blockers as well as acetylcholine receptor antagonists (AChR blockers, mecamylamine hydrochloride, 10 µM, #2843, Tocris; atropine, 10 µM, #A0132,

Sigma Aldrich). Concentrations were chosen based on previous published studies (Baptista et al., 2005; Choi et al., 2016; Hanna et al., 2017; Joshi et al., 2016). Finally, tetrodotoxin (TTX, 1 µM, Sigma Aldrich, T8024) was bath-applied to the tissue for 10 min to confirm the recorded signals were synaptic in origin. Drugs were stored as aliquots at -18 °C and freshly prepared to appropriate concentrations in pre-warmed recording aCSF immediately before application. All drugs were bath-applied via the perfusion cannula.

4.3.5.3 *Data analysis*

Anatomical location was assigned to each channel by overlaying reconstructions of the known recording array geometry and histological images, in combination with the known anatomical landmarks on the slice as described in Chapter 3. We identified cells that responded to the optogenetic-activating pulse and were presumably cholinergic (ChAT+ve) based on whether the average spike counts across multiple stimulus repeats (typically ~ 180 presentations across a 30 min period), exceeded the upper or lower bounds of the 99% confidence limits for prestimulus spike counts (within at least one 10 ms bin < 100 ms after stimulus onset). For ChAT+ve cells, we then compared the average firing rate during the 100 ms immediately preceding the optogenetic-activating pulse (baseline) with the average firing rate during the 50 ms following LED flash onset (response), to compare how cells changed their responses following application of antagonists. Proportions of opto-responsive cells were compared between anatomical regions using a two-tailed Fisher's exact test, and the effects of drugs on the opto-responses were tested using a two-way repeat measures (RM) ANOVA. Statistical analysis was performed using GraphPad Prism v9.1.2 (USA).

4.3.6 ***In vivo* electrophysiology**

Previous work outlined in Chapter 3 had highlighted that *in vitro* analysis of circadian rhythms could be complicated by the MHb resetting its phase. Therefore, having verified our optogenetic approach was reliably stimulating responses in ChAT+ve cells, we performed the rest of our experiments using an *in vivo* approach.

A total of 10 ChAT-Cre;Ai32 mice (4 female, 6 male, equally weighted across experimental groups) aged 71 - 153 days were used for these experiments. Animals were anaesthetized with 1.55 g / kg urethane in 0.9% sterile saline (20%, w / v), delivered via intraperitoneal injection. Injections were performed between ZT1 - 3 for ‘day’ experiments or ZT9 – 11 for ‘night’ experiments in order that surgical procedures could be performed under normal lighting conditions without resetting the circadian system. Urethane was used as it induces a stable period of anaesthesia for several hours

(Haumesser et al., 2017), with minimal CNS depression (Maggi and Meli, 1986) and has better spike-sorting outcomes than other anaesthetic agents (Hildebrandt et al., 2017). Once sufficient depth of anaesthesia was reached, mice were securely head-fixed in a stereotaxic frame (SR-15M; Narishige International Ltd, London, UK) with bite and ear bars. Mice were maintained at 37 ˚C by placing them over a homeothermic mat (Harvard Apparatus, Cambridge, UK). A scalpel was used to expose the surface of the skull, and Lambda and Bregma were measured and the head adjusted to ensure the skull was level. A hole was drilled in the skull at coordinates based on the Paxinos and Franklin mouse reference atlas (Paxinos and Franklin, 2003), 1.6 mm posterior from Bregma and 0.7 mm lateral to the midline on the right hand side, and the dura was removed to expose the brain (see Figure 4.6A). Eyes were coated first with atropine (1% in saline, Sigma Aldrich) to dilate the pupils, and then mineral oil (Sigma Aldrich) to protect the cornea for the duration of the recording. Due to variation in the length of surgical preparation time, data collection began between ZT4 – 7.5 for experiments classified as 'day' (collected from 4 mice) or ZT12.5 – 17 for experiments classed as 'night' (collected from 6 mice). Experimental data collection varied between 1 – 4 hr in length.

4.3.6.1 *Data acquisition*

A 32-site recording electrode (three parallel rows of 10 – 12 sites at 50 µm spacing; site area: 121 μm^2; OALPPoly3; Neuronexus, Figure 4.6B-C) with connected optical fibre was used to both record and optogenetically stimulate cells within the same site. The recording electrode was coated with fluorescent dye (CM-DII V22888; Fisher Scientific, Loughborough, UK) to facilitate visualisation of the position of the electrode following histological processing. The electrode was angled at 12 ˚ relative to the dorsal-ventral axis in order to avoid the superior sagittal sinus, a major blood vessel located along the surface of the brain at the midline (Xiong et al., 2017). A fluid-filled micromanipulator (MO-10; Narishige International Ltd) was employed to slowly lower the electrode to a depth of 2.7 mm from the pial surface, in order to record from sites located across the right MHb.

The electrode was left in place for 30 min before data collection to allow neural activity to stabilize. We used a Recorder64 system (Plexon, US) to acquire wideband neural signals, which were then amplified for a gain of 3500X and digitized at 40 kHz and stored for offline analysis. Single unit activity was extracted from the data using Kilosort, an automated template-matching based algorithm (Pachitariu et al., 2016). Identified single units were exported as 'virtual tetrodes' (spike waveforms detected across 4 adjacent channels) for manual refinement in Offline Sorter

x64 v3.3.5 (Plexon, US). Successfully isolated units displayed a distinct refractory period (> 1.5 ms) in the interspike interval histogram.

4.3.6.2 *Optogenetic stimuli*

ChR2 was activated through optogenetic photostimulation using a blue 465 nm table-top PlexBright LED module (Plexon, USA), 634 mW / mm^2 intensity at the tip of the 200 µm fibre, terminating 100 µm above the dorsal-most recording site. Light pulses (3 – 300 ms delivered every 2s) were controlled through custom written LabView programs (National Instruments, TX, USA), with each flash duration presented at least 50 times. This protocol was performed either in darkness or under binocular illumination.

4.3.6.3 *Visual stimuli*

Binocular visual stimuli were delivered through two flexible fibre optic light cables (7 mm diameter, Edmund Optics, York, UK) attached to a custom lightsource (components from Thorlabs: NJ, USA and Edmund Optics; York, UK). Light stimuli were generated by 405 nm LEDs, calibrated to provide equal irradiance to either eye. The choice of 405 nm LED ensured each of the mouse photoreceptor classes (which exhibit very similar relative sensitivities at 405 nm) also experienced equivalent irradiance (Sakhi et al., 2014b). The light guides terminated in two internally reflective plastic cones, each positioned snugly over the mouse's eye to prevent light scatter and provide approximately full field illumination (see Figure 4.7A). Neutral density (ND) filter wheels (Thorlabs) allowed for spectrally neutral 10 – 1000 fold reductions in light intensity (ND -3 – ND 0) from the brightest lightstep (15.4 log photons cm^{-2} s^{-1}). Light stimuli were controlled through custom written LabVIEW programs (National Instruments, Austin, TX, USA) such that a 60 s period of dark was followed by a 60 s light step, and then a further 60 s dark. This was repeated at least 3 times at each light intensity used.

4.3.6.4 *Histology*

Following completion of *in vivo* electrophysiology experiments, mice were decapitated and the brains were extracted. Brains were incubated overnight in 4 % PFA at 4 °C before being transferred to 30 % sucrose for cryoprotection. Immunohistochemical processing was performed as described above, staining for ChAT and EYFP. CaseViewer V2.4 software (3DHISTECH, Hungary) was used to visualize and capture images of the processed tissue. The anatomical coordinates of the electrode tip was estimated based on visualisation of CM-DiI fluorescence, in combination with best-matching coronal panels from the Paxinos and Franklin mouse reference atlas (2003).

Projected anatomical locations of each recorded cell was then determined based on the known geometry of the electrode and mapped onto a single coronal anatomical template.

4.3.6.5 *Data analysis*

Optogenetic responses: Cells were classified as ChAT+ve if the mean change in spike rate in the 50 ms following optogenetic stimulation (relative to that in the preceding 100 ms) was significantly greater than zero (one sample t-tests across 50 - 100 trials each; $P < 0.05$). For quantification of response amplitude across stimulus durations we defined 'Peak' response as the average change in spike rate occurring within the same 50 ms window (which captured the initial phasic responses even when stimulus durations were shorter than 50 ms). We also quantified 'Mean' responses, defined as the average increase in spike counts across a 300 ms following stimulus onset (i.e. a window of equal duration to the longest stimulation employed). Where average population peristimulus response data is presented, responses for individual cells were baseline corrected by subtracting the mean spike count in the 100 ms window preceding stimulation.

Visual responses: Basic procedures for analysis of visual responses were similar to the above. In this case cells were defined as light activated or suppressed when the mean change in firing rate during the 60 s stimulus presentation (relative to the preceding 60 s) for the two highest light intensities was significantly above or below 0 respectively (one sample t-tests across 6 trials/stimulus; $P<0.05$). For quantification we calculated mean response (as above) across intensities as well as the average change in baseline firing during the first 500 ms following light onset (a window where neurons in major retinorecipient structures exhibit robust light-driven changes in firing; Howarth et al., 2014; Walmsley and Brown, 2015). Where average population peristimulus response data is presented, responses for individual cells were baseline corrected by subtracting the mean spike count in the 60 s window light presentation.

Synaptic connectivity: A cross-correlation histogram (CCH) was generated for each pair of simultaneously recorded neurons, such that we calculated the spike probability for each test cell as a function of time relative to a spike from a reference cell. We excluded spikes that were triggered by the optogenetic photostimulation (within 500 ms of the start of each optogenetic stimulus), so as to avoid spurious correlations. CCHs were analysed with a conservative threshold for significance ($P < 0.01$ after correction for multiple comparisons) with the peaks or troughs with the shortest lag relative to the reference cell spike used to define the putative type of connectivity. Significant peaks that did not decay by more than 75% after crossing the lag=0ms boundary (i.e. where there was substantially increased spike probability both before and after a reference cell spike) were considered to exhibit shared-input.

4.3.6.6 *Statistical analysis*

Most grouped data were analysed by two-way mixed effects ANOVA, followed by Holm-Šídák's test. However, when data was missing, it was instead analysed by fitting a mixed model as implemented in GraphPad Prism v9.1.2. This uses a compound symmetry covariance matrix, and is fit using Restricted Maximum Likelihood. Proportions were compared using Fisher's exact two-tailed test or Chi-square tests. Statistical analysis was performed using Graphpad Prism v9.1.2 (USA), apart from post-hoc analysis for Chi-squared tests, which were analysed using the 'chisq.posthoc.test' package in R (Ebbert, 2019). This package computes Bonferroni-corrected p values for the analysis of standardized residuals (Beasley and Schumacker, 1995).

As is conventional in electrophysiological studies (Society for Neuroscience, 2018), we treat individual isolated units as independent statistical observations. However, all cells collected from a single animal are not truly independent from each other, as they are all dependent on the physiology of that particular animal (and may be driven by factors such as the animals prior mood, light history, and response to anaesthesia). Results were scrutinized to ensure that any conclusions we draw here were not reliant on the underlying data drawn from a single animal, and so we remain confident in the reliability of our results using this approach.

4.4 Results

4.4.1 **Characterization of ChAT-Cre;Ai32 transgenic mice**

In order to validate our transgenic mouse line and determine its suitability for investigations into diurnal variation in cholinergic signalling and optogenetic manipulation, we first sought to characterize the expression profile of the ChR2 protein in the ChAT-Cre;Ai32 mice and to check for off-target expression of opsins, as well as to confirm that these animals had similar activity levels and circadian-driven behaviour by examining their wheel-running behaviour.

4.4.1.1 *Channelrhodopsin-2 expression in ChAT-Cre;Ai32 mice*

We characterized expression of the ChR2-EYFP reporter protein in both coronal and sagittal sections of the entire mouse brain, simultaneously identifying cholinergic neurons through immunoreactivity for ChAT (Figure 4.2). We found expected co-localisation of ChAT and EYFP immunofluorescence in areas known to have high ChAT expression, including the caudate putamen, medial septum, nucleus of the diagonal band, MHb, oculomotor nucleus and areas in

the cortex. Importantly, we did not observe any off-target EYFP expression, indicating suitability for use in our experiments.

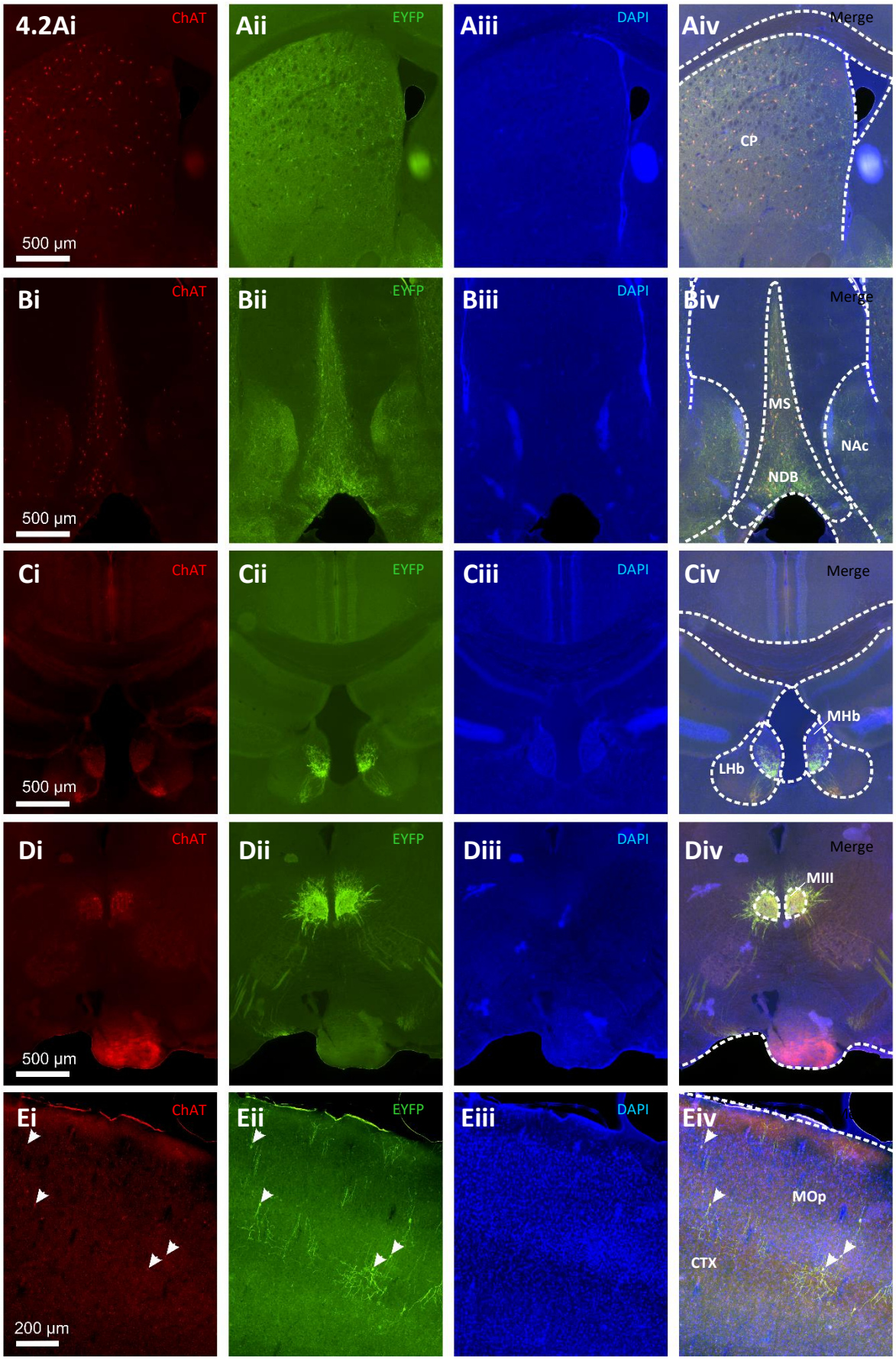
4.2Ai
ChAT
500 μm
Aii
EYFP
Aiii
DAPI
Aiv
Merge
CP
Bi
ChAT
500 μm
Bii
EYFP
Biii
DAPI
Biv
Merge
MS
NAc
NDB
Ci
ChAT
500 μm
Cii
EYFP
Ciii
DAPI
Civ
Merge
MHb
LHb
Di
ChAT
500 μm
Dii
EYFP
Diii
DAPI
Div
Merge
MIII
Ei
ChAT
200 μm
Eii
EYFP
Eiii
DAPI
Eiv
MOp
CTX

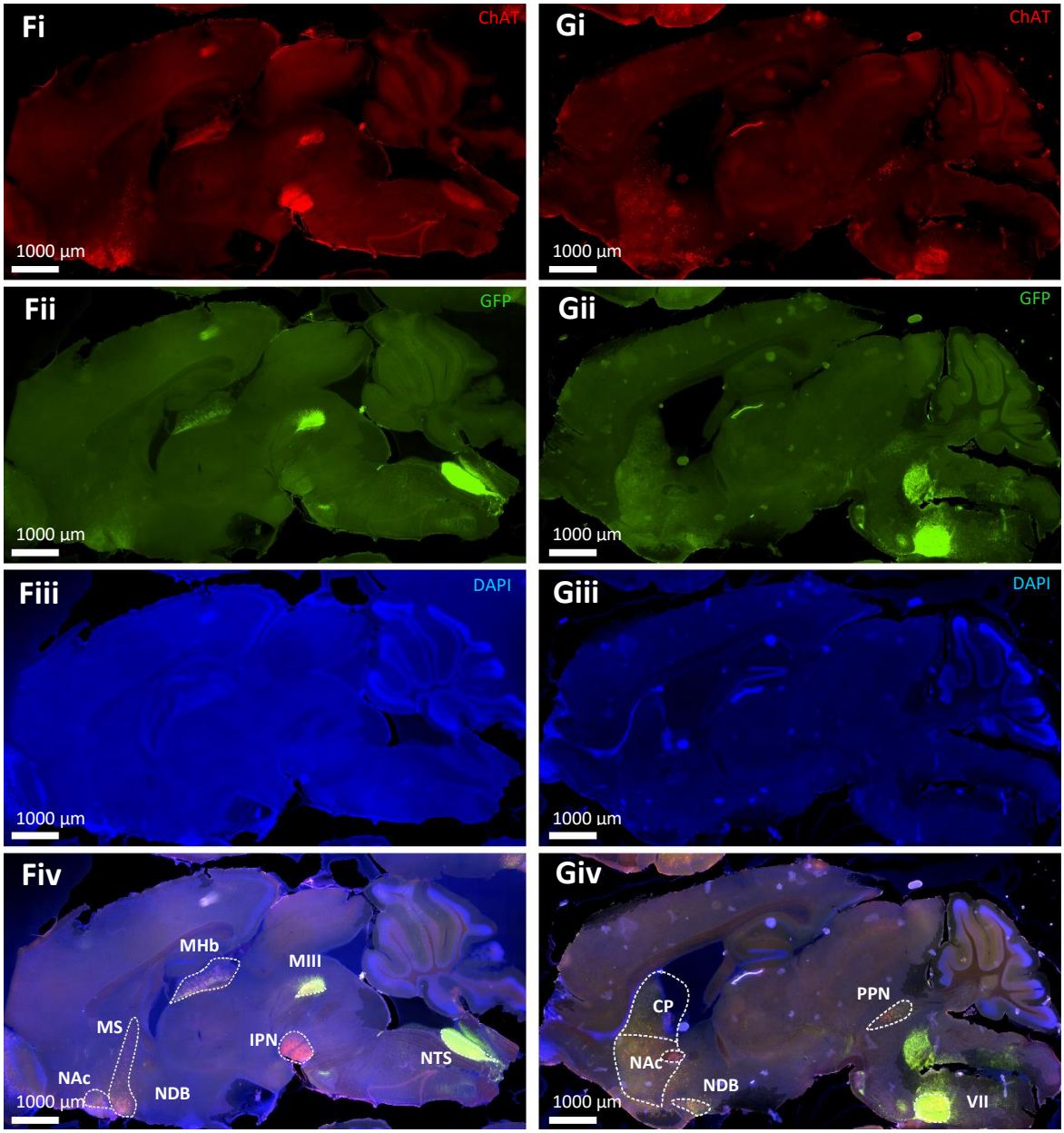

Figure 4.2 Immunofluorescent co-localisation of ChAT and ChR2-EYFP in the brains of ChAT-Cre;Ai32 mice. 40 µm thick brain sections were labelled for ChAT (i), EYFP (ii) and DAPI (iii) to check for co-expression of ChAT and ChR2 in expected brain regions. Panel iv is the composite image of the three channels with anatomical landmarks overlaid. White arrows are examples of co-localization in individual cells.

A – E) Coronal sections demonstrating restricted co-localization of ChAT and EYFP signal in expected areas including A) the caudate putamen (CP), B) the medial septum (MS), nucleus of the diagonal band (NDB) and the nucleus accumbens (NAc), C) the MHb, D) the oculomotor nucleus (MIII) and E) the primary motor area of the cortex (MOp).
F – G) Sagittal sections demonstrating demonstrating restricted co-localization of ChAT and EYFP signal in expected areas including F) the nucleus of the solitary tract (NTS), and G) the pedunculopontine nucleus (PPN) and facial motor nucleus (VII).
Slides were processed using a slidescanner and images were acquired with CaseViewer software at 2X objective (F-G), 5X objective (A – D) or 10X (E).

4.4.1.2 *Circadian wheel-running behaviour*

For reporter mice to be useful tools for studying the cholinergic system, it is important that they drive expression of reporter proteins without perturbing normal mouse behaviour. We assessed the circadian behaviour of both male and female Ai32 and ChAT-Cre;Ai32 mice, as shown in Figure 4.3. The average free-running tau period was calculated for each group, and a two-way ANOVA did not reveal any significant main effects of either sex (Figure 4.3E; F (1, 12) = 0.04, p = 0.84) or genotype (F (1, 12) = 0.70, p = 0.42). There was no evidence of any interaction between these factors (F (1, 12) = 0.19, p = 0.67), suggesting all animals had similar endogenous circadian periods.

We also quantified the robustness of circadian rhythms to investigate if groups had similar levels of rhythmic activity. We did not detect any sex or genotype differences for activity rhythms generated under LD conditions (Figure 4.3F; two-way ANOVA; Sex: F (1, 12) = 0.0342, p = 0.86; Genotype: F (1, 12) = 1.42, p = 0.26; Sex x Genotype: F (1, 12) = 0.394, p = 0.54) or DD conditions (Fig 4.3G; two-way ANOVA; Sex: F (1, 12) = 4.27, p = 0.061; Genotype: F (1, 12) = 0.644, p = 0.44; Sex x Genotype: F (1, 12) = 0.00004, p = 0.99). Together, both the histological analysis and the circadian wheel-running behaviour of the ChAT-cre;Ai32 mice indicated their suitability as tools for investigating the diurnal modulation of cholinergic neurons within the MHb.

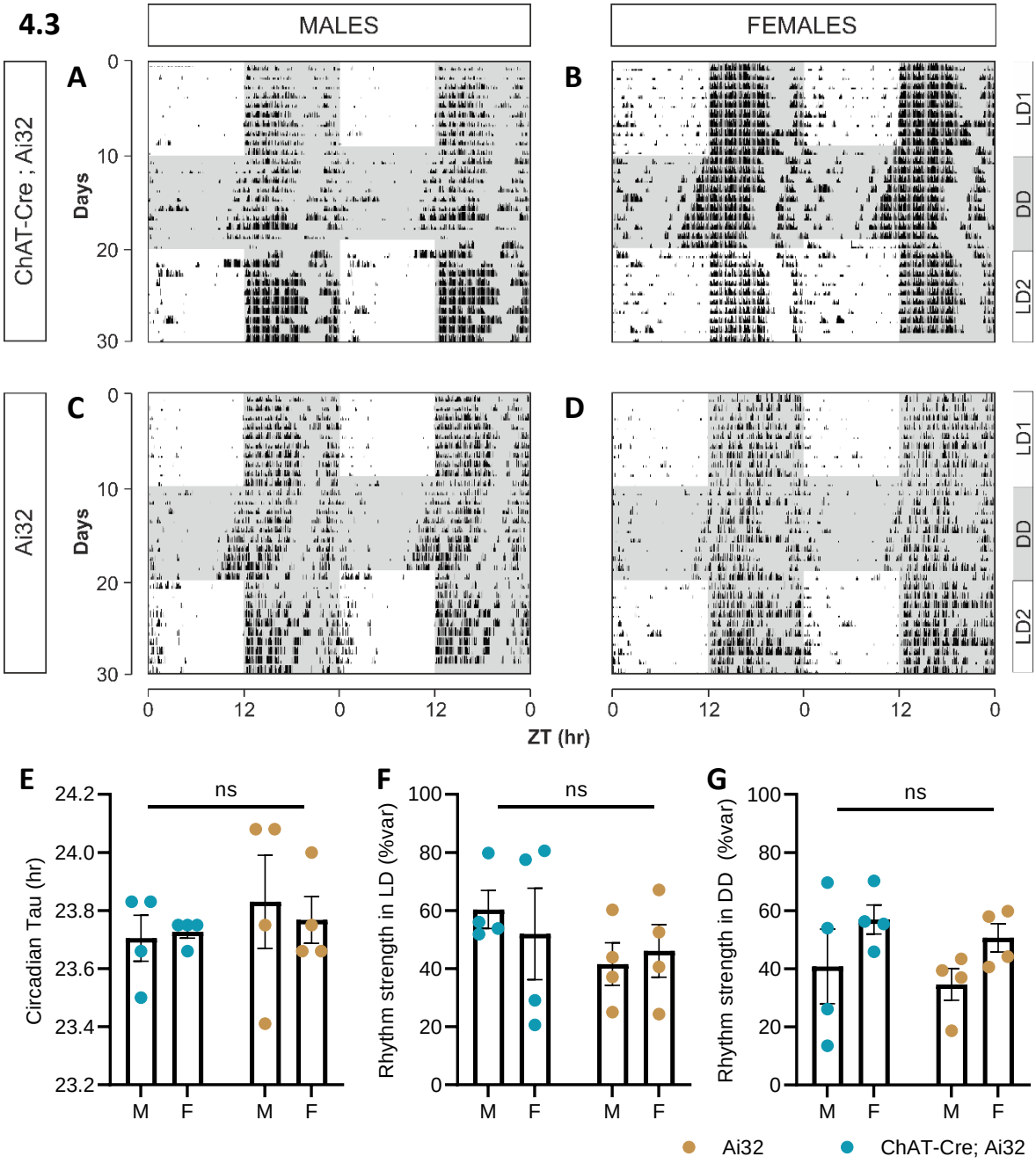

Figure 4.3 Circadian wheel-running activity of ChAT-Cre;Ai32 mice and Ai32 wildtype littermates.

A – D) Representative double-plotted wheel-running actogram for age-matched ChAT-Cre;Ai32 male (A) or female (B) mice or Ai32 males (C) and females (D) under 10 days of 12 hr light / 12 hr dark (LD1); 10 days of complete darkness (DD); and a further 10 days of 12 hr light / 12 hr dark (LD2). Data is presented as percentile distribution in 5 min bins, successive days of activity are plotted top to bottom. Shaded areas represented time spent in dark.

E) Average free-running tau period for each group, with 4 mice per group. There was no significant effect of genotype (two-way ANOVA; F (1, 12) = 0.70, p = 0.42) or sex (F (1, 12) = 0.0411, p = 0.84) on the average tau measurement for each group.

F - G) Quantification of rhythm robustness for each group (n = 4) either under LD (F) or DD (G) conditions. There were no significant differences detected between any of the groups in either condition (two-way ANOVA).

4.4.2 **Viral tracing cholinergic inputs to the MHb**

We injected a retrograde Cre-dependent viral tracer in order to identify an upstream source of cholinergic input to the MHb, as illustrated in Figure 4.4A-B. Three of the four mice we used showed no apparent EYFP expression within either the cell bodies or fibre tracts of any neurons near the MHb. However, EYFP expression was co-localized to ChAT expressing neurons in the cortex, matching the route of the injection, suggesting viral delivery had been off-target in these cases. However, one mouse showed clear and abundant ChR2 expression within the MHb (Figure 4.4C). EYFP expression within cell bodies was restricted exclusively to the ventral portion of the MHb, matching the pattern of ChAT expression in this structure. We also saw clear EYFP expression within neuronal fibres extending to the IPN, the downstream target of the MHb (Figure 4.4D). This suggests that cholinergic neurons within the MHb may exhibit extensive synaptic connections to one another, since the AAV2retro construct used here typically produces minimal anterograde/direct labelling (Tervo et al., 2016).

It should be noted that we were unable to identify any other cell bodies or fibres expressing EYFP in any of the other sections collected from this animal. In particular, we did not observe any EYFP expression in the neural structures which have been hypothesized as the likely upstream sources of cholinergic input to the MHb, including the medial septum, nucleus of the diagonal band, triangular septum or septofimbrial nucleus (see Figure 4.4E-F). This aligns with data from the mouse brain connectivity atlas (Oh et al., 2014), where Cre-dependent anterograde tracer injections into these structures in ChAT-Cre mice fail to produce labelled fibres in the MHb.

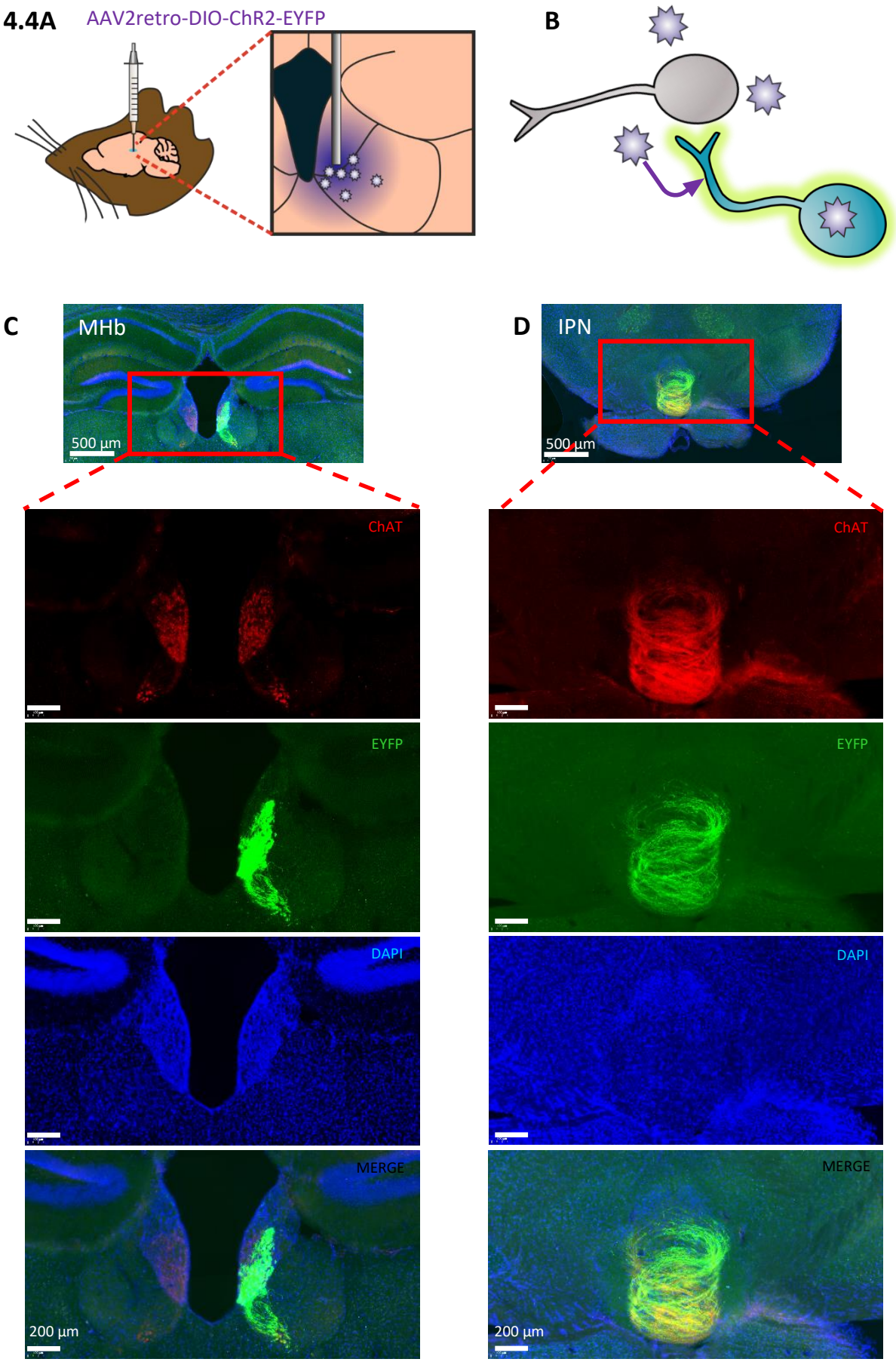
4.4A
AAV2retro-DIO-ChR2-EYFP
B
C
MHb
500 µm
D
IPN
500 µm
ChAT
EYFP
DAPI
MERGE
200 µm
ChAT
EYFP
DAPI
MERGE
200 µm

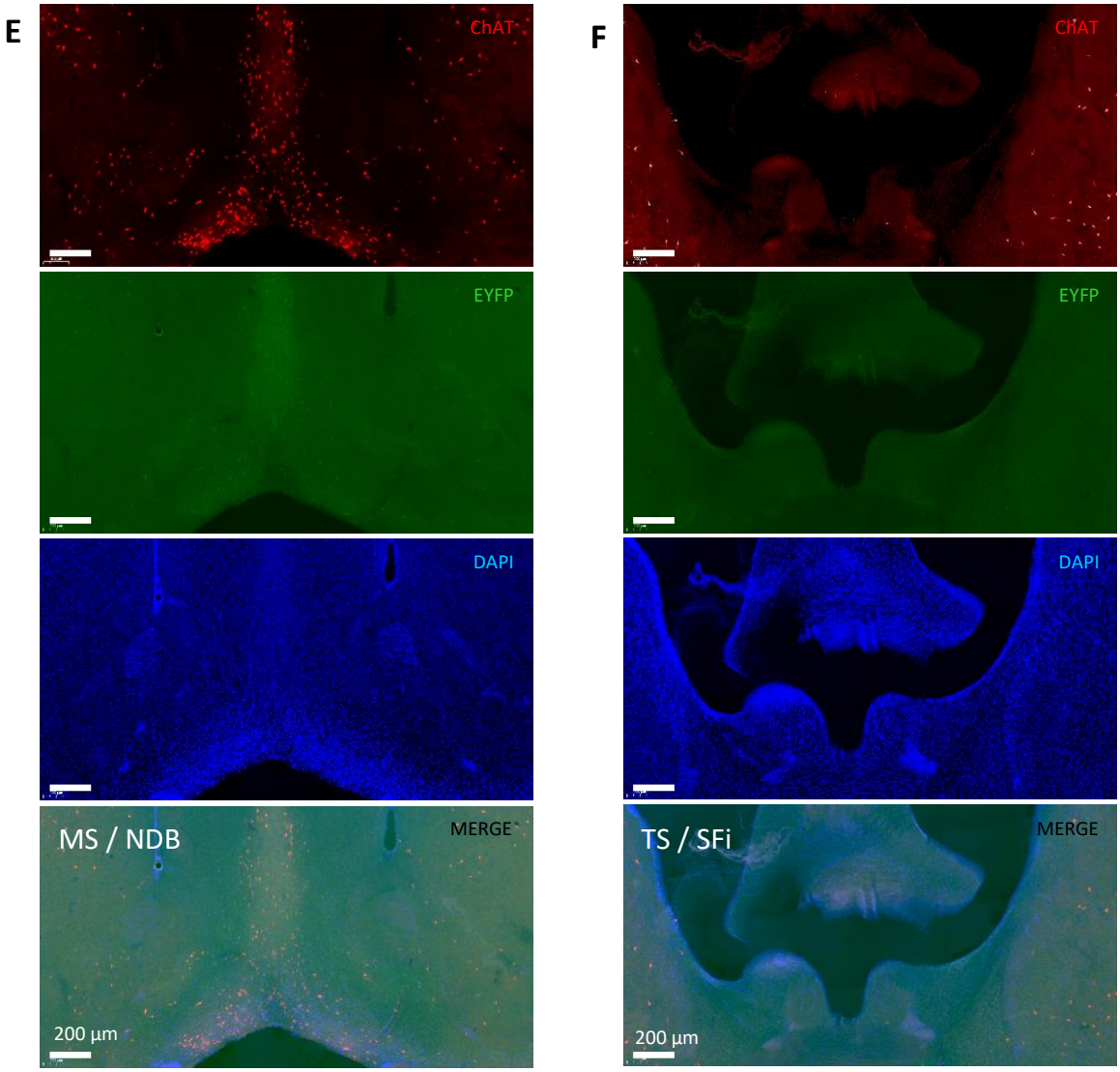

Figure 4.4 Retrograde labelling studies did not reveal an upstream source of cholinergic inputs to the MHb.

A - B) Schematic illustrating the experimental approach for labelling cholinergic neurons that project to the MHb. The double floxed AAV-RG-ChR2-EYFP was injected into the right MHb of ChAT-Cre mice (A). The viral particles are taken up by axonal terminals in the injection site and are then transported back to the cell soma where they transduce the neurons, producing stable expression of ChR2-EYFP in neurons expressing ChAT-cre (B). Histology was performed 4 weeks later to allow transfection.
C – F) Coronal sections were labelled for ChAT (red), EYFP (green), and DAPI (blue) to produce composite images. Clear EYFP expression was restricted to cell bodies found in the MHb (C), and cell fibres located in the fasciculus retroflexus and IPN (D). No EYFP expression was observed in the putative upstream sources of cholinergic input to the MHb, including E) the medial septum (MS) or nucleus of the diagonal band (NDB), or F) the triangular septum (TS) or septofimbrial nucleus (SFi).
Slides were processed using a slidescanner and images were acquired with CaseViewer software at 5X (A – D) or 10X (E) objective.

4.4.3 *In vitro* modulation of cholinergic MHb neurons

To verify that optogenetic stimulation would allow us to functionally identify cholinergic neurons, we performed *in vitro* electrophysiological recordings with acute brain slices from ChAT-Cre;Ai32 mice. pMEAs were used to record from sites spread across both the LHb and the MHb in both hemispheres, and 10 ms ramped optogenetic pulses (Paul et al., 2020) were delivered to the surface of the tissue to activate ChR2 (see Figure 4.5A-C). Figure 4.5D-K illustrates how cells in the MHb and LHb responded to the optogenetic pulse after application of both GluR antagonists and AChR antagonists.

We recorded a total of 46 cells from 10 animals, of which photostimulation only produced an excitatory response in a subset of cells located in the MHb (23.8 % of cells located in the MHb). These responses were absent from any cells recorded in the LHb, which indicated ChAT+ve cells were significantly enriched in the MHb (Figure 4.5L; $p = 0.018$, Fisher's exact test), as expected.

For MHb ChAT+ve cells, delivery of the optogenetic pulse reliably led to a significant increase in average firing rates when compared with the activity immediately preceding the photostimulation (Figure 4.5M; two-way RM ANOVA; Photostimulation: $F(1, 4) = 18.5$, $p = 0.013$). These responses were unchanged by the application of pharmacological modulators (Drugs: $F(2, 8) = 0.902$, $p = 0.44$; Photostimulation x Drugs: $F(2, 8) = 0.597$, $p = 0.57$), indicating that responses were recorded exclusively from ChAT+ve neurons which were directly activated by the photostimulation, rather than through indirect synaptic connections. Together these results confirmed the ChR2 expression within the MHb was functional, and could be reliably identified through photostimulation.

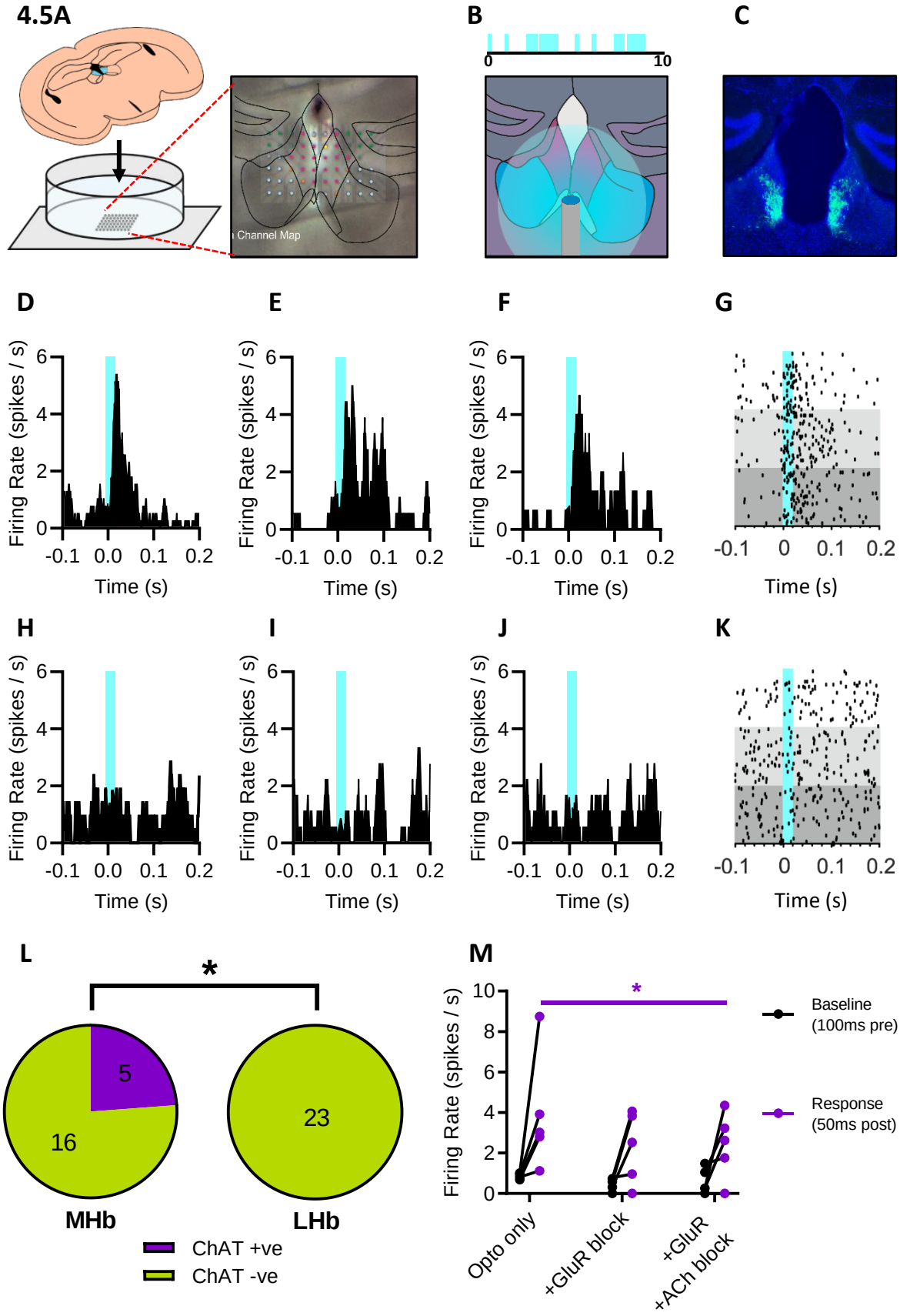
4.5A
Channel Map
B
0
10
C
D
E
F
G
H
I
J
K
Firing Rate (spikes / s)
Time (s)
-0.1 0.0 0.1 0.2
L
*
5
16
23
MHb
LHb
ChAT +ve
ChAT -ve
M
Firing Rate (spikes / s)
Baseline
(100ms pre)
Response
(50ms post)
Opto only
+GluR block
+GluR
+ACh block

Figure 4.5 MHb cholinergic cells were targeted optogenetically and isolated pharmacologically using the pMEA system.

A - B) Schematic diagram demonstrating how cells from the MHb were recorded using the pMEA underneath the slice, with recording contacts spread across both LHb and MHb (A), and B) an optogenetic fibre was placed above the tissue to allow light activation of ChR2 expressing cells. Inset illustrates the photostimulation protocol used (ramped train of light pulses over 10ms).
C) Immunofluorescence microscope image demonstrating how the ChR2 is distributed in the MHb tissue, visualized through EYFP labelling.
D - F) Representative peristimulus histograms from an opto-responsive (and presumed ChAT+ve) cell in the MHb, demonstrating activation of the cell following a 10 ms opto pulse alone (D), in the presence of glutamate receptor blockers alone (E) or in combination with cholinergic receptor blockers (F). Data is presented in 5 ms bins.
G) Corresponding peristimulus raster plot of the MHb cell shown in D – F, demonstrating firing in response to the opto pulse (white), with GluR blockers (light grey) or GluR blockers and AChR blockers (dark grey).
H - J) Representative peristimulus histograms from a cell in the LHb which did not respond to the photostimulation, demonstrating spontaneous behaviour of the neuron following a 10ms opto pulse (H) in the presence of glutamate receptor blockers alone (I) or in combination with cholinergic receptor blockers (J). Data is presented in 5 ms bins.
K) Corresponding peristimulus raster plot of the LHb cell shown in H – J, demonstrating firing in response to the opto pulse alone (white), with GluR blockers (light grey) or GluR blockers and AChR blockers (dark grey).
L) Proportion of opto-responsive cells (presumed to be ChAT+ve) recorded from the MHb and the LHb. There was a significantly greater proportion of ChAT+ve cells recorded in the MHb (Fisher's exact test, p = 0.019).
(M) MHb ChAT+ve cells reliably increased their firing activity in response to the photostimulation protocol (n = 5 ChAT+ve cells from a total of 10 mice, two-way RM ANOVA, Photostimulation: F (1, 4) = 18.5, p = 0.013) and this response was unchanged following the application of the pharmacological treatment (Drugs: F (2, 8) = 0.90, p = 0.44).
Data is presented as the mean ± SEM; *, p<0.05. Presentation of optogenetic photostimulation shown as blue shading on the graphs.

4.4.4 *In vivo* electrophysiology

We next aimed to investigate the activity of cholinergic MHb neurons *in vivo*, in particular to determine whether these cells were visually responsive and how these cells varied according to the time of day. To this end, we performed a series of electrophysiological recordings in anaesthetised ChAT-Cre;Ai32 mice (see Figure 4.6A-C). Direct photostimulation of neurons expressing ChR2 allowed identification of ChAT+ve cells based on their intrinsic photosensitivity.

4.4.4.1 *Optogenetic stimulation of MHb cholinergic neurons in ChAT-Cre;Ai32 mice*

We delivered a series of LED flashes of increasing duration between 3 – 300 ms in order to selectively activate ChAT+ve neurons. We recorded a total of 177 isolated cells, from locations across the MHb and surrounding tissue as shown in Figure 4.6D. ChAT+ve neurons were found

only within the projected boundaries of the MHb. ChAT+ve neurons reliably produced increases in firing activity to photostimulation (Figure 4.6E-H). The average responses from all ChAT+ve neurons shows that responses were sustained for the duration of photostimulation, terminating when the opto pulse ended (Figure 4.6I-M). Approximately a quarter of all cells we recorded were classified as ChAT+ve (Figure 4.6N).

We next examined the effect of different LED pulse durations on the firing of the cells. As expected, ChAT+ve neurons produced significantly greater peak responses in comparison to ChAT-ve neurons at all flash durations tested, even with just 3ms photostimulation (Figure 4.6O; two-way mixed effects ANOVA; Flash duration: F (4, 700) = 70.5, p < 0.0001; Cell type: F (1, 175) = 108.5, p < 0.0001; Flash duration x Cell type: F (4, 700) = 61.1, p <0.0001; Holm-Šídák's post hoc test). We also performed similar analysis on the mean responses of neurons calculated from across the 300 ms following onset of photostimulation (Figure 4.6P). Longer pulse durations produced larger responses in ChAT+ve neurons, which showed significant increases in firing rate relative to ChAT-ve cells at flash durations of 10 ms and longer (two-way mixed effects ANOVA; Flash duration: F (4, 700) = 116.5, p < 0.0001; Cell type: F (1, 175) = 118.1, p < 0.0001; Flash duration x Cell type: F (4, 700) = 106.3, p <0.0001; Holm-Šídák's post hoc test).

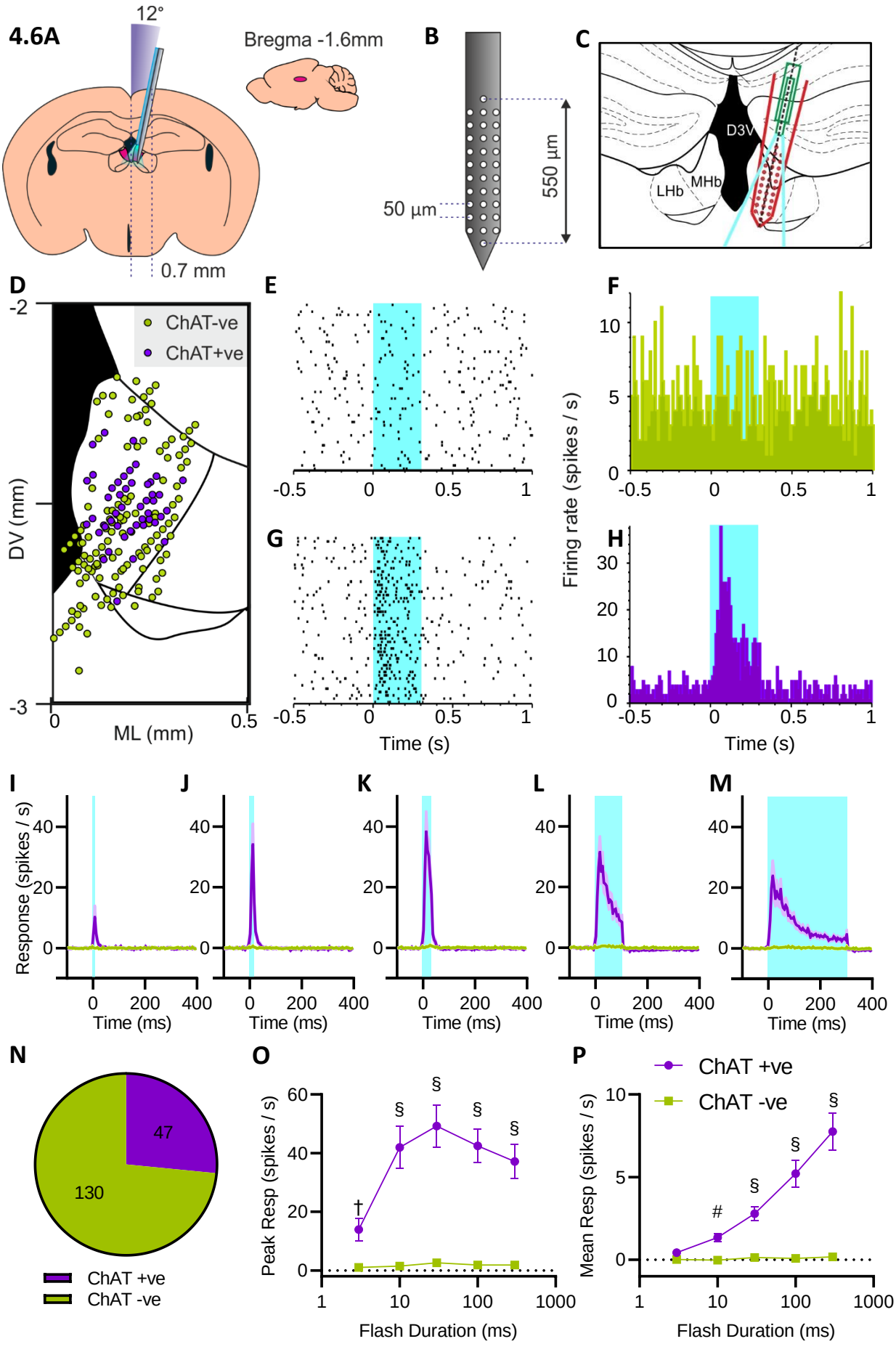
4.6A
12°
Bregma -1.6mm
0.7 mm
B
50 µm
550 µm
C
D3V
MHb
LHb
D
-2
-3
DV (mm)
ML (mm)
0
0.5
ChAT-ve
ChAT+ve
E
F
G
H
Firing rate (spikes / s)
Time (s)
I
J
K
L
M
Response (spikes / s)
Time (ms)
N
47
130
ChAT +ve
ChAT -ve
O
Peak Resp (spikes / s)
Flash Duration (ms)
P
ChAT +ve
ChAT -ve
Mean Resp (spikes / s)
Flash Duration (ms)

Figure 4.6 Optogenetic stimulation reliably activates a subset of MHb neurons in anaesthetized ChAT-Cre; Ai32 mice.

A - C) Schematics demonstrating the stereotactic coordinates used to target the MHb for the *in vivo* electrophysiological recordings (A), the layout of recording contacts on the electrode (B), and the target electrode placement within the MHb (C).
D) Projected anatomical locations of recorded cells classified either as presumed cholinergic cells (ChAT+ve) or non-cholinergic cells (ChAT–ve) depending on whether or not the cell responded to our optogenetic photostimulation. ChAT+ve cells were restricted to the MHb.
E – H) Representative peristimulus raster plots (left) and corresponding peristimulus time histograms (right) showing responses from a single cell in response to 300 ms blue light flashes (100 trials). (E) and (F) depict a cell that was not optogenetically activated and therefore presumed ChAT-ve. (G) and (H) are responses from a cell that was optogenetically activated and therefore presumed ChAT+ve. Histograms are presented with 10 ms bin width.
I - M) Average response profile of cells classified as ChAT+ve or ChAT-ve in response to LED flashes of either I) 3 ms, J) 10 ms, K) 30 ms, L) 100 ms, or M) 300 ms duration.
N) Proportion of total recorded cells that were classified either as ChAT+ve or ChAT –ve.
O) Average peak responses to photostimulation (peak firing rate during flash in 5 ms bin) were significantly greater in ChAT +ve cells than ChAT-ve cells at every flash duration tested (two-way mixed ANOVA, Flash Duration x Cell group: F (4, 700) = 61.1, p = < 0.0001; Holm-Šídák's post-hoc test). Graph displays significant differences between cell types.
P) We also calculated the mean response of the cell across 300 ms (the duration of the longest photosimulation). ChAT+ve cells showed a significantly greater response than ChAT-ve cells only at flash durations of 10 ms and above (two-way mixed effects ANOVA, Flash Duration x Cell group: F (4, 700) = 106.3, p < 0.0001; Holm-Šídák's post-hoc test). Graph displays significant differences between cell types. Data is presented as the mean ± SEM; #, p <0.01; †, p<0.001; §, p<0.0001. Presentation of optogenetic photostimulation shown as blue shading on the graphs.

4.4.4.2 *Binocular illumination drives visual responses in cells of the MHb*

Our next aim was to determine whether neurons in the MHb receive information about external illumination, as has been suggested in previous electrophysiological studies in rats (Zhao and Rusak, 2005). We evaluated how cells responded to 60 s of full field binocular illumination across four logarithmically spaced background light levels (ND -3 to ND 0), delivered via cones fitted over the mouse' eyes as shown in Figure 4.7A. We found robust changes in firing in response to this stimulus in both the MHb, LHb and the paraventricular nucleus of the thalamus. Visually responsive cells did not appear to be restricted to any particular anatomical location (Figure 4.7B) and were either activated or inhibited by the illumination (Figure 4.7C). We found similar proportions of activated and inhibited visual responses in both ChAT+ve and ChAT-ve MHb cells (Figure 4.7D-E; $\chi^2(2, N = 148) = 3.08$, $p = 0.21$). Across all the anatomical locations we examined, the majority of cells were not visually responsive, and the proportions of light-activated and light-inhibited cells were similar (Figure 4.7F).

Both light-activated and light-inhibited cells exhibited sluggish but sustained responses, as shown in Figure G-N, which often lasted beyond the termination of the light stimulus. In order to identify if visual responses were a result of direct retinal innervation, we examined how both ChAT+ve and ChAT-ve neurons responded to visual illumination in the first 500 ms following light onset at varying light intensities. Neither light-activated (Figure 4.7O; two-way mixed effects ANOVA; ND: F (3, 60) = 0.84, p = 0.48) nor light-inhibited responses were significantly altered by increasing the light intensity (Figure 4.7Q; F (3, 51) = 0.358, p = 0.78), and activity was similar between cell types (Activated, Cell type: F (1, 20) = 0.189, p = 0.67; Inhibited, Cell type: F (1, 17) = 0.0289, p = 0.86). There was no significant interaction between these factors (Activated, ND x Cell type: F (3, 60) = 0.19, p = 0.90; Inhibited, ND x Cell type: F (3, 51) = 0.375, p = 0.77). This suggests that information about light did not reach the MHb via a direct synaptic circuit, as neurons in major retinorecipient structures are robustly activated within the first 500 ms of such light steps (Howarth et al., 2014; Walmsley and Brown, 2015).

In contrast, when we examined average responses from MHb neurons across the duration of the binocular illumination we found that both light-activated (Figure 4.7P; two-way mixed effects ANOVA; ND: F (3, 60) = 17.6, p < 0.0001) and light-inhibited cells (Figure 4.7R; two-way mixed effects ANOVA; ND: F (3, 51) = 6.22, p = 0.0011) demonstrated a significant main effect of increasing light intensity on their response size. In both cases, responses were similar between ChAT+ve and ChAT-ve cells (Activated, Cell type: F (1, 20) = 1.707, p = 0.21; Inhibited, Cell type: F (1, 17) = 0.0737, p = 0.79). There was no significant interaction between light intensity and cell type (Activated, ND x Cell type: F (3, 60) = 0.328, p = 0.81; Inhibited, ND x Cell type: F (3, 51) = 0.502, p = 0.68). Holm-Šídák's post-hoc tests indicated that only the two brightest illumination intensities used were sufficient to drive either significantly activated or suppressed responses compared to neural activity recorded at the dimmest light intensity.

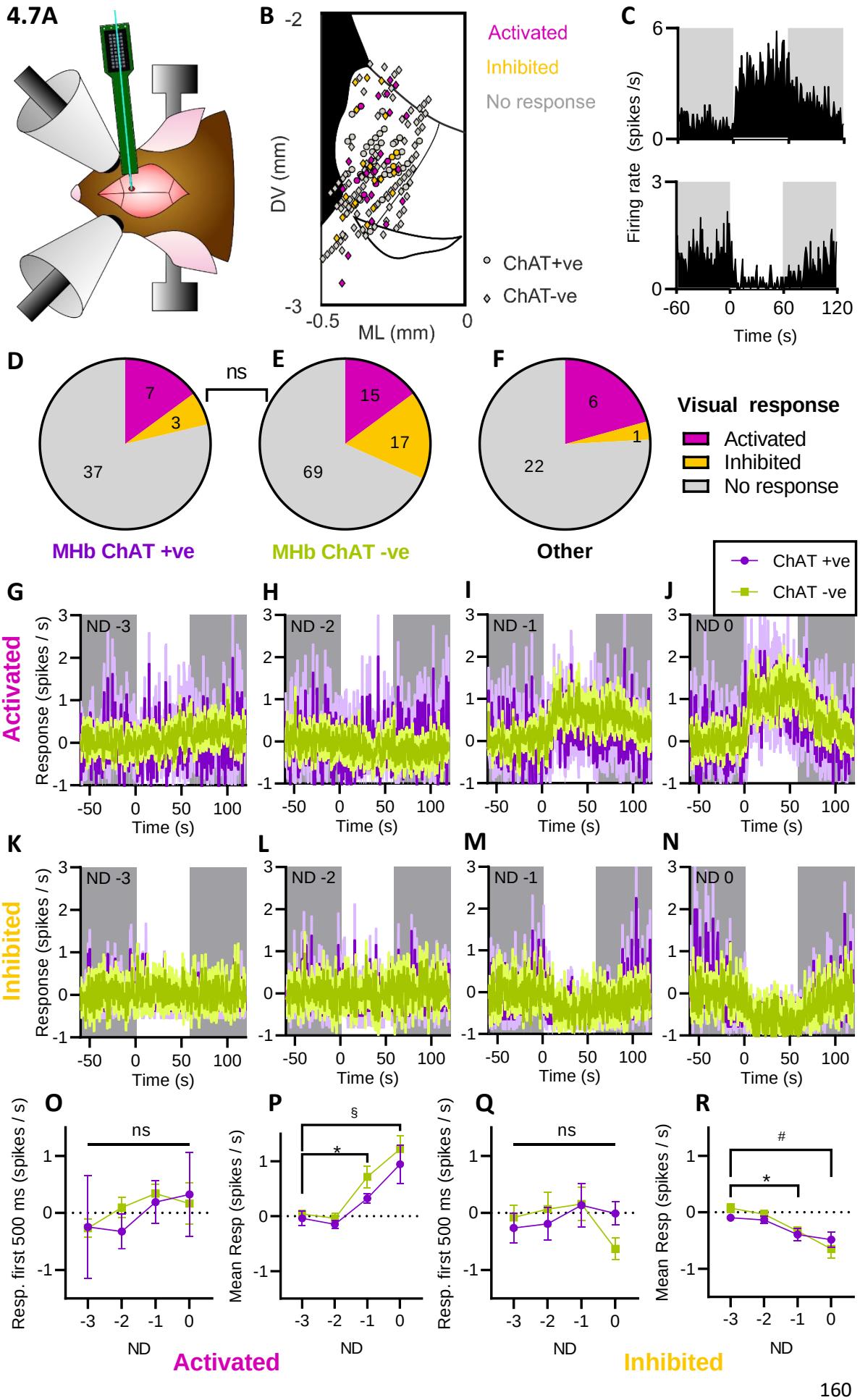
4.7A
B
-2
DV (mm)
-3
-0.5
ML (mm)
0
Activated
Inhibited
No response
ChAT+ve
ChAT-ve
C
6
0
Firing rate (spikes /s)
3
0
-60
0
60
120
Time (s)
D
7
3
37
ns
E
15
17
69
F
6
1
22
Visual response
Activated
Inhibited
No response
MHb ChAT +ve
MHb ChAT -ve
Other
ChAT +ve
ChAT -ve
G
H
I
J
Activated
ND -3
ND -2
ND -1
ND 0
Response (spikes / s)
Time (s)
K
L
M
N
Inhibited
O
P
Q
R
Resp. first 500 ms (spikes / s)
Mean Resp (spikes / s)
ns
*
§
#
ND
Activated
Inhibited

Figure 4.7 Binocular illumination produced both light-activated and light-suppressed visual responses in cells located across the MHb.

A) Schematic demonstrating how binocular illumination was achieved. The mouse was head-fixed using ear and bite-bars, and two flexible fibre optic light cables terminated in internally reflective plastic cones fitted over the mouse's eyes delivered full field illumination. An electrode with connected optical fibre was used to both record and optogenetically stimulate cells within the right MHb.
B) Projected anatomical locations of cells classified either as light-activated (pink), light-inhibited (yellow) or not visually responsive (grey). ChAT+ve cells are shown as circles and ChAT-ve cells are diamonds.
C) Representative peristimulus time histograms showing responses to binocular illumination of 60 s light at the highest light intensity (ND 0) from a light-activated (top) and a light-inhibited (bottom) cell in the mouse MHb. Data is the response from 6 trials with bin width 1s.
D – F) Proportions of cells classified as light-activated, light-inhibited, or no response to binocular illumination for MHb ChAT+ve cells (D), MHb ChAT-ve cells (E), or cells recorded outside the projected boundaries of the MHb (F). There was no difference in the proportions of responses between MHb cells (Chi-square test, $\chi_2(2, N = 148) = 3.08$, $p = 0.21$).
G – J) Mean ± SEM peristimulus time histograms from either ChAT+ve (purple) or ChAT-ve (green) cells that were classified as light-activated (ChAT+ve, $n = 7$; ChAT-ve, $n = 21$) in response to 60 s binocular illumination at varying light intensities: ND -3 (G); ND -2 (H); ND -1 (I); or ND 0 (J).
K – N) Mean ± SEM peristimulus time histograms from either ChAT+ve (purple) or ChAT-ve (green) cells that were classified as light-inhibited (ChAT+ve, $n = 3$; ChAT-ve, $n = 18$) in response to 60 s binocular illumination at varying light intensities: ND -3 (K); ND -2 (L); ND -1 (M); or ND 0 (N).
O) There was no significant effect of cell type or light intensity on the average MHb light-activated responses recorded during the initial 500 ms of binocular illumination (two-way mixed effects ANOVA, Cell type: $F(1, 20) = 0.189$, $p = 0.18$; Light intensity: $F(3, 60) = 0.841$, $p = 0.48$).
P) Light-activated ChAT+ve and ChAT-ve cells in the MHb responded similarly to binocular illumination, significantly increasing their responses compared to ND -3 at light intensities of ND -1 and above (two-way mixed effects ANOVA; Cell type: $F(1, 20) = 1.707$, $p=0.206$, ND: $F(3, 60) = 17.6$, $p < 0.0001$; Holm-Šídák's post-hoc test).
Q) Light-inhibited ChAT+ve and ChAT-ve cells in the MHb responded similarly across all light intensities during the first 500 ms of the illumination (two-way mixed effects ANOVA, Cell type: $F(1, 17) = 0.0289$, $p = 0.87$; Light intensity: $F(3, 51) = 0.358$, $p = 0.78$).
R) Light-activated ChAT+ve and ChAT-ve cells in the MHb responded similarly to binocular illumination, significantly increasing their responses compared to ND -3 at light intensities of ND -1 and above (two-way mixed effects ANOVA; $F(3, 51) = 6.22$, $p = 0.0011$; Holm-Šídák's post-hoc test).
Data is presented as the mean ± SEM; *, $p<0.05$; #, $p<0.01$; §, $p<0.0001$. Grey shaded areas represent periods of darkness in figures C, G-N.

4.4.4.3 *Light environment does not modulate cholinergic neuron responses to photostimulation*

As we saw that a subset of ChAT+ve neurons were responsive to binocular illumination, we then investigated whether changing the light environment might alter the responses to optogenetic photostimulation. MHb ChAT+ve neurons were activated with LED pulses of increasing duration, either whilst the mouse was left in darkness or receiving constant full field binocular illumination (ND 0). The two-way RM ANOVA revealed the expected main effect of flash duration on both

light-activated (Figure 4.8A-B; Peak response, Flash duration: F (4, 24) = 3.87, p = 0.015; Mean response, Flash duration: F (4, 24) = 6.19, p = 0.0014) and light-inhibited photostimulation-driven peak and mean responses (Figure 4.8C-D; Peak response, Flash duration: F (4, 8) = 9.72, p = 0.0037; Mean response, Flash duration: F (4, 8) = 6.46, p = 0.013). However, there was no significant main effect of light environment on any of these responses in either light-activated (Peak response, Light environment: F (1, 6) = 0.50, p = 0.51; Mean response, Light environment: F (1, 6) = 2.01, p = 0.21) or light-inhibited cells (Peak response, Light environment: F (1, 2) = 5.43, p = 0.15; Mean response, Light environment: F (1, 2) = 1.74, p = 0.32). There was no evidence of a significant interaction between these terms on the peak responses (Activated, Flash duration x Light environment: F (4, 24) = 1.76, p = 0.17; Inhibited, Flash duration x Light environment: F (4, 8) = 0.31, p = 0.86) or mean responses (Activated, Flash duration x Light environment: F (4, 24) = 0.38, p =0.82; Inhibited, Flash duration x Light environment: F (4, 8) = 1.01, p = 0.46). This indicates that light-modulated activity of MHb cholinergic neurons does not noticeably influence their intrinsic excitability.

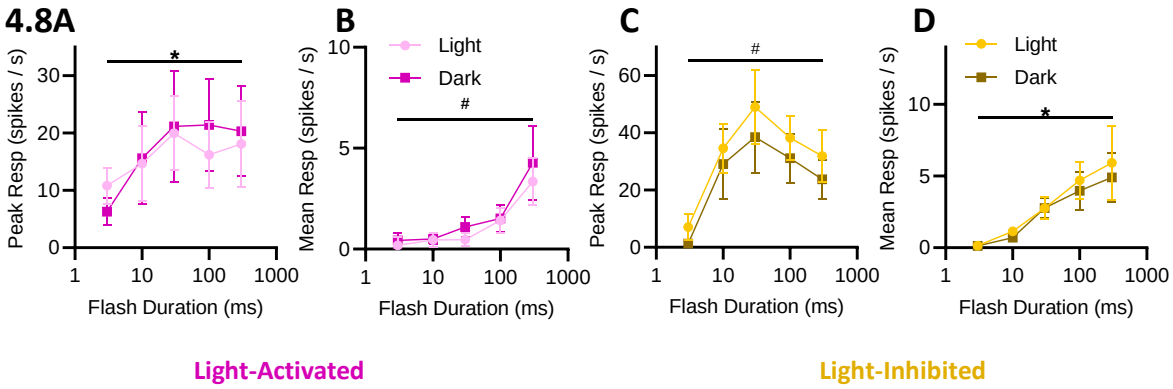

Figure 4.8 Visually-responsive MHb cholinergic neuron responses to optogenetic photostimulation are not modulated by the light environment. Mice received optogenetic LED flashes either in darkness or under constant binocular illumination.

A - B) Two-way RM ANOVAs revealed that there was a significant effect of flash duration on both peak (C; F (4, 24) = 3.8, p =0.015) and mean responses (F (4, 24) = 6.19; p = 0.0014) of light-activated ChAT+ve MHb neurons (n = 7) but there was no significant effect of binocular illumination.
C - D) Similarly, two-way RM ANOVAs showed that light-inhibited MHb ChAT+ve cells (n = 3) peak and mean responses to optogenetic photostimulation were significantly affected by flash duration (peak responses, F (4, 8) = 9.72, p = 0.0037; mean responses F (4, 8) = 6.46, p = 0.013) but not by binocular illumination
Data is presented as the mean ± SEM; *, p<0.05; #, p<0.01.

4.4.4.4 *Time of day modulates MHb neuronal properties*

We also wanted to know whether there was a time of day influence on cholinergic neurons of the MHb. Experiments were performed either during the day (n = 23 cells from 4 mice) or during the night (n = 24 cells from 6 mice), and so initially we compared the opto-responses between these two time points (Figure 4.9A-E). Interestingly, a significantly greater proportion of the cells we isolated were ChAT+ve cells, when recording from the MHb during the day compared to the night (Figure 4.9F-G; p = 0.0084, Fisher's exact test), potentially suggesting a greater subset of non-cholinergic MHb neurons were silent during the day. Further, among ChAT+ve cells, a two-way mixed effects ANOVA revealed that there was a significant main effect of Flash duration on both the peak (Figure 4.9H; F (4, 180) = 25.6, p < 0.0001) and mean responses (Figure 4.9I; F (4, 180) = 42.5, p < 0.0001) with increased pulse widths producing increased responses at both time points as anticipated. Visual inspection of the data suggested greater peak responses from ChAT+ve neurons recorded during the night than the day, but this main effect did not reach significance (Time of day: F (1, 45) = 3.83, p = 0.056), nor did the interaction with Flash duration (Time of day x Flash duration: F (4, 180) = 1.90, p = 0.11). Mean responses calculated from across the duration of the flash were very similar between night and day (Time of day: F (1, 45) = 0.069, p = 0.79), and again there was no evidence of any interaction effects (F (4, 180) = 0.823, p = 0.51).

Since the precise recording times for 'day' and 'night' experiments analysed above varied somewhat across recordings, we next performed a higher resolution examination of how neuronal peak responses vary according to the time of day. Data from all the experiments was divided into 2 hr bins which corresponded to the projected circadian time of recording. There was a tendency for peak responses to increase across the late projected day and into the early night, before decreasing during the middle of the night (Figure 4.9J). A two-way mixed effects ANOVA was employed to investigate how responses were affected by time of day and flash duration, revealing a significant interaction effect (ZT: F (6, 86) = 2.61, p = 0.02; Flash duration: F (4, 344) = 47.1, p < 0.0001; ZT x Flash duration: F (24, 344) = 1.72, p = 0.02). Holm-Šídák's post-hoc test identified peak responses that significantly differed from those recorded at ZT 5 using flash durations of both 30 and 100 ms, as indicated on the graph. Similarly, there was a significant interaction between ZT and Flash duration on the mean responses (Figure 4.9K; ZT: F (6, 86) = 1.60, p = 0.15; Flash duration: F (4, 344) = 53.5, p < 0.0001; ZT x Flash duration: F (24, 344) = 2.25, p = 0.0009). Mean responses varied significantly from those collected at ZT 5 at various points across the circadian cycle, but only using the longest duration of optogenetic stimulation (Holm-Šídák's post-hoc test). Collectively, these data suggest intrinsic excitability of MHb ChAT+ve neurons is enhanced around the dusk-transition.

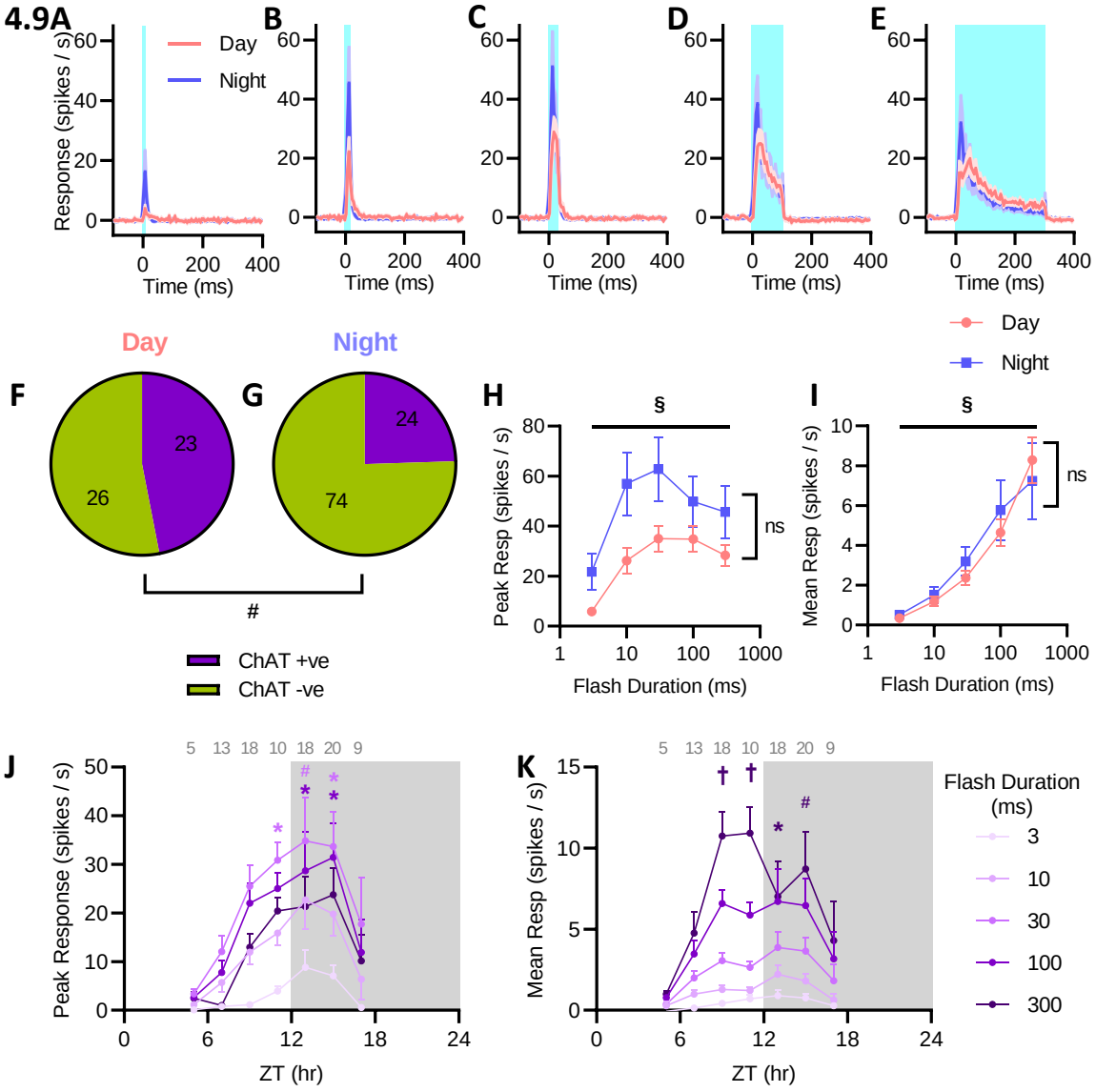

Figure 4.9 MHb cholinergic neuronal response properties are modulated by the time of day.

A – E) Average peristimulus time histograms of ChAT+ve MHb cells recorded during the day (*n* = 23) or night (*n* = 24) in response to LED flashes of either A) 3 ms, B) 10 ms, C) 30 ms, D) 100 ms, or E) 300 ms duration.
F - G) Pie charts showing how the proportion of cholinergic cells varied between day (F) and night (G; Fisher's exact test).
H) There was a significant main effect of flash duration on the peak responses (two-way mixed ANOVA; Flash Duration: F (4, 180) = 25.6, p < 0.0001), but no main effect of Time of day (F (1, 45) = 3.83, p = 0.056).
I) There was a significant main effect of flash duration (two-way mixed effects ANOVA; Flash Duration: F (4, 180) = 42.46, p < 0.0001) but not of time of day (F (1, 45) = 0.0689, p = 0.79) on the mean response of the neurons across the duration of the flash driven by optogenetic photostimulation.
J – K) The data was collapsed into 2 hr bins to examine how ChAT+ve neuronal responses to LED photostimulation varied according to the projected time of day. Shaded areas represent the projected night. There was a significant interaction between ZT and Flash Duration on both the peak (J; F (24, 344) = 1.72, p = 0.02) and mean responses (K; F (24, 344) = 2.25, p = 0.0009). Graphs display significant differences from ZT 5 at each flash duration (Holm-Šídák's post-hoc test), numbers in grey above the graph represent number of cells contributing to each data point.
Data is presented as the mean ± SEM; *, p<0.05; #, p<0.01; †, p<0.001.

Previous studies have shown that MHb neuronal spontaneous firing rates exhibit diurnal variation (Sakhi et al., 2014a; Zhao and Rusak, 2005) and so we investigated how steady state firing from cells recorded in the MHb varied according to the time of day. Again, we portioned the data collected from across the experiment into 2 hr bins, this time examining the spontaneous firing collected during epochs of darkness (i.e., without visual illumination) and without optogenetic stimulation. We examined the activity of both ChAT+ve and ChAT-ve MHb cells, and found that there was significant variation in firing rates across the projected day (Figure 4.10A; mixed effects model, ZT: F (5, 132) = 8.05, $p < 0.0001$; Holm-Šídák's post-hoc tests illustrated graphically), although there was no evidence that cholinergic neurons had a different profile of diurnal variation compared to other MHb neurons (Cell type: F (1, 174) = 2.20, $p = 0.14$; Cell type x ZT: F (5, 132) = 0.426, $p = 0.83$). Across the 12 hours of data collected, we observed maximal firing rates occurring during the mid-projected day and a nadir following the transition between projected day and night.

We also compared diurnal profiles of steady state firing rates between the two classes of visually responsive MHb cells (including ChAT+ve and –ve examples). A mixed effects model showed that light-activated and light-inhibited cells did not differ significantly from each other in their diurnal firing activity (Figure 4.10B; Cell type: F (1, 40) = 0.035, $p = 0.85$). There was no evidence that firing rates varied significantly across the projected day (ZT: F (5, 11) = 1.63, $p = 0.23$), and the interaction between ZT and Cell type was not significant (F (5, 11) = 1.18, $p = 0.38$).

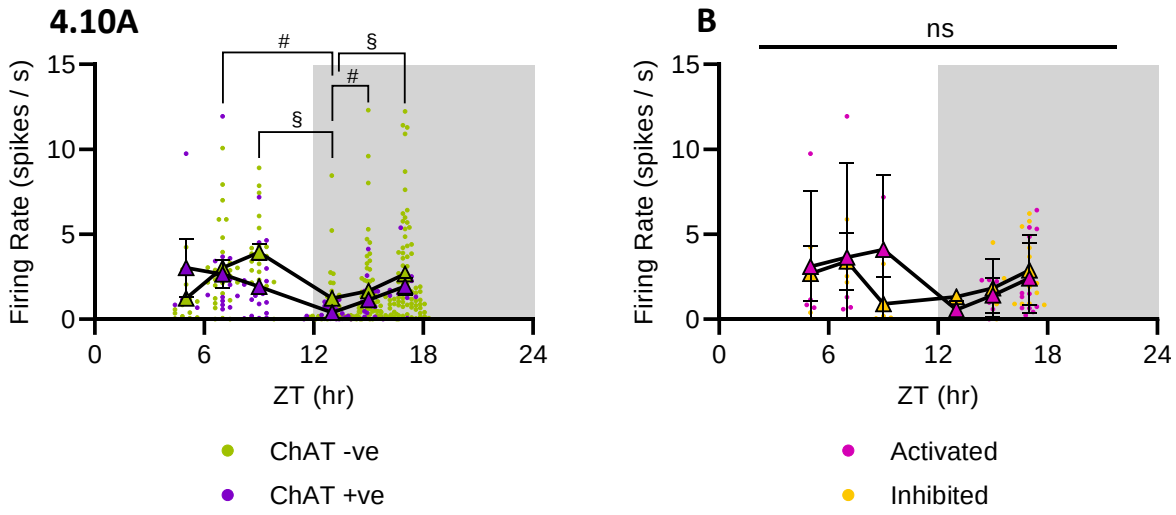

Figure 4.10 Steady state firing rates of MHb neurons are modulated by the projected time of day.

A) Firing rates from cells recorded without environmental illumination across the recordings were collapsed into 2 hr bins to examine the diurnal profile of both ChAT+ve (*n* = 47) and ChAT-ve (*n* = 101) MHb neurons. A mixed-effects analysis showed that MHb cells modulated their firing according to the time of day ($F(5, 115) = 7.94$, $p < 0.0001$) and this activity did not significantly differ between ChAT+ve and ChAT-ve cells ($F(1, 146) = 2.35$, $p = 0.13$). The results of Holm-Šídák's post-hoc tests examining the main effect of ZT on MHb neurons are shown on the graph. There were no ChAT-ve cells recorded during ZT11 and so this timepoint was excluded to allow analysis.
B) Similarly, steady state firing rates from both light-activated (*n* = 22) and light-inhibited cells (*n* = 20) were collapsed into 2hr bins to examine diurnal variation in these groups. A mixed-effects analysis showed that visually responsive cells modulated their firing according to the time of day ($F(6, 14) = 3.46$, $p = 0.026$), and this was similar between light-activated and light-inhibited cells ($F(1, 40) = 0.855$, $p = 0.36$). Holm-Šídák's post-hoc analysis did not reveal any significant differences between firing rates at any ZT. Data from ZT11 was excluded as few cells were recorded at this time point.
Data is presented as the mean ± SEM; *, $p<0.05$; #, $p<0.01$; §, $p<0.0001$.

4.4.4.5 *Synaptic communication across MHb cells*

The final investigation we undertook examined the synaptic connectivity of neurons simultaneously recorded in our dataset. We calculated the cross-correlation histograms (CCH) of 2076 pairs of neurons, grouped according to whether the cells were cholinergic or not. The pattern of CCH indicated the putative (direct or indirect) functional communication between the pairs of cells, as shown in Figure 4.11A-E. The majority of cell interactions showed no correlation and therefore indicated a lack of functional connection (ChAT+ve x ChAT+ve, 156/388; ChAT+ve x ChAT-ve, 259/362; ChAT-ve x ChAT-ve, 930/1326), and were not included in the subsequent analysis.

There was a diversity in the profiles of the CCHs for different pairs of neurons, grouped into five types based on the nature and direction of influence between the two cells. Figure 4.11F demonstrates the proportion of synaptic connectivity patterns observed within each group of paired neurons, which was shown to be unequally distributed between groups (X^2 (10, N = 731) = 198.6, $p < 0.0001$). Post hoc comparisons of synaptic connectivity patterns by cell pair types revealed that the ChAT+ve x ChAT+ve cell pairs had a significantly greater than expected proportion of shared input connectivity patterns ($p < 0.0001$), nearly half of all pairs of ChAT+ve cells. Conversely, within the ChAT-ve x ChAT-ve pairings, cells were connected via shared inputs less than the expected proportion ($p = 0.00013$). Other types of connectivity, likely reflecting mono- or polysynaptic connections between neurons pairs were generally rare across all populations examined (<5% of pairs tested). Nonetheless, ChAT+ve x ChAT+ve cell pairs also had a significantly smaller proportion of correlation patterns consistent with inhibitory inputs or outputs (-veIN, $p = 0.00076$; -veOUT, $p = 0.0025$).

We compared the average latency of the peak or trough in the CCH for each group of paired neurons (Figure 4.11G). A two-way ANOVA revealed a significant interaction between the synaptic connectivity pattern and the groups of neuron pairs (Connectivity pattern x Group: F (8, 716) = 2.55, $p = 0.0097$; Connectivity pattern: F (4, 716) = 163.1, $p < 0.0001$; Group: F (2, 716) = 0.021, $p = 0.98$). Post-hoc analysis indicated that for ChAT+ve cells receiving inhibitory influence from other ChAT+ve cells, the lag time was significantly slower (M = -40.1 ± 6.3 ms) than for either ChAT+ve x ChAT-ve pairs (M = -22.5 ± 4.8 ms, $p = 0.0024$; Holm-Šídák's post-hoc test) or ChAT-ve x ChAT-ve pairs (M = -31.5 ± 3.1 ms, $p = 0.049$). Such inhibitory influences were also substantially slower than excitatory influences between ChAT+ve neurons pairs which had an average latency of 3.1 ± 0.59 ms. The latter is more in line with what one might expect for a monosynaptic connection, while the inhibitory connections are presumably less direct in nature (in at least some cases).

We also calculated the average change in spike probability of the peak or trough in the CCH for each group of paired neurons (Figure 4.11H). There was no evidence that the cell type of the paired neurons influenced the amplitude (two-way ANOVA; group: F (2, 716) = 0.021, $p = 0.98$; interaction: F (8, 716) = 1.49, $p = 0.16$), although there was significant effect of the type of synaptic connectivity (Connectivity pattern: F (4, 716) = 163.1, $p < 0.0001$), with the shared connection type associated with more pronounced changes in spike probability relative to other types of connections.

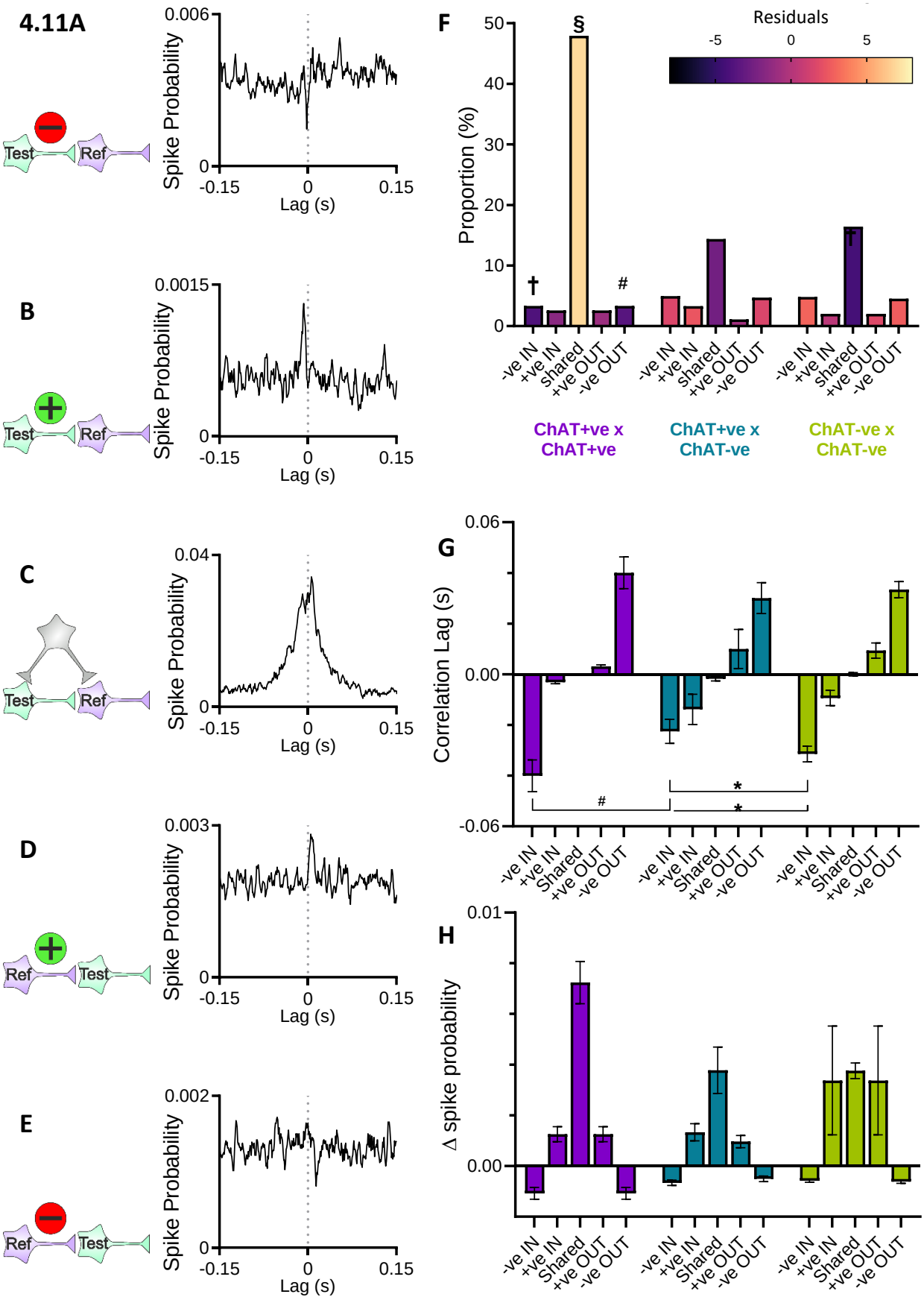
4.11A
Test
Ref
Spike Probability
Lag (s)
B
C
D
E
F
Residuals
Proportion (%)
-ve IN
+ve IN
Shared
+ve OUT
-ve OUT
ChAT+ve x ChAT+ve
ChAT+ve x ChAT-ve
ChAT-ve x ChAT-ve
G
Correlation Lag (s)
H
Δ spike probability

Figure 4.11 Synaptic connectivity of cells within the MHb. Each pair of simultaneously recorded neurons from across the 10 *in vivo* experiments was analyzed to determine the pattern of connectivity by generating cross-correlation histograms (CCHs), with a conservative threshold for significance (P < 0.01). Spikes triggered by optogenetic photostimulation were not included.

A) Representative CCH showing a -veIN connection between two ChAT-ve cells. Left, schematic depicting the relationship between the test (aqua) and the reference cell (mauve) for this classification: the test cell tends to decrease firing before reference cell fires a spike, consistent with inhibitory input to reference cell.
B) Representative CCH showing a +veIN connection between two ChAT-ve cells. The test cell tends to increase firing before reference cell fires a spike, consistent with excitatory input to reference cell.
C) Representative CCH of two ChAT+ve cells with a shared input. Test and reference cells tend to be active at similar times.
D) Representative CCH of +veOUT relationship between a ChAT+ve cell (reference) and ChAT-ve cell (test). Test cell tends to increase firing after reference cell fires a spike, consistent with excitatory input from reference cell.
E) Representative CCH of -veOUT relationship between a ChAT+ve cell (reference) and ChAT-ve cell (test). Test cell tends to decrease firing after reference cell fires a spike, consistent with inhibitory input from reference cell.
F) Proportion of connectivity patterns observed for each group of paired neurons (non correlated relationships were not included on the graph or in subsequent analysis). A Chi square test revealed that there was a significant association between these variables (X^2 (10, N = 731) = 198.6, p < 0.0001; post-hoc tests Bonferroni-adjusted). Bars are coloured according to the size of their residual values, as shown in the heatmap (inset above).
G) Average latency of the peak or trough in the CCH for each group of paired neurons. –veIN cell latencies were significantly larger in ChAT+ve x ChAT+ve pairs than the other groups of neuron pairs (two-way ANOVA; connectivity pattern x group: F (8, 716) = 2.55, p = 0.0097, Holm-Šídák's post-hoc test).
H) Average change in spike probability of the peak or trough in the CCH for each group of paired neurons. There was no evidence that the type of paired neurons influenced the amplitude (two-way ANOVA; group: F (2, 716) = 0.021, p = 0.98), although this was significantly affected by the type of synaptic connectivity (connectivity pattern: F (4, 716) = 163.1, p < 0.0001).
Data is presented as the mean ± SEM; *, p<0.05; #, p<0.01; §, p<0.0001.

4.5 Discussion

Previous studies involving the MHb have suggested that, in rats, some MHb cells may be photo-responsive and/or exhibit day-night variations in firing. This study set out to further examine the extent to which this was true also of the mouse MHb and further establish whether these properties differed between cholinergic and other neural subpopulations in the habenula. We find that approximately a quarter of cells within the MHb displayed light-driven changes in firing, which included a subset of cholinergic neurons. We also find evidence of diurnal variation in steady state firing of cells within the MHb, and evidence of time of day modulation of cholinergic neuronal responses. Collectively these indicate that the responsiveness of cholinergic neurons to excitatory input vary in an opposing manner to spontaneous activity, with a nadir in firing

occurring around the day-night transition and a corresponding increase in response to optogenetic stimulation. Finally, we find that cholinergic neuronal activity shows a high degree of correlation, indicative of a shared excitatory drive and indicating that this population tends to provide strongly coordinated neuronal output to its downstream targets.

4.5.1 ChAT-Cre;Ai32 mice as a tool for investigating diurnal rhythms in cholinergic neurons

To be a useful tool for studying cholinergic neurons, ChAT-Cre;Ai32 mice must express ChR2 in ChAT cells exclusively, and this expression should match the expected distribution of cholinergic neurons in the mouse brain. Previous studies have suggested that the Ai32 mouse line may be susceptible to low levels of 'leaky' expression of ChR2 (Prabhakar et al., 2019). Where observed (in animals homozygous for the Ai32 allele), expression levels were too low to drive functional optogenetic responses. Nonetheless, it is important to remain vigilant to the potential for off-target effects. In the mice used here (heterozygote for the Ai32 allele), we found no evidence of any such aberrant expression. Instead, we found that ChR2 expression was reliably expressed in cells which also expressed ChAT. Our immunofluorescence images were consistent with previous work characterizing ChAT expression within the mouse brain (Harris et al., 2014; Li et al., 2018), including the Allen Mouse Brain Atlas (Lein et al., 2007), indicating that these mice are suitable for purpose in this study.

In addition, as we aimed to investigate how cholinergic neurons are modulated by the time of day, these mice needed to display circadian rhythms that were comparable to their wildtype counterparts. We found that all male ChAT-Cre;Ai32 mice studied in our wheel-running paradigm displayed free-running periods of 23.71 ± 0.079 hr. This matches previous studies investigating wheel-running activity in C57BL/6J male mice, which reported a tau of 23.77 ± 0.02 (Schwartz and Zimmerman, 1990). Both males and females had similar free running tau which is also consistent with previous work (Loh et al., 2014). In addition, robustness of activity rhythms were equivalent between both ChAT-Cre;Ai32 and Ai32 mice, indicating that expression of ChR2 did not significantly perturb circadian rhythmicity. Therefore, we can conclude that at least at the behavioural level, the circadian system is unperturbed in ChAT-Cre;Ai32 mice, making them suitable for investigations into circadian rhythmicity.

Having observed established ChR2 expression in the expected regions, the next step in our validation process was to verify that optogenetic stimulation allowed us to reliably identify cholinergic neurons. We performed these initial experiments *in vitro*, to facilitate pharmacological

analysis and investigate the possibility of transynaptic excitatory responses, and found that we were able to reliably activate ChAT+ve neurons within the MHb. When initially planning this study we had intended to go on to characterise neuronal rhythms in ChAT+ve population *ex vivo*. However given our concurrent discovery that MHb rhythms are reset *ex vivo* (see Chapter 3), we next went on to characterise rhythmic properties using *in vivo* approaches for the remainder of the study.

4.5.2 Light responses in MHb neurons

Here, we demonstrated both light-activated and light-inhibited responses in many cells across the MHb, in roughly equal proportions between cholinergic and non-cholinergic cells. We found approximately a quarter of all MHb neurons exhibited light responses, which is largely in agreement with Zhao and Rusak's observations of 19 % of all rat MHb cells being photically responsive (2005), although they found a greater proportion of light-inhibited than light-activated MHb neurons *in vivo*. We extend these findings by demonstrating that responses were not apparent during the first 500 ms following light exposure, indicating an indirect synaptic route for this light information to reach the MHb. Such sluggish light responses appear similar in nature to those previously identified in the mouse LHb (Sakhi et al., 2014b) and also hypothalamic/ventral thalamic regions that do not receive direct retinal input (Brown et al., 2011). The temporal profile and sensitivity of MHb light responses also matches that seen in the thalamus and pretectum of rodless/coneless mice (Allen et al., 2011; Brown et al., 2013), suggesting melanopsin as the primary photoreceptor driving such responses.

Currently, the exact route by which the MHb receives light information remains unclear (Jesuthasan, 2018). The mouse MHb neither receives direct retinal input (Morin & Studholme, 2014) nor is it known to receive any significant direct input from other major retinorecipient regions (lateral geniculate nucleus [LGN], pretectum, superior colliculus, suprachiasmatic nucleus; Oh et al., 2014). There are potentially less studied circuits which may be responsible for driving light responses in the habenula, however. The peri-habenular nucleus of the thalamus (pHb), a region directly adjacent the LHb, receives direct input from intrinsically-photosensitive retinal ganglion cells (ipRGCs; Hattar et al., 2006), which produces excitatory responses (Sakhi et al., 2014b) and is capable of driving light-mediated changes in behaviour and mood (An et al., 2020; Fernandez et al., 2018). A very recent, unpublished study has reported that a subset of GABAergic axon terminals from the pHb terminate in the MHb, and further that these GABAergic pHb neurons are innervated by neurons in the retinorecipient IGL/vLGN region (Brock et al., 2022). The presence of a direct pHb-MHb projection therefore raises the possibility that this is also a route by

which cells in the MHb can receive information about light from other directly retinorecipient pHb neurons (Fernandez et al., 2018).

Another potential route for light information to reach the MHb is via the LHb. The LHb reportedly regulates the anti-depressive effects of light therapy via an ipRGC- ventral LGN/intergeniculate leaflet-LHb pathway (Huang et al., 2019), and studies from zebrafish have indicated that the thalamus mediates responses to illumination in the dorsal habenula, the fish equivalent to the MHb (Cheng et al., 2017). Again, it remains unclear as to whether the LHb communicates with the MHb, although MHb to LHb connections have been suggested (Hu et al., 2020; Kim and Chang, 2005), and the MHb and LHb can interact with each other indirectly through the IPN (Lima et al., 2017). In sum, further work is needed to identify the circuits driving visual responses in the MHb.

It is also worth noting that at present, the functional significance of light-dependent responses in the MHb remains unclear. Whilst there was a significant proportion of cholinergic cells that exhibited such responses, this was true also for non-cholinergic cells in the MHb (and indeed the cells outside of the MHb). Thus, such responses certainly do not seem to be a specific characteristic of particular neuronal types and could serve a range of functions in modulating behaviours associated with the epithalamus. In particular, the MHb is implicated in mood-associated behaviours such as anxiety (Otsu et al., 2018), motivation (Hsu et al., 2014), and fear (Yamaguchi et al., 2013). It is certainly plausible that increased signalling in the MHb stimulated by light could produce enhanced aversive responses which could offer enhanced chances of survival to a mouse – indeed, optogenetic activation of MHb cholinergic neurons has been shown to control expression of aversive memories (Soria-Gómez et al., 2015) or the motivation to explore novel stimuli (Molas et al., 2017b).

4.5.3 MHb neurons properties are influenced by the time of day

Our finding that mouse MHb neurons exhibit diurnal variation in their steady state firing extends earlier reports which also found time of day influences on MHb spontaneous firing activity. Zhao and Rusak (2005) found diurnal differences in rat MHb neuronal firing *in vivo*, with firing rates tending to be higher during the subjective day than the night, but do not provide detailed timing information as to precisely when such cells were recorded. Sakhi et al (2014a) demonstrated diurnal variation in mouse MHb neuronal activity via *ex vivo* patch clamp recordings, with peak firing rates around the day-night transition among active neurons but also a significantly increased proportion of silent neurons at that time. This latter effect may be a more significant determinant of overall MHb activity, since we found population firing rates in the MHb acutely *ex*

vivo were reduced at the beginning of the projected night (Chapter 3). Moreover, those findings coincide with the present observation that MHb cell firing *in vivo* (for both ChAT+ve and –ve neurons) was lowest in recordings occurring just following the start of subjective night.

In addition to confirming diurnal variation in spontaneous activity levels of MHb neurons in general, this study provides evidence that cholinergic neurons of the MHb similarly vary their steady state firing over the course of the day. We found that MHb cholinergic neurons followed a similar pattern of firing activity as the population of non-cholinergic cells, indicating that the rhythmic activity detected here is likely driven by the same mechanism for both populations. Under basal conditions MHb cholinergic neurons had lowest spontaneous firing at ZT13, implying that ACh release from the MHb might also be lowest at this time. Rhythmic ACh release has previously been demonstrated in the cortex, demonstrating higher ACh release during the dark phase than the light phase (Jiménez-Capdeville and Dykes, 1993; Kametani and Kawamura, 1991). However, as the cortex and the MHb have different functions, it is reasonable to assume they may have different rhythms in neurotransmitter release. As increased signalling through MHb cholinergic neurons decreases fear responses in mice (Zhang et al., 2016), we speculate that the increase in spontaneous firing activity across the dark phase we demonstrated in MHb cholinergic neurons could conceivably lead to reduced fear responses at this time. This aligns with the known diurnal rhythms in fear expected in a nocturnal prey animal who would be least at risk to predation during the night (Valentinuzzi et al., 2001).

We also demonstrated that cholinergic neurons modulate their responses to stimulation according to the time of day, with an increased response to excitatory input around dusk. Again, this is intriguing when considered in terms of the known functions of inputs to the MHb. A recent study showed that activation of the MHb via optogenetic stimulation of inputs from the triangular septum produced anxiolysis and promoted locomotion in mice (Otsu et al., 2018) – both behaviours known to be promoted with the onset of the dark phase (Nakano et al., 2016; Siepka and Takahashi, 2005), coinciding with the time of increased responsiveness of MHb cholinergic neurons.

It is interesting to note that we identified a decreased proportion of ChAT+ve cells during recordings targeted to the night compared with the projected day. Unlike in other passive electrophysiological recordings which are biased against detecting the activity of sparsely firing or silent neurons (Siegle et al., 2021), the optogenetic stimulation employed here means that this is less likely to impact our identification of cholinergic neurons. A more likely possibility would be that ChAT+ve cells formed a greater proportion of the sample during the day because other

neuronal classes were more likely to be silent at that time. Such a possibility would not directly align with the *ex vivo* findings of Sakhi et al (2014a), however, whose data suggest that similar proportions of MHb cells overall were silent across the epochs we recorded. This discrepancy could reflect differences in circadian (or general) regulation of membrane properties between *in* and *ex-vivo* preparations and/or may be indicative of different biases in the two approaches toward which neurons are sampled.

4.5.4 **MHb cholinergic neuron activity is strongly coordinated**

In this study we presented evidence that pairs of ChAT+ve neurons have a significantly higher proportion of CCH profiles consistent with a shared drive: nearly half of all ChAT+ve x ChAT+ve pairs we identified were likely to be firing at the same time, in greater synchrony than the other neuron pairs. In addition, we found that excitatory inputs had shorter latencies with decreased variability, consistent with monosynaptic inputs from a more homogenous synapse type, whilst inhibitory drives were much longer, with increased variability, indicative of polysynaptic connections and a heterogeneity in synapses. Given the very strong coordinated activity across almost half of all ChAT+ve cell pairs it is interesting to consider where this shared excitatory drive originates. The MHb (and in particular the region containing cholinergic cells) is the site of remarkably dense nicotinic AChR expression (Grady et al., 2009). It is tempting to speculate then that local (perhaps paracrine) communication between the ChAT+ve cells could be the origin of this coordinated activity. It remains possible, however, that this rather reflects shared input from one or more external cell population(s). In part consistent with the latter possibility, a previous slice recording study (where such external inputs would have been lacking) did not find evidence of synchronised activity among adjacent cholinergic MHb neurons (Görlich et al., 2013). However, it should be noted that the results from Görlich et al are based only on five neuronal pairs and it is unclear whether the duration of recordings and/or analysis techniques employed would have been sufficient to detect the nature of coupling observed here.

Considering inputs to the MHb more generally, early studies from the 1980s suggested the posterior septum or the nucleus of the diagonal band (Contestabile and Fonnum, 1983; Fonnum and Contestabile, 1984) as upstream sources of cholinergic input to the MHb, and are still widely referenced in more recent papers (Klemm, 2004; Qin and Luo, 2009). While such inputs, acting via nicotinic receptors on cholinergic neurons could plausibly result in the coordinated activity of such cells observed in the present study, more recent evidence raises doubt around those earlier anatomical findings. Hence, one tracing study failed to find any evidence of cholinergic terminals from the triangular septum (a component of the posterior septum) terminating in the MHb

(Kawaja et al., 1990), and a later report failed to identify any cholinergic axon terminals in the MHb at all (Sperlágh et al., 1998). It should also be noted that we scrutinised the Allen Mouse Brain Connectivity Atlas (Oh et al., 2014) and could not identify ChAT-expressing neurons from any structure (including the posterior septum or nucleus of the diagonal band) that projected to the MHb. We sought to clarify this issue within this report. Accordingly, our retrograde tracing study failed to identify any cholinergic inputs to the MHb other than MHb cholinergic neurons themselves. While the latter result admittedly derives from a single injection in this case, taken together, the available data strongly points to the possibility that there is no direct upstream source of cholinergic inputs to the MHb.

4.5.5 **Conclusion**

Having demonstrated that MHb neurons are modulated both by time of day and visual responses, it is important to consider the functional implications of these findings. MHb neurons are implicated in a range of functions, including fear (Yamaguchi et al., 2013; Zhang et al., 2016), depression (Han et al., 2017; Xu et al., 2018), anxiety (Otsu et al., 2018), nicotine withdrawal (Lee et al., 2019; Zhao-Shea et al., 2013) and reward signalling (Boulos et al., 2017). There are rhythmic aspects to all of these behaviours (Albrecht and Stork, 2017; Ketchesin et al., 2020; Landgraf et al., 2014; McClung, 2013; Parekh and McClung, 2016; Perkins et al., 2009), although as yet the exact mechanism driving these rhythms is largely undefined. In this report we highlight a potential role for the MHb cholinergic neurons in driving the timing of some of these behaviours, demonstrating rhythms in both spontaneous firing and increased responsiveness to excitatory inputs. The timing of these signals align with promoting anxiolysis and decreased fear responses during the dark phase, known functions of the MHb (Otsu et al., 2018; Yamaguchi et al., 2013; Zhang et al., 2016). Further studies are needed to fully elucidate the function of diurnal variation and visual inputs to cholinergic signalling in the MHb, which could represent a useful target for regulating nicotine addiction behaviours and indeed other mood-associated disorders.

4.6 References

Aizawa, H., Kobayashi, M., Tanaka, S., Fukai, T., Okamoto, H., 2012. Molecular characterization of the subnuclei in rat habenula. J. Comp. Neurol. 520, 4051–4066. https://doi.org/10.1002/cne.23167

Albrecht, A., Stork, O., 2017. Circadian Rhythms in Fear Conditioning: An Overview of Behavioral, Brain System, and Molecular Interactions. Neural Plast 2017, 3750307. https://doi.org/10.1155/2017/3750307

Allen, A.E., Brown, T.M., Lucas, R.J., 2011. A Distinct Contribution of Short-Wavelength-Sensitive Cones to Light-Evoked Activity in the Mouse Pretectal Olivary Nucleus. J Neurosci 31, 16833–16843. https://doi.org/10.1523/JNEUROSCI.2505-11.2011

An, K., Zhao, H., Miao, Y., Xu, Q., Li, Y.-F., Ma, Y.-Q., Shi, Y.-M., Shen, J.-W., Meng, J.-J., Yao, Y.-G., Zhang, Z., Chen, J.-T., Bao, J., Zhang, M., Xue, T., 2020. A circadian rhythm-gated subcortical pathway for nighttime-light-induced depressive-like behaviors in mice. Nat Neurosci 23, 869–880. https://doi.org/10.1038/s41593-020-0640-8

Andres, K.H., von Düring, M., Veh, R.W., 1999. Subnuclear organization of the rat habenular complexes. J. Comp. Neurol. 407, 130–150.

Baptista, V., Ogawa, W.N., Aguiar, J.F., Varanda, W.A., 2005. Electrophysiological evidence for the presence of NR2C subunits of N-methyl-D-aspartate receptors in rat neurons of the nucleus tractus solitarius. Braz J Med Biol Res 38, 105–110. https://doi.org/10.1590/S0100-879X2005000100016

Beasley, T.M., Schumacker, R.E., 1995. Multiple Regression Approach to Analyzing Contingency Tables: Post Hoc and Planned Comparison Procedures. The Journal of Experimental Education 64, 79–93. https://doi.org/10.1080/00220973.1995.9943797

Boulos, L.-J., Darcq, E., Kieffer, B.L., 2017. Translating the Habenula—From Rodents to Humans. Biological Psychiatry, Depression: Genes, Circuits, and Treatments 81, 296–305. https://doi.org/10.1016/j.biopsych.2016.06.003

Brock, O., Gelegen, C.E., Salgarella, I., Sully, P., Jager, P., Menage, L., Mehta, I., Jęczmień-Łazur, J., Djama, D., Strother, L., Coculla, A., Vernon, A., Brickley, S., Holland, P., Cooke, S., Delogu, A., 2022. A role for thalamic projection GABAergic neurons in circadian responses to light. bioRxiv.

Brown, T.M., Allen, A.E., al-Enezi, J., Wynne, J., Schlangen, L., Hommes, V., Lucas, R.J., 2013. The Melanopic Sensitivity Function Accounts for Melanopsin-Driven Responses in Mice under Diverse Lighting Conditions. PLoS One 8, e53583. https://doi.org/10.1371/journal.pone.0053583

Brown, T.M., Wynne, J., Piggins, H.D., Lucas, R.J., 2011. Multiple hypothalamic cell populations encoding distinct visual information. The Journal of Physiology 589, 1173–1194. https://doi.org/10.1113/jphysiol.2010.199877

Chandra, S., Scharf, D., Shiffman, S., 2011. Within-day temporal patterns of smoking, withdrawal symptoms, and craving. Drug Alcohol Depend 117, 118–125. https://doi.org/10.1016/j.drugalcdep.2010.12.027

Chaudhury, D., Colwell, C.S., 2002. Circadian modulation of learning and memory in fear-conditioned mice. Behavioural Brain Research 133, 95–108. https://doi.org/10.1016/S0166-4328(01)00471-5

Chen, E., Lallai, V., Sherafat, Y., Grimes, N.P., Pushkin, A.N., Fowler, J.P., Fowler, C.D., 2018. Altered Baseline and Nicotine-Mediated Behavioral and Cholinergic Profiles in ChAT-Cre Mouse Lines. J. Neurosci. 38, 2177–2188. https://doi.org/10.1523/JNEUROSCI.1433-17.2018

Cheng, R.-K., Krishnan, S., Lin, Q., Kibat, C., Jesuthasan, S., 2017. Characterization of a thalamic nucleus mediating habenula responses to changes in ambient illumination. BMC Biol 15. https://doi.org/10.1186/s12915-017-0431-1

Choi, K., Lee, Y., Lee, C., Hong, S., Lee, S., Kang, S.J., Shin, K.S., 2016. Optogenetic activation of septal GABAergic afferents entrains neuronal firing in the medial habenula. Sci Rep 6, 34800. https://doi.org/10.1038/srep34800

Contestabile, A., Fonnum, F., 1983. Cholinergic and GABAergic forebrain projections to the habenula and nucleus interpeduncularis: Surgical and kainic acid lesions. Brain Research 275, 287–297. https://doi.org/10.1016/0006-8993(83)90989-7

Cui, L.-J., Chen, W.-H., Liu, A.-L., Han, X., Jiang, S.-X., Yuan, F., Zhong, Y.-M., Yang, X.-L., Weng, S.-J., 2020. nGnG Amacrine Cells and Brn3b-negative M1 ipRGCs are Specifically Labeled in the ChAT-ChR2-EYFP Mouse. Invest Ophthalmol Vis Sci 61, 14. https://doi.org/10.1167/iovs.61.2.14

Ebbert, D., 2019. chisq.posthoc.test: A Post Hoc Analysis for Pearson's Chi-Squared Test for Count Data.

Fernandez, D.C., Fogerson, P.M., Ospri, L.L., Thomsen, M.B., Layne, R.M., Severin, D., Zhan, J., Singer, J.H., Kirkwood, A., Zhao, H., Berson, D., Hattar, S., 2018. Light affects mood and learning through distinct retina-brain pathways. Cell 175, 71-84.e18. https://doi.org/10.1016/j.cell.2018.08.004

Fonnum, F., Contestabile, A., 1984. Colchicine neurotoxicity demonstrates the cholinergic projection from the supracommissural septum to the habenula and the nucleus interpeduncularis in the rat. J Neurochem 43, 881–884. https://doi.org/10.1111/j.1471-4159.1984.tb12814.x

Fowler, C.D., Tuesta, L., Kenny, P.J., 2013. Role of α5* nicotinic acetylcholine receptors in the effects of acute and chronic nicotine treatment on brain reward function in mice. Psychopharmacology (Berl). https://doi.org/10.1007/s00213-013-3235-1

Frahm, S., Antolin-Fontes, B., Görlich, A., Zander, J.-F., Ahnert-Hilger, G., Ibañez-Tallon, I., 2015. An essential role of acetylcholine-glutamate synergy at habenular synapses in nicotine dependence. Elife 4, e11396. https://doi.org/10.7554/eLife.11396

Görlich, A., Antolin-Fontes, B., Ables, J.L., Frahm, S., Ślimak, M.A., Dougherty, J.D., Ibañez-Tallon, I., 2013. Reexposure to nicotine during withdrawal increases the pacemaking activity of cholinergic habenular neurons. Proc Natl Acad Sci U S A 110, 17077–17082. https://doi.org/10.1073/pnas.1313103110

Grady, S.R., Moretti, M., Zoli, M., Marks, M.J., Zanardi, A., Pucci, L., Clementi, F., Gotti, C., 2009. Rodent habenulo-interpeduncular pathway expresses a large variety of uncommon nAChR subtypes, but only the alpha3beta4* and alpha3beta3beta4* subtypes mediate acetylcholine release. J. Neurosci. 29, 2272–2282. https://doi.org/10.1523/JNEUROSCI.5121-08.2009

Han, S., Yang, S.H., Kim, J.Y., Mo, S., Yang, E., Song, K.M., Ham, B.-J., Mechawar, N., Turecki, G., Lee, H.W., Kim, H., 2017. Down-regulation of cholinergic signaling in the habenula induces anhedonia-like behavior. Sci Rep 7, 900. https://doi.org/10.1038/s41598-017-01088-6

Hanna, L., Walmsley, L., Pienaar, A., Howarth, M., Brown, T.M., 2017. Geniculohypothalamic GABAergic projections gate suprachiasmatic nucleus responses to retinal input. J. Physiol. (Lond.). https://doi.org/10.1113/JP273850

Harris, J.A., Hirokawa, K.E., Sorensen, S.A., Gu, H., Mills, M., Ng, L.L., Bohn, P., Mortrud, M., Ouellette, B., Kidney, J., Smith, K.A., Dang, C., Sunkin, S., Bernard, A., Oh, S.W., Madisen, L., Zeng, H., 2014. Anatomical characterization of Cre driver mice for neural circuit mapping and manipulation. Frontiers in Neural Circuits 8, 76. https://doi.org/10.3389/fncir.2014.00076

Hattar, S., Kumar, M., Park, A., Tong, P., Tung, J., Yau, K.-W., Berson, D.M., 2006. Central projections of melanopsin-expressing retinal ganglion cells in the mouse. J. Comp. Neurol. 497, 326–349. https://doi.org/10.1002/cne.20970

Haumesser, J.K., Kühn, J., Güttler, C., Nguyen, D.-H., Beck, M.H., Kühn, A.A., van Riesen, C., 2017. Acute In Vivo Electrophysiological Recordings of Local Field Potentials and Multi-unit

Activity from the Hyperdirect Pathway in Anesthetized Rats. J Vis Exp 55940. https://doi.org/10.3791/55940
Herkenham, M., Nauta, W.J., 1977. Afferent connections of the habenular nuclei in the rat. A horseradish peroxidase study, with a note on the fiber-of-passage problem. J Comp Neurol 173, 123–146. https://doi.org/10.1002/cne.901730107
Hildebrandt, K.J., Sahani, M., Linden, J.F., 2017. The Impact of Anesthetic State on Spike-Sorting Success in the Cortex: A Comparison of Ketamine and Urethane Anesthesia. Frontiers in Neural Circuits 11, 95. https://doi.org/10.3389/fncir.2017.00095
Howarth, M., Walmsley, L., Brown, T.M., 2014. Binocular integration in the mouse lateral geniculate nuclei. Curr Biol 24, 1241–1247. https://doi.org/10.1016/j.cub.2014.04.014
Hsu, Y.-W.A., Wang, S.D., Wang, S., Morton, G., Zariwala, H.A., de la Iglesia, H.O., Turner, E.E., 2014. Role of the dorsal medial habenula in the regulation of voluntary activity, motor function, hedonic state, and primary reinforcement. J. Neurosci. 34, 11366–11384. https://doi.org/10.1523/JNEUROSCI.1861-14.2014
Hu, H., Cui, Y., Yang, Y., 2020. Circuits and functions of the lateral habenula in health and in disease. Nat Rev Neurosci 21, 277–295. https://doi.org/10.1038/s41583-020-0292-4
Huang, L., Xi, Y., Peng, Y., Yang, Y., Huang, X., Fu, Y., Tao, Q., Xiao, J., Yuan, T., An, K., Zhao, H., Pu, M., Xu, F., Xue, T., Luo, M., So, K.-F., Ren, C., 2019. A Visual Circuit Related to Habenula Underlies the Antidepressive Effects of Light Therapy. Neuron 102, 128-142.e8. https://doi.org/10.1016/j.neuron.2019.01.037
Jesuthasan, S., 2018. The thalamo-habenula projection revisited. Seminars in Cell & Developmental Biology, The cancer secretome and secreted biomarkers 78, 116–119. https://doi.org/10.1016/j.semcdb.2017.08.023
Jiménez-Capdeville, M.E., Dykes, R.W., 1993. Daily changes in the release of acetylcholine from rat primary somatosensory cortex. Brain Research 625, 152–158. https://doi.org/10.1016/0006-8993(93)90148-G
Joshi, A., Kalappa, B.I., Anderson, C.T., Tzounopoulos, T., 2016. Cell-Specific Cholinergic Modulation of Excitability of Layer 5B Principal Neurons in Mouse Auditory Cortex. J. Neurosci. 36, 8487–8499. https://doi.org/10.1523/JNEUROSCI.0780-16.2016
Kametani, H., Kawamura, H., 1991. Circadian rhythm of cortical acetylcholine release as measured by in vivo microdialysis in freely moving rats. Neuroscience Letters 132, 263–266. https://doi.org/10.1016/0304-3940(91)90316-L
Kawaja, M.D., Flumerfelt, B.A., Hrycyshyn, A.W., 1990. Synaptic organization of septal projections in the rat medial habenula: a wheat germ agglutinin-horseradish peroxidase and immunohistochemical study. Synapse 6, 45–54. https://doi.org/10.1002/syn.890060106
Ketchesin, K.D., Becker-Krail, D., McClung, C.A., 2020. Mood-related central and peripheral clocks. Eur J Neurosci 51, 326–345. https://doi.org/10.1111/ejn.14253
Kim, U., Chang, S.-Y., 2005. Dendritic morphology, local circuitry, and intrinsic electrophysiology of neurons in the rat medial and lateral habenular nuclei of the epithalamus. J. Comp. Neurol. 483, 236–250. https://doi.org/10.1002/cne.20410
Klemm, W.R., 2004. Habenular and interpeduncularis nuclei: shared components in multiple-function networks. Med. Sci. Monit. 10, RA261-273.
Koppensteiner, P., Galvin, C., Ninan, I., 2016. Development- and experience-dependent plasticity in the dorsomedial habenula. Molecular and Cellular Neuroscience 77, 105–112. https://doi.org/10.1016/j.mcn.2016.10.006
Landgraf, D., McCarthy, M.J., Welsh, D.K., 2014. The role of the circadian clock in animal models of mood disorders. Behav Neurosci 128, 344–359. https://doi.org/10.1037/a0036029
Lee, H.W., Yang, S.H., Kim, J.Y., Kim, H., 2019. The Role of the Medial Habenula Cholinergic System in Addiction and Emotion-Associated Behaviors. Front Psychiatry 10. https://doi.org/10.3389/fpsyt.2019.00100

LeGates, T.A., Fernandez, D.C., Hattar, S., 2014. Light as a central modulator of circadian rhythms, sleep and affect. Nat Rev Neurosci 15, 443–454. https://doi.org/10.1038/nrn3743

Lein, E.S., Hawrylycz, M.J., Ao, N., Ayres, M., Bensinger, A., Bernard, A., Boe, A.F., Boguski, M.S., Brockway, K.S., Byrnes, E.J., Chen, Lin, Chen, Li, Chen, T.-M., Chi Chin, M., Chong, J., Crook, B.E., Czaplinska, A., Dang, C.N., Datta, S., Dee, N.R., Desaki, A.L., Desta, T., Diep, E., Dolbeare, T.A., Donelan, M.J., Dong, H.-W., Dougherty, J.G., Duncan, B.J., Ebbert, A.J., Eichele, G., Estin, L.K., Faber, C., Facer, B.A., Fields, R., Fischer, S.R., Fliss, T.P., Frensley, C., Gates, S.N., Glattfelder, K.J., Halverson, K.R., Hart, M.R., Hohmann, J.G., Howell, M.P., Jeung, D.P., Johnson, R.A., Karr, P.T., Kawal, R., Kidney, J.M., Knapik, R.H., Kuan, C.L., Lake, J.H., Laramee, A.R., Larsen, K.D., Lau, C., Lemon, T.A., Liang, A.J., Liu, Y., Luong, L.T., Michaels, J., Morgan, J.J., Morgan, R.J., Mortrud, M.T., Mosqueda, N.F., Ng, L.L., Ng, R., Orta, G.J., Overly, C.C., Pak, T.H., Parry, S.E., Pathak, S.D., Pearson, O.C., Puchalski, R.B., Riley, Z.L., Rockett, H.R., Rowland, S.A., Royall, J.J., Ruiz, M.J., Sarno, N.R., Schaffnit, K., Shapovalova, N.V., Sivisay, T., Slaughterbeck, C.R., Smith, S.C., Smith, K.A., Smith, B.I., Sodt, A.J., Stewart, N.N., Stumpf, K.-R., Sunkin, S.M., Sutram, M., Tam, A., Teemer, C.D., Thaller, C., Thompson, C.L., Varnam, L.R., Visel, A., Whitlock, R.M., Wohnoutka, P.E., Wolkey, C.K., Wong, V.Y., Wood, M., Yaylaoglu, M.B., Young, R.C., Youngstrom, B.L., Feng Yuan, X., Zhang, B., Zwingman, T.A., Jones, A.R., 2007. Genome-wide atlas of gene expression in the adult mouse brain. Nature 445, 168–176. https://doi.org/10.1038/nature05453

Li, X., Yu, B., Sun, Q., Zhang, Y., Ren, M., Zhang, X., Li, A., Yuan, J., Madisen, L., Luo, Q., Zeng, H., Gong, H., Qiu, Z., 2018. Generation of a whole-brain atlas for the cholinergic system and mesoscopic projectome analysis of basal forebrain cholinergic neurons. PNAS 115, 415–420. https://doi.org/10.1073/pnas.1703601115

Lima, L.B., Bueno, D., Leite, F., Souza, S., Gonçalves, L., Furigo, I.C., Donato, J., Metzger, M., 2017. Afferent and efferent connections of the interpeduncular nucleus with special reference to circuits involving the habenula and raphe nuclei. J Comp Neurol 525, 2411–2442. https://doi.org/10.1002/cne.24217

Loh, D.H.-W., Kuljis, D.A., Azuma, L., Wu, Y., Truong, D., Wang, H.-B., Colwell, C.S., 2014. Disrupted reproduction, estrous cycle, and circadian rhythms in female vasoactive intestinal peptide deficient mice. J Biol Rhythms 29, 355–369. https://doi.org/10.1177/0748730414549767

Madisen, L., Mao, T., Koch, H., Zhuo, J., Berenyi, A., Fujisawa, S., Hsu, Y.-W.A., Garcia, A.J., Gu, X., Zanella, S., Kidney, J., Gu, H., Mao, Y., Hooks, B.M., Boyden, E.S., Buzsáki, G., Ramirez, J.M., Jones, A.R., Svoboda, K., Han, X., Turner, E.E., Zeng, H., 2012. A toolbox of Cre-dependent optogenetic transgenic mice for light-induced activation and silencing. Nat Neurosci 15, 793–802. https://doi.org/10.1038/nn.3078

Maggi, C.A., Meli, A., 1986. Suitability of urethane anesthesia for physiopharmacological investigations in various systems. Part 1: General considerations. Experientia 42, 109–114. https://doi.org/10.1007/BF01952426

McClung, C.A., 2013. How might circadian rhythms control mood? Let me count the ways….. Biol Psychiatry 74, 242–249. https://doi.org/10.1016/j.biopsych.2013.02.019

McLaughlin, I., Dani, J.A., De Biasi, M., 2017. The medial habenula and interpeduncular nucleus circuitry is critical in addiction, anxiety, and mood regulation. J. Neurochem. 142, 130–143. https://doi.org/10.1111/jnc.14008

Milosavljevic, N., 2019. How Does Light Regulate Mood and Behavioral State? Clocks Sleep 1, 319–331. https://doi.org/10.3390/clockssleep1030027

Molas, S., DeGroot, S.R., Zhao-Shea, R., Tapper, A.R., 2017a. Anxiety and Nicotine Dependence: Emerging Role of the Habenulo-Interpeduncular Axis. Trends Pharmacol. Sci. 38, 169–180. https://doi.org/10.1016/j.tips.2016.11.001

Molas, S., Zhao-Shea, R., Liu, L., DeGroot, S.R., Gardner, P.D., Tapper, A.R., 2017b. A circuit-based mechanism underlying familiarity signaling and the preference for novelty. Nat Neurosci 20, 1260–1268. https://doi.org/10.1038/nn.4607

Mouland, J.W., Martial, F., Watson, A., Lucas, R.J., Brown, T.M., 2019. Cones Support Alignment to an Inconsistent World by Suppressing Mouse Circadian Responses to the Blue Colors Associated with Twilight. Current Biology 29, 4260-4267.e4. https://doi.org/10.1016/j.cub.2019.10.028

Mrosovsky, N., 1988. Phase response curves for social entrainment. J Comp Physiol A 162, 35–46. https://doi.org/10.1007/BF01342701

Naciff, J.M., Behbehani, M.M., Misawa, H., Dedman, J.R., 1999. Identification and transgenic analysis of a murine promoter that targets cholinergic neuron expression. J Neurochem 72, 17–28. https://doi.org/10.1046/j.1471-4159.1999.0720017.x

Nakano, J.J., Shimizu, K., Shimba, S., Fukada, Y., 2016. SCOP/PHLPP1β in the basolateral amygdala regulates circadian expression of mouse anxiety-like behavior. Sci Rep 6, 33500. https://doi.org/10.1038/srep33500

O'Dell, L.E., Chen, S.A., Smith, R.T., Specio, S.E., Balster, R.L., Paterson, N.E., Markou, A., Zorrilla, E.P., Koob, G.F., 2007. Extended access to nicotine self-administration leads to dependence: Circadian measures, withdrawal measures, and extinction behavior in rats. J. Pharmacol. Exp. Ther. 320, 180–193. https://doi.org/10.1124/jpet.106.105270

Oh, S.W., Harris, J.A., Ng, L., Winslow, B., Cain, N., Mihalas, S., Wang, Q., Lau, C., Kuan, L., Henry, A.M., Mortrud, M.T., Ouellette, B., Nguyen, T.N., Sorensen, S.A., Slaughterbeck, C.R., Wakeman, W., Li, Y., Feng, D., Ho, A., Nicholas, E., Hirokawa, K.E., Bohn, P., Joines, K.M., Peng, H., Hawrylycz, M.J., Phillips, J.W., Hohmann, J.G., Wohnoutka, P., Gerfen, C.R., Koch, C., Bernard, A., Dang, C., Jones, A.R., Zeng, H., 2014. A mesoscale connectome of the mouse brain. Nature 508, 207–214. https://doi.org/10.1038/nature13186

Otsu, Y., Lecca, S., Pietrajtis, K., Rousseau, C.V., Marcaggi, P., Dugué, G.P., Mailhes-Hamon, C., Mameli, M., Diana, M.A., 2018. Functional Principles of Posterior Septal Inputs to the Medial Habenula. Cell Reports 22, 693–705. https://doi.org/10.1016/j.celrep.2017.12.064

Pachitariu, M., Steinmetz, N., Kadir, S., Carandini, M., D, H.K., 2016. Kilosort: realtime spike-sorting for extracellular electrophysiology with hundreds of channels. https://doi.org/10.1101/061481

Pang, X., Liu, L., Ngolab, J., Zhao-Shea, R., McIntosh, J.M., Gardner, P.D., Tapper, A.R., 2016. Habenula cholinergic neurons regulate anxiety during nicotine withdrawal via nicotinic acetylcholine receptors. Neuropharmacology 107, 294–304. https://doi.org/10.1016/j.neuropharm.2016.03.039

Parekh, P.K., McClung, C.A., 2016. Circadian Mechanisms Underlying Reward-Related Neurophysiology and Synaptic Plasticity. Front Psychiatry 6, 187. https://doi.org/10.3389/fpsyt.2015.00187

Paul, S., Hanna, L., Harding, C., Hayter, E.A., Walmsley, L., Bechtold, D.A., Brown, T.M., 2020. Output from VIP cells of the mammalian central clock regulates daily physiological rhythms. Nat Commun 11, 1453. https://doi.org/10.1038/s41467-020-15277-x

Paxinos, G., Franklin, K.B.J., 2003. The mouse brain in stereotaxic coordinates, 2nd Edition. ed. San Diego : Academic Press.

Perkins, K.A., Briski, J., Fonte, C., Scott, J., Lerman, C., 2009. Severity of tobacco abstinence symptoms varies by time of day. Nicotine Tob. Res. 11, 84–91. https://doi.org/10.1093/ntr/ntn003

Prabhakar, A., Vujovic, D., Cui, L., Olson, W., Luo, W., 2019. Leaky expression of channelrhodopsin-2 (ChR2) in Ai32 mouse lines. PLOS ONE 14, e0213326. https://doi.org/10.1371/journal.pone.0213326

Qin, C., Luo, M., 2009. Neurochemical phenotypes of the afferent and efferent projections of the mouse medial habenula. Neuroscience 161, 827–837. https://doi.org/10.1016/j.neuroscience.2009.03.085

Ren, J., Qin, C., Hu, F., Tan, J., Qiu, L., Zhao, S., Feng, G., Luo, M., 2011. Habenula "cholinergic" neurons co-release glutamate and acetylcholine and activate postsynaptic neurons via distinct transmission modes. Neuron 69, 445–452. https://doi.org/10.1016/j.neuron.2010.12.038

Rossi, J., Balthasar, N., Olson, D., Scott, M., Berglund, E., Lee, C.E., Choi, M.J., Lauzon, D., Lowell, B.B., Elmquist, J.K., 2011. Melanocortin-4-receptors Expressed by Cholinergic Neurons Regulate Energy Balance and Glucose Homeostasis. Cell Metab 13, 195–204. https://doi.org/10.1016/j.cmet.2011.01.010

Sakhi, K., Belle, M.D.C., Gossan, N., Delagrange, P., Piggins, H.D., 2014a. Daily variation in the electrophysiological activity of mouse medial habenula neurones. J Physiol 592, 587–603. https://doi.org/10.1113/jphysiol.2013.263319

Sakhi, K., Wegner, S., Belle, M.D.C., Howarth, M., Delagrange, P., Brown, T.M., Piggins, H.D., 2014b. Intrinsic and extrinsic cues regulate the daily profile of mouse lateral habenula neuronal activity. J Physiol 592, 5025–5045. https://doi.org/10.1113/jphysiol.2014.280065

Salas, R., Sturm, R., Boulter, J., De Biasi, M., 2009. Nicotinic receptors in the habenulo-interpeduncular system are necessary for nicotine withdrawal in mice. J. Neurosci. 29, 3014–3018. https://doi.org/10.1523/JNEUROSCI.4934-08.2009

Schwartz, W., Zimmerman, P., 1990. Circadian timekeeping in BALB/c and C57BL/6 inbred mouse strains. J. Neurosci. 10, 3685–3694. https://doi.org/10.1523/JNEUROSCI.10-11-03685.1990

Sheffield, E.B., Quick, M.W., Lester, R.A., 2000. Nicotinic acetylcholine receptor subunit mRNA expression and channel function in medial habenula neurons. Neuropharmacology 39, 2591–2603.

Shih, P.-Y., Engle, S.E., Oh, G., Deshpande, P., Puskar, N.L., Lester, H.A., Drenan, R.M., 2014. Differential expression and function of nicotinic acetylcholine receptors in subdivisions of medial habenula. J. Neurosci. 34, 9789–9802. https://doi.org/10.1523/JNEUROSCI.0476-14.2014

Siegle, J.H., Ledochowitsch, P., Jia, X., Millman, D.J., Ocker, G.K., Caldejon, S., Casal, L., Cho, A., Denman, D.J., Durand, S., Groblewski, P.A., Heller, G., Kato, I., Kivikas, S., Lecoq, J., Nayan, C., Ngo, K., Nicovich, P.R., North, K., Ramirez, T.K., Swapp, J., Waughman, X., Williford, A., Olsen, S.R., Koch, C., Buice, M.A., de Vries, S.E., 2021. Reconciling functional differences in populations of neurons recorded with two-photon imaging and electrophysiology. eLife 10, e69068. https://doi.org/10.7554/eLife.69068

Siepka, S.M., Takahashi, J.S., 2005. Methods to Record Circadian Rhythm Wheel Running Activity in Mice. Methods Enzymol 393, 230–239. https://doi.org/10.1016/S0076-6879(05)93008-5

Society for Neuroscience, 2018. Recommendations for the Design and Analysis of In Vivo Electrophysiology Studies. J. Neurosci. 38, 5837–5839. https://doi.org/10.1523/JNEUROSCI.1480-18.2018

Sokolove, P.G., Bushell, W.N., 1978. The chi square periodogram: Its utility for analysis of circadian rhythms. Journal of Theoretical Biology 72, 131–160. https://doi.org/10.1016/0022-5193(78)90022-X

Soria-Gómez, E., Busquets-Garcia, A., Hu, F., Mehidi, A., Cannich, A., Roux, L., Louit, I., Alonso, L., Wiesner, T., Georges, F., Verrier, D., Vincent, P., Ferreira, G., Luo, M., Marsicano, G., 2015. Habenular CB1 Receptors Control the Expression of Aversive Memories. Neuron 88, 306–313. https://doi.org/10.1016/j.neuron.2015.08.035

Sperlágh, B., Maglóczky, Z., Vizi, E.S., Freund, T.F., 1998. The triangular septal nucleus as the major source of ATP release in the rat habenula: a combined neurochemical and morphological study. Neuroscience 86, 1195–1207.

Teneggi, V., Tiffany, S.T., Squassante, L., Milleri, S., Ziviani, L., Bye, A., 2002. Smokers deprived of cigarettes for 72 h: effect of nicotine patches on craving and withdrawal. Psychopharmacology (Berl.) 164, 177–187. https://doi.org/10.1007/s00213-002-1176-1

Tervo, D.G.R., Huang, B.-Y., Viswanathan, S., Gaj, T., Lavzin, M., Ritola, K.D., Lindo, S., Michael, S., Kuleshova, E., Ojala, D., Huang, C.-C., Gerfen, C.R., Schiller, J., Dudman, J.T., Hantman, A.W., Looger, L.L., Schaffer, D.V., Karpova, A.Y., 2016. A designer AAV variant permits efficient retrograde access to projection neurons. Neuron 92, 372–382. https://doi.org/10.1016/j.neuron.2016.09.021

Valentinuzzi, V.S., Kolker, D.E., Vitaterna, M.H., Ferrari, E.A.M., Takahashi, J.S., Turek, F.W., 2001. Effect of circadian phase on context and cued fear conditioning in C57BL/6J mice. Animal Learning & Behavior 29, 133–142. https://doi.org/10.3758/BF03192822

Viswanath, H., Carter, A.Q., Baldwin, P.R., Molfese, D.L., Salas, R., 2013. The medial habenula: still neglected. Front Hum Neurosci 7, 931. https://doi.org/10.3389/fnhum.2013.00931

Walmsley, L., Brown, T.M., 2015. Eye-specific visual processing in the mouse suprachiasmatic nuclei. The Journal of Physiology 593, 1731–1743. https://doi.org/10.1113/jphysiol.2014.288225

Xiong, B., Li, A., Lou, Y., Chen, S., Long, B., Peng, J., Yang, Z., Xu, T., Yang, X., Li, X., Jiang, T., Luo, Q., Gong, H., 2017. Precise Cerebral Vascular Atlas in Stereotaxic Coordinates of Whole Mouse Brain. Frontiers in Neuroanatomy 11, 128. https://doi.org/10.3389/fnana.2017.00128

Xu, C., Sun, Y., Cai, X., You, T., Zhao, Hongzhe, Li, Y., Zhao, Hua, 2018. Medial Habenula-Interpeduncular Nucleus Circuit Contributes to Anhedonia-Like Behavior in a Rat Model of Depression. Frontiers in Behavioral Neuroscience 12, 238. https://doi.org/10.3389/fnbeh.2018.00238

Yamaguchi, T., Danjo, T., Pastan, I., Hikida, T., Nakanishi, S., 2013. Distinct Roles of Segregated Transmission of the Septo-Habenular Pathway in Anxiety and Fear. Neuron 78, 537–544. https://doi.org/10.1016/j.neuron.2013.02.035

Zhang, J., Tan, L., Ren, Y., Liang, J., Lin, R., Feng, Q., Zhou, J., Hu, F., Ren, J., Wei, C., Yu, T., Zhuang, Y., Bettler, B., Wang, F., Luo, M., 2016. Presynaptic Excitation via GABAB Receptors in Habenula Cholinergic Neurons Regulates Fear Memory Expression. Cell 166, 716–728. https://doi.org/10.1016/j.cell.2016.06.026

Zhao, H., Rusak, B., 2005. Circadian firing-rate rhythms and light responses of rat habenular nucleus neurons in vivo and in vitro. Neuroscience 132, 519–528. https://doi.org/10.1016/j.neuroscience.2005.01.012

Zhao-Shea, R., Liu, L., Pang, X., Gardner, P.D., Tapper, A.R., 2013. Activation of GABAergic neurons in the interpeduncular nucleus triggers physical nicotine withdrawal symptoms. Curr. Biol. 23, 2327–2335. https://doi.org/10.1016/j.cub.2013.09.041

5 Diurnal rhythms in the transcriptome of the medial habenula

5.1 Abstract

Intrinsic rhythmic changes with a period of approximately 24 hours is a property of circadian timekeepers that are present in a number of structures in the mammalian brain. Previous work suggests that the medial habenula (MHb) is one such circadian oscillator, as it displays daily variation in both electrophysiological properties and gene expression. We sought to determine whether transcriptional changes in clock genes as well as other transcripts occurs in the MHb. We collected MHb tissue at four time points equally spread across the day-night cycle under diurnal conditions. Using RNA sequencing to identify rhythmic patterns in transcript expression, we classified 330 transcripts as rhythmic, and found that most tended to peak during the night. Only two clock genes, *Nr1d2* (*Rev-Erbβ*) and *Nr1F1* (RAR-related orphan receptor α or *RorA*) were identified as rhythmic. Pathway analysis indicated that nocturnally peaking rhythmic genes were associated with pathways that regulate synaptic plasticity and insulin signalling. From this, we identify HNF4A as a potential upstream regulator of these genes. These results indicate that daily variation in gene expression occurs in the MHb and raise the possibility that this temporal variation is not directly driven by canonical local molecular clockwork. Instead, it is possible that the observed time effects are driven by the light / dark cycle and are not strictly 'circadian'.

5.2 Introduction

Circadian rhythms are prevalent throughout almost all lifeforms, and allow an organism to anticipate and adapt to the changing conditions arising from the Earth's 24 hour rotation on its axis (Patke et al., 2020). In the mammalian brain, the central clock responsible for driving most of these rhythms is contained within the suprachiasmatic nuclei of the hypothalamus (SCN; Hastings et al., 2018). The SCN sustains a near 24 hour rhythm in molecular and cellular activity and this is sustained in the absence of external cues as it is underpinned by a cell autonomous transcriptional/translational feedback loop of core clock genes (Buhr and Takahashi, 2013). This enables the SCN to communicate time of day information to the rest of the body and the brain through both direct neuronal circuitry and paracrine mechanisms (Begemann et al., 2020).

However, the SCN is not alone in its capacity for rhythmic clock gene expression and circadian variation in its physiology. 'Extra-SCN oscillators' are found at sites throughout the mammalian brain (Begemann et al., 2020; Guilding and Piggins, 2007) and a number of studies have implicated the habenula as one of these. The mammalian habenula is a small but complex bilateral structure of the epithalamus and acts as a relay site linking the basal forebrain with the midbrain. The habenula can be divided into two major substructures, the lateral (LHb) and the medial habenula (MHb). While these substructures differ in molecular and neurochemical profile, both have been implicated in signalling the aversive properties of "drugs of abuse" and mood disorders due to their direct and indirect connections with the reward circuitry of the brain (Boulos et al., 2017) .

Currently, the LHb is held to be the substructure of the habenula that can express semi-autonomous rhythms in clock genes and neural activity (Baño-Otálora and Piggins, 2017; Salaberry and Mendoza, 2015). However, the possibility that the MHb can function as an extra-SCN circadian oscillator is under-explored. Current evidence suggests that MHb neurons vary in their electrical state across the 24 hour cycle, with firing rate increasing from morning to early evening (Zhao and Rusak, 2005). Furthermore, this day-night change in discharge rate seemingly depends on a functional molecular clock as it is absent in recordings from the MHb of *Cry1-2* knockout mice (Sakhi et al., 2014). Further, there is evidence of rhythmic expression of clock gene in the mouse MHb (Landgraf et al., 2016; Olejniczak et al., 2021). In addition there are many studies which have demonstrated that there is circadian activity in the habenula in general, although it is not certain which substructure is driving these changes (Guilding et al., 2010; Paul et al., 2011; Zhang et al., 2016). The evidence for circadian activity in these parameters raises the

question as to where this circadian control might originate from and whether the MHb itself is another semi-autonomous clock of the mammalian nervous system.

To address this, we performed a genome wide assay of the MHb to investigate if and when genes exhibit daily variation in their expression. We then used pathway analysis to identify which pathways potentially underlie this variation in gene expression. Our results indicate that while some genes within the MHb vary in expression over the 24 hour cycle, it is not clear that this is driven through rhythmic expression of clock genes. Instead, our analysis indicates a potential role for synaptic plasticity and insulin signalling, pathways which are enriched for our rhythmic genes.

5.3 Methods

5.3.1 **Animals**

All animal studies were performed in accordance with the 1986 UK Home Office Animal Procedures Act, with approval provided by local ethics review. Procedures were carried out under the authority of Project Licences 70/7843. A total of 20 male C57BL/6J mice (Envigo, Hillcrest, UK) aged between 101-108 days old were group-housed (6 animals per home cage, including companion mice not used for this study), provided with *ad libitum* access to food and water and maintained at controlled ambient temperature (21±2°C) and humidity (55±5%) conditions. Animals were kept in purpose-built light-tight cabinets to allow precise control of their light / dark cycle. All animals received 12 hr of light followed by 12 hr of dark (where lights-on = Zeitgeber Time (ZT) 0 and lights-off = ZT 12), the timings of which were adjusted to allow tissue collection to be performed during the standard working day. In total there were three separate light / dark cycles: lights on at 03:00 and off at 15:00 for tissue collection between 08:40-09:00 (ZT 18); lights on at 05:00 and off at 17:00 for tissue collection between 12:00-12:20 (ZT 0) or 16:40-17:00 (ZT 12); lights on at 12:00 and off at 00:00 for tissue collection at 17:50-18:10 (ZT 6). Animals were left to entrain to these light / dark cycles for at least 4 weeks before tissue collection.

5.3.2 **Tissue harvesting**

Tissue was harvested at 4 time points chosen to cover the spread of a circadian day, using tissue from 5 animals at each time point (ZT 0, ZT 6, ZT 12, and ZT 18). Each dissection took ~ 20 min and consequently, animals were culled over a 48 hr period. Mice were culled by cervical dislocation, which was performed either under standard room lighting conditions or in complete darkness with the aid of night vision goggles (ATN NVG-7, Armasight Inc., USA) for those procedures carried out during ZT 18. Therefore, the data presented here investigates the

physiologically relevant day-night variations in gene expression, rather than performing the experiments under constant conditions to investigate the free-running clock (Pembroke et al., 2015).

Following decapitation, the brain was rapidly removed and snap frozen through placement on foil pre-chilled with dry ice and covered with more dry ice. Tissue was immediately stored at -80°C until subsequent cryosectioning (which was performed within 1 month of tissue collection).

5.3.3 Tissue sectioning

To avoid RNA degradation, all equipment was treated with RNAseZap (Sigma-Aldrich, UK) and left under UV light for at least 30 min prior to use**.** Whole frozen brains acclimated to the cryostat at -19 °C (Leica CM3050 S) for 30 min. Coronal sections (15 µm thick) were cut and mounted onto Polyethylene naphthalate glass membrane slides (Thermofisher Scientific, UK). Sections were taken from across the full extent of the rostral-caudal axis of the habenula, corresponding sections between -0.7 mm and -2.18 mm from Bregma as determined using Paxinos and Franklin mouse brain atlas (Paxinos and Franklin, 2003). Following sectioning, slides were chilled on dry ice and stored in the freezer at -80 °C.

5.3.4 Laser capture microdissection

Immediately prior to laser dissection, each slide was warmed to ambient room temperature for approximately 1 min. Sections were then dehydrated with graded descending ethanol washes (100%, 1 min; 95%, 30 s; 75 %, 30s), Nissl stained (1% cresyl violet in 75% ethanol, 1min, Sigma-Aldrich, UK) and then rehydrated with further ascending ethanol washes (75%, 30 s; 95%, 30 s; 100%). All solutions were made up fresh immediately before use, using RNAse-free water and kept on ice. Once stained, the slides were kept submerged in chilled 100% ethanol until they were placed into the laser capture microscope, preventing endogenous RNAse activity (Clément-Ziza et al., 2008).

All visualization and microdissection was performed using a Leica LMD-6000 upright microscope (Leica Microsystems, Germany). Prior to each dissection, the microscope stage and surrounding workbench was pre-treated with RNAseZAP (Sigma-Aldrich, UK). Nissl staining enabled identification of cell bodies and delineation of the MHb since the density of cells is much higher in the MHb than in the adjacent LHb or subjacent paraventricular thalamus (Zhang and Oorschot, 2006)**.** The portion of tissue containing the MHb was individually identified and cutting outlines were meticulously drawn for each section through visualization of both anatomical landmarks (including the dorsal third ventricle, 3V, and the white matter of the fasciculus retroflexus, FR, and

stria medullaris, SM) as well as the increased density of the cell bodies (see Figure 5.1). If the LHb / MHb border was unclear, the area surrounding the MHb was drawn conservatively to prevent sampling LHb tissue. The lack of contact between experimenter, equipment and the sample further reduced the risk of contamination.

Once the area was outlined, a high powered 50 mW nitrogen laser producing 355 nm light was used to cut through the tissue which was collected directly into lysis buffer in the cap of a standard 0.5 ml thin-wall PCR tube. As the habenula is a long structure (at least 1.4 mm on its rostro-caudal axis**;** Paxinos & Franklin, 2003), approximately 70 - 80 sections were used per animal. This took a total of 1.5 hr dissection time, with each slide being at room temperature for about 20 min each.

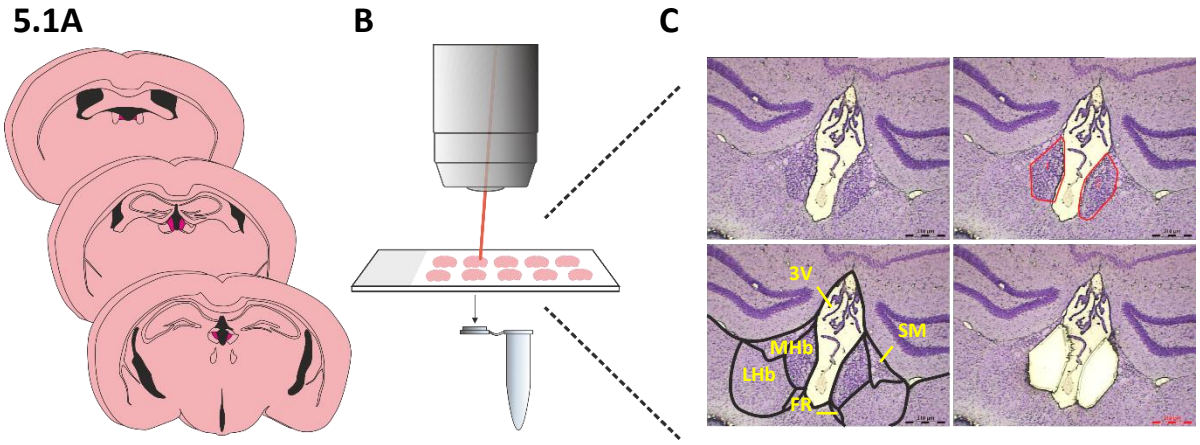

Figure 5.1 Schematic illustrating how MHb tissue was isolated from brain tissue using laser capture microdissection.

A) 15 µm thick coronal serial sections spanning the entire rostro-caudal length of the habenula were collected from each brain using a cryostat.
B) The MHb in each section was individually microdissected using a laser capture microscope, and tissue from the entire MHb was collected into the cap of a standard 0.5 ml PCR tube.
C) Nissl staining allowed for easier delineation of the MHb through identification of the third ventricle (3V), lateral habenula (LHb), stria medullaris (SM) and fasciculus retroflexus (FR). After carefully drawing around the medial habenula (MHb; red outline), the high-powered laser would cut along this guideline, allowing accurate isolation of this area only and avoiding contamination from surrounding tissue.

5.3.5 **RNA extraction**

RNA was immediately isolated from the sample once the tissue from an entire habenula was collected into one cap, using the ReliaPrep RNA Tissue Miniprep System (Promega, USA) to lyse cells and to purify RNA out of cell lysates according to the manufacturer's instructions as follows. The PCR tube was briefly spun in a centrifuge to ensure all the tissue was collected into the buffer.

Cells were lysed with bacterial lysis buffer with added 1-Thioglycerol, and genomic DNA was sheared first by disruption with a needle and syringe followed by pipette. Tubes were centrifuged for 3 min at 14000 g, and the lysate was transferred to a clean PCR tube. 100 % isopropanol (Fisher Scientific, UK) was added and the solution briefly vortexed (5 s) before being passed through a mini-column in the centrifuge to bind RNA to the binding matrix (1 min, 14000 g). The resulting solution in the collection tube was discarded, and RNA wash solution was added to the mini-column before a further centrifugation step (30 s, 14000 g). DNAse (deoxyribonuclease) solution was added to the miniprep and left to incubate for 15 min to remove impurities and contaminating genomic DNA. After further washing and centrifugation steps (column wash solution, 15 s, 14000 g; RNA wash, 30 s, 14000g; RNA wash, 2 min, 16000g) the mini-column was transferred to an elution tube. Nuclease-free water was added to cover the binding matrix and put through the centrifuge for a further minute (14000g), and this step was repeated. The elutant containing RNA was snap-frozen on dry ice and stored at -80 °C. Once all the tissue had been processed, samples were shipped on dry ice to Qiagen Genomic Services, Germany for RNA sequencing steps. The concentration of RNA ranged between 1.67 - 8.57 ng / µL, apart from one sample which was below 1.4 ng / µL and was therefore excluded from the analysis (collected during ZT 18).

5.3.6 **RNA sequencing**

All sequencing steps were performed by Qiagen Genomic Services (Hilden, Germany) as described below. To account for the low yield of RNA collected for each sample, RNA sequencing was performed using the QIAseq ultraplex (UPX 3' Transcriptome Kit, QIAGEN, 2021). With this approach, each sample receives a unique ID, and each RNA molecule is tagged with a unique molecular index (UMI) during reverse transcription before conversion to cDNA (see Figure 5.2). Following reverse transcription with integrated template switching, all the cDNA molecules can be combined without loss of sample information, and all library construction steps can be performed in one step. This allows for more accurate quantification of cDNA molecules after PCR amplification in spite of sequence-dependent bias (Kivioja et al., 2012). After cDNA amplification, samples were purified and library preparation quality control was performed using TapeStation 4200 (Agilent) or Agent Bioanalyzer. Libraries were pooled in equimolar ratios, quantified using qPCR and sequenced on an Illumina NextSeq 500 sequencer. Raw data was de-multiplexed and bcl2fastq software (Illumina inc.) generated FASTQ files for each sample. Reads were aligned to the mouse GRCm38 genome using the STAR aligner.

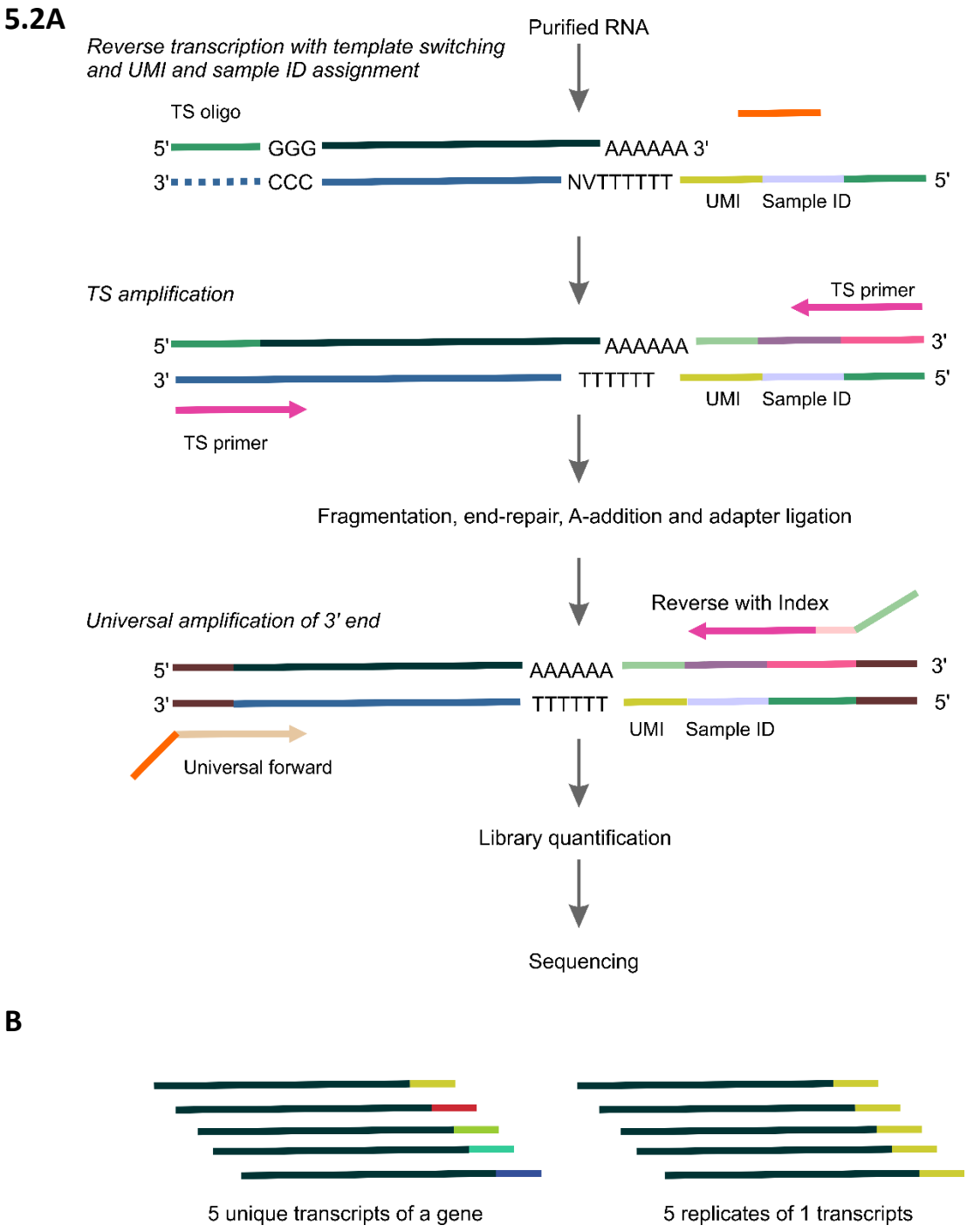

Figure 5.2 Schematic illustrating the principles behind unique molecular indexing in RNA sequencing.

A) Individual reverse transcription reactions are performed for each sample, which tags all the cDNA with a unique sample ID, and each molecule is given a unique molecular index (UMI). After reverse transcription, samples are pooled for downstream processing.
B) Barcoded cDNA molecules are amplified by PCR. Sequence dependent bias and noise can lead to uneven amplification. Sequence reads with different UMIs can easily be attributed to the original molecules, whereas sequence reads which share the same UMI are due to PCR duplication from the original molecule. Figure adapted from QIAGEN, 2021.

5.3.7 Expression quantification

Genes that had low expression across all the samples were filtered out and removed from the analysis (i.e. if the total number of UMI read counts across all samples was less than or equal to 5 x number of samples = 85). The raw counts for each gene were then normalized to account for factors such as read length and unequal dispersion using the R package DESeq2 (Love et al., 2014), which is commonly employed for differential expression analyses and performs well in most contexts (Schurch et al., 2016). All further analysis was performed using normalised count data. Unsupervised principal components analysis was performed on variance stabilizing transformed (VST) expression values in order to diminish the number of variables and summarize the data. Initial examination showed that 2 data points were shown to be outliers (2 samples collected during ZT 12), and were therefore removed from subsequent analysis. Ensemble IDs as generated through the Qiagen workflow were then assigned to gene symbols for further analysis using the biomaRt package in R, calling the dataset="mmusculus_gene_ensembl" (Durinck et al., 2021).

5.3.8 Identification of cycling genes

There are several statistical approaches which are commonly used to identify circadian rhythms in gene expression, including JTK cycle (Hughes et al., 2010), ARSER (Yang and Su, 2010) and RAIN (Thaben and Westermark, 2014). However, several review studies have discussed that these methods are not best suited to the small sample size as used in this study (Hughes et al., 2017; Laloum and Robinson-Rechavi, 2020; Wu et al., 2020). Therefore, we employed the R package diffCircadian (v0.0.0), which employs a likelihood-based method to identify cycling genes whose expression significantly alters over time with a sinusoidal oscillatory pattern (Ding et al., 2021). This approach employs finite sample corrections to improve performance with small sample sizes, and thus is appropriate for analysis here. As this study was designed to be exploratory and this method yields a low false-positive error, we deemed a significance threshold of $p < 0.05$ to be appropriate. This was based on the approach used by Ding and colleagues who developed this statistical method (Ding et al., 2021). This statistical package also allowed us to calculate an estimate of the time of the peak expression for each gene, with the estimation of goodness of fit (R^2).

Heatmaps of rhythmic transcripts were generated using Pheatmap package in R (Kolde, 2019), with samples ordered according to the time of cull. We applied a z-transformation for each gene, whereby the normalized expression counts are converted to heat map colour using the mean and maximum values. The intensity scale of the standardized expression values ranges from dark green (low expression) to dark pink (high expression).

As we were interested in whether cells in the MHb were driven by the molecular circadian clock, we also specifically examined core canonical circadian clock-regulating genes, focussing on the following genes (Takahashi, 2017): *Clock* (clock circadian regulator), *Per1-3* (Period Circadian Clock 1-3), *Cry1-2* (Cryptochrome 1-2), *Npas2* (neuronal PAS domain protein 2), *Csnkle* (casein kinase 1 epsilon), *Csnk1a1* (casein kinase 1 alpha 1), *Arntl* (aryl hydrocarbon receptor nuclear translocator-like, also known as *Bmal1*), *Nr1d1-2* (nuclear receptor subfamily 1 group D member 1-2, also known as *Rev-Erbα-β*), *Rora-c* (RAR-related orphan receptor A-C).

5.3.9 Pathway and upstream regulator analysis with Ingenuity Pathway Analysis

In addition to changes in expression of individual genes that are evident from the RNA sequencing data, the coordinate regulation of multiple genes allows predictions to be made about the pathways involved in the rhythmic variation in the MHb across the circadian day. Having identified a group of rhythmic genes, the rhythmic transcripts were classified as "day-peaking" and "night-peaking" genes, based on whether their peak expression as calculated through diffCircadian was predicted to be during the light phase (ZT 0 – 12; day-peaking) or the dark phase (ZT 12 – 24; night-peaking). We then used Ingenuity Pathway Analysis (IPA) software (Ingenuity IPA Version 68752261, QIAGEN) to investigate whether these genes were enriched for specific biological pathways, and to identify upstream modulators of our list of rhythmic genes (Krämer et al., 2014). Upstream regulator analysis identifies molecules which might explain gene expression patterns in the dataset. The software utilizes a broad definition of the upstream regulator for this analysis, so that any type of regulatory molecule, from microRNA to a drug, can be included in the results.

In the pathway analysis, gene lists were analyzed as follows: the Ingenuity Knowledge Base (Genes only) was used as the reference set. Predictions used in this study were based on experimentally observed interactions within all datasets in IPA with the stringent filter setting applied. Interactions from all nodes, data sources, species, and mutations were used to predict both regulators and enriched pathways, considering both direct and indirect relationships. Statistical significance for each pathway/regulator was determined by Fisher's exact right-tailed test through the software. For canonical pathways, we also calculated the ratio for each canonical pathway, which is the number of genes from the gene list that mapped to the pathway divided by the total number of molecules that make up the pathway. As this was an exploratory study, and we had no *a priori* expectations about which pathways and upstream regulators might be enriched in our gene lists, we corrected P-values for multiple testing using the Benjamini-Hochberg (BH) false discovery rate. For all analyses, pathways and upstream regulators were

considered enriched if they met a threshold $q < 0.05$ (for visualisation, p values are given using –log[p-value], so the threshold is equivalent to 1.3 in figures), where upstream regulators were connected to 2 or more genes within our datasets. Setting a 5% false discovery rate is the standard approach recommended for this type of pathway analysis by Qiagen, and means that if we detected 100 significant pathways, we expect that at most 5 would be falsely identified as significant. This was selected as an appropriate level of false positives for an exploratory study. All bar charts demonstrating the significance of canonical pathways and upstream regulators were produced in R using ggplot2 (Wickham et al., 2021).

5.4 Results

5.4.1 Assessment of sample collection

The total number of detected genes per sample and raw UMI counts, representing the absolute number of observed transcripts per sample prior to normalization, are visualized in Figure 5.2. As absolute counts, they are not normalized for sequencing depth, technical variation or RNA content per cell. To compare UMI counts across samples, data was normalized according to DeSeq2 methods (Figure 5.3C). Excluding transcripts with < 85 UMI counts across all the samples resulted in 7412 transcripts being further analysed.

Principal components analysis was performed on all the samples, using the variance stabilizing transformation on the normalized count data for each sample. Figure 5.2D shows that there was a moderate degree of separation between the groups, with principal components 1 and 2 both combined explaining 69% of the variance. In general, day time points (ZT 0 and ZT 6) are clustered in the left hand portion, while night time points are clustered toward the right hand portion of the graph. However, there was considerable overlap between groups, suggesting that the majority of gene expression is not noticeably altered by time of day.

We also assessed the accuracy of our laser capture microdissection by assessing expression of genes known to be enriched in the MHb (*VACht*, *Tac1*, *Tac2* and *ChAT*) and comparing these with expression of LHb enriched genes (*Chrm2*, *Kcnc2*, *Gpr83*, and *Cacna1b*; Hashikawa et al., 2020; Hsu et al., 2016; Wagner et al., 2016b). Normalized gene counts indicated that MHb enriched genes were expressed in our samples, while those of the LHb were not present in the final transcript list. Therefore, this suggests that our samples were likely an accurate representation of MHb tissue alone and were unlikely to be unduly contaminated by inclusion of neighbouring LHb tissue.

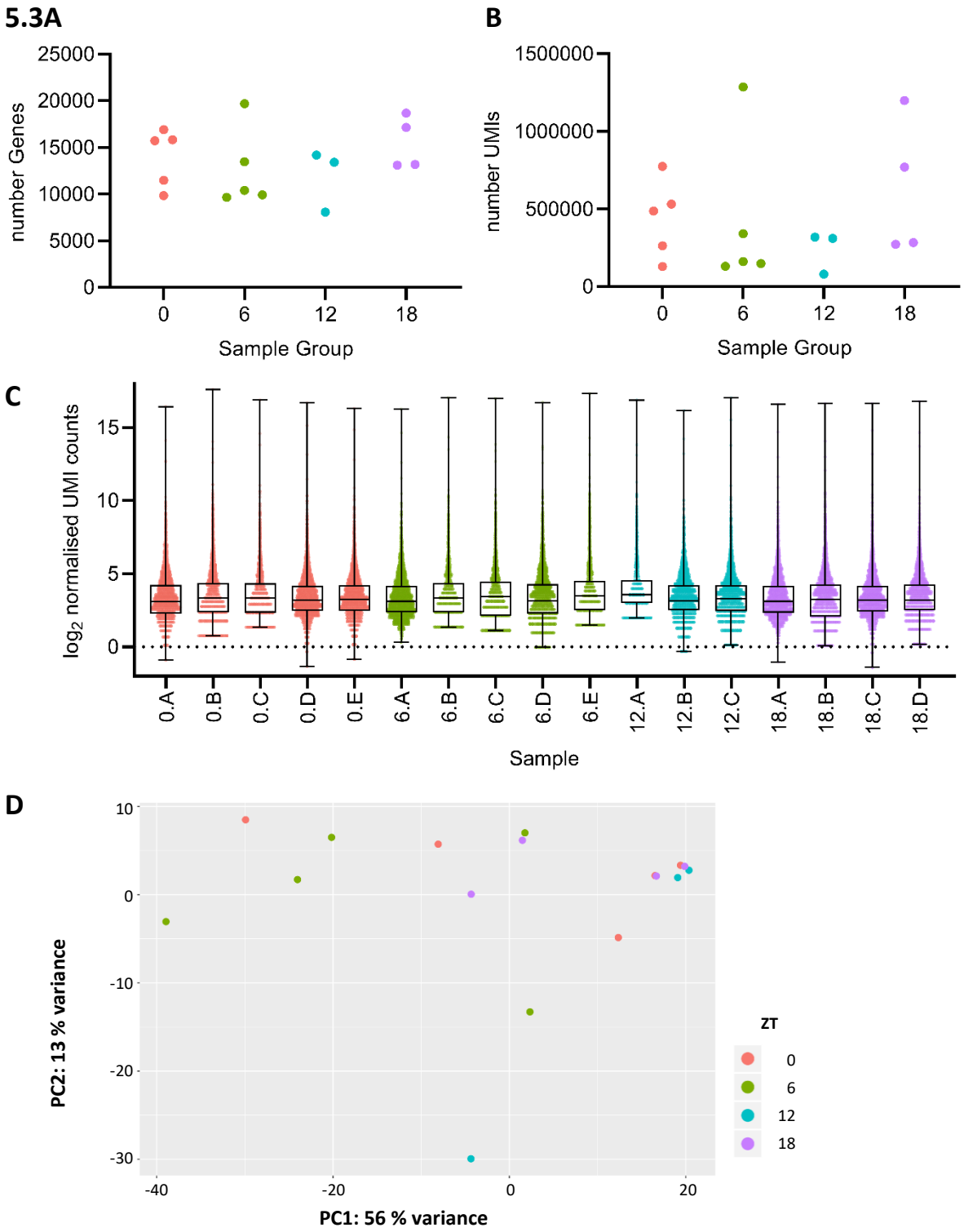

Figure 5.3 Distribution of gene expression values and primary sample analysis

A - B) Scatter plots of the number of the number of genes (A) and unique molecular identifiers (UMIs) (B) per sample at each ZT.
C) Visualization of the distribution of normalised UMI read counts per sample using a boxplot. The UMI counts were normalized using size factor normalization method from the DESeq2 R package.
D) Principal component analysis (PCA) plot showing separation of RNA sequencing data by ZT. The PCA was performed on all samples using the DESeq2 transformed counts (using variance stabilizing transformation) of all genes.

5.4.2 **Rhythmic gene expression within the MHb**

We identified a total of 330 genes whose expression varied in a sinusoidal manner (as determined through diffCircadian) (Table 7.1, Appendix). Figure 5.4A demonstrates the top 12 genes identified as rhythmic and demonstrating the highest levels of significance. These mRNAs encoded proteins involved in actin regulation, transcriptional control and protein binding. Of the transcripts identified as rhythmic, we observe that some peak during the day and some peak during the night, as can be seen in Figure 5.4B.

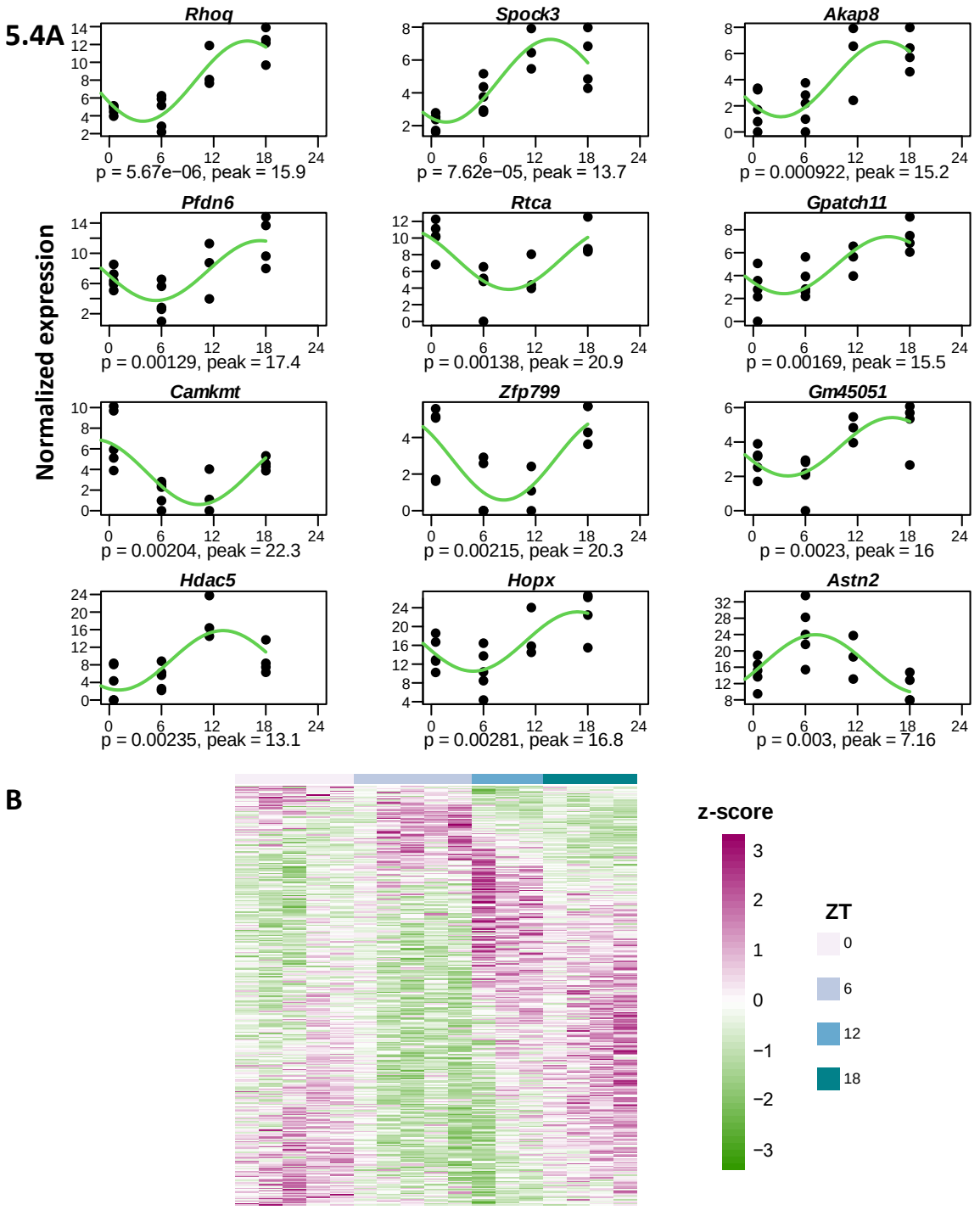

Figure 5.4 Rhythmic transcripts were identified within the MHb transcriptome

A) Top 12 rhythmic transcripts whose expression significantly altered over time with a sinusoidal oscillatory pattern as identified through diffCircadian. In the scatterplots, each dot represents a sample with the x-axis indicating time of tissue collection on a ZT scale and the y-axis indicating level of transcript expression. The green line is the fitted sinusoidal curve. Estimated peak time and p-values are located below each scatterplot.

B) Heatmap displaying each of the 330 transcripts identified as significantly rhythmic by diffCircadian, ordered by the time at which they peak. Each column represents a sample and the samples were ordered by the time of tissue extraction (ZT, denoted in blue as shown in legend). Cells are coloured according to the level of expression following z-transformation for each transcript.

We also examined our dataset for expression of core circadian clock genes. Of the six core circadian genes expressed above threshold, only *Nr1d2* (*Rev-Erbβ*) and *Rora* (RAR-related orphan receptor α) passed our criteria for rhythmicity (Figure 5.5). These were estimated to show peak expression at ZT 15.5 (R^2 = 0.48) and ZT 20.5 (R^2 = 0.36) respectively. However, we did not find expression of other clock genes, including *Per1-2, Cry1-2, Csnkle*, *Npas2*, *Arntl*, *Nr1d1* or *Rorc* within our dataset, and thus these were not analysed for rhythmicity.

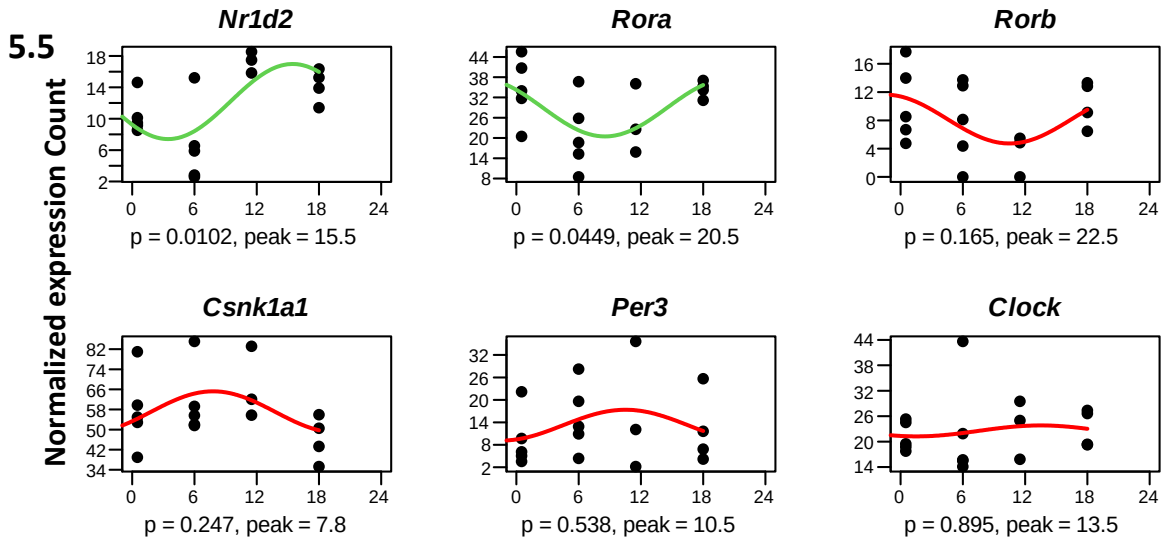

Figure 5.5 Expression patterns of the five core circadian genes detected within the samples.

Only Nr1d2 and Rora showed significant rhythmic oscillation as identified through diffCircadian. In the scatterplots, each dot represents a sample with the x-axis indicating time of tissue collection on a ZT scale and the y-axis indicating level of transcript expression. The line is the fitted sinusoidal curve, green indicating significant oscillation and red indicating non-significant oscillation. Estimated peak time and p-values are located below each scatterplot. Other clock gene transcripts were not detected above threshold levels within this dataset.

5.4.3 Rhythmic genes that peaked in the night were associated with synaptic plasticity and hormone signalling

The 330 genes identified as rhythmic were subsequently divided into 'day-peaking' (*n* = 80) and night-peaking (*n* = 250). We successfully mapped 78 day-peaking genes and 248 night-peaking genes within the software, and in all cases the unmapped genes were sequences corresponding to predicted genes only. Ingenuity software identified 14 canonical pathways that were significantly linked to the day-peaking rhythmic genes (Table 7.2, Appendix), but none passed our threshold for significance following correction for multiple testing. In contrast, 71 canonical pathways were significantly linked with the night-peaking genes, of which 5 were considered significantly enriched according to our threshold Benjamini-Hochberg corrected threshold (Table 7.3, Appendix). Figure 5.6A-B shows the top 10 canonical pathways as identified through IPA for both day and night-peaking rhythmic genes.

EIF2 (eukaryotic initiation factor 2) signalling is involved with protein synthesis and has been implicated in synaptic plasticity (Oliveira et al., 2021), as has Reelin signalling in neurons through its role in neuronal migration and dendritic growth (Jossin, 2020). Clathrin-mediated endocytosis is a key component of synaptic transmission and thus has been implicated as important in synaptic plasticity (Granseth et al., 2006). Interestingly, both insulin receptor signalling and insulin-like growth factor 1 (IGF-1) signalling were indicated to be significantly enriched within the night-peaking dataset, indicating the possibility of time of day modulation of hormone signalling within the MHb. Figure 5.6C-G shows the heat maps for each of the significant canonical pathways, demonstrating the underlying rhythm of the genes involved.

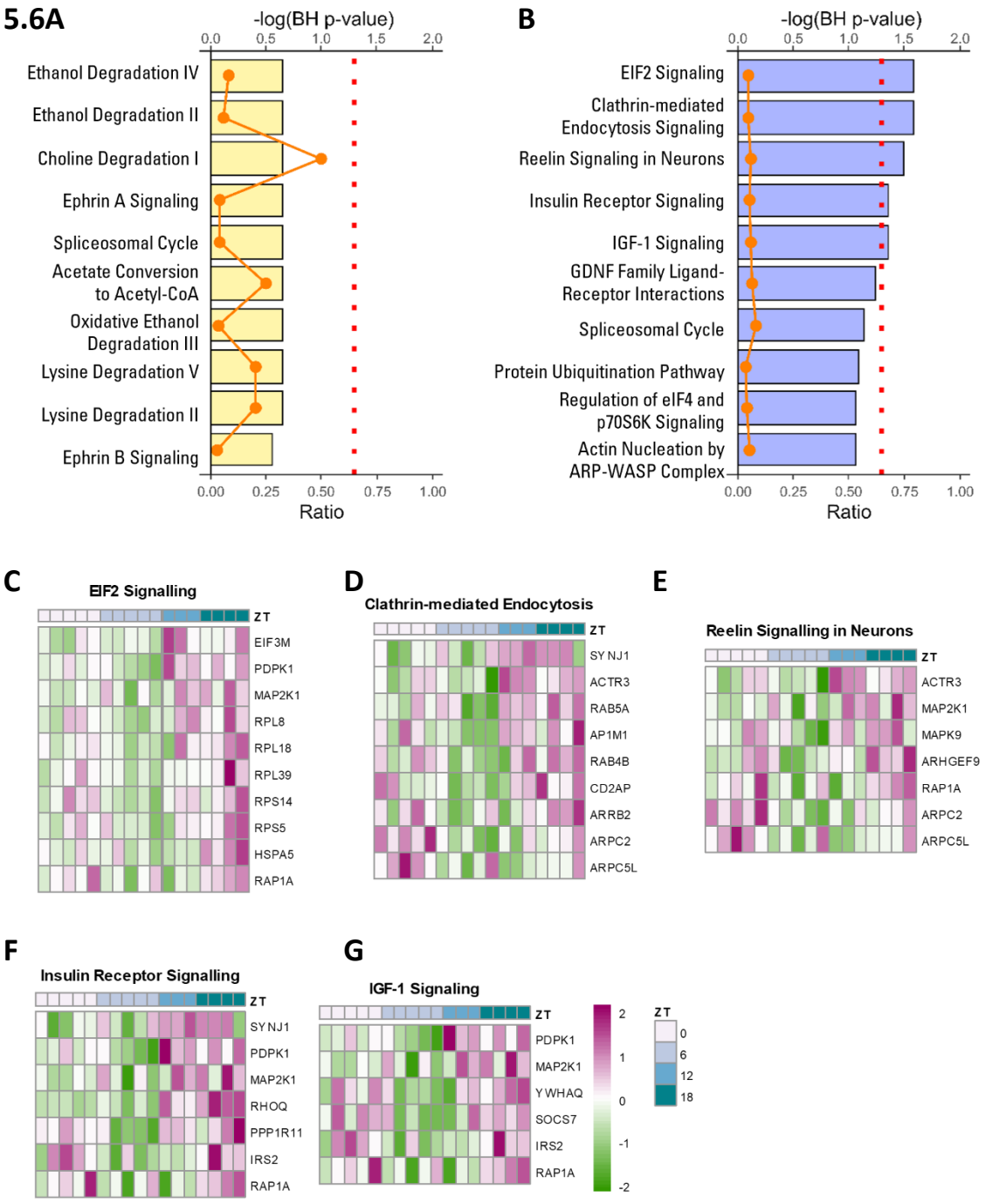

Figure 5.6 Canonical pathways enriched within MHb rhythmic genes.

A - B) Top 10 canonical pathways identified by IPA software for both the day-peaking rhythmic genes (A) and night-peaking (B) rhythmic genes. Canonical pathways were ordered by the -log (p-value) derived from Fisher's exact test. The top x axis displays the – log of the Benjamini-Hochberg (BH) corrected p-value. The bottom x axis displays the ratio (number of genes derived from our dataset, divided by the total number of genes in the pathway). The bar graph represents the -log(BH p-value). The red line indicates the threshold at a BH corrected $p < 0.05$. No canonical pathways were identified as significantly associated with the day peaking rhythmic genes.

C – G) Heatmaps showing the z-transformed transcripts involved in each of the 5 canonical pathways significantly associated with the night-peaking rhythmic genes. Each column represents a sample and the samples were ordered by the time of tissue extraction, ZT, as identified by the shade of blue as shown in the legend.

5.4.4 **HNF4A is identified as a potential upstream regulator of MHb rhythmic genes**

Next, the analysis of predicted upstream regulators was conducted using the IPA software. Thirty-one terms with $p < 0.05$ and connected to two or more rhythmic genes were identified as potential upstream regulators of the day-peaking rhythmic genes (Table 7.4, Appendix), and 81 terms were identified for the night-peaking genes (Table 7.5, Appendix). Figure 5.7A-B shows the top 10 most significant predicted upstream regulators ordered by *p* value as identified through IPA for both day and night-peaking rhythmic genes. Across both groups, only one regulator passed the criteria for significance following Benjamini-Hochberg correction. HNF4A (hepatocyte nuclear factor-4-alpha, an orphan nuclear receptor) was identified as a possible upstream regulator of night-peaking rhythmic genes ($p = 0.00495$), and was linked to 46 target molecules within the night-peaking rhythmic gene dataset (Figure 5.7C). HNF4A has recently been implicated in regulating genes involved in hormone activity, immunological functions and amine synthesis in the brain (Yamanishi et al., 2015) as well as dendritic spine morphology (Liu et al., 2017).

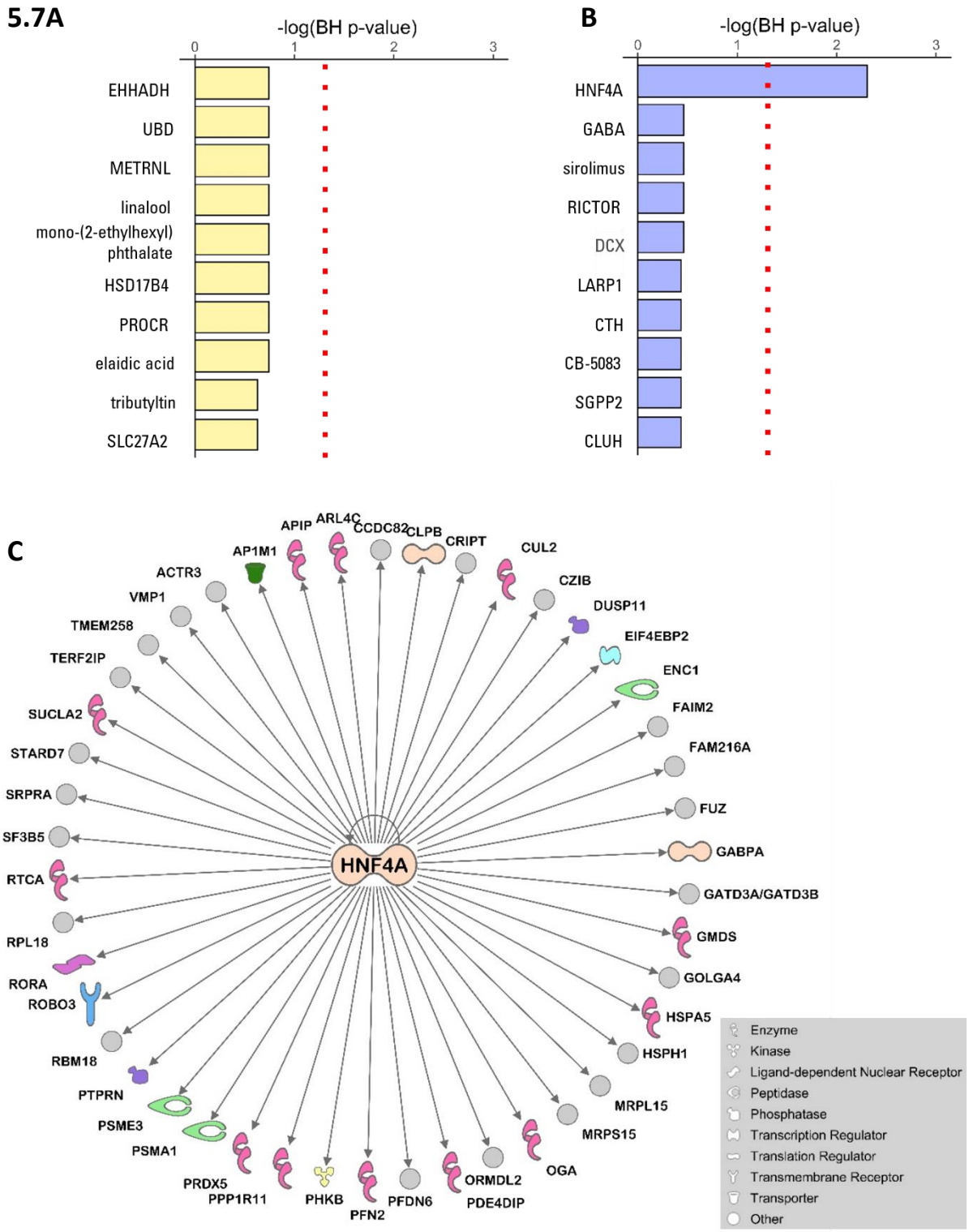

Figure 5.7 Upstream regulators of MHb rhythmic genes

A-B) Top 10 upstream regulators identified by IPA software for both the day-peaking rhythmic genes (A) and night-peaking (B) rhythmic genes. Upstream regulators were ordered by the -log (p-value) derived from Fisher's exact test. The top x axis displays the – log of the Benjamini-Hochberg (BH) corrected p-value. The red line indicates the threshold at a BH corrected $p < 0.05$. No canonical pathways were identified as significantly associated with the day-peaking rhythmic genes, and only HNF4A was identified as a potential upstream regulator of the rhythmic genes that peak in the night.

C) Network visualizing all the target molecules of HNF4A present in the set of night-peaking rhythmic genes.

5.5 Discussion

There is a wealth of circadian transcriptome studies which identify oscillating genes in peripheral tissues (Akhtar et al., 2002; Greenwell et al., 2019; Hughes et al., 2007; Lu et al., 2021; Oster et al., 2006; Perelis et al., 2015; Solanas et al., 2017; Storch et al., 2002; Welz et al., 2019; Zhang et al., 2014), and it is estimated that 5 to 45 % of all protein coding genes in the mouse transcriptome are rhythmic in expression in at least one area of the body (Li and Zhang, 2015; Panda et al., 2002). However, this abundance in circadian transcriptome investigations of peripheral tissues greatly surpasses those assessing circadian gene expression in the brain (Wu et al., 2020). As an area previously identified as exhibiting diurnal variation in both electrophysiological activity (Sakhi et al., 2014; Zhao and Rusak, 2005) and rhythmic clock gene expression (Landgraf et al., 2016), we sought to investigate whether the transcriptional activity of the MHb varied across the 24 hr day-night cycle. Somewhat surprisingly, while we found evidence of rhythmic gene expression within this structure, we did not observe this in the core clock genes. Interestingly, a greater proportion of the rhythmic transcriptome tended to peak in expression at night. We identified that these night-peaking rhythmic genes are significantly enriched for pathways involved in synaptic plasticity and hormone signalling. Finally, we implicate a potential upstream regulator of these, HNF4A, which is also implicated in hormone signalling. Thus, this presents an alternative route by which daily variation in the MHb molecular programs is driven by extrinsic factors, rather than arising from intrinsic canonical clock gene expression in this structure.

5.5.1 Rhythmic transcripts may reflect both circadian and diurnal driven genes

In this study, we found that 330 genes displayed rhythmic variation in their expression patterns. Previous studies investigating the circadian transcriptome in other mouse brain regions have estimated the number of cycling genes to be approximately 100 in hypothalamus, brainstem, and cerebellum (Zhang et al., 2014). At first then, our estimate seems perhaps overly generous. However, as we are examining under light / dark conditions, while Zhang et al examined rhythmic expression in constant dark conditions, one explanation for this apparent disparity is that we are also detecting transcripts whose expression is influenced by light exposure, rather than the circadian system *per se* (Leming et al., 2014; Pembroke et al., 2015). The observation that the MHb is at least indirectly photoresponsive adds credence to this possibility (Zhao and Rusak, 2005). In addition, a recent study which performed whole genome microarray profiling of mouse ventral tegmental area (using tissue harvested every 6 hr under diel conditions as in this study) identified 10 % of their transcripts as rhythmic, equating to over 2500 rhythmic transcripts (Koch

et al., 2020). Therefore, we consider our estimate of rhythmic transcripts to be of an appropriate magnitude.

5.5.2 Clock genes are unlikely to be driving diurnal variation within the MHb

In this study, we did not find rhythmic expression of the majority of the core clock genes. Two core clock genes, *Nr1d2* and *Rora*, were identified as rhythmic, and it is interesting to note that their expression in the MHb is phase delayed in comparison to that reported in the mouse SCN where *Nr1d2* transcription peaked at ZT 6 and *Rora* at ZT 10 (Pembroke et al., 2015). In our study, we also observed a difference in the expression of these genes, with *Nr1d2* peaking at ZT 15.5 and *Rora* following at ZT 20.5. Of course, it should be noted that with only four time points we cannot be certain of the precision of our phase estimates but broadly our data suggest expression is in antiphase to the SCN. The four other clock genes that were expressed within our samples (*Rorb*, *Csnk1a1, Per3* and *Clock*) did not meet our criteria for rhythmicity.

It is plausible that the low resolution of our time sampling in combination with the known heterogeneity of gene expression of cells within the MHb, decreases the signal to noise ratio and masks the rhythms of the clock genes we detected in our samples. Recent single-cell RNA sequencing investigations of the MHb have revealed not only multiple non-neuronal subtypes within the MHb, such as microglia and astrocytes, but also identified at least 5 clusters of neuronal cells, which differ in their spatial and gene expression profiles (Hashikawa et al., 2020; Wallace et al., 2020). In addition, there is little correlation in the rhythmic expression of genes across brain regions (Zhang et al., 2014), and thus heterogeneous clusters of cells in the MHb may rhythmically express clock genes but out of phase with one another, resulting in overall reduced oscillation amplitudes for these genes.

However, the majority of the clock genes we queried were not detected significantly within our dataset at all, including *Per1-2, Cry1-2, Csnkle*, *Npas2*, *Arntl*, *Nr1d1* and *Rorc*. This contrasts with a previous study in which PER2 (as reported by luciferase) varied rhythmically in the mouse MHb *in vitro* (Landgraf et al., 2016), and a previous *in situ* hybridization study which demonstrated rhythmic expression of both *Per1* and *Per2* mRNA expression in mouse MHb (Olejniczak et al., 2021). One explanation might be that only a small subset of MHb cells may contain the molecular clock, preventing detection of their expression above the noise threshold, although alternative mechanisms driving the rhythmicity of gene expression within the MHb cannot ruled out. Furthermore, it is possible that protein products of canonical clock genes may be rhythmic in the absence of rhythmic transcripts. For example, a number of studies have identified rhythmic proteins encoded by non rhythmic mRNAs (Mauvoisin et al., 2014; Reddy et al., 2006; Robles et

al., 2014), with rhythms in protein abundance generated through posttranslational mechanisms instead (Green, 2018).

Ours is not the first study to find evidence of daily variation in the transcriptome in the absence of cycling clock genes. Staehle et al (2020) performed high throughput qPCR on a number of transcripts extracted from both the dorsal vagal complex and the central nucleus of the amygdala (two brain regions not previously flagged as rhythmic) and found that a significant proportion of genes displayed diurnal variation in expression, indicating a role for daily rhythmicity without input from the molecular circadian clock. Other studies have shown cellular circadian rhythmicity even in the absence of core molecular clock genes (Putker et al., 2021). However, even in the absence of any local clock, the MHb is likely to receive rhythmic inputs (either directly from other clock containing structures, or indirectly due to behavioural rhythms in the animals), which may also drive the rhythmic gene expression observed within the present study.

5.5.3 Pathway analysis implicates insulin signalling as a potential rhythmic process within the MHb

The rhythmic MHb genes identified here were enriched for insulin signalling pathways, which are proposed as a mechanism to signal food intake time to clocks in the body (Crosby et al., 2019). Intriguingly, previous work suggests the MHb may be involved in regulating feeding behaviour. Fasting increases expression of leptin receptor mRNA in the MHb of mice (Lin and Huang, 1997). Insulin receptors are expressed with high density in the MHb (Unger et al., 1989), and in fact insulin signalling in the MHb through TCF7L2 (activated by insulin; Ip et al., 2012) provides polysynaptic input to the pancreas and can control blood glucose levels (Duncan et al., 2019). Food restriction alters opioid binding within this brain structure (Wolinsky et al., 1994), and many feeding-related neuropeptides including cholecystokinin, neuronatin, neuropeptide Y and its corresponding receptor NPYR1 are highly expressed within the MHb (Wagner et al., 2016a). An antisense oligodeoxynucleotide directed against the insulin receptor precursor protein into the third ventricle reduced insulin receptor protein within the MHb and caused hyperphagia (Obici et al., 2002). That study also highlights that the MHb has access to factors through the ventricular system due to its anatomical position, which is another mechanism for signalling across the brain (Rodríguez et al., 1999; Tomé et al., 2007). Further, the MHb can modulate the reward centres of the brain (Mathis and Kenny, 2019), and so could be involved in integrating the signals associated with feeding into this circuitry. Most recently, a study by London et al (2020) showed that cAMP-dependent protein kinase signalling in the MHb modulates both exercise motivation and hedonic

eating in opposing directions. Therefore, further work is merited to assess the potential roles of these signalling pathways within the MHb in regulating appetite.

Hormonal signalling within the brain is known to be a route through which information about the time of day is sent to “slave” oscillators to keep clocks in sync (Kriegsfeld and Silver, 2006). Therefore it is intriguing that HNF4A, which is a critical metabolic regulator involved in the regulation of the hormone insulin (Rhee et al., 2003), was identified as a potential upstream regulator of our night-peaking rhythmic gene set. As yet, there are few studies investigating the role of this gene within the mammalian brain, although it is known as an upstream regulator of signalling pathways which control neurite growth (Wang et al., 2013) and has been linked to regulation of dendritic spine morphology (Liu et al., 2017). Further, HNF4A has recently been implicated in regulating genes involved in hormone activity, immunological functions and amine synthesis in several brain regions in mice experiencing chronic mild stress, a model of depression (Yamanishi et al., 2015). It remains to be determined if HNF4A has a role in rhythmic gene expression within the MHb.

5.5.4 Pathways involved with synaptic transmission and neuronal morphology could underlie diurnal variation in MHb electrophysiology

The MHb exhibits daily variation in its electrophysiological response properties (Sakhi et al., 2014; Zhao and Rusak, 2005). Clathrin-mediated endocytosis is a crucial component of synaptic transmission (Chanaday et al., 2019; Liang et al., 2017), and is further regulated through actin dynamics (Cingolani and Goda, 2008). These present a potential means of sustaining the rhythms of electrical firing seen in the MHb. Indeed, rhythmic rates of vesicle recycling occurs in the SCN and suggests a mechanism of clock cell regulation in mammals (Deery et al., 2009). In the current study, the rhythmic genes in the MHb were also enriched for pathways which are involved in regulating various aspects of the actin cytoskeleton. Reelin accumulates at synaptic contacts and influences dendritic growth as well as modulating the postsynaptic ionotropic receptors directly involved in synaptic plasticity (Jossin, 2020). EIF2 controls translation which critically impacts the synaptic plasticity. This has been demonstrated primarily in pyramidal neurons of the hippocampus and prefrontal cortex (Trinh and Klann, 2013), so it remains uncertain how this would translate within the MHb. Synaptic plasticity can vary according to the time of day (Frank, 2016), and the enrichment of pathways involved in synaptic plasticity in the rhythmic genes suggests a rhythmic component to these functions within the MHb. This also presents a potential mechanism driving the daily changes in excitability observed within the MHb.

5.5.5 **Limitations of the study**

By nature of the quantity of genes and statistical comparisons, we anticipate the inclusion of some false positives within this dataset, and it should be noted that it is likely that only the genes with the strongest rhythmic signals are biologically relevant (Laloum and Robinson-Rechavi, 2020). Therefore, these findings must be interpreted with caution. Further, recent reviews have advised that lower temporal resolution such as that used here (only 4 timepoints) results in higher rates of false negatives and reduces the ability to accurately determine rhythmic parameters (Wu et al., 2020). Due to cost restraints, we were also limited to relatively low numbers of biological replicates used here (*n* = 3-5 in each group), and may therefore lack statistical power to identify some rhythmic genes (Hughes et al., 2017). These factors are perhaps reflected in our inability to identify any canonical pathways that were significantly enriched for our day-peaking rhythmic genes. At a superficial level, this seems to suggest that rhythmic day-peaking genes do not perform a coherent function. However, instead this is likely attributable to the relatively small number of genes (80) that were assessed through the IPA software. The performance of this package is best when 200 – 3000 genes are considered (Krämer et al., 2014). Therefore, the likelihood of rhythmic day-peaking genes being functionally important cannot be ruled out and thus merits future study.

One further limitation of this study is that as the tissue collection was performed under diurnal conditions, we do not know how the rhythmic transcripts identified in this report might persist in constant darkness. Therefore, it must be noted that we have not been able to identify transcripts with true circadian oscillation, and further work is needed to identify whether the oscillations in transcript abundance are driven through independent timekeeping mechanisms or through the light / dark cycle.

5.5.6 **Conclusions**

While the above limitations reduce the generalizability of the results, they do not impair the overall suggestions of these findings. Taken together, our results certainly indicate that the MHb varies transcription according to the time of day. Our analysis has identified that daily variation within the MHb may be driven in part through hormone signalling, and mechanisms regulating synaptic plasticity. In addition, we find that HNF4A may regulate a subset of night-peaking rhythmic genes and therefore signpost this as an interesting direction for future investigation. These pathways are further warranted as they are congruent with the known biology of the MHb.

5.6 References

Akhtar, R.A., Reddy, A.B., Maywood, E.S., Clayton, J.D., King, V.M., Smith, A.G., Gant, T.W., Hastings, M.H., Kyriacou, C.P., 2002. Circadian Cycling of the Mouse Liver Transcriptome, as Revealed by cDNA Microarray, Is Driven by the Suprachiasmatic Nucleus. Current Biology 12, 540–550. https://doi.org/10.1016/S0960-9822(02)00759-5

Baño-Otálora, B., Piggins, H.D., 2017. Contributions of the lateral habenula to circadian timekeeping. Pharmacology Biochemistry and Behavior, The lateral habenula. From the neuroanatomy to the implication in CNS disorders 162, 46–54. https://doi.org/10.1016/j.pbb.2017.06.007

Begemann, K., Neumann, A.-M., Oster, H., 2020. Regulation and function of extra-SCN circadian oscillators in the brain. Acta Physiologica 229, e13446. https://doi.org/10.1111/apha.13446

Boulos, L.-J., Darcq, E., Kieffer, B.L., 2017. Translating the Habenula—From Rodents to Humans. Biological Psychiatry, Depression: Genes, Circuits, and Treatments 81, 296–305. https://doi.org/10.1016/j.biopsych.2016.06.003

Buhr, E.D., Takahashi, J.S., 2013. Molecular components of the Mammalian circadian clock. Handb Exp Pharmacol 3–27. https://doi.org/10.1007/978-3-642-25950-0_1

Chanaday, N.L., Cousin, M.A., Milosevic, I., Watanabe, S., Morgan, J.R., 2019. The Synaptic Vesicle Cycle Revisited: New Insights into the Modes and Mechanisms. J. Neurosci. 39, 8209–8216. https://doi.org/10.1523/JNEUROSCI.1158-19.2019

Cingolani, L.A., Goda, Y., 2008. Actin in action: the interplay between the actin cytoskeleton and synaptic efficacy. Nat Rev Neurosci 9, 344–356. https://doi.org/10.1038/nrn2373

Clément-Ziza, M., Munnich, A., Lyonnet, S., Jaubert, F., Besmond, C., 2008. Stabilization of RNA during laser capture microdissection by performing experiments under argon atmosphere or using ethanol as a solvent in staining solutions. RNA 14, 2698–2704. https://doi.org/10.1261/rna.1261708

Crosby, P., Hamnett, R., Putker, M., Hoyle, N.P., Reed, M., Karam, C.J., Maywood, E.S., Stangherlin, A., Chesham, J.E., Hayter, E.A., Rosenbrier-Ribeiro, L., Newham, P., Clevers, H., Bechtold, D.A., O'Neill, J.S., 2019. Insulin/IGF-1 Drives PERIOD Synthesis to Entrain Circadian Rhythms with Feeding Time. Cell 177, 896-909.e20. https://doi.org/10.1016/j.cell.2019.02.017

Deery, M.J., Maywood, E.S., Chesham, J.E., Sládek, M., Karp, N.A., Green, E.W., Charles, P.D., Reddy, A.B., Kyriacou, C.P., Lilley, K.S., Hastings, M.H., 2009. Proteomic Analysis Reveals the Role of Synaptic Vesicle Cycling in Sustaining the Suprachiasmatic Circadian Clock. Current Biology 19, 2031–2036. https://doi.org/10.1016/j.cub.2009.10.024

Ding, H., Meng, L., Liu, A.C., Gumz, M.L., Bryant, A.J., Mcclung, C.A., Tseng, G.C., Esser, K.A., Huo, Z., 2021. Likelihood-based tests for detecting circadian rhythmicity and differential circadian patterns in transcriptomic applications. Briefings in Bioinformatics. https://doi.org/10.1093/bib/bbab224

Duncan, A., Heyer, M.P., Ishikawa, M., Caligiuri, S.P.B., Liu, X., Chen, Z., Micioni Di Bonaventura, M.V., Elayouby, K.S., Ables, J.L., Howe, W.M., Bali, P., Fillinger, C., Williams, M., O'Connor, R.M., Wang, Z., Lu, Q., Kamenecka, T.M., Ma'ayan, A., O'Neill, H.C., Ibanez-Tallon, I., Geurts, A.M., Kenny, P.J., 2019. Habenular TCF7L2 links nicotine addiction to diabetes. Nature 574, 372–377. https://doi.org/10.1038/s41586-019-1653-x

Durinck, S., Huber, W., Davis, S., Pepin, F., Buffalo, V.S., Smith, M., 2021. biomaRt: Interface to BioMart databases (i.e. Ensembl). Bioconductor version: Release (3.14). https://doi.org/10.18129/B9.bioc.biomaRt

Frank, M.G., 2016. Circadian Regulation of Synaptic Plasticity. Biology (Basel) 5, 31. https://doi.org/10.3390/biology5030031

Granseth, B., Odermatt, B., Royle, S.J., Lagnado, L., 2006. Clathrin-Mediated Endocytosis Is the Dominant Mechanism of Vesicle Retrieval at Hippocampal Synapses. Neuron 51, 773–786. https://doi.org/10.1016/j.neuron.2006.08.029

Green, C.B., 2018. Circadian Posttranscriptional Regulatory Mechanisms in Mammals. Cold Spring Harb Perspect Biol 10, a030692. https://doi.org/10.1101/cshperspect.a030692

Greenwell, B.J., Trott, A.J., Beytebiere, J.R., Pao, S., Bosley, A., Beach, E., Finegan, P., Hernandez, C., Menet, J.S., 2019. Rhythmic Food Intake Drives Rhythmic Gene Expression More Potently than the Hepatic Circadian Clock in Mice. Cell Rep 27, 649-657.e5. https://doi.org/10.1016/j.celrep.2019.03.064

Guilding, C., Hughes, A.T.L., Piggins, H.D., 2010. Circadian oscillators in the epithalamus. Neuroscience 169, 1630–1639. https://doi.org/10.1016/j.neuroscience.2010.06.015

Guilding, C., Piggins, H.D., 2007. Challenging the omnipotence of the suprachiasmatic timekeeper: are circadian oscillators present throughout the mammalian brain? European Journal of Neuroscience 25, 3195–3216. https://doi.org/10.1111/j.1460-9568.2007.05581.x

Hashikawa, Y., Hashikawa, K., Rossi, M.A., Basiri, M.L., Liu, Y., Johnston, N.L., Ahmad, O.R., Stuber, G.D., 2020. Transcriptional and Spatial Resolution of Cell Types in the Mammalian Habenula. Neuron. https://doi.org/10.1016/j.neuron.2020.03.011

Hastings, M.H., Maywood, E.S., Brancaccio, M., 2018. Generation of circadian rhythms in the suprachiasmatic nucleus. Nat Rev Neurosci 19, 453–469. https://doi.org/10.1038/s41583-018-0026-z

Hsu, Y.-W.A., Morton, G., Guy, E.G., Wang, S.D., Turner, E.E., 2016. Dorsal Medial Habenula Regulation of Mood-Related Behaviors and Primary Reinforcement by Tachykinin-Expressing Habenula Neurons. eNeuro 3. https://doi.org/10.1523/ENEURO.0109-16.2016

Hughes, M., DeHaro, L., Pulivarthy, S.R., Gu, J., Hayes, K., Panda, S., Hogenesch, J.B., 2007. High-resolution Time Course Analysis of Gene Expression from Pituitary. Cold Spring Harb Symp Quant Biol 72, 381–386.

Hughes, M.E., Abruzzi, K.C., Allada, R., Anafi, R., Arpat, A.B., Asher, G., Baldi, P., de Bekker, C., Bell-Pedersen, D., Blau, J., Brown, S., Ceriani, M.F., Chen, Z., Chiu, J.C., Cox, J., Crowell, A.M., DeBruyne, J.P., Dijk, D.-J., DiTacchio, L., Doyle, F.J., Duffield, G.E., Dunlap, J.C., Eckel-Mahan, K., Esser, K.A., FitzGerald, G.A., Forger, D.B., Francey, L.J., Fu, Y.-H., Gachon, F., Gatfield, D., de Goede, P., Golden, S.S., Green, C., Harer, J., Harmer, S., Haspel, J., Hastings, M.H., Herzel, H., Herzog, E.D., Hoffmann, C., Hong, C., Hughey, J.J., Hurley, J.M., de la Iglesia, H.O., Johnson, C., Kay, S.A., Koike, N., Kornacker, K., Kramer, A., Lamia, K., Leise, T., Lewis, S.A., Li, J., Li, X., Liu, A.C., Loros, J.J., Martino, T.A., Menet, J.S., Merrow, M., Millar, A.J., Mockler, T., Naef, F., Nagoshi, E., Nitabach, M.N., Olmedo, M., Nusinow, D.A., Ptáček, L.J., Rand, D., Reddy, A.B., Robles, M.S., Roenneberg, T., Rosbash, M., Ruben, M.D., Rund, S.S.C., Sancar, A., Sassone-Corsi, P., Sehgal, A., Sherrill-Mix, S., Skene, D.J., Storch, K.-F., Takahashi, J.S., Ueda, H.R., Wang, H., Weitz, C., Westermark, P.O., Wijnen, H., Xu, Y., Wu, G., Yoo, S.-H., Young, M., Zhang, E.E., Zielinski, T., Hogenesch, J.B., 2017. Guidelines for Genome-Scale Analysis of Biological Rhythms. J Biol Rhythms 32, 380–393. https://doi.org/10.1177/0748730417728663

Hughes, M.E., Hogenesch, J.B., Kornacker, K., 2010. JTK_CYCLE: an efficient nonparametric algorithm for detecting rhythmic components in genome-scale data sets. J Biol Rhythms 25, 372–380. https://doi.org/10.1177/0748730410379711

Ip, W., Shao, W., Chiang, Y.A., Jin, T., 2012. The Wnt signaling pathway effector TCF7L2 is upregulated by insulin and represses hepatic gluconeogenesis. Am J Physiol Endocrinol Metab 303, E1166-1176. https://doi.org/10.1152/ajpendo.00249.2012

Jossin, Y., 2020. Reelin Functions, Mechanisms of Action and Signaling Pathways During Brain Development and Maturation. Biomolecules 10, E964. https://doi.org/10.3390/biom10060964

Kivioja, T., Vähärautio, A., Karlsson, K., Bonke, M., Enge, M., Linnarsson, S., Taipale, J., 2012. Counting absolute numbers of molecules using unique molecular identifiers. Nat Methods 9, 72–74. https://doi.org/10.1038/nmeth.1778

Koch, C.E., Begemann, K., Kiehn, J.T., Griewahn, L., Mauer, J., M. E. Hess, Moser, A., Schmid, S.M., Brüning, J.C., Oster, H., 2020. Circadian regulation of hedonic appetite in mice by clocks in dopaminergic neurons of the VTA. Nat Commun 11, 3071. https://doi.org/10.1038/s41467-020-16882-6

Kolde, R., 2019. pheatmap: Pretty Heatmaps.

Krämer, A., Green, J., Pollard, J., Tugendreich, S., 2014. Causal analysis approaches in Ingenuity Pathway Analysis. Bioinformatics 30, 523–530. https://doi.org/10.1093/bioinformatics/btt703

Kriegsfeld, L.J., Silver, R., 2006. The regulation of neuroendocrine function: Timing is everything. Horm Behav 49, 557–574. https://doi.org/10.1016/j.yhbeh.2005.12.011

Laloum, D., Robinson-Rechavi, M., 2020. Methods detecting rhythmic gene expression are biologically relevant only for strong signal. PLOS Computational Biology 16, e1007666. https://doi.org/10.1371/journal.pcbi.1007666

Landgraf, D., Long, J.E., Welsh, D.K., 2016. Depression-like behaviour in mice is associated with disrupted circadian rhythms in nucleus accumbens and periaqueductal grey. European Journal of Neuroscience 43, 1309–1320. https://doi.org/10.1111/ejn.13085

Leming, M.T., Rund, S.S.C., Behura, S.K., Duffield, G.E., O'Tousa, J.E., 2014. A database of circadian and diel rhythmic gene expression in the yellow fever mosquito Aedes aegypti. BMC Genomics 15, 1128. https://doi.org/10.1186/1471-2164-15-1128

Li, S., Zhang, L., 2015. Circadian Control of Global Transcription. BioMed Research International 2015, e187809. https://doi.org/10.1155/2015/187809

Liang, K., Wei, L., Chen, L., 2017. Exocytosis, Endocytosis, and Their Coupling in Excitable Cells. Frontiers in Molecular Neuroscience 10, 109. https://doi.org/10.3389/fnmol.2017.00109

Lin, S., Huang, X.F., 1997. Fasting increases leptin receptor mRNA expression in lean but not obese (ob/ob) mouse brain. NeuroReport 8, 3624–3629.

Liu, D., Tang, H., Li, X.-Y., Deng, M.-F., Wei, N., Wang, X., Zhou, Y.-F., Wang, D.-Q., Fu, P., Wang, J.-Z., Hébert, S.S., Chen, J.-G., Lu, Y., Zhu, L.-Q., 2017. Targeting the HDAC2/HNF-4A/miR-101b/AMPK Pathway Rescues Tauopathy and Dendritic Abnormalities in Alzheimer's Disease. Mol Ther 25, 752–764. https://doi.org/10.1016/j.ymthe.2017.01.018

London, E., Wester, J.C., Bloyd, M., Bettencourt, S., McBain, C.J., Stratakis, C.A., 2020. Loss of habenular Prkar2a reduces hedonic eating and increases exercise motivation. JCI Insight 5, 141670. https://doi.org/10.1172/jci.insight.141670

Love, M.I., Huber, W., Anders, S., 2014. Moderated estimation of fold change and dispersion for RNA-seq data with DESeq2. Genome Biology 15, 550. https://doi.org/10.1186/s13059-014-0550-8

Lu, Y., Liu, B., Ma, J., Yang, S., Huang, J., 2021. Disruption of Circadian Transcriptome in Lung by Acute Sleep Deprivation. Frontiers in Genetics 12.

Mathis, V., Kenny, P.J., 2019. From controlled to compulsive drug-taking: The role of the habenula in addiction. Neuroscience & Biobehavioral Reviews, Addiction: a neurobiological and cognitive brain disorder 106, 102–111. https://doi.org/10.1016/j.neubiorev.2018.06.018

Mauvoisin, D., Wang, J., Jouffe, C., Martin, E., Atger, F., Waridel, P., Quadroni, M., Gachon, F., Naef, F., 2014. Circadian clock-dependent and -independent rhythmic proteomes implement distinct diurnal functions in mouse liver. Proc Natl Acad Sci U S A 111, 167–172. https://doi.org/10.1073/pnas.1314066111

Obici, S., Feng, Z., Karkanias, G., Baskin, D.G., Rossetti, L., 2002. Decreasing hypothalamic insulin receptors causes hyperphagia and insulin resistance in rats. Nat Neurosci 5, 566–572. https://doi.org/10.1038/nn0602-861

Olejniczak, I., Ripperger, J.A., Sandrelli, F., Schnell, A., Mansencal-Strittmatter, L., Wendrich, K., Hui, K.Y., Brenna, A., Fredj, N.B., Albrecht, U., 2021. Light affects behavioral despair involving the clock gene Period 1. PLOS Genetics 17, e1009625. https://doi.org/10.1371/journal.pgen.1009625

Oliveira, M.M., Lourenco, M.V., Longo, F., Kasica, N.P., Yang, W., Ureta, G., Ferreira, D.D.P., Mendonça, P.H.J., Bernales, S., Ma, T., De Felice, F.G., Klann, E., Ferreira, S.T., 2021. Correction of eIF2-dependent defects in brain protein synthesis, synaptic plasticity, and memory in mouse models of Alzheimer's disease. Science Signaling 14, eabc5429. https://doi.org/10.1126/scisignal.abc5429

Oster, H., Damerow, S., Hut, R.A., Eichele, G., 2006. Transcriptional profiling in the adrenal gland reveals circadian regulation of hormone biosynthesis genes and nucleosome assembly genes. J Biol Rhythms 21, 350–361. https://doi.org/10.1177/0748730406293053

Panda, S., Antoch, M.P., Miller, B.H., Su, A.I., Schook, A.B., Straume, M., Schultz, P.G., Kay, S.A., Takahashi, J.S., Hogenesch, J.B., 2002. Coordinated Transcription of Key Pathways in the Mouse by the Circadian Clock. Cell 109, 307–320. https://doi.org/10.1016/S0092-8674(02)00722-5

Patke, A., Young, M.W., Axelrod, S., 2020. Molecular mechanisms and physiological importance of circadian rhythms. Nat Rev Mol Cell Biol 21, 67–84. https://doi.org/10.1038/s41580-019-0179-2

Paul, M.J., Indic, P., Schwartz, W.J., 2011. A role for the habenula in the regulation of locomotor activity cycles. European Journal of Neuroscience 34, 478–488. https://doi.org/10.1111/j.1460-9568.2011.07762.x

Paxinos, G., Franklin, K.B.J., 2003. The mouse brain in stereotaxic coordinates, 2nd Edition. ed. San Diego : Academic Press.

Pembroke, W.G., Babbs, A., Davies, K.E., Ponting, C.P., Oliver, P.L., 2015. Temporal transcriptomics suggest that twin-peaking genes reset the clock. eLife 4, e10518. https://doi.org/10.7554/eLife.10518

Perelis, M., Marcheva, B., Ramsey, K.M., Schipma, M.J., Hutchison, A.L., Taguchi, A., Peek, C.B., Hong, H., Huang, W., Omura, C., Allred, A.L., Bradfield, C.A., Dinner, A.R., Barish, G.D., Bass, J., 2015. Pancreatic β cell enhancers regulate rhythmic transcription of genes controlling insulin secretion. Science 350, aac4250. https://doi.org/10.1126/science.aac4250

Putker, M., Wong, D.C.S., Seinkmane, E., Rzechorzek, N.M., Zeng, A., Hoyle, N.P., Chesham, J.E., Edwards, M.D., Feeney, K.A., Fischer, R., Peschel, N., Chen, K.-F., Vanden Oever, M., Edgar, R.S., Selby, C.P., Sancar, A., O'Neill, J.S., 2021. CRYPTOCHROMES confer robustness, not rhythmicity, to circadian timekeeping. EMBO J 40, e106745. https://doi.org/10.15252/embj.2020106745

QIAGEN, 2021. QIAseq® UPX 3' Transcriptome Handbook (No. HB-2485-007). USA.

Reddy, A.B., Karp, N.A., Maywood, E.S., Sage, E.A., Deery, M., O'Neill, J.S., Wong, G.K.Y., Chesham, J., Odell, M., Lilley, K.S., Kyriacou, C.P., Hastings, M.H., 2006. Circadian orchestration of the hepatic proteome. Curr Biol 16, 1107–1115. https://doi.org/10.1016/j.cub.2006.04.026

Rhee, J., Inoue, Y., Yoon, J.C., Puigserver, P., Fan, M., Gonzalez, F.J., Spiegelman, B.M., 2003. Regulation of hepatic fasting response by PPARγ coactivator-1α (PGC-1): Requirement for hepatocyte nuclear factor 4α in gluconeogenesis. PNAS 100, 4012–4017. https://doi.org/10.1073/pnas.0730870100

Robles, M.S., Cox, J., Mann, M., 2014. In-vivo quantitative proteomics reveals a key contribution of post-transcriptional mechanisms to the circadian regulation of liver metabolism. PLoS Genet 10, e1004047. https://doi.org/10.1371/journal.pgen.1004047

Rodríguez, S., Vio, K., Wagner, C., Barría, M., Navarrete, E.H., Ramírez, V.D., Pérez-Fígares, J.M., Rodríguez, E.M., 1999. Changes in the cerebrospinal-fluid monoamines in rats with an

immunoneutralization of the subcommissural organ-Reissner's fiber complex by maternal delivery of antibodies. Exp Brain Res 128, 278–290. https://doi.org/10.1007/s002210050848

Sakhi, K., Belle, M.D.C., Gossan, N., Delagrange, P., Piggins, H.D., 2014. Daily variation in the electrophysiological activity of mouse medial habenula neurones. J Physiol 592, 587–603. https://doi.org/10.1113/jphysiol.2013.263319

Salaberry, N.L., Mendoza, J., 2015. Insights into the Role of the Habenular Circadian Clock in Addiction. Front Psychiatry 6, 179. https://doi.org/10.3389/fpsyt.2015.00179

Schurch, N.J., Schofield, P., Gierliński, M., Cole, C., Sherstnev, A., Singh, V., Wrobel, N., Gharbi, K., Simpson, G.G., Owen-Hughes, T., Blaxter, M., Barton, G.J., 2016. How many biological replicates are needed in an RNA-seq experiment and which differential expression tool should you use? RNA 22, 839–851. https://doi.org/10.1261/rna.053959.115

Solanas, G., Peixoto, F.O., Perdiguero, E., Jardí, M., Ruiz-Bonilla, V., Datta, D., Symeonidi, A., Castellanos, A., Welz, P.-S., Caballero, J.M., Sassone-Corsi, P., Muñoz-Cánoves, P., Benitah, S.A., 2017. Aged Stem Cells Reprogram Their Daily Rhythmic Functions to Adapt to Stress. Cell 170, 678-692.e20. https://doi.org/10.1016/j.cell.2017.07.035

Staehle, M.M., O'Sullivan, S., Vadigepalli, R., Kernan, K.F., Gonye, G.E., Ogunnaike, B.A., Schwaber, J.S., 2020. Diurnal Patterns of Gene Expression in the Dorsal Vagal Complex and the Central Nucleus of the Amygdala – Non-rhythm-generating Brain Regions. Frontiers in Neuroscience 14, 375. https://doi.org/10.3389/fnins.2020.00375

Storch, K.-F., Lipan, O., Leykin, I., Viswanathan, N., Davis, F.C., Wong, W.H., Weitz, C.J., 2002. Extensive and divergent circadian gene expression in liver and heart. Nature 417, 78–83. https://doi.org/10.1038/nature744

Takahashi, J.S., 2017. Transcriptional architecture of the mammalian circadian clock. Nat Rev Genet 18, 164–179. https://doi.org/10.1038/nrg.2016.150

Thaben, P.F., Westermark, P.O., 2014. Detecting rhythms in time series with RAIN. J Biol Rhythms 29, 391–400. https://doi.org/10.1177/0748730414553029

Tomé, M., Moreira, E., Pérez-Fígares, J.-M., Jiménez, A.J., 2007. Presence of D1- and D2-like dopamine receptors in the rat, mouse and bovine multiciliated ependyma. J Neural Transm (Vienna) 114, 983–994. https://doi.org/10.1007/s00702-007-0666-z

Trinh, M.A., Klann, E., 2013. Translational Control by eIF2α Kinases in Long-lasting Synaptic Plasticity and Long-term Memory. Neurobiol Learn Mem 105, 93–99. https://doi.org/10.1016/j.nlm.2013.04.013

Unger, J., McNeill, T.H., Moxley, R.T., White, M., Moss, A., Livingston, J.N., 1989. Distribution of insulin receptor-like immunoreactivity in the rat forebrain. Neuroscience 31, 143–157. https://doi.org/10.1016/0306-4522(89)90036-5

Wagner, F., Bernard, R., Derst, C., French, L., Veh, R.W., 2016a. Microarray analysis of transcripts with elevated expressions in the rat medial or lateral habenula suggest fast GABAergic excitation in the medial habenula and habenular involvement in the regulation of feeding and energy balance. Brain Struct Funct 221, 4663–4689. https://doi.org/10.1007/s00429-016-1195-z

Wagner, F., French, L., Veh, R.W., 2016b. Transcriptomic-anatomic analysis of the mouse habenula uncovers a high molecular heterogeneity among neurons in the lateral complex, while gene expression in the medial complex largely obeys subnuclear boundaries. Brain Struct Funct 221, 39–58. https://doi.org/10.1007/s00429-014-0891-9

Wallace, M.L., Huang, K.W., Hochbaum, D., Hyun, M., Radeljic, G., Sabatini, B.L., 2020. Anatomical and single-cell transcriptional profiling of the murine habenular complex. eLife 9, e51271. https://doi.org/10.7554/eLife.51271

Wang, J., Cheng, H., Li, X., Lu, W., Wang, K., Wen, T., 2013. Regulation of Neural Stem Cell Differentiation by Transcription Factors HNF4-1 and MAZ-1. Mol Neurobiol 47, 228–240. https://doi.org/10.1007/s12035-012-8335-0

Welz, P.-S., Zinna, V.M., Symeonidi, A., Koronowski, K.B., Kinouchi, K., Smith, J.G., Guillén, I.M., Castellanos, A., Furrow, S., Aragón, F., Crainiciuc, G., Prats, N., Caballero, J.M., Hidalgo, A., Sassone-Corsi, P., Benitah, S.A., 2019. BMAL1-Driven Tissue Clocks Respond Independently to Light to Maintain Homeostasis. Cell 177, 1436-1447.e12. https://doi.org/10.1016/j.cell.2019.05.009

Wickham, H., Chang, W., Henry, L., Pedersen, T.L., Takahashi, K., Wilke, C., Woo, K., Yutani, H., Dunnington, D., RStudio, 2021. ggplot2: Create Elegant Data Visualisations Using the Grammar of Graphics.

Wolinsky, T.D., Carr, K.D., Hiller, J.M., Simon, E.J., 1994. Effects of chronic food restriction on mu and kappa opioid binding in rat forebrain: a quantitative autoradiographic study. Brain Res 656, 274–280. https://doi.org/10.1016/0006-8993(94)91470-2

Wu, G., Ruben, M.D., Lee, Y., Li, J., Hughes, M.E., Hogenesch, J.B., 2020. Genome-wide studies of time of day in the brain: Design and analysis. Brain Science Advances 6, 92–105. https://doi.org/10.26599/BSA.2020.9050005

Yamanishi, K., Doe, N., Sumida, M., Watanabe, Y., Yoshida, M., Yamamoto, H., Xu, Y., Li, W., Yamanishi, H., Okamura, H., Matsunaga, H., 2015. Hepatocyte Nuclear Factor 4 Alpha Is a Key Factor Related to Depression and Physiological Homeostasis in the Mouse Brain. PLOS ONE 10, e0119021. https://doi.org/10.1371/journal.pone.0119021

Yang, R., Su, Z., 2010. Analyzing circadian expression data by harmonic regression based on autoregressive spectral estimation. Bioinformatics 26, i168-174. https://doi.org/10.1093/bioinformatics/btq189

Zhang, B., Gao, Y., Li, Y., Yang, J., Zhao, H., 2016. Sleep Deprivation Influences Circadian Gene Expression in the Lateral Habenula [WWW Document]. Behavioural Neurology. https://doi.org/10.1155/2016/7919534

Zhang, R., Lahens, N.F., Ballance, H.I., Hughes, M.E., Hogenesch, J.B., 2014. A circadian gene expression atlas in mammals: implications for biology and medicine. Proc Natl Acad Sci U S A 111, 16219–16224. https://doi.org/10.1073/pnas.1408886111

Zhang, R., Oorschot, D.E., 2006. Total number of neurons in the habenular nuclei of the rat epithalamus: a stereological study. J Anat 208, 577–585. https://doi.org/10.1111/j.1469-7580.2006.00573.x

Zhao, H., Rusak, B., 2005. Circadian firing-rate rhythms and light responses of rat habenular nucleus neurons in vivo and in vitro. Neuroscience 132, 519–528. https://doi.org/10.1016/j.neuroscience.2005.01.012

6 General Discussion

Whilst there is ample evidence indicating that the reward circuitry of the brain may be under circadian control, as yet there are limited studies into whether there are circadian influences on mechanisms driving nicotine intake. This thesis set out to investigate diurnal variation in cholinergic signalling within the rodent brain, using a multilevel approach which encompassed: i) a whole animal level exploration of daily variation in behavioural responses to nicotine; ii) network level investigations of circadian variation in MHb activity and cholinergic signalling through the use of *ex-* and *in vivo* electrophysiological approaches; and iii) molecular level assessment of daily variations in the MHb transcriptome. This chapter summarises the key findings of this thesis, discusses how together they alter our understanding of both the medial habenula (MHb) and the interactions between time of day modulation and cholinergic signalling and considers how these new insights might have translational benefit for humans in the future. Finally, potential limitations of the experimental approaches are discussed, alongside likely directions for future work arising from the results presented in this thesis.

6.1 Key findings of this thesis

6.1.1 Chapter 2

This thesis began investigating the interaction between time of day and cholinergic signalling at the whole animal level, through behavioural studies. Although various drugs of abuse are known to vary in their effective potency over the circadian day (Abarca et al., 2002), this possibility has not been extensively investigated for nicotine. Therefore, in Chapter 2, we set out to determine how acute nicotine challenge influenced locomotor responses in rats, as a function of time of day. In addition, we chose to perform our experiments using female rats as there are a limited number of studies investigating the acute effects of nicotine in female animals, despite known sex differences in the behavioural effects of nicotine (Moen and Lee, 2021). We found that acute nicotine challenge alters spontaneous ambulatory activity, but the direction and magnitude of this effect is dependent on the time of day, such that activity tends to be suppressed at times when the rats are at their most spontaneously active and conversely, ambulation is activated during the rats' rest phase. In contrast, we showed that acute nicotine challenge tended to suppress rearing behaviour, but these effects were only apparent at times in the day when animals were at their most spontaneously active. These results indicated distinct signalling pathways mediating these

two behaviours, which differentially interact with the circadian system to produce these daily rhythms in nicotine sensitivity.

6.1.2 **Chapter 3**

Having established evidence for circadian variation in responses to nicotine at the behavioural level, our next aim was to determine the underlying neural mechanisms. These studies focussed specifically on the MHb, an area known to be highly important in nicotinic cholinergic signalling in the rodent brain where previous studies have suggested a major role in nicotine addiction (Lee et al., 2019) and also demonstrated circadian oscillatory properties (Sakhi et al., 2014a; Zhao and Rusak, 2005). We performed a series of *in vitro* electrophysiological experiments, revealing higher spontaneous firing rates and responses to nicotine in brain slice recordings performed during the early projected day compared to the late day. In recordings lasting for the entirety of a circadian cycle, we also saw evidence of circadian rhythmicity in the activity of many individual MHb neurons. However, the phase of peak firing across these MHb neurons did not reliably reflect the animal's prior light history but, rather, was correlated with the time of slice preparation. In sum, these data suggest circadian rhythms in MHb activity are rapidly reset *ex vivo*, precluding longitudinal study. Nonetheless the data also provide clear evidence consistent with the idea that circadian rhythms in MHb activity and responses to nicotinic receptor stimulation could underlie daily variations in neurobehavioural responses to nicotine.

6.1.3 **Chapter 4**

The *ex vivo* work discussed above indicated that MHb cells had rhythmic properties, but the potential insights available from such experiments were complicated by the MHb resetting its phase *ex vivo*. Therefore, subsequent studies were designed to explore rhythms in the MHb further using *in vivo* electrophysiological techniques. These experiments employed optogenetics in order to identify cholinergic neurons of the MHb and distinguish these from other MHb cell types, and consequently examine both the spontaneous and light-evoked activity of these subpopulations at different times of day. We showed diurnal variation in steady state firing and excitability of MHb cholinergic neurons, with reduced spontaneous activity but enhanced evoked responses during the early night. In addition, we confirmed previous work which had showed the MHb is light responsive (Zhao and Rusak, 2005), and further found that this property is shared with subset of cholinergic neurons. Finally, we found that the cholinergic neurons of the MHb had a higher than expected degree of correlated activity compared to other MHb cell types, indicative of shared synaptic inputs. Thus, we established that MHb cholinergic neurons integrate both

circadian and photic information, which could contribute to the rhythmic drive in nicotine addiction behaviours.

6.1.4 Chapter 5

Our final aim was to elucidate the molecular mechanisms driving the diurnal variation in MHb properties we had observed in Chapters 3 & 4. Therefore, we employed RNA sequencing at four time points across the day / night cycle to generate a diurnal transcriptomic profile of mouse MHb tissue. Somewhat unexpectedly, we did not find evidence for robust rhythms in molecular clock genes nor in nicotinic receptor expression. We did, however, find a group of rhythmic transcripts, primarily with peak expression during the dark phase. Of these, a subset with peak expression during the dark phase were associated with insulin signalling and mechanisms regulating synaptic plasticity. We further identify HNF4A, a metabolic regulator of insulin regulation, as a potential upstream regulator of a subset of night-peaking rhythmic genes. Therefore, this final chapter implies that rhythmic activity of the MHb may well be driven by mechanisms other than local canonical molecular clockwork such as from other clock containing structures or due to behavioural rhythms.

6.2 Implications of this work

6.2.1 The importance of considering time of day modulation when designing experiments studying nicotine

Chronobiologists have long been fascinated by the temporal organisation of physiology, and the 2017 Nobel Prize in Physiology or Medicine being awarded for circadian rhythm research indicates just how important this aspect of biology is viewed as today. A wealth of knowledge has shown that there are time of day modulations in processes as wide ranging as gene expression in cyanobacteria (Johnson, 2007), regulation of flowering in plants (Creux and Harmer, 2019) and even mood regulation in mammals (Albrecht, 2017). Therefore it is essential that biologists across all fields consider circadian rhythmicity as a possible contributing factor in their own work. However, research indicates that in spite of this, the majority of publications still fail to report the time of day (Nelson et al., 2021). The work described in this thesis reveals significant effects of time of day encompassing behavioural and neurophysiological responses to nicotine (Chapters 2 and 3) as well as basic cellular excitability (Chapters 3 and 4) and gene expression in the MHb (Chapter 5). Importantly such variation could lead to substantially different outcomes for experiments performed within the typical range of working hours (e.g., between early and late day) for laboratory scientists who are not directly considering circadian control mechanisms as

part of their research. Failure to consider such actions is likely then to lead to increased variability within studies (and increased animal usage) and/or heterogeneity in results reported across different studies. With research into neurobehavioural responses and addiction to nicotine remaining a major field of investigation and growing interest in habenula contributions to this and other aspects of brain function (Lee et al., 2019; Mathuru, 2017; Molas et al., 2017a), but few studies characterising how these aspects of biology are altered by the time of day, these data highlight a need for researchers to consider diurnal variation in their own studies.

6.2.2 Where might the rhythms in nicotine-evoked locomotor behaviour originate?

Chapter 2 establishes a potential interplay between circadian/diurnal rhythmicity and nicotine-evoked changes in locomotor activity, and provides further evidence that nicotine-evoked modulation of rearing and ambulation are driven by distinct pathways. The locomotor stimulant effects of nicotine are attributed to dopamine signalling within the mesolimbic system (Di Chiara, 2000), with the ventral tegmental area (VTA; Panagis et al., 1996) or the nucleus accumbens (NAc; Louis & Clarke, 1998) implicated more specifically. Nicotine's effects on rearing are less well characterized but have been linked to the NAc as well (Adermark et al., 2015; Casarrubea et al., 2015). Our results confirm that both of these behaviours are modulated by the time of day, which indicates there must certainly be a site integrating circadian signals with the effects of nicotine on locomotor activity. The VTA has been shown to be a major area involved in the nicotine-elicited hyperlocomotion in rats, following studies infusing nicotinic acetylcholine receptor (nAChR) blockers into the VTA which attenuated this response (Gotti et al., 2010). In addition, neurons in the VTA are known to display rhythmic activity, demonstrating diurnal variation in spontaneous firing activity in dopaminergic neurons in rats (Domínguez-López et al., 2014) and tissue-level diurnal gene expression rhythmicity in mice (Koch et al., 2020). Alternatively, the NAc has been reported to exhibit circadian expression of *Per2 ex vivo*, using a luciferase reporter (Landgraf et al., 2016b) as well as rhythms in electrophysiological activity, via *in vivo* recordings in hamsters (Yamazaki et al., 1998) and *ex vivo* recordings from mouse brain slices (Parekh et al., 2018). However, with the MHb known to indirectly influence activity of both the VTA (Balcita-Pedicino et al., 2011; Cuello et al., 1978) and the NAc (Eggan and McCallum, 2016), in addition to the rhythmic properties revealed here in this thesis, together suggests that the MHb is also well-placed to modulate the locomotor effects according to the time of day.

Certainly the MHb is able to influence motor activity in rodents. Early studies in rats with lesions of the fasciculus retroflexus (the efferent pathway of the habenula) showed increased locomotor activity, implicating either lateral habenula (LHb) or MHb (or both) in this action (Murphy et al.,

1996). Hamsters with transected fasciculus retroflexus show altered period in circadian rest-activity rhythms as measured through wheel-running behaviour (Paul et al., 2011). Loss of dorsal MHb in mice attenuated spontaneous wheel-running activity compared with controls (Hsu et al., 2017), whilst optogenetic activation of this area increased distance travelled in the open field (Hsu et al., 2014). Mice with postnatal ablation of the MHb did not exhibit the normal locomotor suppressant effects of habituation when continually exposed to the same environment, perhaps indicating an increased drive to explore novelty (Kobayashi et al., 2013), although selective ablation of habenula cholinergic neurons did not affect general locomotor activity in mice (J. Zhang et al., 2016). Finally, infusion of α3β4 nAChR-specific antagonists into rat MHb attenuated both the hyperactivity associated with acute nicotine challenge (McCallum et al., 2012) as well as the locomotor sensitization effects of nicotine (Eggan and McCallum, 2017, 2016). Therefore, the work in Chapter 2 indicates a potential role for the MHb in regulating the time of day modulation of nicotine's effects on locomotor activity, which justify further investigation.

6.2.3 Rhythms in MHb cell and tissue function and their potential origins

Work performed by Sakhi et al (2014a) and Zhao and Rusak (2005) indicated that the MHb shows evidence of daily variation in electrophysiological output and excitability. The work presented in Chapters 3, 4 and 5 confirms the rhythmic capacity of the MHb, but the origin of these rhythms remains unclear. Our *in vitro* experiments showed that the MHb exhibits circadian rhythms in spontaneous population-level activity and that a sizeable proportion of MHb neurons displayed evidence of a rhythm in firing without input from the suprachiasmatic nucleus (SCN) for the duration of a circadian cycle. However, we also saw that the phase of these rhythms appeared to be reset according to the time of the slice preparation, rather than the prior light history of the animals. This observation explains the previous finding from Zhao and Rusak (2005), where discontinuous sampling from MHb neurons *ex vivo* failed to reveal a population rhythm in spontaneous activity in a dataset that pooled neurons across slices prepared 12 hours apart. The resetting of MHb rhythms detected here is in stark contrast to the SCN, however, where *ex vivo* neuronal firing retains a predictable phase relative to the prior light / dark cycle (Brown et al., 2006; S. Paul et al., 2020; vanderLeest et al., 2009). By contrast, such *ex vivo* resetting of MHb neuronal rhythms is more in keeping with that observed in extra-SCN brain regions with less robust internal clocks (Chrobok et al., 2021; Harding et al., 2020). These data highlight the importance of appropriate controls and caution when assessing the rhythmic function of clocks outside the SCN, in order to confirm that phasing observed *ex vivo* provides a true indication of the timing of rhythmic activity in the intact animal.

Importantly, however, analysis of data across the acute phase (first hour) of recordings performed at different times of day did indicate the presence of a coordinated rhythm in MHb activity that was detectable, with high firing in the morning and reduced spontaneous activity during the early night. This aligns with data from Sakhi et al (2014a) on circadian variation in the proportion of silent MHb neurons as well as *in vivo* recordings performed here (and previously in rats; Zhao and Rusak, 2005) revealing daily variations in MHb firing. On aggregate these data are consistent with the view that rhythms in MHb activity detectable in the intact animal are transiently retained *ex vivo* and therefore reflect some intrinsic variations in MHb cell/tissue function. Accordingly, investigation of the diurnal transcriptomic profile of the MHb certainly indicated rhythmic gene expression in this tissue that could potentially underlie such changes in MHb neuronal activity.

Interestingly, we did not find rhythmic expression of many core molecular clock genes in the MHb. In particular, we did not detect *Per2* expression within our transcriptional dataset, although rhythmic *Per2* expression has previously been demonstrated within this tissue *ex vivo* using a bioluminescent reporter in mice (Landgraf et al., 2016b), and *Per2* mRNA has been detected in rat MHb using *in situ* hybridisation (Shieh, 2003). However, there is conflicting evidence regarding clock gene expression in the MHb. Hence another study, also using *Per2* reporter, found that oscillations in the mouse MHb to be very weak and potentially driven by the ependymal cell layer (Guilding et al., 2010).

It remains a possibility that clock gene expression is detected only weakly in the MHb, in such low quantities that it was not detected above noise thresholds in our transcriptional dataset. Certainly our finding that individual neurons of the MHb are capable of sustaining rhythmic pattern in their firing rates for up to 24 hours is indicative of a local clock. However, recent work by Putker et al has shown that circadian rhythmicity in some cells occurs even in the absence of molecular clock genes (Putker et al., 2021). Alternatively, in the absence of a local molecular clock, the rhythms we observed in the MHb might be driven through rhythmic inputs either from other clock containing structures or time of day–dependent behavioural rhythms. As we detected electrophysiological rhythms in our *ex vivo* tissue slices, this suggests the clock structure would have to be local, and within the slice. Of course, as an adjacent structure also capable of maintaining rhythms independent of the SCN (Mendoza, 2017), the LHb presents a potential driver of the MHb. There is evidence for reciprocal connections between the MHb and LHb (Lima et al., 2017) although this is purported to be driven through the IPN which was not contained within our slices. Nonetheless, the rhythms we demonstrated in LHb and MHb neurons were broadly in phase in our long-term slices (with the LHb following MHb rhythms with a four hour delay), which supports the idea of crosstalk between these structures.

Extending the work of Zhao and Rusak (2005), our *in vivo* experimental work confirmed that neurons across the MHb are light responsive, and further suggested melanopsin as the likely photoreceptor of origin. This presents another route by which rhythms may be conferred on the MHb, and in particular may drive the rhythmic gene expression observed in Chapter 5. Changes in gene expression following light exposure has been demonstrated in the cortex (Hrvatin et al., 2018), and the SCN (Wen et al., 2020), and some of these light-dependent transcription changes in the SCN are dependent on the time of day (Alzate-Correa et al., 2021; Wen et al., 2020).

The anatomical position of the MHb, positioned directly adjacent to the third ventricle, means that this structure is also well placed to receive diffuse clock signals through the ventricular system. The arcuate nucleus is an extra-SCN oscillator (Guilding et al., 2009) and is similarly located lateral to the third ventricle. The arcuate receives information about circulating leptin hormone via tanycyte mediated transport (García-Cáceres et al., 2019; Müller-Fielitz et al., 2017), demonstrating one way that behavioural/feeding rhythms could be signalled to the MHb. Interestingly, tanycytes have also been identified within rat MHb tissue (Cupédo and de Weerd, 1985). Diffusible substances from the SCN are also able to convey clock signals through this ventricular system: SCN tissue transplants into the third ventricle can restore locomotor activity rhythms in hamsters lacking SCN (Silver et al., 1996). In a recent study, Chrobok et al demonstrated rhythmic penetration of blood borne molecules into the nucleus of the solitary tract, a rhythmic structure within the brainstem (Chrobok et al., 2020). As insulin signalling was identified as a possible rhythmic process within the MHb in Chapter 5, circulating factors relating to metabolic status provide a plausible source of external timing signals for the MHb.

6.2.4 What adaptive purpose might rhythms serve for MHb function?

Given that the MHb clearly exhibits daily variation in neuronal activity and gene expression it is worth considering what potential functions such rhythmicity may serve. Previous work has implicated the MHb in a range of behaviours including anxiety, fear and depression (Lee et al., 2019; McLaughlin et al., 2017; Molas et al., 2017a) all of which have demonstrated diurnal variation (Albrecht and Stork, 2017; Ketchesin et al., 2020; Landgraf et al., 2014; McClung, 2013). Certainly, rhythms in the MHb could contribute to these diurnal patterns in mood. In addition, the MHb is well placed to receive information about daily rhythms in satiety signalling, and we presented tentative links to feeding behaviour as suggested through our RNA experiments. Food is often considered the primary 'natural' reward (DePoy et al., 2017a), and it is easy to see how a circadian drive in food seeking behaviours could be advantageous for a nocturnal prey animal such as the mouse. Indeed, rhythmic drives over food seeking behaviour have been demonstrated

previously in rodents (Mistlberger, 2011). In order to seek food, animals must be motivated both to perform locomotor activity and perhaps have increased drive for exploring novel stimuli, both behaviours linked to the MHb (Hsu et al., 2014; London et al., 2020; Molas et al., 2017b). As a potential site of integration between circulating hormone signals and time of day information, the work presented in this thesis raises the possibility that the MHb may modulate the downstream reward centres to drive motivation to seek food to appropriate times of day. Activation of cholinergic MHb neurons is known to reduce the expression (and promote the extinction) of fear memories in mice (J. Zhang et al., 2016). Accordingly our finding that such cells exhibit diurnal variation in firing provides a route by which the MHb could shape rhythms in exploratory activity in mice, for example by reducing risky exploratory activity around the beginning of the mouse' active phase (dusk) when risk of predation may be especially high.

6.2.5 Implications for MHb-mediated nicotine addiction behaviours

Much research into the MHb has focussed on its role in nicotine addiction (Lee et al., 2019), and previous studies have indicated that MHb cholinergic neurons may contribute to smoking relapses. In abstinent mice previously subject to chronic nicotine administration, MHb cholinergic neurons show increased spontaneous firing if re-exposed to nicotine (Görlich et al., 2013). MHb cholinergic neurons also moderate the aversive properties of nicotine, thus regulating self-administration (Souter et al., 2021), as well as mediating the anxiogenic effects associated with nicotine withdrawal (Pang et al., 2016; Zhao-Shea et al., 2015). Interestingly, self-administration of nicotine in rats follows a circadian pattern (O'Dell et al., 2007), and humans have both diurnal variation in smoking, representative of nicotine intake (Chandra et al., 2011; Grainge et al., 2009; Mooney et al., 2006), and also show time of day variation in severity of withdrawal symptoms following tobacco abstinence (Parrott, 1995; Perkins et al., 2009; Teneggi et al., 2002). The time of day modulation of MHb cholinergic neuron firing activity demonstrated within this thesis could contribute to the rhythms underlying these behaviours. We have also shown that neurons of the MHb modulate their responses to nicotine in a time of day dependent manner *ex vivo*, with increased firing in the early day compared to the late day. Furthermore, our behavioural studies indicate a switch between more suppressive actions of nicotine on locomotion during the early day, to greater stimulatory effects during the late day. As such, it is tempting to speculate that the MHb is driving the suppressive effects of nicotine on activity. However, as these particular experiments did not span the entirety of the circadian cycle, we are unable to fully extrapolate the hours at which MHb may be most sensitive to nicotine signalling, or most likely to drive nicotine-evoked behaviours. Further work investigating how this rhythmicity is altered following

chronic nicotine exposure is needed in order to determine how circadian control of nicotine signalling could be harnessed for translational benefit to humans.

Studies into the human habenula have been challenging until recently, as both the MHb and LHb have a combined total volume between 30 – 36 mm^3 (Savitz et al., 2011). The pea-sized proportions of this structure meant that distinguishing between LHb and MHb was challenging in non-invasive imaging techniques, although recent advances in Ultra-high resolution Magnetic Resonance Imaging (hr-MRI) have made this possible (Boulos et al., 2017). Application of this technique has indicated similar topography of the habenula in rodents and humans (Strotmann et al., 2014, 2013). So far human research has confirmed several findings from rodent studies, including habenula contributions to mood disorders. Post–mortem histological studies of patients diagnosed with major depression disorder or bipolar disorder showed reduced volume in both MHb and LHb (Ranft et al., 2010). Hr-MRI of unmedicated patients with bipolar disorder or depression confirmed this reduction in habenula volume (Savitz et al., 2011). Human habenula is also activated during aversive learning, although these studies do not differentiate between LHb and MHb (Hennigan et al., 2015; Lawson et al., 2014). Studies in humans have also shown a consistent role of the MHb in mediating addiction behaviours. Transcriptional examination of human MHb identified genes associated with nicotine response and genetic tendency for smoking were enriched in the MHb (Le Foll and French, 2018). Finally, a recent study has shown that human habenula is responsive to luminance, and moreover this response is dependent on the time of day (Kaiser et al., 2019). These studies indicate that findings in the rodent habenula, including the results illustrated within this thesis, have a good translational potential for human therapies due to the conserved nature of the habenula complex.

Depression remains a significant risk factor for developing nicotine dependence (Dierker et al., 2015) and decreases the likelihood of a successful attempt to quit smoking (McClave et al., 2009). This is thought to be in part driven by attempts to self-medicate and relieve the symptoms of depression through nicotine consumption (Yao et al., 2021). Depression is also strongly linked to circadian disruption (Difrancesco et al., 2019; Jagannath et al., 2013), and there is evidence for diurnal variation in the efficacy of some antidepressant therapies (Swanson et al., 2017). MHb cholinergic neurons are thought to regulate the midbrain monoaminergic neurons and are associated with anhedonic behaviours (McLaughlin et al., 2017; Xu et al., 2018; Yamaguchi et al., 2013). Therefore, the MHb may be one locus mediating interactions between circadian disruption, depression and nicotine addiction. It is plausible that circadian disruption at the MHb leads to mistimed outputs which produce inappropriate anxiety and fear responses, contributing

to the pathology of depression and promoting nicotine dependence in an attempt to alleviate the symptoms of depression.

6.3 Discussion of experimental strategies

6.3.1 Translational potential of nocturnal rodents

Many of the experimental design choices of this thesis were considered with the eventual translational capability of this work in mind, such as the decision to study rhythms using animals maintained under the more physiologically/practically relevant situation of exposure to a 24 hour light / dark cycle, rather than the constant conditions that would more specifically isolate circadian influences. As discussed previously, the function and structure of the MHb at least appears to be broadly conserved across species (Fakhoury, 2017), suggesting that discoveries in the rodent may apply to humans as well. However, in using nocturnal rodents to investigate rhythmic activity, there are some limitations which must be considered if the eventual goal is translation to a diurnal species.

Much of the current research into circadian biology has been performed using nocturnal rodents. Whilst the phase expression of the majority of molecular clock components (Takahashi et al., 2008; Yan et al., 2018) and the daily patterns in firing rate seen within the SCN are in phase regardless of the active period of the animal (Inouye and Kawamura, 1979; Sato and Kawamura, 1984; Schwartz et al., 1983; Smale et al., 2008), there are important differences in the circadian system between diurnal and nocturnal rodents. The most obvious of course, are the behavioural outputs in sleep, locomotor activity, neuroendocrine and autonomic function which are largely reversed between chronotypes (Becker et al., 2019; Kumar Jha et al., 2015; Paul and Brown, 2019; Wang et al., 2020), with the notable exception of the hormone melatonin (Johnston and Skene, 2015). Other studies have shown photic induction in c-fos in retinorecipient regions including the subparaventricular zone, intergeniculate leaflet, and LHb of diurnal Nile grass rats, which was absent in nocturnal mice (Shuboni et al., 2015). There are other differences in habenula circuitry which differ between diurnal and nocturnal rodents, such as the presence of GABAergic interneurons in the LHb in diurnal Nile Grass rats which are absent in nocturnal Norway rats (Langel et al., 2018). Interestingly, in humans, luminance produced a decrease in habenula activation (Kaiser et al., 2019), whereas the results presented in this thesis and in previous studies show nocturnal rodents tended to display increased habenula activation in response to light exposure (Sakhi et al., 2014b; Zhao and Rusak, 2005), perhaps indicating hard-wired differences in light processing within the habenula between chronotypes. Therefore, it is plausible that there

will be differences in the activity of MHb between diurnal and nocturnal species which could in turn differentially regulate mood-related behaviours or the other behaviours with which the MHb is linked.

In addition, it is well known that C57Bl/6J mice (as used throughout this thesis) are melatonin deficient (Dubocovich et al., 2005). Whilst this hormone is neither necessary nor sufficient for driving rhythmic activity in mice (Kasahara et al., 2010), some studies have shown that a lack of melatonin does have marked effects on circadian behaviours, including less stable locomotor rhythms under steady entrained conditions (Pfeffer et al., 2017). Whilst we do not anticipate the lack of melatonin in the mice used in this thesis to dramatically alter our findings when compared to animals with functional melatonin signalling, we instead suggest caution when extrapolating the phases of rhythms reported in this thesis to such animals.

6.3.2 **Limitations of *in vitro* electrophysiology**

In vitro electrophysiological recordings offer a number of potential benefits for understanding rhythmic control mechanisms in the brain in that i) they allow neurons to be studied while isolated from external sources of input, including inputs from other brain regions as well as indirect rhythmic signals associated with physiological and behavioural rhythms in the intact animal; ii) they are amenable to long-term recording over the timescales required to assess circadian rhythmicity and iii) they facilitate pharmacological manipulations to dissect responses to neurochemicals of interest and underlying mechanisms. Often, *in vitro* electrophysiological approaches rely on the recording of individual neurons, which can be particularly useful for isolating cell intrinsic mechanisms but usually precludes longitudinal monitoring and investigations of neural circuit dynamics (Accardi et al., 2016). The use of multielectrode arrays however, allowed us to record simultaneously from sites across the MHb over the extended epochs necessary to assess circadian rhythmicity in Chapters 3 & 4. As our primary aim for the *in vitro* investigations was to characterise the diurnal patterns in rhythmic firing activity of neurons in the MHb, it is important that this technique is a close approximation of activity seen *in vivo.*

Plenty of evidence indicates that rhythms in firing in acute *ex vivo* slices of SCN tissue are true reflections of *in vivo* timing (Meijer and Schwartz, 2003; vanderLeest et al., 2009; Vansteensel et al., 2003). As noted above, however, in keeping with reports focussing on other potential extra-SCN brain clock sites (Chrobok et al., 2021; Harding et al., 2020), rhythms in the MHb appear to be rapidly reset *ex vivo*. While the mechanism underlying this resetting is currently unclear, it seems that while long-term MEA recordings such as those used here can provide a useful indication of the capacity of individual cells to sustain rhythms in neuronal activity, they are potentially less

useful for revealing the 'true' phase of such rhythms in the intact animal. Importantly, our data (alongside results from other studies; Sakhi et al., 2014a; Zhao and Rusak, 2005) indicate that, at least at the population level, rhythmic activity in the MHb transiently retains its *in vivo* timing information in acute slice preparations. Hence, data obtained *ex vivo* can still inform our understanding of population-level circadian control mechanisms involving the MHb, although future studies need to be appropriately designed such that recordings are limited to the first few hours post slice preparation.

6.3.3 Limitations of *in vivo* electrophysiology

The work presented in Chapter 4 employed *in vivo* electrophysiological methods. Thus, recording from the MHb in this way we preserve the full complement of direct and indirect signalling pathways acting upon the structure (including from the SCN, for example), thus allowing us to draw more firm conclusions about the phase of rhythmic activity we identified here. However, there remains an important question: is rhythmic brain activity observed in anaesthetized animals representative of awake behaving animals? Of course, brain states under anaesthesia are not identical to animals perceiving and responding to stimuli (Sorrenti et al., 2021). Some studies have shown that mice under urethane have brain state alterations that are similar to sleep (Pagliardini et al., 2013), highlighting the depressive actions of this anaesthetic (Shumkova et al., 2021).

We chose urethane as our anaesthetic to enable stable recordings over prolonged periods of time. Urethane has limited effects on GABAergic signalling (Hara and Harris, 2002; Maggi and Meli, 1986), which is critical for time of day investigation as circadian network oscillations are maintained by GABA (Buzsáki, 2002). In addition, it is often the anaesthetic of choice for electrophysiological examination of visual activity as it does not alter sensory-evoked responses to the same degree as other agents (Simons et al., 1992). However, there are some drawbacks with this anaesthetic agent. Urethane was found to potentiate the functions of nAChRs, although this study found that urethane had effects on several other neurotransmitter-gated ion channels also transfected in Xenopus oocytes (Hara and Harris, 2002). It is unclear exactly how this might relate to the experiments presented in this thesis, although it highlights that performing experiments in awake animals would provide the most physiologically sound results (although this would be true regardless of the choice of anaesthetic).

One final consideration of our *in vivo* electrophysiological studies is our transgenic mouse line. Previous work has shown that in a different ChAT-Cre line, generated via bacterial artificial chromosome (BAC) method, mice had deficits in locomotor activity and nicotine-mediated responses (Chen et al., 2018). Therefore, our first goal was to characterize the daily locomotor

activity of the ChAT-Cre mice used in this thesis to check for normal circadian function. We showed that both rhythm robustness and circadian phase was the same between ChAT-Cre;Ai32 mice and our controls. Similarly, a previous study has indicated that the ChAT-Cre mice as used in this thesis have similar sleep-wake state duration and temporal profile to littermate mice not expressing Cre (Anaclet et al., 2015). This gave us confidence that rhythms *in vivo* would likely be similar to the rhythms of wildtype mice.

We also confirmed that ChR2 expression in this line faithfully recapitulated the endogenous pattern of ChAT expression, which is not the case for BAC-generated ChAT-ChR2 mice (Cui et al., 2020). This then allowed us to identify putative cholinergic neurons during *in vivo* multielectrode recordings, based on their direct responses to brief light flashes, and characterise their spontaneous and light evoked activity as a function of time of day. One caveat that should be considered when interpreting these data is that ChAT is expressed in starburst amacrine cells in the retina (Ivanova et al., 2010). Accordingly, it is formally possible that our binocular illumination inadvertently activated this group of neurons and generated light-evoked responses. However, the light intensities used here were at least two orders of magnitude lower than the threshold for evoking ChR2-driven responses (Madisen et al., 2012). Moreover, starburst amacrine cells signal through the image-forming visual system of the brain, which typically relies on the actions of fast signals (Taylor and Smith, 2012). As we detected only sluggish responses characteristic of melanopsin-driven signalling in our experiments, it seems unlikely that optogenetically activated cells in the retina contributed to the results presented in this thesis.

6.3.4 Methodological considerations of RNA-sequencing

In Chapter 5, we use RNA-sequencing in combination with laser-capture microdissection of the entire MHb tissue in order to produce a diurnal profile of gene expression within this tissue. RNA-sequencing allows an unbiased approach to the quantification of RNA abundance within a tissue sample at a whole-genome scale, in comparison to targeted profiling of genes of interests through microarray techniques for example. The use of laser-capture dissection results in increased precision and dramatically reduced variability compared with manual dissection or tissue punches (Farris et al., 2017). As such, we can be relatively confident that contamination of our sample from surrounding areas was minimal, and therefore the results are representative of the population of MHb cells. However, there are a number of points which must be considered when assessing the results of our experiments.

In particular, the lack of detection of many of the core clock gene transcripts across our samples, in spite of previous work demonstrating their expression within the MHb (Landgraf et al., 2014;

Olejniczak et al., 2021; Shieh, 2003), suggests that these transcripts may have been expressed at very low levels within our samples. One disadvantage of the bulk RNA sequencing we employed is that it reflects the average RNA abundance across the entire tissue sample. Like other brain structures, the MHb is composed of multiple different cell types (such as astrocytes, microglia, ependymal cells and neurons), and the MHb can be further divided into at least two functionally different substructures (for example the dorsal and ventral portions of the MHb), which differ in both neurotransmitter expression and behavioural output (C.-H. Cho et al., 2019; Hsu et al., 2014). Other studies have divided the MHb even further based on gene expression (Wagner et al., 2014). Indeed, each single brain cell may be characterized by a unique transcriptional profile (Harbom et al., 2016; Keil et al., 2018). Therefore, the high degree of heterogeneity within the MHb may obfuscate the populations of rare cell types in bulk sequencing (Tasic et al., 2018). Further, if clock gene-expressing cells in the MHb are rare, this may lead to inaccurate quantification as RNA sequencing is less able to quantify transcripts that are very low in abundance (Keil et al., 2018). Nonetheless, the unique molecular index barcoding approach as employed in this thesis improves reproducibility of quantification of low abundance transcripts (Islam et al., 2014).

Single-cell RNA sequencing is hailed as the methodological advancement which circumvents the issues of tissue heterogeneity present with bulk sequencing techniques (Cembrowski, 2019; Kulkarni et al., 2019; Ofengeim et al., 2017). Indeed, two recent studies have used this approach in the habenula to demonstrate the diversity of cells type and gene expression within this tissue, identifying between 12 – 20 cell clusters with distinct transcriptional profiles (Hashikawa et al., 2020; Wallace et al., 2020). However, single-cell sequencing presents its own difficulties: isolating single neurons is particularly challenging, as axonal and dendritic processes increase the likelihood of cell membrane rupture during dissociation (Cardona-Alberich et al., 2021) with losses resulting from single-cell RNA collection and reverse transcription steps limiting somatic RNA sampling to between 20 - 30% (Cembrowski, 2019; Tasic et al., 2018). In addition, the requirement for multiple time points for circadian analysis present a significant financial hurdle.

One final limitation to note is the low sampling frequency of our study, as we collected tissue at only four time points. Certainly, increasing the sampling resolution would improve accuracy and facilitate reliable identification of rhythmic genes (Hughes et al., 2017; Wu et al., 2020). However, a recent review highlighted the lack of circadian transcriptome studies focussed within the brain (Wu et al., 2020): only the SCN, pituitary, hypothalamus, brain stem, and cerebellum have currently been examined for circadian profiles of gene expression (Hughes et al., 2007; Pembroke et al., 2015; Zhang et al., 2014). Therefore, despite some of the limitations associated with bulk

sequencing, the work presented in this thesis nonetheless makes a valuable contribution to the field. The identification of rhythmic components within the MHb transcriptome should be further investigated, in particular as there is good evidence to suggest that there is high conservation of gene expression between human and mouse brain tissues (Breschi et al., 2017; Wang and Wang, 2019).

6.4 Key areas for follow up work

The collective work presented in this thesis has served to confirm that there are time of day influences on nicotinic cholinergic signalling mechanisms. The data demonstrate that behavioural and electrophysiological responses to nicotine are modulated by the time of day, and further shown the oscillatory capacity of cells in the MHb through both *in vitro* and *in vivo* approaches. Finally, we identify a subset of rhythmic genes expressed within the MHb. In turn, these findings prompt several avenues for further research, which will now be discussed below.

6.4.1 Origins of MHb rhythms

The results presented in this thesis were not able to conclude whether the rhythms within the MHb were driven through endogenous molecular clocks. One method to assess the possibility of a local clock would be through the use of transgenic mice engineered to have conditional deletion of the molecular clock within the MHb. For example, injecting an adeno-associated virus (AAV) vector vector to deliver Cre recombinase to the MHb of floxxed *Bmal1* mice (as generated by Storch et al., 2007) would inhibit molecular clock function in these cells. A lack of rhythmicity in the MHb following this procedure would indicate the reliance of MHb neurons on a local clock. Alternatively, we could 'switch off' inputs from other oscillatory structures, via injections of a retrograde AAV vector into the MHb alongside Cre-dependent inhibitory constructs (such as Lamplight, which enables optogenetic silencing; Rodgers et al., 2021), and determine whether MHb rhythmicity is retained.

6.4.2 Could the MHb contribute to diurnal variation in nicotine-evoked locomotor activity?

The work presented in this thesis indicates a time of day modulation over nicotine-evoked changes in locomotor activity in rats. However, the origin of this time of day modulation remains as yet undetermined. As discussed, recent studies involving mice have indicated that the MHb modulates exercise motivation, and the work of this thesis indicates the oscillatory properties of this structure. Therefore, an interesting avenue for investigation would be investigating whether

the MHb is the site of time of day influences on nicotine-evoked locomotion. Previous work has shown that this may not be driven exclusively by cholinergic neurons of the MHb, as selective ablation of these neurons did not affect locomotor activity within a novel open field or in the chamber used for fear conditioning experiments (J. Zhang et al., 2016). Instead it is likely that neurons in the dorsal portion of the MHb are likely to be involved due to their known involvement in regulating voluntary locomotor behaviours (Hsu et al., 2014).

One of the reasons we used this species, rather than mouse, was to facilitate comparison with previous published work, which has largely been carried out in rats. However, we propose that future experiments could be performed in mice, to allow the use of genetic tools available for the species, as mice also show diurnal variation in nicotine-evoked locomotion (Mexal et al., 2012). For example, mice with a conditional null mutation in *Pou4f1* of the dorsal MHb leads to restricted post-natal ablation of this tissue, as described in Hsu et al (2014). Performing the experiments as described in Chapter 2 in these animals would indicate whether this area of the MHb is involved in the diurnal variation in nicotine's effects on locomotion. In addition, this approach could be used to investigate how the MHb might modulate other rhythmic behaviours as discussed; for example fear responses and feeding behaviours.

However, genetic lesion studies cannot rule out the possible compensatory effects of other brain regions and network reorganisation contributing to the observed effects (Eisener-Dorman et al., 2009). Therefore, these studies could be followed up with DREADD-based chemogenetic tools (designer receptors exclusively activated by designer drugs) or optogenetic manipulations of this system. For example, directly injecting a Cre-inducible recombinant AAV vector containing ChR2 into the brains of mice expressing Cre-recombinase in neurons expressing a marker of dorsal MHb (synaptotagmin-6 BAC Cre line, $Syt6^{Cre}$; Hsu et al., 2014) would allow for specific activation of dorsal MHb using optogenetic photostimulation. Similarly, injecting Cre-dependent DREADDs would allow either activation or inhibition of these neurons, following administration of the otherwise inert drug CNO (Zhu et al., 2016). Optogenetics offers high temporal control but often requires cumbersome implanted fibreoptic probes to allow behavioural assessments (Canales et al., 2018). DREADDs eliminate the need for such equipment and are minimally invasive, but are subject to a delay following administration of CNO (Smith et al., 2016). Therefore, ideally such investigations would employ both techniques. Of course, equivalent approaches could also be used to assess the role of cholinergic MHb cells by delivering Cre-dependent DREADDs to the MHb of ChAT-Cre mice. Additionally, *in vivo* fibre photometry using genetically encoded calcium indicators to label these MHb cell populations would allow for long-term monitoring of neuronal activity (Patel et al., 2020). If used in conjunction with behavioural assessments, we could

determine whether changes in the activity of neuronal populations correlate with behavioural changes.

Furthermore, as investigating the acute effects of nicotine challenge on locomotion as presented in this thesis was a minimally invasive procedure, and relied only on the animal's spontaneous behaviour rather than a learned response, it would be both interesting and relatively straightforward to carry out this experiment with a diurnal rodent, such as *Rhabdomys pumilio.* Interestingly, one study investigating the effects of acute nicotine on guinea pigs, a diurnal rodent, showed reduced locomotor activation relative to rats (Simmons et al., 2010). However, as the authors did not include information about the times of day these experiments took place, experiments were likely performed during the active phase of the guinea pig, a time point we have shown is less likely to lead to strong activating effects of nicotine.

6.4.3 Origins of ACh input to the MHb

In Chapter 4, we discussed the conflicting evidence in the literature pertaining to the source of cholinergic inputs to the MHb. The evidence from our retrograde tracing study failed to identify any cholinergic inputs to the MHb other than MHb cholinergic neurons themselves, indicating that there may not be a direct upstream source of cholinergic inputs to the MHb. We propose performing further viral tracing experiments: injecting anterograde Cre-dependent tracer into the triangular septum or nucleus of the diagonal band of ChAT-Cre mice (two sites indicated as potential sources of cholinergic input to the MHb; Klemm, 2004; Qin & Luo, 2009) would further validate the findings presented in this thesis. In addition, non-selective retrograde tracing from the MHb in wildtype mice alongside immunohistochemistry for ChAT would further rule out presence of cholinergic input.

6.4.4 Confirmation of key transcriptomics findings

Chapter 5 was designed to be a broad exploratory investigation to identify rhythmic transcripts expressed within the MHb. As such, we endeavoured to report only those transcripts identified after meeting stringent statistical thresholds, and identified a number of key avenues for further investigation. Whilst following RNA sequencing results with a real time quantitative PCR investigation is traditional, it is not essential (Coenye, 2021), and was not performed for the completion of this thesis. Nonetheless, a quantitative PCR measurement of the top rhythmic transcripts identified in this report could offer a useful way to confirm our findings and indeed provide a more economical way to examine expression levels with a finer time scale - a 2 hr sampling resolution has been recommended for accurate assessment of the phases of rhythmic

transcripts (Hughes et al., 2017; Wu et al., 2020). Further, combining single-cell sequencing with circadian analysis would allow isolation of different neuronal subpopulations which may be differentially contributing to the rhythmicity of the MHb. For example, a recent study employed single-cell sequencing of the SCN to identify 11 neuronal subpopulations, and demonstrated circadian regulation of neuropeptidergic signalling between these subpopulations (Morris et al., 2021).

Transcriptomics data, including RNA sequencing, is often used to infer protein expression (Keil et al., 2018). However, final protein levels depend on a combination of transcriptional, translational and post-translational regulatory mechanisms. As such, the exact degree of correlation between transcript and protein abundance remains controversial (Edfors et al., 2016; Liu et al., 2016). Western blots, ELISAs and immunostaining offer protein level quantification (Keil et al., 2018), and could be used to determine how the transcriptional rhythms we observed in the MHb might translate into rhythms in protein levels.

6.4.5 Exploring the function of specific nAChRs in rhythmic signalling

In Chapter 3, we explored the contribution of just one nAChR subtype, α4β2, and found some evidence that signalling through this receptor was modulated by the time of day. However, we know that many other nAChR subtypes are expressed within the MHb (Grady et al., 2009). In particular, signalling through the α5 nAChR subunit in the MHb mediates the aversive properties of nicotine (Frahm et al., 2011), whilst MHb α3β4 nAChRs mediate nicotine self-administration in mice (Görlich et al., 2013). These present interesting candidates to once again investigate how time of day might influence mechanisms driving nicotine behaviours. Pharmacological investigations performed *ex vivo* seem to be the most straightforward starting point for investigating the contributions of these receptors. Whilst multielectrode recordings provide a convenient rapid screen, ultimately patch clamp recordings could prove a useful additional tool here. In particular, this technique allows observation of the direct effects of pharmacological manipulation on the cell in question, in isolation from indirect network mediated effects, for example in the presence of tetrodotoxin to eliminate spiking activity driven by action potentials.

6.4.6 Studying the MHb in an awake, behaving animal

Finally, as discussed previously, there are drawbacks of performing experiments on anaesthetized animals. Recording electrophysiological activity of the MHb in awake animals presents the most physiologically relevant approach. This could be achieved in head-fixed animals, but would be challenging to record for longer durations of time due to the stressful nature of the technique

(Juczewski et al., 2020). Instead, performing long-term recording of MHb neurons in freely moving animals would allow us to determine the diurnal rhythms of these neurons across a full circadian cycle. Previous studies have performed *in vivo* recordings of SCN electrophysiological activity in freely moving animals to demonstrate diurnal variation in firing rates in SCN (Inouye and Kawamura, 1979; Yamazaki et al., 1998), VTA (Fifel et al., 2018) and hippocampus (Munn et al., 2015). However, a limitation of these approaches is that they usually preclude isolation of the activity of individual cells. *In vivo c*alcium imaging potentially provides a way to measure neural activity in a freely-behaving animal, and is able to monitor specific cell populations (fibre photometry; Cui et al., 2014)) or even single cells (miniscope; Ghosh et al., 2011).

6.5 Summary

Figure 6.1 summarises the key results of this thesis, and attempts to relate how the main findings from each chapter might interact with each other, and puts these findings into the context with some of the known functions of the MHb. For the purpose of this summary, we assume that rat and mouse MHb are likely to have similar function (Fakhoury, 2017).

The MHb can receive information about the time of day through several possible routes, including innervation from other oscillatory brain structures (such as the LHb for example); through indirect innervation from the retina providing photic information which may signal information about the light / dark cycle (via inputs from the pHb for example; Chapter 4); or through diffuse circulating factors in the ventricular system which may signal timing information about feeding rhythms (Chapter 5). The MHb may also be the site inherent rhythmicity, as it remains a possibility that a subset of MHb neurons express the molecular clock, conferring the capacity for self-sustained oscillations in firing activity (Chapter 3). Finally, under diel conditions as was used throughout the majority of this thesis, the changes in the environment associated with the day / night cycle will produce other behavioural rhythms that can feedback rhythmic signals to the brain.

Reflecting these rhythmic inputs to the MHb, there is diurnal variation in the transcription of some genes within the MHb (Chapter 5). A greater proportion of these rhythmic transcripts have peak mRNA abundance during the night. A subset of these night-peaking rhythmic transcripts are associated with hormone signalling and synaptic plasticity, suggesting these are rhythmic processes within the MHb. The rhythms in mRNA which have been associated with mechanisms regulating synaptic plasticity may contribute to the rhythms in MHb electrophysiology observed in Chapters 3 & 4, although it is not clear how the rhythms in mRNA abundance translate to rhythms in protein products.

As a general population, MHb neuron spontaneous firing activity is rhythmic with lowest firing activity at the day / night transition (Chapters 3 & 4). The work in Chapter 3 indicates that MHb neuronal excitatory responses to nicotine are likely to follow the same pattern, with greatest increases in firing in response to nicotine at times when the spontaneous firing activity is greatest. As the MHb has been linked to exercise and motivation (Hsu et al., 2014), a possible behavioural consequence of this rhythm in firing activity could result in the diurnal variation in the locomotor suppressing actions of nicotine we characterized in Chapter 2: the greater increase in firing in response to nicotine during the dark phase / early light phase could drive greatest suppression of motor activity at this time.

Similarly, the cholinergic subpopulation of MHb neurons also have underlying diurnal variation in spontaneous firing activity, which follows the same rhythm as the rest of the MHb neuronal population (Chapter 4). Acetylcholine release from these neurons presumably also follows a similar pattern. Previous work has shown that the firing of MHb cholinergic neurons promotes the extinction of fear memories (J. Zhang et al., 2016), so this could be one way in which the MHb contributes to diurnal variation in fear and mood regulation. At dusk, the nadir in MHb cholinergic firing means that fear memories are still heightened, and the subsequent increase in firing during the dark phase promotes the extinction of fear memories during the animal's active phase, promoting riskier behaviours to occur under cover of darkness. Interestingly, MHb cholinergic neurons have a rhythm in their response to excitatory inputs which is antiphase with the rhythm in spontaneous firing activity (Chapter 4). This is another route by which nicotine could mediate its rhythmic effects on behaviour. The excitatory inputs to the MHb have been shown to promote anxiolysis and locomotor stimulating effects (Otsu et al., 2018). Nicotine may act in an excitatory manner here to stimulate the same outputs, with greatest nicotine-evoked anxiolysis at dusk for example. These same cholinergic MHb neurons mediate the aversive properties of nicotine (Pang et al., 2016; Souter et al., 2021) and rhythms in these neurons likely contribute to the daily rhythms in nicotine intake and withdrawal symptoms seen in humans (Chandra et al., 2011; Grainge et al., 2009; Mooney et al., 2006; Perkins et al., 2009; Teneggi et al., 2002).

Together, this highlights the numerous rhythmic processes feeding into and arising from the MHb, that could contribute both to daily rhythms in normal behaviour and physiology, as well as nicotine-evoked behaviours.

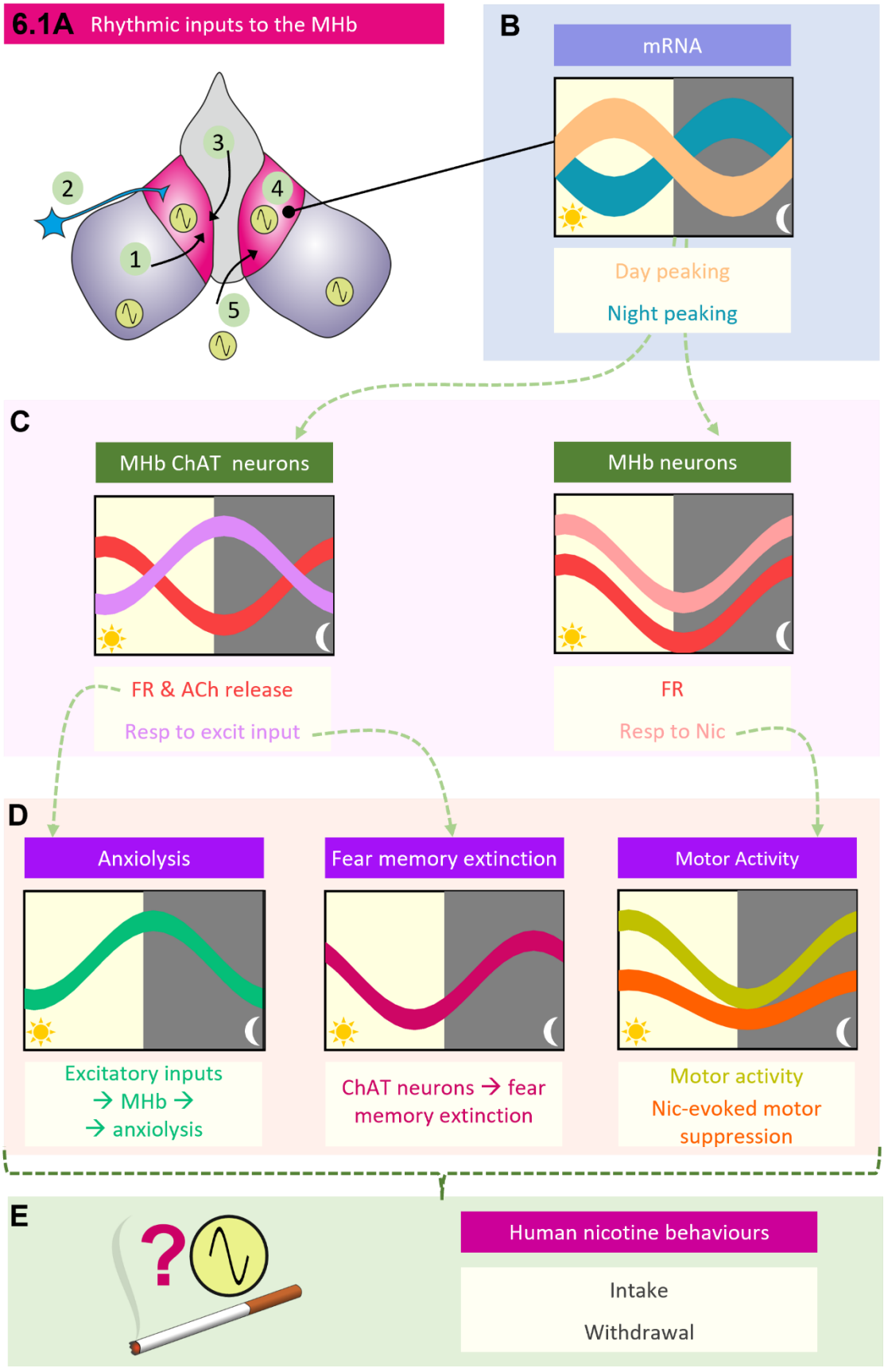
6.1A Rhythmic inputs to the MHb
B
mRNA
Day peaking
Night peaking
C
MHb ChAT neurons
MHb neurons
FR & ACh release
Resp to excit input
FR
Resp to Nic
D
Anxiolysis
Fear memory extinction
Motor Activity
Excitatory inputs → MHb → → anxiolysis
ChAT neurons → fear memory extinction
Motor activity
Nic-evoked motor suppression
E
Human nicotine behaviours
Intake
Withdrawal

Figure 6.1 Thesis summary

A) The MHb can receive rhythmic information from a variety of sources including (1) other rhythmic brain areas; (2) photic information; (3) circulatory factors; (4) inherent molecular rhythmicity in the MHb; (5) other behavioural rhythms.
B) There are both day-peaking and night-peaking mRNA transcripts in the MHb, which likely contribute to rhythms in electrophysiology and behaviour.
C) MHb neurons have rhythms in both firing rate (FR) and responses to nicotine (nic). MHb cholinergic neurons (ChAT) have the same rhythm in spontaneous FR as other MHb neurons, and are likely to have the same rhythm in ACh release. MHb neuron responses to excitatory inputs is rhythmic, and peaks at dusk.
D) The rhythms in the MHb may contribute to both rhythms in inherent behaviours (including anxiolysis and extinction of fear memories) but also rhythms in nicotine-evoked behaviours (including locomotor activity suppression).
E) The MHb is therefore likely contributing to rhythms in nicotine behaviour in humans, including nicotine intake and withdrawal symptoms.

6.6 Conclusions

Overall, these results indicate that there is certainly rhythmic control of nicotinic cholinergic signalling within the rodent brain, and one locus integrating time of day information with the cholinergic system is the MHb. The present data leave open the question of whether such rhythms are endogenously generated within cholinergic neurons of the MHb and/or other local neurons in this structure. Regardless, these data highlight the MHb as a potential site for diurnal modulation of goal-directed behaviours including those related to nicotine addiction. As a brain region of critical importance for mediating the withdrawal effects of nicotine, future studies in this area would benefit strongly from considering the time of day. Indeed, it is possible that tailoring nicotine cessation treatments to account for the time of day may yet yield more successful therapies in the future. More generally, the present findings provide a potential route by which time of day-dependent variations might be imposed onto other aspects of mammalian behaviour and cognition, for example relating to fear, anxiety and depression. Given growing evidence for associations between circadian dysfunction and neuropsychiatric disorders in humans, the MHb is therefore a promising site for future studies aimed at identifying underlying mechanisms of these disorders.

7 References

References from Chapters 1 and 6 are included below. References for Chapters 2-5 are included at the end of individual chapters.

Abarca, C., Albrecht, U., Spanagel, R., 2002. Cocaine sensitization and reward are under the influence of circadian genes and rhythm. Proc. Natl. Acad. Sci. U.S.A. 99, 9026–9030. https://doi.org/10.1073/pnas.142039099

Abe, M., Herzog, E.D., Yamazaki, S., Straume, M., Tei, H., Sakaki, Y., Menaker, M., Block, G.D., 2002. Circadian rhythms in isolated brain regions. J. Neurosci. 22, 350–356.

Ables, J.L., Görlich, A., Antolin-Fontes, B., Wang, C., Lipford, S.M., Riad, M.H., Ren, J., Hu, F., Luo, M., Kenny, P.J., Heintz, N., Ibañez-Tallon, I., 2017. Retrograde inhibition by a specific subset of interpeduncular α5 nicotinic neurons regulates nicotine preference. Proc Natl Acad Sci U S A 114, 13012–13017. https://doi.org/10.1073/pnas.1717506114

Abrahamson, E.E., Moore, R.Y., 2001. Suprachiasmatic nucleus in the mouse: retinal innervation, intrinsic organization and efferent projections. Brain Res 916, 172–191. https://doi.org/10.1016/s0006-8993(01)02890-6

Accardi, M.V., Pugsley, M.K., Forster, R., Troncy, E., Huang, H., Authier, S., 2016. The emerging role of in vitro electrophysiological methods in CNS safety pharmacology. Journal of Pharmacological and Toxicological Methods, Focused Issue on Safety Pharmacology 81, 47–59. https://doi.org/10.1016/j.vascn.2016.03.008

Acosta, J., Bussi, I.L., Esquivel, M., Höcht, C., Golombek, D.A., Agostino, P.V., 2020. Circadian modulation of motivation in mice. Behav Brain Res 382, 112471. https://doi.org/10.1016/j.bbr.2020.112471

Adan, A., 1994. Chronotype and personality factors in the daily consumption of alcohol and psychostimulants. Addiction 89, 455–462. https://doi.org/10.1111/j.1360-0443.1994.tb00926.x

Adermark, L., Morud, J., Lotfi, A., Jonsson, S., Söderpalm, B., Ericson, M., 2015. Age-contingent influence over accumbal neurotransmission and the locomotor stimulatory response to acute and repeated administration of nicotine in Wistar rats. Neuropharmacology 97, 104–112. https://doi.org/10.1016/j.neuropharm.2015.06.001

Agetsuma, M., Aizawa, H., Aoki, T., Nakayama, R., Takahoko, M., Goto, M., Sassa, T., Amo, R., Shiraki, T., Kawakami, K., Hosoya, T., Higashijima, S., Okamoto, H., 2010. The habenula is crucial for experience-dependent modification of fear responses in zebrafish. Nat Neurosci 13, 1354–1356. https://doi.org/10.1038/nn.2654

Agostinelli, L.J., Geerling, J.C., Scammell, T.E., 2019. Basal Forebrain Subcortical Projections. Brain Struct Funct 224, 1097–1117. https://doi.org/10.1007/s00429-018-01820-6

Ahmed, N.Y., Knowles, R., Dehorter, N., 2019. New Insights Into Cholinergic Neuron Diversity. Frontiers in Molecular Neuroscience 12, 204. https://doi.org/10.3389/fnmol.2019.00204

Aizawa, H., Amo, R., Okamoto, H., 2011. Phylogeny and Ontogeny of the Habenular Structure. Front Neurosci 5. https://doi.org/10.3389/fnins.2011.00138

Aizawa, H., Kobayashi, M., Tanaka, S., Fukai, T., Okamoto, H., 2012. Molecular characterization of the subnuclei in rat habenula. J. Comp. Neurol. 520, 4051–4066. https://doi.org/10.1002/cne.23167

Aizawa, H., Zhu, M., 2019. Toward an understanding of the habenula's various roles in human depression. Psychiatry and Clinical Neurosciences 73, 607–612. https://doi.org/10.1111/pcn.12892

Albrecht, A., Stork, O., 2017. Circadian Rhythms in Fear Conditioning: An Overview of Behavioral, Brain System, and Molecular Interactions. Neural Plast 2017, 3750307. https://doi.org/10.1155/2017/3750307

Albrecht, U., 2017. Molecular Mechanisms in Mood Regulation Involving the Circadian Clock. Front Neurol 8, 30. https://doi.org/10.3389/fneur.2017.00030
Albus, H., Vansteensel, M.J., Michel, S., Block, G.D., Meijer, J.H., 2005. A GABAergic mechanism is necessary for coupling dissociable ventral and dorsal regional oscillators within the circadian clock. Curr Biol 15, 886–893. https://doi.org/10.1016/j.cub.2005.03.051
Allen, S.S., Bade, T., Hatsukami, D., Center, B., 2008. Craving, withdrawal, and smoking urges on days immediately prior to smoking relapse. Nicotine Tob. Res. 10, 35–45. https://doi.org/10.1080/14622200701705076
Alzate-Correa, D., Aten, S., Campbell, M.J., Hoyt, K.R., Obrietan, K., 2021. Light-induced changes in the suprachiasmatic nucleus transcriptome regulated by the ERK/MAPK pathway. PLOS ONE 16, e0249430. https://doi.org/10.1371/journal.pone.0249430
An, K., Zhao, H., Miao, Y., Xu, Q., Li, Y.-F., Ma, Y.-Q., Shi, Y.-M., Shen, J.-W., Meng, J.-J., Yao, Y.-G., Zhang, Z., Chen, J.-T., Bao, J., Zhang, M., Xue, T., 2020. A circadian rhythm-gated subcortical pathway for nighttime-light-induced depressive-like behaviors in mice. Nat Neurosci 23, 869–880. https://doi.org/10.1038/s41593-020-0640-8
Anaclet, C., Pedersen, N.P., Ferrari, L.L., Venner, A., Bass, C.E., Arrigoni, E., Fuller, P.M., 2015. Basal forebrain control of wakefulness and cortical rhythms. Nat Commun 6, 8744. https://doi.org/10.1038/ncomms9744
Andersen, N., Corradi, J., Sine, S.M., Bouzat, C., 2013. Stoichiometry for activation of neuronal α7 nicotinic receptors. PNAS 110, 20819–20824. https://doi.org/10.1073/pnas.1315775110
Antolin-Fontes, B., Ables, J.L., Görlich, A., Ibañez-Tallon, I., 2015. The habenulo-interpeduncular pathway in nicotine aversion and withdrawal. Neuropharmacology 96, 213–222. https://doi.org/10.1016/j.neuropharm.2014.11.019
Arfken, C.L., 1988. Temporal pattern of alcohol consumption in the United States. Alcohol Clin Exp Res 12, 137–142. https://doi.org/10.1111/j.1530-0277.1988.tb00147.x
Arvin, M.C., Jin, X.-T., Yan, Y., Wang, Y., Ramsey, M.D., Kim, V.J., Beckley, N.A., Henry, B.A., Drenan, R.M., 2019. Chronic Nicotine Exposure Alters the Neurophysiology of Habenulo-Interpeduncular Circuitry. J Neurosci 39, 4268–4281. https://doi.org/10.1523/JNEUROSCI.2816-18.2019
Astiz, M., Heyde, I., Oster, H., 2019. Mechanisms of Communication in the Mammalian Circadian Timing System. Int J Mol Sci 20, 343. https://doi.org/10.3390/ijms20020343
Bae, M.-J., Song, Y.-M., Shin, J.-Y., Choi, B.-Y., Keum, J.-H., Lee, E.-A., 2017. The Association Between Shift Work and Health Behavior: Findings from the Korean National Health and Nutrition Examination Survey. Korean J Fam Med 38, 86–92. https://doi.org/10.4082/kjfm.2017.38.2.86
Balcita-Pedicino, J.J., Omelchenko, N., Bell, R., Sesack, S.R., 2011. The inhibitory influence of the lateral habenula on midbrain dopamine cells: Ultrastructural evidence for indirect mediation via the rostromedial mesopontine tegmental nucleus. Journal of Comparative Neurology 519, 1143–1164. https://doi.org/10.1002/cne.22561
Bano-Otalora, B., Martial, F., Harding, C., Bechtold, D.A., Allen, A.E., Brown, T.M., Belle, M.D.C., Lucas, R.J., 2021a. Bright daytime light enhances circadian amplitude in a diurnal mammal. Proc Natl Acad Sci U S A 118, e2100094118. https://doi.org/10.1073/pnas.2100094118
Bano-Otalora, B., Moye, M.J., Brown, T., Lucas, R.J., Diekman, C.O., Belle, M.D., 2021b. Daily electrical activity in the master circadian clock of a diurnal mammal. eLife 10, e68179. https://doi.org/10.7554/eLife.68179
Baño-Otálora, B., Piggins, H.D., 2017. Contributions of the lateral habenula to circadian timekeeping. Pharmacology Biochemistry and Behavior, The lateral habenula. From the neuroanatomy to the implication in CNS disorders 162, 46–54. https://doi.org/10.1016/j.pbb.2017.06.007

Barrington-Trimis, J.L., Urman, R., Berhane, K., Unger, J.B., Cruz, T.B., Pentz, M.A., Samet, J.M., Leventhal, A.M., McConnell, R., 2016. E-Cigarettes and Future Cigarette Use. Pediatrics 138, e20160379. https://doi.org/10.1542/peds.2016-0379

Barth, M., Schultze, M., Schuster, C.M., Strauss, R., 2010. Circadian plasticity in photoreceptor cells controls visual coding efficiency in Drosophila melanogaster. PLoS One 5, e9217. https://doi.org/10.1371/journal.pone.0009217

Bass, C.E., Jansen, H.T., Roberts, D.C.S., 2010. Free-running rhythms of cocaine self-administration in rats held under constant lighting conditions. Chronobiol Int 27, 535–548. https://doi.org/10.3109/07420521003664221

Basu, P., Wensel, A.L., McKibbon, R., Lefebvre, N., Antle, M.C., 2016. Activation of M1/4 receptors phase advances the hamster circadian clock during the day. Neurosci Lett 621, 22–27. https://doi.org/10.1016/j.neulet.2016.04.012

Becker, B.K., Zhang, D., Soliman, R., Pollock, D.M., 2019. Autonomic nerves and circadian control of renal function. Autonomic Neuroscience 217, 58–65. https://doi.org/10.1016/j.autneu.2019.01.003

Begemann, K., Neumann, A.-M., Oster, H., 2020. Regulation and function of extra-SCN circadian oscillators in the brain. Acta Physiologica 229, e13446. https://doi.org/10.1111/apha.13446

Beiranvand, F., Zlabinger, C., Orr-Urtreger, A., Ristl, R., Huck, S., Scholze, P., 2014. Nicotinic acetylcholine receptors control acetylcholine and noradrenaline release in the rodent habenulo-interpeduncular complex. Br. J. Pharmacol. 171, 5209–5224. https://doi.org/10.1111/bph.12841

Belle, M.D.C., Diekman, C.O., Forger, D.B., Piggins, H.D., 2009a. Daily electrical silencing in the mammalian circadian clock. Science 326, 281–284. https://doi.org/10.1126/science.1169657

Belle, M.D.C., Diekman, C.O., Forger, D.B., Piggins, H.D., 2009b. Daily Electrical Silencing in the Mammalian Circadian Clock. Science 326, 281–284. https://doi.org/10.1126/science.1169657

Bell-Pedersen, D., Cassone, V.M., Earnest, D.J., Golden, S.S., Hardin, P.E., Thomas, T.L., Zoran, M.J., 2005. Circadian rhythms from multiple oscillators: lessons from diverse organisms. Nat. Rev. Genet. 6, 544–556. https://doi.org/10.1038/nrg1633

Benowitz, N.L., 2010. Nicotine Addiction. N Engl J Med 362, 2295–2303. https://doi.org/10.1056/NEJMra0809890

Benowitz, N.L., 2009. Pharmacology of Nicotine: Addiction, Smoking-Induced Disease, and Therapeutics. Annu Rev Pharmacol Toxicol 49, 57–71. https://doi.org/10.1146/annurev.pharmtox.48.113006.094742

Benowitz, N.L., 2008. Clinical pharmacology of nicotine: implications for understanding, preventing, and treating tobacco addiction. Clin. Pharmacol. Ther. 83, 531–541. https://doi.org/10.1038/clpt.2008.3

Benowitz, N.L., Jacob, P., III, 1984. Daily intake of nicotine during cigarette smoking. Clinical Pharmacology & Therapeutics 35, 499–504. https://doi.org/10.1038/clpt.1984.67

Benowitz, N.L., Kuyt, F., Jacob, P., 1982. Circadian blood nicotine concentrations during cigarette smoking. Clin. Pharmacol. Ther. 32, 758–764.

Benwell, M.E., Balfour, D.J., Anderson, J.M., 1988. Evidence that tobacco smoking increases the density of (-)-[3H]nicotine binding sites in human brain. J. Neurochem. 50, 1243–1247.

Beretta, C.A., Dross, N., Guiterrez-Triana, J.A., Ryu, S., Carl, M., 2012. Habenula circuit development: past, present, and future. Front Neurosci 6, 51. https://doi.org/10.3389/fnins.2012.00051

Berrard, S., Varoqui, H., Cervini, R., Israël, M., Mallet, J., Diebler, M.-F., 1995. Coregulation of Two Embedded Gene Products, Choline Acetyltransferase and the Vesicular Acetylcholine

Transporter. Journal of Neurochemistry 65, 939–942. https://doi.org/10.1046/j.1471-4159.1995.65020939.x
Berrettini, W.H., Doyle, G.A., 2012. The CHRNA5-A3-B4 gene cluster in nicotine addiction. Mol. Psychiatry 17, 856–866. https://doi.org/10.1038/mp.2011.122
Berson, D.M., 2003. Strange vision: ganglion cells as circadian photoreceptors. Trends in Neurosciences 26, 314–320. https://doi.org/10.1016/S0166-2236(03)00130-9
Bhadra, U., Thakkar, N., Das, P., Pal Bhadra, M., 2017. Evolution of circadian rhythms: from bacteria to human. Sleep Medicine 35, 49–61. https://doi.org/10.1016/j.sleep.2017.04.008
Bierut, L.J., 2011. Genetic Vulnerability and Susceptibility to Substance Dependence. Neuron 69, 618–627. https://doi.org/10.1016/j.neuron.2011.02.015
Bina, K.G., Rusak, B., Semba, K., 1993. Localization of cholinergic neurons in the forebrain and brainstem that project to the suprachiasmatic nucleus of the hypothalamus in rat. Journal of Comparative Neurology 335, 295–307. https://doi.org/10.1002/cne.903350212
Boulos, L.-J., Darcq, E., Kieffer, B.L., 2017. Translating the Habenula—From Rodents to Humans. Biological Psychiatry, Depression: Genes, Circuits, and Treatments 81, 296–305. https://doi.org/10.1016/j.biopsych.2016.06.003
Bovet, D., Bovet-Nitti, F., Oliverio, A., 1967. Action of Nicotine on Spontaneous and Acquired Behavior in Rats and Mice*. Annals of the New York Academy of Sciences 142, 261–267. https://doi.org/10.1111/j.1749-6632.1967.tb13728.x
Breschi, A., Gingeras, T.R., Guigó, R., 2017. Comparative transcriptomics in human and mouse. Nat Rev Genet 18, 425–440. https://doi.org/10.1038/nrg.2017.19
Brody, A.L., Mandelkern, M.A., Olmstead, R.E., Allen-Martinez, Z., Scheibal, D., Abrams, A.L., Costello, M.R., Farahi, J., Saxena, S., Monterosso, J., London, E.D., 2009. Ventral striatal dopamine release in response to smoking a regular vs a denicotinized cigarette. Neuropsychopharmacology 34, 282–289. https://doi.org/10.1038/npp.2008.87
Broms, U., Kaprio, J., Hublin, C., Partinen, M., Madden, P. a. F., Koskenvuo, M., 2011. Evening types are more often current smokers and nicotine-dependent—a study of Finnish adult twins. Addiction 106, 170–177. https://doi.org/10.1111/j.1360-0443.2010.03112.x
Brower, K.J., 2003. Insomnia, alcoholism and relapse. Sleep Med Rev 7, 523–539. https://doi.org/10.1016/s1087-0792(03)90005-0
Brown, D.A., 2019. Acetylcholine and cholinergic receptors. Brain Neurosci Adv 3, 2398212818820506. https://doi.org/10.1177/2398212818820506
Brown, T.M., Banks, J.R., Piggins, H.D., 2006. A novel suction electrode recording technique for monitoring circadian rhythms in single and multiunit discharge from brain slices. Journal of Neuroscience Methods 156, 173–181. https://doi.org/10.1016/j.jneumeth.2006.02.024
Bruijnzeel, A.W., Bishnoi, M., van Tuijl, I.A., Keijzers, K.F.M., Yavarovich, K.R., Pasek, T.M., Ford, J., Alexander, J.C., Yamada, H., 2010. Effects of prazosin, clonidine, and propranolol on the elevations in brain reward thresholds and somatic signs associated with nicotine withdrawal in rats. Psychopharmacology (Berl.) 212, 485–499. https://doi.org/10.1007/s00213-010-1970-0
Brum, M.C.B., Filho, F.F.D., Schnorr, C.C., Bottega, G.B., Rodrigues, T.C., 2015. Shift work and its association with metabolic disorders. Diabetol Metab Syndr 7, 45. https://doi.org/10.1186/s13098-015-0041-4
Buchanan, G.F., Gillette, M.U., 2005. New light on an old paradox: site-dependent effects of carbachol on circadian rhythms. Exp Neurol 193, 489–496. https://doi.org/10.1016/j.expneurol.2005.01.008
Buhr, E.D., Takahashi, J.S., 2013. Molecular components of the Mammalian circadian clock. Handb Exp Pharmacol 3–27. https://doi.org/10.1007/978-3-642-25950-0_1

Buijs, F.N., León-Mercado, L., Guzmán-Ruiz, M., Guerrero-Vargas, N.N., Romo-Nava, F., Buijs, R.M., 2016. The Circadian System: A Regulatory Feedback Network of Periphery and Brain. Physiology (Bethesda) 31, 170–181. https://doi.org/10.1152/physiol.00037.2015

Buzsáki, G., 2002. Theta Oscillations in the Hippocampus. Neuron 33, 325–340. https://doi.org/10.1016/S0896-6273(02)00586-X

Byrne, J.E.M., Hughes, M.E., Rossell, S.L., Johnson, S.L., Murray, G., 2017. Time of Day Differences in Neural Reward Functioning in Healthy Young Men. J. Neurosci. 37, 8895–8900. https://doi.org/10.1523/JNEUROSCI.0918-17.2017

Byrne, J.E.M., Tremain, H., Leitan, N.D., Keating, C., Johnson, S.L., Murray, G., 2019. Circadian modulation of human reward function: Is there an evidentiary signal in existing neuroimaging studies? Neuroscience & Biobehavioral Reviews 99, 251–274. https://doi.org/10.1016/j.neubiorev.2019.01.025

Calarco, C.A., Picciotto, M.R., 2020. Nicotinic Acetylcholine Receptor Signaling in the Hypothalamus: Mechanisms Related to Nicotine's Effects on Food Intake. Nicotine Tob Res 22, 152–163. https://doi.org/10.1093/ntr/ntz010

Canales, A., Park, S., Kilias, A., Anikeeva, P., 2018. Multifunctional Fibers as Tools for Neuroscience and Neuroengineering. Acc Chem Res 51, 829–838. https://doi.org/10.1021/acs.accounts.7b00558

Cardona-Alberich, A., Tourbez, M., Pearce, S.F., Sibley, C.R., 2021. Elucidating the cellular dynamics of the brain with single-cell RNA sequencing. RNA Biol 18, 1063–1084. https://doi.org/10.1080/15476286.2020.1870362

Casarrubea, M., Davies, C., Faulisi, F., Pierucci, M., Colangeli, R., Partridge, L., Chambers, S., Cassar, D., Valentino, M., Muscat, R., Benigno, A., Crescimanno, G., Di Giovanni, G., 2015. Acute nicotine induces anxiety and disrupts temporal pattern organization of rat exploratory behavior in hole-board: a potential role for the lateral habenula. Frontiers in Cellular Neuroscience 9, 197. https://doi.org/10.3389/fncel.2015.00197

Cembrowski, M.S., 2019. Single-cell transcriptomics as a framework and roadmap for understanding the brain. Journal of Neuroscience Methods 326, 108353. https://doi.org/10.1016/j.jneumeth.2019.108353

Chandra, S., Scharf, D., Shiffman, S., 2011. Within-day temporal patterns of smoking, withdrawal symptoms, and craving. Drug Alcohol Depend 117, 118–125. https://doi.org/10.1016/j.drugalcdep.2010.12.027

Chandra, S., Shiffman, S., Scharf, D.M., Dang, Q., Shadel, W.G., 2007. Daily smoking patterns, their determinants, and implications for quitting. Exp Clin Psychopharmacol 15, 67–80. https://doi.org/10.1037/1064-1297.15.1.67

Changeux, J.-P., 2010. Nicotine addiction and nicotinic receptors: lessons from genetically modified mice. Nat. Rev. Neurosci. 11, 389–401. https://doi.org/10.1038/nrn2849

Chaudhury, D., Colwell, C.S., 2002. Circadian modulation of learning and memory in fear-conditioned mice. Behavioural Brain Research 133, 95–108. https://doi.org/10.1016/S0166-4328(01)00471-5

Chaudhury, D., Wang, L.M., Colwell, C.S., 2005. Circadian Regulation of Hippocampal Long-Term Potentiation. J Biol Rhythms 20, 225–236. https://doi.org/10.1177/0748730405276352

Chen, A., Machiorlatti, M., Krebs, N.M., Muscat, J.E., 2019. Socioeconomic differences in nicotine exposure and dependence in adult daily smokers. BMC Public Health 19, 375. https://doi.org/10.1186/s12889-019-6694-4

Chen, E., Lallai, V., Sherafat, Y., Grimes, N.P., Pushkin, A.N., Fowler, J.P., Fowler, C.D., 2018. Altered Baseline and Nicotine-Mediated Behavioral and Cholinergic Profiles in ChAT-Cre Mouse Lines. J. Neurosci. 38, 2177–2188. https://doi.org/10.1523/JNEUROSCI.1433-17.2018

Chen, L., Chatterjee, M., Li, J.Y.H., 2010. The Mouse Homeobox Gene Gbx2 Is Required for the Development of Cholinergic Interneurons in the Striatum. J. Neurosci. 30, 14824–14834. https://doi.org/10.1523/JNEUROSCI.3742-10.2010

Cheng, R.-K., Krishnan, S., Lin, Q., Kibat, C., Jesuthasan, S., 2017. Characterization of a thalamic nucleus mediating habenula responses to changes in ambient illumination. BMC Biol 15. https://doi.org/10.1186/s12915-017-0431-1

Cho, C.-H., Lee, S., Kim, A., Yarishkin, O., Ryoo, K., Lee, Y.-S., Jung, H.-G., Yang, E., Lee, D.Y., Lee, B., Kim, H., Oh, U., Im, H.-I., Hwang, E.M., Park, J.-Y., 2019. TMEM16A expression in cholinergic neurons of the medial habenula mediates anxiety-related behaviors. EMBO reports. https://doi.org/10.15252/embr.201948097

Cho, Y.-M., Kim, H.-R., Kang, M.-Y., Myong, J.-P., Koo, J.W., 2019. Fixed night workers and failed smoking cessation. Journal of Occupational Medicine and Toxicology 14, 23. https://doi.org/10.1186/s12995-019-0243-z

Choi, K., Lee, Y., Lee, C., Hong, S., Lee, S., Kang, S.J., Shin, K.S., 2016. Optogenetic activation of septal GABAergic afferents entrains neuronal firing in the medial habenula. Sci Rep 6, 34800. https://doi.org/10.1038/srep34800

Chrobok, L., Northeast, R.C., Myung, J., Cunningham, P.S., Petit, C., Piggins, H.D., 2020. Timekeeping in the hindbrain: a multi-oscillatory circadian centre in the mouse dorsal vagal complex. Commun Biol 3, 1–12. https://doi.org/10.1038/s42003-020-0960-y

Chrobok, L., Pradel, K., Janik, M.E., Sanetra, A.M., Bubka, M., Myung, J., Ridla Rahim, A., Klich, J.D., Jeczmien-Lazur, J.S., Palus-Chramiec, K., Lewandowski, M.H., 2021. Intrinsic circadian timekeeping properties of the thalamic lateral geniculate nucleus. J Neurosci Res. https://doi.org/10.1002/jnr.24973

Coenye, T., 2021. Do results obtained with RNA-sequencing require independent verification? Biofilm 3, 100043. https://doi.org/10.1016/j.bioflm.2021.100043

Colangelo, C., Shichkova, P., Keller, D., Markram, H., Ramaswamy, S., 2019. Cellular, Synaptic and Network Effects of Acetylcholine in the Neocortex. Frontiers in Neural Circuits 13.

Concha, M.L., Wilson, S.W., 2001. Asymmetry in the epithalamus of vertebrates. Journal of Anatomy 199, 63–84. https://doi.org/10.1046/j.1469-7580.2001.19910063.x

Conroy, D.A., Hairston, I.S., Arnedt, J.T., Hoffmann, R.F., Armitage, R., Brower, K.J., 2012. Dim light melatonin onset in alcohol-dependent men and women compared with healthy controls. Chronobiol Int 29, 35–42. https://doi.org/10.3109/07420528.2011.636852

Contestabile, A., Flumerfelt, B.A., 1981. Afferent connections of the interpeduncular nucleus and the topographic organization of the habenulo-interpeduncular pathway: an HRP study in the rat. J. Comp. Neurol. 196, 253–270. https://doi.org/10.1002/cne.901960206

Contestabile, A., Fonnum, F., 1983. Cholinergic and GABAergic forebrain projections to the habenula and nucleus interpeduncularis: Surgical and kainic acid lesions. Brain Research 275, 287–297. https://doi.org/10.1016/0006-8993(83)90989-7

Contestabile, A., Villani, L., Fasolo, A., Franzoni, M.F., Gribaudo, L., Oktedalen, O., Fonnum, F., 1987. Topography of cholinergic and substance P pathways in the habenulo-interpeduncular system of the rat. An immunocytochemical and microchemical approach. Neuroscience 21, 253–270. https://doi.org/10.1016/0306-4522(87)90337-x

Cooper, S.Y., Henderson, B.J., 2020. The Impact of Electronic Nicotine Delivery System (ENDS) Flavors on Nicotinic Acetylcholine Receptors and Nicotine Addiction-Related Behaviors. Molecules 25, 4223. https://doi.org/10.3390/molecules25184223

Covernton, P.O.J., Lester, R.A.J., 2002. Prolonged stimulation of presynaptic nicotinic acetylcholine receptors in the rat interpeduncular nucleus has differential effects on transmitter release. Int. J. Dev. Neurosci. 20, 247–258.

Creux, N., Harmer, S., 2019. Circadian Rhythms in Plants. Cold Spring Harb Perspect Biol 11, a034611. https://doi.org/10.1101/cshperspect.a034611

Crnko, S., Du Pré, B.C., Sluijter, J.P.G., Van Laake, L.W., 2019. Circadian rhythms and the molecular clock in cardiovascular biology and disease. Nat Rev Cardiol 16, 437–447. https://doi.org/10.1038/s41569-019-0167-4

Cuello, A.C., Emson, P.C., Paxinos, G., Jessell, T., 1978. Substance P containing and cholinergic projections from the habenula. Brain Res. 149, 413–429.

Cui, G., Jun, S.B., Jin, X., Luo, G., Pham, M.D., Lovinger, D.M., Vogel, S.S., Costa, R.M., 2014. Deep brain optical measurements of cell type–specific neural activity in behaving mice. Nat Protoc 9, 1213–1228. https://doi.org/10.1038/nprot.2014.080

Cui, L.-J., Chen, W.-H., Liu, A.-L., Han, X., Jiang, S.-X., Yuan, F., Zhong, Y.-M., Yang, X.-L., Weng, S.-J., 2020. nGnG Amacrine Cells and Brn3b-negative M1 ipRGCs are Specifically Labeled in the ChAT-ChR2-EYFP Mouse. Invest Ophthalmol Vis Sci 61, 14. https://doi.org/10.1167/iovs.61.2.14

Cupédo, R.N., de Weerd, H., 1985. Tanycytes in the medial habenular nucleus of the rat. Anat Embryol (Berl) 172, 7–10. https://doi.org/10.1007/BF00318938

Czoli, C.D., Fong, G.T., Mays, D., Hammond, D., 2017. How do consumers perceive differences in risk across nicotine products? A review of relative risk perceptions across smokeless tobacco, e-cigarettes, nicotine replacement therapy and combustible cigarettes. Tobacco Control 26, e49–e58. https://doi.org/10.1136/tobaccocontrol-2016-053060

Dani, J.A., 2015. Neuronal Nicotinic Acetylcholine Receptor Structure and Function and Response to Nicotine. Int Rev Neurobiol 124, 3–19. https://doi.org/10.1016/bs.irn.2015.07.001

Dani, J.A., Bertrand, D., 2007. Nicotinic acetylcholine receptors and nicotinic cholinergic mechanisms of the central nervous system. Annu. Rev. Pharmacol. Toxicol. 47, 699–729. https://doi.org/10.1146/annurev.pharmtox.47.120505.105214

Dani, J.A., De Biasi, M., 2013. Mesolimbic Dopamine and Habenulo-Interpeduncular Pathways in Nicotine Withdrawal. Cold Spring Harb Perspect Med 3. https://doi.org/10.1101/cshperspect.a012138

Dannenberg, H., Young, K., Hasselmo, M., 2017. Modulation of Hippocampal Circuits by Muscarinic and Nicotinic Receptors. Frontiers in Neural Circuits 11, 102. https://doi.org/10.3389/fncir.2017.00102

Day, J., Damsma, G., Fibiger, H.C., 1991. Cholinergic activity in the rat hippocampus, cortex and striatum correlates with locomotor activity: An in vivo microdialysis study. Pharmacology Biochemistry and Behavior 38, 723–729. https://doi.org/10.1016/0091-3057(91)90233-R

De Biasi, M., 2002. Nicotinic mechanisms in the autonomic control of organ systems. J Neurobiol 53, 568–579. https://doi.org/10.1002/neu.10145

De Biasi, M., Dani, J.A., 2011. Reward, Addiction, Withdrawal to Nicotine. Annu Rev Neurosci 34, 105–130. https://doi.org/10.1146/annurev-neuro-061010-113734

de Kloet, S.F., Mansvelder, H.D., De Vries, T.J., 2015. Cholinergic modulation of dopamine pathways through nicotinic acetylcholine receptors. Biochemical Pharmacology, Nicotinic Acetylcholine Receptors as Therapeutic Targets: Emerging Frontiers in Basic Research and Clinical Science (Satellite to the 2015 Meeting of the Society for Neuroscience) Oct 14-15, Chicago, IL USA 97, 425–438. https://doi.org/10.1016/j.bcp.2015.07.014

Deneau, G., Yanagita, T., Seevers, M.H., 1969. Self-administration of psychoactive substances by the monkey. Psychopharmacologia 16, 30–48. https://doi.org/10.1007/BF00405254

DePoy, L.M., McClung, C.A., Logan, R.W., 2017a. Neural Mechanisms of Circadian Regulation of Natural and Drug Reward [WWW Document]. Neural Plasticity. https://doi.org/10.1155/2017/5720842

DePoy, L.M., McClung, C.A., Logan, R.W., 2017b. Neural Mechanisms of Circadian Regulation of Natural and Drug Reward. Neural Plasticity 2017, e5720842. https://doi.org/10.1155/2017/5720842

Descarries, L., Gisiger, V., Steriade, M., 1997. Diffuse transmission by acetylcholine in the CNS. Progress in Neurobiology 53, 603–625. https://doi.org/10.1016/S0301-0082(97)00050-6

Di Chiara, G., 2000. Role of dopamine in the behavioural actions of nicotine related to addiction. European Journal of Pharmacology 393, 295–314. https://doi.org/10.1016/S0014-2999(00)00122-9
Dierker, L., Rose, J., Selya, A., Piasecki, T.M., Hedeker, D., Mermelstein, R., 2015. Depression and Nicotine Dependence from Adolescence to Young Adulthood. Addict Behav 41, 124–128. https://doi.org/10.1016/j.addbeh.2014.10.004
Difrancesco, S., Lamers, F., Riese, H., Merikangas, K.R., Beekman, A.T.F., van Hemert, A.M., Schoevers, R.A., Penninx, B.W.J.H., 2019. Sleep, circadian rhythm, and physical activity patterns in depressive and anxiety disorders: A 2-week ambulatory assessment study. Depression and Anxiety 36, 975–986. https://doi.org/10.1002/da.22949
Dojo, K., Yamaguchi, Y., Fustin, J.-M., Doi, M., Kobayashi, M., Okamura, H., 2017. Carbachol Induces Phase-dependent Phase Shifts of Per1 Transcription Rhythms in Cultured Suprachiasmatic Nucleus Slices. J Biol Rhythms 32, 101–108. https://doi.org/10.1177/0748730417691205
Domínguez-López, S., Howell, R.D., López-Canúl, M.G., Leyton, M., Gobbi, G., 2014. Electrophysiological characterization of dopamine neuronal activity in the ventral tegmental area across the light–dark cycle. Synapse 68, 454–467. https://doi.org/10.1002/syn.21757
Dubocovich, M.L., Hudson, R.L., Sumaya, I.C., Masana, M.I., Manna, E., 2005. Effect of MT1 melatonin receptor deletion on melatonin-mediated phase shift of circadian rhythms in the C57BL/6 mouse. J Pineal Res 39, 113–120. https://doi.org/10.1111/j.1600-079X.2005.00230.x
Duchemin, A.-M., Zhang, H., Neff, N.H., Hadjiconstantinou, M., 2009. Increased expression of VMAT2 in dopaminergic neurons during nicotine withdrawal. Neurosci. Lett. 467, 182–186. https://doi.org/10.1016/j.neulet.2009.10.038
Earnest, D.J., Turek, F.W., 1985. Neurochemical basis for the photic control of circadian rhythms and seasonal reproductive cycles: role for acetylcholine. Proc Natl Acad Sci U S A 82, 4277–4281. https://doi.org/10.1073/pnas.82.12.4277
Eckel-Mahan, K.L., Phan, T., Han, S., Wang, H., Chan, G.C.-K., Scheiner, Z.S., Storm, D.R., 2008. Circadian oscillation of hippocampal MAPK activity and cAMP: implications for memory persistence. Nat Neurosci 11, 1074–1082. https://doi.org/10.1038/nn.2174
Edfors, F., Danielsson, F., Hallström, B.M., Käll, L., Lundberg, E., Pontén, F., Forsström, B., Uhlén, M., 2016. Gene-specific correlation of RNA and protein levels in human cells and tissues. Mol Syst Biol 12, 883. https://doi.org/10.15252/msb.20167144
Edwards, F.A., Gibb, A.J., Colquhoun, D., 1992. ATP receptor-mediated synaptic currents in the central nervous system. Nature 359, 144–147. https://doi.org/10.1038/359144a0
Eggan, B.L., McCallum, S.E., 2017. α3β4 nicotinic receptors in the medial habenula and substance P transmission in the interpeduncular nucleus modulate nicotine sensitization. Behavioural Brain Research 316, 94–103. https://doi.org/10.1016/j.bbr.2016.08.028
Eggan, B.L., McCallum, S.E., 2016. 18-Methoxycoronaridine acts in the medial habenula to attenuate behavioral and neurochemical sensitization to nicotine. Behav. Brain Res. 307, 186–193. https://doi.org/10.1016/j.bbr.2016.04.008
Eilertsen, M., Clokie, B.G.J., Ebbesson, L.O.E., Tanase, C., Migaud, H., Helvik, J.V., 2021. Neural activation in photosensitive brain regions of Atlantic salmon (Salmo salar) after light stimulation. PLoS One 16, e0258007. https://doi.org/10.1371/journal.pone.0258007
Eisener-Dorman, A.F., Lawrence, D.A., Bolivar, V.J., 2009. Cautionary Insights on Knockout Mouse Studies: The Gene or Not the Gene? Brain Behav Immun 23, 318–324. https://doi.org/10.1016/j.bbi.2008.09.001
Elayouby, K.S., Ishikawa, M., Dukes, A.J., Smith, A.C.W., Lu, Q., Fowler, C.D., Kenny, P.J., 2021. α3* Nicotinic Acetylcholine Receptors in the Habenula-Interpeduncular Nucleus Circuit

Regulate Nicotine Intake. J Neurosci 41, 1779–1787. https://doi.org/10.1523/JNEUROSCI.0127-19.2020
El-Boraie, A., Tyndale, R.F., 2021. The Role of Pharmacogenetics in Smoking. Clin Pharmacol Ther. https://doi.org/10.1002/cpt.2345
Engmann, O., 2021. How Psychoactive Drugs and the Circadian Clock Are Enlightening One Another, in: Engmann, O., Brancaccio, M. (Eds.), Circadian Clock in Brain Health and Disease, Advances in Experimental Medicine and Biology. Springer International Publishing, Cham, pp. 129–152. https://doi.org/10.1007/978-3-030-81147-1_8
Erickson, T.B., Lee, J., Zautcke, J.L., Morris, R., 1998. Analysis of cocaine chronotoxicology in an urban ED. Am J Emerg Med 16, 568–571.
Erren, T.C., Morfeld, P., Groß, J.V., Wild, U., Lewis, P., 2019. IARC 2019: "Night shift work" is probably carcinogenic: What about disturbed chronobiology in all walks of life? Journal of Occupational Medicine and Toxicology 14, 29. https://doi.org/10.1186/s12995-019-0249-6
Etchegaray, J.-P., Machida, K.K., Noton, E., Constance, C.M., Dallmann, R., Napoli, M.N.D., DeBruyne, J.P., Lambert, C.M., Yu, E.A., Reppert, S.M., Weaver, D.R., 2009. Casein Kinase 1 Delta Regulates the Pace of the Mammalian Circadian Clock. Molecular and Cellular Biology. https://doi.org/10.1128/MCB.00338-09
Evans, H.L., Ghiselli, W.B., Patton, R.A., 1973. Diurnal rhythm in behavioral effects of methamphetamine, p-chloramethamphetamine and scopolamine. J Pharmacol Exp Ther 186, 10–17.
Fakhoury, M., 2018. The dorsal diencephalic conduction system in reward processing: Spotlight on the anatomy and functions of the habenular complex. Behavioural Brain Research 348, 115–126. https://doi.org/10.1016/j.bbr.2018.04.018
Fakhoury, M., 2017. The habenula in psychiatric disorders: More than three decades of translational investigation. Neuroscience & Biobehavioral Reviews. https://doi.org/10.1016/j.neubiorev.2017.02.010
Fakier, N., Wild, L.G., 2011. Associations among sleep problems, learning difficulties and substance use in adolescence. J Adolesc 34, 717–726. https://doi.org/10.1016/j.adolescence.2010.09.010
Falk, S., Lund, C., Clemmensen, C., 2020. Muscarinic receptors in energy homeostasis: Physiology and pharmacology. Basic & Clinical Pharmacology & Toxicology 126, 66–76. https://doi.org/10.1111/bcpt.13311
Farris, S., Wang, Y., Ward, J.M., Dudek, S.M., 2017. Optimized Method for Robust Transcriptome Profiling of Minute Tissues Using Laser Capture Microdissection and Low-Input RNA-Seq. Frontiers in Molecular Neuroscience 10, 185. https://doi.org/10.3389/fnmol.2017.00185
Feltenstein, M.W., See, R.E., 2008. The neurocircuitry of addiction: an overview. Br J Pharmacol 154, 261–274. https://doi.org/10.1038/bjp.2008.51
Fernandez, D.C., Fogerson, P.M., Ospri, L.L., Thomsen, M.B., Layne, R.M., Severin, D., Zhan, J., Singer, J.H., Kirkwood, A., Zhao, H., Berson, D., Hattar, S., 2018. Light affects mood and learning through distinct retina-brain pathways. Cell 175, 71-84.e18. https://doi.org/10.1016/j.cell.2018.08.004
Fifel, K., Meijer, J.H., Deboer, T., 2018. Circadian and Homeostatic Modulation of Multi-Unit Activity in Midbrain Dopaminergic Structures. Sci Rep 8, 7765. https://doi.org/10.1038/s41598-018-25770-5
Fisk, A.S., Tam, S.K.E., Brown, L.A., Vyazovskiy, V.V., Bannerman, D.M., Peirson, S.N., 2018. Light and Cognition: Roles for Circadian Rhythms, Sleep, and Arousal. Front Neurol 9, 56. https://doi.org/10.3389/fneur.2018.00056
Fisk, J.E., Montgomery, C., 2009. Sleep impairment in ecstasy/polydrug and cannabis-only users. Am J Addict 18, 430–437. https://doi.org/10.3109/10550490903077762

Flumerfelt, B.A., Contestabile, A., 1982. Acetylcholinesterase Histochemistry of the habenulo-interpeduncular pathway in the rat and the effects of electrolytic and kainic acid lesions. Anat. Embryol. 163, 435–446.

Fonnum, F., Contestabile, A., 1984. Colchicine neurotoxicity demonstrates the cholinergic projection from the supracommissural septum to the habenula and the nucleus interpeduncularis in the rat. J Neurochem 43, 881–884. https://doi.org/10.1111/j.1471-4159.1984.tb12814.x

Fowler, C.D., Lu, Q., Johnson, P.M., Marks, M.J., Kenny, P.J., 2011. Habenular α5 nicotinic receptor subunit signalling controls nicotine intake. Nature 471, 597–601. https://doi.org/10.1038/nature09797

Frahm, S., Antolin-Fontes, B., Görlich, A., Zander, J.-F., Ahnert-Hilger, G., Ibañez-Tallon, I., 2015. An essential role of acetylcholine-glutamate synergy at habenular synapses in nicotine dependence. Elife 4, e11396. https://doi.org/10.7554/eLife.11396

Frahm, S., Slimak, M.A., Ferrarese, L., Santos-Torres, J., Antolin-Fontes, B., Auer, S., Filkin, S., Pons, S., Fontaine, J.-F., Tsetlin, V., Maskos, U., Ibañez-Tallon, I., 2011. Aversion to nicotine is regulated by the balanced activity of β4 and α5 nicotinic receptor subunits in the medial habenula. Neuron 70, 522–535. https://doi.org/10.1016/j.neuron.2011.04.013

Francis, T.C., Lobo, M.K., 2017. Emerging Role for Nucleus Accumbens Medium Spiny Neuron Subtypes in Depression. Biological Psychiatry, Stress and Neuroplasticity 81, 645–653. https://doi.org/10.1016/j.biopsych.2016.09.007

Fuller, P.M., Gooley, J.J., Saper, C.B., 2006. Neurobiology of the Sleep-Wake Cycle: Sleep Architecture, Circadian Regulation, and Regulatory Feedback , Neurobiology of the Sleep-Wake Cycle: Sleep Architecture, Circadian Regulation, and Regulatory Feedback. J Biol Rhythms 21, 482–493. https://doi.org/10.1177/0748730406294627

Gahring, L.C., Persiyanov, K., Rogers, S.W., 2004. Neuronal and astrocyte expression of nicotinic receptor subunit beta4 in the adult mouse brain. J. Comp. Neurol. 468, 322–333. https://doi.org/10.1002/cne.10942

Gallardo, C.M., Darvas, M., Oviatt, M., Chang, C.H., Michalik, M., Huddy, T.F., Meyer, E.E., Shuster, S.A., Aguayo, A., Hill, E.M., Kiani, K., Ikpeazu, J., Martinez, J.S., Purpura, M., Smit, A.N., Patton, D.F., Mistlberger, R.E., Palmiter, R.D., Steele, A.D., 2014. Dopamine receptor 1 neurons in the dorsal striatum regulate food anticipatory circadian activity rhythms in mice. Elife 3, e03781. https://doi.org/10.7554/eLife.03781

Gallego, X., Molas, S., Amador-Arjona, A., Marks, M.J., Robles, N., Murtra, P., Armengol, L., Fernández-Montes, R.D., Gratacòs, M., Pumarola, M., Cabrera, R., Maldonado, R., Sabrià, J., Estivill, X., Dierssen, M., 2012. Overexpression of the CHRNA5/A3/B4 genomic cluster in mice increases the sensitivity to nicotine and modifies its reinforcing effects. Amino Acids 43, 897–909. https://doi.org/10.1007/s00726-011-1149-y

García-Cáceres, C., Balland, E., Prevot, V., Luquet, S., Woods, S.C., Koch, M., Horvath, T.L., Yi, C.-X., Chowen, J.A., Verkhratsky, A., Araque, A., Bechmann, I., Tschöp, M.H., 2019. Role of astrocytes, microglia, and tanycytes in brain control of systemic metabolism. Nat Neurosci 22, 7–14. https://doi.org/10.1038/s41593-018-0286-y

Gaytan, O., Swann, A., Dafny, N., 1998. Diurnal differences in rat's motor response to amphetamine. Eur J Pharmacol 345, 119–128. https://doi.org/10.1016/s0014-2999(97)01558-6

Gekakis, N., Staknis, D., Nguyen, H.B., Davis, F.C., Wilsbacher, L.D., King, D.P., Takahashi, J.S., Weitz, C.J., 1998. Role of the CLOCK protein in the mammalian circadian mechanism. Science 280, 1564–1569. https://doi.org/10.1126/science.280.5369.1564

Ghosh, K.K., Burns, L.D., Cocker, E.D., Nimmerjahn, A., Ziv, Y., Gamal, A.E., Schnitzer, M.J., 2011. Miniaturized integration of a fluorescence microscope. Nat Methods 8, 871–878. https://doi.org/10.1038/nmeth.1694

Gielow, M.R., Zaborszky, L., 2017. The Input-Output Relationship of the Cholinergic Basal Forebrain. Cell Reports 18, 1817–1830. https://doi.org/10.1016/j.celrep.2017.01.060

Giniatullin, R., Nistri, A., Yakel, J.L., 2005. Desensitization of nicotinic ACh receptors: shaping cholinergic signaling. Trends in Neurosciences 28, 371–378. https://doi.org/10.1016/j.tins.2005.04.009

Girardet, C., Blanchard, M.-P., Ferracci, G., Lévêque, C., Moreno, M., François-Bellan, A.-M., Becquet, D., Bosler, O., 2010. Daily changes in synaptic innervation of VIP neurons in the rat suprachiasmatic nucleus: contribution of glutamatergic afferents. European Journal of Neuroscience 31, 359–370. https://doi.org/10.1111/j.1460-9568.2009.07071.x

Girod, R., Barazangi, N., McGehee, D., Role, L.W., 2000. Facilitation of glutamatergic neurotransmission by presynaptic nicotinic acetylcholine receptors. Neuropharmacology 39, 2715–2725.

Glick, S.D., Ramirez, R.L., Livi, J.M., Maisonneuve, I.M., 2006. 18-Methoxycoronaridine acts in the medial habenula and/or interpeduncular nucleus to decrease morphine self-administration in rats. Eur. J. Pharmacol. 537, 94–98. https://doi.org/10.1016/j.ejphar.2006.03.045

Görlich, A., Antolin-Fontes, B., Ables, J.L., Frahm, S., Ślimak, M.A., Dougherty, J.D., Ibañez-Tallon, I., 2013. Reexposure to nicotine during withdrawal increases the pacemaking activity of cholinergic habenular neurons. Proc Natl Acad Sci U S A 110, 17077–17082. https://doi.org/10.1073/pnas.1313103110

Gottesfeld, Z., 1983. Origin and distribution of noradrenergic innervation in the habenula: A neurochemical study. Brain Research 275, 299–304. https://doi.org/10.1016/0006-8993(83)90990-3

Gotti, C., Clementi, F., Fornari, A., Gaimarri, A., Guiducci, S., Manfredi, I., Moretti, M., Pedrazzi, P., Pucci, L., Zoli, M., 2009. Structural and functional diversity of native brain neuronal nicotinic receptors. Biochem. Pharmacol. 78, 703–711. https://doi.org/10.1016/j.bcp.2009.05.024

Gotti, C., Guiducci, S., Tedesco, V., Corbioli, S., Zanetti, L., Moretti, M., Zanardi, A., Rimondini, R., Mugnaini, M., Clementi, F., Chiamulera, C., Zoli, M., 2010. Nicotinic Acetylcholine Receptors in the Mesolimbic Pathway: Primary Role of Ventral Tegmental Area α6β2* Receptors in Mediating Systemic Nicotine Effects on Dopamine Release, Locomotion, and Reinforcement. J. Neurosci. 30, 5311–5325. https://doi.org/10.1523/JNEUROSCI.5095-09.2010

Grabus, S.D., Martin, B.R., Imad Damaj, M., 2005. Nicotine physical dependence in the mouse: involvement of the alpha7 nicotinic receptor subtype. Eur. J. Pharmacol. 515, 90–93. https://doi.org/10.1016/j.ejphar.2005.03.044

Grady, S.R., Moretti, M., Zoli, M., Marks, M.J., Zanardi, A., Pucci, L., Clementi, F., Gotti, C., 2009. Rodent habenulo-interpeduncular pathway expresses a large variety of uncommon nAChR subtypes, but only the alpha3beta4* and alpha3beta3beta4* subtypes mediate acetylcholine release. J. Neurosci. 29, 2272–2282. https://doi.org/10.1523/JNEUROSCI.5121-08.2009

Grainge, M.J., Shahab, L., Hammond, D., O'Connor, R.J., McNeill, A., 2009. First cigarette on waking and time of day as predictors of puffing behaviour in UK adult smokers. Drug Alcohol Depend 101, 191–195. https://doi.org/10.1016/j.drugalcdep.2009.01.013

Grandin, L.D., Alloy, L.B., Abramson, L.Y., 2006. The social zeitgeber theory, circadian rhythms, and mood disorders: review and evaluation. Clin Psychol Rev 26, 679–694. https://doi.org/10.1016/j.cpr.2006.07.001

Greenbaum, L., Lerer, B., 2009. Differential contribution of genetic variation in multiple brain nicotinic cholinergic receptors to nicotine dependence: recent progress and emerging open questions. Mol. Psychiatry 14, 912–945. https://doi.org/10.1038/mp.2009.59

Grigsby, K.B., Kelty, T.J., Booth, F.W., 2018. Medial habenula maturational deficits associate with low motivation for voluntary physical activity. Brain Res 1698, 187–194. https://doi.org/10.1016/j.brainres.2018.08.016
Grippo, R.M., Güler, A.D., 2019. Dopamine Signaling in Circadian Photoentrainment: Consequences of Desynchrony. Yale J Biol Med 92, 271–281.
Grippo, R.M., Purohit, A.M., Zhang, Q., Zweifel, L.S., Güler, A.D., 2017. Direct Midbrain Dopamine Input to the Suprachiasmatic Nucleus Accelerates Circadian Entrainment. Curr Biol 27, 2465-2475.e3. https://doi.org/10.1016/j.cub.2017.06.084
Guilding, C., Hughes, A.T.L., Brown, T.M., Namvar, S., Piggins, H.D., 2009. A riot of rhythms: neuronal and glial circadian oscillators in the mediobasal hypothalamus. Mol Brain 2, 28. https://doi.org/10.1186/1756-6606-2-28
Guilding, C., Hughes, A.T.L., Piggins, H.D., 2010. Circadian oscillators in the epithalamus. Neuroscience 169, 1630–1639. https://doi.org/10.1016/j.neuroscience.2010.06.015
Guilding, C., Piggins, H.D., 2007. Challenging the omnipotence of the suprachiasmatic timekeeper: are circadian oscillators present throughout the mammalian brain? European Journal of Neuroscience 25, 3195–3216. https://doi.org/10.1111/j.1460-9568.2007.05581.x
Guilding, C., Scott, F., Bechtold, D.A., Brown, T.M., Wegner, S., Piggins, H.D., 2013. Suppressed cellular oscillations in after-hours mutant mice are associated with enhanced circadian phase-resetting. The Journal of Physiology 591, 1063–1080. https://doi.org/10.1113/jphysiol.2012.242198
Haam, J., Yakel, J.L., 2017. Cholinergic modulation of the hippocampal region and memory function. J Neurochem 142, 111–121. https://doi.org/10.1111/jnc.14052
Hadjiconstantinou, M., Neff, N.H., 2011. Nicotine and endogenous opioids: neurochemical and pharmacological evidence. Neuropharmacology 60, 1209–1220. https://doi.org/10.1016/j.neuropharm.2010.11.010
Hall, F.S., Drgonova, J., Jain, S., Uhl, G.R., 2013. Implications of genome wide association studies for addiction: Are our a priori assumptions all wrong? Pharmacology & Therapeutics 140, 267–279. https://doi.org/10.1016/j.pharmthera.2013.07.006
Hampp, G., Ripperger, J.A., Houben, T., Schmutz, I., Blex, C., Perreau-Lenz, S., Brunk, I., Spanagel, R., Ahnert-Hilger, G., Meijer, J.H., Albrecht, U., 2008. Regulation of monoamine oxidase A by circadian-clock components implies clock influence on mood. Curr. Biol. 18, 678–683. https://doi.org/10.1016/j.cub.2008.04.012
Han, S., Yang, S.H., Kim, J.Y., Mo, S., Yang, E., Song, K.M., Ham, B.-J., Mechawar, N., Turecki, G., Lee, H.W., Kim, H., 2017. Down-regulation of cholinergic signaling in the habenula induces anhedonia-like behavior. Sci Rep 7, 900. https://doi.org/10.1038/s41598-017-01088-6
Hanin, I., Massarelli, R., Costa, E., 1970. Acetylcholine concentrations in rat brain: diurnal oscillation. Science 170, 341–342. https://doi.org/10.1126/science.170.3955.341
Hao, H., Allen, D.L., Hardin, P.E., 1997. A circadian enhancer mediates PER-dependent mRNA cycling in Drosophila melanogaster. Molecular and Cellular Biology. https://doi.org/10.1128/MCB.17.7.3687
Hara, K., Harris, R.A., 2002. The anesthetic mechanism of urethane: the effects on neurotransmitter-gated ion channels. Anesth Analg 94, 313–318, table of contents. https://doi.org/10.1097/00000539-200202000-00015
Harbom, L.J., Chronister, W.D., McConnell, M.J., 2016. Single neuron transcriptome analysis can reveal more than cell type classification: Does it matter if every neuron is unique? Bioessays 38, 157–161. https://doi.org/10.1002/bies.201500097
Harding, C., Bechtold, D.A., Brown, T.M., 2020. Suprachiasmatic nucleus-dependent and independent outputs driving rhythmic activity in hypothalamic and thalamic neurons. BMC Biol 18, 134. https://doi.org/10.1186/s12915-020-00871-8
Harrington, L., Viñals, X., Herrera-Solís, A., Flores, A., Morel, C., Tolu, S., Faure, P., Maldonado, R., Maskos, U., Robledo, P., 2016. Role of β4* Nicotinic Acetylcholine Receptors in the

Habenulo-Interpeduncular Pathway in Nicotine Reinforcement in Mice. Neuropsychopharmacology 41, 1790–1802. https://doi.org/10.1038/npp.2015.346
Hartsock, M.J., Spencer, R.L., 2020. Memory and the circadian system: identifying candidate mechanisms by which local clocks in the brain may regulate synaptic plasticity. Neurosci Biobehav Rev 118, 134–162. https://doi.org/10.1016/j.neubiorev.2020.07.023
Hashikawa, Y., Hashikawa, K., Rossi, M.A., Basiri, M.L., Liu, Y., Johnston, N.L., Ahmad, O.R., Stuber, G.D., 2020. Transcriptional and Spatial Resolution of Cell Types in the Mammalian Habenula. Neuron. https://doi.org/10.1016/j.neuron.2020.03.011
Hastings, M.H., Maywood, E.S., Brancaccio, M., 2019. The Mammalian Circadian Timing System and the Suprachiasmatic Nucleus as Its Pacemaker. Biology (Basel) 8, 13. https://doi.org/10.3390/biology8010013
Hastings, M.H., Maywood, E.S., Brancaccio, M., 2018. Generation of circadian rhythms in the suprachiasmatic nucleus. Nat Rev Neurosci 19, 453–469. https://doi.org/10.1038/s41583-018-0026-z
Hatori, M., Panda, S., 2010. CRY links the circadian clock and CREB-mediated gluconeogenesis. Cell Res 20, 1285–1288. https://doi.org/10.1038/cr.2010.152
Hattar, S., Kumar, M., Park, A., Tong, P., Tung, J., Yau, K.-W., Berson, D.M., 2006. Central projections of melanopsin-expressing retinal ganglion cells in the mouse. J. Comp. Neurol. 497, 326–349. https://doi.org/10.1002/cne.20970
Haynie, D.L., Lewin, D., Luk, J.W., Lipsky, L.M., O'Brien, F., Iannotti, R.J., Liu, D., Simons-Morton, B.G., 2017. Beyond Sleep Duration: Bidirectional Associations Among Chronotype, Social Jetlag, and Drinking Behaviors in a Longitudinal Sample of US High School Students. Sleep 41, zsx202. https://doi.org/10.1093/sleep/zsx202
He, C., Chen, F., Li, B., Hu, Z., 2014. Neurophysiology of HCN channels: from cellular functions to multiple regulations. Prog. Neurobiol. 112, 1–23. https://doi.org/10.1016/j.pneurobio.2013.10.001
Hegazi, S., Lowden, C., Rios Garcia, J., Cheng, A.H., Obrietan, K., Levine, J.D., Cheng, H.-Y.M., 2019. A Symphony of Signals: Intercellular and Intracellular Signaling Mechanisms Underlying Circadian Timekeeping in Mice and Flies. Int J Mol Sci 20, E2363. https://doi.org/10.3390/ijms20092363
Heikkinen, A.M., Broms, U., Pitkäniemi, J., Koskenvuo, M., Meurman, J., 2009. Key factors in smoking cessation intervention among 15-16-year-olds. Behav Med 35, 93–99. https://doi.org/10.1080/08964280903232035
Hemmendinger, L.M., Moore, R.Y., 1984. Interpeduncular nucleus organization in the rat: cytoarchitecture and histochemical analysis. Brain Res. Bull. 13, 163–179.
Henderson, B.J., Lester, H.A., 2015. Inside-out neuropharmacology of nicotinic drugs. Neuropharmacology, The Nicotinic Acetylcholine Receptor: From Molecular Biology to Cognition 96, 178–193. https://doi.org/10.1016/j.neuropharm.2015.01.022
Hennigan, K., D'Ardenne, K., McClure, S.M., 2015. Distinct midbrain and habenula pathways are involved in processing aversive events in humans. J Neurosci 35, 198–208. https://doi.org/10.1523/JNEUROSCI.0927-14.2015
Herkenham, M., Nauta, W.J., 1979. Efferent connections of the habenular nuclei in the rat. J. Comp. Neurol. 187, 19–47. https://doi.org/10.1002/cne.901870103
Herkenham, M., Nauta, W.J., 1977. Afferent connections of the habenular nuclei in the rat. A horseradish peroxidase study, with a note on the fiber-of-passage problem. J Comp Neurol 173, 123–146. https://doi.org/10.1002/cne.901730107
Hikosaka, O., 2010. The habenula: from stress evasion to value-based decision-making. Nat Rev Neurosci 11, 503–513. https://doi.org/10.1038/nrn2866
Hikosaka, O., Sesack, S.R., Lecourtier, L., Shepard, P.D., 2008. Habenula: Crossroad between the Basal Ganglia and the Limbic System. J. Neurosci. 28, 11825–11829. https://doi.org/10.1523/JNEUROSCI.3463-08.2008

Hildebrand, B.E., Nomikos, G.G., Bondjers, C., Nisell, M., Svensson, T.H., 1997. Behavioral manifestations of the nicotine abstinence syndrome in the rat: peripheral versus central mechanisms. Psychopharmacology (Berl.) 129, 348–356.

Hofman, M.A., Zhou, J.N., Swaab, D.F., 1996. Suprachiasmatic nucleus of the human brain: an immunocytochemical and morphometric analysis. Anat Rec 244, 552–562. https://doi.org/10.1002/(SICI)1097-0185(199604)244:4<552::AID-AR13>3.0.CO;2-O

Honma, S., Ikeda, M., Abe, H., Tanahashi, Y., Namihira, M., Honma, K., Nomura, M., 1998. Circadian oscillation of BMAL1, a partner of a mammalian clock gene Clock, in rat suprachiasmatic nucleus. Biochem Biophys Res Commun 250, 83–87. https://doi.org/10.1006/bbrc.1998.9275

Hood, S., Cassidy, P., Cossette, M.-P., Weigl, Y., Verwey, M., Robinson, B., Stewart, J., Amir, S., 2010. Endogenous dopamine regulates the rhythm of expression of the clock protein PER2 in the rat dorsal striatum via daily activation of D2 dopamine receptors. J. Neurosci. 30, 14046–14058. https://doi.org/10.1523/JNEUROSCI.2128-10.2010

Horowitz, T.S., Cade, B.E., Wolfe, J.M., Czeisler, C.A., 2003. Searching Night and Day: A Dissociation of Effects of Circadian Phase and Time Awake on Visual Selective Attention and Vigilance. Psychol Sci 14, 549–557. https://doi.org/10.1046/j.0956-7976.2003.psci_1464.x

Houben, T., Coomans, C.P., Meijer, J.H., 2014. Regulation of circadian and acute activity levels by the murine suprachiasmatic nuclei. PLoS One 9, e110172. https://doi.org/10.1371/journal.pone.0110172

Hrvatin, S., Hochbaum, D.R., Nagy, M.A., Cicconet, M., Robertson, K., Cheadle, L., Zilionis, R., Ratner, A., Borges-Monroy, R., Klein, A.M., Sabatini, B.L., Greenberg, M.E., 2018. Single-cell analysis of experience-dependent transcriptomic states in the mouse visual cortex. Nat Neurosci 21, 120–129. https://doi.org/10.1038/s41593-017-0029-5

Hsu, Y.-W.A., Gile, J.J., Perez, J.G., Morton, G., Ben-Hamo, M., Turner, E.E., de la Iglesia, H.O., 2017. The Dorsal Medial Habenula Minimally Impacts Circadian Regulation of Locomotor Activity and Sleep. J. Biol. Rhythms 32, 444–455. https://doi.org/10.1177/0748730417730169

Hsu, Y.-W.A., Tempest, L., Quina, L.A., Wei, A.D., Zeng, H., Turner, E.E., 2013. Medial habenula output circuit mediated by α5 nicotinic receptor-expressing GABAergic neurons in the interpeduncular nucleus. J. Neurosci. 33, 18022–18035. https://doi.org/10.1523/JNEUROSCI.2927-13.2013

Hsu, Y.-W.A., Wang, S.D., Wang, S., Morton, G., Zariwala, H.A., de la Iglesia, H.O., Turner, E.E., 2014. Role of the dorsal medial habenula in the regulation of voluntary activity, motor function, hedonic state, and primary reinforcement. J. Neurosci. 34, 11366–11384. https://doi.org/10.1523/JNEUROSCI.1861-14.2014

Hu, H., Cui, Y., Yang, Y., 2020. Circuits and functions of the lateral habenula in health and in disease. Nat Rev Neurosci 21, 277–295. https://doi.org/10.1038/s41583-020-0292-4

Huang, L., Xi, Y., Peng, Y., Yang, Y., Huang, X., Fu, Y., Tao, Q., Xiao, J., Yuan, T., An, K., Zhao, H., Pu, M., Xu, F., Xue, T., Luo, M., So, K.-F., Ren, C., 2019. A Visual Circuit Related to Habenula Underlies the Antidepressive Effects of Light Therapy. Neuron 102, 128-142.e8. https://doi.org/10.1016/j.neuron.2019.01.037

Hughes, M.E., Abruzzi, K.C., Allada, R., Anafi, R., Arpat, A.B., Asher, G., Baldi, P., de Bekker, C., Bell-Pedersen, D., Blau, J., Brown, S., Ceriani, M.F., Chen, Z., Chiu, J.C., Cox, J., Crowell, A.M., DeBruyne, J.P., Dijk, D.-J., DiTacchio, L., Doyle, F.J., Duffield, G.E., Dunlap, J.C., Eckel-Mahan, K., Esser, K.A., FitzGerald, G.A., Forger, D.B., Francey, L.J., Fu, Y.-H., Gachon, F., Gatfield, D., de Goede, P., Golden, S.S., Green, C., Harer, J., Harmer, S., Haspel, J., Hastings, M.H., Herzel, H., Herzog, E.D., Hoffmann, C., Hong, C., Hughey, J.J., Hurley, J.M., de la Iglesia, H.O., Johnson, C., Kay, S.A., Koike, N., Kornacker, K., Kramer, A., Lamia, K., Leise, T., Lewis, S.A., Li, J., Li, X., Liu, A.C., Loros, J.J., Martino, T.A., Menet, J.S., Merrow,

M., Millar, A.J., Mockler, T., Naef, F., Nagoshi, E., Nitabach, M.N., Olmedo, M., Nusinow, D.A., Ptáček, L.J., Rand, D., Reddy, A.B., Robles, M.S., Roenneberg, T., Rosbash, M., Ruben, M.D., Rund, S.S.C., Sancar, A., Sassone-Corsi, P., Sehgal, A., Sherrill-Mix, S., Skene, D.J., Storch, K.-F., Takahashi, J.S., Ueda, H.R., Wang, H., Weitz, C., Westermark, P.O., Wijnen, H., Xu, Y., Wu, G., Yoo, S.-H., Young, M., Zhang, E.E., Zielinski, T., Hogenesch, J.B., 2017. Guidelines for Genome-Scale Analysis of Biological Rhythms. J Biol Rhythms 32, 380–393. https://doi.org/10.1177/0748730417728663

Hughes, M.E., DiTacchio, L., Hayes, K., Pullivarthy, S.R., Panda, S., Hogenesch, J., 2007. High resolution time course analysis of gene expression from the liver and pituitary. Cold Spring Harb Symp Quant Biol 72, 381–386. https://doi.org/10.1101/sqb.2007.72.011

Hurst, R., Rollema, H., Bertrand, D., 2013. Nicotinic acetylcholine receptors: From basic science to therapeutics. Pharmacology & Therapeutics 137, 22–54. https://doi.org/10.1016/j.pharmthera.2012.08.012

Hut, R.A., Van der Zee, E.A., 2011. The cholinergic system, circadian rhythmicity, and time memory. Behav. Brain Res. 221, 466–480. https://doi.org/10.1016/j.bbr.2010.11.039

Hwang, B.H., Suzuki, R., Lumeng, L., Li, T.-K., McBride, W.J., 2004. Innate differences in neuropeptide Y (NPY) mRNA expression in discrete brain regions between alcohol-preferring (P) and -nonpreferring (NP) rats: a significantly low level of NPY mRNA in dentate gyrus of the hippocampus and absence of NPY mRNA in the medial habenular nucleus of P rats. Neuropeptides 38, 359–368. https://doi.org/10.1016/j.npep.2004.09.004

Ikeda, M., Hojo, Y., Komatsuzaki, Y., Okamoto, M., Kato, A., Takeda, T., Kawato, S., 2015. Hippocampal spine changes across the sleep–wake cycle: corticosterone and kinases. Journal of Endocrinology 226, M13–M27. https://doi.org/10.1530/JOE-15-0078

Inouye, S.T., Kawamura, H., 1979. Persistence of circadian rhythmicity in a mammalian hypothalamic “island” containing the suprachiasmatic nucleus. Proc Natl Acad Sci U S A 76, 5962–5966. https://doi.org/10.1073/pnas.76.11.5962

Ishihara, K., Miyasita, A., Inugami, M., Fukuda, K., Yamazaki, K., Miyata, Y., 1985. Differences in the time or frequency of meals, alcohol and caffeine ingestion, and smoking found between “morning” and “evening” types. Psychol Rep 57, 391–396. https://doi.org/10.2466/pr0.1985.57.2.391

Islam, S., Zeisel, A., Joost, S., La Manno, G., Zajac, P., Kasper, M., Lönnerberg, P., Linnarsson, S., 2014. Quantitative single-cell RNA-seq with unique molecular identifiers. Nature Methods 11, 163–166. https://doi.org/10.1038/nmeth.2772

Ito, H.T., Schuman, E.M., 2008. Frequency-dependent signal transmission and modulation by neuromodulators. Front Neurosci 2, 138–144. https://doi.org/10.3389/neuro.01.027.2008

Ivanova, E., Hwang, G.-S., Pan, Z.-H., 2010. Characterization of transgenic mouse lines expressing Cre-recombinase in the retina. Neuroscience 165, 233–243. https://doi.org/10.1016/j.neuroscience.2009.10.021

Jagannath, A., Peirson, S.N., Foster, R.G., 2013. Sleep and circadian rhythm disruption in neuropsychiatric illness. Curr Opin Neurobiol 23, 888–894. https://doi.org/10.1016/j.conb.2013.03.008

Janik, D., Mrosovsky, N., 1994. Intergeniculate leaflet lesions and behaviorally-induced shifts of circadian rhythms. Brain Res 651, 174–182. https://doi.org/10.1016/0006-8993(94)90695-5

Jansen, H.T., Sergeeva, A., Stark, G., Sorg, B.A., 2012. Circadian Discrimination of Reward: Evidence for Simultaneous Yet Separable Food- and Drug-Entrained Rhythms in the Rat. Chronobiology International 29, 454–468. https://doi.org/10.3109/07420528.2012.667467

Jenni-Eiermann, S., Hahn, H.P. von, Honegger, C.G., 1985. Circadian Variations of Neurotransmitter Binding in Three Age Groups of Rats. GER 31, 138–149. https://doi.org/10.1159/000212695
Jiménez-Capdeville, M.E., Dykes, R.W., 1993. Daily changes in the release of acetylcholine from rat primary somatosensory cortex. Brain Research 625, 152–158. https://doi.org/10.1016/0006-8993(93)90148-G
Jin, X.-T., Tucker, B.R., Drenan, R.M., 2020. Nicotine Self-Administration Induces Plastic Changes to Nicotinic Receptors in Medial Habenula. eNeuro 7, ENEURO.0197-20.2020. https://doi.org/10.1523/ENEURO.0197-20.2020
Johnson, C.H., 2007. Bacterial Circadian Programs. Cold Spring Harb Symp Quant Biol 72, 395–404. https://doi.org/10.1101/sqb.2007.72.027
Johnson, C.H., Golden, S.S., 1999. Circadian programs in cyanobacteria: adaptiveness and mechanism. Annu. Rev. Microbiol. 53, 389–409. https://doi.org/10.1146/annurev.micro.53.1.389
Johnson, S.W., North, R.A., 1992. Two types of neurone in the rat ventral tegmental area and their synaptic inputs. J Physiol 450, 455–468. https://doi.org/10.1113/jphysiol.1992.sp019136
Johnston, J.D., Skene, D.J., 2015. 60 YEARS OF NEUROENDOCRINOLOGY: Regulation of mammalian neuroendocrine physiology and rhythms by melatonin. J Endocrinol 226, T187-198. https://doi.org/10.1530/JOE-15-0119
Jones, B.E., 2020. Arousal and sleep circuits. Neuropsychopharmacology 45, 6–20. https://doi.org/10.1038/s41386-019-0444-2
Jones, B.E., 2008. Modulation of cortical activation and behavioral arousal by cholinergic and orexinergic systems. Ann. N. Y. Acad. Sci. 1129, 26–34. https://doi.org/10.1196/annals.1417.026
Jones, J.R., Simon, T., Lones, L., Herzog, E.D., 2018. SCN VIP Neurons Are Essential for Normal Light-Mediated Resetting of the Circadian System. J. Neurosci. 38, 7986–7995. https://doi.org/10.1523/JNEUROSCI.1322-18.2018
Juczewski, K., Koussa, J.A., Kesner, A.J., Lee, J.O., Lovinger, D.M., 2020. Stress and behavioral correlates in the head-fixed method: stress measurements, habituation dynamics, locomotion, and motor-skill learning in mice. Sci Rep 10, 12245. https://doi.org/10.1038/s41598-020-69132-6
Kaiser, C., Kaufmann, C., Leutritz, T., Arnold, Y.L., Speck, O., Ullsperger, M., 2019. The human habenula is responsive to changes in luminance and circadian rhythm. NeuroImage 189, 581–588. https://doi.org/10.1016/j.neuroimage.2019.01.064
Kametani, H., Kawamura, H., 1991. Circadian rhythm of cortical acetylcholine release as measured by in vivo microdialysis in freely moving rats. Neuroscience Letters 132, 263–266. https://doi.org/10.1016/0304-3940(91)90316-L
Karkowski, L.M., Prescott, C.A., Kendler, K.S., 2000. Multivariate assessment of factors influencing illicit substance use in twins from female-female pairs. Am. J. Med. Genet. 96, 665–670.
Kasahara, T., Abe, K., Mekada, K., Yoshiki, A., Kato, T., 2010. Genetic variation of melatonin productivity in laboratory mice under domestication. Proc Natl Acad Sci U S A 107, 6412–6417. https://doi.org/10.1073/pnas.0914399107
Keil, J.M., Qalieh, A., Kwan, K.Y., 2018. Brain Transcriptome Databases: A User's Guide. J Neurosci 38, 2399–2412. https://doi.org/10.1523/JNEUROSCI.1930-17.2018
Kenny, P.J., Markou, A., 2006. Nicotine Self-Administration Acutely Activates Brain Reward Systems and Induces a Long-Lasting Increase in Reward Sensitivity. Neuropsychopharmacology 31, 1203. https://doi.org/10.1038/sj.npp.1300905
Ketchesin, K.D., Becker-Krail, D., McClung, C.A., 2020. Mood-related central and peripheral clocks. Eur J Neurosci 51, 326–345. https://doi.org/10.1111/ejn.14253

Kim, U., Chang, S.-Y., 2005. Dendritic morphology, local circuitry, and intrinsic electrophysiology of neurons in the rat medial and lateral habenular nuclei of the epithalamus. J. Comp. Neurol. 483, 236–250. https://doi.org/10.1002/cne.20410

Kim, U., Chung, L., 2007. Dual GABAergic synaptic response of fast excitation and slow inhibition in the medial habenula of rat epithalamus. J. Neurophysiol. 98, 1323–1332. https://doi.org/10.1152/jn.00575.2007

King, S.L., Caldarone, B.J., Picciotto, M.R., 2004. β2-subunit-containing nicotinic acetylcholine receptors are critical for dopamine-dependent locomotor activation following repeated nicotine administration. Neuropharmacology, Frontiers in Addiction Research: Celebrating the 30th Anniversary of the National Institute on Drug Abuse. 47, 132–139. https://doi.org/10.1016/j.neuropharm.2004.06.024

Kita, T., Nakashima, T., Kurogochi, Y., 1986. Circadian variation of nicotine-induced ambulatory activity in rats. Jpn. J. Pharmacol. 41, 55–60.

Kiyatkin, E.A., 2014. Critical role of peripheral sensory systems in mediating the neural effects of nicotine following its acute and repeated exposure. Rev Neurosci 25, 207–221. https://doi.org/10.1515/revneuro-2013-0067

Klemm, W.R., 2004. Habenular and interpeduncularis nuclei: shared components in multiple-function networks. Med. Sci. Monit. 10, RA261-273.

Kobayashi, Y., Sano, Y., Vannoni, E., Goto, H., Ikeda, T., Suzuki, H., Oba, A., Kawasaki, H., Kanba, S., Lipp, H.-P., Murphy, N., Wolfer, D., Itohara, S., 2013. Genetic dissection of medial habenula–interpeduncular nucleus pathway function in mice. Frontiers in Behavioral Neuroscience 7, 17. https://doi.org/10.3389/fnbeh.2013.00017

Koch, C.E., Begemann, K., Kiehn, J.T., Griewahn, L., Mauer, J., M. E. Hess, Moser, A., Schmid, S.M., Brüning, J.C., Oster, H., 2020. Circadian regulation of hedonic appetite in mice by clocks in dopaminergic neurons of the VTA. Nat Commun 11, 3071. https://doi.org/10.1038/s41467-020-16882-6

Koob, G.F., Le Moal, M., 2001. Drug addiction, dysregulation of reward, and allostasis. Neuropsychopharmacology 24, 97–129. https://doi.org/10.1016/S0893-133X(00)00195-0

Kovanen, L., Saarikoski, S.T., Haukka, J., Pirkola, S., Aromaa, A., Lönnqvist, J., Partonen, T., 2010. Circadian clock gene polymorphisms in alcohol use disorders and alcohol consumption. Alcohol Alcohol 45, 303–311. https://doi.org/10.1093/alcalc/agq035

Kuipers, M.A.G., West, R., Beard, E.V., Brown, J., 2020. Impact of the “Stoptober” Smoking Cessation Campaign in England From 2012 to 2017: A Quasiexperimental Repeat Cross-Sectional Study. Nicotine Tob Res 22, 1453–1459. https://doi.org/10.1093/ntr/ntz108

Kulkarni, A., Anderson, A.G., Merullo, D.P., Konopka, G., 2019. Beyond bulk: a review of single cell transcriptomics methodologies and applications. Current Opinion in Biotechnology, Systems Biology • Nanobiotechnology 58, 129–136. https://doi.org/10.1016/j.copbio.2019.03.001

Kumar Jha, P., Challet, E., Kalsbeek, A., 2015. Circadian rhythms in glucose and lipid metabolism in nocturnal and diurnal mammals. Mol Cell Endocrinol 418 Pt 1, 74–88. https://doi.org/10.1016/j.mce.2015.01.024

Kume, K., Zylka, M.J., Sriram, S., Shearman, L.P., Weaver, D.R., Jin, X., Maywood, E.S., Hastings, M.H., Reppert, S.M., 1999. mCRY1 and mCRY2 are essential components of the negative limb of the circadian clock feedback loop. Cell 98, 193–205. https://doi.org/10.1016/s0092-8674(00)81014-4

Kurtuncu, M., Arslan, A.D., Akhisaroglu, M., Manev, H., Uz, T., 2004. Involvement of the pineal gland in diurnal cocaine reward in mice. Eur. J. Pharmacol. 489, 203–205. https://doi.org/10.1016/j.ejphar.2004.03.010

Kutlu, M.G., Parikh, V., Gould, T.J., 2015. Nicotine Addiction and Psychiatric Disorders. Int Rev Neurobiol 124, 171–208. https://doi.org/10.1016/bs.irn.2015.08.004

Landgraf, D., Long, J.E., Welsh, D.K., 2016a. Depression-like behaviour in mice is associated with disrupted circadian rhythms in nucleus accumbens and periaqueductal grey. European Journal of Neuroscience 43, 1309–1320. https://doi.org/10.1111/ejn.13085

Landgraf, D., Long, J.E., Welsh, D.K., 2016b. Depression-like behaviour in mice is associated with disrupted circadian rhythms in nucleus accumbens and periaqueductal grey. Eur J Neurosci 43, 1309–1320. https://doi.org/10.1111/ejn.13085

Landgraf, D., McCarthy, M.J., Welsh, D.K., 2014. The role of the circadian clock in animal models of mood disorders. Behav Neurosci 128, 344–359. https://doi.org/10.1037/a0036029

Langel, J., Ikeno, T., Yan, L., Nunez, A.A., Smale, L., 2018. Distributions of GABAergic and glutamatergic neurons in the brains of a diurnal and nocturnal rodent. Brain Res 1700, 152–159. https://doi.org/10.1016/j.brainres.2018.08.019

Lawson, R.P., Seymour, B., Loh, E., Lutti, A., Dolan, R.J., Dayan, P., Weiskopf, N., Roiser, J.P., 2014. The habenula encodes negative motivational value associated with primary punishment in humans. Proc Natl Acad Sci U S A 111, 11858–11863. https://doi.org/10.1073/pnas.1323586111

Le Foll, B., French, L., 2018. Transcriptomic Characterization of the Human Habenula Highlights Drug Metabolism and the Neuroimmune System. Front Neurosci 12. https://doi.org/10.3389/fnins.2018.00742

Lebois, E.P., Thorn, C., Edgerton, J.R., Popiolek, M., Xi, S., 2018. Muscarinic receptor subtype distribution in the central nervous system and relevance to aging and Alzheimer's disease. Neuropharmacology, Neuropharmacology on Muscarinic Receptors 136, 362–373. https://doi.org/10.1016/j.neuropharm.2017.11.018

Lecourtier, L., Kelly, P.H., 2007. A conductor hidden in the orchestra? Role of the habenular complex in monoamine transmission and cognition. Neuroscience & Biobehavioral Reviews 31, 658–672. https://doi.org/10.1016/j.neubiorev.2007.01.004

Lee, C., Etchegaray, J.-P., Cagampang, F.R.A., Loudon, A.S.I., Reppert, S.M., 2001. Posttranslational Mechanisms Regulate the Mammalian Circadian Clock. Cell 107, 855–867. https://doi.org/10.1016/S0092-8674(01)00610-9

Lee, H., Choi, T.-I., Kim, Y.-M., Lee, S., Han, B., Bak, I.S., Moon, S.A., Yu, D.-Y., Shin, K.S., Kwon, Y.K., Moon, C., Ryu, J.H., Hoe, H.-S., Kim, C.-H., Shim, I., 2021. Regulation of habenular G-protein gamma 8 on learning and memory via modulation of the central acetylcholine system. Mol Psychiatry 26, 3737–3750. https://doi.org/10.1038/s41380-020-00893-2

Lee, H.W., Yang, S.H., Kim, J.Y., Kim, H., 2019. The Role of the Medial Habenula Cholinergic System in Addiction and Emotion-Associated Behaviors. Front Psychiatry 10. https://doi.org/10.3389/fpsyt.2019.00100

Lein, E.S., Hawrylycz, M.J., Ao, N., Ayres, M., Bensinger, A., Bernard, A., Boe, A.F., Boguski, M.S., Brockway, K.S., Byrnes, E.J., Chen, Lin, Chen, Li, Chen, T.-M., Chi Chin, M., Chong, J., Crook, B.E., Czaplinska, A., Dang, C.N., Datta, S., Dee, N.R., Desaki, A.L., Desta, T., Diep, E., Dolbeare, T.A., Donelan, M.J., Dong, H.-W., Dougherty, J.G., Duncan, B.J., Ebbert, A.J., Eichele, G., Estin, L.K., Faber, C., Facer, B.A., Fields, R., Fischer, S.R., Fliss, T.P., Frensley, C., Gates, S.N., Glattfelder, K.J., Halverson, K.R., Hart, M.R., Hohmann, J.G., Howell, M.P., Jeung, D.P., Johnson, R.A., Karr, P.T., Kawal, R., Kidney, J.M., Knapik, R.H., Kuan, C.L., Lake, J.H., Laramee, A.R., Larsen, K.D., Lau, C., Lemon, T.A., Liang, A.J., Liu, Y., Luong, L.T., Michaels, J., Morgan, J.J., Morgan, R.J., Mortrud, M.T., Mosqueda, N.F., Ng, L.L., Ng, R., Orta, G.J., Overly, C.C., Pak, T.H., Parry, S.E., Pathak, S.D., Pearson, O.C., Puchalski, R.B., Riley, Z.L., Rockett, H.R., Rowland, S.A., Royall, J.J., Ruiz, M.J., Sarno, N.R., Schaffnit, K., Shapovalova, N.V., Sivisay, T., Slaughterbeck, C.R., Smith, S.C., Smith, K.A., Smith, B.I., Sodt, A.J., Stewart, N.N., Stumpf, K.-R., Sunkin, S.M., Sutram, M., Tam, A., Teemer, C.D., Thaller, C., Thompson, C.L., Varnam, L.R., Visel, A., Whitlock, R.M., Wohnoutka, P.E., Wolkey, C.K., Wong, V.Y., Wood, M., Yaylaoglu, M.B., Young, R.C., Youngstrom, B.L., Feng Yuan, X., Zhang, B., Zwingman, T.A., Jones, A.R., 2007. Genome-wide atlas of gene

expression in the adult mouse brain. Nature 445, 168–176. https://doi.org/10.1038/nature05453
Lenn, N.J., Wong, V., Hamill, G.S., 1983. Left-right pairing at the crest synapses of rat interpeduncular nucleus. Neuroscience 9, 383–389.
Leslie, F.M., Mojica, C.Y., Reynaga, D.D., 2013. Nicotinic receptors in addiction pathways. Mol. Pharmacol. 83, 753–758. https://doi.org/10.1124/mol.112.083659
Li, S., Liu, L., Jiang, W., Sun, L., Zhou, S., Le Foll, B., Zhang, X.Y., Kosten, T.R., Lu, L., 2010. Circadian alteration in neurobiology during protracted opiate withdrawal in rats. J. Neurochem. 115, 353–362. https://doi.org/10.1111/j.1471-4159.2010.06941.x
Li, X., Yu, B., Sun, Q., Zhang, Y., Ren, M., Zhang, X., Li, A., Yuan, J., Madisen, L., Luo, Q., Zeng, H., Gong, H., Qiu, Z., 2018. Generation of a whole-brain atlas for the cholinergic system and mesoscopic projectome analysis of basal forebrain cholinergic neurons. PNAS 115, 415–420. https://doi.org/10.1073/pnas.1703601115
Li, Y., Ma, W., Kang, Q., Qiao, L., Tang, D., Qiu, J., Zhang, Q., Li, H., 2015. Night or darkness, which intensifies the feeling of fear? International Journal of Psychophysiology 97, 46–57. https://doi.org/10.1016/j.ijpsycho.2015.04.021
Lima, L.B., Bueno, D., Leite, F., Souza, S., Gonçalves, L., Furigo, I.C., Donato, J., Metzger, M., 2017. Afferent and efferent connections of the interpeduncular nucleus with special reference to circuits involving the habenula and raphe nuclei. J Comp Neurol 525, 2411–2442. https://doi.org/10.1002/cne.24217
Liston, C., Cichon, J.M., Jeanneteau, F., Jia, Z., Chao, M.V., Gan, W.-B., 2013. Circadian glucocorticoid oscillations promote learning-dependent synapse formation and maintenance. Nat Neurosci 16, 698–705. https://doi.org/10.1038/nn.3387
Liu, Y., Beyer, A., Aebersold, R., 2016. On the Dependency of Cellular Protein Levels on mRNA Abundance. Cell 165, 535–550. https://doi.org/10.1016/j.cell.2016.03.014
Logan, R.W., Hasler, B.P., Forbes, E.E., Franzen, P.L., Torregrossa, M.M., Huang, Y.H., Buysse, D.J., Clark, D.B., McClung, C.A., 2018. Impact of sleep and circadian rhythms on addiction vulnerability in adolescents. Biol Psychiatry 83, 987–996. https://doi.org/10.1016/j.biopsych.2017.11.035
Logan, R.W., Williams, W.P., McClung, C.A., 2014. Circadian rhythms and addiction: Mechanistic insights and future directions. Behav Neurosci 128, 387–412. https://doi.org/10.1037/a0036268
London, E., Wester, J.C., Bloyd, M., Bettencourt, S., McBain, C.J., Stratakis, C.A., 2020. Loss of habenular Prkar2a reduces hedonic eating and increases exercise motivation. JCI Insight 5, 141670. https://doi.org/10.1172/jci.insight.141670
López, A.J., Jia, Y., White, A.O., Kwapis, J.L., Espinoza, M., Hwang, P., Campbell, R., Alaghband, Y., Chitnis, O., Matheos, D.P., Lynch, G., Wood, M.A., 2019. Medial habenula cholinergic signaling regulates cocaine-associated relapse-like behavior. Addict Biol 24, 403–413. https://doi.org/10.1111/adb.12605
Louis, M., Clarke, P.B.S., 1998. Effect of ventral tegmental 6-hydroxydopamine lesions on the locomotor stimulant action of nicotine in rats. Neuropharmacology 37, 1503–1513. https://doi.org/10.1016/S0028-3908(98)00151-8
Luchicchi, A., Bloem, B., Viaña, J.N.M., Mansvelder, H.D., Role, L.W., 2014. Illuminating the role of cholinergic signaling in circuits of attention and emotionally salient behaviors. Front. Synaptic Neurosci. 6. https://doi.org/10.3389/fnsyn.2014.00024
Lüscher, C., 2016. The Emergence of a Circuit Model for Addiction. Annu. Rev. Neurosci. 39, 257–276. https://doi.org/10.1146/annurev-neuro-070815-013920
Lynch, W.J., Carroll, M.E., 2001. Regulation of drug intake. Exp Clin Psychopharmacol 9, 131–143.
Madisen, L., Mao, T., Koch, H., Zhuo, J., Berenyi, A., Fujisawa, S., Hsu, Y.-W.A., Garcia, A.J., Gu, X., Zanella, S., Kidney, J., Gu, H., Mao, Y., Hooks, B.M., Boyden, E.S., Buzsáki, G., Ramirez, J.M., Jones, A.R., Svoboda, K., Han, X., Turner, E.E., Zeng, H., 2012. A toolbox of Cre-

dependent optogenetic transgenic mice for light-induced activation and silencing. Nat Neurosci 15, 793–802. https://doi.org/10.1038/nn.3078
Maggi, C.A., Meli, A., 1986. Suitability of urethane anesthesia for physiopharmacological investigations in various systems. Part 1: General considerations. Experientia 42, 109–114. https://doi.org/10.1007/BF01952426
Malin, D.H., Goyarzu, P., 2009. Rodent models of nicotine withdrawal syndrome. Handb Exp Pharmacol 401–434. https://doi.org/10.1007/978-3-540-69248-5_14
Mansvelder, H.D., Keath, J.R., McGehee, D.S., 2002. Synaptic mechanisms underlie nicotine-induced excitability of brain reward areas. Neuron 33, 905–919.
Mansvelder, H.D., McGehee, D.S., 2000. Long-Term Potentiation of Excitatory Inputs to Brain Reward Areas by Nicotine. Neuron 27, 349–357. https://doi.org/10.1016/S0896-6273(00)00042-8
Mao, D., Gallagher, K., McGehee, D.S., 2011. Nicotine potentiation of excitatory inputs to ventral tegmental area dopamine neurons. J Neurosci 31, 6710–6720. https://doi.org/10.1523/JNEUROSCI.5671-10.2011
Marchand, E.R., Riley, J.N., Moore, R.Y., 1980. Interpeduncular nucleus afferents in the rat. Brain Res. 193, 339–352.
Maruani, J., Geoffroy, P.A., 2022. Multi-Level Processes and Retina-Brain Pathways of Photic Regulation of Mood. J Clin Med 11, 448. https://doi.org/10.3390/jcm11020448
Mathis, V., Barbelivien, A., Majchrzak, M., Mathis, C., Cassel, J.-C., Lecourtier, L., 2017. The Lateral Habenula as a Relay of Cortical Information to Process Working Memory. Cereb Cortex 27, 5485–5495. https://doi.org/10.1093/cercor/bhw316
Mathuru, A.S., 2017. A little rein on addiction. Semin. Cell Dev. Biol. https://doi.org/10.1016/j.semcdb.2017.09.030
Matsumoto, M., Hikosaka, O., 2007. Lateral habenula as a source of negative reward signals in dopamine neurons. Nature 447, 1111–1115. https://doi.org/10.1038/nature05860
Maywood, E.S., 2020. Synchronization and maintenance of circadian timing in the mammalian clockwork. Eur J Neurosci 51, 229–240. https://doi.org/10.1111/ejn.14279
Maywood, E.S., Chesham, J.E., O'Brien, J.A., Hastings, M.H., 2011. A diversity of paracrine signals sustains molecular circadian cycling in suprachiasmatic nucleus circuits. Proc Natl Acad Sci U S A 108, 14306–14311. https://doi.org/10.1073/pnas.1101767108
McCallum, S.E., Cowe, M.A., Lewis, S.W., Glick, S.D., 2012. α3β4 nicotinic acetylcholine receptors in the medial habenula modulate the mesolimbic dopaminergic response to acute nicotine in vivo. Neuropharmacology 63, 434–440. https://doi.org/10.1016/j.neuropharm.2012.04.015
McClave, A.K., Dube, S.R., Strine, T.W., Kroenke, K., Caraballo, R.S., Mokdad, A.H., 2009. Associations between smoking cessation and anxiety and depression among U.S. adults. Addict Behav 34, 491–497. https://doi.org/10.1016/j.addbeh.2009.01.005
McClung, C.A., 2013. How might circadian rhythms control mood? Let me count the ways….. Biol Psychiatry 74, 242–249. https://doi.org/10.1016/j.biopsych.2013.02.019
McClung, C.A., 2007. Circadian rhythms, the mesolimbic dopaminergic circuit, and drug addiction. ScientificWorldJournal 7, 194–202. https://doi.org/10.1100/tsw.2007.213
McClung, C.A., Sidiropoulou, K., Vitaterna, M., Takahashi, J.S., White, F.J., Cooper, D.C., Nestler, E.J., 2005. Regulation of dopaminergic transmission and cocaine reward by the Clock gene. Proc. Natl. Acad. Sci. U.S.A. 102, 9377–9381. https://doi.org/10.1073/pnas.0503584102
McGehee, D.S., Heath, M.J., Gelber, S., Devay, P., Role, L.W., 1995. Nicotine enhancement of fast excitatory synaptic transmission in CNS by presynaptic receptors. Science 269, 1692–1696. https://doi.org/10.1126/science.7569895

McKay, B.E., Placzek, A.N., Dani, J.A., 2007. Regulation of synaptic transmission and plasticity by neuronal nicotinic acetylcholine receptors. Biochem. Pharmacol. 74, 1120–1133. https://doi.org/10.1016/j.bcp.2007.07.001

McLaughlin, I., Dani, J.A., De Biasi, M., 2017. The medial habenula and interpeduncular nucleus circuitry is critical in addiction, anxiety, and mood regulation. J. Neurochem. 142, 130–143. https://doi.org/10.1111/jnc.14008

Meijer, J.H., Schwartz, W.J., 2003. In search of the pathways for light-induced pacemaker resetting in the suprachiasmatic nucleus. J. Biol. Rhythms 18, 235–249. https://doi.org/10.1177/0748730403018003006

Melani, R., Von Itter, R., Jing, D., Koppensteiner, P., Ninan, I., 2019. Opposing effects of an atypical glycinergic and substance P transmission on interpeduncular nucleus plasticity. Neuropsychopharmacol. 44, 1828–1836. https://doi.org/10.1038/s41386-019-0396-6

Mendoza, J., 2017. Circadian neurons in the lateral habenula: Clocking motivated behaviors. Pharmacol. Biochem. Behav. 162, 55–61. https://doi.org/10.1016/j.pbb.2017.06.013

Mendoza, J., Challet, E., 2014. Circadian insights into dopamine mechanisms. Neuroscience, The Ventral Tegmentum and Dopamine: A New Wave of Diversity 282, 230–242. https://doi.org/10.1016/j.neuroscience.2014.07.081

Meng, C., Brandl, F., Tahmasian, M., Shao, J., Manoliu, A., Scherr, M., Schwerthöffer, D., Bäuml, J., Förstl, H., Zimmer, C., Wohlschläger, A.M., Riedl, V., Sorg, C., 2014. Aberrant topology of striatum's connectivity is associated with the number of episodes in depression. Brain 137, 598–609. https://doi.org/10.1093/brain/awt290

Metzger, M., Souza, R., Lima, L.B., Bueno, D., Gonçalves, L., Sego, C., Donato, J., Shammah-Lagnado, S.J., 2021. Habenular connections with the dopaminergic and serotonergic system and their role in stress-related psychiatric disorders. Eur J Neurosci 53, 65–88. https://doi.org/10.1111/ejn.14647

Mexal, S., Horton, W.J., Crouch, E.L., Maier, S.I.B., Wilkinson, A.L., Marsolek, M., Stitzel, J.A., 2012. Diurnal variation in nicotine sensitivity in mice: role of genetic background and melatonin. Neuropharmacology 63, 966–973. https://doi.org/10.1016/j.neuropharm.2012.06.065

Meyer-Bernstein, E.L., Morin, L.P., 1996. Differential serotonergic innervation of the suprachiasmatic nucleus and the intergeniculate leaflet and its role in circadian rhythm modulation. J Neurosci 16, 2097–2111.

Michael, A.K., Fribourgh, J.L., Chelliah, Y., Sandate, C.R., Hura, G.L., Schneidman-Duhovny, D., Tripathi, S.M., Takahashi, J.S., Partch, C.L., 2017. Formation of a repressive complex in the mammalian circadian clock is mediated by the secondary pocket of CRY1. Proc Natl Acad Sci U S A 114, 1560–1565. https://doi.org/10.1073/pnas.1615310114

Milosavljevic, N., 2019. How Does Light Regulate Mood and Behavioral State? Clocks Sleep 1, 319–331. https://doi.org/10.3390/clockssleep1030027

Mistlberger, R.E., 2011. Neurobiology of food anticipatory circadian rhythms. Physiology & Behavior, Proceedings from the 2010 meeting of the Society for the Study of Ingestive Behavior (SSIB) 104, 535–545. https://doi.org/10.1016/j.physbeh.2011.04.015

Mizumori, S.J.Y., Baker, P.M., 2017. The Lateral Habenula and Adaptive Behaviors. Trends Neurosci 40, 481–493. https://doi.org/10.1016/j.tins.2017.06.001

Moen, J.K., Lee, A.M., 2021. Sex Differences in the Nicotinic Acetylcholine Receptor System of Rodents: Impacts on Nicotine and Alcohol Reward Behaviors. Front Neurosci 15, 745783. https://doi.org/10.3389/fnins.2021.745783

Molas, S., DeGroot, S.R., Zhao-Shea, R., Tapper, A.R., 2017a. Anxiety and Nicotine Dependence: Emerging Role of the Habenulo-Interpeduncular Axis. Trends Pharmacol. Sci. 38, 169–180. https://doi.org/10.1016/j.tips.2016.11.001

Molas, S., Zhao-Shea, R., Liu, L., DeGroot, S.R., Gardner, P.D., Tapper, A.R., 2017b. A circuit-based mechanism underlying familiarity signaling and the preference for novelty. Nat Neurosci 20, 1260–1268. https://doi.org/10.1038/nn.4607

Mooney, M., Green, C., Hatsukami, D., 2006. Nicotine self-administration: cigarette versus nicotine gum diurnal topography. Hum Psychopharmacol 21, 539–548. https://doi.org/10.1002/hup.808
Moore, R.Y., 1983. Organization and function of a central nervous system circadian oscillator: the suprachiasmatic hypothalamic nucleus. Fed Proc 42, 2783–2789.
Moore, R.Y., Lenn, N.J., 1972. A retinohypothalamic projection in the rat. Journal of Comparative Neurology 146, 1–14. https://doi.org/10.1002/cne.901460102
Morin, L.P., Studholme, K.M., 2014. Retinofugal Projections in the Mouse. J Comp Neurol 522, 3733–3753. https://doi.org/10.1002/cne.23635
Morley, B.J., 1986. The interpeduncular nucleus. Int. Rev. Neurobiol. 28, 157–182.
Morley, B.J., Garner, L.L., 1990. Light-dark variation in response to chronic nicotine treatment and the density of hypothalamic alpha-bungarotoxin receptors. Pharmacol. Biochem. Behav. 37, 239–245.
Morris, E.L., Patton, A.P., Chesham, J.E., Crisp, A., Adamson, A., Hastings, M.H., 2021. Single-cell transcriptomics of suprachiasmatic nuclei reveal a Prokineticin-driven circadian network. EMBO J 40, e108614. https://doi.org/10.15252/embj.2021108614
Mulle, C., Vidal, C., Benoit, P., Changeux, J.P., 1991. Existence of different subtypes of nicotinic acetylcholine receptors in the rat habenulo-interpeduncular system. J. Neurosci. 11, 2588–2597.
Müller-Fielitz, H., Stahr, M., Bernau, M., Richter, M., Abele, S., Krajka, V., Benzin, A., Wenzel, J., Kalies, K., Mittag, J., Heuer, H., Offermanns, S., Schwaninger, M., 2017. Tanycytes control the hormonal output of the hypothalamic-pituitary-thyroid axis. Nat Commun 8, 484. https://doi.org/10.1038/s41467-017-00604-6
Munn, R.G.K., Tyree, S.M., McNaughton, N., Bilkey, D.K., 2015. The frequency of hippocampal theta rhythm is modulated on a circadian period and is entrained by food availability. Front Behav Neurosci 9, 61. https://doi.org/10.3389/fnbeh.2015.00061
Murakami, N., Takahashi, K., Kawashima, K., 1984. Effect of light on the acetylcholine concentrations of the suprachiasmatic nucleus in the rat. Brain Res 311, 358–360. https://doi.org/10.1016/0006-8993(84)90100-8
Mure, L.S., Le, H.D., Benegiamo, G., Chang, M.W., Rios, L., Jillani, N., Ngotho, M., Kariuki, T., Dkhissi-Benyahya, O., Cooper, H.M., Panda, S., 2018. Diurnal transcriptome atlas of a primate across major neural and peripheral tissues. Science 359. https://doi.org/10.1126/science.aao0318
Murphy, C.A., DiCamillo, A.M., Haun, F., Murray, M., 1996. Lesion of the habenular efferent pathway produces anxiety and locomotor hyperactivity in rats: a comparison of the effects of neonatal and adult lesions. Behavioural Brain Research 81, 43–52. https://doi.org/10.1016/S0166-4328(96)00041-1
Murray, G., Nicholas, C.L., Kleiman, J., Dwyer, R., Carrington, M.J., Allen, N.B., Trinder, J., 2009. Nature's clocks and human mood: the circadian system modulates reward motivation. Emotion 9, 705–716. https://doi.org/10.1037/a0017080
Nakamura, M., Gao, S., Okamura, H., Nakahara, D., 2011. Intrathecal cocaine delivery enables long-access self-administration with binge-like behavior in mice. Psychopharmacology (Berl.) 213, 119–129. https://doi.org/10.1007/s00213-010-2021-6
Nelson, R.J., Bumgarner, J.R., Walker, W.H., DeVries, A.C., 2021. Time-of-day as a critical biological variable. Neuroscience & Biobehavioral Reviews 127, 740–746. https://doi.org/10.1016/j.neubiorev.2021.05.017
Neugebauer, N.M., Einstein, E.B., Lopez, M.B., McClure-Begley, T.D., Mineur, Y.S., Picciotto, M.R., 2013. Morphine dependence and withdrawal induced changes in cholinergic signaling. Pharmacol. Biochem. Behav. 109, 77–83. https://doi.org/10.1016/j.pbb.2013.04.015

NHS Digital, 2020. Statistics on Smoking, England 2020 [WWW Document]. URL https://digital.nhs.uk/data-and-information/publications/statistical/statistics-on-smoking/statistics-on-smoking-england-2020 (accessed 8.18.21).
Nordberg, A., Wahlström, G., 1980. Diurnal fluctuation in striatal choline acetyltransferase activity and strain difference in brain protein content of the rat. Acta Physiologica Scandinavica 108, 385–388. https://doi.org/10.1111/j.1748-1716.1980.tb06548.x
O'Dell, L.E., Chen, S.A., Smith, R.T., Specio, S.E., Balster, R.L., Paterson, N.E., Markou, A., Zorrilla, E.P., Koob, G.F., 2007. Extended access to nicotine self-administration leads to dependence: Circadian measures, withdrawal measures, and extinction behavior in rats. J. Pharmacol. Exp. Ther. 320, 180–193. https://doi.org/10.1124/jpet.106.105270
Ofengeim, D., Giagtzoglou, N., Huh, D., Zou, C., Yuan, J., 2017. Single-Cell RNA Sequencing: Unraveling the Brain One Cell at a Time. Trends Mol Med 23, 563–576. https://doi.org/10.1016/j.molmed.2017.04.006
Ogawa, S.K., Cohen, J.Y., Hwang, D., Uchida, N., Watabe-Uchida, M., 2014. Organization of monosynaptic inputs to the serotonin and dopamine neuromodulatory systems. Cell Rep 8, 1105–1118. https://doi.org/10.1016/j.celrep.2014.06.042
O'Hara, B.F., Edgar, D.M., Cao, V.H., Wiler, S.W., Craig Heller, H., Kilduff, T.S., Miller, J.D., 1998. Nicotine and nicotinic receptors in the circadian system. Psychoneuroendocrinology, Effects of Nicotine on the Hypothalamic-Pituitary-Axis (HPA) and Immune Function 23, 161–173. https://doi.org/10.1016/S0306-4530(97)00077-2
Olejniczak, I., Ripperger, J.A., Sandrelli, F., Schnell, A., Mansencal-Strittmatter, L., Wendrich, K., Hui, K.Y., Brenna, A., Fredj, N.B., Albrecht, U., 2021. Light affects behavioral despair involving the clock gene Period 1. PLOS Genetics 17, e1009625. https://doi.org/10.1371/journal.pgen.1009625
Ostroumov, A., Dani, J.A., 2018. Convergent Neuronal Plasticity and Metaplasticity Mechanisms of Stress, Nicotine, and Alcohol. Annu Rev Pharmacol Toxicol 58, 547–566. https://doi.org/10.1146/annurev-pharmtox-010617-052735
Otsu, Y., Lecca, S., Pietrajtis, K., Rousseau, C.V., Marcaggi, P., Dugué, G.P., Mailhes-Hamon, C., Mameli, M., Diana, M.A., 2018. Functional Principles of Posterior Septal Inputs to the Medial Habenula. Cell Reports 22, 693–705. https://doi.org/10.1016/j.celrep.2017.12.064
Pagliardini, S., Gosgnach, S., Dickson, C.T., 2013. Spontaneous Sleep-Like Brain State Alternations and Breathing Characteristics in Urethane Anesthetized Mice. PLoS One 8, e70411. https://doi.org/10.1371/journal.pone.0070411
Panagis, G., Nisell, M., Nomikos, G.G., Chergui, K., Svensson, T.H., 1996. Nicotine injections into the ventral tegmental area increase locomotion and Fos-like immunoreactivity in the nucleus accumbens of the rat. Brain Research 730, 133–142. https://doi.org/10.1016/0006-8993(96)00432-5
Pang, X., Liu, L., Ngolab, J., Zhao-Shea, R., McIntosh, J.M., Gardner, P.D., Tapper, A.R., 2016. Habenula cholinergic neurons regulate anxiety during nicotine withdrawal via nicotinic acetylcholine receptors. Neuropharmacology 107, 294–304. https://doi.org/10.1016/j.neuropharm.2016.03.039
Parekh, P.K., Becker-Krail, D., Sundaravelu, P., Ishigaki, S., Okado, H., Sobue, G., Huang, Y., McClung, C.A., 2018. Altered GluA1 (Gria1) Function and Accumbal Synaptic Plasticity in the ClockΔ19 Model of Bipolar Mania. Biol Psychiatry 84, 817–826. https://doi.org/10.1016/j.biopsych.2017.06.022
Park, H., Cheon, M., Kim, S., Chung, C., 2017. Temporal variations in presynaptic release probability in the lateral habenula. Sci Rep 7, 1–8. https://doi.org/10.1038/srep40866
Parrott, A.C., 1995. Stress modulation over the day in cigarette smokers. Addiction 90, 233–244.
Patel, A.A., McAlinden, N., Mathieson, K., Sakata, S., 2020. Simultaneous Electrophysiology and Fiber Photometry in Freely Behaving Mice. Frontiers in Neuroscience 14, 148. https://doi.org/10.3389/fnins.2020.00148

Patton, A.P., Chesham, J.E., Hastings, M.H., 2016. Combined Pharmacological and Genetic Manipulations Unlock Unprecedented Temporal Elasticity and Reveal Phase-Specific Modulation of the Molecular Circadian Clock of the Mouse Suprachiasmatic Nucleus. J Neurosci 36, 9326–9341. https://doi.org/10.1523/JNEUROSCI.0958-16.2016

Paul, J.R., Davis, J.A., Goode, L.K., Becker, B.K., Fusilier, A., Meador-Woodruff, A., Gamble, K.L., 2020. Circadian regulation of membrane physiology in neural oscillators throughout the brain. European Journal of Neuroscience 51, 109–138. https://doi.org/10.1111/ejn.14343

Paul, M.J., Indic, P., Schwartz, W.J., 2011. A role for the habenula in the regulation of locomotor activity cycles. European Journal of Neuroscience 34, 478–488. https://doi.org/10.1111/j.1460-9568.2011.07762.x

Paul, S., Brown, T., 2019. Direct effects of the light environment on daily neuroendocrine control. J Endocrinol JOE-19-0302.R1. https://doi.org/10.1530/JOE-19-0302

Paul, S., Hanna, L., Harding, C., Hayter, E.A., Walmsley, L., Bechtold, D.A., Brown, T.M., 2020. Output from VIP cells of the mammalian central clock regulates daily physiological rhythms. Nat Commun 11, 1453. https://doi.org/10.1038/s41467-020-15277-x

Pembroke, W.G., Babbs, A., Davies, K.E., Ponting, C.P., Oliver, P.L., 2015. Temporal transcriptomics suggest that twin-peaking genes reset the clock. eLife 4, e10518. https://doi.org/10.7554/eLife.10518

Perkins, K.A., Briski, J., Fonte, C., Scott, J., Lerman, C., 2009. Severity of tobacco abstinence symptoms varies by time of day. Nicotine Tob. Res. 11, 84–91. https://doi.org/10.1093/ntr/ntn003

Perreau-Lenz, S., Vengeliene, V., Noori, H.R., Merlo-Pich, E.V., Corsi, M.A., Corti, C., Spanagel, R., 2012. Inhibition of the Casein-Kinase-1-Epsilon/Delta Prevents Relapse-Like Alcohol Drinking. Neuropsychopharmacology 37, 2121–2131. https://doi.org/10.1038/npp.2012.62

Perry, D.C., Dávila-García, M.I., Stockmeier, C.A., Kellar, K.J., 1999. Increased nicotinic receptors in brains from smokers: membrane binding and autoradiography studies. J. Pharmacol. Exp. Ther. 289, 1545–1552.

Perry, D.C., Xiao, Y., Nguyen, H.N., Musachio, J.L., Dávila-García, M.I., Kellar, K.J., 2002. Measuring nicotinic receptors with characteristics of alpha4beta2, alpha3beta2 and alpha3beta4 subtypes in rat tissues by autoradiography. J. Neurochem. 82, 468–481.

Perry, E.K., Perry, R.H., Tomlinson, B.E., 1977. Circadian variations in cholinergic enzymes and muscarinic receptor binding in human cerebral cortex. Neuroscience Letters 4, 185–189. https://doi.org/10.1016/0304-3940(77)90136-7

Petsakou, A., Sapsis, T.P., Blau, J., 2015. Circadian Rhythms in Rho1 Activity Regulate Neuronal Plasticity and Network Hierarchy. Cell 162, 823–835. https://doi.org/10.1016/j.cell.2015.07.010

Pfeffer, M., Korf, H.-W., Wicht, H., 2017. The Role of the Melatoninergic System in Light-Entrained Behavior of Mice. Int J Mol Sci 18. https://doi.org/10.3390/ijms18030530

Piasecki, T.M., Richardson, A.E., Smith, S.M., 2007. Self-monitored motives for smoking among college students. Psychol Addict Behav 21, 328–337. https://doi.org/10.1037/0893-164X.21.3.328

Picciotto, M.R., Higley, M.J., Mineur, Y.S., 2012. Acetylcholine as a neuromodulator: cholinergic signaling shapes nervous system function and behavior. Neuron 76, 116–129. https://doi.org/10.1016/j.neuron.2012.08.036

Picciotto, M.R., Kenny, P.J., 2021. Mechanisms of Nicotine Addiction. Cold Spring Harb Perspect Med 11, a039610. https://doi.org/10.1101/cshperspect.a039610

Picciotto, M.R., Lewis, A.S., van Schalkwyk, G.I., Mineur, Y.S., 2015. Mood and anxiety regulation by nicotinic acetylcholine receptors: A potential pathway to modulate aggression and related behavioral states. Neuropharmacology 96, 235–243. https://doi.org/10.1016/j.neuropharm.2014.12.028

Picciotto, M.R., Mineur, Y.S., 2014. Molecules and circuits involved in nicotine addiction: The many faces of smoking. Neuropharmacology 76 Pt B, 545–553. https://doi.org/10.1016/j.neuropharm.2013.04.028

Pidoplichko, V.I., Noguchi, J., Areola, O.O., Liang, Y., Peterson, J., Zhang, T., Dani, J.A., 2004. Nicotinic cholinergic synaptic mechanisms in the ventral tegmental area contribute to nicotine addiction. Learn. Mem. 11, 60–69. https://doi.org/10.1101/lm.70004

Pietila, K., Laakso, I., Ahtee, L., 1995. Chronic oral nicotine administration affects the circadian rhythm of dopamine and 5-hydroxytryptamine metabolism in the striata of mice. Naunyn Schmiedebergs Arch. Pharmacol. 353, 110–115.

Preitner, N., Damiola, F., Lopez-Molina, L., Zakany, J., Duboule, D., Albrecht, U., Schibler, U., 2002. The orphan nuclear receptor REV-ERBalpha controls circadian transcription within the positive limb of the mammalian circadian oscillator. Cell 110, 251–260. https://doi.org/10.1016/s0092-8674(02)00825-5

Proulx, C.D., Hikosaka, O., Malinow, R., 2014. Reward processing by the lateral habenula in normal and depressive behaviors. Nat Neurosci 17, 1146–1152. https://doi.org/10.1038/nn.3779

Putker, M., Wong, D.C.S., Seinkmane, E., Rzechorzek, N.M., Zeng, A., Hoyle, N.P., Chesham, J.E., Edwards, M.D., Feeney, K.A., Fischer, R., Peschel, N., Chen, K.-F., Vanden Oever, M., Edgar, R.S., Selby, C.P., Sancar, A., O'Neill, J.S., 2021. CRYPTOCHROMES confer robustness, not rhythmicity, to circadian timekeeping. EMBO J 40, e106745. https://doi.org/10.15252/embj.2020106745

Qin, C., Luo, M., 2009. Neurochemical phenotypes of the afferent and efferent projections of the mouse medial habenula. Neuroscience 161, 827–837. https://doi.org/10.1016/j.neuroscience.2009.03.085

Quick, M.W., Ceballos, R.M., Kasten, M., McIntosh, J.M., Lester, R.A.J., 1999. α3β4 subunit-containing nicotinic receptors dominate function in rat medial habenula neurons. Neuropharmacology 38, 769–783. https://doi.org/10.1016/S0028-3908(99)00024-6

Ranft, K., Dobrowolny, H., Krell, D., Bielau, H., Bogerts, B., Bernstein, H.-G., 2010. Evidence for structural abnormalities of the human habenular complex in affective disorders but not in schizophrenia. Psychol Med 40, 557–567. https://doi.org/10.1017/S0033291709990821

Rawashdeh, O., Jilg, A., Maronde, E., Fahrenkrug, J., Stehle, J.H., 2016. Period1 gates the circadian modulation of memory-relevant signaling in mouse hippocampus by regulating the nuclear shuttling of the CREB kinase pP90RSK. Journal of Neurochemistry 138, 731–745. https://doi.org/10.1111/jnc.13689

Rawashdeh, O., Parsons, R., Maronde, E., 2018. Clocking In Time to Gate Memory Processes: The Circadian Clock Is Part of the Ins and Outs of Memory. Neural Plasticity 2018, e6238989. https://doi.org/10.1155/2018/6238989

Raymond, R.C., Warren, M., Morris, R.W., Leikin, J.B., 1992. Periodicity of presentations of drugs of abuse and overdose in an emergency department. J Toxicol Clin Toxicol 30, 467–478. https://doi.org/10.3109/15563659209021561

Reid, K.J., Abbott, S.M., 2015. Jet Lag and Shift Work Disorder. Sleep Med Clin 10, 523–535. https://doi.org/10.1016/j.jsmc.2015.08.006

Ren, J., Qin, C., Hu, F., Tan, J., Qiu, L., Zhao, S., Feng, G., Luo, M., 2011. Habenula "cholinergic" neurons co-release glutamate and acetylcholine and activate postsynaptic neurons via distinct transmission modes. Neuron 69, 445–452. https://doi.org/10.1016/j.neuron.2010.12.038

Ren, Z.-Y., Zhang, X.-L., Liu, Y., Zhao, L.-Y., Shi, J., Bao, Y., Zhang, X.Y., Kosten, T.R., Lu, L., 2009. Diurnal variation in cue-induced responses among protracted abstinent heroin users. Pharmacology Biochemistry and Behavior 91, 468–472. https://doi.org/10.1016/j.pbb.2008.08.023

Ripperger, J.A., Schibler, U., 2006. Rhythmic CLOCK-BMAL1 binding to multiple E-box motifs drives circadian Dbp transcription and chromatin transitions. Nat Genet 38, 369–374. https://doi.org/10.1038/ng1738

Rodgers, J., Bano-Otalora, B., Belle, M.D.C., Paul, S., Hughes, R., Wright, P., McDowell, R., Milosavljevic, N., Orlowska-Feuer, P., Martial, F.P., Wynne, J., Ballister, E.R., Storchi, R., Allen, A.E., Brown, T., Lucas, R.J., 2021. Using a bistable animal opsin for switchable and scalable optogenetic inhibition of neurons. EMBO Rep 22, e51866. https://doi.org/10.15252/embr.202051866

Rosenwasser, A.M., 2010. Circadian clock genes: non-circadian roles in sleep, addiction, and psychiatric disorders? Neurosci Biobehav Rev 34, 1249–1255. https://doi.org/10.1016/j.neubiorev.2010.03.004

Rusak, B., Bina, K.G., 1990. Neurotransmitters in the mammalian circadian system. Annu Rev Neurosci 13, 387–401. https://doi.org/10.1146/annurev.ne.13.030190.002131

Saccone, S.F., Hinrichs, A.L., Saccone, N.L., Chase, G.A., Konvicka, K., Madden, P.A.F., Breslau, N., Johnson, E.O., Hatsukami, D., Pomerleau, O., Swan, G.E., Goate, A.M., Rutter, J., Bertelsen, S., Fox, L., Fugman, D., Martin, N.G., Montgomery, G.W., Wang, J.C., Ballinger, D.G., Rice, J.P., Bierut, L.J., 2007. Cholinergic nicotinic receptor genes implicated in a nicotine dependence association study targeting 348 candidate genes with 3713 SNPs. Hum. Mol. Genet. 16, 36–49. https://doi.org/10.1093/hmg/ddl438

Sadacca, L.A., Lamia, K.A., deLemos, A.S., Blum, B., Weitz, C.J., 2011. An intrinsic circadian clock of the pancreas is required for normal insulin release and glucose homeostasis in mice. Diabetologia 54, 120–124. https://doi.org/10.1007/s00125-010-1920-8

Sakhi, K., Belle, M.D.C., Gossan, N., Delagrange, P., Piggins, H.D., 2014a. Daily variation in the electrophysiological activity of mouse medial habenula neurones. J Physiol 592, 587–603. https://doi.org/10.1113/jphysiol.2013.263319

Sakhi, K., Wegner, S., Belle, M.D.C., Howarth, M., Delagrange, P., Brown, T.M., Piggins, H.D., 2014b. Intrinsic and extrinsic cues regulate the daily profile of mouse lateral habenula neuronal activity. J Physiol 592, 5025–5045. https://doi.org/10.1113/jphysiol.2014.280065

Salaberry, N.L., Hamm, H., Felder-Schmittbuhl, M.-P., Mendoza, J., 2019. A suprachiasmatic-independent circadian clock(s) in the habenula is affected by Per gene mutations and housing light conditions in mice. Brain Struct Funct 224, 19–31. https://doi.org/10.1007/s00429-018-1756-4

Salaberry, N.L., Mendoza, J., 2015. Insights into the Role of the Habenular Circadian Clock in Addiction. Front Psychiatry 6, 179. https://doi.org/10.3389/fpsyt.2015.00179

Salas, R., Sturm, R., Boulter, J., De Biasi, M., 2009. Nicotinic receptors in the habenulo-interpeduncular system are necessary for nicotine withdrawal in mice. J. Neurosci. 29, 3014–3018. https://doi.org/10.1523/JNEUROSCI.4934-08.2009

Sartor, C.E., Lessov-Schlaggar, C.N., Scherrer, J.F., Bucholz, K.K., Madden, P.A.F., Pergadia, M.L., Grant, J.D., Jacob, T., Xian, H., 2010. Initial response to cigarettes predicts rate of progression to regular smoking: findings from an offspring-of-twins design. Addict Behav 35, 771–778. https://doi.org/10.1016/j.addbeh.2010.03.004

Sato, T., Kawamura, H., 1984. Circadian rhythms in multiple unit activity inside and outside the suprachiasmatic nucleus in the diurnal chipmunk (Eutamias sibiricus). Neurosci Res 1, 45–52. https://doi.org/10.1016/0168-0102(84)90029-4

Sato, T.K., Panda, S., Miraglia, L.J., Reyes, T.M., Rudic, R.D., McNamara, P., Naik, K.A., FitzGerald, G.A., Kay, S.A., Hogenesch, J.B., 2004. A Functional Genomics Strategy Reveals Rora as a Component of the Mammalian Circadian Clock. Neuron 43, 527–537. https://doi.org/10.1016/j.neuron.2004.07.018

Savitz, J.B., Nugent, A.C., Bogers, W., Roiser, J.P., Bain, E.E., Neumeister, A., Zarate, C.A., Manji, H.K., Cannon, D.M., Marrett, S., Henn, F., Charney, D.S., Drevets, W.C., 2011. Habenula

volume in bipolar disorder and major depressive disorder: a high-resolution magnetic resonance imaging study. Biol Psychiatry 69, 336–343. https://doi.org/10.1016/j.biopsych.2010.09.027

Schwartz, W.J., Klerman, E.B., 2019. Circadian Neurobiology and the Physiological Regulation of Sleep and Wakefulness. Neurol Clin 37, 475–486. https://doi.org/10.1016/j.ncl.2019.03.001

Schwartz, W.J., Reppert, S.M., Eagan, S.M., Moore-Ede, M.C., 1983. In vivo metabolic activity of the suprachiasmatic nuclei: a comparative study. Brain Res 274, 184–187. https://doi.org/10.1016/0006-8993(83)90538-3

Semm, P., Demaine, C., 1984. Electrophysiology of the pigeon's habenular nuclei: evidence for pineal connections and input from the visual system. Brain Res Bull 12, 115–121. https://doi.org/10.1016/0361-9230(84)90222-3

Shearman, L.P., Sriram, S., Weaver, D.R., Maywood, E.S., Chaves, I., Zheng, B., Kume, K., Lee, C.C., van der Horst, G.T., Hastings, M.H., Reppert, S.M., 2000. Interacting molecular loops in the mammalian circadian clock. Science 288, 1013–1019. https://doi.org/10.1126/science.288.5468.1013

Sheffield, E.B., Quick, M.W., Lester, R.A.J., 2000. Nicotinic acetylcholine receptor subunit mRNA expression and channel function in medial habenula neurons. Neuropharmacology 39, 2591–2603. https://doi.org/10.1016/S0028-3908(00)00138-6

Shelton, L., Becerra, L., Borsook, D., 2012. Unmasking the mysteries of the habenula in pain and analgesia. Prog. Neurobiol. 96, 208–219. https://doi.org/10.1016/j.pneurobio.2012.01.004

Shibata, H., Suzuki, T., Matsushita, M., 1986. Afferent projections to the interpeduncular nucleus in the rat, as studied by retrograde and anterograde transport of wheat germ agglutinin conjugated to horseradish peroxidase. J. Comp. Neurol. 248, 272–284. https://doi.org/10.1002/cne.902480210

Shieh, K.R., 2003. Distribution of the rhythm-related genes rPERIOD1, rPERIOD2, and rCLOCK, in the rat brain. Neuroscience 118, 831–843. https://doi.org/10.1016/S0306-4522(03)00004-6

Shiffman, S., Engberg, J.B., Paty, J.A., Perz, W.G., Gnys, M., Kassel, J.D., Hickcox, M., 1997. A day at a time: Predicting smoking lapse from daily urge. Journal of Abnormal Psychology 106, 104–116. https://doi.org/10.1037/0021-843X.106.1.104

Shih, P.-Y., Engle, S.E., Oh, G., Deshpande, P., Puskar, N.L., Lester, H.A., Drenan, R.M., 2014. Differential Expression and Function of Nicotinic Acetylcholine Receptors in Subdivisions of Medial Habenula. J Neurosci 34, 9789–9802. https://doi.org/10.1523/JNEUROSCI.0476-14.2014

Shrestha, P., Mousa, A., Heintz, N., 2015. Layer 2/3 pyramidal cells in the medial prefrontal cortex moderate stress induced depressive behaviors. Elife 4. https://doi.org/10.7554/eLife.08752

Shuboni, D.D., Cramm, S.L., Yan, L., Ramanathan, C., Cavanaugh, B.L., Nunez, A.A., Smale, L., 2015. Acute effects of light on the brain and behavior of diurnal Arvicanthis niloticus and nocturnal Mus musculus. Physiol Behav 138, 75–86. https://doi.org/10.1016/j.physbeh.2014.09.006

Shuboni-Mulligan, D.D., Cavanaugh, B.L., Tonson, A., Shapiro, E.M., Gall, A.J., 2019. Functional and anatomical variations in retinorecipient brain areas in Arvicanthis niloticus and Rattus norvegicus: Implications for the circadian and masking systems. Chronobiol Int 36, 1464–1481. https://doi.org/10.1080/07420528.2019.1651325

Shumkova, V., Sitdikova, V., Rechapov, I., Leukhin, A., Minlebaev, M., 2021. Effects of urethane and isoflurane on the sensory evoked response and local blood flow in the early postnatal rat somatosensory cortex. Sci Rep 11, 9567. https://doi.org/10.1038/s41598-021-88461-8

Sidor, M.M., Spencer, S.M., Dzirasa, K., Parekh, P.K., Tye, K.M., Warden, M.R., Arey, R.N., Enwright, J.F., Jacobsen, J.P.R., Kumar, S., Remillard, E.M., Caron, M.G., Deisseroth, K., McClung, C.A., 2015. Daytime spikes in dopaminergic activity drive rapid mood-cycling in mice. Mol. Psychiatry 20, 1406–1419. https://doi.org/10.1038/mp.2014.167

Siemann, J.K., Grueter, B.A., McMahon, D.G., 2021. Rhythms, Reward, and Blues: Consequences of Circadian Photoperiod on Affective and Reward Circuit Function. Neuroscience 457, 220–234. https://doi.org/10.1016/j.neuroscience.2020.12.010

Silman, I., Sussman, J.L., 2008. Acetylcholinesterase: how is structure related to function? Chem Biol Interact 175, 3–10. https://doi.org/10.1016/j.cbi.2008.05.035

Silver, R., LeSauter, J., Tresco, P.A., Lehman, M.N., 1996. A diffusible coupling signal from the transplanted suprachiasmatic nucleus controlling circadian locomotor rhythms. Nature 382, 810–813. https://doi.org/10.1038/382810a0

Simmons, M.A., Werkheiser, J.L., Hudzik, T.J., 2010. Acute nicotine and phencyclidine increase locomotor activity of the guinea pig with attenuated potencies relative to their effects on rat or mouse. Pharmacology Biochemistry and Behavior 94, 410–415. https://doi.org/10.1016/j.pbb.2009.10.002

Simons, D.J., Carvell, G.E., Hershey, A.E., Bryant, D.P., 1992. Responses of barrel cortex neurons in awake rats and effects of urethane anesthesia. Exp Brain Res 91, 259–272. https://doi.org/10.1007/BF00231659

Sjöholm, L.K., Kovanen, L., Saarikoski, S.T., Schalling, M., Lavebratt, C., Partonen, T., 2010. CLOCK is suggested to associate with comorbid alcohol use and depressive disorders. J Circadian Rhythms 8, 1. https://doi.org/10.1186/1740-3391-8-1

Ślimak, M.A., Ables, J.L., Frahm, S., Antolin-Fontes, B., Santos-Torres, J., Moretti, M., Gotti, C., Ibañez-Tallon, I., 2014. Habenular expression of rare missense variants of the β4 nicotinic receptor subunit alters nicotine consumption. Front Hum Neurosci 8, 12. https://doi.org/10.3389/fnhum.2014.00012

Smale, L., Nunez, A.A., Schwartz, M.D., 2008. Rhythms in a diurnal brain. Biological Rhythm Research 39, 305–318. https://doi.org/10.1080/09291010701682666

Smith, K.S., Bucci, D.J., Luikart, B.W., Mahler, S.V., 2016. DREADDs: Use and Application in Behavioral Neuroscience. Behav Neurosci 130, 137–155. https://doi.org/10.1037/bne0000135

Snider, K.H., Sullivan, K.A., Obrietan, K., 2018. Circadian Regulation of Hippocampal-Dependent Memory: Circuits, Synapses, and Molecular Mechanisms [WWW Document]. Neural Plasticity. https://doi.org/10.1155/2018/7292540

Soria-Gómez, E., Busquets-Garcia, A., Hu, F., Mehidi, A., Cannich, A., Roux, L., Louit, I., Alonso, L., Wiesner, T., Georges, F., Verrier, D., Vincent, P., Ferreira, G., Luo, M., Marsicano, G., 2015. Habenular CB1 Receptors Control the Expression of Aversive Memories. Neuron 88, 306–313. https://doi.org/10.1016/j.neuron.2015.08.035

Sorrenti, V., Cecchetto, C., Maschietto, M., Fortinguerra, S., Buriani, A., Vassanelli, S., 2021. Understanding the Effects of Anesthesia on Cortical Electrophysiological Recordings: A Scoping Review. Int J Mol Sci 22, 1286. https://doi.org/10.3390/ijms22031286

Souter, E.A., Chen, Y.-C., Zell, V., Lallai, V., Steinkellner, T., Conrad, W.S., Wisden, W., Harris, K.D., Fowler, C.D., Hnasko, T.S., 2021. Disruption of VGLUT1 in cholinergic medial habenula projections increases nicotine self-administration. eNeuro ENEURO.0481-21.2021. https://doi.org/10.1523/ENEURO.0481-21.2021

Sperlágh, B., Maglóczky, Z., Vizi, E.S., Freund, T.F., 1998. The triangular septal nucleus as the major source of ATP release in the rat habenula: a combined neurochemical and morphological study. Neuroscience 86, 1195–1207.

Stephan, F.K., Swann, J.M., Sisk, C.L., 1979. Anticipation of 24-hr feeding schedules in rats with lesions of the suprachiasmatic nucleus. Behav Neural Biol 25, 346–363. https://doi.org/10.1016/s0163-1047(79)90415-1

Stephenson-Jones, M., Floros, O., Robertson, B., Grillner, S., 2012. Evolutionary conservation of the habenular nuclei and their circuitry controlling the dopamine and 5-hydroxytryptophan (5-HT) systems. PNAS 109, E164–E173. https://doi.org/10.1073/pnas.1119348109

Stevens, V.L., Bierut, L.J., Talbot, J.T., Wang, J.C., Sun, J., Hinrichs, A.L., Thun, M.J., Goate, A., Calle, E.E., 2008. Nicotinic receptor gene variants influence susceptibility to heavy smoking. Cancer Epidemiol. Biomarkers Prev. 17, 3517–3525. https://doi.org/10.1158/1055-9965.EPI-08-0585

Stokkan, K.A., Yamazaki, S., Tei, H., Sakaki, Y., Menaker, M., 2001. Entrainment of the circadian clock in the liver by feeding. Science 291, 490–493. https://doi.org/10.1126/science.291.5503.490

Storch, K.-F., Paz, C., Signorovitch, J., Raviola, E., Pawlyk, B., Li, T., Weitz, C.J., 2007. Intrinsic circadian clock of the mammalian retina: importance for retinal processing of visual information. Cell 130, 730–741. https://doi.org/10.1016/j.cell.2007.06.045

Stratmann, M., Stadler, F., Tamanini, F., van der Horst, G.T.J., Ripperger, J.A., 2010. Flexible phase adjustment of circadian albumin D site-binding protein (DBP) gene expression by CRYPTOCHROME1. Genes Dev 24, 1317–1328. https://doi.org/10.1101/gad.578810

Strotmann, B., Heidemann, R.M., Anwander, A., Weiss, M., Trampel, R., Villringer, A., Turner, R., 2014. High-resolution MRI and diffusion-weighted imaging of the human habenula at 7 tesla. J Magn Reson Imaging 39, 1018–1026. https://doi.org/10.1002/jmri.24252

Strotmann, B., Kögler, C., Bazin, P.-L., Weiss, M., Villringer, A., Turner, R., 2013. Mapping of the internal structure of human habenula with ex vivo MRI at 7T. Front Hum Neurosci 7, 878. https://doi.org/10.3389/fnhum.2013.00878

Sun, L., Ma, J., Turck, C.W., Xu, P., Wang, G.-Z., 2020. Genome-wide circadian regulation: A unique system for computational biology. Computational and Structural Biotechnology Journal 18, 1914–1924. https://doi.org/10.1016/j.csbj.2020.07.002

Sutherland, R.J., 1982. The dorsal diencephalic conduction system: a review of the anatomy and functions of the habenular complex. Neurosci Biobehav Rev 6, 1–13.

Swanson, L.M., Burgess, H.J., Huntley, E.D., Bertram, H., Mooney, A., Zollars, J., Dopp, R., Hoffmann, R., Armitage, R., Todd Arnedt, J., 2017. Relationships between circadian measures, depression, and response to antidepressant treatment: A preliminary investigation. Psychiatry Research 252, 262–269. https://doi.org/10.1016/j.psychres.2017.03.010

Tahara, Y., Aoyama, S., Shibata, S., 2017. The mammalian circadian clock and its entrainment by stress and exercise. J Physiol Sci 67, 1–10. https://doi.org/10.1007/s12576-016-0450-7

Takagishi, M., Chiba, T., 1991. Efferent projections of the infralimbic (area 25) region of the medial prefrontal cortex in the rat: an anterograde tracer PHA-L study. Brain Res. 566, 26–39.

Takahashi, J.S., 2017. Transcriptional architecture of the mammalian circadian clock. Nat Rev Genet 18, 164–179. https://doi.org/10.1038/nrg.2016.150

Takahashi, J.S., Hong, H.-K., Ko, C.H., McDearmon, E.L., 2008. The genetics of mammalian circadian order and disorder: implications for physiology and disease. Nat Rev Genet 9, 764–775. https://doi.org/10.1038/nrg2430

Tamura, E.K., Oliveira-Silva, K.S., Ferreira-Moraes, F.A., Marinho, E.A.V., Guerrero-Vargas, N.N., 2021. Circadian rhythms and substance use disorders: A bidirectional relationship. Pharmacology Biochemistry and Behavior 201, 173105. https://doi.org/10.1016/j.pbb.2021.173105

Tasic, B., Yao, Z., Graybuck, L.T., Smith, K.A., Nguyen, T.N., Bertagnolli, D., Goldy, J., Garren, E., Economo, M.N., Viswanathan, S., Penn, O., Bakken, T., Menon, V., Miller, J., Fong, O., Hirokawa, K.E., Lathia, K., Rimorin, christine, Tieu, M., Larsen, R., casper, T., Barkan, E., Kroll, M., Parry, S., Shapovalova, N.V., Hirschstein, D., Pendergraft, J., Sullivan, H.A., Kim, T.K., Szafer, A., Dee, N., Groblewski, P., Wickersham, ian, cetin, A., Harris, J.A., Levi, B.P.,

Sunkin, S.M., Madisen, L., Daigle, T.L., Looger, L., Bernard, A., Phillips, J., Lein, E., Hawrylycz, M., Svoboda, K., Jones, A.R., Koch, christof, Zeng, H., 2018. Shared and distinct transcriptomic cell types across neocortical areas. Nature 563, 72–78. https://doi.org/10.1038/s41586-018-0654-5

Tavakoli-Nezhad, M., Schwartz, W.J., 2006. Hamsters running on time: is the lateral habenula a part of the clock? Chronobiol Int 23, 217–224. https://doi.org/10.1080/07420520500521947

Tavernier, R., Munroe, M., Willoughby, T., 2015. Perceived morningness-eveningness predicts academic adjustment and substance use across university, but social jetlag is not to blame. Chronobiol Int 32, 1233–1245. https://doi.org/10.3109/07420528.2015.1085062

Taylor, W.R., Smith, R.G., 2012. The role of starburst amacrine cells in visual signal processing. Vis Neurosci 29, 73–81. https://doi.org/10.1017/S0952523811000393

Tega, Y., Yamazaki, Y., Akanuma, S., Kubo, Y., Hosoya, K., 2018. Impact of Nicotine Transport across the Blood–Brain Barrier: Carrier-Mediated Transport of Nicotine and Interaction with Central Nervous System Drugs. Biological and Pharmaceutical Bulletin 41, 1330–1336. https://doi.org/10.1248/bpb.b18-00134

Teneggi, V., Tiffany, S.T., Squassante, L., Milleri, S., Ziviani, L., Bye, A., 2002. Smokers deprived of cigarettes for 72 h: effect of nicotine patches on craving and withdrawal. Psychopharmacology (Berl.) 164, 177–187. https://doi.org/10.1007/s00213-002-1176-1

Teplin, D., Raz, B., Daiter, J., Varenbut, M., Tyrrell, M., 2006. Screening for substance use patterns among patients referred for a variety of sleep complaints. Am J Drug Alcohol Abuse 32, 111–120. https://doi.org/10.1080/00952990500328695

Thorgeirsson, T.E., Geller, F., Sulem, P., Rafnar, T., Wiste, A., Magnusson, K.P., Manolescu, A., Thorleifsson, G., Stefansson, H., Ingason, A., Stacey, S.N., Bergthorsson, J.T., Thorlacius, S., Gudmundsson, J., Jonsson, T., Jakobsdottir, M., Saemundsdottir, J., Olafsdottir, O., Gudmundsson, L.J., Bjornsdottir, G., Kristjansson, K., Skuladottir, H., Isaksson, H.J., Gudbjartsson, T., Jones, G.T., Mueller, T., Gottsäter, A., Flex, A., Aben, K.K.H., de Vegt, F., Mulders, P.F.A., Isla, D., Vidal, M.J., Asin, L., Saez, B., Murillo, L., Blondal, T., Kolbeinsson, H., Stefansson, J.G., Hansdottir, I., Runarsdottir, V., Pola, R., Lindblad, B., van Rij, A.M., Dieplinger, B., Haltmayer, M., Mayordomo, J.I., Kiemeney, L.A., Matthiasson, S.E., Oskarsson, H., Tyrfingsson, T., Gudbjartsson, D.F., Gulcher, J.R., Jonsson, S., Thorsteinsdottir, U., Kong, A., Stefansson, K., 2008. A variant associated with nicotine dependence, lung cancer and peripheral arterial disease. Nature 452, 638–642. https://doi.org/10.1038/nature06846

Tsai, M., Byun, M.K., Shin, J., Crotty Alexander, L.E., 2020. Effects of e-cigarettes and vaping devices on cardiac and pulmonary physiology. J Physiol 598, 5039–5062. https://doi.org/10.1113/JP279754

Ueda, H.R., Hayashi, S., Chen, W., Sano, M., Machida, M., Shigeyoshi, Y., Iino, M., Hashimoto, S., 2005. System-level identification of transcriptional circuits underlying mammalian circadian clocks. Nat Genet 37, 187–192. https://doi.org/10.1038/ng1504

Ussher, M., West, R., 2003. Diurnal variations in first lapses to smoking for nicotine patch users. Hum Psychopharmacol 18, 345–349. https://doi.org/10.1002/hup.493

Valdez, P., 2019. Circadian Rhythms in Attention. Yale J Biol Med 92, 81–92.

Valdez, P., Ramírez, C., García, A., Talamantes, J., Armijo, P., Borrani, J., 2005. Circadian rhythms in components of attention. Biological Rhythm Research 36, 57–65. https://doi.org/10.1080/09291010400028633

van Amelsvoort, L.G.P.M., Jansen, N.W.H., Kant, Ij., 2006. Smoking among Shift Workers: More Than a Confounding Factor. Chronobiology International 23, 1105–1113. https://doi.org/10.1080/07420520601089539

Van Erum, J., Van Dam, D., De Deyn, P.P., 2019. Alzheimer's disease: Neurotransmitters of the sleep-wake cycle. Neuroscience & Biobehavioral Reviews 105, 72–80. https://doi.org/10.1016/j.neubiorev.2019.07.019

vanderLeest, H.T., Vansteensel, M.J., Duindam, H., Michel, S., Meijer, J.H., 2009. Phase of the Electrical Activity Rhythm in the Scn in Vitro Not Influenced by Preparation Time. Chronobiology International 26, 1075–1089. https://doi.org/10.3109/07420520903227746

Vansteensel, M.J., Yamazaki, S., Albus, H., Deboer, T., Block, G.D., Meijer, J.H., 2003. Dissociation between circadian Per1 and neuronal and behavioral rhythms following a shifted environmental cycle. Curr Biol 13, 1538–1542. https://doi.org/10.1016/s0960-9822(03)00560-8

Velasquez, K.M., Molfese, D.L., Salas, R., 2014. The role of the habenula in drug addiction. Front Hum Neurosci 8, 174. https://doi.org/10.3389/fnhum.2014.00174

Vescovi, P.P., Coiro, V., Volpi, R., Passeri, M., 1992. Diurnal variations in plasma ACTH, cortisol and beta-endorphin levels in cocaine addicts. Horm Res 37, 221–224. https://doi.org/10.1159/000182316

Villano, I., Messina, A., Valenzano, A., Moscatelli, F., Esposito, T., Monda, V., Esposito, M., Precenzano, F., Carotenuto, M., Viggiano, A., Chieffi, S., Cibelli, G., Monda, M., Messina, G., 2017. Basal Forebrain Cholinergic System and Orexin Neurons: Effects on Attention. Frontiers in Behavioral Neuroscience 11.

Viswanath, H., Carter, A.Q., Baldwin, P.R., Molfese, D.L., Salas, R., 2013. The medial habenula: still neglected. Front Hum Neurosci 7, 931. https://doi.org/10.3389/fnhum.2013.00931

Vitaterna, M.H., Takahashi, J.S., Turek, F.W., 2001. Overview of Circadian Rhythms. Alcohol Res Health 25, 85–93.

Wagner, F., French, L., Veh, R.W., 2016. Transcriptomic-anatomic analysis of the mouse habenula uncovers a high molecular heterogeneity among neurons in the lateral complex, while gene expression in the medial complex largely obeys subnuclear boundaries. Brain Struct Funct 221, 39–58. https://doi.org/10.1007/s00429-014-0891-9

Wagner, F., Stroh, T., Veh, R.W., 2014. Correlating habenular subnuclei in rat and mouse by using topographic, morphological, and cytochemical criteria. Journal of Comparative Neurology 522, 2650–2662. https://doi.org/10.1002/cne.23554

Wallace, M.L., Huang, K.W., Hochbaum, D., Hyun, M., Radeljic, G., Sabatini, B.L., 2020. Anatomical and single-cell transcriptional profiling of the murine habenular complex. eLife 9, e51271. https://doi.org/10.7554/eLife.51271

Wang, C., Guerriero, L.E., Huffman, D.M., Ajwad, A.A., Brooks, T.C., Sunderam, S., Seifert, A.W., O'Hara, B.F., 2020. A comparative study of sleep and diurnal patterns in house mouse (Mus musculus) and Spiny mouse (Acomys cahirinus). Sci Rep 10, 10944. https://doi.org/10.1038/s41598-020-67859-w

Wang, H.-L., Morales, M., 2009. Pedunculopontine and laterodorsal tegmental nuclei contain distinct populations of cholinergic, glutamatergic and GABAergic neurons in the rat. Eur. J. Neurosci. 29, 340–358. https://doi.org/10.1111/j.1460-9568.2008.06576.x

Wang, J., Lindstrom, J., 2018. Orthosteric and allosteric potentiation of heteromeric neuronal nicotinic acetylcholine receptors. Br J Pharmacol 175, 1805–1821. https://doi.org/10.1111/bph.13745

Wang, W., Wang, G.-Z., 2019. Understanding Molecular Mechanisms of the Brain Through Transcriptomics. Front Physiol 10, 214. https://doi.org/10.3389/fphys.2019.00214

Webb, I.C., Baltazar, R.M., Wang, X., Pitchers, K.K., Coolen, L.M., Lehman, M.N., 2009. Diurnal variations in natural and drug reward, mesolimbic tyrosine hydroxylase, and clock gene expression in the male rat. J. Biol. Rhythms 24, 465–476. https://doi.org/10.1177/0748730409346657

Webb, I.C., Lehman, M.N., Coolen, L.M., 2015. Diurnal and circadian regulation of reward-related neurophysiology and behavior. Physiol. Behav. 143, 58–69. https://doi.org/10.1016/j.physbeh.2015.02.034

Weber, P., Kula-Eversole, E., Pyza, E., 2009. Circadian Control of Dendrite Morphology in the Visual System of Drosophila melanogaster. PLOS ONE 4, e4290. https://doi.org/10.1371/journal.pone.0004290

Weiss, R.B., Baker, T.B., Cannon, D.S., von Niederhausern, A., Dunn, D.M., Matsunami, N., Singh, N.A., Baird, L., Coon, H., McMahon, W.M., Piper, M.E., Fiore, M.C., Scholand, M.B., Connett, J.E., Kanner, R.E., Gahring, L.C., Rogers, S.W., Hoidal, J.R., Leppert, M.F., 2008. A candidate gene approach identifies the CHRNA5-A3-B4 region as a risk factor for age-dependent nicotine addiction. PLoS Genet. 4, e1000125. https://doi.org/10.1371/journal.pgen.1000125

Wen, S., Ma, D., Zhao, M., Xie, L., Wu, Q., Gou, L., Zhu, C., Fan, Y., Wang, H., Yan, J., 2020. Spatiotemporal single-cell analysis of gene expression in the mouse suprachiasmatic nucleus. Nat Neurosci 23, 456–467. https://doi.org/10.1038/s41593-020-0586-x

West, R.J., Hajek, P., Belcher, M., 1989. Severity of withdrawal symptoms as a predictor of outcome of an attempt to quit smoking. Psychol Med 19, 981–985.

Whitton, A.E., Mehta, M., Ironside, M.L., Murray, G., Pizzagalli, D.A., 2018. Evidence of a diurnal rhythm in implicit reward learning. Chronobiology International 35, 1104–1114. https://doi.org/10.1080/07420528.2018.1459662

Williams, R.L., Soliman, K.F., Mizinga, K.M., 1993. Circadian variation in tolerance to the hypothermic action of CNS drugs. Pharmacol. Biochem. Behav. 46, 283–288.

Wills, L., Kenny, P.J., 2021. Addiction-related neuroadaptations following chronic nicotine exposure. J Neurochem 157, 1652–1673. https://doi.org/10.1111/jnc.15356

Wittenberg, R.E., Wolfman, S.L., De Biasi, M., Dani, J.A., 2020. Nicotinic acetylcholine receptors and nicotine addiction: A brief introduction. Neuropharmacology 177, 108256. https://doi.org/10.1016/j.neuropharm.2020.108256

Wittmann, M., Dinich, J., Merrow, M., Roenneberg, T., 2006. Social Jetlag: Misalignment of Biological and Social Time. Chronobiology International 23, 497–509. https://doi.org/10.1080/07420520500545979

Wolfman, S.L., Gill, D.F., Bogdanic, F., Long, K., Al-Hasani, R., McCall, J.G., Bruchas, M.R., McGehee, D.S., 2018. Nicotine aversion is mediated by GABAergic interpeduncular nucleus inputs to laterodorsal tegmentum. Nat Commun 9, 2710. https://doi.org/10.1038/s41467-018-04654-2

Wonnacott, S., 1997. Presynaptic nicotinic ACh receptors. Trends in Neurosciences 20, 92–98. https://doi.org/10.1016/S0166-2236(96)10073-4

World Health Organization, 2021. Tobacco Fact Sheet [WWW Document]. URL https://www.who.int/news-room/fact-sheets/detail/tobacco (accessed 8.18.21).

World Health Organization, 2019. WHO global report on trends in prevalence of tobacco use 2000-2025, third edition, 3rd ed. WHO, Geneva.

Wu, G., Ruben, M.D., Lee, Y., Li, J., Hughes, M.E., Hogenesch, J.B., 2020. Genome-wide studies of time of day in the brain: Design and analysis. Brain Science Advances 6, 92–105. https://doi.org/10.26599/BSA.2020.9050005

Xia, L., Nygard, S.K., Sobczak, G.G., Hourguettes, N.J., Bruchas, M.R., 2017. Dorsal-CA1 Hippocampal Neuronal Ensembles Encode Nicotine-Reward Contextual Associations. Cell Rep 19, 2143–2156. https://doi.org/10.1016/j.celrep.2017.05.047

Xu, C., Sun, Y., Cai, X., You, T., Zhao, Hongzhe, Li, Y., Zhao, Hua, 2018. Medial Habenula-Interpeduncular Nucleus Circuit Contributes to Anhedonia-Like Behavior in a Rat Model of Depression. Frontiers in Behavioral Neuroscience 12, 238. https://doi.org/10.3389/fnbeh.2018.00238

Xu, Z., Feng, Z., Zhao, M., Sun, Q., Deng, L., Jia, X., Jiang, T., Luo, P., Chen, W., Tudi, A., Yuan, J., Li, X., Gong, H., Luo, Q., Li, A., 2021. Whole-brain connectivity atlas of glutamatergic and GABAergic neurons in the mouse dorsal and median raphe nuclei. eLife 10, e65502. https://doi.org/10.7554/eLife.65502

Yamaguchi, T., Danjo, T., Pastan, I., Hikida, T., Nakanishi, S., 2013. Distinct Roles of Segregated Transmission of the Septo-Habenular Pathway in Anxiety and Fear. Neuron 78, 537–544. https://doi.org/10.1016/j.neuron.2013.02.035

Yamakawa, G.R., Basu, P., Cortese, F., MacDonnell, J., Whalley, D., Smith, V.M., Antle, M.C., 2016. The cholinergic forebrain arousal system acts directly on the circadian pacemaker. Proc Natl Acad Sci U S A 113, 13498–13503. https://doi.org/10.1073/pnas.1610342113

Yamamoto, S., Shigeyoshi, Y., Ishida, Y., Fukuyama, T., Yamaguchi, S., Yagita, K., Moriya, T., Shibata, S., Takashima, N., Okamura, H., 2001. Expression of the Per1 gene in the hamster: brain atlas and circadian characteristics in the suprachiasmatic nucleus. J. Comp. Neurol. 430, 518–532.

Yamazaki, S., Kerbeshian, M.C., Hocker, C.G., Block, G.D., Menaker, M., 1998. Rhythmic Properties of the Hamster Suprachiasmatic NucleusIn Vivo. J. Neurosci. 18, 10709–10723. https://doi.org/10.1523/JNEUROSCI.18-24-10709.1998

Yan, L., Smale, L., Nunez, A.A., 2018. Circadian and photic modulation of daily rhythms in diurnal mammals. Eur J Neurosci 10.1111/ejn.14172. https://doi.org/10.1111/ejn.14172

Yang, J.-J., Wang, Y.-T., Cheng, P.-C., Kuo, Y.-J., Huang, R.-C., 2010. Cholinergic modulation of neuronal excitability in the rat suprachiasmatic nucleus. J. Neurophysiol. 103, 1397–1409. https://doi.org/10.1152/jn.00877.2009

Yang, Y., Xu, T., Zhang, Y., Qin, X., 2017. Molecular basis for the regulation of the circadian clock kinases CK1δ and CK1ε. Cellular Signalling 31, 58–65. https://doi.org/10.1016/j.cellsig.2016.12.010

Yao, Y., Xu, Y., Cai, Z., Liu, Q., Ma, Y., Li, A.N., Payne, T.J., Li, M.D., 2021. Determination of shared genetic etiology and possible causal relations between tobacco smoking and depression. Psychological Medicine 51, 1870–1879. https://doi.org/10.1017/S003329172000063X

Zatz, M., Brownstein, M.J., 1979. Intraventricular carbachol mimics the effects of light on the circadian rhythm in the rat pineal gland. Science 203, 358–361. https://doi.org/10.1126/science.32619

Zhang, B., Gao, Y., Li, Y., Yang, J., Zhao, H., 2016. Sleep Deprivation Influences Circadian Gene Expression in the Lateral Habenula [WWW Document]. Behavioural Neurology. https://doi.org/10.1155/2016/7919534

Zhang, E.E., Liu, Y., Dentin, R., Pongsawakul, P.Y., Liu, A.C., Hirota, T., Nusinow, D.A., Sun, X., Landais, S., Kodama, Y., Brenner, D.A., Montminy, M., Kay, S.A., 2010. Cryptochrome mediates circadian regulation of cAMP signaling and hepatic gluconeogenesis. Nat Med 16, 1152–1156. https://doi.org/10.1038/nm.2214

Zhang, G.-W., Shen, L., Zhong, W., Xiong, Y., Zhang, L.I., Tao, H.W., 2018. Transforming Sensory Cues into Aversive Emotion via Septal-Habenular Pathway. Neuron 99, 1016-1028.e5. https://doi.org/10.1016/j.neuron.2018.07.023

Zhang, J., Tan, L., Ren, Y., Liang, J., Lin, R., Feng, Q., Zhou, J., Hu, F., Ren, J., Wei, C., Yu, T., Zhuang, Y., Bettler, B., Wang, F., Luo, M., 2016. Presynaptic Excitation via GABAB Receptors in Habenula Cholinergic Neurons Regulates Fear Memory Expression. Cell 166, 716–728. https://doi.org/10.1016/j.cell.2016.06.026

Zhang, R., Lahens, N.F., Ballance, H.I., Hughes, M.E., Hogenesch, J.B., 2014. A circadian gene expression atlas in mammals: implications for biology and medicine. Proc Natl Acad Sci U S A 111, 16219–16224. https://doi.org/10.1073/pnas.1408886111

Zhang, T., Zhang, L., Liang, Y., Siapas, A.G., Zhou, F.-M., Dani, J.A., 2009. Dopamine signaling differences in the nucleus accumbens and dorsal striatum exploited by nicotine. J. Neurosci. 29, 4035–4043. https://doi.org/10.1523/JNEUROSCI.0261-09.2009

Zhao, H., Rusak, B., 2005. Circadian firing-rate rhythms and light responses of rat habenular nucleus neurons in vivo and in vitro. Neuroscience 132, 519–528. https://doi.org/10.1016/j.neuroscience.2005.01.012

Zhao, Z., Xu, H., Liu, Y., Mu, L., Xiao, J., Zhao, H., 2015. Diurnal Expression of the Per2 Gene and Protein in the Lateral Habenular Nucleus. Int J Mol Sci 16, 16740–16749. https://doi.org/10.3390/ijms160816740

Zhao-Shea, R., DeGroot, S.R., Liu, L., Vallaster, M., Pang, X., Su, Q., Gao, G., Rando, O.J., Martin, G.E., George, O., Gardner, P.D., Tapper, A.R., 2015. Increased CRF signalling in a ventral tegmental area-interpeduncular nucleus-medial habenula circuit induces anxiety during nicotine withdrawal. Nat Commun 6, 6770. https://doi.org/10.1038/ncomms7770

Zhao-Shea, R., Liu, L., Pang, X., Gardner, P.D., Tapper, A.R., 2013. Activation of GABAergic neurons in the interpeduncular nucleus triggers physical nicotine withdrawal symptoms. Curr. Biol. 23, 2327–2335. https://doi.org/10.1016/j.cub.2013.09.041

Zhu, H., Aryal, D.K., Olsen, R.H.J., Urban, D.J., Swearingen, A., Forbes, S., Roth, B.L., Hochgeschwender, U., 2016. Cre dependent DREADD (Designer Receptors Exclusively Activated by Designer Drugs) mice. Genesis 54, 439–446. https://doi.org/10.1002/dvg.22949

Zoli, M., Pistillo, F., Gotti, C., 2015. Diversity of native nicotinic receptor subtypes in mammalian brain. Neuropharmacology 96, 302–311. https://doi.org/10.1016/j.neuropharm.2014.11.003

Zoli, M., Pucci, S., Vilella, A., Gotti, C., 2018. Neuronal and Extraneuronal Nicotinic Acetylcholine Receptors. Curr Neuropharmacol 16, 338–349. https://doi.org/10.2174/1570159X15666170912110450

8 Appendix: Tables from Chapter 5

Table 8.1 MHb genes classified as rhythmic using diffCircadian.

Rank	Gene symbol	Entrez Gene Name	Location	peakTime	R^2	pvalue
1	Rhoq	ras homolog family member Q	Plasma Membrane	15.86	0.82	5.67E-06
2	Spock3	SPARC (osteonectin), cwcv and kazal like domains proteoglycan 3	Extracellular Space	13.71	0.74	7.62E-05
3	Akap8	A-kinase anchoring protein 8	Nucleus	15.17	0.63	0.000922
4	Pfdn6	prefoldin subunit 6	Cytoplasm	17.35	0.61	0.001288
5	Rtca	RNA 3'-terminal phosphate cyclase	Nucleus	20.92	0.61	0.001379
6	Gpatch11	G-patch domain containing 11	Nucleus	15.53	0.60	0.00169
7	Camkmt	calmodulin-lysine N-methyltransferase	Nucleus	22.28	0.59	0.002038
8	Zfp799	zinc finger protein 799	Other	20.33	0.58	0.00215
9	Gm45051	NA	NA	15.98	0.58	0.002304
10	Hdac5	histone deacetylase 5	Nucleus	13.08	0.58	0.002354
11	Hopx	HOP homeobox	Nucleus	16.81	0.57	0.002807
12	Astn2	astrotactin 2	Cytoplasm	7.16	0.56	0.002999
13	Avl9	AVL9 cell migration associated	Other	17.99	0.55	0.003951
14	Stard7	StAR related lipid transfer domain containing 7	Cytoplasm	17.40	0.55	0.004026
15	Enpp4	ectonucleotide pyrophosphatase/phosphodiesterase 4	Cytoplasm	20.60	0.54	0.004321
16	0610010K14Rik	chromosome 17 open reading frame 49	Nucleus	21.54	0.54	0.004338
17	Cacna1d	calcium voltage-gated channel subunit alpha1 D	Plasma Membrane	7.20	0.54	0.00434
18	Cuta	cutA divalent cation tolerance homolog	Cytoplasm	15.84	0.54	0.004343
19	Nova1	NOVA alternative splicing regulator 1	Nucleus	2.26	0.54	0.004552
20	Btbd1	BTB domain containing 1	Cytoplasm	19.72	0.53	0.004793
21	Vav3	vav guanine nucleotide exchange factor 3	Extracellular Space	11.22	0.53	0.005054
22	St7	suppression of tumorigenicity 7	Other	22.16	0.53	0.005347
23	Psme3	proteasome activator subunit 3	Cytoplasm	20.80	0.52	0.005786
24	Magi3	membrane associated guanylate kinase, WW and PDZ domain containing 3	Cytoplasm	0.58	0.52	0.005811
25	Gm36529	predicted gene, 36529	Other	23.51	0.52	0.006293
26	Ubap2l	ubiquitin-associated protein 2-like	Nucleus	15.40	0.52	0.006298
27	Exoc7	exocyst complex component 7	Cytoplasm	11.39	0.52	0.006302
28	Cdip1	cell death inducing p53 target 1	Nucleus	0.51	0.51	0.006334
29	Emg1	EMG1 N1-specific pseudouridine methyltransferase	Nucleus	10.79	0.51	0.006662
30	Sfxn3	sideroflexin 3	Cytoplasm	11.00	0.51	0.006732
31	Trpc4	transient receptor potential cation channel subfamily C member 4	Plasma Membrane	11.27	0.50	0.007705
32	Vps45	vacuolar protein sorting 45 homolog	Cytoplasm	12.37	0.50	0.007725
33	Arhgef9	Cdc42 guanine nucleotide exchange factor 9	Cytoplasm	18.25	0.50	0.007779
34	Mxd4	MAX dimerization protein 4	Nucleus	15.39	0.50	0.007912
35	Mpi	mannose phosphate isomerase	Cytoplasm	13.48	0.50	0.008263

36	Ino80d	INO80 complex subunit D	Nucleus	5.76	0.50	0.008278
37	Ppp1r11	protein phosphatase 1 regulatory inhibitor subunit 11	Cytoplasm	17.98	0.49	0.008422
38	Hspa5	heat shock protein family A (Hsp70) member 5	Cytoplasm	18.75	0.49	0.008506
39	Ilrun	inflammation and lipid regulator with UBA-like and NBR1-like domains	Cytoplasm	20.67	0.49	0.008538
40	Higd1a	HIG1 hypoxia inducible domain family member 1A	Cytoplasm	21.58	0.49	0.008703
41	Appl2	adaptor protein, phosphotyrosine interacting with PH domain and leucine zipper 2	Cytoplasm	19.33	0.49	0.008854
42	Acadm	acyl-CoA dehydrogenase medium chain	Cytoplasm	15.39	0.49	0.009034
43	Arhgap12	Rho GTPase activating protein 12	Cytoplasm	19.25	0.49	0.00914
44	Taf1	TATA-box binding protein associated factor 1	Nucleus	23.85	0.49	0.009382
45	Syt15	synaptotagmin 15	Cytoplasm	8.83	0.48	0.009617
46	Mrps6	mitochondrial ribosomal protein S6	Cytoplasm	12.13	0.48	0.009639
47	Pdpk1	3-phosphoinositide dependent protein kinase 1	Cytoplasm	15.57	0.48	0.01004
48	Miga1	mitoguardin 1	Plasma Membrane	13.52	0.48	0.010166
49	Nr1d2	nuclear receptor subfamily 1 group D member 2	Nucleus	15.47	0.48	0.010227
50	Ly6e	lymphocyte antigen 6 family member E	Plasma Membrane	21.14	0.48	0.010561
51	Vta1	vesicle trafficking 1	Cytoplasm	21.98	0.48	0.010621
52	Acsl1	acyl-CoA synthetase long chain family member 1	Cytoplasm	11.14	0.48	0.010626
53	Msantd4	Myb/SANT DNA binding domain containing 4 with coiled-coils	Nucleus	16.80	0.48	0.01082
54	Trip12	thyroid hormone receptor interactor 12	Cytoplasm	13.09	0.48	0.010932
55	Rprd2	regulation of nuclear pre-mRNA domain containing 2	Nucleus	9.09	0.47	0.011383
56	Cul2	cullin 2	Nucleus	22.23	0.46	0.012612
57	Shtn1	shootin 1	Plasma Membrane	23.96	0.46	0.012794
58	Rida	reactive intermediate imine deaminase A homolog	Cytoplasm	20.62	0.46	0.012902
59	Clasp1	cytoplasmic linker associated protein 1	Cytoplasm	8.50	0.46	0.012927
60	Ube2k	ubiquitin conjugating enzyme E2 K	Cytoplasm	12.61	0.46	0.013017
61	Dph7	diphthamide biosynthesis 7	Cytoplasm	20.34	0.46	0.013047
62	Rab5a	RAB5A, member RAS oncogene family	Cytoplasm	16.43	0.46	0.013333
63	Tmcc3	transmembrane and coiled-coil domain family 3	Cytoplasm	22.43	0.46	0.013676
64	Ptar1	protein prenyltransferase alpha subunit repeat containing 1	Other	13.74	0.46	0.013725
65	Mrps15	mitochondrial ribosomal protein S15	Cytoplasm	17.30	0.46	0.013767
66	Eif3m	eukaryotic translation initiation factor 3 subunit M	Cytoplasm	13.77	0.46	0.014262
67	Gm5577	predicted gene 5577	Other	7.31	0.46	0.014275
68	Soga3	SOGA family member 3	Other	14.85	0.45	0.01436
69	Brms1l	BRMS1 like transcriptional repressor	Other	14.37	0.45	0.014381
70	Lyar	Ly1 antibody reactive	Plasma Membrane	22.67	0.45	0.014528
71	Mtch1	mitochondrial carrier 1	Cytoplasm	17.46	0.45	0.014609
72	Snx14	sorting nexin 14	Cytoplasm	14.99	0.45	0.014615
73	Cript	CXXC repeat containing interactor of PDZ3 domain	Cytoplasm	22.21	0.45	0.015045
74	Vamp1	vesicle associated membrane protein 1	Cytoplasm	6.58	0.45	0.01549
75	Klhl22	kelch like family member 22	Cytoplasm	12.87	0.45	0.015513

76	Dhx15	DEAH-box helicase 15	Nucleus	14.93	0.45	0.015575
77	Ccdc82	coiled-coil domain containing 82	Other	16.17	0.45	0.01559
78	Actr3	actin related protein 3	Plasma Membrane	14.89	0.45	0.015779
79	Dnai4	dynein axonemal intermediate chain 4	Cytoplasm	17.39	0.45	0.016006
80	Hspb6	heat shock protein family B (small) member 6	Cytoplasm	19.84	0.45	0.016032
81	Cmas	cytidine monophosphate N-acetylneuraminic acid synthetase	Nucleus	12.63	0.44	0.016287
82	Zfp637	zinc finger protein 32	Nucleus	0.27	0.44	0.016606
83	Scn3b	sodium voltage-gated channel beta subunit 3	Plasma Membrane	14.66	0.44	0.016753
84	Arpc2	actin related protein 2/3 complex subunit 2	Cytoplasm	21.68	0.44	0.016765
85	Pcmtd1	protein-L-isoaspartate (D-aspartate) O-methyltransferase domain containing 1	Cytoplasm	14.29	0.44	0.017342
86	Npcd	neuronal pentraxin chromo domain	Plasma Membrane	18.90	0.44	0.017417
87	Lyrm2	LYR motif containing 2	Cytoplasm	1.93	0.44	0.01791
88	Faim2	Fas apoptotic inhibitory molecule 2	Plasma Membrane	21.31	0.44	0.018025
89	Hacd1	3-hydroxyacyl-CoA dehydratase 1	Cytoplasm	19.01	0.44	0.018058
90	Irs2	insulin receptor substrate 2	Cytoplasm	20.17	0.44	0.018137
91	Mpp5	protein associated with LIN7 1, MAGUK family member	Plasma Membrane	17.46	0.43	0.018384
92	Cd2ap	CD2 associated protein	Cytoplasm	18.55	0.43	0.018523
93	Dusp11	dual specificity phosphatase 11	Nucleus	12.43	0.43	0.018675
94	Gm20390	NA	NA	20.12	0.43	0.018722
95	Magohb	mago homolog B, exon junction complex subunit	Nucleus	14.20	0.43	0.019012
96	Gm4525	ribosomal protein S27 pseudogene	Other	18.82	0.43	0.019014
97	Rimklb	ribosomal modification protein rimK like family member B	Cytoplasm	5.96	0.43	0.019461
98	Kash5	KASH domain containing 5	Nucleus	4.79	0.43	0.019775
99	Znhit2	zinc finger HIT-type containing 2	Other	17.33	0.43	0.019963
100	Sf3b5	splicing factor 3b subunit 5	Nucleus	19.46	0.43	0.020085
101	Ptprn	protein tyrosine phosphatase receptor type N	Plasma Membrane	15.22	0.43	0.020209
102	Acox1	acyl-CoA oxidase 1	Cytoplasm	11.22	0.43	0.020218
103	Ufsp2	UFM1 specific peptidase 2	Other	14.28	0.43	0.020252
104	Golga4	golgin A4	Cytoplasm	19.83	0.43	0.020692
105	Tsn	translin	Nucleus	4.33	0.43	0.020706
106	P2ry12	purinergic receptor P2Y12	Plasma Membrane	19.59	0.42	0.021006
107	Ubr5	ubiquitin protein ligase E3 component n-recognin 5	Nucleus	13.11	0.42	0.021157
108	Ptrh2	peptidyl-tRNA hydrolase 2	Cytoplasm	9.84	0.42	0.021218
109	Ywhaq	tyrosine 3-monooxygenase/tryptophan 5-monooxygenase activation protein theta	Cytoplasm	19.25	0.42	0.021257
110	Foxj1	forkhead box J1	Nucleus	22.01	0.42	0.021268
111	Tceal3	transcription elongation factor A like 6	Other	23.50	0.42	0.021321
112	Rnf103	ring finger protein 103	Cytoplasm	12.61	0.42	0.021345
113	Podxl2	podocalyxin like 2	Plasma Membrane	16.71	0.42	0.021437
114	Kif5c	kinesin family member 5C	Cytoplasm	16.06	0.42	0.021496
115	Dnaja4	DnaJ heat shock protein family (Hsp40) member A4	Nucleus	20.39	0.42	0.021505

116	Stim1	stromal interaction molecule 1	Plasma Membrane	8.63	0.42	0.021516
117	Nsf	N-ethylmaleimide sensitive factor, vesicle fusing ATPase	Cytoplasm	10.67	0.42	0.021682
118	Fam131a	family with sequence similarity 131 member A	Other	21.09	0.42	0.021684
119	Timm50	translocase of inner mitochondrial membrane 50	Cytoplasm	17.88	0.42	0.021878
120	Dnttip1	deoxynucleotidyltransferase terminal interacting protein 1	Nucleus	0.82	0.42	0.02188
121	Glcci1	glucocorticoid induced 1	Cytoplasm	11.91	0.42	0.021934
122	Synj1	synaptojanin 1	Cytoplasm	13.90	0.42	0.021994
123	Fnta	farnesyltransferase, CAAX box, alpha	Cytoplasm	18.11	0.42	0.022244
124	Sucla2	succinate-CoA ligase ADP-forming subunit beta	Cytoplasm	16.62	0.42	0.02263
125	Zfp704	zinc finger protein 704	Nucleus	19.35	0.42	0.022805
126	Cav2	caveolin 2	Plasma Membrane	19.66	0.42	0.022817
127	Eif4ebp2	eukaryotic translation initiation factor 4E binding protein 2	Cytoplasm	20.73	0.42	0.023044
128	Stx5a	syntaxin 5	Cytoplasm	16.80	0.42	0.023337
129	Fndc9	fibronectin type III domain containing 9	Other	8.25	0.41	0.023559
130	Banf1	BAF nuclear assembly factor 1	Nucleus	21.06	0.41	0.023739
131	Otud7a	OTU deubiquitinase 7A	Cytoplasm	16.67	0.41	0.023807
132	Arpc5l	actin related protein 2/3 complex subunit 5 like	Cytoplasm	23.06	0.41	0.023925
133	Scg3	secretogranin III	Extracellular Space	14.00	0.41	0.023957
134	Chic2	cysteine rich hydrophobic domain 2	Plasma Membrane	1.91	0.41	0.024455
135	Zcchc24	zinc finger CCHC-type containing 24	Other	17.51	0.41	0.024637
136	Frmd5	FERM domain containing 5	Plasma Membrane	22.70	0.41	0.024637
137	Abr	ABR activator of RhoGEF and GTPase	Cytoplasm	14.39	0.41	0.024794
138	Commd10	COMM domain containing 10	Nucleus	4.04	0.41	0.025048
139	Amn1	antagonist of mitotic exit network 1 homolog	Plasma Membrane	15.62	0.41	0.025104
140	Nrg3os	neuregulin 3, opposite strand	Other	7.25	0.41	0.02516
141	Czib	CXXC motif containing zinc binding protein	Cytoplasm	14.75	0.41	0.025265
142	Cept1	choline/ethanolamine phosphotransferase 1	Cytoplasm	14.28	0.41	0.025283
143	Sox11	SRY-box transcription factor 11	Nucleus	4.18	0.41	0.025286
144	Mpdz	multiple PDZ domain crumbs cell polarity complex component	Plasma Membrane	18.73	0.41	0.025698
145	Gm10421	predicted gene 10421	Other	22.29	0.41	0.025745
146	Manf	mesencephalic astrocyte derived neurotrophic factor	Extracellular Space	20.38	0.41	0.025764
147	Stip1	stress induced phosphoprotein 1	Cytoplasm	14.19	0.41	0.025819
148	Smarcd1	SWI/SNF related, matrix associated, actin dependent regulator of chromatin, subfamily d, member 1	Nucleus	15.14	0.41	0.026158
149	Rtf1	RTF1 homolog, Paf1/RNA polymerase II complex component	Nucleus	5.65	0.41	0.02636
150	Kcnn2	potassium intermediate/small conductance calcium-activated channel, subfamily N, member 2	Plasma Membrane	12.54	0.40	0.026518
151	Pigq	phosphatidylinositol glycan anchor biosynthesis class Q	Cytoplasm	14.78	0.40	0.026716
152	Cnnm2	cyclin and CBS domain divalent metal cation transport mediator 2	Plasma Membrane	10.76	0.40	0.026762
153	Pfn2	profilin 2	Cytoplasm	16.78	0.40	0.026926
154	Spata7	spermatogenesis associated 7	Cytoplasm	20.57	0.40	0.027148

155	Gabpa	GA binding protein transcription factor subunit alpha	Nucleus	20.51	0.40	0.02716
156	Ythdf3	YTH N6-methyladenosine RNA binding protein 3	Cytoplasm	13.92	0.40	0.0272
157	Frg1	FSHD region gene 1	Nucleus	6.67	0.40	0.027485
158	Npdc1	neural proliferation, differentiation and control 1	Extracellular Space	19.81	0.40	0.027539
159	Snrpg	small nuclear ribonucleoprotein polypeptide G	Nucleus	12.76	0.40	0.027708
160	Rars2	arginyl-tRNA synthetase 2, mitochondrial	Cytoplasm	16.68	0.40	0.027796
161	Arl6ip6	ADP ribosylation factor like GTPase 6 interacting protein 6	Nucleus	3.21	0.40	0.027965
162	Dhx30	DExH-box helicase 30	Nucleus	14.72	0.40	0.028182
163	Wdfy2	WD repeat and FYVE domain containing 2	Cytoplasm	6.06	0.40	0.028273
164	Pde4dip	phosphodiesterase 4D interacting protein	Cytoplasm	12.76	0.40	0.028289
165	Nolc1	nucleolar and coiled-body phosphoprotein 1	Nucleus	1.43	0.40	0.02841
166	Adgrv1	adhesion G protein-coupled receptor V1	Plasma Membrane	14.71	0.40	0.029001
167	Pex2	peroxisomal biogenesis factor 2	Cytoplasm	19.33	0.40	0.029098
168	Tiprl	TOR signaling pathway regulator	Cytoplasm	13.26	0.40	0.029182
169	Dalrd3	DALR anticodon binding domain containing 3	Other	21.05	0.40	0.029438
170	Lrif1	ligand dependent nuclear receptor interacting factor 1	Nucleus	2.64	0.40	0.029481
171	Dtd1	D-aminoacyl-tRNA deacylase 1	Cytoplasm	1.21	0.40	0.029537
172	Usp33	ubiquitin specific peptidase 33	Cytoplasm	14.62	0.40	0.029542
173	Fuz	fuzzy planar cell polarity protein	Plasma Membrane	18.03	0.40	0.029645
174	Srpr	SRP receptor subunit alpha	Cytoplasm	18.96	0.39	0.029923
175	Frs2	fibroblast growth factor receptor substrate 2	Plasma Membrane	20.48	0.39	0.029955
176	Tubgcp5	tubulin gamma complex associated protein 5	Cytoplasm	12.00	0.39	0.030055
177	Ap1m1	adaptor related protein complex 1 subunit mu 1	Cytoplasm	17.10	0.39	0.030093
178	Amy1	amylase alpha 2A	Extracellular Space	13.37	0.39	0.030165
179	Rbm8a	RNA binding motif protein 8A	Nucleus	0.90	0.39	0.030202
180	Gm43112	NA	NA	11.27	0.39	0.03033
181	Trmt10b	tRNA methyltransferase 10B	Cytoplasm	23.75	0.39	0.030643
182	Gm14325	zinc finger protein 442	Nucleus	17.44	0.39	0.030717
183	Mrpl20	mitochondrial ribosomal protein L20	Cytoplasm	19.33	0.39	0.030927
184	Jam3	junctional adhesion molecule 3	Plasma Membrane	21.74	0.39	0.031074
185	Lamtor4	late endosomal/lysosomal adaptor, MAPK and MTOR activator 4	Cytoplasm	14.47	0.39	0.031131
186	Gm6563	SAP domain containing ribonucleoprotein pseudogene	Other	20.02	0.39	0.031242
187	Coil	coilin	Nucleus	13.67	0.39	0.031467
188	Sar1b	secretion associated Ras related GTPase 1B	Cytoplasm	19.30	0.39	0.031566
189	Mydgf	myeloid derived growth factor	Extracellular Space	1.06	0.39	0.031852
190	Clic4	chloride intracellular channel 4	Plasma Membrane	18.77	0.39	0.031907
191	Sf3b2	splicing factor 3b subunit 2	Nucleus	5.69	0.39	0.031935
192	Pcp4l1	Purkinje cell protein 4-like 1	Other	5.40	0.39	0.032304
193	Paip2b	poly(A) binding protein interacting protein 2B	Other	14.09	0.39	0.032389
194	Clpb	caseinolytic mitochondrial matrix peptidase chaperone subunit B	Nucleus	21.98	0.39	0.032479

195	Pcsk1	proprotein convertase subtilisin/kexin type 1	Cytoplasm	15.02	0.39	0.0325
196	Ormdl2	ORMDL sphingolipid biosynthesis regulator 2	Cytoplasm	19.42	0.39	0.032724
197	Rpl8	ribosomal protein L8	Cytoplasm	16.73	0.39	0.032804
198	Rnf13	ring finger protein 13	Cytoplasm	15.23	0.39	0.032947
199	Enah	ENAH actin regulator	Plasma Membrane	16.17	0.39	0.032962
200	Mcrip1	MAPK regulated corepressor interacting protein 1	Nucleus	20.65	0.39	0.033086
201	Zmym4	zinc finger MYM-type containing 4	Nucleus	22.82	0.39	0.033256
202	Saxo2	stabilizer of axonemal microtubules 2	Nucleus	14.67	0.38	0.033413
203	Rnf150	ring finger protein 150	Other	21.58	0.38	0.033507
204	Zfyve1	zinc finger FYVE-type containing 1	Cytoplasm	17.77	0.38	0.033624
205	Upp2	uridine phosphorylase 2	Cytoplasm	5.96	0.38	0.033687
206	Krt10	keratin 10	Cytoplasm	14.67	0.38	0.033696
207	Fam234b	family with sequence similarity 234 member B	Other	9.23	0.38	0.034123
208	Gm26418		Other	17.41	0.38	0.034362
209	Rbm18	RNA binding motif protein 18	Other	18.15	0.38	0.034365
210	Gatd3a	glutamine amidotransferase like class 1 domain containing 3A	Cytoplasm	15.51	0.38	0.034373
211	Rgcc	regulator of cell cycle	Cytoplasm	17.39	0.38	0.034614
212	Babam1	BRISC and BRCA1 A complex member 1	Nucleus	20.56	0.38	0.034717
213	Adgrl1	adhesion G protein-coupled receptor L1	Plasma Membrane	23.93	0.38	0.034743
214	Aamdc	adipogenesis associated Mth938 domain containing	Cytoplasm	11.11	0.38	0.034917
215	Mrpl15	mitochondrial ribosomal protein L15	Cytoplasm	21.90	0.38	0.03514
216	2310057M21Rik	chromosome 10 open reading frame 88	Other	19.84	0.38	0.035171
217	Map2k1	mitogen-activated protein kinase kinase 1	Cytoplasm	15.60	0.38	0.035249
218	Wdr18	WD repeat domain 18	Nucleus	17.23	0.38	0.03536
219	Rap1a	RAP1A, member of RAS oncogene family	Cytoplasm	20.81	0.38	0.035377
220	Kcnb2	potassium voltage-gated channel subfamily B member 2	Plasma Membrane	9.98	0.38	0.03542
221	Serf2	small EDRK-rich factor 2	Other	15.60	0.38	0.03543
222	Rpl18	ribosomal protein L18	Cytoplasm	17.51	0.38	0.035526
223	Arl4c	ADP ribosylation factor like GTPase 4C	Nucleus	14.87	0.38	0.035541
224	Acyp1	acylphosphatase 1	Cytoplasm	20.17	0.38	0.03561
225	Pdzd4	PDZ domain containing 4	Cytoplasm	1.60	0.38	0.035704
226	Eipr1	EARP complex and GARP complex interacting protein 1	Cytoplasm	18.69	0.38	0.035714
227	Gfap	glial fibrillary acidic protein	Cytoplasm	23.09	0.38	0.035721
228	Sf3b6	splicing factor 3b subunit 6	Nucleus	20.44	0.38	0.035897
229	Atp11b	ATPase phospholipid transporting 11B (putative)	Plasma Membrane	18.72	0.38	0.035913
230	Spcs1	signal peptidase complex subunit 1	Cytoplasm	17.11	0.38	0.036085
231	1500009C09Rik	long intergenic non-protein coding RNA 634	Other	22.94	0.38	0.03651
232	Tsc22d2	TSC22 domain family member 2	Nucleus	4.05	0.38	0.036686
233	Mapk9	mitogen-activated protein kinase 9	Cytoplasm	18.22	0.38	0.036697
234	Bin1	bridging integrator 1	Nucleus	14.66	0.38	0.036884
235	Zfp740		Other	17.35	0.38	0.036916
236	Fam216a	family with sequence similarity 216 member A	Other	16.41	0.38	0.037026

237	Ciao2a	cytosolic iron-sulfur assembly component 2A	Extracellular Space	15.91	0.38	0.037151
238	Arrb2	arrestin beta 2	Cytoplasm	19.57	0.37	0.037314
239	Tsr2	TSR2 ribosome maturation factor	Other	23.43	0.37	0.037402
240	Uba52	ubiquitin A-52 residue ribosomal protein fusion product 1	Cytoplasm	16.08	0.37	0.037413
241	Fgfr1op2	FGFR1 oncogene partner 2	Cytoplasm	12.13	0.37	0.03748
242	Peli1	pellino E3 ubiquitin protein ligase 1	Cytoplasm	0.37	0.37	0.037577
243	Abhd11os	abhydrolase domain containing 11, opposite strand	Other	18.93	0.37	0.038184
244	Vmp1	vacuole membrane protein 1	Plasma Membrane	16.48	0.37	0.039227
245	Prdx5	peroxiredoxin 5	Cytoplasm	15.49	0.37	0.039316
246	Ncdn	neurochondrin	Cytoplasm	15.43	0.37	0.039514
247	Megf9	multiple EGF like domains 9	Extracellular Space	17.59	0.37	0.039525
248	Gm15258	NA	NA	3.45	0.37	0.039731
249	Ap3m2	adaptor related protein complex 3 subunit mu 2	Cytoplasm	5.02	0.37	0.039762
250	Oga	O-GlcNAcase	Cytoplasm	15.54	0.37	0.039877
251	Aldh7a1	aldehyde dehydrogenase 7 family member A1	Cytoplasm	4.52	0.37	0.039912
252	Exoc6b	exocyst complex component 6B	Other	19.66	0.37	0.039919
253	Magi2	membrane associated guanylate kinase, WW and PDZ domain containing 2	Plasma Membrane	10.13	0.37	0.039932
254	Casc3	CASC3 exon junction complex subunit	Nucleus	19.63	0.37	0.03996
255	Rnf214	ring finger protein 214	Other	9.66	0.37	0.040047
256	Babam2	BRISC and BRCA1 A complex member 2	Cytoplasm	16.62	0.37	0.040118
257	Zfyve16	zinc finger FYVE-type containing 16	Nucleus	21.14	0.37	0.040791
258	Enc1	ectodermal-neural cortex 1	Nucleus	18.65	0.37	0.040844
259	Pi4ka	phosphatidylinositol 4-kinase alpha	Cytoplasm	3.58	0.37	0.041009
260	Rps14	ribosomal protein S14	Cytoplasm	18.48	0.37	0.041304
261	Zfas1	zinc finger, NFX1-type containing 1, antisense RNA 1	Other	22.97	0.37	0.041438
262	Hnmt	histamine N-methyltransferase	Cytoplasm	23.73	0.37	0.041441
263	Snx29	sorting nexin 29	Cytoplasm	9.95	0.37	0.041495
264	Stmn4	stathmin 4	Cytoplasm	17.92	0.36	0.041633
265	Robo3	roundabout guidance receptor 3	Plasma Membrane	20.27	0.36	0.041743
266	Tmem258	transmembrane protein 258	Cytoplasm	19.57	0.36	0.04177
267	Psma1	proteasome 20S subunit alpha 1	Cytoplasm	13.77	0.36	0.042302
268	2310011J03Rik	chromosome 19 open reading frame 25	Other	13.38	0.36	0.042482
269	Fancm	FA complementation group M	Nucleus	11.31	0.36	0.042623
270	Phkb	phosphorylase kinase regulatory subunit beta	Cytoplasm	12.33	0.36	0.042956
271	Socs7	suppressor of cytokine signaling 7	Cytoplasm	19.99	0.36	0.04299
272	Eml4	EMAP like 4	Cytoplasm	23.04	0.36	0.043057
273	Ncapd3	non-SMC condensin II complex subunit D3	Nucleus	17.18	0.36	0.043095
274	Hsph1	heat shock protein family H (Hsp110) member 1	Cytoplasm	18.91	0.36	0.043173
275	Snx13	sorting nexin 13	Cytoplasm	22.11	0.36	0.043377
276	Tnrc6c	trinucleotide repeat containing adaptor 6C	Cytoplasm	5.75	0.36	0.043741
277	Spg21	SPG21 abhydrolase domain containing, maspardin	Plasma Membrane	21.03	0.36	0.043911
278	Tlcd2	TLC domain containing 2	Plasma Membrane	6.34	0.36	0.043942

279	Hint1	histidine triad nucleotide binding protein 1	Nucleus	16.59	0.36	0.044089
280	U2af1	U2 small nuclear ribonucleoprotein auxiliary factor (U2AF) 1	Nucleus	19.16	0.36	0.044336
281	Catspere2	catsper channel auxiliary subunit epsilon	Extracellular Space	7.77	0.36	0.044393
282	Lrrfip1	LRR binding FLII interacting protein 1	Cytoplasm	17.00	0.36	0.044403
283	Gpn1	GPN-loop GTPase 1	Nucleus	19.52	0.36	0.044507
284	Ndufs7	NADH:ubiquinone oxidoreductase core subunit S7	Cytoplasm	18.07	0.36	0.044696
285	Lpcat1	lysophosphatidylcholine acyltransferase 1	Cytoplasm	23.02	0.36	0.044883
286	Rora	RAR related orphan receptor A	Nucleus	20.54	0.36	0.044894
287	Rab4b	RAB4B, member RAS oncogene family	Plasma Membrane	18.31	0.36	0.044928
288	Gmds	GDP-mannose 4,6-dehydratase	Cytoplasm	15.33	0.36	0.044934
289	Map7d1	MAP7 domain containing 1	Cytoplasm	13.82	0.36	0.044974
290	Top2b	DNA topoisomerase II beta	Nucleus	14.10	0.36	0.045015
291	Rps5	ribosomal protein S5	Cytoplasm	18.49	0.36	0.045074
292	Btbd7	BTB domain containing 7	Nucleus	12.47	0.36	0.045199
293	Ptcd3	pentatricopeptide repeat domain 3	Cytoplasm	16.12	0.36	0.045297
294	Rpl39	ribosomal protein L39	Cytoplasm	18.24	0.36	0.04535
295	Prxl2c	peroxiredoxin like 2C	Other	8.49	0.36	0.045355
296	Serpini1	serpin family I member 1	Extracellular Space	21.79	0.36	0.045393
297	Hsd17b12	hydroxysteroid 17-beta dehydrogenase 12	Cytoplasm	6.37	0.36	0.045502
298	Rock2	Rho associated coiled-coil containing protein kinase 2	Cytoplasm	8.01	0.36	0.04566
299	Cep162	centrosomal protein 162	Nucleus	13.66	0.36	0.045735
300	Ppia	peptidylprolyl isomerase A	Cytoplasm	17.07	0.36	0.045982
301	Uimc1	ubiquitin interaction motif containing 1	Nucleus	7.75	0.36	0.04605
302	Morf4l1	mortality factor 4 like 1	Nucleus	5.36	0.36	0.046275
303	Ndufb4	NADH:ubiquinone oxidoreductase subunit B4	Cytoplasm	19.02	0.36	0.046357
304	Pou2f2	POU class 2 homeobox 2	Nucleus	6.37	0.36	0.046368
305	Obi1	ORC ubiquitin ligase 1	Nucleus	8.06	0.35	0.047189
306	Sacm1l	SAC1 like phosphatidylinositide phosphatase	Cytoplasm	20.88	0.35	0.047233
307	Camk1	calcium/calmodulin dependent protein kinase I	Cytoplasm	17.20	0.35	0.047295
308	Luc7l3	LUC7 like 3 pre-mRNA splicing factor	Nucleus	4.62	0.35	0.047296
309	Dync1i1	dynein cytoplasmic 1 intermediate chain 1	Cytoplasm	16.22	0.35	0.047348
310	Cenpx	centromere protein X	Nucleus	18.64	0.35	0.047385
311	Cx3cr1	C-X3-C motif chemokine receptor 1	Plasma Membrane	22.69	0.35	0.047494
312	Crppa	CDP-L-ribitol pyrophosphorylase A	Cytoplasm	7.72	0.35	0.047873
313	Pard3b	par-3 family cell polarity regulator beta	Plasma Membrane	10.92	0.35	0.048161
314	Terf2ip	TERF2 interacting protein	Nucleus	16.41	0.35	0.048339
315	Usp14	ubiquitin specific peptidase 14	Cytoplasm	13.84	0.35	0.048418
316	Ncbp2	nuclear cap binding protein subunit 2	Nucleus	8.11	0.35	0.048424
317	Ranbp6	RAN binding protein 6	Cytoplasm	15.06	0.35	0.048503
318	Ankrd46	ankyrin repeat domain 46	Nucleus	17.95	0.35	0.048825
319	Dbp	D-box binding PAR bZIP transcription factor	Nucleus	11.15	0.35	0.049075
320	Psmc5	proteasome 26S subunit, ATPase 5	Nucleus	18.70	0.35	0.049169

321	Gm27021	predicted gene, 27021	Other	20.81	0.35	0.049409
322	Rpe	ribulose-5-phosphate-3-epimerase	Cytoplasm	16.97	0.35	0.049439
323	Ap3s2	adaptor related protein complex 3 subunit sigma 2	Cytoplasm	22.60	0.35	0.049532
324	Apip	APAF1 interacting protein	Cytoplasm	22.63	0.35	0.049555
325	Zic1	Zic family member 1	Nucleus	19.87	0.35	0.049566
326	Relch	RAB11 binding and LisH domain, coiled-coil and HEAT repeat containing	Cytoplasm	5.72	0.35	0.049589
327	Mrpl39	mitochondrial ribosomal protein L39	Cytoplasm	20.61	0.35	0.049691
328	Cck	cholecystokinin	Extracellular Space	17.63	0.35	0.049739
329	Gm15773	PC4 and SFRS1 interacting protein 1 pseudogene	Other	4.71	0.35	0.049746
330	Tmie	transmembrane inner ear	Plasma Membrane	8.17	0.35	0.049819

Table 8.2 Canonical pathways enriched in day-peaking rhythmic MHb genes

Ingenuity Canonical Pathways	-log(p value)	-log(BH p value)	Ratio	Molecules
Ethanol Degradation IV	2.6	0.654	0.0833	ACSL1,ALDH7A1
Ethanol Degradation II	2.3	0.654	0.0588	ACSL1,ALDH7A1
Choline Degradation I	2.21	0.654	0.5	ALDH7A1
Ephrin A Signaling	2.02	0.654	0.0426	ROCK2,VAV3
Spliceosomal Cycle	1.99	0.654	0.0408	RBM8A,SF3B2
Acetate Conversion to Acetyl-CoA	1.91	0.654	0.25	ACSL1
Oxidative Ethanol Degradation III	1.88	0.654	0.0357	ACSL1,ALDH7A1
Lysine Degradation II	1.81	0.654	0.2	ALDH7A1
Lysine Degradation V	1.81	0.654	0.2	ALDH7A1
Ephrin B Signaling	1.67	0.561	0.0278	ROCK2,VAV3
Role of BRCA1 in DNA Damage Response	1.59	0.517	0.025	FANCM,UIMC1
Neurovascular Coupling Signaling Pathway	1.48	0.445	0.0133	CACNA1D,ROCK2,STIM1
Fatty Acid Activation	1.34	0.409	0.0667	ACSL1
LPS/IL-1 Mediated Inhibition of RXR Function	1.34	0.409	0.0118	ACOX1,ACSL1,ALDH7A1

Table 8.3 Canonical pathways enriched night-peaking rhythmic MHb genes

Ingenuity Canonical Pathways	-log(p value)	-log(BH p value)	Ratio	Molecules
EIF2 Signaling	4.04	1.59	0.0446	EIF3M, HSPA5, MAP2K1, PDPK1, RAP1A, RPL18, RPL39, RPL8, RPS14, RPS5
Clathrin-mediated Endocytosis Signaling	3.83	1.59	0.0466	ACTR3, AP1M1, ARPC2, ARPC5L, ARRB2, CD2AP, RAB4B, RAB5A, SYNJ1
Reelin Signaling in Neurons	3.55	1.49	0.0556	ACTR3, ARHGEF9, ARPC2, ARPC5L, MAP2K1, MAPK9, RAP1A
Insulin Receptor Signaling	3.27	1.36	0.05	IRS2, MAP2K1, PDPK1, PPP1R11, RAP1A, RHOQ, SYNJ1
IGF-1 Signaling	3.2	1.36	0.0577	IRS2, MAP2K1, PDPK1, RAP1A, SOCS7, YWHAQ
GDNF Family Ligand-Receptor Interactions	3	1.24	0.0658	FRS2, IRS2, MAP2K1, MAPK9, RAP1A
Spliceosomal Cycle	2.84	1.14	0.0816	CASC3, DHX15, MAGOHB, SF3B6
Protein Ubiquitination Pathway	2.73	1.09	0.0327	CUL2, HSPA5, HSPB6, HSPH1, PSMA1, PSMC5, UBE2K, USP14, USP33
Regulation of eIF4 and p70S6K Signaling	2.66	1.07	0.0391	EIF3M, EIF4EBP2, MAP2K1, PDPK1, RAP1A, RPS14, RPS5
Actin Nucleation by ARP-WASP Complex	2.61	1.07	0.0538	ACTR3, ARPC2, ARPC5L, RAP1A, RHOQ
NRF2-mediated Oxidative Stress Response	2.56	1.06	0.0338	DNAJA4, ENC1, MAP2K1, MAPK9, RAP1A, STIP1, UBE2K, USP14
Telomerase Signaling	2.35	0.907	0.0467	HDAC5, MAP2K1, PDPK1, RAP1A, TERF2IP
Remodeling of Epithelial Adherens Junctions	2.32	0.907	0.0588	ACTR3, ARPC2, ARPC5L, RAB5A
mTOR Signaling	2.25	0.907	0.033	EIF3M, EIF4EBP2, PDPK1, RAP1A, RHOQ, RPS14, RPS5
Integrin Signaling	2.24	0.907	0.0329	ACTR3, ARPC2, ARPC5L, MAP2K1, PFN2, RAP1A, RHOQ
Signaling by Rho Family GTPases	2.24	0.907	0.0299	ACTR3, ARHGEF9, ARPC2, ARPC5L, GFAP, MAP2K1, MAPK9, RHOQ
Regulation of Actin-based Motility by Rho	2.2	0.907	0.0431	ACTR3, ARPC2, ARPC5L, PFN2, RHOQ
Fc Epsilon RI Signaling	2.17	0.907	0.0424	MAP2K1, MAPK9, PDPK1, RAP1A, SYNJ1
Cholecystokinin/Gastrin-mediated Signaling	2.16	0.907	0.042	CCK, MAP2K1, MAPK9, RAP1A, RHOQ
Neurotrophin/TRK Signaling	2.15	0.907	0.0526	FRS2, MAP2K1, PDPK1, RAP1A
RHOA Signaling	2.09	0.876	0.0403	ACTR3, ARHGAP12, ARPC2, ARPC5L, PFN2
Colanic Acid Building Blocks Biosynthesis	2.08	0.876	0.143	GMDS, MPI
14-3-3-mediated Signaling	2.04	0.86	0.0394	GFAP, MAP2K1, MAPK9, RAP1A, YWHAQ
BAG2 Signaling Pathway	2	0.86	0.0476	HSPA5, PSMA1, PSMC5, PSME3
D-mannose Degradation	2	0.86	1	MPI
fMLP Signaling in Neutrophils	1.99	0.86	0.0382	ACTR3, ARPC2, ARPC5L, MAP2K1, RAP1A
Prolactin Signaling	1.96	0.851	0.0465	MAP2K1, PDPK1, RAP1A, SOCS7
RAC Signaling	1.9	0.801	0.0362	ACTR3, ARPC2, ARPC5L, MAP2K1, RAP1A

Cell Cycle: G2/M DNA Damage Checkpoint Regulation	1.86	0.793	0.06	TOP2B, TRIP12, YWHAQ
UVC-Induced MAPK Signaling	1.84	0.793	0.0588	MAP2K1, MAPK9, RAP1A
ERBB Signaling	1.83	0.793	0.0426	MAP2K1, MAPK9, PDPK1, RAP1A
Non-Small Cell Lung Cancer Signaling	1.83	0.793	0.0426	HDAC5, MAP2K1, PDPK1, RAP1A
FAT10 Signaling Pathway	1.73	0.712	0.0536	PSMA1, PSMC5, PSME3
GDP-L-fucose Biosynthesis I (from GDP-D-mannose)	1.7	0.712	0.5	GMDS
S-methyl-5-thio-?-D-ribose 1-phosphate Degradation	1.7	0.712	0.5	APIP
Thrombin Signaling	1.7	0.712	0.0283	ARHGEF9, CAMK1, MAP2K1, PDPK1, RAP1A, RHOQ
Epithelial Adherens Junction Signaling	1.68	0.712	0.0318	ACTR3, ARPC2, ARPC5L, RAP1A, YWHAQ
RHOGDI Signaling	1.67	0.712	0.0279	ACTR3, ARHGAP12, ARHGEF9, ARPC2, ARPC5L, RHOQ
Protein Kinase A Signaling	1.66	0.712	0.0221	AKAP8, DUSP11, MAP2K1, PHKB, PPP1R11, PTPRN, RAP1A, TIMM50, YWHAQ
Endometrial Cancer Signaling	1.65	0.712	0.05	MAP2K1, PDPK1, RAP1A
Huntington's Disease Signaling	1.63	0.701	0.0249	HDAC5, HSPA5, MAPK9, PDPK1, PSMA1, PSMC5, PSME3
Aldosterone Signaling in Epithelial Cells	1.61	0.688	0.0305	HSPA5, HSPB6, HSPH1, MAP2K1, PDPK1
Thrombopoietin Signaling	1.6	0.688	0.0476	IRS2, MAP2K1, RAP1A
Prostate Cancer Signaling	1.58	0.684	0.0357	HDAC5, MAP2K1, PDPK1, RAP1A
CDK5 Signaling	1.56	0.678	0.0351	MAP2K1, MAPK9, PPP1R11, RAP1A
ERB2-ERBB3 Signaling	1.56	0.678	0.0462	MAP2K1, PDPK1, RAP1A
Germ Cell-Sertoli Cell Junction Signaling	1.54	0.668	0.0292	MAP2K1, MAPK9, PDPK1, RAP1A, RHOQ
ERBB4 Signaling	1.51	0.658	0.0441	MAP2K1, PDPK1, RAP1A
NGF Signaling	1.51	0.658	0.0339	MAP2K1, MAPK9, PDPK1, RAP1A
Agrin Interactions at Neuromuscular Junction	1.48	0.638	0.0429	GABPA, MAPK9, RAP1A
D-myo-inositol (1, 4, 5, 6)-Tetrakisphosphate Biosynthesis	1.47	0.638	0.0279	DUSP11, PPP1R11, PTPRN, SACM1L, SYNJ1
D-myo-inositol (3, 4, 5, 6)-tetrakisphosphate Biosynthesis	1.47	0.638	0.0279	DUSP11, PPP1R11, PTPRN, SACM1L, SYNJ1
Glioma Signaling	1.44	0.625	0.0323	CAMK1, HDAC5, MAP2K1, RAP1A
Actin Cytoskeleton Signaling	1.43	0.622	0.0245	ACTR3, ARPC2, ARPC5L, MAP2K1, PFN2, RAP1A
Acute Phase Response Signaling	1.41	0.613	0.027	MAP2K1, MAPK9, PDPK1, RAP1A, SOCS7
3-phosphoinositide Degradation	1.36	0.613	0.0262	DUSP11, PPP1R11, PTPRN, SACM1L, SYNJ1
p70S6K Signaling	1.36	0.613	0.0303	MAP2K1, PDPK1, RAP1A, YWHAQ
Production of Nitric Oxide and Reactive Oxygen Species in Macrophages	1.36	0.613	0.0262	MAP2K1, MAPK9, PPP1R11, RAP1A, RHOQ
Thyroid Cancer Signaling	1.35	0.613	0.038	IRS2, MAP2K1, RAP1A
4-1BB Signaling in T Lymphocytes	1.34	0.613	0.0588	MAP2K1, MAPK9
Chemokine Signaling	1.34	0.613	0.0375	CAMK1, MAP2K1, RAP1A
FLT3 Signaling in Hematopoietic Progenitor Cells	1.34	0.613	0.0375	MAP2K1, PDPK1, RAP1A
Renal Cell Carcinoma Signaling	1.34	0.613	0.0375	CUL2, MAP2K1, RAP1A
Role of BRCA1 in DNA Damage Response	1.34	0.613	0.0375	BABAM1, BABAM2, SMARCD1

Role of JAK2 in Hormone-like Cytokine Signaling	1.34	0.613	0.0588	IRS2, SOCS7
D-myo-inositol-5-phosphate Metabolism	1.33	0.613	0.0256	DUSP11, PPP1R11, PTPRN, SACM1L, SYNJ1
STAT3 Pathway	1.33	0.613	0.0296	MAP2K1, MAPK9, RAP1A, SOCS7
CMP-N-acetylneuraminate Biosynthesis I (Eukaryotes)	1.31	0.611	0.2	CMAS
JAK/STAT Signaling	1.31	0.611	0.0366	MAP2K1, RAP1A, SOCS7
Role of MAPK Signaling in the Pathogenesis of Influenza	1.31	0.611	0.0366	MAP2K1, MAPK9, RAP1A
PI3K/AKT Signaling	1.3	0.609	0.0251	MAP2K1, PDPK1, RAP1A, SYNJ1, YWHAQ

Table 8.4 Upstream regulators associated with day-peaking rhythmic MHb genes

Upstream Regulator	Molecule Type	-log(p value)	-log(BH p value)	molecule count	Target molecules in dataset
EHHADH	enzyme	2.950782	0.744727	2	ACOX1, ACSL1
UBD	other	2.89279	0.744727	2	ACOX1, ACSL1
METRNL	other	2.838632	0.744727	2	ACOX1, ACSL1
linalool	chemical - endogenous non-mammalian	2.655608	0.744727	2	ACOX1, ACSL1
mono-(2-ethylhexyl)phthalate	chemical toxicant	2.653647	0.744727	4	ACOX1, ACSL1, PTRH2, ROCK2
HSD17B4	enzyme	2.50307	0.744727	2	ACOX1, ACSL1
PROCR	other	2.437707	0.744727	2	PELI1, ROCK2
elaidic acid	chemical - endogenous mammalian	2.428291	0.744727	3	ACOX1, ACSL1, HSD17B12
tributyltin	chemical reagent	2.053057	0.619789	3	ACOX1, ACSL1, ROCK2
SLC27A2	transporter	2.041914	0.619789	2	ACOX1, ACSL1
GBX2	transcription regulator	2.041914	0.619789	2	ACSL1, KCNB2
ATN1	transcription regulator	1.9914	0.619789	3	DBP, SOX11, VAMP1
fish oils	chemical drug	1.917215	0.619789	2	ACOX1, ACSL1
ACOX1	enzyme	1.896196	0.619789	3	ACOX1, ACSL1, UPP2
KLF15	transcription regulator	1.835647	0.610834	2	ACOX1, ACSL1
Calmodulin	group	1.764472	0.610834	2	NSF, VAMP1
IL4R	transmembrane receptor	1.737549	0.610834	2	ACOX1, ACSL1
PNPLA2	enzyme	1.688246	0.610834	2	ACOX1, ACSL1
miR-21-5p (and other miRNAs w/seed AGCUUAU)	mature microRNA	1.640165	0.610834	2	GLCCI1, PELI1
RIPK2	kinase	1.628932	0.610834	2	ACOX1, ACSL1
RXRB	ligand-dependent nuclear receptor	1.605548	0.610834	2	ACOX1, ACSL1
topotecan	chemical drug	1.595166	0.610834	3	ACSL1, ASTN2, PARD3B
HNF4A	transcription regulator	1.573489	0.610834	13	AAMDC, ACOX1, ACSL1, CHIC2, DBP, EMG1, NCBP2, NSF, PARD3B, STIM1, TSN, VAMP1, WDFY2
ARNTL	transcription regulator	1.562249	0.605548	2	ACOX1, DBP
beta-estradiol	chemical - endogenous mammalian	1.464706	0.578396	14	ACOX1, ACSL1, ALDH7A1, CACNA1D, EMG1, HSD17B12, MAGI2, Pcp4l1, SFXN3, SOX11, TMIE, TSC22D2, VAMP1, VAV3
isobutylmethylxanthine	chemical toxicant	1.437707	0.576754	3	ACOX1, ACSL1, ROCK2
G protein alpha	group	1.395774	0.576754	2	HSD17B12, LYRM2
bezafibrate	chemical drug	1.379864	0.576754	2	ACOX1, ACSL1
TO-901317	chemical reagent	1.342944	0.576754	3	ACOX1, ACSL1, HSD17B12
PSEN2	peptidase	1.332547	0.576754	2	ACSL1, DBP
MMP3	peptidase	1.310691	0.576754	2	NCBP2, RBM8A

Table 8.5 Upstream regulators associated with night-peaking rhythmic MHb genes

Upstream Regulator	Molecule Type	-log(p value)	-log(BH p value)	molecule count	Target molecules in dataset
HNF4A	transcription regulator	5.517126	2.305395	46	ACTR3, AP1M1, APIP, ARL4C, CCDC82, CLPB, CRIPT, CUL2, CZIB, DUSP11, EIF4EBP2, ENC1, FAIM2, FAM216A, FUZ, GABPA, GATD3A/GATD3B, GMDS, GOLGA4, HSPA5, HSPH1, MRPL15, MRPS15, OGA, ORMDL2, PDE4DIP, PFDN6, PFN2, PHKB, PPP1R11, PRDX5, PSMA1, PSME3, PTPRN, RBM18, ROBO3, RORA, RPL18, RTCA, SF3B5, SRPRA, STARD7, SUCLA2, TERF2IP, TMEM258, VMP1
GABA	chemical - endogenous mammalian	3.198596	0.455932	13	ACADM, CEPT1, HSPA5, LPCAT1, MAPK9, NDUFB4, PDPK1, RPL18, RPL39, Snrpg, SUCLA2, Uba52, YWHAQ
sirolimus	chemical drug	3.116339	0.455932	16	ACADM, CX3CR1, HDAC5, HSPA5, IRS2, PDPK1, PEX2, PPIA, PRDX5, PSME3, RHOQ, RPL18, RPL8, RPS14, RPS5, VMP1
RICTOR	other	3.007446	0.455932	10	IRS2, NDUFB4, NDUFS7, PSMA1, PSMC5, PSME3, RPL18, RPL8, RPS5, Uba52
DCX	other	2.966576	0.455932	2	ACTR3, GFAP
LARP1	translation regulator	2.714443	0.428291	5	RPL18, RPL39, RPL8, RPS14, RPS5
CTH	enzyme	2.651695	0.428291	2	CX3CR1, HSPA5
CB-5083	chemical drug	2.651695	0.428291	2	GABPA, HSPA5
SGPP2	phosphatase	2.603801	0.428291	3	DNAJA4, HSPA5, HSPH1
CLUH	translation regulator	2.490797	0.428291	4	MRPL15, MRPL39, NDUFS7, SUCLA2
dichlorovinylcysteine	chemical toxicant	2.467246	0.428291	3	PRDX5, PSMA1, STIP1
1, 2-dithiol-3-thione	chemical reagent	2.183096	0.428291	7	LY6E, PFN2, PSMA1, RPL18, STIP1, UBE2K, USP14
Mt	group	2.170053	0.428291	2	GFAP, HSPA5
TSC2	other	2.130768	0.428291	6	DYNC1I1, GFAP, HSPA5, IRS2, PDPK1, PSMA1
CPT1B	enzyme	2.118045	0.428291	7	ACADM, IRS2, MAP2K1, MAPK9, PDPK1, PHKB, RHOQ
anandamide	chemical - endogenous mammalian	2.101824	0.428291	3	HSPA5, MAP2K1, STIP1
PCSK2	peptidase	2.100727	0.428291	2	CCK, PCSK1
ATG5	other	2.035269	0.428291	4	HSPA5, LAMTOR4, PSME3, ROBO3
SAHM1	chemical reagent	2.012781	0.428291	3	JAM3, LY6E, MPI
PCK1	kinase	1.978811	0.428291	2	ACADM, IRS2
FSH	complex	1.958607	0.428291	10	ARL4C, DHX15, ENC1, HDAC5, MAP2K1, PTPRN, RAB5A, RPL39, SMARCD1, STIP1
geldanamycin	chemical drug	1.950782	0.428291	8	ARRB2, BIN1, CUL2, HSPA5, IRS2, PDPK1, RAB5A, YWHAQ
2-amino-1-methyl-6-phenylimidazo-4-5-b-pyridine	chemical toxicant	1.931814	0.428291	3	HSPA5, HSPH1, RAP1A
GFAP	other	1.920819	0.428291	2	GFAP, HSPA5
Lh	complex	1.920819	0.428291	9	ARL4C, MAP2K1, PTPRN, RAB5A, RPL39, RPL8, RPS5, SMARCD1, STIP1
tetrachlorodibenzodioxin	chemical toxicant	1.850781	0.428291	11	CCK, CUL2, EIF4EBP2, ENC1, HACD1, HDAC5, MANF, PCSK1, PSMA1, TRMT10B, ZIC1
torin1	chemical reagent	1.832683	0.428291	6	NDUFS7, RPL18, RPL39, RPL8, RPS14, RPS5
FABP5	transporter	1.823909	0.428291	2	PDPK1, RORA
SLC13A1	transporter	1.793174	0.428291	4	HNMT, HSPA5, RPL8, SRPRA

miR-1-3p (and other miRNAs w/seed GGAAUGU)	mature microRNA	1.793174	0.428291	6	COIL, DHX15, EML4, MXD4, SHTN1, YWHAQ
MAPKAPK3	kinase	1.777284	0.428291	2	HSPA5, HSPB6
UBQLN2	other	1.761954	0.428291	3	NR1D2, PSMA1, PSMC5
desmopressin	biologic drug	1.761954	0.428291	4	HINT1, HSPH1, PPIA, YWHAQ
G protein alpha	group	1.747147	0.428291	4	CMAS, RPE, SPCS1, SRPRA
NCD-38	chemical reagent	1.735182	0.428291	2	GFAP, HSPA5
(1S, 2R)-NCL-1	chemical reagent	1.735182	0.428291	2	GFAP, HSPA5
PTEN	phosphatase	1.718967	0.428291	14	CX3CR1, GMDS, HDAC5, IRS2, LRRFIP1, MXD4, NDUFB4, PDPK1, RAB5A, RAP1A, SOGA3, STX5, SUCLA2, SYNJ1
CREB1	transcription regulator	1.712198	0.428291	12	CCK, GABPA, HSPA5, IRS2, MIGA1, PCSK1, PTPRN, SCN3B, SERPINI1, SHTN1, SPOCK3, TCEAL6
HDL	complex	1.696804	0.428291	3	CX3CR1, GFAP, HSPA5
MLXIPL	transcription regulator	1.694649	0.428291	5	RPL18, RPL39, RPL8, RPS14, RPS5
STEAP3	transporter	1.675718	0.428291	3	FRMD5, PDPK1, RGCC
TRIM2	enzyme	1.655608	0.428291	2	GABPA, NDUFB4
BPIFB1	other	1.655608	0.428291	2	MAP2K1, MAPK9
IND S1	chemical - kinase inhibitor	1.655608	0.428291	2	PSMA1, STIP1
GW9662	chemical reagent	1.645892	0.428291	4	CX3CR1, HSPA5, IRS2, RORA
ELL2	transcription regulator	1.636388	0.428291	3	MANF, SPCS1, SRPRA
CCK	other	1.619789	0.428291	2	GFAP, HSPA5
mir-33	microRNA	1.619789	0.428291	2	FRS2, IRS2
TP53	transcription regulator	1.619789	0.428291	30	ACADM, ARRB2, CAV2, CLIC4, DNAJA4, GABPA, GOLGA4, HDAC5, HSPA5, HSPH1, Krt10, MAP2K1, MPDZ, MPI, MRPL15, MRPL39, NCAPD3, PEX2, PSMA1, PSME3, PTPRN, RAB5A, RPE, RPS5, SCN3B, STIP1, SUCLA2, TOP2B, USP14, VMP1
FGF21	growth factor	1.617983	0.428291	3	ACADM, HSPA5, IRS2
PSEN1	peptidase	1.603801	0.428291	9	AMY2A, GFAP, HINT1, HSPA5, PPIA, PRDX5, RHOQ, STIP1, TOP2B
GnRH analog	biologic drug	1.596879	0.428291	8	AP3S2, ARHGEF9, ATP11B, BABAM2, GATD3A/GATD3B, HINT1, NDUFS7, PPIA
FGFR1	kinase	1.59176	0.428291	4	EIF4EBP2, HSPA5, PCSK1, PDPK1
D-glucose	chemical - endogenous mammalian	1.590067	0.428291	14	ACADM, GABPA, GFAP, HSPA5, IRS2, KIF5C, LAMTOR4, PCSK1, PDPK1, PSME3, PTPRN, RPS14, SRPRA, SUCLA2
miR-16-5p (and other miRNAs w/seed AGCAGCA)	mature microRNA	1.58838	0.428291	6	MAP2K1, MRPL20, PHKB, RIDA, SRPRA, VPS45
ANGPT2	growth factor	1.562249	0.428291	6	APIP, ARL4C, HDAC5, HSPA5, MAP2K1, SOCS7
RRP1B	transcription regulator	1.540608	0.428291	4	RHOQ, RPL39, RPS14, RPS5
LHX2	transcription regulator	1.519993	0.428291	2	FOXJ1, ROBO3
MAPT	other	1.517126	0.428291	11	FUZ, GFAP, HINT1, HSPA5, HSPH1, PFN2, PPIA, PRDX5, STIP1, SYNJ1, TOP2B
DTX1	transcription regulator	1.489455	0.414539	2	HIGD1A, LY6E
NR4A1	ligand-dependent nuclear receptor	1.482804	0.411168	7	BABAM2, LY6E, NDUFB4, NDUFS7, PHKB, RPE, SUCLA2

PRKAA1	kinase	1.4698	0.41005	5	FGFR1OP2, HIGD1A, HSPA5, PTPRN, SERPINI1
IND S7	chemical - kinase inhibitor	1.459671	0.41005	2	PSMA1, STIP1
MMP12	peptidase	1.458421	0.41005	3	ACTR3, PSMA1, PSME3
MEL S3	chemical - kinase inhibitor	1.431798	0.41005	2	PSMA1, STIP1
epoxomicin	chemical - protease inhibitor	1.431798	0.41005	2	HSPA5, IRS2
CX3CR1	G-protein coupled receptor	1.423659	0.41005	5	ADGRV1, ATP11B, DNAI4, FUZ, SPATA7
5-hydroxytryptamine	chemical - endogenous mammalian	1.421361	0.41005	4	AP1M1, BABAM2, BIN1, STX5
GCK	kinase	1.404504	0.41005	2	ACADM, IRS2
IFRD1	other	1.378824	0.41005	2	PPIA, RPL39
bufalin	chemical reagent	1.378824	0.41005	2	HSPA5, YWHAQ
linoleic acid	chemical - endogenous mammalian	1.366532	0.401209	3	ACADM, CCK, HSPA5
ADIPOR1	transmembrane receptor	1.353596	0.396856	2	ACADM, GFAP
metribolone	chemical reagent	1.341035	0.396856	9	CAV2, HSPA5, HSPH1, IRS2, MRPL15, MRPS15, NCAPD3, NDUFS7, PPIA
RB1	transcription regulator	1.335358	0.396856	10	APPL2, CLIC4, CMAS, IRS2, Krt10, NDUFS7, OGA, ROBO3, SRPRA, TIMM50
HAVCR2	other	1.329754	0.396856	2	CX3CR1, PRDX5
sodium tungstate	chemical drug	1.329754	0.396856	2	GFAP, MAP2K1
UCHL1	peptidase	1.324222	0.396856	3	EIF3M, HACD1, HSPA5
THBS4	other	1.306273	0.396856	2	HSPA5, MANF
4-(2-aminoethyl) benzenesulfonylfluoride	chemical - protease inhibitor	1.306273	0.396856	2	HSPA5, SERPINI1
IRF4	transcription regulator	1.304518	0.396856	5	CX3CR1, MANF, MAPK9, PSMA1, RORA